frontiers | Research Topics

Forces in biology: Cell and developmental mechanobiology and its implications in disease, volume II

Edited by
Selwin K. Wu, Guillermo Alberto Gomez, Samantha Jane Stehbens, Anne Karine Lagendijk, Bipul R. Acharya, Aparna Ratheesh, Rashmi Priya and Alexander Bershadsky

Published in
Frontiers in Cell and Developmental Biology

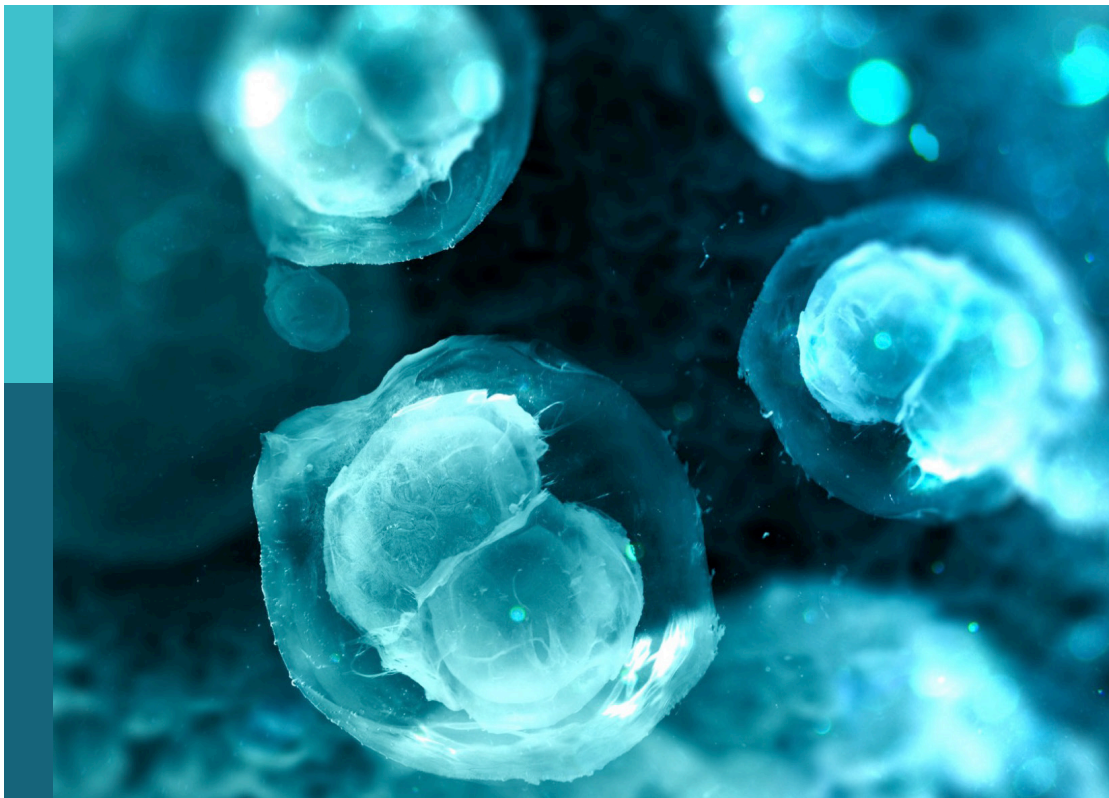

ISSN 1664-8714
ISBN 978-2-83251-063-6
DOI 10.3389/978-2-83251-063-6

About Frontiers

Frontiers is more than just an open access publisher of scholarly articles: it is a pioneering approach to the world of academia, radically improving the way scholarly research is managed. The grand vision of Frontiers is a world where all people have an equal opportunity to seek, share and generate knowledge. Frontiers provides immediate and permanent online open access to all its publications, but this alone is not enough to realize our grand goals.

Frontiers journal series

The Frontiers journal series is a multi-tier and interdisciplinary set of open-access, online journals, promising a paradigm shift from the current review, selection and dissemination processes in academic publishing. All Frontiers journals are driven by researchers for researchers; therefore, they constitute a service to the scholarly community. At the same time, the *Frontiers journal series* operates on a revolutionary invention, the tiered publishing system, initially addressing specific communities of scholars, and gradually climbing up to broader public understanding, thus serving the interests of the lay society, too.

Dedication to quality

Each Frontiers article is a landmark of the highest quality, thanks to genuinely collaborative interactions between authors and review editors, who include some of the world's best academicians. Research must be certified by peers before entering a stream of knowledge that may eventually reach the public - and shape society; therefore, Frontiers only applies the most rigorous and unbiased reviews. Frontiers revolutionizes research publishing by freely delivering the most outstanding research, evaluated with no bias from both the academic and social point of view. By applying the most advanced information technologies, Frontiers is catapulting scholarly publishing into a new generation.

What are Frontiers Research Topics?

Frontiers Research Topics are very popular trademarks of the *Frontiers journals series*: they are collections of at least ten articles, all centered on a particular subject. With their unique mix of varied contributions from Original Research to Review Articles, Frontiers Research Topics unify the most influential researchers, the latest key findings and historical advances in a hot research area.

Find out more on how to host your own Frontiers Research Topic or contribute to one as an author by contacting the Frontiers editorial office: frontiersin.org/about/contact

Forces in biology: Cell and developmental mechanobiology and its implications in disease, volume II

Topic editors

Selwin K. Wu — National University of Singapore, Singapore
Guillermo Alberto Gomez — University of South Australia, Australia
Samantha Jane Stehbens — The University of Queensland, Australia
Anne Karine Lagendijk — The University of Queensland, Australia
Bipul R. Acharya — University of Virginia, United States
Aparna Ratheesh — University of Warwick, United Kingdom
Rashmi Priya — Francis Crick Institute, United Kingdom
Alexander Bershadsky — Weizmann Institute of Science, Israel

Citation

Wu, S. K., Gomez, G. A., Stehbens, S. J., Lagendijk, A. K., Acharya, B. R., Ratheesh, A., Priya, R., Bershadsky, A., eds. (2023). *Forces in biology: Cell and developmental mechanobiology and its implications in disease, volume II*. Lausanne: Frontiers Media SA. doi: 10.3389/978-2-83251-063-6

Table of contents

frontiers | Frontiers in Cell and Developmental Biology

TYPE Editorial
PUBLISHED 01 December 2022
DOI 10.3389/fcell.2022.1082857

OPEN ACCESS

EDITED AND REVIEWED BY
Akihiko Ito,
Kindai University, Japan

*CORRESPONDENCE
Selwin K. Wu,
selwin_wu@mail.dfci.harvard.edu

SPECIALTY SECTION
This article was submitted to Cell Adhesion and Migration, a section of the journal Frontiers in Cell and Developmental Biology

RECEIVED 28 October 2022
ACCEPTED 07 November 2022
PUBLISHED 01 December 2022

CITATION
Wu SK, Gomez GA, Stehbens S, Acharya BR, Ratheesh A, Priya R, Lagendijk A and Bershadsky A (2022), Editorial: Forces in biology - Cell and developmental mechanobiology and its implications in disease - Volume II. *Front. Cell Dev. Biol.* 10:1082857. doi: 10.3389/fcell.2022.1082857

Editorial: Forces in biology - Cell and developmental mechanobiology and its implications in disease - Volume II

Selwin K. Wu[1,2]*, Guillermo A. Gomez[3], Samantha Stehbens[4], Bipul R. Acharya[5], Aparna Ratheesh[6], Rashmi Priya[7], Anne Lagendijk[4,8] and Alexander Bershadsky[1,9]

[1]Mechanobiology Institute, National University of Singapore, Singapore, Singapore, [2]Department of Biological Sciences, National University of Singapore, Singapore, Singapore, [3]Centre for Cancer Biology, SA Pathology and University of South Australia, Adelaide, SA, Australia, [4]Cell and Developmental Biology Division, Institute for Molecular Bioscience, The University of Queensland, Brisbane, QLD, Australia, [5]Wellcome Centre for Cell-Matrix Research, Faculty of Biology, Medicine & Health, Manchester Academic Health Science Centre, University of Manchester, Manchester, United Kingdom, [6]Warwick Medical School, University of Warwick, Coventry, United Kingdom, [7]Francis Crick Institute, London, United Kingdom, [8]School of Biomedical Sciences, The University of Queensland, Brisbane, QLD, Australia, [9]Department of Molecular Cell Biology, Weizmann Institute of Science, Rehovot, Israel

KEYWORDS

forces, brain, cancer, bones and cartilage, immunology

Editorial on the Research Topic
Forces in biology - Cell and developmental mechanobiology and its implications in disease - Volume II

Cellular biomechanics underlie a diversity of cellular processes and behaviours, simultaneously being a fundamental determinant of tissue patterning. Core cellular activities, from differentiation and proliferation to migration and apoptosis, are influenced by the cell's mechanical properties and the ability to discern mechanical signals from their environment. The intrinsic cell machinery internalizes exogenous physical signals from their environment, and a high-precision regulation from a molecular to multicellular level ensures each cell interpret such signals and meets its designated fate. Thus, cells within tissues constantly acquire sensory inputs from their neighbours and the extracellular matrix—detecting, transducing and processing mechanochemical signals to modulate processes and coordinate responses. In this issue, we highlight recent developments in three areas of cell biomechanics in these chapters: 1) Cell and Developmental Biology, 2) Cancer and 3) Bones & Connective Tissues.

In the first chapter, Alvarez and Smutny reviewed the recent advancements on how actomyosin-contractile forces affect tissue morphogenesis and regulate cell fate in mouse and zebrafish embryonic development. Next, Procès et al. developed a comprehensive review of the heterogenous mechanobiology of the brain, from a molecular to organ level, to help engineer early interventional therapies or treatments for traumatic brain injury, neurodegenerative diseases, and glioblastoma.

As the complexity of our understanding of mechanobiology grows, theoretical modelling can help interweave existing experimental data and consolidate various parameters into a singular, quantitative system. These computational models can help to form new hypotheses or to unify concepts. Khataee et al. put forward a general model based on the Cellular Potts Model to encapsulate and analyze the interplay between cellular mechanical properties and dynamical transitions in epithelial cell shapes and structures. Interestingly, cell extrusion promotes monolayer-to-multilayer transition based on the mechanical properties of cells and the orientation of cell division.

While mechanochemical signalling pathways can control both cellular dynamics (at a short timescale) and gene expression (at longer time scales), their co-regulation is critical for the self-organization of cells into tissues. Afzal et al. studied how the interaction of placenta and the endometrium eventually results in the deep invasion of placental extravillous trophoblasts into the maternal stroma. They demonstrated that paracrine HB-EGF signalling reduces activated decidual fibroblasts' enhanced contractility and energetic state by rebalancing the SRF-MRTF-TCF transcriptional axis.

Further, misregulation of the aforementioned mechanobiological mechanisms can lead to pathological consequences such as cancer and suppressed immunity. In Chapter 2, we focus on cancer mechanobiology. Dobrokhotov et al. found that actomyosin activity is impaired in cutaneous squamous cell carcinoma (cSCC). External application of tensile loads to adherens junctions by sustained mechanical stretch attenuates the proliferation of cSCC cells. Force-dependent activation of actomyosin in cSCC cells also inhibits their proliferation in a cell-cell contact-dependent manner. Taken together, the malignancy of cSCC cells may be reduced by applying tensile loads to adherens junctions.

Besides the adherens junctions, cancer progression also involves remodelling the extracellular matrix (ECM). Vahala and Choi review current platforms and biomaterials engineered to mimic the micro and nano-properties of the tumour microenvironment, and subsequent understanding of mechanically regulated pathways in cancer. In essence, cancer cells morphologically adapt to survive in altered environments. Thus, changing tumour ECM properties, including stiffness and ligand chemistry and spacing, are factors that should be considered and incorporated when designing future tools.

Next, how contractile forces regulate non-adherent natural killer (NK) cells during cancer surveillance was addressed by Wong et al.

They found that lung cancer cells can provoke NK cells and enhance their actomyosin-mediated contractility as a potential early phase activation mechanism. This action shuttles Eomes, an evolutionarily conserved NK cell transcription factor, into the nucleus. NK cells responded to the presumed immunosuppressive TGFβ in the NK-lung cancer coculture medium to sustain its intracellular contractility through myosin light chain phosphorylation, thereby promoting the nuclear localization of Eomes, which likely responds downstream to mechanical stimuli for increased NK cytotoxicity.

In the final chapter, we focus on the study of bones and connective tissues, which lies precisely at the interface of biomechanics and mechanobiology. The chapter commences with Choi et al. reviewing the current knowledge of the osteocyte's role in maintaining bone health and the key regulatory pathways of these mechanosensitive cells. Subsequently, they highlighted the therapeutic opportunities offered by existing treatments and the potential for targeting osteocyte-directed signalling.

Delving into the cartilage, Boos et al. reviewed the different cartilages and chondrocyte mechanosensing types, then moved on to the multiscale strain transfer through cartilage tissue the involvement of individual ECM components before finally outlining insights to understand multiscale strain transfer in cartilage further. Essentially, the heterogeneity in the spatial variation of ECM molecules leads to a non-uniform, depth-dependent strain transfer and alters the magnitude of forces sensed by cells in articular cartilage and fibrocartilage, influencing chondrocyte metabolism and biochemical response.

We end the issue with a review of Ehlers-Danlos Syndromes (EDSs), a group of connective tissue disorders characterized by skin stretchability, joint hypermobility and instability. Though EDS patients typically exhibit lowered elasticity, recent evidence suggests that comorbidities of EDS could also be associated with reduced tissue stiffness. Royer and Han discussed the potential mechanobiological pathways involved in the two most popular types of EDS: classical and hypermobile, and their respective, associated comorbidities: mast cell activation syndrome and impaired wound healing—finding that altered mechanosensitive proteins and the lack of collagen V to be main contributors respectively.

Extending the traditions of our first issue (Forces in Biology) (Wu et al., 2020), we hope that this issue will also be of exceptional interest to students and researchers studying molecular and cellular mechanisms in development and diseases; To understand and appreciate their complex, yet cohesive inner workings, and ideally inspire better designs in therapeutics and diagnostics.

Author contributions

SW wrote the manuscript. GG edited the manuscript. All authors provided intellectual input to the editorial.

Funding

SW is supported by a MOE Research Scholarship Block Research Fellow Scheme by the Singapore Ministry of Education (C141000207532) and a Young Individual Research Grant (MOH-OFYIRG20nov-0019) by the National Medical Research Council of Singapore. GG and SS are supported by Australian Research Council Future Fellowships (FT160100366 and FT190100516). GG is also supported the National Health and Medical Research Council of Australia (Ideas grant 2021/GNT2013180); the Charlie Teo Fundation, the Cure Brain Cancer Foundation; the University of South Australia, The Medical Advances Without Animals Trust (MAWA) and the NeuroSurgical Research Foundation (NRF). BA is supported by BBSRC, United Kingdom (BB/V001140/1).

Reference

Wu, S. K., Gomez, G. A., Stehbens, S. J., and Smutny, M. (2020). Editorial: Forces in Biology - cell and developmental mechanobiology and its Implications in disease. *Front. Cell. Dev. Biol.* 8, 598179. doi:10.3389/fcell.2020.598179

Acknowledgments

We thank Tay Shu Chian for co-writing the introduction and editing the manuscript. We are also grateful for all reviewers for their immense effort to review all manuscripts in this issue.

Conflict of interest

The authors declare that the research was conducted in the absence of any commercial or financial relationships that could be construed as a potential conflict of interest.

Publisher's note

frontiers in Cell and Developmental Biology

ORIGINAL RESEARCH
published: 11 November 2021
doi: 10.3389/fcell.2021.728383

Anti-Malignant Effect of Tensile Loading to Adherens Junctions in Cutaneous Squamous Cell Carcinoma Cells

Oleg Dobrokhotov[1], Masaki Sunagawa[2,3], Takeru Torii[4], Shinji Mii[2], Keiko Kawauchi[4], Atsushi Enomoto[2], Masahiro Sokabe[1] and Hiroaki Hirata[1]**

[1]Mechanobiology Laboratory, Nagoya University Graduate School of Medicine, Nagoya, Japan, [2]Department of Pathology, Nagoya University Graduate School of Medicine, Nagoya, Japan, [3]Division of Surgical Oncology, Department of Surgery, Nagoya University Graduate School of Medicine, Nagoya, Japan, [4]Frontiers of Innovative Research in Science and Technology, Konan University, Kobe, Japan

OPEN ACCESS

Edited by:
Bipul R. Acharya, University of Virginia, United States

Reviewed by:
René-Marc Mège, Centre National de la Recherche Scientifique (CNRS), France
Srikala Raghavan, Institute for Stem Cell Science and Regenerative Medicine (inStem), India

***Correspondence:**
Hiroaki Hirata
hhirata@med.nagoya-u.ac.jp
Masahiro Sokabe
msokabe@med.nagoya-u.ac.jp

Specialty section:
This article was submitted to Cell Adhesion and Migration, a section of the journal Frontiers in Cell and Developmental Biology

Received: *22 June 2021*
Accepted: *19 October 2021*
Published: *11 November 2021*

Citation:
Dobrokhotov O, Sunagawa M, Torii T, Mii S, Kawauchi K, Enomoto A, Sokabe M and Hirata H (2021) Anti-Malignant Effect of Tensile Loading to Adherens Junctions in Cutaneous Squamous Cell Carcinoma Cells. Front. Cell Dev. Biol. 9:728383. doi: 10.3389/fcell.2021.728383

Actomyosin contractility regulates various cellular processes including proliferation and differentiation while dysregulation of actomyosin activity contributes to cancer development and progression. Previously, we have reported that actomyosin-generated tension at adherens junctions is required for cell density-dependent inhibition of proliferation of normal skin keratinocytes. However, it remains unclear how actomyosin contractility affects the hyperproliferation ability of cutaneous squamous cell carcinoma (cSCC) cells. In this study, we find that actomyosin activity is impaired in cSCC cells both *in vitro* and *in vivo*. External application of tensile loads to adherens junctions by sustained mechanical stretch attenuates the proliferation of cSCC cells, which depends on intact adherens junctions. Forced activation of actomyosin of cSCC cells also inhibits their proliferation in a cell-cell contact-dependent manner. Furthermore, the cell cycle arrest induced by tensile loading to adherens junctions is accompanied by epidermal differentiation in cSCC cells. Our results show that the degree of malignant properties of cSCC cells can be reduced by applying tensile loads to adherens junctions, which implies that the mechanical status of adherens junctions may serve as a novel therapeutic target for cSCC.

Keywords: actomyosin, adherens junction, contact inhibition, mechanosensing, mechanotransduction, epidermoid carcinoma

INTRODUCTION

The great significance of actomyosin cytoskeleton and actomyosin-generated tension in epithelia development, morphogenesis, and homeostasis is well appreciated. Actomyosin network regulates cell-cell and cell-extracellular matrix (ECM) adhesions, cell division, and delamination, as well as modulates critical regulatory gene networks controlling cell proliferation, apoptosis, stemness, and differentiation (Humphrey et al., 2014; Heer and Martin, 2017; Pinheiro and Bellaïche, 2018). Given the importance of actomyosin in normal epithelial functions, failures in the regulation of the actomyosin cytoskeleton potentially cause various diseases including cancers (Dobrokhotov et al., 2018). Many studies have shown the role of actomyosin in cancer progression; however, these studies have mainly focused on the effect of mechanical forces at the cell-ECM interface rather than cell-cell

interaction (Butcher et al., 2009; Provenzano et al., 2009; Yu et al., 2011; Chaudhuri et al., 2018). As most of the solid tumors originate in epithelia in which cells form epithelial sheets (Hanahan and Weinberg, 2011), the mechanical interaction between cells may also influence tumor cell behaviors.

Loss of cell density-dependent inhibition of proliferation (termed contact inhibition of proliferation, CIP) is a characteristic feature of cancer cells (Hanahan and Weinberg, 2011). CIP depends on the formation of the cell-cell adhesion structure, adherens junction (AJ) (McClatchey and Yap, 2012), and dysregulation of AJs is associated with carcinogenesis (Vasioukhin, 2012; Wong et al., 2018). At AJs, the transmembrane protein E-cadherin binds *trans*-homophilically *via* its extracellular domain, which mediates adhesion between the neighboring cells. The cytoplasmic tail of E-cadherin connects to the actomyosin cytoskeleton at AJs through linker proteins, including α- and β-catenins (Mège and Ishiyama, 2017; Bruner and Derksen, 2018). Interestingly, the homophilic binding of E-cadherin *per se* does not inhibit but promotes the proliferation of cells (Liu et al., 2006; Hirata et al., 2017), and actomyosin-generated tension at AJs is essential for CIP in normal human keratinocytes (Hirata et al., 2017). However, the role of tensile forces at AJs in cell proliferation may be context- and cell-type-dependent because it has been reported that tensile loads at AJs induce both promotion and inhibition of proliferation of MDCK cells (Benham-Pyle et al., 2015; Furukawa et al., 2017). In the case of cutaneous squamous cell carcinoma (cSCC), some studies implied the tumorigenic effect of actomyosin contractility (Samuel et al., 2011; García-Mariscal et al., 2018; Carley et al., 2021), while others suggested its tumor-suppressive function (Sugai et al., 1992; McMullan et al., 2003; Strudwick et al., 2015). Notably, neither of the studies directly compared the level of actomyosin contractility in cSCC cells against normal keratinocytes. Hence, it remains unclear whether and how the tensile status at AJs contributes to the malignant proliferation of cSCC cells.

Skin homeostasis depends not only on the regulation of cell proliferation but also on the differentiation of keratinocytes. The epidermis is composed of stratified layers of cells; among them, only cells in the stratum basale, the innermost layer, have the proliferative ability, while cells that lack contact with the basement membrane, form the suprabasal layers and undergo terminal differentiation (Simpson et al., 2011) depending on tension in the nuclear lamina (Carley et al., 2021). In cancer, histological differentiation grade, which assesses how much the cancer cells lose the differentiated phenotype (including expression of differentiation markers and typical morphologies of differentiated cells) of the original tissue cells, is a major prognostic parameter. Less-differentiated cancers generally exhibit more aggressive and drug-resistant phenotypes (Karantza, 2011; Dmello et al., 2019). In the case of cSCC, the low differentiation group shows over three times higher metastatic rate and over two times higher recurrence rate than the high differentiation group (Rowe et al., 1992; Barksdale et al., 1997; Alam and Ratner, 2001). However, it remains unknown whether actomyosin activity affects the differentiation status of cSCC cells.

In this study, we investigate the role of actomyosin contractility in cSCC cell proliferation and differentiation. We find that the overproliferation of cSCC cells is associated with impairment in actomyosin contractility, both *in vivo* and *in vitro*. Exogenous induction of tensile loads at AJs by pharmacological activation of actomyosin or mechanical stretch of confluent cSCC cells attenuated proliferation and induced epidermal differentiation of cSCC cells. Our results suggest that tensile loads at AJs have an anti-malignant effect in cSCC.

RESULTS

Overproliferation of cSCC Cells Concurs with Impaired Actomyosin Contractility

We first examined actomyosin contractility in cSCC *in vivo* by using mouse skin tumors that were induced chemically by application of 9,10-dimethyl-1,2-benzanthracene (DMBA) followed by tetradecanoyl-phorbol acetate (TPA), which causes mutations that are highly similar to somatic mutations in human cSCC (Nassar et al., 2015). Samples of the tumor-free back skin and DMBA/TPA-induced skin tumors from wild-type FVB/N mice were immunohistochemically (IHC) stained for Ki-67, a cell proliferation marker (Gerdes et al., 1984), and myosin regulatory light chain (MLC) phosphorylated at Ser19 site (pS19-MLC), as the pS19-MLC level reflects the contractile activity of actomyosin (Riento and Ridley, 2003) (**Figure 1A**), wherein smooth and skeletal muscle cells were used as the internal positive control for pS19-MLC staining (**Supplementary Figures S1A,B**). Since cSCC cells are deemed to originate from the quiescent suprabasal keratinocytes (Ratushny et al., 2012), we compared cSCC cells with the normal keratinocytes of suprabasal layers. As expected, the tumor-free skin showed typical stratification of cells and Ki-67-positive cells were not detected in suprabasal layers, i.e., keratinocytes in the suprabasal layers were cell cycle-arrested (**Figure 1A**). By contrast, skin tumors did not show a layered organization, and Ki-67 positive cells were distributed throughout the tumors. The higher ability of cell proliferation in the skin tumors concurred with lower actomyosin contractility in comparison to the suprabasal layers of the healthy epidermis (**Figure 1A**). We further noted that, in the papilloma tissue, which is a benign tumor that represents an early stage of cancerogenesis and may progress to cSCC (Neagu et al., 2016), MLC phosphorylation and Ki-67 expression had an apparent negative correlation. A high level of pS19-MLC in the superficial region coincided with almost exclusively Ki-67-negative cells, while in the deeper regions MLC phosphorylation was largely reduced and Ki-67-positive cells were abundant (**Supplementary Figure S1C**). These results demonstrate that the high proliferation ability is closely associated with the low actomyosin activity throughout normal keratinocytes, papilloma, and cSCC cells *in vivo*, and suggest that the reduction in MLC phosphorylation first occurs at a relatively early stage of skin cancer development.

To recapitulate our *in vivo* findings in a cell culture model, we used the cSCC cell line, A431, commonly used for skin cancer studies. As expected and in contrast to primary

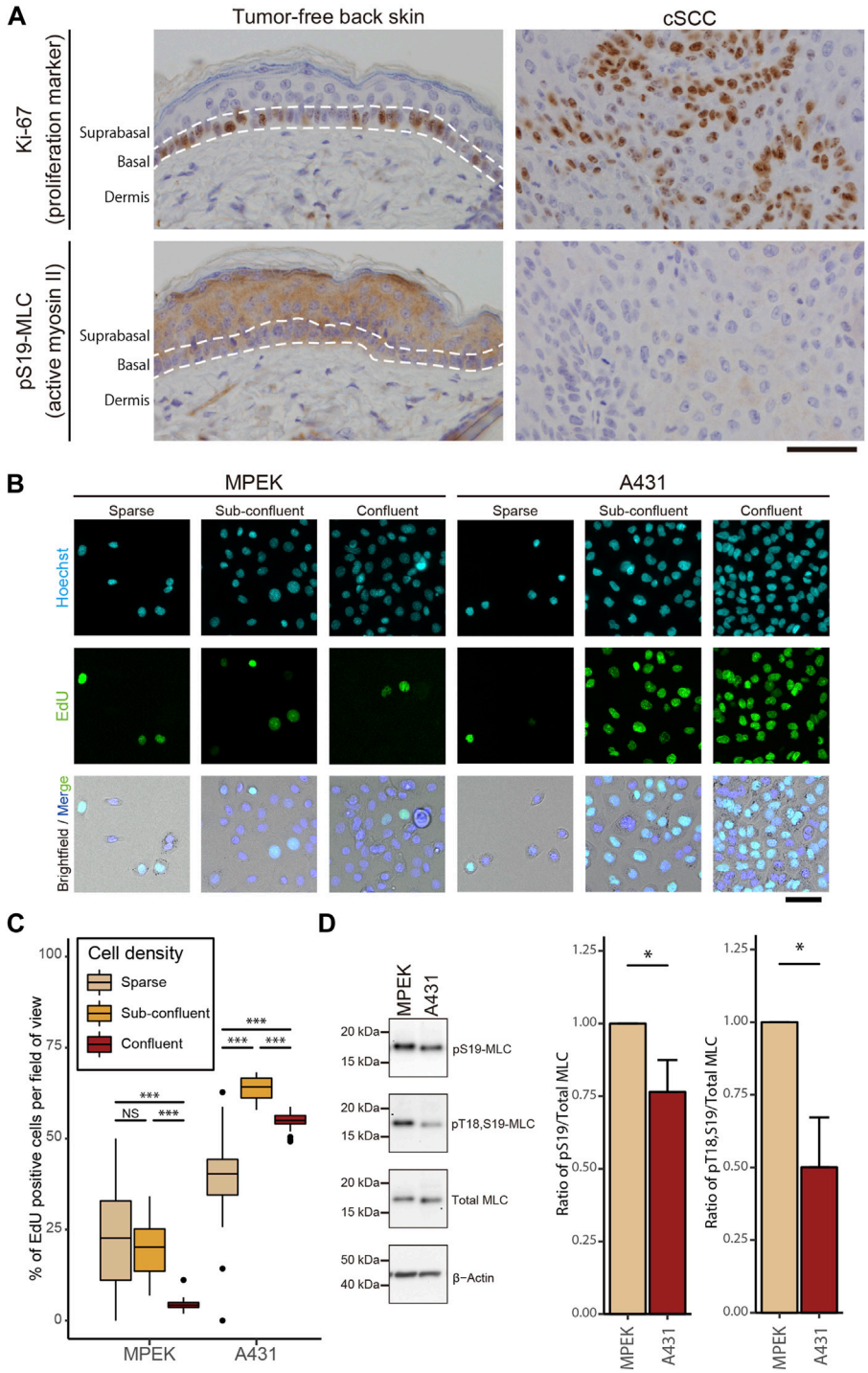

FIGURE 1 | Impairment of actomyosin contractility is associated with hyperproliferation of cSCC cells both *in vitro* and *in vivo*. **(A)** DMBA/TPA-treated tumor-free mouse back skin and cSCC were subjected to IHC staining for Ki-67 and pS19-MLC. Scale bar, 50 μm. **(B)** Fluorescence microscopy analysis of EdU incorporation (green) in MPEK and A431 cells under sparse, sub-confluent, and confluent conditions. Under the sparse condition, only sequestered cells lacking any cell-cell contact were used for the analyses. Cell nuclei were labeled with Hoechst 33342 (cyan). Scale bar, 50 μm. **(C)** Percentages of EdU-positive nuclei in MPEK and A431 cells at different cell densities. Box-and-whisker plots show the median, the interquartile range, and the tenth and ninetieth percentiles. $n = 40$ fields of view from two independent experiments (>1500 cells per condition) were pooled for the analysis. ***$p < 0.001$; NS, $p > 0.05$. **(D)** Whole-cell lysates of confluent MPEK and A431 cells were immunoblotted for pS19-MLC, Thr18-and Ser19-doublephosphorylated MLC (pT18,S19-MLC), total MLC, and β-actin. Bar graphs show the quantification of the densitometric ratio of pS19-MLC or pT18,S19-MLC against total MLC. Values were normalized with the mean values in MPEK cells. Each bar represents mean ± SD from three independent experiments. *$p < 0.05$.

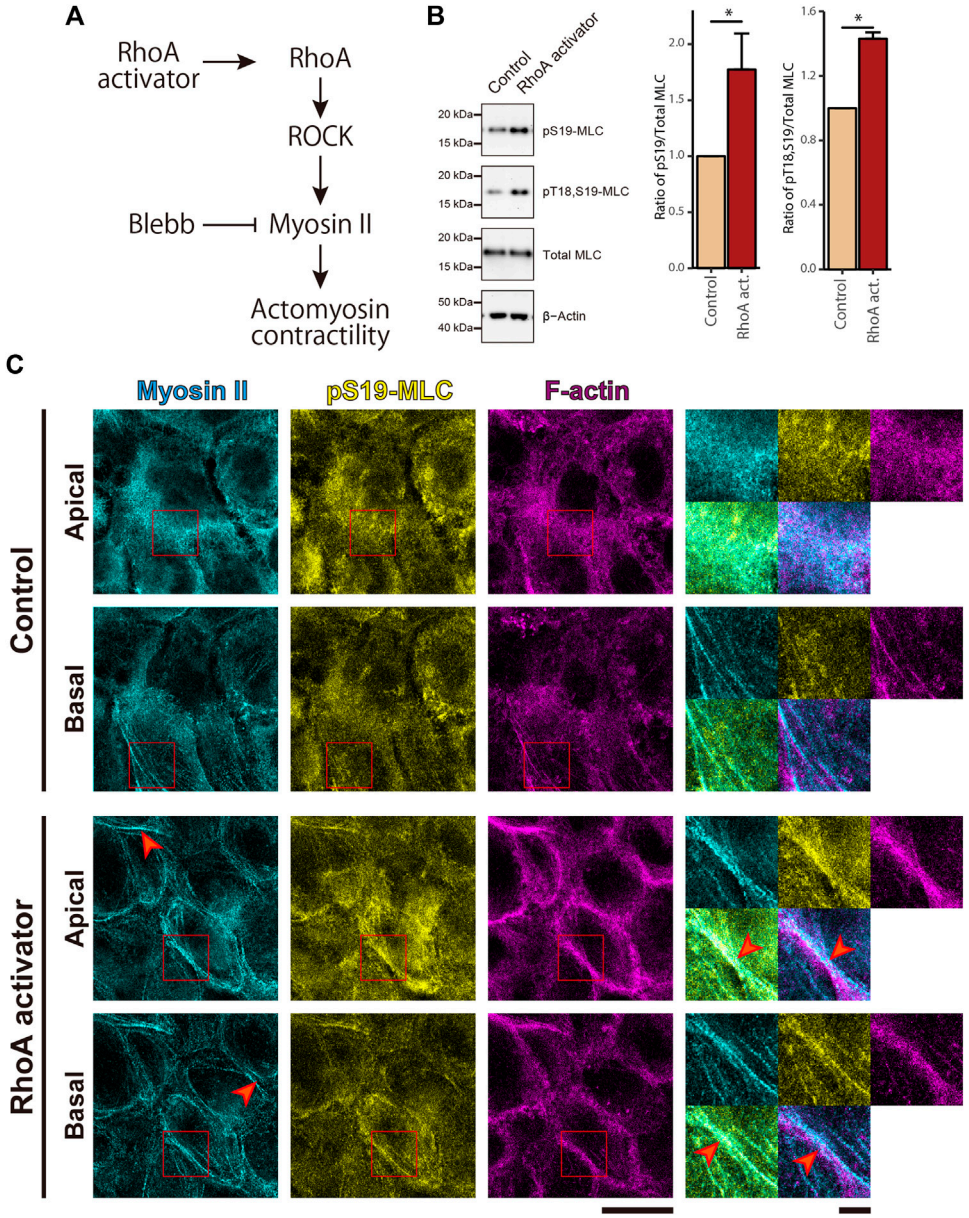

FIGURE 2 | RhoA activation induces MLC phosphorylation and enrichment of actomyosin fibers at the cell-cell junctional regions in cSCC cells. **(A)** The RhoA-ROCK-myosin II signaling cascade for actomyosin activation. **(B)** Whole-cell lysates of control A431 cells and A431 cells treated with 5 μg/ml RhoA activator (RhoA act.) were immunoblotted for pS19-MLC, pT18,S19-MLC, total MLC, and β-actin. Bar graphs show the quantification of the densitometric ratio of pS19-MLC or pT18,S19-MLC against total MLC. Values were normalized with the mean values in control cells. Each bar represents mean ± SD from three independent experiments. *$p <$ 0.05. **(C)** Confluent A431 cells were treated as in **(B)** and stained for non-muscle myosin IIA (cyan), pS19-MLC (yellow), and F-actin (magenta). Apical and basal focal planes of the cells are shown. Magnified images of the boxed regions are also shown. Red arrowheads indicate accumulated actomyosin at the lateral part of the cell cortex in the RhoA activator-treated cells. Scale bars, 5 μm for magnified images, and 20 μm for others.

epidermal keratinocytes (MPEK), A431 cancer cells showed impairment in CIP; even at the confluent cell density, A431 cells continued proliferating (**Figures 1B,C**). The proliferation of A431 cells was greater at the confluent cell density than that for sequestered cells lacking cell-cell contact, with the maximum reached at the sub-confluent cell density (**Figure 1C**). Following the assessment of proliferation, levels of MLC phosphorylation were evaluated by western blotting (WB). Consistent with the IHC results *in vivo*, A431 cSCC cells showed a lower level of MLC phosphorylation at both Thr18 and Ser19 residues than normal MPEK keratinocytes, while total MLC expression stayed unaltered (**Figure 1D**). Taken together, our results reveal that cSCC cells with a high proliferation

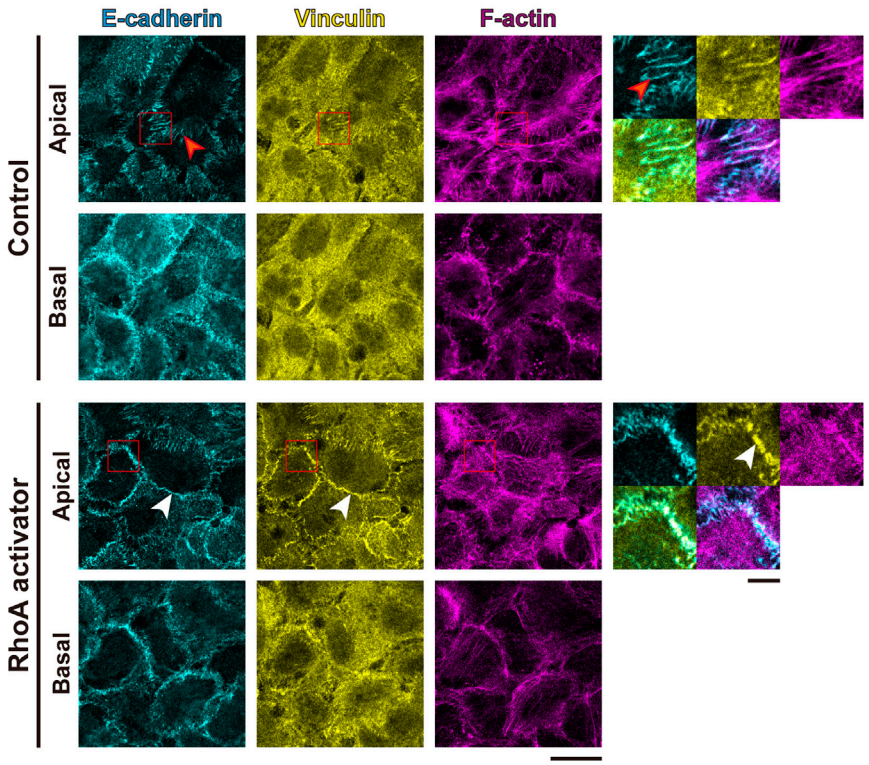

FIGURE 3 | RhoA activation increases tensile loads at adherens junctions but not focal adhesions in cSCC cells. Confluent A431 cells were treated with or without 5 μg/ml RhoA activator (RhoA act.) and stained for E-cadherin (cyan), F-actin (magenta), and vinculin (yellow). Apical and basal focal planes of the cells are shown. Magnified images of the boxed regions are also shown. The red arrowheads indicate zipper-like AJs, and the white arrowheads indicate continuous AJs. Scale bars, 5 μm for magnified images, and 20 μm for others.

ability have a reduced level of actomyosin contractility in comparison to normal keratinocytes both *in vivo* and *in vitro*.

Both Activation of Actomyosin Contractility and Mechanical Stretch Inhibit Cell Cycle Progression in cSCC Cells

Given that the high ability of cell proliferation coincides with low actomyosin contractility in cSCC cells, it is natural to ask whether the low level of actomyosin contractility contributes to the overproliferation of cSCC cells. To address this question, we activated the small GTPase RhoA in the RhoA-ROCK-myosin II signaling cascade by treating cells with the membrane-permeable derivative of the bacterial cytotoxic necrotizing factor which selectively deamidates Gln63 of RhoA to constitutively activate RhoA (Flatau et al., 1997; Schmidt et al., 1997) (**Figure 2A**). Upon RhoA activation in confluent A431 cells, we observed elevated actomyosin contractility as revealed by an increase in Thr18 and Ser19 phosphorylation of MLC (**Figure 2B**). Activation of actomyosin potentially elevates the tensile status not only at AJs but also at focal adhesions (FAs), which may facilitate autophosphorylation of focal adhesion kinase (FAK) and thus promote cell proliferation (Schwartz and Assoian, 2001; Wang et al., 2005; Pasapera et al., 2010; Hirata et al., 2015). To discriminate actomyosin activities at these distinct adhesion classes, we conducted an immunofluorescence (IF) analysis of actomyosin distribution in the cells. Interestingly, in non-treated control samples, actomyosin was rather dispersed with only few distinct filaments at the basal part of the cortex (**Figure 2C**). By contrast, RhoA activation induced formation of prominent actomyosin fibers and their accumulation along the lateral membrane at cell-cell boundaries (**Figure 2C**, red arrowheads). However, this treatment did not apparently promote formation of stress fibers at the basal cortex (**Figure 2C**).

To further evaluate the tensile status at cell adhesion structures, we examined the intracellular distribution of vinculin, because vinculin localizes to AJs and FAs when these adhesive structures suffer tensile force (Yonemura et al., 2010; Hirata et al., 2014; Bays and DeMali, 2017). Consistent with the impairment in MLC phosphorylation, in the non-treated confluent A431 cells, vinculin was mainly cytoplasmic with only occasional localization at AJs and without noticeable localization at FAs (**Figure 3**). However, treatment with the RhoA activator induced vinculin accumulation at AJs (**Figure 3**). Even though a faint vinculin-positive FAs could be observed in some RhoA activator-treated cells (**Supplementary Figure S2A**), in majority of the cells vinculin accumulation at FAs was not detected. Similar to vinculin, zyxin (another force-responsive marker of FAs; Hirata et al., 2008; Schiller et al., 2011) also showed only slight accumulation at FAs in small

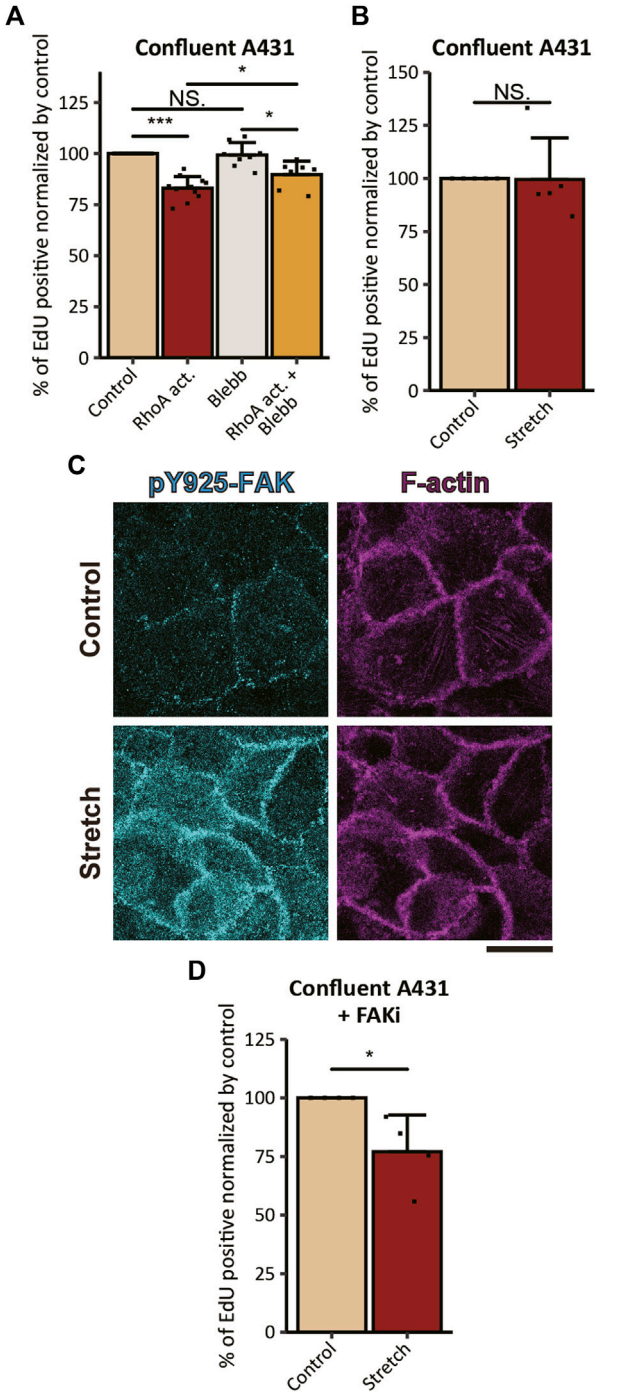

FIGURE 4 | Actomyosin activation and mechanical stretch inhibit the proliferation of cSCC cells. **(A)** Ratios of EdU-positive nuclei in confluent A431 cells treated with 5 μg/ml RhoA activator (RhoA act.), 100 μM *p*-aminoblebbistatin (Blebb) or combination of both drugs (RhoA act. + Blebb) for 6 h followed by incubation with EdU for 2 h in the presence of the same compounds. Values were normalized with the mean value in control cells. Each bar represents mean ± SD. $n \geq 8$ independent experiments. $^{*}p < 0.05$; $^{***}p < 0.001$; NS, $p > 0.05$. **(B)** Ratios of EdU-positive nuclei in confluent A431 cells without FAKi treatment under static (Control) and 20% UPS (Stretch) conditions. Values were normalized with the mean value in the static control. Each bar represents mean ± SD. $n = 5$ independent experiments. NS, $p > 0.05$. **(C)** Non-treated confluent A431 cells under static (Control) and 20% UPS (Stretch) conditions were stained for pY925-FAK (cyan) and F-actin (magenta). Basal focal planes of the cells are shown. Scale bars, 20 μm. **(D)** Ratios of EdU-positive nuclei in confluent A431 cells with FAKi treatment under static (Control) and 20% UPS (Stretch) conditions. Values were normalized with the mean value in the static control. Each bar represents mean ± SD. $n = 4$ independent experiments. $^{*}p < 0.05$; NS, $p > 0.05$.

subpopulation of RhoA activator-treated cells (**Supplementary Figure S2A**). In contrast to A431 cells, C2C12 myoblasts, which were used as a positive control, showed obvious localization of vinculin and zyxin at FAs (**Supplementary Figure S2B**). In line with these observations, RhoA activation in confluent A431 cells did not altered phosphorylation at Tyr925 site of FAK (**Supplementary Figure S3**). Taken together, these results suggest that RhoA activation significantly increased tensile loads at the AJs but not at the FAs in confluent A431 cells, which is consistent with the previous finding that actomyosin-generated tension is differentially regulated in distinct subcellular compartments (Gayrard et al., 2018; Déjardin et al., 2020). Notably, while only zipper-like AJs connected to the tips of radial actin bundles were observed in apical portions of control A431 cells (**Figure 3**, red arrowheads), treatment with the RhoA activator caused the formation of continuous lines of E-cadherin staining associated with the cortical actin and vinculin (**Figure 3**, white arrowheads), which was reminiscent of the development of honeycomb lattice of continuous AJs in differentiating keratinocytes (Vaezi et al., 2002). Consistently, the length of continuous vinculin-positive AJs was significantly higher under the RhoA activator treatment, in comparison to the control (**Supplementary Figures S4A,B**).

Next, we assessed the effect of RhoA activation on cell cycle progression. We found that the proliferation of A431 cells was inhibited by 6-h treatment with the RhoA activator, as revealed by a reduction in the ratio of EdU positive cells in comparison to the non-treated control (**Figure 4A**). The RhoA-induced inhibitory effect on cell proliferation was diminished by combined treatment with the direct inhibitor of myosin II ATPase activity, *p*-aminoblebbistatin (hereafter Blebb; Várkuti et al., 2016), indicating that RhoA activation attenuates proliferation of cSCC cells *via* activation of actomyosin contractility. However, since the Blebb treatment failed to fully abrogate the effect of RhoA activation (**Figure 4A**), some additional myosin II-independent mechanism(s) might also be involved in RhoA-induced inhibition of cell proliferation. Notably, Blebb treatment alone did not have any statistically significant effect on the proliferation of confluent A431 cSCC cells (**Figure 4A**), whereas the same treatment led to the promotion of cell proliferation in normal keratinocytes under the confluent condition (Hirata et al., 2017). These opposing results are likely to be caused by the difference in endogenous levels of actomyosin contractility in these two cell types; in contrast to the case of normal keratinocytes with the high actomyosin activity, the low level

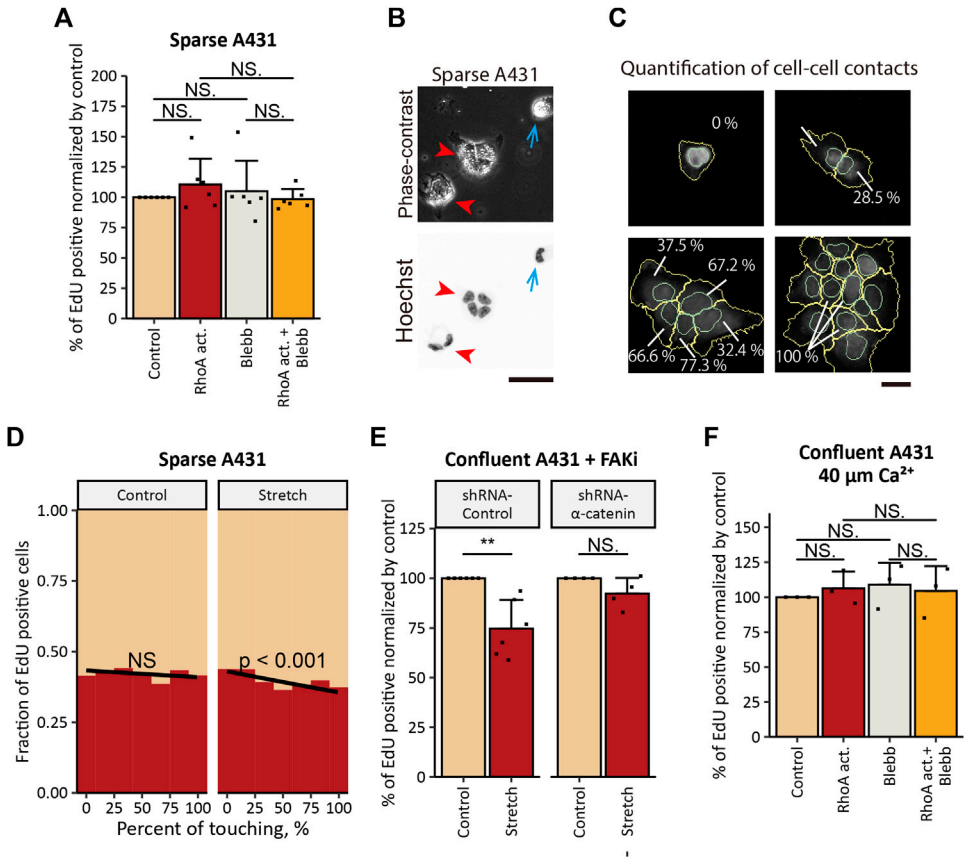

FIGURE 5 | Tensile loading-induced inhibition of the proliferation depends on the intact AJs in cSCC cells. **(A)** Ratios of EdU-positive nuclei in sparse A431 cells treated with 5 μg/ml RhoA activator (RhoA act.), 100 μM *p*-aminoblebbistatin (Blebb) or combination of both drugs (RhoA act. + Blebb) for 6 h followed by incubation with EdU for 2 h in the presence of the same compounds. Sequestered cells lacking any cell-cell contact were used for the analyses. Values were normalized with the mean value in control cells. Each bar represents mean ± SD. $n = 6$ independent experiments (>900 cells each). NS, $p > 0.05$. **(B)** Phase-contrast and fluorescence images of A431 cells seeded at a low cell density. Cell nuclei were labeled with Hoechst 33342. Blue arrows indicate sequestered cell, and red arrowheads indicate cell clusters. Scale bar, 50 μm. **(C)** Graphical representation of the quantification of cell-cell contact. In cells stained for nuclei (with Hoechst 33342) and β-catenin, nuclei (cyan) and whole-cells (yellow) were outlined, and the percentage of the cell perimeter contacting to neighboring cells was quantified using CellProfiler software. Scale bar, 50 μm. **(D)** Under 20% UPS (Stretch, **right panel**), but not under the static condition (Control, **left panel**), the fraction of A431 cells that transited into S-phase decreased with the increase in the percentage of the cell perimeter that was in direct contact with neighboring cells. Results of logistic regression fitting are presented as black lines with the corresponding *p*-values (NS, $p > 0.05$). Results of four independent experiments (>800 cells each) were pooled for the analysis. **(E)** Ratios of EdU-positive nuclei in FAKi-treated A431 cells expressing control-shRNA or α-catenin-shRNA under static (Control) and 20% UPS (Stretch) conditions. Values were normalized with the mean values in static controls. Each bar represents mean ± SD. $n \geq 4$ independent experiments. $^{**}p < 0.01$; NS, $p > 0.05$. **(F)** Ratios of EdU-positive nuclei in confluent A431 cells treated as in **(A)** under the low-Ca^{2+} condition. Values were normalized with the mean value in control cells. Each bar represents mean ± SD. $n = 3$ independent experiments. NS, $p > 0.05$.

of actomyosin contractility in cSCC cells would abrogate additional effects of myosin II inhibition on cell proliferation, whilst the increase in actomyosin contractility upon RhoA activation would sensitize cSCC cells to Blebb treatment. Of note, when duration of treatment was extended to 24 h, the proliferation inhibitory effect of RhoA activation was further enhanced (**Supplementary Figure S5A**). However, 24-h treatment with Blebb caused nuclear fragmentation in a number of cells (**Supplementary Figure S5B**), which was consistent with the previous report showing that long-term (>15 h) treatment with Blebb had a cytotoxic effect in keratinocytes (Hirata et al., 2017). Hence, 6-h treatment duration was exploited in further experiments.

While RhoA activation upregulates actomyosin contractility through the RhoA-ROCK-myosin II signaling cascade, ROCK is not the sole effector of RhoA (Wheeler and Ridley, 2004) and MLC is not the sole substrate of ROCK (Riento and Ridley, 2003). Hence, RhoA activation potentially brings multiple consequences apart from the induction of actomyosin contractility, which might be reflected by the observation that the proliferation-inhibitory effect of RhoA on cSCC cells was not completely abrogated by Blebb treatment, as discussed above. Another way to induce tension at AJs is a mechanical planar stretch of cell culture (Borghi et al., 2012). However, the application of 20% uniaxial planar stretch (UPS) to the cells seeded on the flexible substrate neither inhibited nor promoted the proliferation of

confluent A431 cells (**Figure 4B**). It is known that substrate stretch increases tension not only at the AJs but also at cell-ECM adhesions (Hirata et al., 2014; Sun et al., 2016; Sethi et al., 2017; Andersen et al., 2018), which might promote cell proliferation through the FAK signaling (Schwartz and Assoian, 2001; Wang et al., 2005). Therefore, the result can be explained by the counteracting effect of tensile loading to the AJs and FAs on the proliferation of stretched A431 cells. Consistently with this assumption, UPS application to confluent A431 cells induced Tyr925 phosphorylation of FAK (**Figure 4C**) which is known to promote cell proliferation through Ras/MAPK signaling (Schlaepfer et al., 1994). To exclude contribution of the cell-ECM tension-dependent mechanism to stretch-induced responses in cell proliferation, we pre-treated confluent A431 cells with the FAK inhibitor PF-573228 (hereafter FAKi; Slack-Davis et al., 2007). In contrast to non-treated cells, cells treated with FAKi showed a significant reduction in EdU incorporation in response to the application of UPS (**Figure 4D**). These results suggest that exogenous tensile loading to AJs has an inhibitory effect on the proliferation of cSCC cells, however, UPS application also induces FAK activation that counteracts this inhibitory effect.

Adherens Junctions are Required for Tensile Loading-Induced Inhibition of the Proliferation in cSCC Cells

In our previous study, actomyosin tension specifically at AJs was shown to inhibit the proliferation of normal keratinocytes (Hirata et al., 2017). Thus, we sought to examine the involvement of AJs in the mechanically induced inhibition of proliferation in A431 cells. Cells that lack cell-cell contact *a priori* do not form AJ complexes. Therefore, we evaluated the effect of RhoA activation on the proliferation of A431 cells under the sparse condition. In contrast to the case of confluent A431 cells, the treatment of sequestered A431 cells with the RhoA activator did not show any statistically significant effect on cell proliferation (**Figure 5A**), which was associated with no apparent promotion of vinculin and zyxin accumulation at FAs (**Supplementary Figure S2C**).

Additional evidence for the role of the tension at AJs in inhibition of cSCC cell proliferation was obtained by UPS application to A431 cells seeded at a low cell density. As A431 cells do not proceed epithelial-mesenchymal transition and retain an epithelial phenotype (Garnier et al., 2012), they tended to form cell clusters (**Figure 5B**, red arrowheads) and only some subpopulation of cells stayed secluded (**Figure 5B**, blue arrows). Using logistic regression analyses, we assessed whether the extent of cell-cell contact (measured as the percentage of the cell perimeter in direct contact with neighboring cells) (**Figure 5C**) would affect cell proliferation under UPS. We found that cells with larger cell-cell contact regions showed a significantly lower probability of S-phase entry under UPS but not under the non-stretched control condition (**Figure 5D**). Taken together these results indicate that cell-cell contacts are indispensable for the tensile loading-induced inhibition of the proliferation in cSCC cells.

Another way to examine the role of tension at AJs is to interfere with the force transmission from the actin cytoskeleton to AJs. α-Catenin, one of the major components of AJs, is essential for the mechanical coupling of the actomyosin network to AJs, and the loss of α-catenin functionally impairs AJs (Mège and Ishiyama, 2017) and prevents transmission of actomyosin-generated forces to AJs (Thomas et al., 2013; Barry et al., 2014; Buckley et al., 2014). Accordingly, we stably knocked down (KD) α-catenin expression in A431 cells by the use of shRNA (**Supplementary Figures S6A,B**). The proliferation inhibitory effect of UPS in confluent A431 cells under FAK inhibition was eliminated by α-catenin KD (**Figure 5E**), indicating involvement of intact AJs in UPS-induced inhibition of A431 cell proliferation. However, treatment with the RhoA activator caused a significant decrease in cell proliferation in both cells expressing non-targeting shRNA and α-catenin-KD cells cultured at confluent densities, and a decrease in cell proliferation upon RhoA activation was abrogated by Blebb treatment (**Supplementary Figure S6C**). Potentially, the residual expression of α-catenin in α-catenin-KD cells was sufficient to form immature AJs (**Supplementary Figure S6D**, red arrowheads), which might trigger proliferation inhibitory signaling downstream of RhoA activation. On the other hand, in contrast to sturdy apical AJs formed in naïve A431 cells (**Supplementary Figure S6D**, yellow arrowheads), these immature AJs would not be stable enough to withstand more acute mechanical stretch. Such a touchy nature of AJs in α-catenin-KD cells might underlie the phenomenon that α-catenin KD eliminated the proliferation inhibitory effect of mechanical stretch but not the effect of RhoA activation.

To further investigate the role of tension at AJs, we disassembled AJs by depleting extracellular Ca^{2+} from the cell culture medium as Ca^{2+} is required for intercellular homophilic interaction of E-cadherin (Lewis et al., 1994; Koch et al., 1997; Kim et al., 2011). Keratinocytes do not form AJs in media containing 30 μM of Ca^{2+}, while AJs rapidly form when Ca^{2+} concentration is raised to 1 mM (Lewis et al., 1994). Consistently with the previous reports, we observed that in the low-Ca^{2+} medium (ca. 40 μM of Ca^{2+}) A431 cells lacked apparent AJs (**Supplementary Figure S7**). Under the low-Ca^{2+} condition, the treatment of A431 cells with the RhoA activator did not show an inhibitory effect on the proliferation of A431 cells (**Figure 5F**). Taken together, the results obtained for A431 cells show that actomyosin contractility and mechanical stretch inhibit cSCC cell proliferation in an AJ-dependent manner.

RhoA-Induced Inhibition of cSCC Cell Proliferation Accompanies Promotion of Keratinocytic Differentiation

Considering that proliferation and differentiation are tightly coordinated in normal keratinocytes (Simpson et al., 2011), we next asked whether RhoA-induced inhibition of cSCC cell proliferation was associated with an alteration in the cell differentiation status. Six-hour treatment with the RhoA activator (under the same conditions as for the EdU incorporation assay) did not significantly affect the expression

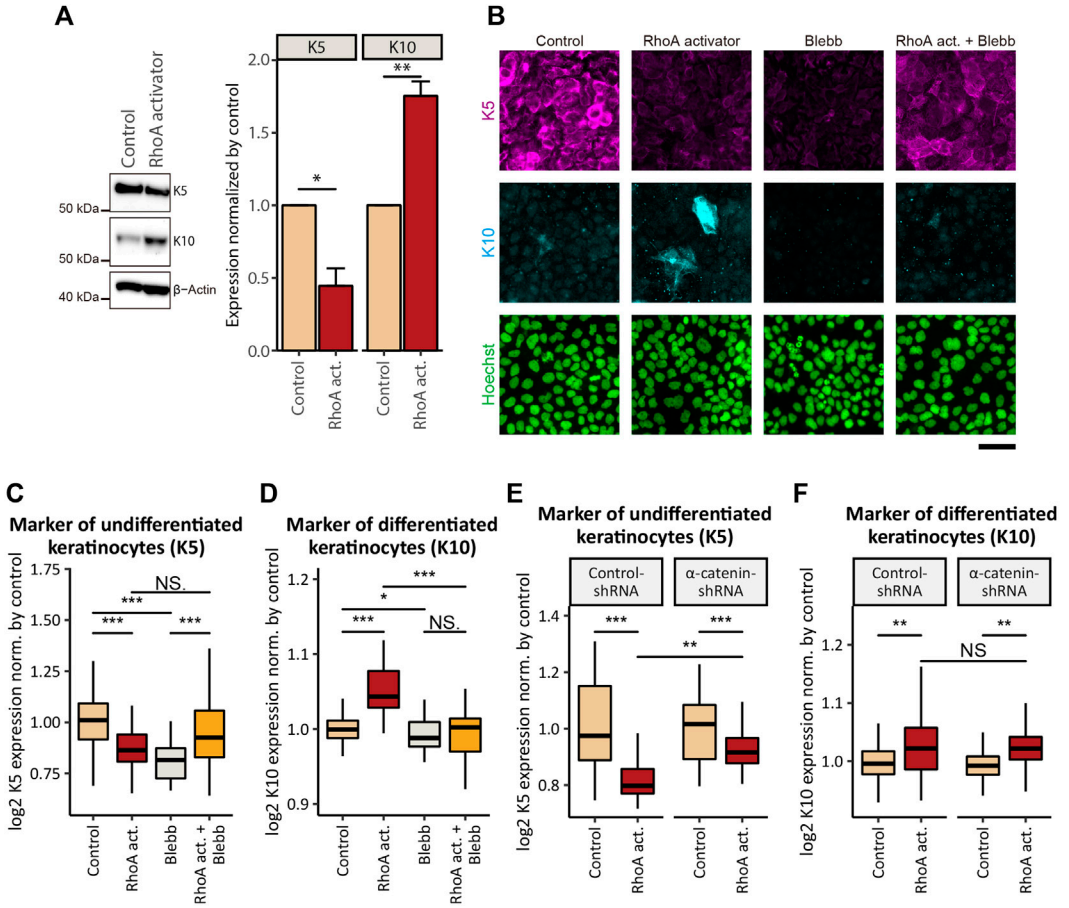

FIGURE 6 | Activation of actomyosin contractility induces epidermal differentiation of cSCC cells. **(A)** Whole-cell lysates of confluent A431 cells treated with or without 5 μg/ml RhoA activator (RhoA act.) for 24 h were immunoblotted for K5, K10, and β-actin. Bar graphs show the result of the densitometric quantification of K5 and K10. Values were normalized with the mean values in control cells. Each bar represents mean ± SD. $n = 3$ independent experiments. $^{*}p < 0.05$; $^{**}p < 0.01$. **(B)** Confluent A431 cells treated with 5 μg/ml RhoA activator (RhoA act.), 100 μM *p*-aminoblebbistatin (Blebb) or combination of both drugs (RhoA act. + Blebb) for 24 h were stained for markers of basal (undifferentiated, K5, magenta) and suprabasal (differentiated, K10, cyan) keratinocytes. Cell nuclei were labeled with Hoechst 33342 (green). Scale bar, 50 μm. **(C, D)** Quantification of **(B)**. Fluorescence intensities of K5 **(C)** and K10 **(D)** in confluent A431 cells treated with indicated compounds for 24 h. Values were normalized with the mean values in control cells. Box-and-whisker plots show the median, the interquartile range, and the tenth and ninetieth percentiles. $n = 60$ fields of view from three independent experiments were pooled for the analysis. $^{*}p < 0.05$; $^{***}p < 0.001$; NS, $p > 0.05$. **(E, F)** Quantification of fluorescence intensities of K5 **(E)** and K10 **(F)** in confluent A431 cells expressing control-shRNA or α-catenin-shRNA treated with indicated compounds for 24 h. Values were normalized with the mean values in non-treated controls. Box-and-whisker plots show the median, the interquartile range, and the tenth and ninetieth percentiles. $n = 60$ fields of view from three independent experiments were pooled for the analysis. $^{**}p < 0.01$; $^{***}p < 0.001$; NS, $p > 0.05$.

of markers for basal undifferentiated keratinocytes-keratin-5 (K5) and differentiated keratinocytes-keratin-10 (K10) (data not shown). However, when the treatment duration was extended to 24 h, RhoA activation led to a significant decrease in the expression of K5 and an increase in the expression of K10 (**Figures 6A–D**). Co-treatment with Blebb eliminated the RhoA-induced elevation in K10 expression (**Figures 6B,D**), indicating that the expression of K10 depends on the actomyosin activity. By contrast, the same co-treatment did not show a statistically significant increase in the K5 expression ($p = 0.094$) in comparison to the treatment with the RhoA activator alone (**Figure 6C**). However, the ratio of cells expressing high levels of K5 was notably increased by co-treatment with Blebb (the upper quartile of the K5 expression in the cells treated with the combination of the RhoA activator and Blebb was approximately equal to the 90th percentile of K5 expression in cells treated with the RhoA activator alone; **Figure 6C**). Hence, K5 expression may also be affected by actomyosin-dependent mechanism(s). While treatment with Blebb alone reduced expression of both K5 and K10 (**Figures 6C,D**), this might be potentially due to the cytotoxic effect of long-term Blebb treatment, as discussed above. Taken together, our results suggest that activation of actomyosin contractility not only inhibits proliferation but also promotes keratinocytic differentiation in cSCC cells.

Next, we assessed the involvement of AJs in the actomyosin-regulated differentiation process. shRNA-mediated KD of α-catenin in A431 cells significantly attenuated the RhoA-induced inhibition of K5 expression in comparison to the cells

expressing control-shRNA (**Figure 6E**), whereas the effect of RhoA activation on K10 expression was not significantly altered by α-catenin KD (**Figure 6F**). These results suggest that promotion of differentiation of cSCC cells downstream of actomyosin activation depends, at least partially, on intact AJs, while distinct differentiation markers may be influenced by different effectors downstream of RhoA.

DISCUSSION

The role of actomyosin contractility in cancer cell proliferation has not been well understood. While we have previously reported that actomyosin-based tension at AJs is required for CIP in normal keratinocytes (Hirata et al., 2017), we find in this study that cSCC cells having a defect in CIP exhibit a low level of MLC phosphorylation, which should cause reduced actomyosin contractility. Furthermore, we provide evidence that the proliferation of cSCC cells is inhibited by pharmacologically (i.e., RhoA activation) or mechanically (i.e., UPS application) induced tensile loads at AJs. Importantly, actomyosin activation in cSCC cells not only inhibits their proliferation but also promotes epidermal differentiation in an AJ-dependent manner. Our results suggest that tension at AJs acts as an anti-malignant factor in cSCC.

Our finding that actomyosin contractility inhibits cell cycle progression in cSCC is in line with some of the previous reports showing that RhoA and ROCK are required for keratinocyte differentiation, while ROCK inhibition promotes keratinocyte proliferation (Sugai et al., 1992; McMullan et al., 2003; Strudwick et al., 2015). Nevertheless, other reports imply pro-proliferative and tumorigenic effects of actomyosin contractility in skin keratinocytes (Samuel et al., 2011; García-Mariscal et al., 2018). It is of note that in contrast to the present study, the previous *in vitro* study (Samuel et al., 2011; García-Mariscal et al., 2018) showing the proliferation-promoting effect of actomyosin activity in primary keratinocytes employed low extracellular Ca^{2+} conditions (at concentrations below 20 μM) for experiments. AJ formation would be abrogated under these low Ca^{2+} conditions, and, therefore, activation of actomyosin might not result in AJ-dependent inhibition of cell proliferation. Since the extracellular Ca^{2+} concentration in the epidermis is normally maintained in the range of 1.1–1.4 mM (Breitwieser, 2008), we believe that the condition used in this study (ca. 2.2 mM of Ca^{2+}) is physiologically relevant. However, extracellular Ca^{2+} may not be the sole factor to bring the inconsistency in the role of actomyosin contractility because *in vivo* studies also showed opposing results for the effect of RhoA-ROCK-myosin II signaling perturbations on tumorigenesis in the skin (Sugai et al., 1992; Samuel et al., 2011; García-Mariscal et al., 2018). Importantly, in the previous *in vivo* studies, actomyosin activity was perturbed by pharmacologically or genetically altering expression/activity of RhoA or ROCK (Sugai et al., 1992; Samuel et al., 2011; García-Mariscal et al., 2018). Since actomyosin is not a sole downstream target of RhoA and ROCK (Riento and Ridley, 2003; Wheeler and Ridley, 2004), these previous approaches may not directly address the role of actomyosin contractility.

Another major limitation in the previous *in vivo* studies is the lack of methodology for evaluating and manipulating the actomyosin-mediated mechanical status in specific subcellular compartments such as cell-ECM and cell-cell adhesion sites. Indeed, tension at FAs and at AJs reportedly have opposing effects on cell proliferation; while tension at FAs promotes proliferation of various cell types (Schwartz and Assoian, 2001; Wang et al., 2005) and inhibits differentiation in normal keratinocytes (Carley et al., 2021), tension at AJs has been suggested to inhibit proliferation of MDCK epithelial cells (Furukawa et al., 2017), keratinocytes (Hirata et al., 2017) and cSCC cells (this study). These opposing effects may counteract each other when the actomyosin activity is globally altered in the skin tissue. Fibrillogenesis and stiffening of ECM induced by tissue-scale stretching of the skin (Verhaegen et al., 2012) may also activate integrin signaling at FAs and counter the anti-proliferative effect of AJ tension. In contrast to the former studies, we have discriminated, in the present study, the role of tension at AJs from that at FAs by combing pharmacological modulation of actomyosin activity, mechanical manipulation of cells, modulation of the cell density, pharmacological inhibition of FA signaling, and genetical perturbation of AJs. With these approaches, we have revealed that tensile loads at AJs have a specific role in inhibiting cSCC cell proliferation.

Considering the well-known proliferation-promoting role of tensile loads at FAs, it might be surprising that RhoA activation in sparse A431 cell culture did not promote cell proliferation. In contrast to RhoA-induced vinculin accumulation at AJs (**Figure 3A**), activation of RhoA in A431 cells did not apparently promote the recruitment of vinculin and zyxin to FAs under both confluent (**Figure 3A**, **Supplementary Figure S2A**) and sparse (**Supplementary Figure S2C**) conditions. These results are consistent with the previous reports that myosin II shows polarized distribution along the apicobasal axis in epithelial cells (Levayer and Lecuit, 2012), which was also observed in the present study (**Figure 2C**). Furthermore, MLC phosphorylation in FA-associated actomyosin stress fibers is differentially regulated by ROCK and MLCK depending on cell types (Totsukawa et al., 2004; Kassianidou et al., 2017; Matsui and Deguchi, 2019). Thus, activation of the RhoA-ROCK pathway in sparse A431 cells might not effectively increase tension at FAs and, therefore, failed to promote cell proliferation.

Since tensile loads at AJs are suggested to have an anti-malignant effect on cSCC cells through inhibition of their proliferation and promotion of their epidermal differentiation, the tensile status of AJs may provide a novel therapeutic target for cSCC. As mentioned above, global activation of actomyosin in the tissue might increase tension not only at AJs but also at FAs, which may cause undesired stimulation of cSCC growth (Sugai et al., 1992; Samuel et al., 2011; Zhou et al., 2015; Ichijo et al., 2017; Purnell et al., 2018). Thus, the development of a methodology for locally increasing tension at AJs would be required for the practical application and RhoA signaling might be a potential target. Furthermore, understanding of the

molecular mechanism for attenuating malignant behaviors (hyperproliferation and poor differentiation) of cSCC cells downstream of tensile loads at AJs would also be needed for developing an effective strategy for the treatment of cSCC.

METHODS

Mice

Wild-type FVB/N mice were purchased from CLEA Japan, Inc. (Tokyo, Japan). FVB/N mice display a high incidence of cSCC after treatment with various tumor-induction protocols (Hennings et al., 1993). All mice were housed in the animal facilities of Nagoya University Graduate School of Medicine. All animal protocols were approved by the Animal Care and Use Committee of Nagoya University Graduate School of Medicine (Approval ID number 28175).

Cell Culture

The human cSCC cells A431 (purchased from ATCC, CRL-1555), C2C12 mouse myoblasts, and HEK293T cells were maintained in high-glucose Dulbecco's modified Eagle's medium (DMEM; Nacalai Tesque, Kyoto, Japan) supplemented with 10% fetal bovine serum (FBS; Life Technologies, Carlsbad, CA). The mouse primary epidermal keratinocytes (MPEK) were isolated as previously described (Sunagawa et al., 2016) and maintained in the KGM-Gold medium (Lonza, Walkersville, MD).

Antibodies and Chemicals

The rabbit polyclonal antibodies (pAbs) against Tyr925-phosphorylated FAK (3284), MLC (3672), Ser19-phosphorylated MLC (3671) and Thr18,Ser19-doublephosphorylated MLC (3674), the rabbit monoclonal antibody (mAb) against E-cadherin (3195), GAPDH (2118), and the mouse mAb against Ser19-phosphorylated MLC (3675) were purchased from Cell Signaling Technology (Danvers, MA). The mouse mAb against keratin-10 (MA5-13705) was from Thermo Fisher Scientific (Waltham, MA). The rabbit pAbs against β-catenin (ab6302) and non-muscle myosin IIA (ab75590), and the rabbit mAb against keratin-5 (ab52635), FAK (ab40794), Tyr397-phosphorylated FAK (ab81298), and Ki-67 (SP6) were from Abcam (Cambridge, United Kingdom). The mouse mAb against β-actin (A5441) and vinculin (V9131), and the rabbit mAb against zyxin (ZRB1408) were from Sigma Chemical (St. Louis, MO). Alexa Fluor 488-goat anti-rabbit IgG, Alexa Fluor 488-goat anti-mouse IgG, Alexa Fluor 546-goat anti-rabbit IgG and Alexa Fluor 555-goat anti-mouse IgG antibodies were from Life Technologies. Horseradish peroxidase-conjugated anti-mouse IgG and anti-rabbit IgG antibodies were from GE Healthcare (Little Chalfont, United Kingdom) and Zymed Laboratories (San Francisco, CA), respectively. Rho activator II (RhoA activator) was from Cytoskeleton (Denver, CO). Para-aminoblebbistatin (Blebb) was from Optopharma (Budapest, Hungary). The FAK inhibitor PF-573228 was from Sigma Chemical. Ethylene glycol-bis (β-aminoethyl ether)-N,N,N′,N′-tetraacetic acid (EGTA) was from Dojindo Laboratories (Kumamoto, Japan). Hoechst 33342 was from Life Technologies.

Skin Tumorigenesis Assay

Murine skin tumors were induced by a standard two-stage chemical carcinogenesis protocol, as previously described (Abel et al., 2009; Aoi et al., 2014). In brief, 6–8-week-old female mice were shaved on the dorsal skin with electric clippers and subjected to a single topical application of 100 nmol 9,10-dimethyl-1,2-benzanthracene (DMBA, Sigma Chemical) in 200 μl acetone 24 h after shaving. One week after DMBA treatment, the mice received topical applications of 5 nmol tetradecanoyl-phorbol acetate (TPA, Sigma Chemical) in 200 μl acetone twice weekly for 15 weeks. All animal protocols were approved by the Animal Care and Use Committee of Nagoya University Graduate School of Medicine (Approval ID number: 28175).

Immunohistochemistry

Skin and tumor tissues were fixed for 24 h in 10% neutral-buffered formalin (Nacalai Tesque), dehydrated, and embedded in paraffin. Sections (4-μm thick) prepared for IHC were deparaffinized in xylene and rehydrated in a graded series of ethanol. For antigen retrieval, the sections were immersed in either Epitope Retrieval Solution (pH 6, Leica Biosystems) or HistoVT One solution (pH 7, Nacalai Tesque) and incubated for 30 min at 98°C in a water bath. Non-specific binding was blocked with Protein Block Serum-Free (Dako) for 30 min at room temperature. Then, the sections were incubated with primary antibodies diluted in 1% BSA/PBS for 2 h at room temperature. Primary antibody dilutions were as follows: anti-pS19-MLC–1:100, anti-Ki-67–1:100. After inhibiting endogenous peroxidase with 0.3% hydrogen peroxide in methanol for 15 min, the sections were further incubated with EnVision+ system-horseradish peroxidase (HRP)-Labelled Polymer (anti-rabbit, Dako) for 30 min at room temperature. Signals were visualized by the Liquid DAB+ Substrate-Chromogen System (Dako) with nuclear counterstaining using hematoxylin. Skeletal and smooth muscle cells from the regions underlying epidermis were used as an internal positive control for pS19-MLC staining (**Supplementary Figures S1A,B**).

shRNA-Mediated Depletion of α-Catenin

shRNAs were introduced into A431 cells using the retrovirus system, as described previously (Hirata et al., 2017). In brief, the sequence of either 5′-GACTTAGGAATCCAGTATA-3′ (for targeting human catenin alpha-1) or 5′-ATAGTCACAGAC ATTAGGT-3′ (for the non-targeting control) was inserted into the pSUPER.retro.puro retroviral vector. The inserted vector was co-transfected with the pE-ampho vector into HEK293T cells using the GeneJuice transfection reagent (Merck Millipore, MA, United States). Supernatants containing viral particles were collected 48 h after transfection, filtered through 0.45-μm syringe filters, and used for infection into A431 cells in the presence of 8 μg/ml Polybrene (Sigma Chemical). Infected A431 cells were selected with 1.5 μg/ml puromycin (Sigma Chemical).

Pharmacological Treatment and EdU Incorporation

Trypsinized cells were seeded at the cell density of 1×10^4 cells/cm^2 (sparse), 1×10^5 cells/cm^2 (sub-confluent), or 2×10^5 cells/cm^2 (confluent) onto glass-bottom or plastic 24-well plates, or elastic polydimethylsiloxane (PDMS) chambers (Strex, Osaka, Japan) precoated with 50 μg/ml collagen (Koken, Tokyo, Japan), and cultured for 40 h before the treatment. When cells were seeded at the confluent cell density (i.e., 2×10^5 cells/cm^2), surfaces of the wells/chambers were completely covered with cells. In sparse cultures, cells forming clusters were excluded from analyses, unless otherwise stated.

In the experiment to compare the proliferation of A431 and MPEK cells, we used the KGM-Gold medium, which promotes the proliferation of primary keratinocytes in serum-free and feeder-free conditions (Borowiec et al., 2013). For the experiments with the low Ca^{2+}-medium, Ca^{2+}-free DMEM (Nacalai Tesque) supplemented with 0.3 mM EGTA and 10% FBS was used (Hirata et al., 2020). Given the concentration of Ca^{2+} in FBS to be 3.4 mM (Gstraunthaler and Lindl, 2013), the free Ca^{2+} concentration in the low Ca^{2+}-medium was estimated as ~40 μM (calculated using Ca-EGTA Calculator v1.3; Bers et al., 2010). In all other experiments, DMEM supplemented with 10% FBS was used.

For the experiments with pharmacological activation/inhibition of actomyosin contractility, cells were treated with either 5 μg/ml of the membrane-permeable form of cytotoxic necrotizing factor-1 from *Escherichia coli* (hereafter RhoA activator), which deamidates glutamine-63 of RhoA to glutamate to constitutively activate RhoA by blocking its GTPase activity (Flatau et al., 1997; Schmidt et al., 1997), 100 μM of the myosin II ATPase inhibitor para-aminoblebbistatin [hereafter Blebb-a water-soluble form of blebbistatin (Straight et al., 2003; Kovács et al., 2004; Várkuti et al., 2016)], or combination of 5 μg/ml RhoA activator and 100 μM Blebb for 6 h or 24 h, followed by further incubation for 2 h with 10 μM EdU in the presence of the same set of the compounds. When indicated, along with the RhoA activator and/or Blebb, 10 μM of the FAK inhibitor PF-573228 (Slack-Davis et al., 2007) was added to the media.

For the experiments with mechanical stretching, cells seeded on the PDMS substrate were subjected to 20% uniaxial planar stretch continuously for 6 h and further incubated for 2 h with 10 μM EdU under the stretch. To stretch cells under inhibition of FAK activity, cells were pre-treated with 10 μM of the FAK inhibitor PF-573228 for 2 h and then stretched in the presence of PF-573228.

After the incubation with EdU, cells were fixed and permeabilized with 4% formaldehyde and 0.5% Triton X-100, respectively, in PBS, and incorporated EdU was visualized with Alexa Fluor 488-azide or Alexa Fluor 647-azide using the "click chemistry" kit (Life Technologies or Click Chemistry Tool, Scottsdale, AZ). Total nuclei were stained with 5 μg/ml Hoechst 33342.

Immunofluorescence

Cells, which were pharmacologically treated when indicated, were fixed and permeabilized for 30 min with 4% formaldehyde and 0.2% Triton X-100 in the cytoskeleton stabilizing buffer (137 mM NaCl, 5 mM KCl, 1.1 mM Na_2HPO_4, 0.4 mM KH_2PO_4, 4 mM $NaHCO_3$, 2 mM $MgCl_2$, 5.5 mM glucose, 2 mM EGTA, and 5 mM PIPES, pH 6.1). This was followed by blocking with 1% BSA in the cytoskeleton stabilizing buffer for 30 min. The cells were then incubated with primary antibodies overnight, washed, and further incubated with secondary antibodies for 40 min. Primary antibodies were diluted in the cytoskeleton stabilizing buffer containing 1% BSA as follows: anti-keratin-5–1:250, anti-keratin-10–1:50, anti-E-cadherin–1:200, anti-vinculin–1:200, anti-zyxin–1:1000, anti-non-muscle Myosin IIA–1:250, pS19-MLC–1:250, and anti-β-catenin–1:3000. Secondary antibodies and Alexa Fluor 647-conjugated phalloidin (to detect F-actin; Thermo Fisher Scientific) were diluted to 1:200 in the cytoskeleton stabilizing buffer containing 1% BSA. Total nuclei were stained with 5 μg/ml Hoechst 33342. All immunofluorescence experiments were repeated at least twice, and typical images are shown in figures.

Microscope Image Acquisition

For fluorescence imaging, cells were observed using an epifluorescence inverted microscope (BZ-X710, Keyence, Osaka, Japan) equipped with an air (NA 0.45, 20x or NA 0.50, 40x ELWD S Plan Fluor, Nikon) or an oil immersion (NA 1.40, 60x, Plan Apo, Nikon) objective and a high-resolution 2.83-megapixel monochrome CCD camera. The BZ-X viewer software (version 1.3.0.5, Keyence) was used for image acquisition. To characterize the adherens junctions, cells were observed using a confocal laser scanning microscope (LSM 510, Zeiss, Oberkochen, Germany) equipped with an oil immersion objective (NA 1.4, 63x Plan-Aphochromat, Zeiss) under control of ZEN 2009 software (version 6.0.0.303, Zeiss).

Image Processing and Analysis

Acquired images were analyzed offline using custom pipelines in ImageJ (ver. 1.53c) and in the automated image analysis software CellProfiler (ver. 4.0.6, Carpenter Lab, Broad Institute of Harvard and MIT, Cambridge, MA; (McQuin et al., 2018). Briefly, images were subjected to nuclei segmentation using the StarDist 2D plugin (Schmidt et al., 2018) for ImageJ based on the Hoechst channel with the versatile (fluorescent nuclei) model. The segmented images were saved and used as an input in CellProfiler. Whenever necessary, whole cells were segmented with the propagation algorithm and the minimum cross-entropy thresholding method in the appropriate secondary staining channel by using nuclei as "seed" objects. Next, the fluorescence intensities of segmented objects were calculated. To identify the region of the cell perimeter that was in direct contact with neighboring cells, the cytoplasm surrounding the segmented nucleus was detected in the β-catenin channel. Then the adjacent objects were identified. For quantification of continuous vinculin staining, the continuous lines of junctional vinculin were manually outlined and their lengths were measured using ImageJ.

Western Blot

Cells, which were pharmacologically treated when indicated, were lysed with the 2x lithium dodecyl sulfate sample buffer (Life

Technologies) containing 2.5% β-mercaptoethanol. The lysate samples were resolved by SDS-PAGE (4–12% Bis-Tris or 3–8% Tris-Acetate gels; Life Technologies), electroblotted onto a polyvinylidene fluoride membrane (Immobilon-P, Millipore, MA, United States), blocked with 1% skim milk in TBS-T (20 mM Tris, 150 mM NaCl, 0.1% Tween-20, pH 7.5), and probed with antibodies. Primary antibodies dilutions were as follows: anti-MLC–1:800, anti-S19-MLC–1:800, anti-T18,S19-MLC–1:800, anti-K5–1:25000, anti-K10–1:2000, anti-α-catenin–1:10000, and anti-β-actin–1:10000 in 0.1% skim milk in TBS-T. Secondary HRP-conjugated antibodies were diluted to 1:2500 in 0.1% skim milk in TBS-T. Immunoreactive bands were detected with the SuperSignal West Femto ECL substrate (Thermo Fisher Scientific). Images were captured using CoolSNAP *fx* CCD camera (Photometrics, AZ, United States) and MetaMorph software (ver. 7.5.0.0, Molecular Devices, CA, United States). Chemiluminescence was quantified using ImageJ (ver. 1.52i; Schindelin et al., 2012). All immunoblot experiments were repeated at least twice, and typical blots are shown in figures.

Statistical Analysis

Statistical analyses were conducted using the free software for statistical computing and graphics R (version 4.0.4; R Core Team, 2019), and graphs were produced using the packages ggplot2 (Wickham, 2016) and ggsignif (Ahlmann-Eltze and Patil, 2021).

Even though the same treatment reproducibly caused a similar effect on the cell proliferation (i.e., inhibited or promoted proliferation) against the control in each experiment, the high variability in the proliferation level of the control cells led to large SD values among experiments. Thus, to unmask the actual effect of a treatment, the ratio of EdU-positive cells under the treatment was normalized by that under the control condition in each experiment. The normalization allowed us to remove the variability in the proliferation of control cells from the analysis and isolate the effect of the treatments.

The bivariate logistic regression analysis was performed to assess the association between the cell-cell contact area and the probability of entry into the S-phase. The percentage of the cell perimeter that was in direct contact with neighboring cells was used as the independent variable. The fluorescence intensity of EdU, used as the dependent variable, was dichotomized into the outcomes "1" for EdU-positive cells or "0" for EdU-negative cells. Results of model fitting were shown graphically on the plots with corresponding *p*-values.

Bar graphs were presented as mean ± SD. In box-and-whisker plots, the line, the box, and the whiskers represent the median, the interquartile range, and the tenth and ninetieth percentiles, respectively. In the EdU incorporation assay and quantitative immunofluorescence (IF), five or more fields of view in each of two or more independent experiments were analyzed for each condition with a total of more than 800 cells (sparse) or more than 10^4 cells (confluent) per condition in each experiment was analyzed. Statistical significance was assessed using Student's two-tailed, unpaired t-test.

DATA AVAILABILITY STATEMENT

The original contributions presented in the study are included in the article/**Supplementary Material**, further inquiries can be directed to the corresponding authors.

ETHICS STATEMENT

The animal study was reviewed and approved by Animal Care and Use Committee of Nagoya University Graduate School of Medicine.

AUTHOR CONTRIBUTIONS

OD and HH designed the research. MSu, SM, and AE performed all of the *in vivo* works. OD, TT, KK, and HH performed all of the *in vitro* works. OD, AE, and HH analyzed the data. OD, MSo, and HH wrote the manuscript. MSo and HH oversaw the project. All authors read and approved the final manuscript.

FUNDING

This work was supported by the grant for collaborative research between Nagoya University and R-Pharm (2614Dj-02b to MSo), JSPS KAKENHI Grant Numbers 15H0936 (to MSo), 19K23748 (to HH), 20K12596 (to HH) and 21H05127 (to HH), and Grant for Basic Science Research Projects from The Sumitomo Foundation (to HH).

ACKNOWLEDGMENTS

We thank Kaori Ushida (Nagoya University) for the technical assistance.

SUPPLEMENTARY MATERIAL

The Supplementary Material for this article can be found online at: https://www.frontiersin.org/articles/10.3389/fcell.2021.728383/full#supplementary-material

REFERENCES

Abel, E. L., Angel, J. M., Kiguchi, K., and DiGiovanni, J. (2009). Multi-stage Chemical Carcinogenesis in Mouse Skin: Fundamentals and Applications. *Nat. Protoc.* 4, 1350–1362. doi:10.1038/nprot.2009.120

Ahlmann-Eltze, C., and Patil, I. (2021). *ggsignif: R Package for Displaying Significance Brackets for "ggplot2"*. PsyArXiv [Preprint]. Available at: https://psyarxiv.com/7awm6 (Accessed October 25, 2021).

Alam, M., and Ratner, D. (2001). Cutaneous Squamous-Cell Carcinoma. *N. Engl. J. Med.* 344, 975–983. doi:10.1056/nejm200103293441306

Andersen, J. I., Pennisi, C. P., Fink, T., and Zachar, V. (2018). Focal Adhesion Kinase Activation Is Necessary for Stretch-Induced Alignment and Enhanced Differentiation of Myogenic Precursor Cells. *Tissue Eng. A* 24, 631–640. doi:10.1089/ten.tea.2017.0137

Aoi, J., Endo, M., Kadomatsu, T., Miyata, K., Ogata, A., Horiguchi, H., et al. (2014). Angiopoietin-like Protein 2 Accelerates Carcinogenesis by Activating Chronic Inflammation and Oxidative Stress. *Mol. Cancer Res.* 12, 239–249. doi:10.1158/1541-7786.mcr-13-0336

Barksdale, S. K., O'Connor, N., and Barnhill, R. (1997). Prognostic Factors for Cutaneous Squamous Cell and Basal Cell Carcinoma. *Surg. Oncol. Clin. North Am.* 6, 625–638. doi:10.1016/s1055-3207(18)30319-3

Barry, A. K., Tabdili, H., Muhamed, I., Wu, J., Shashikanth, N., Gomez, G. A., et al. (2014). α-Catenin Cytomechanics - Role in Cadherin-dependent Adhesion and Mechanotransduction. *J. Cel. Sci.* 127, 1779–1791. doi:10.1242/jcs.139014

Bays, J. L., and DeMali, K. A. (2017). Vinculin in Cell-Cell and Cell-Matrix Adhesions. *Cell. Mol. Life Sci.* 74, 2999–3009. doi:10.1007/s00018-017-2511-3

Benham-Pyle, B. W., Pruitt, B. L., and Nelson, W. J. (2015). Cell Adhesion. Mechanical Strain Induces E-Cadherin-Dependent Yap1 and β-Catenin Activation to Drive Cell Cycle Entry. *Science* 348, 1024–1027. doi:10.1126/science.aaa4559

Bers, D. M., Patton, C. W., and Nuccitelli, R. (2010). A Practical Guide to the Preparation of Ca(2+) Buffers. *Methods Cel. Biol.* 99, 1–26. doi:10.1016/b978-0-12-374841-6.00001-3

Borghi, N., Sorokina, M., Shcherbakova, O. G., Weis, W. I., Pruitt, B. L., Nelson, W. J., et al. (2012). E-cadherin Is under Constitutive Actomyosin-Generated Tension that Is Increased at Cell-Cell Contacts upon Externally Applied Stretch. *Proc. Natl. Acad. Sci.* 109, 12568–12573. doi:10.1073/pnas.1204390109

Borowiec, A.-S., Delcourt, P., Dewailly, E., and Bidaux, G. (2013). Optimal Differentiation of *In Vitro* Keratinocytes Requires Multifactorial External Control. *PLoS One* 8, e77507. doi:10.1371/journal.pone.0077507

Breitwieser, G. E. (2008). Extracellular Calcium as an Integrator of Tissue Function. *Int. J. Biochem. Cel. Biol.* 40, 1467–1480. doi:10.1016/j.biocel.2008.01.019

Bruner, H. C., and Derksen, P. W. B. (2018). Loss of E-Cadherin-Dependent Cell-Cell Adhesion and the Development and Progression of Cancer. *Cold Spring Harb. Perspect. Biol.* 10, a029330. doi:10.1101/cshperspect.a029330

Buckley, C. D., Tan, J., Anderson, K. L., Hanein, D., Volkmann, N., Weis, W. I., et al. (2014). Cell Adhesion. The Minimal Cadherin-Catenin Complex Binds to Actin Filaments under Force. *Science* 346, 1254211. doi:10.1126/science.1254211

Butcher, D. T., Alliston, T., and Weaver, V. M. (2009). A Tense Situation: Forcing Tumour Progression. *Nat. Rev. Cancer* 9, 108–122. doi:10.1038/nrc2544

Carley, E., Stewart, R. M., Zieman, A., Jalilian, I., King, D. E., Zubek, A., et al. (2021). The LINC Complex Transmits Integrin-dependent Tension to the Nuclear Lamina and Represses Epidermal Differentiation. *Elife* 10, e58541. doi:10.7554/eLife.58541

Chaudhuri, P. K., Low, B. C., and Lim, C. T. (2018). Mechanobiology of Tumor Growth. *Chem. Rev.* 118, 6499–6515. doi:10.1021/acs.chemrev.8b00042

Déjardin, T., Carollo, P. S., Sipieter, F., Davidson, P. M., Seiler, C., Cuvelier, D., et al. (2020). Nesprins Are Mechanotransducers that Discriminate Epithelial-Mesenchymal Transition Programs. *J. Cel. Biol.* 219, e201908036. doi:10.1083/jcb.201908036

Dmello, C., Srivastava, S. S., Tiwari, R., Chaudhari, P. R., Sawant, S., and Vaidya, M. M. (2019). Multifaceted Role of Keratins in Epithelial Cell Differentiation and Transformation. *J. Biosci.* 44, 190. doi:10.1007/s12038-019-9864-8

Dobrokhotov, O., Samsonov, M., Sokabe, M., and Hirata, H. (2018). Mechanoregulation and Pathology of YAP/TAZ via Hippo and Non-hippo Mechanisms. *Clin. Transl. Med.* 7, 23. doi:10.1186/s40169-018-0202-9

Flatau, G., Lemichez, E., Gauthier, M., Chardin, P., Paris, S., Fiorentini, C., et al. (1997). Toxin-induced Activation of the G Protein P21 Rho by Deamidation of Glutamine. *Nature* 387, 729–733. doi:10.1038/42743

Furukawa, K. T., Yamashita, K., Sakurai, N., and Ohno, S. (2017). The Epithelial Circumferential Actin Belt Regulates YAP/TAZ through Nucleocytoplasmic Shuttling of Merlin. *Cel. Rep.* 20, 1435–1447. doi:10.1016/j.celrep.2017.07.032

García-Mariscal, A., Li, H., Pedersen, E., Peyrollier, K., Ryan, K. M., Stanley, A., et al. (2018). Loss of RhoA Promotes Skin Tumor Formation and Invasion by Upregulation of RhoB. *Oncogene* 37, 847–860. doi:10.1038/onc.2017.333

Garnier, D., Magnus, N., Lee, T. H., Bentley, V., Meehan, B., Milsom, C., et al. (2012). Cancer Cells Induced to Express Mesenchymal Phenotype Release Exosome-like Extracellular Vesicles Carrying Tissue Factor. *J. Biol. Chem.* 287, 43565–43572. doi:10.1074/jbc.m112.401760

Gayrard, C., Bernaudin, C., Déjardin, T., Seiler, C., and Borghi, N. (2018). Src- and Confinement-dependent FAK Activation Causes E-Cadherin Relaxation and β-catenin Activity. *J. Cel. Biol.* 217, 1063–1077. doi:10.1083/jcb.201706013

Gerdes, J., Lemke, H., Baisch, H., Wacker, H. H., Schwab, U., and Stein, H. (1984). Cell Cycle Analysis of a Cell Proliferation-Associated Human Nuclear Antigen Defined by the Monoclonal Antibody Ki-67. *J. Immunol.* 133, 1710–1715.

Gstraunthaler, G., and Lindl, T. (2013). *Zell- und Gewebekultur: Allgemeine Grundlagen und spezielle Anwendungen*. Berlin, Heidelberg: Springer-Verlag.

Hanahan, D., and Weinberg, R. A. (2011). Hallmarks of Cancer: the Next Generation. *Cell* 144, 646–674. doi:10.1016/j.cell.2011.02.013

Heer, N. C., and Martin, A. C. (2017). Tension, Contraction and Tissue Morphogenesis. *Development* 144, 4249–4260. doi:10.1242/dev.151282

Hennings, H., Glick, A. B., Lowry, D. T., Krsmanovic, L. S., Sly, L. M., and Yuspa, S. H. (1993). FVB/N Mice: an Inbred Strain Sensitive to the Chemical Induction of Squamous Cell Carcinomas in the Skin. *Carcinogenesis* 14, 2353–2358. doi:10.1093/carcin/14.11.2353

Hirata, H., Tatsumi, H., and Sokabe, M. (2008). Mechanical Forces Facilitate Actin Polymerization at Focal Adhesions in a Zyxin-dependent Manner. *J. Cel. Sci.* 121, 2795–2804. doi:10.1242/jcs.030320

Hirata, H., Tatsumi, H., Lim, C. T., and Sokabe, M. (2014). Force-dependent Vinculin Binding to Talin in Live Cells: a Crucial Step in Anchoring the Actin Cytoskeleton to Focal Adhesions. *Am. J. Physiol. Cell Physiol.* 306, C607–C620. doi:10.1152/ajpcell.00122.2013

Hirata, H., Gupta, M., Vedula, S. R. K., Lim, C. T., Ladoux, B., and Sokabe, M. (2015). Actomyosin Bundles Serve as a Tension Sensor and a Platform for ERK Activation. *EMBO Rep.* 16, 250–257. doi:10.15252/embr.201439140

Hirata, H., Samsonov, M., and Sokabe, M. (2017). Actomyosin Contractility Provokes Contact Inhibition in E-Cadherin-Ligated Keratinocytes. *Sci. Rep.* 7, 46326. doi:10.1038/srep46326

Hirata, H., Dobrokhotov, O., and Sokabe, M. (2020). Coordination between Cell Motility and Cell Cycle Progression in Keratinocyte Sheets via Cell-Cell Adhesion and Rac1. *iScience* 23, 101729. doi:10.1016/j.isci.2020.101729

Humphrey, J. D., Dufresne, E. R., and Schwartz, M. A. (2014). Mechanotransduction and Extracellular Matrix Homeostasis. *Nat. Rev. Mol. Cel Biol.* 15, 802–812. doi:10.1038/nrm3896

Ichijo, R., Kobayashi, H., Yoneda, S., Iizuka, Y., Kubo, H., Matsumura, S., et al. (2017). Tbx3-dependent Amplifying Stem Cell Progeny Drives Interfollicular Epidermal Expansion during Pregnancy and Regeneration. *Nat. Commun.* 8, 508. doi:10.1038/s41467-017-00433-7

Karantza, V. (2011). Keratins in Health and Cancer: More Than Mere Epithelial Cell Markers. *Oncogene* 30, 127–138. doi:10.1038/onc.2010.456

Kassianidou, E., Hughes, J. H., and Kumar, S. (2017). Activation of ROCK and MLCK Tunes Regional Stress Fiber Formation and Mechanics via Preferential Myosin Light Chain Phosphorylation. *Mol. Biol. Cell* 28, 3832–3843. doi:10.1091/mbc.e17-06-0401

Kim, S. A., Tai, C.-Y., Mok, L.-P., Mosser, E. A., and Schuman, E. M. (2011). Calcium-dependent Dynamics of Cadherin Interactions at Cell-Cell Junctions. *Proc. Natl. Acad. Sci.* 108, 9857–9862. doi:10.1073/pnas.1019003108

Koch, A. W., Pokutta, S., Lustig, A., and Engel, J. (1997). Calcium Binding and Homoassociation of E-Cadherin Domains. *Biochemistry* 36, 7697–7705. doi:10.1021/bi9705624

Kovács, M., Tóth, J., Hetényi, C., Málnási-Csizmadia, A., and Sellers, J. R. (2004). Mechanism of Blebbistatin Inhibition of Myosin II. *J. Biol. Chem.* 279, 35557–35563. doi:10.1074/jbc.m405319200

Levayer, R., and Lecuit, T. (2012). Biomechanical Regulation of Contractility: Spatial Control and Dynamics. *Trends Cel. Biol.* 22, 61–81. doi:10.1016/j.tcb.2011.10.001

Lewis, J. E., Jensen, P. J., Johnson, K. R., and Wheelock, M. J. (1994). E-Cadherin Mediates Adherens Junction Organization through Protein Kinase C. *J. Cel. Sci.* 107 (Pt 12), 3615–3621. doi:10.1242/jcs.107.12.3615

Liu, W. F., Nelson, C. M., Pirone, D. M., and Chen, C. S. (2006). E-Cadherin Engagement Stimulates Proliferation via Rac1. *J. Cel. Biol.* 173, 431–441. doi:10.1083/jcb.200510087

Matsui, T. S., and Deguchi, S. (2019). Spatially Selective Myosin Regulatory Light Chain Regulation Is Absent in Dedifferentiated Vascular Smooth Muscle Cells but Is Partially Induced by Fibronectin and Klf4. *Am. J. Physiol. Cell Physiol.* 316, C509–C521. doi:10.1152/ajpcell.00251.2017

McClatchey, A. I., and Yap, A. S. (2012). Contact Inhibition (Of Proliferation) Redux. *Curr. Opin. Cel. Biol.* 24, 685–694. doi:10.1016/j.ceb.2012.06.009

McMullan, R., Lax, S., Robertson, V. H., Radford, D. J., Broad, S., Watt, F. M., et al. (2003). Keratinocyte Differentiation Is Regulated by the Rho and ROCK Signaling Pathway. *Curr. Biol.* 13, 2185–2189. doi:10.1016/j.cub.2003.11.050

McQuin, C., Goodman, A., Chernyshev, V., Kamentsky, L., Cimini, B. A., Karhohs, K. W., et al. (2018). CellProfiler 3.0: Next-Generation Image Processing for Biology. *Plos Biol.* 16, e2005970. doi:10.1371/journal.pbio.2005970

Mège, R. M., and Ishiyama, N. (2017). Integration of Cadherin Adhesion and Cytoskeleton at Adherens Junctions. *Cold Spring Harb. Perspect. Biol.* 9, a028738. doi:10.1101/cshperspect.a028738

Nassar, D., Latil, M., Boeckx, B., Lambrechts, D., and Blanpain, C. (2015). Genomic Landscape of Carcinogen-Induced and Genetically Induced Mouse Skin Squamous Cell Carcinoma. *Nat. Med.* 21, 946–954. doi:10.1038/nm.3878

Neagu, M., Caruntu, C., Constantin, C., Boda, D., Zurac, S., Spandidos, D. A., et al. (2016). Chemically Induced Skin Carcinogenesis: Updates in Experimental Models (Review). *Oncol. Rep.* 35, 2516–2528. doi:10.3892/or.2016.4683

Pasapera, A. M., Schneider, I. C., Rericha, E., Schlaepfer, D. D., and Waterman, C. M. (2010). Myosin II Activity Regulates Vinculin Recruitment to Focal Adhesions through FAK-Mediated Paxillin Phosphorylation. *J. Cel. Biol.* 188, 877–890. doi:10.1083/jcb.200906012

Pinheiro, D., and Bellaïche, Y. (2018). Mechanical Force-Driven Adherens Junction Remodeling and Epithelial Dynamics. *Dev. Cel.* 47, 3–19. doi:10.1016/j.devcel.2018.09.014

Provenzano, P. P., Inman, D. R., Eliceiri, K. W., and Keely, P. J. (2009). Matrix Density-Induced Mechanoregulation of Breast Cell Phenotype, Signaling and Gene Expression through a FAK-ERK Linkage. *Oncogene* 28, 4326–4343. doi:10.1038/onc.2009.299

Purnell, C. A., Gart, M. S., Buganza-Tepole, A., Tomaszewski, J. P., Topczewska, J. M., Kuhl, E., et al. (2018). Determining the Differential Effects of Stretch and Growth in Tissue-Expanded Skin: Combining Isogeometric Analysis and Continuum Mechanics in a Porcine Model. *Dermatol. Surg.* 44, 48–52. doi:10.1097/dss.0000000000001228

R Core Team (2019). *R: A Language and Environment for Statistical Computing*. Vienna: R Foundation for statistical computing.

Ratushny, V., Gober, M. D., Hick, R., Ridky, T. W., and Seykora, J. T. (2012). From Keratinocyte to Cancer: the Pathogenesis and Modeling of Cutaneous Squamous Cell Carcinoma. *J. Clin. Invest.* 122, 464–472. doi:10.1172/jci57415

Riento, K., and Ridley, A. J. (2003). Rocks: Multifunctional Kinases in Cell Behaviour. *Nat. Rev. Mol. Cel. Biol.* 4, 446–456. doi:10.1038/nrm1128

Rowe, D. E., Carroll, R. J., and Day, C. L., Jr (1992). Prognostic Factors for Local Recurrence, Metastasis, and Survival Rates in Squamous Cell Carcinoma of the Skin, Ear, and Lip. *J. Am. Acad. Dermatol.* 26, 976–990. doi:10.1016/0190-9622(92)70144-5

Samuel, M. S., Lopez, J. I., McGhee, E. J., Croft, D. R., Strachan, D., Timpson, P., et al. (2011). Actomyosin-Mediated Cellular Tension Drives Increased Tissue Stiffness and β-Catenin Activation to Induce Epidermal Hyperplasia and Tumor Growth. *Cancer Cell* 19, 776–791. doi:10.1016/j.ccr.2011.05.008

Schiller, H. B., Friedel, C. C., Boulegue, C., and Fässler, R. (2011). Quantitative Proteomics of the Integrin Adhesome Show a Myosin II-dependent Recruitment of LIM Domain Proteins. *EMBO Rep.* 12, 259–266. doi:10.1038/embor.2011.5

Schindelin, J., Arganda-Carreras, I., Frise, E., Kaynig, V., Longair, M., Pietzsch, T., et al. (2012). Fiji: an Open-Source Platform for Biological-Image Analysis. *Nat. Methods* 9, 676–682. doi:10.1038/nmeth.2019

Schlaepfer, D. D., Hanks, S. K., Hunter, T., and Geer, P. v. d. (1994). Integrin-mediated Signal Transduction Linked to Ras Pathway by GRB2 Binding to Focal Adhesion Kinase. *Nature* 372, 786–791. doi:10.1038/372786a0

Schmidt, G., Sehr, P., Wilm, M., Selzer, J., Mann, M., and Aktories, K. (1997). Gln 63 of Rho Is Deamidated by *Escherichia coli* Cytotoxic Necrotizing Factor-1. *Nature* 387, 725–729. doi:10.1038/42735

Schmidt, U., Weigert, M., Broaddus, C., and Myers, G. (2018). "Cell Detection with star-convex Polygons," in *Medical Image Computing and Computer Assisted Intervention – MICCAI 2018 Lecture Notes in Computer Science* (Cham: Springer International Publishing), 265–273. doi:10.1007/978-3-030-00934-2_30

Schwartz, M. A., and Assoian, R. K. (2001). Integrins and Cell Proliferation: Regulation of Cyclin-Dependent Kinases via Cytoplasmic Signaling Pathways. *J. Cel. Sci.* 114, 2553–2560. doi:10.1242/jcs.114.14.2553

Sethi, K., Cram, E. J., and Zaidel-Bar, R. (2017). Stretch-induced Actomyosin Contraction in Epithelial Tubes: Mechanotransduction Pathways for Tubular Homeostasis. *Semin. Cel. Dev. Biol.* 71, 146–152. doi:10.1016/j.semcdb.2017.05.014

Simpson, C. L., Patel, D. M., and Green, K. J. (2011). Deconstructing the Skin: Cytoarchitectural Determinants of Epidermal Morphogenesis. *Nat. Rev. Mol. Cel. Biol.* 12, 565–580. doi:10.1038/nrm3175

Slack-Davis, J. K., Martin, K. H., Tilghman, R. W., Iwanicki, M., Ung, E. J., Autry, C., et al. (2007). Cellular Characterization of a Novel Focal Adhesion Kinase Inhibitor. *J. Biol. Chem.* 282, 14845–14852. doi:10.1074/jbc.m606695200

Straight, A. F., Cheung, A., Limouze, J., Chen, I., Westwood, N. J., Sellers, J. R., et al. (2003). Dissecting Temporal and Spatial Control of Cytokinesis with a Myosin II Inhibitor. *Science* 299, 1743–1747. doi:10.1126/science.1081412

Strudwick, X. L., Lang, D. L., Smith, L. E., and Cowin, A. J. (2015). Combination of Low Calcium with Y-27632 Rock Inhibitor Increases the Proliferative Capacity, Expansion Potential and Lifespan of Primary Human Keratinocytes while Retaining Their Capacity to Differentiate into Stratified Epidermis in a 3D Skin Model. *Plos One* 10, e0123651. doi:10.1371/journal.pone.0123651

Sugai, M., Hashimoto, K., Kikuchi, A., Inoue, S., Okumura, H., Matsumoto, K., et al. (1992). Epidermal Cell Differentiation Inhibitor ADP-Ribosylates Small GTP-Binding Proteins and Induces Hyperplasia of Epidermis. *J. Biol. Chem.* 267, 2600–2604. doi:10.1016/s0021-9258(18)45923-6

Sun, Z., Guo, S. S., and Fässler, R. (2016). Integrin-mediated Mechanotransduction. *J. Cel Biol.* 215, 445–456. doi:10.1083/jcb.201609037

Sunagawa, M., Mii, S., Enomoto, A., Kato, T., Murakumo, Y., Shiraki, Y., et al. (2016). Suppression of Skin Tumorigenesis in CD109-Deficient Mice. *Oncotarget* 7, 82836–82850. doi:10.18632/oncotarget.12653

Thomas, W. A., Boscher, C., Chu, Y.-S., Cuvelier, D., Martinez-Rico, C., Seddiki, R., et al. (2013). α-Catenin and Vinculin Cooperate to Promote High E-Cadherin-Based Adhesion Strength. *J. Biol. Chem.* 288, 4957–4969. doi:10.1074/jbc.m112.403774

Totsukawa, G., Wu, Y., Sasaki, Y., Hartshorne, D. J., Yamakita, Y., Yamashiro, S., et al. (2004). Distinct Roles of MLCK and ROCK in the Regulation of Membrane Protrusions and Focal Adhesion Dynamics during Cell Migration of Fibroblasts. *J. Cel. Biol.* 164, 427–439. doi:10.1083/jcb.200306172

Várkuti, B. H., Képiró, M., Horváth, I. Á., Végner, L., Ráti, S., Zsigmond, Á., et al. (2016). A Highly Soluble, Non-phototoxic, Non-fluorescent Blebbistatin Derivative. *Sci. Rep.* 6, 26141. doi:10.1038/srep26141

Vaezi, A., Bauer, C., Vasioukhin, V., and Fuchs, E. (2002). Actin cable Dynamics and Rho/Rock Orchestrate a Polarized Cytoskeletal Architecture in the Early Steps of Assembling a Stratified Epithelium. *Dev. Cel.* 3, 367–381. doi:10.1016/s1534-5807(02)00259-9

Vasioukhin, V. (2012). Adherens Junctions and Cancer. *Subcell. Biochem.* 60, 379–414. doi:10.1007/978-94-007-4186-7_16

Verhaegen, P. D., Schouten, H. J., Tigchelaar-Gutter, W., van Marle, J., van Noorden, C. J., Middelkoop, E., et al. (2012). Adaptation of the Dermal Collagen Structure of Human Skin and Scar Tissue in Response to Stretch: an Experimental Study. *Wound Repair Regen.* 20, 658–666. doi:10.1111/j.1524-475x.2012.00827.x

Wang, J. G., Miyazu, M., Xiang, P., Li, S. N., Sokabe, M., and Naruse, K. (2005). Stretch-induced Cell Proliferation Is Mediated by FAK-MAPK Pathway. *Life Sci.* 76, 2817–2825. doi:10.1016/j.lfs.2004.10.050

Wheeler, A., and Ridley, A. (2004). Why Three Rho Proteins? RhoA, RhoB, RhoC, and Cell Motility. *Exp. Cel. Res.* 301, 43–49. doi:10.1016/j.yexcr.2004.08.012

Wickham, H. (2016). *ggplot2: Elegant Graphics for Data Analysis*. New-York: Springer-Verlag.

Wong, S. H. M., Fang, C. M., Chuah, L.-H., Leong, C. O., and Ngai, S. C. (2018). E-Cadherin: Its Dysregulation in Carcinogenesis and Clinical Implications. *Crit. Rev. Oncol. Hematol.* 121, 11–22. doi:10.1016/j.critrevonc.2017.11.010

Yonemura, S., Wada, Y., Watanabe, T., Nagafuchi, A., and Shibata, M. (2010). α-Catenin as a Tension Transducer that Induces Adherens junction Development. *Nat. Cel. Biol.* 12, 533–542. doi:10.1038/ncb2055

Yu, H., Mouw, J. K., and Weaver, V. M. (2011). Forcing Form and Function: Biomechanical Regulation of Tumor Evolution. *Trends Cel. Biol.* 21, 47–56. doi:10.1016/j.tcb.2010.08.015

Zhou, J., Wang, J., Zhang, N., Zhang, Y., and Li, Q. (2015). Identification of Biomechanical Force as a Novel Inducer of Epithelial-Mesenchymal Transition Features in Mechanical Stretched Skin. *Am. J. Transl. Res.* 7, 2187–2198.

Conflict of Interest: The authors declare that the research was conducted in the absence of any commercial or financial relationships that could be construed as a potential conflict of interest.

Publisher's Note: All claims expressed in this article are solely those of the authors and do not necessarily represent those of their affiliated organizations, or those of the publisher, the editors and the reviewers. Any product that may be evaluated in this article, or claim that may be made by its manufacturer, is not guaranteed or endorsed by the publisher.

frontiers in Cell and Developmental Biology

REVIEW
published: 04 February 2022
doi: 10.3389/fcell.2022.795522

Multiscale Strain Transfer in Cartilage

Manuela A. Boos[1], *Shireen R. Lamandé*[2,3] *and Kathryn S. Stok*[1]*

[1]Department of Biomedical Engineering, The University of Melbourne, Parkville, VIC, Australia, [2]Musculoskeletal Research, Murdoch Children's Research Institute, Parkville, VIC, Australia, [3]Department of Paediatrics, The University of Melbourne, Parkville, VIC, Australia

The transfer of stress and strain signals between the extracellular matrix (ECM) and cells is crucial for biochemical and biomechanical cues that are required for tissue morphogenesis, differentiation, growth, and homeostasis. In cartilage tissue, the heterogeneity in spatial variation of ECM molecules leads to a depth-dependent non-uniform strain transfer and alters the magnitude of forces sensed by cells in articular and fibrocartilage, influencing chondrocyte metabolism and biochemical response. It is not fully established how these nonuniform forces ultimately influence cartilage health, maintenance, and integrity. To comprehend tissue remodelling in health and disease, it is fundamental to investigate how these forces, the ECM, and cells interrelate. However, not much is known about the relationship between applied mechanical stimulus and resulting spatial variations in magnitude and sense of mechanical stimuli within the chondrocyte's microenvironment. Investigating multiscale strain transfer and hierarchical structure-function relationships in cartilage is key to unravelling how cells receive signals and how they are transformed into biosynthetic responses. Therefore, this article first reviews different cartilage types and chondrocyte mechanosensing. Following this, multiscale strain transfer through cartilage tissue and the involvement of individual ECM components are discussed. Finally, insights to further understand multiscale strain transfer in cartilage are outlined.

Keywords: cartilage, chondrocytes, mechanotransduction, tissue strain, ECM, heterogeneity

OPEN ACCESS

Edited by:
Selwin K. Wu,
National University of Singapore, Singapore

Reviewed by:
Corey Neu,
University of Colorado Boulder, United States
Christian Hiepen,
Freie Universität Berlin, Germany

***Correspondence:**
Kathryn S. Stok
kstok@unimelb.edu.au

Specialty section:
This article was submitted to Cell Adhesion and Migration, a section of the journal Frontiers in Cell and Developmental Biology

Received: *15 October 2021*
Accepted: *19 January 2022*
Published: *04 February 2022*

Citation:
Boos MA, Lamandé SR and Stok KS (2022) Multiscale Strain Transfer in Cartilage. Front. Cell Dev. Biol. 10:795522. doi: 10.3389/fcell.2022.795522

INTRODUCTION

All tissues in the body contain cells and a well organised extracellular matrix (ECM) compartment. The ECM is tissue-specific and the constituents, such as collagens, proteoglycans (PGs), and elastin, vary between different tissues. The ECM provides physical support and scaffolding for the cells, and also regulates crucial biochemical and biomechanical cues that are required for tissue morphogenesis, differentiation, growth, and homeostasis (Frantz et al. 2010; Theocharis et al. 2016). The cells within these tissues establish the ECM during development, maintain it in healthy tissue, and repair it in response to disease and injury (Lu et al. 2011; Humphrey et al. 2014). This reciprocal relationship between the cells and the ECM is based on the ability of cells to sense physical signals and transduce them into biochemical responses. Converting mechanical signals into chemical signals is called mechanotransduction (Mofrad et al. 2010; Wang 2017). Cross talk between cells and ECM creates a local environment where matrix stiffness and the physical forces sensed by the cells play an essential role in biological functions of cell and tissue physiology, and lead to constant tissue remodelling. Given the finite life span of cells and ECM components, this remodelling ensures a homeostatic balance in the tissue, e.g. structural integrity and functionality. This homeostasis is thus achieved by balanced matrix degradation and deposition of new

constituents. Disruption of these homeostatic processes leads to tissue degeneration, fibrosis or other pathologies.

Cartilage is a connective tissue providing mechanical and structural support in different anatomical locations in the human body. Its ECM is produced by the relatively scarce specialised cells, chondrocytes, and is mainly composed of PGs, different collagen types, and elastin. It is classified into three different types, hyaline cartilage (articular joints, nose, ribs), elastic cartilage (ears, larynx), and fibrocartilage (menisci, intervertebral discs). These different types vary in their histological and physiological appearance and also in the magnitude of physical daily load they experience (Homicz et al. 2003; Heinegard et al. 2011; McNulty et al. 2015; Nimeskern et al. 2015). Furthermore, different cartilage types have a distinct ECM composition, with a highly heterogeneous accumulation of different proteins, molecules, and fibres. This variation in tissue composition between cartilage types leads to heterogeneous transfer of mechanical stimuli and influences cell morphology and biochemical response. Our knowledge about the mechanoresponse of cartilage has tremendously increased. Single cell responses to mechanical stimuli are well studied in health and disease. However, mechanical signals do not originate in the immediate vicinity of the cells. Rather they result from movements of the whole body and forces from body weight and joint movement. Even though we know well how chondrocytes respond to mechanical stimuli, we do not fully understand how these signals reach the cells, as it is a multiscale process. Furthermore, it is not well known how different ECM compositions and arrangements influence load transfer to cells. Specifically, how heterogeneous strain in the ECM influences chondrocytes and therefore long-term remodelling of cartilage in both health and disease, is not known.

Understanding these processes and mechanisms is as critical to progress in tissue regeneration and repair strategies as it is to engineering cartilage tissues. Gaining further insights into multiscale strain transfer and mechanotransduction in different cartilage types would provide a benchmark by which to compare tissue engineered constructs, and feed into developing effective treatment strategies to address cartilage pathologies. Therefore, this article first reviews different cartilage types and chondrocyte mechanosensing. Following this, multiscale strain transfer through cartilage tissue and the involvement of individual ECM components are discussed. Finally, insights to further understand multiscale strain transfer in cartilage are outlined.

DIFFERENT CARTILAGE TYPES

Hyaline Cartilage

In hyaline cartilage, the so-called 'solid' phase of the ECM is mainly composed of collagen II (15%–22%) and PGs (4%–7%). The PGs are comprised of different glycosaminoglycans (GAG) chains attached to a core protein. The fluid phase on the other hand consists of up to 80% water (Eyre 2002; Heinegard 2009; Sophia Fox et al. 2009). This water content is a result of the fixed charge density created by the negatively charged sulphated GAGs. Their charge attracts cations which leads to osmotic pressure in the tissue. As the PGs with the attached GAGs swell, they are physically limited by the collagen network which gives articular cartilage a high compressive resilience. This feature is further increased under physical load as the repulsive forces of the PGs are pushed closer together and swelling is hindered by the tension in the collagen fibres (Roth et al. 1980). This effect enables articular cartilage to withstand significant loads up to multiple times body weight (Mansour, 2003; Lu et al. 2009; Sophia Fox et al. 2009; Thielen et al. 2019). The experienced physical load of the cartilage varies depending on anatomical location.

Articular cartilage is divided into a superficial zone, a middle zone, and a deep zone, which vary in their ECM composition, cell orientation and morphology (**Figure 1**). In the superficial zone chondrocytes are more abundant and have a flattened, elongated form compared to the deeper zones where they are less densely populated. In deeper zones the chondrocytes are more spherical and are arranged in columns. The PG content in articular cartilage increases with depth. The collagen content however remains constant with increasing depth, but fibres change from being arranged parallel to the surface in the superficial zone to a perpendicular orientation in the deeper zones (Eggli et al. 1988; Guilak, 1995; Wong et al. 1996; Poole et al. 2001; Athanasiou et al. 2009; Quinn et al. 2013). Elastin is present in the superficial zone of articular cartilage (Mansfield et al. 2009). The elastin fibres run parallel to the surface and roughly in the same direction as the collagen fibres (Yeh et al. 2005; Yu et al. 2010).

All chondrocytes in the tissue are surrounded by a PG-rich pericellular matrix (PCM) (**Figure 1**) (Poole 1997). The PCM has a crucial function in absorbing, redistributing, and transmitting mechanical forces in articular and meniscal cartilage (Poole 1997; Sanchez-Adams et al. 2013; Gilbert et al. 2018) (Millward-Sadler et al. 2004). It shields chondrocytes from extensive stress, and because it is a direct link between the cells and the ECM makes an important contribution to transmitting biomechanical signals to the cells (Quinn et al. 1998). The PCM has a high concentration of aggrecan and other PGs such as perlecan, biglycan and decorin which play an important role in its integrity (Gomes et al. 2002; Vincent et al. 2007; Wilusz et al. 2014; Shu et al. 2016). In addition to PGs, collagen type VI in articular cartilage is highly concentrated in the PCM and plays an important role in its mechanical integrity. It connects the chondrocytes to the PCM through β-integrin receptors and transmembrane PGs (Marcelino et al. 1995; Wilusz et al. 2012). The PCM in the articular cartilage superficial zone also contains elastin and lipids (Poole 1997; Mansfield et al. 2009). As the tensile and shear stresses are higher in this zone, this composition would protect the chondrocytes from these stresses.

Fibrocartilage

Located in the knee joint, the menisci, composed of fibrocartilage (**Figure 1**), are responsible for increasing the contact area and distributing forces across the joint. In contrast to hyaline and elastic cartilage, the main collagen type in the menisci is type I (Fox et al. 2015). Collagen fibres are oriented circumferentially in the interior layers of meniscal cartilage compared to radially oriented fibres in the outer

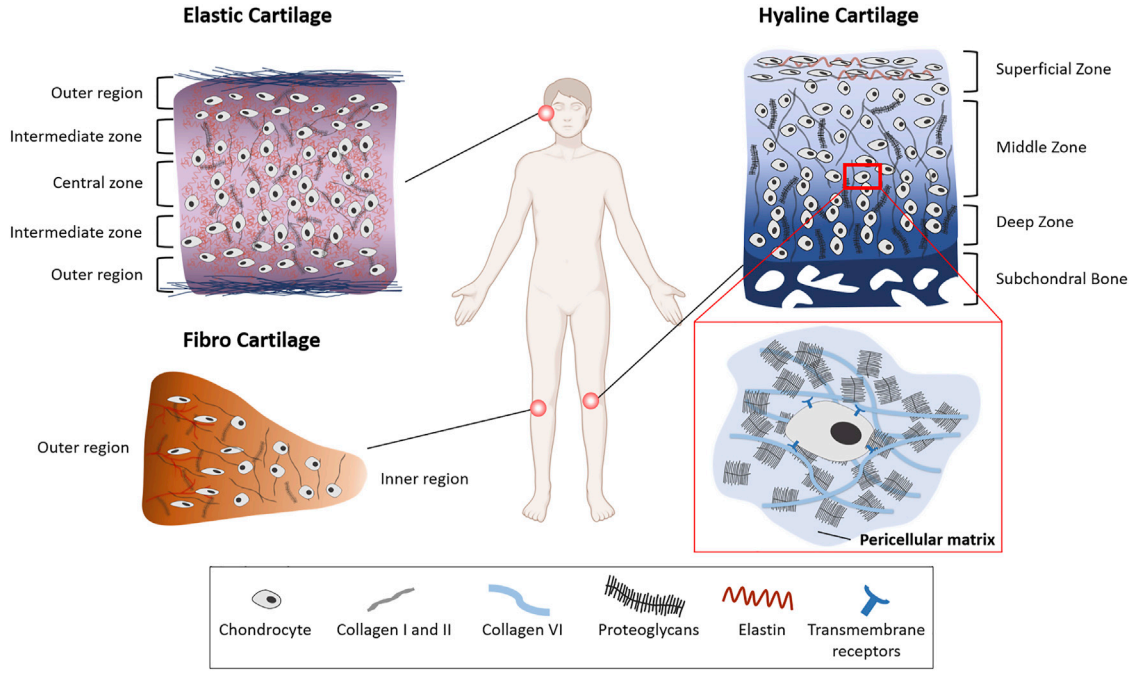

FIGURE 1 | Extracellular matrix heterogeneity of different cartilage types. The three cartilage types vary in ECM composition and arrangement. Elastic cartilage and hyaline articular cartilage are arranged in different zones with the chondrocyte shape becoming smaller and flatter towards the outer region and superficial zone, respectively. Proteoglycan (PG) concentration articular cartilage in the knee joint increases with depth of the tissue. In meniscal cartilage (fibro cartilage) the PG concentration is highest in the outer region. The pericellular matrix (PCM) surrounds the chondrocytes and contains a high amount of PGs such as aggrecan and perlecan, and collagen type VI in articular and meniscal cartilage.

regions (Amis 2010). The circumferential alignment of these collagen fibres contributes to the load bearing properties of the menisci by converting compressive axial stresses to tensile hoop stresses (McDermott et al. 2008; Sanchez-Adams et al. 2013; Fox et al. 2015). Like articular chondrocytes, cells in meniscal cartilage differ in their appearance depending on their location within the tissue. Cells in the outer region of meniscal cartilage have an oval, fusiform shape, whereas cells in the inner region have a round shape (Hellio Le Graverand et al. 2001; Makris et al. 2011). In contrast to the large amount of collagen type I in outer regions of the meniscus, the inner region has more collagen type II (60%) than type I (40%) (McDermott, 2010; Sanchez-Adams et al. 2013). PG-rich regions are interspersed between these collagen fibres, leading to a highly inhomogeneous tissue (Upton et al. 2008; Han et al. 2013; Han et al. 2016). Similarly to the PCM in hyaline cartilage, the PCM in meniscal cartilage is mainly composed of perlecan and collagen type VI (Sanchez-Adams et al. 2013) (**Figure 1**).

Elastic Cartilage

Elastic cartilage is not exposed to large biomechanical forces, as it is found in the head and neck region. It contains a high amount of elastin which is arranged around the chondrocytes and contributes to maintaining anatomic shape *via* complex heterogeneous arrangement of tensile compressive fibre networks (**Figure 1**) (Culav et al. 1999; He et al. 2013; Nimeskern et al. 2016). Elastic ear cartilage is arranged in different zones as well. Similar to articular cartilage, the chondrocytes in the outer regions are smaller and flatter than the cells in the intermediate and central zones, where the chondrocytes are larger and further apart (Keith et al. 1977; Jessop et al. 2016). Collagen type II in auricular cartilage is arranged together with a dense elastin fibre network surrounding the chondrocytes in a honeycomb like structure (Chen et al. 2014; Bos et al. 2018). The composition of the PCM of elastic cartilage has not been reported.

Despite their differences in ECM structure, all three cartilage types are avascular (except the outer region of the menisci), aneural, and alymphatic, resulting in a tissue with limited intrinsic repair capabilities (Khan et al. 2008; Makris et al. 2011). These variations in the cartilage ECM make it a highly heterogeneous tissue on a macrostructural as well as microstructural level. These structural differences in cartilage types directly influence the mechanical environments experienced by the chondrocytes and this heterogeneity leads to nonuniform strain and stress in cartilage. This in turn, changes how mechanical signals are transmitted and received by the cells in these different tissues.

CHONDROCYTE MECHANOSENSING

Chondrocytes establish the cartilage ECM during development and maintain it in healthy tissue (Lu et al. 2011; Humphrey et al.

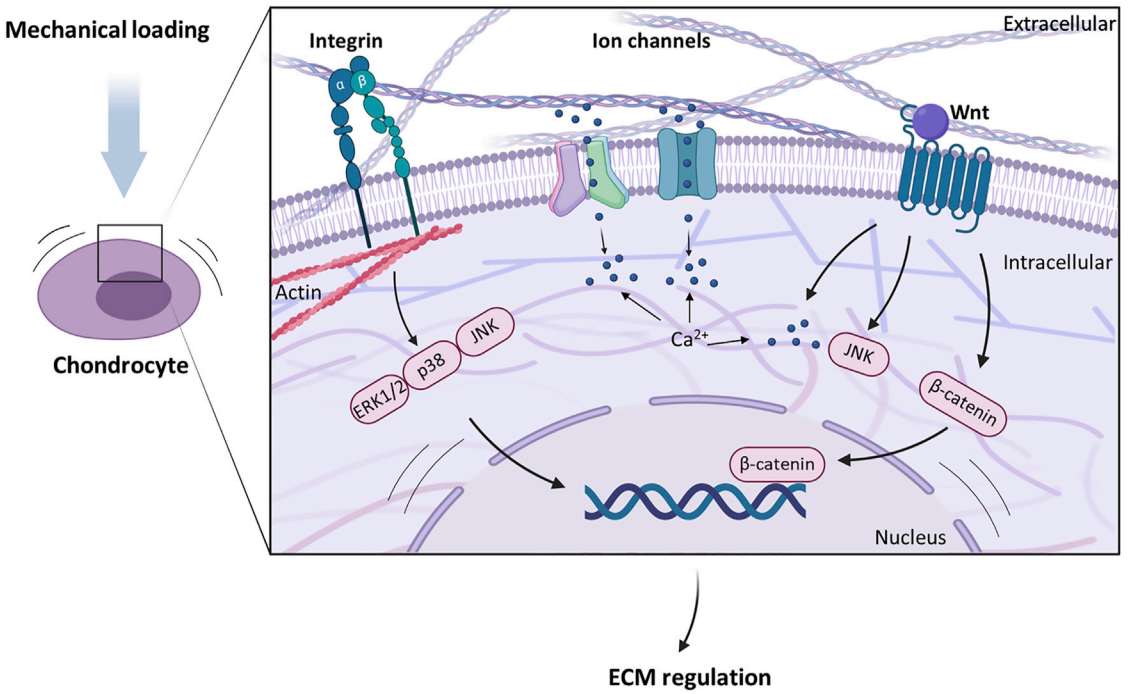

FIGURE 2 | Different cell membrane receptors and signalling molecules are involved in chondrocyte mechanotransduction. Transmembrane ion channels induce intracellular Ca^{2+} signalling upon mechanical stimulation of cartilage and regulate extracellular matrix (ECM) biosynthesis. Integrins serve as a link between ECM molecules and the cytoskeleton and lead to an activation of the MAPK pathway. Signalling molecules such as Wnt activate intracellular signalling cascades that are important for cartilage homeostasis.

2014). This reciprocal relationship between the chondrocytes and ECM is based on their ability to sense physical signals and transduce them into biochemical responses, making them highly mechanosensitive. This conversion of mechanical signals into chemical signals is called mechanotransduction (Mofrad et al. 2010; Wang 2017) and this allows chondrocytes to sense changes in ECM properties. The response of articular chondrocytes to mechanical stimuli is well studied. They have several cell surface mechanoreceptors, e.g. ion channels, integrin receptors, and primary cilia, that are sensitive to changes in intrinsic tissue stiffness and external tissue compression (**Figure 2**) and initiate intracellular signalling cascades that modulate gene expression leading to ECM remodelling (Gilbert et al. 2018). Furthermore, intracellular deformation and signalling molecules enable responses to changes in mechanical environment.

Ion Channels

Ion channels such as transient receptor potential vanilloid 4 (TRPV4) and Piezo channels are Ca^{2+}-permeable and situated in the plasma membrane where they play a role in mechanically induced Ca^{2+} signalling. Mechanical perturbations such as changes in membrane tension, lipid bilayer distortion and osmotic stress activate these channels. This facilitates Ca^{2+} influx into the chondrocyte and initiates intracellular signalling pathways (Guilak et al. 1999; Pingguan-Murphy et al. 2006). TRPV4 is highly expressed in chondrocytes and promotes anabolic responses. It provides an essential link between mechanical loading and ECM synthesis (Phan et al. 2009; O'Conor et al. 2014; Zelenski et al. 2015). Piezo 1 and 2 channels however are involved in transducing hyperphysiological mechanical stimuli resulting from injuries or overload (Lee et al. 2014; Lee et al. 2017). Mechanical integrity of the ECM and mechanical stimuli experienced by the cells are therefore tightly related to the resulting cellular response.

Integrins

Integrins also play an important role in chondrocyte mechanosensing. They are a family of transmembrane proteins comprised of α and β subunits. Their large extracellular domains bind to PCM ligands such as fibronectin and collagen type VI, whereas the cytoplasmic domains bind to the actin skeleton of the chondrocytes, making integrins a transmembrane link between ECM molecules and the cytoskeleton (Millward-Sadler et al. 2000; Hynes 2002; Wolfenson et al. 2013). Mechanical stimulation activates integrins, and also increases their expression in chondrocytes (Lucchinetti et al. 2004). Furthermore, cell death resulting from cartilage injuries and overload has been associated with integrin-mediated signalling. Integrins transduce mechanical signals from the ECM to the chondrocytes and are sensitive to changes in mechanical properties and stimuli.

The activation of integrins can result in activation and phosphorylation of mitogen-activated protein kinases

(MAPKs). MAPKs comprise ERK1/2, p38 and JNK (Fitzgerald et al. 2008). Their activation leads to many intracellular processes like cell division, differentiation, apoptosis, and transcription. A shear strain of 3% applied at 0.1 Hz for up to 24 h has led to an activation of ERK1/2 and p38K in bovine cartilage explants. The inhibition of ERK1/2 or p38K however abolished the mechanically induced transcription of aggrecan and type II collagen (Fitzgerald et al. 2008). JNK is thought to have role in load-induced matrix anabolism. Cyclic loading at 0.33 Hz for up to 3 h induced JNK activation together with increased PG synthesis in human chondrocyte monolayers (Zhou et al. 2007).

Primary Cilia

Primary cilia are microtubule-based structures extending from the chondrocyte surface into the PCM where they sense matrix deformation and osmotic changes through integrins in the primary cilia membrane and extracellular matrix components, and through mechanosensing ion channels. (McGlashan et al. 2006; Ruhlen et al. 2014). In chondrocytes under 15% compressive strain primary cilia were involved in upregulated PG synthesis (Wann et al. 2012). Furthermore, they have been shown to transduce mechanical signals *via* activation of the MAPK/ERK pathway. A loss of cilia leads to inhibition of downstream cartilage matrix gene expression such as type II collagen (COL-II), type X collagen (COL-X) and BMP-2 (Irianto et al. 2014). As a result, primary cilia play a crucial role in cartilage ECM formation.

Intracellular Deformation

Cytoskeletal organisation and cell shape likewise influence chondrocyte metabolism and activate intrinsic signalling (Ingber et al. 1994; Guilak 1995). Tissue compression as well as changed mechanical properties can lead to compressive deformation of the cellular components, including the nucleus, endoplasmic reticulum, cytoskeleton, and integrins (Guilak 1995; Mobasheri et al. 2002; Wong et al. 2003; Szafranski et al. 2004). These events either lead to direct changes in gene expression or protein synthesis or induce other signalling cascades like intracellular calcium signalling (D'Andrea et al. 2000; Guilak et al. 2000; Roberts et al. 2001; Martins et al. 2012; Hall 2019).

The actin skeleton and the vimentin network are responsible for cell integrity. Disrupting actin leads to a 90% reduction in cell stiffness (Trickey et al. 2004). Following actin disruption, nuclear height and shape are severely changed, which is likely to have an effect on the biochemical response of the cells (Guilak 1995; Martins et al. 2012). Furthermore, the actin skeleton is highly sensitive to mechanical stimulation. High hydrostatic pressure (15–30 MPa) can break down the actin network, and dynamic or static loading has resulted in actin remodelling in bovine chondrocyte monolayers (Parkkinen et al. 1995). This sensitivity of actin to loading and the resulting changes in cell stiffness likely influence chondrocyte gene expression and protein biosynthesis. The vimentin network is prominent in weight-bearing areas of rabbit articular cartilage, whereas it is disassembled in unloaded rat articular cartilage explants (Eggli et al. 1988; Durrant et al. 1999). This suggests a similarly important role of vimentin in chondrocyte homeostasis (Blain et al. 2006).

Wnt Signalling

Biomechanical effects in cartilage are mediated through activating and/or suppressing intracellular signalling pathways. Wnts are a family of signalling molecules that are essential during chondrogenesis and chondrocyte homeostasis (Tamamura et al. 2005; Yuasa et al. 2008). Wnt is bound to the ECM, mainly to heparan sulphate, a specific GAG chain (Takada et al. 2017)and its activation is thought to occur through mechanical as well as enzymatic activity (Scholtes et al. 2018; Thielen et al. 2019). The downstream effects of Wnt ligands include translocation of b-catenin to the nucleus to effect transcription, regulation of Ca^{2+} release, and cytoskeleton reorganisation. *In vivo* both excessive activation and lack of Wnt leads to cartilage breakdown, therefore the mechanoregulation of Wnt signalling is essential for cartilage integrity and homeostasis (Zhu et al. 2008; Zhu et al. 2009; Nalesso et al. 2011).

Mechanosensing in Meniscal Cartilage

How chondrocytes in meniscal cartilage respond to mechanical forces remains largely unknown. Like articular chondrocytes, meniscal chondrocytes are highly mechanosensitive. Physiological compression of porcine *ex vivo* meniscus explants at a strain rate of 10% increases aggrecan gene expression (Aufderheide et al. 2006; Zielinska et al. 2009). However, 20% strain induces a catabolic response and increased PG breakdown (McHenry et al. 2006; Zielinska et al. 2009). Even though we have gained more insight into biochemical activities in meniscal cartilage under load, many underlying mechanisms still need to be investigated.

Mechanosensing in Elastic Cartilage

Elastic cartilage is not exposed to constant high loading, and so, although they are mechanosensitive, mechanotransduction processes in elastic cartilage chondrocytes have not been established. When subjected to dynamic compression, porcine auricular chondrocytes upregulate collagen I, collagen II, and aggrecan gene expression (Chung et al. 2008); however, hese cells were seeded in hyaluronan hydrogels which do not mimic the native ECM components of elastic cartilage. An ECM that lacks elastin may therefore not be an ideal scaffold to study cellular response of chondrocytes from elastic cartilage. The influence of this distinct ECM in auricular cartilage on the chondrocytes remains to be investigated.

We have a good understanding of how articular chondrocytes respond to mechanical stimuli *in vitro* and which mechanosensitive channels, receptors and signalling pathways are activated upon stimulation. However, it is also essential to comprehend how stress and strain resulting from movement and body weight are transferred through the ECM to the cells *in situ*. Mechanical stimulation upregulates ECM biosynthesis and deposition. Therefore, there is likely a direct relationship between ECM composition, mechanical properties and resulting cellular response which should be further explored.

STRAIN TRANSFER AND INDIVIDUAL ECM COMPONENTS

Body movements are complex resulting in different stresses and strains in all cartilage tissues. In the knee strains in articular cartilage can reach up to around 20% depending on the movements and are higher in more load bearing regions (Eckstein et al. 1999; Liu et al. 2010; Coleman et al. 2013). Even though compression is the main force experienced by joints, their movements also include sliding and rotation. Therefore, articular cartilage is also subjected to shear forces (Wong et al. 2008).

Meniscal cartilage is important for absorbing shock and distributes more than 50% of the axial load on the knee joint (Fukubayashi et al. 1980; Fithian et al. 1990). The strains measured in meniscal cartilage under physiological loading are in the range of 3–8% (Kolaczek et al. 2016).

Strain transfer involves organs, tissues, and cells, originating at a macro level, then travelling through the tissues to reach the cells and elicit a response. The cartilage ECM is highly heterogeneous (**Figure 1**) ensuring that force transfer is a complex, nonlinear and nonuniform process.

Bulk Cartilage Tissue Strain is Heterogeneous

The heterogeneity in articular and fibrous cartilage leads to non-uniform compressive strain gradients that are depth-dependent (Eckstein et al. 1999; Erne et al. 2005; Upton et al. 2008). Articular cartilage explants exhibit distinct depth-dependent strain distributions in response to uniaxial compression. The tissue strain in the superficial layer is significantly higher compared to strain in the middle and deep zones in response to tensile and compressive forces (Erne et al. 2005; Mansfield et al. 2015). The higher compressive modulus in deeper zones of articular cartilage correlates with the higher PG content in these zones. Swelling pressure determines the tissue's response to compression. Therefore, in the superficial zone with a lower PG concentration, water is lost more easily as the swelling pressure is lower (Chen et al. 2001).

In meniscal cartilage, strain transfer through the tissue was also heterogeneous and tissue specific (Han et al. 2013). The strain was less attenuated through the tissue at low applied strains (3%–6%) and more attenuated with higher applied strains (6%–15%).

In non-load bearing cartilage, i.e., elastic cartilage, the specific strain distribution has not been reported. Only the mechanical properties of the bulk tissue have been analysed (Nimeskern et al. 2016; Chang et al. 2020).

Despite our good understanding of the mechanics of different zones, the underlying mechanisms and micromechanics of the local tissue composition around the cells remain to be fully investigated. A wide range of cellular responses in the same zone of articular cartilage indicates that cells might not experience the same mechanical loading on a microscale level (Mansfield et al. 2015; Kwon et al. 2016). Microscale strain is also highly heterogeneous in fibrocartilage (**Figure 3**) (Mansfield et al. 2015; Han et al. 2016). Looking beyond bulk tissue mechanics has revealed mechanical loading produces highly heterogeneous microscale strains potentially influencing chondrocyte responses and tissue remodelling. Investigating this local microscale environment is key to unravelling how forces from tissue scale are transmitted to cell level. Therefore, exploring the contribution of the individual ECM components and their interaction under bulk load is essential to understand the micromechanics and investigate the influence of heterogeneous strain on tissue health and disease.

Collagen

Collagen fibres in articular cartilage have been widely explored in relation to tissue mechanics. They are able to resist very high tensile loads. Tensile modulus is largest in the direction parallel to the long axis of collagen fibres and up to 5 times higher in the superficial zone of articular cartilage compared to deeper zones (**Figure 1**). Tensile modulus is related to the degree of crosslinking between collagen fibres (Huang et al. 2005; Responte et al. 2007). In the superficial zone of articular cartilage, where collagen fibres are parallel to the surface, the strain following tensile load is highly heterogeneous. Tensile strain of 6% either applied along the main axis of the collagen fibres or transverse to the main collagen axis in the superficial zone resulted in heterogeneous strain distribution (Mansfield et al. 2015). This heterogeneity in the tensile strain field is thought to be due to the leaf-like organisation of the collagen layers (Nickien et al. 2013; Mansfield et al. 2015).

Proteoglycans

Under compression, the swelling pressure resulting from the GAGs is resisted by the tensile forces of the collagen fibres. The PG concentration increases with tissue depth (**Figure 1**) and correlates with the compressive modulus (Mansfield et al. 2015). On a microscale level, while Irwin *et al.* observed only a weak correlation between GAG content and strain magnitude (Irwin et al. 2021) they acknowledged it is difficult to distinguish GAGs from collagen fibres using Raman spectroscopy and so the measured strain might not have resulted from GAGs solely. Furthermore, strain transfer in PG-rich regions in meniscal cartilage was significantly attenuated compared to fibre rich regions which suggests an intimate and direct involvement of the PGs in strain attenuation and distribution (Han et al. 2016). Diseases like osteoarthritis are related to PG loss and impaired mechanical tissue integrity, which leads to a cascade of deteriorating events. Therefore, a clear understanding of the role of PGs in stress and strain transfer at the microscale is important.

Elastin

The elastin fibres in the superficial zone of articular cartilage are always under tension and a strain of around 15% even in unloaded tissue. Under compression, the fibres show minimal deformation or movement and there is no difference in compressive response when elastin is depleted from articular cartilage (Mansfield et al. 2015; Nimeskern et al. 2016). Therefore, elastic fibres are thought to be involved in recovery after shear and

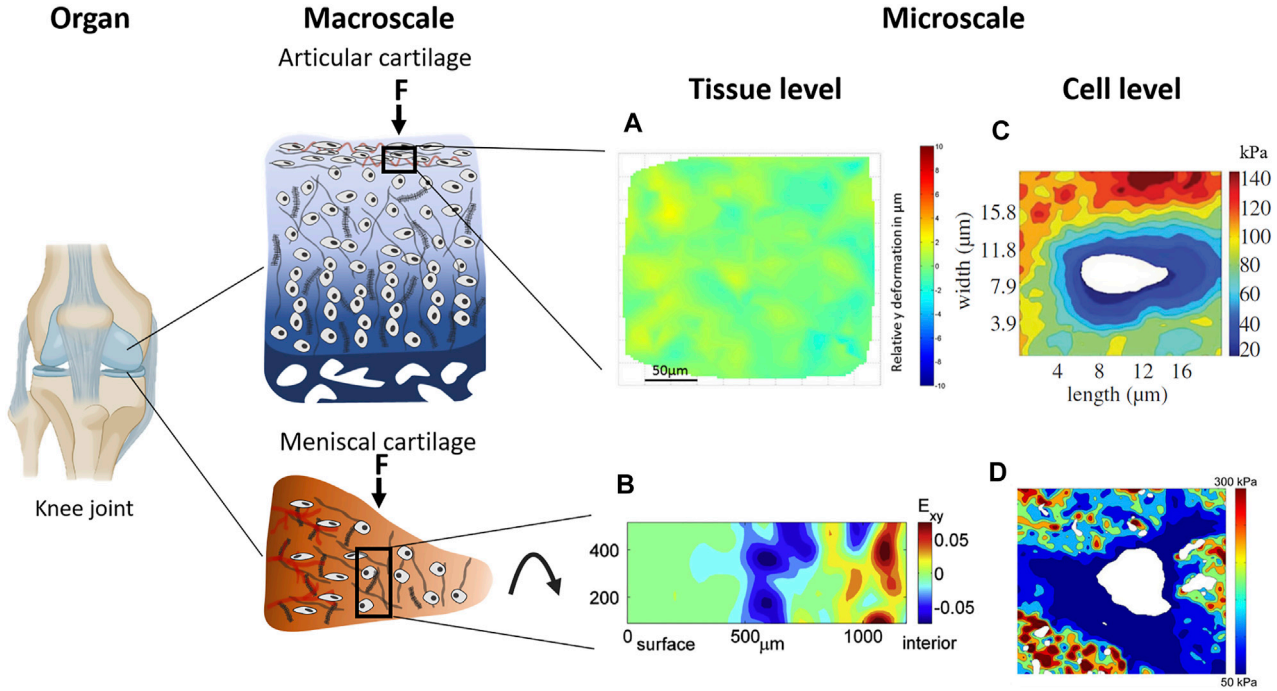

FIGURE 3 | Multiscale strain transfer in articular and meniscal cartilage occurs from the organ to macroscale and microscale. Tissue strains resulting from mechanical compression and tensile loading are non-uniform. **(A)** Heterogeneous strain in the superficial zone of *ex vivo* equine articular cartilage at 38% compressive strain demonstrated by (Mansfield et al. 2015), and **(B)** heterogeneous strain distribution in the central region of *ex vivo* bovine medial meniscal cartilage at 10% compressive strain demonstrated by (Lai et al. 2010). Stiffness maps of the PCM measured with atomic force microcopy reveal a softer PCM compared to the surrounding ECM in both **(C)** the superficial zone of human articular cartilage and **(D)** the middle zone of human meniscal cartilage. Panel **(A)** from (Lai et al. 2010), **(B)** from (Han et al. 2016), **(C)** from (Wilusz et al. 2012), and **(D)** from (Sanchez-Adams et al. 2013) used with permission.

tensile stress (Mansfield et al. 2015). These stresses are highest in the superficial zone of articular cartilage, where the majority of the elastin fibres are present. In auricular cartilage, however, elastin is a major ECM component. Extensive mechanical evaluation has highlighted its importance in the viscoelastic response of auricular cartilage. The tissue loses its compressive and tensile integrity following elastin depletion (Nimeskern et al. 2016).

Pericellular Matrix

The high PG concentration in the PCM produces a high negative charge which attracts counterions therefore providing immediate Ca^{2+} sources for channel activation and swelling, giving it its distinct mechanical properties. The ECM in articular cartilage outside the PCM has a stiffness of up to 1000 kPa, whereas the stiffness of the PCM is only around 50 kPa with a decrease of stiffness in towards deeper zones of the tissue (**Figure 3**) (Darling et al. 2010; Wilusz et al. 2012). In meniscal cartilage the PCM stiffness is around 150 kPa in the outer region gradually decreasing towards the inner region where the stiffness is around 30 kPa (Sanchez-Adams et al. 2013). The chondrocytes themselves have the lowest stiffness, which is 0.1 kPa (Alexopoulos et al. 2003; Steklov et al. 2009; Darling et al. 2010; Nia et al. 2015; Carlson et al. 2017; Chery et al. 2020).

The PCM mechanical properties vary with changes in protein and PG composition. Reduced PG content results in a less negative environment and thus less Ca^{2+} leading to reduced osmotic swelling, ultimately changing the stiffness (Guilak et al. 2006; Danalache et al. 2019; Zhou et al. 2019; Chery et al. 2020). Intact PCMs exhibited a lower elastic modulus compared to PCMs that were depleted of perlecan and were mainly composed of collagen type VI (Wilusz et al. 2012). However, a lack of collagen type VI also decreases the PCM mechanical properties (Alexopoulos et al. 2009; Zelenski et al. 2015; Chery et al. 2020).

These changes in PCM mechanical properties directly influence the chondrocytes. Several studies have shown that a loss of the PCM or a decreased PG content in the PCM leads to increased cell deformation (Millward-Sadler et al. 2004) (Guilak et al. 2006; Danalache et al. 2019; Chery et al. 2020). Recent *in silico studies* have revealed that the softening of the PCM resulted in an increase of strain in the PCM as well as the chondrocyte, even when the macroscale mechanical properties of the tissue did not change (Khoshgoftar et al. 2017). This highlights the importance of the PCM in attenuating mechanical stress and strain shielding of the chondrocytes especially in the superficial zone of articular cartilage where stresses are higher. In a study subjecting bovine articular cartilage explants to hyperphysiological impact loading resulting in cell death due to high strain on integrins. However, when the cell-matrix adhesion was inhibited the cells did not die under injury loading (Sauter et al. 2012; Jang et al. 2014).

Mechanical integrity of the PCM is necessary for physiological mechanotransduction and cartilage health. It is crucial in providing the right mechanical cues for chondrocytes homeostasis and is imperative for the cell-matrix connection. A change in mechanical properties of the PCM seems to have a more direct influence on the cells than bulk tissue strain. It is however not well understood how the heterogeneous strain from the tissue is received by the PCM on the microscale and how this impacts the cells.

Chondrocytes

There is evidence that the nonuniform ECM and resulting strain transfer through the tissue influences chondrocyte deformation and morphology. Cell shape is influenced by the ECM composition which is different in the different zones (**Figure 1**) (Benya 1988; Guilak, 1995). Chondrocytes in the superficial zone, where there is a lower compressive modulus, experience larger changes in volume compared to chondrocytes in the other zones (Mansfield et al. 2015). There can be a wide range of changes in cell thickness in the same zone under compression, indicating that even in the same zone, cells might not experience the same mechanical load (Mansfield et al. 2015; Kwon et al. 2016). Under compression no significant chondrocyte shape changes or displacement were detected in the plane parallel to the surface, whereas under tensile load, all chondrocytes deformed parallel to the articular surface. At a tissue strain of 38%, the median compressive strain in the chondrocytes was 46% (Mansfield et al. 2015). These deformation differences could be due to the original shape of the chondrocytes before mechanical stimulation. In meniscal cartilage, spherical cells deform less than elongated cells which readily deform (Han et al. 2013). Besides *in vitro* experiments, different *in silico* models have highlighted this relationship between cellular deformation and tissue heterogeneity (Breuls et al. 2002; Klika et al. 2019; Tanska et al. 2020).

In addition to variable changes in cell morphology, intracellular strains are also nonuniform. Chondrocyte deformation generates heterogeneous intracellular strain fields which appear to be dependent on cell organelle organisation (Knight et al. 2006). Cell nuclei deform less than the cytoplasm as they have a higher stiffness (Gilchrist et al. 2007). Chondrocyte metabolism is influenced by ECM composition and zonal arrangement (Benya 1988; Guilak et al. 1995; Hall 2019). Elevated strain magnitudes, especially in the superficial zone of articular cartilage, are associated with mitochondrial dysfunction, apoptosis, and cell death (Bonnevie et al. 2018). Although this demonstrates that the mechanical environment influences chondrocyte metabolism, it remains unknown what effects this has in the long term and how this heterogeneous strain affects tissue remodelling over time. Furthermore, it is unclear how stress and strain reach cells and are distributed through the whole heterogeneous tissue, and further how a change in matrix composition and integrity influences the forces sensed in the microenvironment of the cell.

FURTHER DIRECTIONS AND OUTLOOK

The transfer of stress and strain signals to and from cells in tissues involves the integration of the ECM. Different cartilage types have a distinct overall ECM molecular composition, that is spatially highly heterogeneous. The heterogeneity in the ratio of ECM molecules is different in cartilage tissues and regions and leads to a depth-dependent non-uniform compressive strain transfer and alters the magnitude of forces sensed by cells in articular and fibrocartilage, influencing chondrocyte metabolism and biochemical response.

As our understanding of how strain and force are transferred through cartilage tissue grows, it is evident that it is a multiscale process. The influence of matrix molecule interaction and distribution is not well understood, and even though single cell responses to mechanical stimuli are well studied, there is a lack of understanding of the long term effects. It will be important to link the cell response to the tissue scale forces and longitudinally investigate remodelling over a longer time span.

Investigation of multiscale strain transfer would further our understanding of the complex mechanisms of mechanobiology and remodelling in different cartilage tissues, not only load bearing types. Furthermore, it would increase our knowledge about native cartilage tissue, providing a benchmark by which to compare tissue engineered constructs and feed into the development of effective treatment strategies to address cartilage pathologies.

AUTHOR CONTRIBUTIONS

MB, SL, and KS contributed to conception and design of the review. MB performed the literature review and wrote the first draft of the manuscript. All authors contributed to manuscript revision, read, and approved the submitted version.

FUNDING

This work was supported by The University of Melbourne.

ACKNOWLEDGMENTS

We thank Brooke Farrugia for providing the illustrations created with BioRender.com.

REFERENCES

Alexopoulos, L. G., Haider, M. A., Vail, T. P., and Guilak, F. (2003). Alterations in the Mechanical Properties of the Human Chondrocyte Pericellular Matrix with Osteoarthritis. *J. Biomech. Eng.* 125 (3), 323–333. doi:10.1115/1.1579047

Alexopoulos, L. G., Youn, I., Bonaldo, P., and Guilak, F. (2009). Developmental and Osteoarthritic Changes inCol6a1-Knockout Mice: Biomechanics of Type VI Collagen in the Cartilage Pericellular Matrix. *Arthritis Rheum.* 60 (3), 771–779. doi:10.1002/art.24293

Amis, A. (2010). ID McDermott, SD Masouros, AMJ Bull, and AA Amis. *The Meniscus* 91 (96), 11. doi:10.1007/978-3-642-02450-4_1.2

Athanasiou, K. A., Darling, E. M., and Hu, J. C. (2009). Articular Cartilage Tissue engineeringSynthesis Lectures on Tissue Engineering. *Synth. Lectures Tissue Eng.* 1 (1), 1–182. doi:10.2200/s00212ed1v01y200910tis003

Aufderheide, A. C., and Athanasiou, K. A. (2006). A Direct Compression Stimulator for Articular Cartilage and Meniscal Explants. *Ann. Biomed. Eng.* 34 (9), 1463–1474. doi:10.1007/s10439-006-9157-x

Benya, P. D. (1988). Modulation and Reexpression of the Chondrocyte Phenotype; Mediation by Cell Shape and Microfilament Modification. *Path Immunopathol Res.* 7 (1-2), 51–54. doi:10.1159/000157093

Blain, E. J., Gilbert, S. J., Hayes, A. J., and Duance, V. C. (2006). Disassembly of the Vimentin Cytoskeleton Disrupts Articular Cartilage Chondrocyte Homeostasis. *Matrix Biol.* 25 (7), 398–408. doi:10.1016/j.matbio.2006.06.002

Bonnevie, E. D., Delco, M. L., Bartell, L. R., Jasty, N., Cohen, I., Fortier, L. A., et al. (2018). Microscale Frictional Strains Determine Chondrocyte Fate in Loaded Cartilage. *J. Biomech.* 74, 72–78. doi:10.1016/j.jbiomech.2018.04.020

Bos, E. J., Pluemeekers, M., Helder, M., Kuzmin, N., van der Laan, K., Groot, M.-L., et al. (2018). Structural and Mechanical Comparison of Human Ear, Alar, and Septal Cartilage. *Plast. Reconstr. Surg. - Glob. Open* 6 (1), e1610. doi:10.1097/GOX.0000000000001610

Breuls, R. G. M., Sengers, B. G., Oomens, C. W. J., Bouten, C. V. C., and Baaijens, F. P. T. (2002). Predicting Local Cell Deformations in Engineered Tissue Constructs: a Multilevel Finite Element Approach. *J. Biomech. Eng.* 124 (2), 198–207. doi:10.1115/1.1449492

Carlson, A. K., McCutchen, C. N., and June, R. K. (2017). Mechanobiological Implications of Articular Cartilage Crystals. *Curr. Opin. Rheumatol.* 29 (2), 157–162. doi:10.1097/BOR.0000000000000368

Chang, B., Reighard, C., Flanagan, C., Hollister, S., and Zopf, D. (2020). Evaluation of Human Nasal Cartilage Nonlinear and Rate Dependent Mechanical Properties. *J. Biomech.* 100, 109549. doi:10.1016/j.jbiomech.2019.109549

Chen, J., Zhu, X., Xu, Y., Tang, Y., Xiong, S., Zhuo, S., et al. (2014). Stereoscopic Visualization and Quantification of Auricular Cartilage Regeneration in Rabbits Using Multiphoton Microscopy. *Scanning* 36 (5), 540–546. doi:10.1002/sca.21153

Chen, S. S., Falcovitz, Y. H., Schneiderman, R., Maroudas, A., and Sah, R. L. (2001). Depth-dependent Compressive Properties of normal Aged Human Femoral Head Articular Cartilage: Relationship to Fixed Charge Density. *Osteoarthritis and Cartilage* 9 (6), 561–569. doi:10.1053/joca.2001.0424

Chery, D. R., Han, B., Li, Q., Zhou, Y., Heo, S.-J., Kwok, B., et al. (2020). Early Changes in Cartilage Pericellular Matrix Micromechanobiology Portend the Onset of post-traumatic Osteoarthritis. *Acta Biomater.* 111, 267–278. doi:10.1016/j.actbio.2020.05.005

Chung, C., Erickson, I. E., Mauck, R. L., and Burdick, J. A. (2008). Differential Behavior of Auricular and Articular Chondrocytes in Hyaluronic Acid Hydrogels. *Tissue Eng. A* 14 (7), 1121–1131. doi:10.1089/tea.2007.029110.1089/ten.tea.2007.0291

Coleman, J. L., Widmyer, M. R., Leddy, H. A., Utturkar, G. M., Spritzer, C. E., Moorman, C. T., et al. (2013). Diurnal Variations in Articular Cartilage Thickness and Strain in the Human Knee. *J. Biomech.* 46 (3), 541–547. doi:10.1016/j.jbiomech.2012.09.013

Culav, E. M., Clark, C. H., and Merrilees, M. J. (1999). Connective Tissues: Matrix Composition and its Relevance to Physical Therapy. *Phys. Ther.* 79 (3), 308–319. doi:10.1093/ptj/79.3.308

D'Andrea, P., Calabrese, A., Capozzi, I., Grandolfo, M., Tonon, R., and Vittur, F. (2000). Intercellular Ca2+ Waves in Mechanically Stimulated Articular Chondrocytes. *Biorheology* 37 (1-2), 75–83.

Danalache, M., Jacobi, L. F., Schwitalle, M., and Hofmann, U. K. (2019). Assessment of Biomechanical Properties of the Extracellular and Pericellular Matrix and Their Interconnection throughout the Course of Osteoarthritis. *J. Biomech.* 97, 109409. doi:10.1016/j.jbiomech.2019.109409

Darling, E. M., Wilusz, R. E., Bolognesi, M. P., Zauscher, S., and Guilak, F. (2010). Spatial Mapping of the Biomechanical Properties of the Pericellular Matrix of Articular Cartilage Measured *In Situ* via Atomic Force Microscopy. *Biophysical J.* 98 (12), 2848–2856. doi:10.1016/j.bpj.2010.03.037

Durrant, L. A., Archer, C. W., Benjamin, M., and Ralphs, J. R. (1999). Organisation of the Chondrocyte Cytoskeleton and its Response to Changing Mechanical Conditions in Organ Culture. *J. Anat.* 194, 343–353. doi:10.1046/j.1469-7580.1999.19430343.x

Eckstein, F., Tieschky, M., Faber, S., Englmeier, K.-H., and Reiser, M. (1999). Functional Analysis of Articular Cartilage Deformation, Recovery, and Fluid Flow Following Dynamic Exercise *In Vivo*. *Anat. Embryol.* 200(4), 419–424. doi:10.1007/s004290050291

Eggli, P. S., Hunzinker, E. B., and Schenk, R. K. (1988). Quantitation of Structural Features Characterizing Weight- and Less-Weight-Bearing Regions in Articular Cartilage: A Stereological Analysis of Medical Femoral Condyles in Young Adult Rabbits. *Anat. Rec.* 222 (3), 217–227. doi:10.1002/ar.1092220302

Erne, O. K., Reid, J. B., Ehmke, L. W., Sommers, M. B., Madey, S. M., and Bottlang, M. (2005). Depth-dependent Strain of Patellofemoral Articular Cartilage in Unconfined Compression. *J. Biomech.* 38 (4), 667–672. doi:10.1016/j.jbiomech.2004.04.005

Eyre, D. (2002). Collagen of Articular Cartilage. *Arthritis Res.* 4(1), 30–35. doi:10.1186/ar380

Fithian, D. C., Kelly, M. A., and Mow, V. C. (1990). Material Properties and Structure-Function Relationships in the Menisci. *Clin. Orthopaedics Relat. Res.* 252, 19–31. doi:10.1097/00003086-199003000-00004

Fitzgerald, J. B., Jin, M., Chai, D. H., Siparsky, P., Fanning, P., and Grodzinsky, A. J. (2008). Shear- and Compression-Induced Chondrocyte Transcription Requires MAPK Activation in Cartilage Explants. *J. Biol. Chem.* 283 (11), 6735–6743. doi:10.1074/jbc.M708670200

Fox, A. J. S., Wanivenhaus, F., Burge, A. J., Warren, R. F., and Rodeo, S. A. (2015). The Human Meniscus: a Review of Anatomy, Function, Injury, and Advances in Treatment. *Clin. Anat.* 28 (2), 269–287. doi:10.1002/ca.22456

Frantz, C., Stewart, K. M., and Weaver, V. M. (2010). The Extracellular Matrix at a Glance. *J. Cel Sci* 123 (Pt 24), 4195–4200. doi:10.1242/jcs.023820

Fukubayashi, T., and Kurosawa, H. (1980). "The Contact Area and Pressure Distribution Pattern of the Knee:A Study of Normal and Osteoarthrotic Knee Joints." *Acta Orthopaedica Scand.* 51(6): 871–879. doi:10.3109/17453678008990887

Gilbert, S. J., and Blain, E. J. (2018). Cartilage Mechanobiology: How Chondrocytes Respond to Mechanical Load. *Mechanobiology Health Dis.* 1, 99–126. doi:10.1016/b978-0-12-812952-4.00004-0

Gilchrist, C. L., Witvoet-Braam, S. W., Guilak, F., and Setton, L. A. (2007). Measurement of Intracellular Strain on Deformable Substrates with Texture Correlation. *J. Biomech.* 40 (4), 786–794. doi:10.1016/j.jbiomech.2006.03.013

Gomes, R., Kirn-Safran, C., Farach-Carson, M. C., and Carson, D. D. (2002). Perlecan: an Important Component of the Cartilage Pericellular Matrix. *J. Musculoskelet. Neuronal Interact* 2 (6), 511–516.

Guilak, F. (1995). Compression-induced Changes in the Shape and Volume of the Chondrocyte Nucleus. *J. Biomech.* 28 (12), 1529–1541. doi:10.1016/0021-9290(95)00100-x

Guilak, F., and Alexopoulos, L. G., Upton, M. L., Youn, I., and Choi, J. B., Cao, L., et al. (2006). The Pericellular Matrix as a Transducer of Biomechanical and Biochemical Signals in Articular Cartilage. *Ann. N.Y Acad. Sci.* 1068, 498–512. doi:10.1196/annals.1346.011

Guilak, F., Ratcliffe, A., and Mow, V. C. (1995). Chondrocyte Deformation and Local Tissue Strain in Articular Cartilage: A Confocal Microscopy Study. *J. Orthop. Res.* 13 (3), 410–421. doi:10.1002/jor.1100130315

Guilak, F., Tedrow, J. R., and Burgkart, R. (2000). Viscoelastic Properties of the Cell Nucleus. *Biochem. Biophysical Res. Commun.* 269 (3), 781–786. doi:10.1006/bbrc.2000.2360

Guilak, F., Zell, R. A., Erickson, G. R., Grande, D. A., Rubin, C. T., McLeod, K. J., et al. (1999). Mechanically Induced Calcium Waves in Articular Chondrocytes Are Inhibited by Gadolinium and Amiloride. *J. Orthop. Res.* 17 (3), 421–429. doi:10.1002/jor.1100170319

Hall, A. C. (2019). The Role of Chondrocyte Morphology and Volume in Controlling Phenotype-Implications for Osteoarthritis, Cartilage Repair, and Cartilage Engineering. *Curr. Rheumatol. Rep.* 21 (8), 38. doi:10.1007/s11926-019-0837-6

Han, W. M., Heo, S.-J., Driscoll, T. P., Delucca, J. F., McLeod, C. M., Smith, L. J., et al. (2016). Microstructural Heterogeneity Directs Micromechanics and Mechanobiology in Native and Engineered Fibrocartilage. *Nat. Mater* 15 (4), 477–484. doi:10.1038/nmat4520

Han, W. M., Heo, S.-J., Driscoll, T. P., Smith, L. J., Mauck, R. L., and Elliott, D. M. (2013). Macro- to Microscale Strain Transfer in Fibrous Tissues Is Heterogeneous and Tissue-specific. *Biophysical J.* 105 (3), 807–817. doi:10.1016/j.bpj.2013.06.023

He, B., Wu, J. P., Chen, H. H., Kirk, T. B., and Xu, J. (2013). Elastin Fibers Display a Versatile Microfibril Network in Articular Cartilage Depending on the Mechanical Microenvironments. *J. Orthop. Res.* 31 (9), 1345–1353. doi:10.1002/jor.22384

Heinegård, D. (2009). Fell-Muir Lecture: Proteoglycans and More - from Molecules to Biology. *Int. J. Exp. Pathol.* 90 (6), 575–586. doi:10.1111/j.1365-2613.2009.00695.x

Heinegård, D., and Saxne, T. (2011). The Role of the Cartilage Matrix in Osteoarthritis. *Nat. Rev. Rheumatol.* 7 (1), 50–56. doi:10.1038/nrrheum.2010.198

Hellio Le Graverand, M.-P., Ou, Y., Schield-yee, T., Barclay, L., Hart, D., Natsume, T., et al. (2001). The Cells of the Rabbit Meniscus: Their Arrangement, Interrelationship, Morphological Variations and Cytoarchitecture. *J. Anat.* 198 (Pt 5), 525–535. doi:10.1046/j.1469-7580.2000.19850525.x

Homicz, M. R., McGowan, K. B., Lottman, L. M., Beh, G., Sah, R. L., and Watson, D. (2003). A Compositional Analysis of Human Nasal Septal Cartilage. *Arch. Facial Plast. Surg.* 5 (1), 53–58. doi:10.1001/archfaci.5.1.53

Huang, C.-Y., Stankiewicz, A., Ateshian, G. A., and Mow, V. C. (2005). Anisotropy, Inhomogeneity, and Tension-Compression Nonlinearity of Human Glenohumeral Cartilage in Finite Deformation. *J. Biomech.* 38 (4), 799–809. doi:10.1016/j.jbiomech.2004.05.006

Humphrey, J. D., Dufresne, E. R., and Schwartz, M. A. (2014). Mechanotransduction and Extracellular Matrix Homeostasis. *Nat. Rev. Mol. Cel Biol* 15 (12), 802–812. doi:10.1038/nrm3896

Hynes, R. O. (2002). Integrins. *Cell* 110 (6), 673–687. doi:10.1016/s0092-8674(02)00971-6

Ingber, D. E., Dike, L., Hansen, L., Karp, S., Liley, H., Maniotis, A., et al. (1994). Cellular Tensegrity: Exploring How Mechanical Changes in the Cytoskeleton Regulate Cell Growth, Migration, and Tissue Pattern during Morphogenesis. *Mech. Eng. Cytoskeleton Develop. Biol.* 150, 173–224. doi:10.1016/s0074-7696(08)61542-9

Irianto, J., Ramaswamy, G., Serra, R., and Knight, M. M. (2014). Depletion of Chondrocyte Primary Cilia Reduces the Compressive Modulus of Articular Cartilage. *J. Biomech.* 47 (2), 579–582. doi:10.1016/j.jbiomech.2013.11.040

Irwin, R. M., Gao, T., Boys, A. J., Ortved, K., Cohen, I., and Bonassar, L. J. (2021). Microscale Strain Mapping Demonstrates the Importance of Interface Slope in the Mechanics of Cartilage Repair. *J. Biomech.* 114, 110159. doi:10.1016/j.jbiomech.2020.110159

Jang, K. W., Buckwalter, J. A., and Martin, J. A. (2014). Inhibition of Cell-Matrix Adhesions Prevents Cartilage Chondrocyte Death Following Impact Injury. *J. Orthop. Res.* 32 (3), 448–454. doi:10.1002/jor.22523

Jessop, Z. M., Javed, M., Otto, I. A., Combellack, E. J., Morgan, S., Breugem, C. C., et al. (2016). Combining Regenerative Medicine Strategies to Provide Durable Reconstructive Options: Auricular Cartilage Tissue Engineering. *Stem Cel Res Ther* 7, 19. doi:10.1186/s13287-015-0273-0

Keith, D. A., Paz, A., Gallop, P. M., and Glimcher, M. J. (1977). Histologic and Biochemical Identification and Characterization of an Elastin in Cartilage. *J. Histochem. Cytochem.* 25 (10), 1154–1162. doi:10.1177/25.10.72098

Khan, I., Gilbert, S., Singhrao, S., Duance, V., and Archer, C. (2008). Evaluation of the Reasons for Failure of Integration during Cartilage Repair. A Reviewe. *Eur. Cell Mater.*, 16, 26–39. doi:10.22203/eCM.v016a04

Khoshgoftar, M., Torzilli, P. A., and Maher, S. A. (2017). Influence of the Pericellular and Extracellular Matrix Structural Properties on Chondrocyte Mechanics. *J. Orthop. Res.* 36 (2), 721-729. doi:10.1002/jor.23774

Klika, V., Whiteley, J. P., Brown, C. P., and Gaffney, E. A. (2019). The Combined Impact of Tissue Heterogeneity and Fixed Charge for Models of Cartilage: the One-Dimensional Biphasic Swelling Model Revisited. *Biomech. Model. Mechanobiol* 18 (4), 953–968. doi:10.1007/s10237-019-01123-7

Knight, M. M., Bomzon, Z., Kimmel, E., Sharma, A. M., Lee, D. A., and Bader, D. L. (2006). Chondrocyte Deformation Induces Mitochondrial Distortion and Heterogeneous Intracellular Strain fields. *Biomech. Model. Mechanobiol* 5 (2-3), 180–191. doi:10.1007/s10237-006-0020-7

Kolaczek, S., Hewison, C., Caterine, S., Ragbar, M. X., Getgood, A., and Gordon, K. D. (2016). Analysis of 3D Strain in the Human Medial Meniscus. *J. Mech. Behav. Biomed. Mater.* 63, 470–475. doi:10.1016/j.jmbbm.2016.06.001

Kwon, H., Paschos, N. K., Hu, J. C., and Athanasiou, K. (2016). Articular Cartilage Tissue Engineering: the Role of Signaling Molecules. *Cell. Mol. Life Sci.* 73 (6), 1173–1194. doi:10.1007/s00018-015-2115-8

Lai, J. H., and Levenston, M. E. (2010). Meniscus and Cartilage Exhibit Distinct Intra-tissue Strain Distributions under Unconfined Compression. *Osteoarthritis and Cartilage* 18 (10), 1291–1299. doi:10.1016/j.joca.2010.05.020

Lee, W., Guilak, F., and Liedtke, W. (2017). Role of Piezo Channels in Joint Health and Injury. *Curr. Top. Membr.* 79, 263–273. doi:10.1016/bs.ctm.2016.10.003

Lee, W., Leddy, H. A., Chen, Y., Lee, S. H., Zelenski, N. A., McNulty, A. L., et al. (2014). Synergy between Piezo1 and Piezo2 Channels Confers High-Strain Mechanosensitivity to Articular Cartilage. *Proc. Natl. Acad. Sci. USA* 111 (47), E5114–E5122. doi:10.1073/pnas.1414298111

Liu, F., Kozanek, M., Hosseini, A., Van de Velde, S. K., Gill, T. J., Rubash, H. E., et al. (2010). *In Vivo* tibiofemoral Cartilage Deformation during the Stance Phase of Gait. *J. Biomech.* 43 (4), 658–665. doi:10.1016/j.jbiomech.2009.10.028

Lu, P., Takai, K., Weaver, V. M., and Werb, Z. (2011). Extracellular Matrix Degradation and Remodeling in Development and Disease. *Cold Spring Harbor Perspect. Biol.* 3 (12), a005058. doi:10.1101/cshperspect.a005058

Lu, X. L., Mow, V. C., and Guo, X. E. (2009). Proteoglycans and Mechanical Behavior of Condylar Cartilage. *J. Dent Res.* 88 (3), 244–248. doi:10.1177/0022034508330432

Lucchinetti, E., Bhargava, M. M., and Torzilli, P. A. (2004). The Effect of Mechanical Load on Integrin Subunits ?5 and ?1 in Chondrocytes from Mature and Immature Cartilage Explants. *Cel Tissue Res.* 315 (3), 385–391. doi:10.1007/s00441-003-0836-8

Makris, E. A., Hadidi, P., and Athanasiou, K. A. (2011). The Knee Meniscus: Structure-Function, Pathophysiology, Current Repair Techniques, and Prospects for Regeneration. *Biomaterials* 32 (30), 7411–7431. doi:10.1016/j.biomaterials.2011.06.037

Mansfield, J. C., Bell, J. S., and Winlove, C. P. (2015). The Micromechanics of the Superficial Zone of Articular Cartilage. *Osteoarthritis and Cartilage* 23 (10), 1806–1816. doi:10.1016/j.joca.2015.05.030

Mansfield, J., Yu, J., Attenburrow, D., Moger, J., Tirlapur, U., Urban, J., et al. (2009). The Elastin Network: its Relationship with Collagen and Cells in Articular Cartilage as Visualized by Multiphoton Microscopy. *J. Anat.* 215 (6), 682–691. doi:10.1111/j.1469-7580.2009.01149.x

Mansour, J. M. (2003). Biomechanics of Cartilage. *Kinesiol. Mech. Pathomech. Hum. Mov.* 2: 66–79.

Marcelino, J., and McDevitt, C. A. (1995). Attachment of Articular Cartilage Chondrocytes to the Tissue Form of Type VI Collagen. *Biochim. Biophys. Acta (Bba) - Protein Struct. Mol. Enzymol.* 1249 (2), 180–188. doi:10.1016/0167-4838(95)00026-q

Martins, R. P., Finan, J. D., Farshid, G., and Lee, D. A. (2012). Mechanical Regulation of Nuclear Structure and Function. *Annu. Rev. Biomed. Eng.* 14, 431–455. doi:10.1146/annurev-bioeng-071910-124638

McDermott, I. D. (2010). "Anatomy"in *The Meniscus*. Editors P Beaufils and R Verdonk (Berlin, Heidelberg: Springer Berlin Heidelberg), 11–18.

McDermott, I. D., Masouros, S. D., and Amis, A. A. (2008). Biomechanics of the Menisci of the Knee. *Curr. Orthopaedics* 22 (3), 193–201. doi:10.1016/j.cuor.2008.04.005

McGlashan, S. R., Jensen, C. G., and Poole, C. A. (2006). Localization of Extracellular Matrix Receptors on the Chondrocyte Primary Cilium. *J. Histochem. Cytochem.* 54 (9), 1005–1014. doi:10.1369/jhc.5A6866.2006

McHenry, J. A., Zielinska, B., and Haut Donahue, T. L. (2006). Proteoglycan Breakdown of Meniscal Explants Following Dynamic Compression Using a Novel Bioreactor. *Ann. Biomed. Eng.* 34 (11), 1758–1766. doi:10.1007/s10439-006-9178-5

McNulty, A. L., and Guilak, F. (2015). Mechanobiology of the Meniscus. *J. Biomech.* 48 (8), 1469–1478. doi:10.1016/j.jbiomech.2015.02.008

Millward-Sadler, S. J., and Salter, D. M. (2004). Integrin-dependent Signal Cascades in Chondrocyte Mechanotransduction. *Ann. Biomed. Eng.* 32 (3), 435–446. doi:10.1023/b:abme.0000017538.72511.48

Millward-Sadler, S. J., Wright, M. O., Lee, H.-S., Caldwell, H., Nuki, G., and Salter, D. M. (2000). Altered Electrophysiological Responses to Mechanical Stimulation and Abnormal Signalling through α5β1 Integrin in Chondrocytes from Osteoarthritic Cartilage. *Osteoarthritis and Cartilage* 8 (4), 272–278. doi:10.1053/joca.1999.0301

Mobasheri, A., Carter, S D., Martín-Vasallo, P., and Shakibaei, M. (2002). Integrins and Stretch Activated Ion Channels; Putative Components of Functional Cell Surface Mechanoreceptors in Articular Chondrocytes. *Cel Biol. Int.* 26 (1), 1–18. doi:10.1006/cbir.2001.0826

Mofrad, M., Mofrad, M. R. K., and Kamm, R. D. (2010). *Cellular Mechanotransduction : Diverse Perspectives from Molecules to Tissues*. Cambridge: Cambridge University Press.

Nalesso, G., Sherwood, J., Bertrand, J., Pap, T., Ramachandran, M., De Bari, C., et al. (2011). WNT-3A Modulates Articular Chondrocyte Phenotype by Activating Both Canonical and Noncanonical Pathways. *J. Cel Biol* 193 (3), 551–564. doi:10.1083/jcb.201011051

Nia, H. T., Gauci, S. J., Azadi, M., Hung, H.-H., Frank, E., Fosang, A. J., et al. (2015). High-bandwidth AFM-Based Rheology Is a Sensitive Indicator of Early Cartilage Aggrecan Degradation Relevant to Mouse Models of Osteoarthritis. *J. Biomech.* 48 (1), 162–165. doi:10.1016/j.jbiomech.2014.11.012

Nickien, M., Thambyah, A., and Broom, N. (2013). How Changes in Fibril-Level Organization Correlate with the Macrolevel Behavior of Articular Cartilage. *Wires Syst. Biol. Med.* 5 (4), 495–509. doi:10.1002/wsbm.1220

Nimeskern, L., Pleumeekers, M. M., Pawson, D. J., Koevoet, W. L. M., Lehtoviita, I., Soyka, M. B., et al. (2015). Mechanical and Biochemical Mapping of Human Auricular Cartilage for Reliable Assessment of Tissue-Engineered Constructs. *J. Biomech.* 48 (10), 1721–1729. doi:10.1016/j.jbiomech.2015.05.019

Nimeskern, L., Utomo, L., Lehtoviita, I., Fessel, G., Snedeker, J. G., van Osch, G. J. V. M., et al. (2016). Tissue Composition Regulates Distinct Viscoelastic Responses in Auricular and Articular Cartilage. *J. Biomech.* 49 (3), 344–352. doi:10.1016/j.jbiomech.2015.12.032

O'Conor, C. J., Leddy, H. A., Benefield, H. C., Liedtke, W. B., and Guilak, F. (2014). TRPV4-mediated Mechanotransduction Regulates the Metabolic Response of Chondrocytes to Dynamic Loading. *Proc. Natl. Acad. Sci.* 111 (4), 1316–1321. doi:10.1073/pnas.1319569111

Parkkinen, J. J., Lammi, M. J., Inkinen, R., Jortikka, M., Tammi, M., Virtanen, I., et al. (1995). Influence of Short-Term Hydrostatic Pressure on Organization of Stress Fibers in Cultured Chondrocytes. *J. Orthop. Res.* 13 (4), 495–502. doi:10.1002/jor.1100130404

Phan, M. N., Leddy, H. A., Votta, B. J., Kumar, S., Levy, D. S., Lipshutz, D. B., et al. (2009). Functional Characterization of TRPV4 as an Osmotically Sensitive Ion Channel in Porcine Articular Chondrocytes. *Arthritis Rheum.* 60 (10), 3028–3037. doi:10.1002/art.24799

Pingguan-Murphy, B., El-Azzeh, M., Bader, D. L., and Knight, M. M. (2006). Cyclic Compression of Chondrocytes Modulates a Purinergic Calcium Signalling Pathway in a Strain Rate- and Frequency-dependent Manner. *J. Cel. Physiol.* 209 (2), 389–397. doi:10.1002/jcp.20747

Poole, A. R., Kojima, T., Yasuda, T., Mwale, F., Kobayashi, M., and Laverty, S. (2001). Composition and Structure of Articular Cartilage. *Clin. Orthopaedics Relat. Res.* 391 (Suppl. l), S26–S33. doi:10.1097/00003086-200110001-00004

Poole, C. A. (1997). Review. Articular Cartilage Chondrons: Form, Function and Failure. *J. Anat.* 191 (Pt 1), 1–13. doi:10.1046/j.1469-7580.1997.19110001.x

Quinn, T. M., Grodzinsky, A. J., Buschmann, M. D., Kim, Y. J., and Hunziker, E. B. (1998). Mechanical Compression Alters Proteoglycan Deposition and Matrix Deformation Around Individual Cells in Cartilage Explants. *J. Cel Sci.* 111, 573–583. doi:10.1242/jcs.111.5.573

Quinn, T. M., Häuselmann, H.-J., Shintani, N., and Hunziker, E. B. (2013). Cell and Matrix Morphology in Articular Cartilage from Adult Human Knee and Ankle Joints Suggests Depth-Associated Adaptations to Biomechanical and Anatomical Roles. *Osteoarthritis and Cartilage* 21 (12), 1904–1912. doi:10.1016/j.joca.2013.09.011

Responte, D. J., Natoli, R. M., and Athanasiou, K. A. (2007). Collagens of Articular Cartilage: Structure, Function, and Importance in Tissue Engineering. *Crit. Rev. Biomed. Eng.* 35 (5), 363–411. doi:10.1615/critrevbiomedeng.v35.i5.20

Roberts, S. R., Knight, M. M., Lee, D. A., and Bader, D. L. (2001). Mechanical Compression Influences Intracellular Ca2+ Signaling in Chondrocytes Seeded in Agarose Constructs. *J. Appl. Physiol.* 90 (4), 1385–1391. doi:10.1152/jappl.2001.90.4.1385

Roth, V., and Mow, V. C. (1980). The Intrinsic Tensile Behavior of the Matrix of Bovine Articular Cartilage and its Variation with ageThe Journal of Bone and Joint Surgery. *J. Bone Jt. Surg.* 62 (7), 1102–1117. doi:10.2106/00004623-198062070-00007

Ruhlen, R., and Marberry, K. (2014). The Chondrocyte Primary Cilium. *Osteoarthritis and Cartilage* 22 (8), 1071–1076. doi:10.1016/j.joca.2014.05.011

Sanchez-Adams, J., Wilusz, R. E., and Guilak, F. (2013). Atomic Force Microscopy Reveals Regional Variations in the Micromechanical Properties of the Pericellular and Extracellular Matrices of the Meniscus. *J. Orthop. Res.* 31 (8), 1218–1225. doi:10.1002/jor.22362

Sauter, E., Buckwalter, J. A., McKinley, T. O., and Martin, J. A. (2012). Cytoskeletal Dissolution Blocks Oxidant Release and Cell Death in Injured Cartilage. *J. Orthop. Res.* 30 (4), 593–598. doi:10.1002/jor.21552

Scholtes, S., Krämer, E., Weisser, M., Roth, W., Luginbühl, R., Grossner, T., et al. (2018). Global Chondrocyte Gene Expression after a Single Anabolic Loading Period: Time Evolution and Re-inducibility of Mechano-responses. *J. Cel Physiol* 233 (1), 699–711. doi:10.1002/jcp.25933

Shu, C. C., Jackson, M. T., Smith, M. M., Smith, S. M., Penm, S., Lord, M. S., et al. (2016). Ablation of Perlecan Domain 1 Heparan Sulfate Reduces Progressive Cartilage Degradation, Synovitis, and Osteophyte Size in a Preclinical Model of Posttraumatic Osteoarthritis. *Arthritis Rheumatol.* 68 (4), 868–879. doi:10.1002/art.39529

Sophia Fox, A. J., Bedi, A., and Rodeo, S. A. (2009). The Basic Science of Articular Cartilage: Structure, Composition, and Function. *Sports Health* 1 (6), 461–468. doi:10.1177/1941738109350438

Steklov, N., Srivastava, A., Sung, K. L., Chen, P. C., Lotz, M. K., and D'Lima, D. D. (2009). Aging-related Differences in Chondrocyte Viscoelastic Properties. *Mol. Cel Biomech* 6 (2), 113–119.

Szafranski, J. D., Grodzinsky, A. J., Burger, E., Gaschen, V., Hung, H.-H., and Hunziker, E. B. (2004). Chondrocyte Mechanotransduction: Effects of Compression on Deformation of Intracellular Organelles and Relevance to Cellular Biosynthesis. *Osteoarthritis and Cartilage* 12 (12), 937–946. doi:10.1016/j.joca.2004.08.004

Takada, S., Fujimori, S., Shinozuka, T., Takada, R., and Mii, Y. (2017). Differences in the Secretion and Transport of Wnt Proteins. *J. Biochem.* 161 (1), 1–7. doi:10.1093/jb/mvw071

Tamamura, Y., Otani, T., Kanatani, N., Koyama, E., Kitagaki, J., Komori, T., et al. (2005). Developmental Regulation of Wnt/β-Catenin Signals Is Required for Growth Plate Assembly, Cartilage Integrity, and Endochondral Ossification. *J. Biol. Chem.* 280 (19), 19185–19195. doi:10.1074/jbc.M414275200

Tanska, P., Venäläinen, M. S., Erdemir, A., and Korhonen, R. K. (2020). A Multiscale Framework for Evaluating Three-Dimensional Cell Mechanics in Fibril-Reinforced Poroelastic Tissues with Anatomical Cell Distribution - Analysis of Chondrocyte Deformation Behavior in Mechanically Loaded Articular Cartilage. *J. Biomech.* 101, 109648. doi:10.1016/j.jbiomech.2020.109648

Theocharis, A. D., Skandalis, S. S., Gialeli, C., and Karamanos, N. K. (2016). Extracellular Matrix Structure. *Adv. Drug Deliv. Rev.* 97, 4–27. doi:10.1016/j.addr.2015.11.001

Thielen, N., van der Kraan, P., and van Caam, A. (2019). TGFβ/BMP Signaling Pathway in Cartilage Homeostasis. *Cells* 8 (9), 969. doi:10.3390/cells8090969

Trickey, W. R., Vail, T. P., and Guilak, F. (2004). The Role of the Cytoskeleton in the Viscoelastic Properties of Human Articular Chondrocytes. *J. Orthop. Res.* 22 (1), 131–139. doi:10.1016/s0736-0266(03)00150-510.1016/s0736-0266(03)0150-5

Upton, M. L., Gilchrist, C. L., Guilak, F., and Setton, L. A. (2008). Transfer of Macroscale Tissue Strain to Microscale Cell Regions in the Deformed Meniscus. *Biophysical J.* 95 (4), 2116–2124. doi:10.1529/biophysj.107.126938

Vincent, T. L., McLean, C. J., Full, L. E., Peston, D., and Saklatvala, J. (2007). FGF-2 Is Bound to Perlecan in the Pericellular Matrix of Articular Cartilage, where it Acts as a Chondrocyte Mechanotransducer. *Osteoarthritis and Cartilage* 15 (7), 752–763. doi:10.1016/j.joca.2007.01.021

Wang, N. (2017). Review of Cellular Mechanotransduction. *J. Phys. D: Appl. Phys.* 50 (23), 233002. doi:10.1088/1361-6463/aa6e18

Wann, A. K. T., Zuo, N., Haycraft, C. J., Jensen, C. G., Poole, C. A., McGlashan, S. R., et al. (2012). Primary Cilia Mediate Mechanotransduction through Control of ATP-induced Ca2+signaling in Compressed Chondrocytes. *FASEB j.* 26 (4), 1663–1671. doi:10.1096/fj.11-193649

Wilusz, R. E., DeFrate, L. E., and Guilak, F. (2012). A Biomechanical Role for Perlecan in the Pericellular Matrix of Articular Cartilage. *Matrix Biol.* 31 (6), 320–327. doi:10.1016/j.matbio.2012.05.002

Wilusz, R. E., Sanchez-Adams, J., and Guilak, F. (2014). The Structure and Function of the Pericellular Matrix of Articular Cartilage. *Matrix Biol.* 39, 25–32. doi:10.1016/j.matbio.2014.08.009

Wolfenson, H., Lavelin, I., and Geiger, B. (2013). Dynamic Regulation of the Structure and Functions of Integrin Adhesions. *Develop. Cel* 24 (5), 447–458. doi:10.1016/j.devcel.2013.02.012

Wong, B. L., Bae, W. C., Chun, J., Gratz, K. R., Lotz, M., and Robert, L. S. (2008). Biomechanics of Cartilage Articulation: Effects of Lubrication and Degeneration on Shear Deformation. *Arthritis Rheum.* 58 (7), 2065–2074. doi:10.1002/art.23548

Wong, M., and Carter, D. R. (2003). Articular Cartilage Functional Histomorphology and Mechanobiology: a Research Perspective. *Bone* 33 (1), 1–13. doi:10.1016/s8756-3282(03)00083-8

Wong, M., Wuethrich, P., Eggli, P., and Hunziker, E. (1996). Zone-specific Cell Biosynthetic Activity in Mature Bovine Articular Cartilage: A New Method Using Confocal Microscopic Stereology and Quantitative Autoradiography. *J. Orthop. Res.* 14(3), 424–432. doi:10.1002/jor.1100140313

Yeh, A. T., Hammer-Wilson, M. J., Van Sickle, D. C., Benton, H. P., Zoumi, A., Tromberg, B. J., et al. (2005). Nonlinear Optical Microscopy of Articular Cartilage. *Osteoarthritis and Cartilage* 13 (4), 345–352. doi:10.1016/j.joca.2004.12.007

Yu, J., and Urban, J. P. G. (2010). The Elastic Network of Articular Cartilage: an Immunohistochemical Study of Elastin Fibres and Microfibrils. *J. Anat.* 216 (4), 533–541. doi:10.1111/j.1469-7580.2009.01207.x

Yuasa, T., Otani, T., Koike, T., Iwamoto, M., and Enomoto-Iwamoto, M. (2008). Wnt/β-catenin Signaling Stimulates Matrix Catabolic Genes and Activity in Articular Chondrocytes: its Possible Role in Joint Degeneration. *Lab. Invest.* 88 (3), 264–274. doi:10.1038/labinvest.3700747

Zelenski, N. A., Leddy, H. A., Sanchez-Adams, J., Zhang, J., Bonaldo, P., Liedtke, W., et al. (2015). Type VI Collagen Regulates Pericellular Matrix Properties, Chondrocyte Swelling, and Mechanotransduction in Mouse Articular Cartilage. *Arthritis Rheumatol.* 67 (5), 1286–1294. doi:10.1002/art.39034

Zhou, Y., Lv, M., Li, T., Zhang, T., Duncan, R., Wang, L., et al. (2019). Spontaneous Calcium Signaling of Cartilage Cells: from Spatiotemporal Features to Biophysical Modeling. *FASEB j.* 33 (4), 4675–4687. doi:10.1096/fj.201801460R

Zhou, Y., Millward-Sadler, S. J., Lin, H., Robinson, H., Goldring, M., Salter, D. M., et al. (2007). Evidence for JNK-dependent Up-Regulation of Proteoglycan Synthesis and for Activation of JNK1 Following Cyclical Mechanical Stimulation in a Human Chondrocyte Culture Model. *Osteoarthritis and Cartilage* 15 (8), 884–893. doi:10.1016/j.joca.2007.02.001

Zhu, M., Chen, M., Zuscik, M., Wu, Q., Wang, Y. J., Rosier, R. N., et al. (2008). Inhibition of β-catenin Signaling in Articular Chondrocytes Results in Articular Cartilage Destruction. *Arthritis Rheum.* 58 (7), 2053–2064. doi:10.1002/art.23614

Zhu, M., Tang, D., Wu, Q., Hao, S., Chen, M., Xie, C., et al. (2009). Activation of β-Catenin Signaling in Articular Chondrocytes Leads to Osteoarthritis-like Phenotype in Adult β-Catenin Conditional Activation Mice. *J. Bone Mineral Res.* 24 (1), 12–21. doi:10.1359/jbmr.080901

Zielinska, B., Killian, M., Kadmiel, M., Nelsen, M., and Haut Donahue, T. L. (2009). Meniscal Tissue Explants Response Depends on Level of Dynamic Compressive Strain. *Osteoarthritis and Cartilage* 17 (6), 754–760. doi:10.1016/j.joca.2008.11.018

Conflict of Interest: The authors declare that the research was conducted in the absence of any commercial or financial relationships that could be construed as a potential conflict of interest.

Publisher's Note: All claims expressed in this article are solely those of the authors and do not necessarily represent those of their affiliated organizations, or those of the publisher, the editors and the reviewers. Any product that may be evaluated in this article, or claim that may be made by its manufacturer, is not guaranteed or endorsed by the publisher.

frontiers in Cell and Developmental Biology

REVIEW
published: 21 February 2022
doi: 10.3389/fcell.2021.770143

The Mechanosensory Role of Osteocytes and Implications for Bone Health and Disease States

Jung Un Ally Choi, Amanda W. Kijas, Jan Lauko and Alan E. Rowan**

Australian Institute for Bioengineering and Nanotechnology, The University of Queensland, Brisbane, QLD, Australia

Bone homeostasis is a dynamic equilibrium between bone-forming osteoblasts and bone-resorbing osteoclasts. This process is primarily controlled by the most abundant and mechanosensitive bone cells, osteocytes, that reside individually, within chambers of porous hydroxyapatite bone matrix. Recent studies have unveiled additional functional roles for osteocytes in directly contributing to local matrix regulation as well as systemic roles through endocrine functions by communicating with distant organs such as the kidney. Osteocyte function is governed largely by both biochemical signaling and the mechanical stimuli exerted on bone. Mechanical stimulation is required to maintain bone health whilst aging and reduced level of loading are known to result in bone loss. To date, both *in vivo* and *in vitro* approaches have been established to answer important questions such as the effect of mechanical stimuli, the mechanosensors involved, and the mechanosensitive signaling pathways in osteocytes. However, our understanding of osteocyte mechanotransduction has been limited due to the technical challenges of working with these cells since they are individually embedded within the hard hydroxyapatite bone matrix. This review highlights the current knowledge of the osteocyte functional role in maintaining bone health and the key regulatory pathways of these mechanosensitive cells. Finally, we elaborate on the current therapeutic opportunities offered by existing treatments and the potential for targeting osteocyte-directed signaling.

Keywords: bone homeostasis, osteocytes, integrins, mechanotransduction, signaling pathway, aging, osteoporosis, bone therapeutics

OPEN ACCESS

Edited by:
Selwin K Wu,
National University of Singapore, Singapore

Reviewed by:
Stefaan Verbruggen,
The University of Sheffield, United Kingdom
Danielle Wu,
University of Texas Health Science Center at Houston, United States

****Correspondence:***
Alan E. Rowan
alan.rowan@uq.edu.au
Jung Un Ally Choi
jung.choi@uq.edu.au

Specialty section:
This article was submitted to Cell Adhesion and Migration, a section of the journal Frontiers in Cell and Developmental Biology

Received: *03 September 2021*
Accepted: *13 December 2021*
Published: *21 February 2022*

Citation:
Choi JUA, Kijas AW, Lauko J and Rowan AE (2022) The Mechanosensory Role of Osteocytes and Implications for Bone Health and Disease States. Front. Cell Dev. Biol. 9:770143. doi: 10.3389/fcell.2021.770143

INTRODUCTION

The most long-lived bone cells, osteocytes are known as the master regulator of bone formation and resorption (Bonewald 2011). The mechanosensory role of osteocytes underlies well-balanced bone homeostasis, which is primarily influenced by matrix strain and fluid shear stress (Weinbaum et al., 1994; Han et al., 2004; Robling and Turner 2009; Wittkowske et al., 2016). Through mechanotransduction processes, osteocytes are able to transduce extracellular signals to elicit cellular responses by initiating different signaling pathways accordingly to bring functional responses. The dysregulation of osteocyte behavior can lead to reduced bone mass and bone fragility observed in osteoporotic patients. For this reason, osteocyte-induced mechanotransduction has been studied extensively, however, the exact mechanisms and signaling pathways are not fully understood. Here we highlight the crucial role of osteocytes in bone homeostasis, including regulation of the overall bone remodeling process, perilacunar/canalicular remodeling, and

systemic regulatory roles on other tissues such as the kidney, parathyroid, and heart (Dallas et al., 2013; Creecy et al., 2021). Furthermore, we summarize the osteocyte mechanosensors and the current state of mechanoresponsive signaling pathways identified in osteocytes with therapeutic implications. To achieve this, we present both *in vivo* and *in vitro* approaches that have been employed to understand the complex regulatory processes that underly osteocytes' quintessential mechanosensory role in bone.

BONE HOMEOSTASIS

Bone is a weight-bearing tissue, which supports locomotion, protects soft tissue, and is also known as a reservoir for calcium and phosphate (Bellido 2014; Florencio-Silva et al., 2015). Bones are composed of both organic matrix, comprising of largely type I collagen (90%), with the remaining protein component including osteocalcin, osteonectin, osteopontin, fibronectin, and thrombospondin-2 (Sroga and Vashishth 2012), as well as inorganic matrix minerals, mainly comprised of hydroxyapatite ($Ca_5(PO_4)_3OH$) but also including small amounts of potassium, magnesium, sodium, strontium, and calcium salts (Lin et al., 2020). The formation of the bone matrix is initiated by the collagen assembly followed by hydroxyapatite deposition and tuned by minerals and amino acids of non-collagenous proteins (Young 2003; Tavafoghi and Cerruti 2016). The balance of mineral content is important and directly relates to mechanical strength (Faibish et al., 2006). For example, bones become brittle when mineral content is too high and less load-bearing if the mineral content is too low. This mineralized tissue undergoes remodeling to maintain its integrity and is tightly regulated by a precise balance of bone formation and resorption under the control of local and systemic factors, such as cytokines, hormones, and mechanical stimulation (Florencio-Silva et al., 2015). This complex process is a cycle of localized bone resorption to remove old or damaged bone followed by a longer phase of bone formation, both in an equilibrium to maintain healthy bone. The imbalance of this regulation often leads to bone diseases such as osteoporosis and is caused by a variety of factors such as aging, menopause, drugs, and changes in physical activity (Feng and McDonald 2011). Imbalance can also stem from genetic mutations, leading to bone overgrowth disorders due to defective signaling pathways that change the equilibrium resulting in van Buchem disease and sclerosteosis (Balemans et al., 1999; Sebastian and Loots 2018).

Bone is a rigid and load-bearing tissue designed to sustain high mechanical loads during exercise (Benedetti et al., 2018). There are two types of bone tissue, the cortical and trabecular bone, which have the same cells and matrix but differ in structural-functional roles (Clarke 2008). Cortical bones are more calcified and hard, and carry out the role of providing mechanical stability and form a protective layer for the internal cavity (Boskey and Coleman 2010). In comparison, the trabecular bones only contain 1/3 of calcified bone compared to the cortical ones and are mainly involved in metabolic as well as biomechanical functions (Clarke 2008). The composition of the bone matrix is important for fracture resistance, which largely depends on the geometric (size and shape) and material properties (mineral content and composition) (Osterhoff et al., 2016). Bones constantly experience mechanical forces created by various stimuli including fluid flow shear stress, hydrostatic pressure, and direct cellular deformation induced by gravitational forces as a weight-bearing tissue and loading-induced stimuli such as compressive force. The calcified bone matrix may induce micro-deformation with a maximum of 3% strain changes (Hart et al., 2017). The matrix deformation during locomotion is between 0.04 and 0.3% but hardly exceeds 0.1%. Surprisingly *in vitro* studies need to apply more than 10 times this mechanical stimulation to observe osteocyte responses, otherwise, the strain amplification at the cellular level is too small to initiate mechanotransduction pathways (Rubin and Lanyon 1984; Fritton et al., 2000). These *in vitro* forces applied back at the tissue level would cause a fracture (Burr et al., 1996; You et al., 2000; Wang et al., 2015). This difference has to be taken into consideration to more accurately capture the differences between *in vivo* and *in vitro* systems and facilitate the accurate interpretation of a translational approach. The externally applied force is transduced by highly mechanosensitive osteocytes that coordinate the effector cells, bone-forming osteoblasts, and bone-resorbing osteoclasts demonstrating the skeletal adaptation response of mechanical cues into biochemical signals (Bonewald 2011; Schaffler and Kennedy 2012). The above highlights the need to understand the mechanisms underlying osteocyte's important regulatory role in bone homeostasis.

OSTEOCYTES, THE MASTER REGULATOR

Osteocytes are the most abundant (~95%) bone cells, which reside in the hard bone matrix (Hellmich and Ulm 2002; Bonewald 2011). Osteocytes are a terminally differentiated post-mitotic cell type from the osteogenic lineage, derived from mesenchymal stem cell progenitors (Pittenger et al., 1999; Day et al., 2005; Gaur et al., 2005; Sudo et al., 2007). Mesenchymal stem cell differentiation leads to osteoblasts, and a subpopulation is known to terminally differentiate into osteocytes that are individually embedded within small chambers called lacunae (Palumbo et al., 1990; Candeliere et al., 2001). After the differentiation process, the most striking morphological change of mature osteocytes is the development of unique dendritic cell processes. These dendritic cell processes create an extensive cellular network in the hard bone matrix, which enables osteocytes to communicate with neighboring osteocytes, and the osteoblasts and osteoclasts on the bone surface by creating a neuron-like network (Palumbo et al., 1990). This highly complex communication network, is created through a space called canaliculi, which are narrow channels in the hydroxyapatite matrix. Osteocytes are separated from the mineralized bone matrix, by a pericellular space filled with proteoglycan-rich matrix (glycocalyx) and interstitial fluid (Termine et al., 1981; Sauren et al., 1992; Aarden et al.,

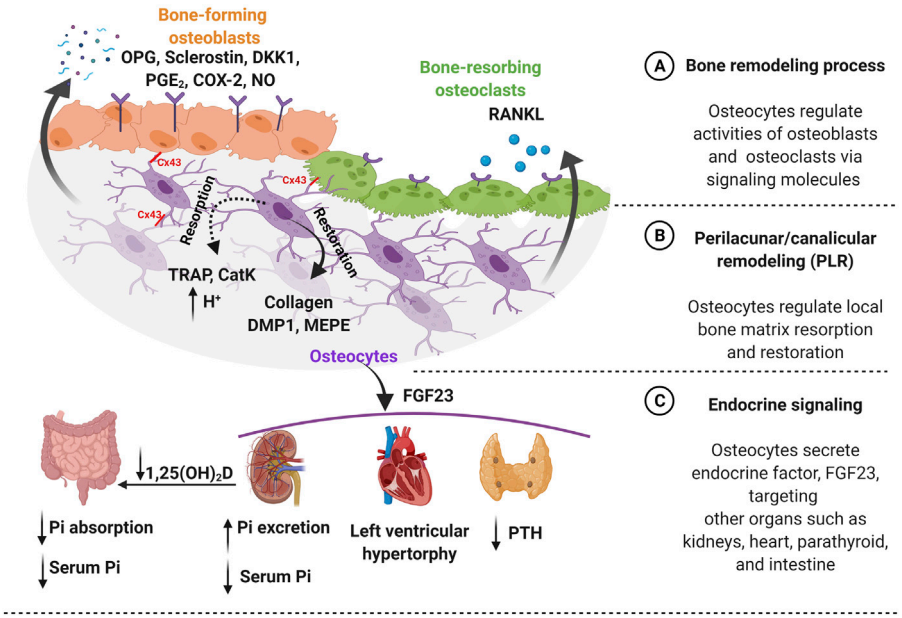

FIGURE 1 | Osteocytes function in both bone homeostasis and endocrine signaling. **(A)** Bone homeostasis is guided by osteocytes, which require a precise balance of bone formation and bone resorption. Osteocytes regulate this dynamic equilibrium by releasing signaling molecules such as osteoprotegerin (OPG), sclerostin, dickkopf-related protein 1 (DKK1), prostaglandin E2 (PGE_2), cyclooxygenase-2 (COX-2), and nitric oxide (NO) for bone-forming osteoblasts. Furthermore, osteocytes secrete receptor activator of nuclear factor-κB ligand (RANKL) for bone-resorbing osteoclasts on the bone surface. Additionally, osteocytes mediate communication with osteoblast and osteoclast via connexin 43 (Cx43) gap junctions. **(B)** Osteocytes regulate the local bone matrix through a process called perilacunar/canalicular remodeling (PLR). Matrix resorption (dotted line) is initiated creating an acidic environment by osteocyte-derived enzymes, such as tartrate-resistant acid phosphatase (TRAP) and cathepsin K (CatK) followed by matrix restoration (solid line), by producing collagen and bone matrix proteins such as dentin matrix protein 1 (DMP1) and matrix extracellular phosphoglycoprotein (MEPE). **(C)** Osteocytes secrete an endocrine factor - fibroblast growth factor (FGF23) to target other organs such as kidneys, heart, and parathyroid. The FGF23 hormone triggers parathyroid to reduce the level of parathyroid hormone (PTH). Moreover, FGF23 increases the risk of heart failure such as left ventricular hypertrophy. Importantly, FGF23 regulates serum phosphate (Pi) level by targeting kidneys by increasing phosphate excretion and also inhibiting the conversion of active vitamin D to 1,25-dihydroxy vitamin D [$1,25(OH)_2D$] in the intestine to decrease phosphate resorption leading to lower serum phosphate level. Figure created using BioRender.

1996). Based on the measurements and mathematical models for branching, these dendritic processes were estimated to form approximately 23 trillion connections and span a total length of over 175000 km within the human body (Buenzli and Sims 2015). *In vivo*, each cell has been shown to have a varying number of dendritic cell processes ranging from 18 to 106, which reduces with aging (Beno et al., 2006; Qin et al., 2020). Initial development of dendritic cell processes from the cell body leads to the formation of subsequent subbranches, which create sufficient surface area for efficient communication with other cells and also serving as a mechanosensory structures. The unique environment for osteocytes is called the lacunocanalicular network (LCN) and is a complicated network within bone tissue with a total surface area of approximately 215 m^2 (Sims 2016; Martin 2019) and is also thought to provide a route for the provision of nutrients, oxygen, and biochemical signals.

Since osteocytes reside in this unique LCN architecture of mineralized matrix, it has been a challenge to study osteocytes. In spite of this challenge, a variety of mechanical stimulations such as fluid flow shear stress, and substrate deformation are known to influence osteocytes functions (You et al., 2000; McGarry et a., 2005; Wittkowske et al., 2016; Qin et al., 2020). It is important to understand that loading-induced matrix deformation not only changes fluid flow velocity, but also the matrix strain, which is closely associated with the LCN architecture. A recent study demonstrated that the LCN architecture is a key determinant for bone adaption in response to mechanical stimulation (van Tol et al., 2020). The fluid flow-induced velocity was strongly dependent on the LCN architecture in a highly dense and connected network (Denisov-Nikol'skiĭ Iu and Doktorov, 1987; Johnson 1984). Another study observed that the fluid flow velocity was not directly correlated to the loading-induced strain deformation, but more associated with the LCN structure based on *in vivo* mice micro-computed tomography (microCT) evaluations (van Tol et al., 2020). The changes in the strain distributions of the LCN upon applying various static and cyclic loads highlighted the diversity of mechanosensors on these cells and complexity of the underlying mechanotransduction pathways (Wang et al., 2015). The dendritic morphology of osteocytes itself is also proposed to be synergistic with the highly-dense LCN network, resulting in an actin-rich cytoskeleton, which enables cell–cell communications between osteocytes allowing a cascade of intracellular events capable of generating a functional response (Burra et al., 2010; Hemmatian et al., 2017).

OSTEOCYTE FUNCTIONS IN BOTH BONE AND EXTRASKELETAL ROLES

As osteocytes are embedded individually within the bone and separated from the effector bone cell types, they utilize secreted signaling molecules to communicate their "instructions" in addition to their broader systemic effects (Dallas et al., 2013; Prideaux et al., 2016). Osteocytes are involved in the secretion of signaling molecules, to regulate osteoblast and osteoclast activities, as well as establishing direct physical connections *via* gap junctions (**Figure 1A**). The quintessential molecule in bone regulation is the osteocyte-specific sclerostin, which is exclusively expressed by mature osteocytes. Sclerostin is an anti-bone formation (antagonist) regulator that directly inhibits the proliferation and differentiation of osteoblasts (Duan and Bonewald 2016). The osteoblast-induced bone formation is initiated by secreted Wnt ligand glycoproteins, which bind to low-density lipoprotein receptors (LRP) 4/5/6 for phosphorylation, leading to suppression of glycogen synthase kinase 3 (GSK3) (Karner and Long 2017). This stabilizes β-catenin, which then translocates into the nucleus, and acts as a transcriptional co-activator. Sclerostin, the protein product of the *SOST* gene expressed by mature osteocytes, binds to the LRP 4/5/6 to inhibit Wnt-binding for the Wnt/β-catenin signaling pathway in osteoblasts. Sclerostin expression is also known to be decreased by mechanical loading and increased in response to unloading conditions such as microgravity and reduced physical levels in bed-ridden patients (Pajevic et al., 2013; Bradbury et al., 2020).

The osteocyte-secreted dickkopf-related protein 1 (DKK1) binds to LRP4/5/6 on osteoblasts and acts as a Wnt competitive inhibitor (Li et al., 2006). Osteocytes also secrete osteoprotegerin (OPG), a soluble decoy receptor for receptor activator of nuclear factor-κB ligand (RANKL), which is a cytokine that binds to osteoclasts, promoting bone resorption (Kearns, Khosla, and Kostenuik 2008). The ratio between OPG and RANKL is commonly used as an indicator of bone mass and decreased RANKL/OPG ratio was reported in response to mechanical stimulation, leading to reduced osteoclast activity (Goldring 2015). Interestingly, proinflammatory cytokines were also observed to be down-regulated by mechanical loading, except interleukin 6 (IL-6) (Pathak et al., 2015; Pathak et al., 2020). Mechanical stimulation modulates the release of other factors such as nitric oxide (NO), prostaglandin E2 (PGE_2), cyclooxygenase-2 (COX-2), and adenosine triphosphate (ATP) in osteocytes (Li et al., 2021). Especially, loading-induced calcium ions (Ca^{2+}) oscillation releases signaling molecules such as NO, PGE_2, insulin-like growth factor-1 (IGF-1), and β-catenin, which are important for osteocyte viability and anabolic effect on bone (Morrell et al., 2018).

Osteocytes, embedded in the hard bone matrix are also known to regulate their local microenvironment through a process called perilacunar/canalicular remodeling (PLR) (**Figure 1B**) (Qing and Bonewald 2009; Lin et al., 2020). Earlier studies observed the enlarged lacunae during lactation to release calcium from a mineralized matrix for high calcium demand situations and also in pathological conditions such as Paget's disease, a bone loss disorder, suggesting the removal of perilacunar matrix by osteocytic osteolysis (Zambonin Zallone et al., 1982; Teti and Zallone 2009; Tsourdi et al., 2018). However, this microenvironment remodeling is also known as a homeostatic mechanism to maintain the perilacunar/canalicular network under healthy conditions such as lactation (Dole et al., 2017). Interestingly, osteocytes are able to remove both minerals and collagen from their surrounding perilacunar matrix by upregulating the H^+ proton pump, creating an acidic microenvironment (Qing et al., 2012; Creecy et al., 2021). The acidic environment can be induced by the parathyroid hormone (PTH) upregulation during lactation (Jähn et al., 2017). Osteocyte-derived matrix removal was observed in lactating mice showing the enlarged lacunar area with upregulation of tartrate-resistant acid phosphatase (TRAP) and cathepsin K (CatK, encoded by the *Ctsk* gene), which were previously thought to be osteoclast-specific (Nakano et al., 2004; Qing et al., 2012; Lotinun et al., 2019). TRAP is an enzyme that is responsible for the dephosphorylation of bone matrix phosphoproteins and CatK is a lysosomal cysteine protease that contains the catalytic mechanism necessary for bone matrix degradation leading to bone resorption (Dai et al., 2020). By increasing osteoclast-like markers, they create an acidic environment via carbonic anhydrase 2 (Car2) and proton-pumping vacuolar ATPases.

Recent research hinted that transforming growth factor beta (TGF-β) is possibly associated with the PLR process (Schurman et al., 2021). *In vitro* studies have demonstrated TGF-β treatment upregulated *Ctsk* and matrix metalloproteinase 14 gene expressions in both osteocytic cell lines, MLO-Y4 and Ocy454 (Dole et al., 2017; Kegelman et al., 2020). Furthermore, intracellular pH (pHi) has been shown to decrease after TGF-β treatment, resulting in cell acidification, inducing PLR resorption that was dependent on the TGF-β receptors on osteocytes (Dole et al., 2017). TGF-β intake by osteocytes was blocked by using type I TGF-β receptor (TβRI) inhibitor (SB-431542), and lead to increased pH levels, equivalent to untreated groups. *In vivo* studies using osteocyte-specific TGF-β receptor knockout mice showed decreased expression of *Ctsk* leading to decreased bone resorption contributing to increased bone mass in these animals. (Dole et al., 2017; Schurman et al., 2021). Furthermore, TGF-β treatment induced changes in gene expression levels of sclerostin in osteocytes. PLR was also induced in osteocytes after recombinant human sclerostin (rhSCL) treatment, which lowers the pHi showing upregulation of catalytic genes (e.g., *Ctsk*, *Car2*, *TRAP*) (Kogawa et al., 2013). This suggests that osteocyte-produced sclerostin promotes catalytic activity to release the minerals. Moreover, rhSCL treatment in human trabecular bone samples showed an increased lacunar area around osteocytes (Kogawa et al., 2018). The activity of sclerostin was also confirmed by Lrp4/5/6 receptors, known for sclerostin binding inhibited osteocyte-mediated catalytic activity for the removal of bone matrix in PLR. However, further investigation is required to understand the mechanisms of PLR, which is different from osteoclast-mediated bone resorption.

It is well known that the increased lacunar area returns to normal after the weaning process suggesting osteocytes play a role in local matrix restoration. It was proposed, that the local PLR remodeling process was independent of mechanical stimulation and was presumed to be hormonally regulated (Qing et al., 2012; Bach-Gansmo et al., 2016). However, a recent study of mice under microgravity conditions, which removes mechanical loading on bones, observed enlarged lacunae size and deformed bone microstructure in these animals (Gerbaix et al., 2017). For osteocytes to perform PLR, both collagen production and mineralization are essential for the matrix restoration process. Previous studies support the osteocyte-driven collagen production using novel GFP-collagen transgenic mice (Baylink and Wergedal 1971; Zambonin Zallone et al., 1982; Kamel-ElSayed et al., 2015). They observed bright collagen production around some osteocytes suggesting heterogeneity in the osteocyte population has a capability of collagen production for PLR restoration. The fact that the collagenous matrix aligned with the axis of the lacunae, suggests collagen orientation and alignment are also coordinated by osteocytes. During this process, the levels of bone matrix proteins such as dentin matrix protein 1 (DMP1) and matrix extracellular phosphoglycoprotein (MEPE) in osteocytes were highly up-regulated to support the mineralization process (Gluhak-Heinrich et al., 2007; Harris et al., 2007; Teti and Zallone 2009; Qing et al., 2012).

PLR contributes to bone quality by altering the mineral to matrix ratio (M/M ratio), which is often used to predict the biomechanical properties of bone (Takata et al., 2011). The M/M ratio often increases with elevated bone mineral density contributing to better bone quality and is significantly increased with exercise (Kohn et al., 2009; Gardinier et al., 2016). *In vivo* studies of mice undertaking treadmill running, showed an increased M/M ratio around the matrix close to osteocytes compared to the bone matrix further away, suggesting localized osteocyte-induced PLR (Gardinier et al., 2016). This finding suggests that PLR regulation takes place predominantly in the mineralized bone matrix such as cortical bone. A better understanding of the mechanism of PLR regulation will aid in developing potential therapeutic applications that could improve cortical bone integrity, which is known to have a lower recovery rate after fracture compared to trabecular fractures (Chen and Sambrook 2011; Rivadeneira and Mäkitie 2016).

Osteocytes are known to secrete signaling factors into the circulatory system to modulate behavior of distant target organs such as parathyroid, kidney, and heart (Martin 2019; Pathak et al., 2020; Florencio-Silva et al., 2015). Particularly, osteocyte-secreted factor, fibroblast growth factor 23 (FGF23) that plays a role in endocrine signaling (**Figure 1C**). FGF23 contributes to kidney functions, maintaining serum phosphate levels by modulating the expression level of sodium/phosphate co-transporters in the kidney (Bonewald and Wacker 2013; Dallas et al., 2013; Dussold et al., 2019). Through this mechanism, FGF23 suppresses the vitamin D hormone (1,25-dihydroxyvitamin D) production in the kidneys by inhibiting the conversion of 25-hydroxyvitamin D to the active form, 1,25-dihydroxyvitamin D by 1-α-hydroxylase (Martin, David, and Quarles 2012; Dallas et al., 2013). The high FGF23 levels inhibit the vitamin D conversion process leading to decreased phosphate absorption in the intestine. This signaling process is tightly regulated by a feedback system between the active form of vitamin D and the level of FGF23 in circulation, where osteocytes play a key role. The elevated levels of circulating FGF23 are known as a risk factor for heart disease such as left ventricular hypertrophy, but further investigation is required to understand the underlying mechanism of FGF23 in this tissue (Mirza et al., 2009; Desjardins et al., 2012). The high prevalence of heart failure is often seen in chronic kidney disease (CKD) patients, which is also associated with elevated levels of FGF23 (Scialla et al., 2014). Furthermore, the parathyroid gland is another target for FGF23, which decreases PTH secretion. Where increased FGF23 levels modulate the downregulation of PTH mRNA expression and secretion *in vitro* (Krajisnik et al., 2007). The important and well-characterized role of PTH is in maintaining systemic calcium levels, where the parathyroid gland-secreted PTH is known to respond to low serum calcium (Bellido et al., 2013). If there is a high calcium demand in the intestine, the PTH levels increase causing mineral release from bones, which is often seen in pathological conditions such as chronic kidney disease. Osteocytes closely coordinate this process by increasing mineral degradation through PLR. Osteocyte-secreted CatK also contributes to the regulation of PTH levels by increasing parathyroid hormone-related peptide (PTHrP) during lactation (Lotinun et al., 2019).

MECHANOSENSORS IN OSTEOCYTES

Osteocytes are known to be one of the most mechanosensitive cells (Jacobs et al., 2010). These cells can be stimulated by various mechanical forces in bone created by gravitational forces and daily activities leading to changes of interstitial fluid flow and matrix deformation at the cellular level in bone. The osteocyte cellular response to mechanical stimulation is crucial in terms of viability, and also for a regulatory role in balanced bone homeostasis (Qin et al., 2020; Wittkowske et al., 2016). The earlier studies primarily focused on fluid flow-induced osteocyte mechanotransduction compared to direct interaction with extracellular matrix (ECM) deformation (Cheng et al., 2001a; Cherian et al., 2005; Kulkarni et al., 2010; Li et al., 2012; Spatz et al., 2015; Qin et al., 2020). The fluid flow rate used in previous *in vitro* studies was between 0.5 and 2 dynes/cm^2 (0.5 and 2 Pa) with some studies using up to 16 dynes/cm^2 (**Table 1**). These studies were demonstrated using both osteocyte cell lines (Cheng et al., 2001b; Cherian et al., 2005; Kulkarni et al., 2010; Litzenberger et al., 2010; Li et al., 2012; Xu et al., 2012; Spatz et al., 2015; Sato et al., 2020) and primary osteocytes (Ajubi et al., 1996; Klein-Nulend et al., 1997; Sterck et al., 1998; Ajubi et al., 1999; Joldersma et al., 2000). However, the exact physiological flow rate remains

TABLE 1 | Summary table for *in vitro* studies on osteocytes in response to mechanical stimulations. Abbreviations: Sclerostin (*Sost*), cyclooxygenase-1 (*COX-1*), osteoprotegerin (*OPG*), receptor activator of nuclear factor-κB ligand (*RANKL*), podoplanin (*E11*), prostaglandin E2 (PGE_2), cyclooxygenase-2 (*COX-2*), connexin 43 (Cx43), matrix extracellular phosphoglycoprotein (*Mepe*), phosphate regulating endopeptidase homologue, X-linked (*Phex*), dentin matrix protein 1 (*Dmp1*).

Cell type	Mechanical stimulation	Gene/Protein expression	Outcome
Osteocyte cell lines			
MLO-Y4	Oscillatory fluid flow, 1 Pa/2 h	*COX-2, RANKL/ OPG*	Response of integrin β1 under oscillatory fluid flow. The absence of β1 showed a reduction in *COX-2* and PGE_2 (Litzenberger et al., 2010)
MLO-Y4	Oscillatory fluid flow, 1 Pa/2 h	*COX-2, Runx-2*, integrin αVβ3, E11	Increased expression of integrin-associated molecules including vinculin, osteopontin, and CD44. Also, more cell spread and fiber stress are formed by fluid flow (Xu et al., 2012; Zhang et al., 2015)
MLO-Y4	Oscillatory fluid flow, 0.5–5 Pa/ 1–4 Pa	*COX-2, RANKL/ OPG*	Cells were exposed to different shear stress amplitude (0.5–5 Pa), oscillating frequency (0.5–2 Hz), and duration (1–4 h). *COX-2* Upregulated gene expression levels for *COX-2* response to higher shear stress amplitudes, faster oscillating frequencies, and longer flow durations, which direct towards bone formation (Li et al., 2012)
MLO-Y4	Fluid shear stress, 16 Pa/ 0.5–2 h	*OPG*, Cx43, PGE_2	Fluid shear stress induces the opening of Cx43 and redistributes Cx43 protein, which promotes PGE_2 release (Chen and Sambrook, 2001; Cherian et al., 2005)
MLO-Y4	Pulsating fluid flow, 0.7 Pa/1 h	*Mepe, RANKL/OPG*	Pulsatile fluid flow induced *Mepe*, but not *Phex*. *RANKL/OPG* gene expression decreased (Kulkarni et al., 2010)
Ocy454	3D fluid shear stress, 0.5–2.0 Pa/2 h or 3 days	*Sost*, *Dmp1*, *RANKL*, *OPG*, *Phex*, *Mepe,* Osteocalcin	Long-term fluid shear stress (3 days) in 2D LS increases *Sost*, *Dmp1*, *RANKL*, *OPG*, *Phex*, *Mepe* (Spatz et al., 2015; Wein et al., 2015)
Ocy454	Laminar fluid flow, 0.8 Pa/ 45 min	*Sost*	Laminar fluid flow downregulated *Sost* gene expression and demonstrated *HDAC5* is required for loading-induced *Sost* suppression (Sato et al., 2020)
Primary osteocytes			
Chicken osteocytes	Pulsating fluid flow, 0.5 Pa/1 h, 0.7 Pa/10 min	PGE_2	Osteocytes rapidly respond to fluid flow to increase PEG_2 (Ajubi et al., 1996) Intracellular Ca^{2+} level was increased through mechanosensitive ion channels (Ajubi et al., 1999)
Mouse calvariae	Pulsating fluid flow, 0.7 Pa/1 h	PGHS-2 (Prostaglandin G/H synthase), PGE_2	After pulsating fluid flow, osteocyte s upregulated *PGHS-2* gene expression, leading to more conversion of arachidonic acid into PGE_2 (Klein-Nulend et al., 1997)
Human calvarial cells/biopsies	Pulsating fluid flow, 0.7 Pa/1h	PGE_2, *COX-2*, Nitric oxide	Pulsating fluid flow upregulated PGE_2, *COX-2*, but not *COX-1* gene expression (Sterck et al., 1998; Klein-Nulend et al., 1998; Joldersma et al., 2000)

unclear. Estimates of the physiological matrix strain that is generated at the cellular level is also lacking. The strain level surrounding osteocytes is heterogeneous, amplifying the strain between the local cellular level and tissue level (Weinbaum et al., 1994; Nicolella et al., 2001; You et al., 2001; Bonivtch et al., 2007; Verbruggen et al., 2012; Hart et al., 2017). Several studies have demonstrated that variations in the size and shape of the LCN geometries are closely associated with non-uniform strain distributions (Canè et al., 1982; Metz et al., 2003). A parametric finite element model used to predict the microstructural response in lacuna showed increased strain with a decreased perilacunar tissue modulus (Bonivtch et al., 2007). The canaliculi diameter was increased by 0.8–1% in response to the applied strain and this deformation directly contributed to the enclosed dendritic process via the tethering elements (e.g., CD44, laminin, and integrins) to the canalicular wall (You et al., 2004). It is postulated that the strain difference between lacunar and canlicular structures may induce significantly different cellular responses in osteocytes (McCreadie and Hollister 1997; Nicolella et al., 2006; Verbruggen et al., 2015). *In vivo* studies revealed that the strain around perilacunar was an order of magnitude greater than the macroscopically applied strains, suggesting that local tissue strain can be magnified by inhomogeneous microstructural features (Nicolella et al., 2006).

There is a wide variety of potential mechanosensors present on osteocytes, which will be discussed in more detail in the following section, that transduce extracellular signals into cellular responses, including pericellular matrix, connexins/ pannexin channels, mechanically-sensitive ion channels, integrins, primary cilium, and caveolae (**Figure 2**) (Bonewald 2011; Qin et al., 2020). There is an ongoing debate around, whether the osteocyte's cell body or the dendritic cell processes are the primary mechanosensitive features of osteocytes. The unique dendritic morphology enables osteocytes to create a massively interconnected network in the human body creating a surface area that increases exposure to the surrounding microenvironment (Buenzli and Sims 2015; Hemmatian et al., 2017). A previous study has shown that the dendritic cell processes are more responsive to fluid shear stress than the cell body, using a transwell filter system to separate the dendritic cell processes from the cell body (Burra et al., 2010). Subsequent studies have also concluded that the more sensitive mechanotransduction occurs through dendritic cell processes, which induces calcium influx and regulate gene

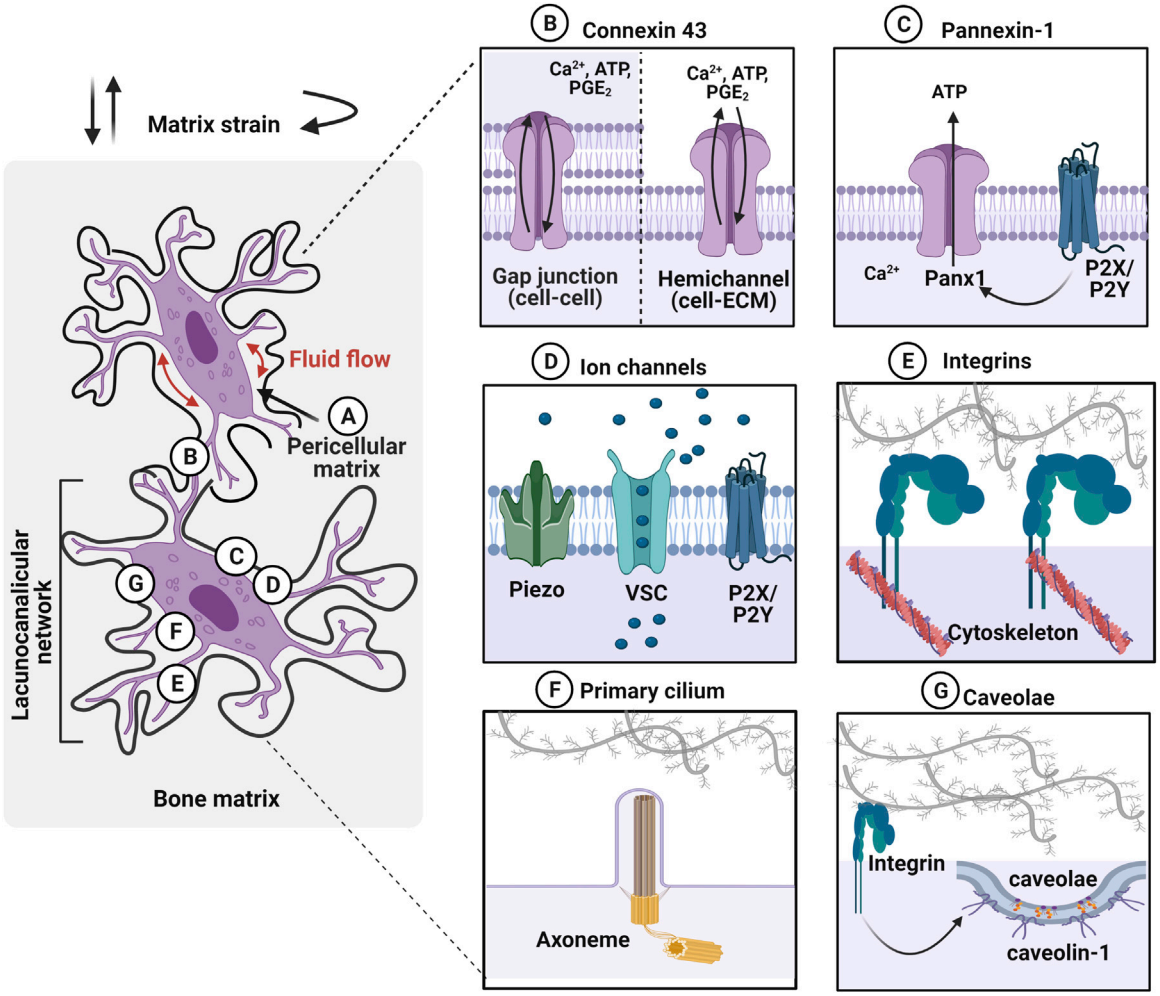

FIGURE 2 | Osteocytes within the lacunocanalicular network express mechanosensors, which can be activated by various mechanical stimuli such as fluid flow in the pericellular matrix and matrix strain (e.g., compressive, tensile, and torsional loading). **(A)** Osteocytes are surrounded by the pericellular matrix, between the cell and the walls of lacunae and canaliculi, which acts as a tether for osteocytes to transduce the mechanical stimulation. **(B)** Gap junctions, expressing on dendritic cell processes, facilitate cell–cell communication between osteocytes. Especially, connexin 43 (Cx43) is highly expressed and these junctions can also function as hemichannels that open to the microenvironment. Mechanical stimuli open these channels and transport calcium ions (Ca^{2+}), adenosine triphosphate (ATP), and prostaglandin E2 (PGE_2) between cells. **(C)** Pannexin-1 (Panx1) hemichannels release ATP to regulate intracellular calcium levels. Panx1 is also associated with purinergic P2X7 receptor to regulate apoptosis. **(D)** Mechanosensing ion channels such as Piezo, voltage-sensitive calcium channel (VSC), and purinergic receptor (P2X/P2Y) are opened in response to the mechanical stimulation and trigger calcium mobilization. **(E)** Integrins, transmembrane receptors that adhere cells to the extracellular matrix through specific motifs, transduce forces into cellular responses by mechanosignaling pathways. **(F)** Primary cilium is a protrusion of the cell membrane that is responsive to stimuli via the ciliary axoneme (microtubules). These immotile membrane protrusions act independently of intracellular Ca^{2+} release. **(G)** Caveolin-1, the structural protein of caveolae is interacting with the integrin β1 subunit to promote mechanotransduction in osteocytes. Figure created using BioRender.

transcription of key secreted signaling molecules such as sclerostin (Wu et al., 2011; Thi et al., 2013).

Pericellular Matrix

Osteocytes are surrounded by a layer of the pericellular matrix (PCM) at the interface between the cell membrane and the hard bone matrix (**Figure 2A**) (Sauren et al., 1992; You et al., 2004). Although the exact composition and structure of PCM are not well defined around the osteocytes, it is considered to be comprised of collagen, fibronectin, proteoglycans, glycoproteins, hyaluronic acid and perlecan/HSPG2 (Sauren et al., 1992; You et al., 2004; Weinbaum et al., 2007; Thompson et al., 2011a; Burra et al., 2011). It was observed that the transverse fibers span the entire PCM, which facilitate the direct interaction of osteocyte dendritic process to the canalicular wall with possible tethering molecules such as integrins, laminin, and CD44 (Noonan et al., 1996; You et al., 2004). It has been proposed that fluid drag forces transduced on the PCM via tethering molecules may induce osteocyte mechanotransduction by amplifying the strain at the cell membrane (You et al., 2001; Han et al., 2004). The strain amplification was further investigated in the context of integrin attachment points along the osteocyte dendritic processes with the collagen hillock traversing the PCM (Wang

et al., 2007). This study demonstrated that the direct interaction of integrin promoted strain amplification by more than two orders of magnitude compared to the tissue-level strain. Hyaluronic acid has been suggested as a major component of the PCM surrounding the osteocytes (Nakamura et al., 1995; Noonan et al., 1996). This was confirmed by diminished osteocyte PGE_2 release with a hyaluronidase treatment after being exposed to oscillating fluid flow under *in vitro* conditions (Reilly et al., 2003). The disappearance of integrin α5 was also observed with hyaluronidase treatment suggesting a tethering element of integrin is closely associated with the hyaluronic acid of PCM (Burra et al., 2011). A reduced volume of hyaluronic acid in PCM was observed with aging, which is possibly associated with the change in mechanoresponse of the osteocytes (Wang et al., 2014; Hagan et al., 2020). Perlecan, a large proteoglycan is also known to regulate solute transport and mechanosensing in PCM (Thompson et al., 2011b). Mice with perlecan deficiency showed decreased anabolic stimuli compared to the control group suggesting osteocytes experienced less fluid drag force, an effect also seen in aged mice (Wang et al., 2014).

Connexin/Pannexin Channels

Connexins are pore structure in the plasma membrane of osteocytes forming either gap junctions (cell–cell) or hemichannels (HC) (cell–matrix) (**Figure 2B**) (Plotkin and Bellido 2013). Although connexin 43 (Cx43) is the most highly expressed connexin in all the bone cell types, Cx37 has also been detected in osteocytes (Jones et al., 1993). This enables osteocytes to communicate with each other by the transfer of small molecules (less than 1 kD) through these gap junctions and respond to the environment via hemichannels that open to the extracellular space. Once osteocytes receive mechanical stimulation, Cx43 is phosphorylated, inducing the opening of connexons, six connexin subunits forming intercellular channels to regulate several effects such as influx of Ca^{2+}, ATP, and PGE_2 from the extracellular environment (Riquelme et al., 2021; Cherian et al., 2005; Genetos et al., 2007; Cheng et al., 2001a; Riquelme and Jiang 2013). This mechanism promotes the extracellular signal-regulated kinase (ERK)1/2-mitogen-activated protein kinase (MAPK) pathway, which regulates the bone remodeling process and is known to inhibit osteocyte apoptosis (Plotkin et al., 2005). Conversely, prolonged closure of connexins due to reduced mechanical loading or aging activates protein kinase B (Akt)/P27/Caspase-3 pathway leading to apoptosis. Pannexin-1 (Panx1) is another mechanosensitive channel expressed in osteocytes that forms only non-junctional channels to exchange small molecules between cell–extracellular space in response to mechanical stimulation (**Figure 2C**) (Aguilar-Perez et al., 2019). During apoptosis, Panx1 channel can be activated by coupling with the purinergic receptor, P2X7 to release ATP to send signals for macrophages (Sandilos et al., 2012). Panx1 knockout mouse model demonstrated that load-induced periosteal bone formation was diminished by dysregulated β-catenin and sclerostin expression in osteocytes (Seref-Ferlengez et al., 2019).

Mechanically-Sensitive Ion Channels

Mechanically-sensitive ion channels (MSICs) in osteocytes are responsive to mechanical stimulation, by opening in response to the tension created in the plasma membrane (**Figure 2D**) (Li et al., 2019a). The role of the mechanosensing ion channel, Piezo 1, which facilitates the exchange of ions between cell and extracellular environment, and leads to the opening of voltage-sensitive calcium channels (VSCs). Osteocytes primarily express more T-type CaV3.2 VSC subunits and a relatively small amount of L-type α1 subunits, which accelerate ATP/Ca^{2+} release in response to fluid shear stress (0.5–4 Pa) (Thompson et al., 2011a; Lu et al., 2012). Piezo 1 has been shown to not only modulate intracellular calcium levels, but also activate downstream signaling pathways such as Akt-sclerostin in response to cyclic stretch-induced mechanical stimulation. Here, sclerostin expression was downregulated by Akt phosphorylation, which was confirmed by the Piezo1 knock-out, which resulted in diminished calcium influx and Wnt, and release of ATP from the cell (Robling and Turner 2009). Osteocytes furthermore regulate mechanically induced ATP *via* P2X/P2Y receptors leading to purinergic signaling (Li et al., 2005; Burnstock et al., 2013).

Integrins

Integrins are heterodimeric transmembrane cell receptors composed of alpha (α) and beta (β) subunits that anchor cells through specific matrix motifs transducing mechanical dynamics from matrix strain and fluid-flow shear stress (**Figure 2E**) (Geoghegan et al., 2019). Osteocytes are known to differentially express integrins, with the α5β1 integrins localizing strongly on the cell body, and αVβ3 integrins along the dendritic cell processes, suggesting site-directed osteocyte mechanotransduction (Haugh et al., 2015; Geoghegan et al., 2019). In extracted mouse bone tissue, integrin αVβ3 binding was observed to localize to the canalicular wall along the periodic protrusions (McNamara et al., 2009). It is proposed that proteoglycan tethering elements bridging the dendritic process of osteocytes to the canalicular wall *via* integrin αVβ3 promotes interaction with the ECM proteins containing Arginine-Glycine-Aspartic acid (RGD) sequence motifs such as fibronectin, osteopontin, von Willebrand factor, sialoprotein, and thrombospondins, but not to collagen (Haugh et al., 2015). The direct adhesion between osteocyte and ECM facilitates the formation of focal adhesions, which link to the actin skeleton to activate cellular responses, such as regulating secreted signaling molecules that are guiding the effector cells. Integrins are known to recruit focal adhesion proteins, including vinculin and paxillin, which link the cytoskeleton to the ECM. Both *in vivo* and *in vitro* studies demonstrated the expression of focal adhesion proteins, such as vinculin, in osteocytes (Zhou et al., 2019; Cao et al., 2020). Another study suggested that integrin αVβ3-mediated mechanotransduction lacks the classic focal adhesion protein recruitment, but rather mediates Ca^{2+} signaling, ATP release

TABLE 2 | The key research demonstrations for mechanosensitive signalling pathways in osteocytes and therapeutic implications.

Signalling pathway	Research	Clinical implications	Reference
Sphinogolipid	SP1 induces osteoclast precursor migration thus increase bone resorption	Increased S1P for osteoporotic fracture/low bone mineral density	(Tian et al., 2021; Thuy et al., 2014; Zhang et al., 2015)
Wnt/β-cat	β-catenin is required for osteocyte viability β-catenin is associate with FoxO transcription to prevent osteocyte apoptosis β-catenin binds to the connexin 43 promoters, promoting cell-cell interaction and enhance the viability	Bisphosphonates, prostaglandin, estrogen are known to prevent osteocyte apoptosis	(Bellido 2014;Xia et al., 2010; Kamel et al., 2010; Plotkin et al., 1999; Kitase et al., 2010; Tomkinson et al., 1998; Duan and Bonewald 2016; Lin et al., 2020)
AMPK	AMPK is the regulator for cellular energy homeostasis AMPK increases cellular AMP/ATP ratio helps to maintain energy homeostasis Protect osteocyte apoptosis by suppressing oxidative stress	Osteoporosis is possibly a disorder of energy metabolism AMPK can be activated by antidiabetic drugs (metformin and thiazolidinediones)	(Tong, Ganta, and Liu 2020; Jeyabalan et al., 2012; Ru and Wang, 2020)
FoxO	FoxO activation inhibits osteocyte apoptosis induced by aging and unloading FoxO signalling associate with Wnt/β-cat for osteocyte viability	Targeting aging-related osteoporosis/bone fragility fractures ROS induce apoptosis; antioxidants such as polyphenols and anthocyanins through diet intake induce anti-osteoclastogenic action	(Kawata and Mikuni-Takagaki 1998; Ru and Wang 2020; Domazetovic et al., 2017)
PTH	Activation of PTH receptor suppressed sclerostin expression Increased level of PTHrP activate PTH receptor for anti-apoptotic effect Deletion of *Mef2C* in osteocytes induced bone formation by decreasing sclerostin; PTH activates Wnt receptor, LRP6 directly, or through FoxO degradation to stabilise beta-catenin in Wnt signalling to induce osteogenesis	Homologous with PTH (N-terminal 1–36) and PTH-related protein (C-terminal 107–109) induce bone formation and also reduce oxidative stress Antioxidant supplement (Resveratrol)	(Kamel et al., 2010; Collette et al., 2012; Wysolmerski 2012; Bellido et al., 2013; Maycas et al., 2015; Portal-Núñez et al., 2016)

and membrane potential through the purinergic channel pannexin 1, the calcium channel CaV3.2-1, and the ATP-gated purinergic receptor P2X7 (Cabahug-Zuckerman et al., 2018). Furthermore, both α5β1 and αVβ3 integrins are known to activate Ca^{2+} channels, but through different mechanisms. An earlier study has identified integrin αVβ3-specific intracellular Ca^{2+} signals, using a novel technique called Stokesian fluid stimulus probe (SFSP). This probe enables the application of hydrodynamic forces (pN range) to the discrete location of the cell body and dendritic cell processes (Thi et al., 2013). The SFSP-stimulated osteocytes (MLO-Y4) showed that dendritic cell processes were more mechanosensitive in the piconewton range of mechanical stimulation, resulting in increased levels of intracellular Ca^{2+}. Using an integrin αVβ3- specific antagonist, Integrisense 750, diminished Ca^{2+} response under SFSP-stimulation was observed (Thi et al., 2013). Thus, integrin αVβ3 is not only involved in activation of focal adhesion protein-mediated mechanotransduction, but also regulates intracellular Ca^{2+} signals through cation and stretch-activated channels in osteocytes. Interestingly, the α5β1 integrins are directly associated with the opening of Cx43 HC to release anabolic molecules from osteocytes (PGE_2), in response to fluid shear stress (Batra et al., 2012). PGE_2 also has an autocrine effect, stimulating the upregulation of Cx43 protein expression in osteocytes, which further induces an increase in formation of gap junctions between cells (Cheng et al., 2001b). The activation of the intracellular mechanotransduction pathway, involving phosphoinositide 3-kinase (PI3K)-Akt signaling to open Cx43 HC by conformational activation of integrin α5β1 is independent of adhesion to the ECM. Especially, the integrin α5 subunit is crucial in establishing the specific interaction with the C termini of Cx43. It was observed that siRNA knockdown of integrin α5 diminished the opening of the Cx43 HC under fluid flow-induced stimulation (Batra et al., 2012; Riquelme et al., 2021). It was argued that not only integrin α5 activates Cx43 HC, but also integrin αVβ3 expressed along the dendritic cell processes can transduce signals to the cell body for Cx43 HC activation *via* PI3K-Akt signaling. This was demonstrated both *in vitro* and *in vivo* under fluid shear stress with steady fluid flow/oscillatory fluid flow and under tibial compression in mice. The results showed that integrin αV was more responsive to low fluid shear stress levels to activate Cx43 HC compared to integrin α5 induced activation. Notably, at a higher fluid shear stress level, integrin α5 was activated independently of integrin αV, implying that the activation of either integrin pair is fluid shear stress level dependent. This study concluded that fluid shear stress could not suppress sclerostin expression without Cx43 HC, which was demonstrated by blocking with antibodies, suggesting Cx43 is essential for the anabolic effects on bone.

Numerous *in vitro* studies have been undertaken to understand targeted integrin-mediated mechanotransduction in osteocytes, with only a few *in vivo* studies, with most of

these using specific integrin β1-deleted transgenic mice (Zimmerman et al., 2000; Litzenberger et al., 2009; Shekaran et al., 2014). In a study investigating the integrin β1-mediated response after cyclic ulna loading for 3 days, osteocyte-specific integrin β1-knockout mice showed reduced bone formation suggesting that the integrin β1 is required to promote mechanically-induced bone formation (Litzenberger et al., 2009). Unfortunately, the osteocyte-specific integrin β3 targeted approach has not been progressed due to technical challenges. For this reason, it is still not clear what the precise functional roles that these integrins play on bone homeostasis are.

Primary Cilium

Cilia are present in both motile and immotile cells, which have microtubule axoneme. Nine sets of microtubules doublets provide structural support and rigidity (Satir et al., 2010). The primary cilium has "9 + 0" pattern with nine doublet microtubules without the central pair, which are seen in the immotile cilia. In contrast, "9 + 2" pattern with 9 doublets plus one central pair of microtubules is often seen in motile cilium. Osteocytes present non-motile primary cilium with "9 + 0" arrangement, 2–9 μm in length, which are mechanoresponsive (**Figure 2F**) (Qin et al., 2020). Primary cilium changes the morphology during mechanical adaptation, which induces expression of cilium-related proteins such as Sperm flagellar protein 2 (Spef2), polycystin -1 or -2 (PC1 or 2), kinesin II intraflagellar transport (Kif3a), and Adenylyl cyclase 6 (AC6) (Xiao et al., 2006; Temiyasathit et al., 2012; Qin et al., 2020). Primary cilium also changes its stiffness in response to mechanical stimulation through an acetylation-mediated mechanism that induces calcium movement. This mechanism is dependent on polycystines (polycystin 1 and 2). These are proteins located at the base of the cilium acting like a cationic change to facilitate Ca^{2+} transfer (Yavropoulou and Yovos 2016). Interestingly, polycystin 1 mutant mice showed reduced bone mineral density due to a lack of response to mechanical stimulation (Xiao et al., 2006). Mice also showed decreased OPG and increased RANKL levels that results in reduced bone mineral density in both trabecular and cortical bones (Temiyasathit and Jacobs 2010). The gene expression level of runt-related transcription factor 2 (*Runx2*), osterix, and osteocalcin were also observed to decrease, where these are all key parameters responsible for bone development, bone density, and mechanical properties.

Caveolae

Although this has been demonstrated to date only in MLO-Y4 osteocytic cells (**Figure 2G**), caveolin-1, the structural protein of caveolae was proposed as a membrane mechanosensor in osteocytes, interacting with the integrin β1 subunit (Gortazar et al., 2013). Caveolae are 60–80 nm plasma membrane pits that are present in many mechanosensitive cells such as myocytes. In osteocytes, caveolae are physically linked to integrin β1 leading to activation of ERK through tyrosine protein kinase (Src) and focal adhesion kinase (FAK) phosphorylation. Thus, it was postulated that caveolin-1 is essential for integrin/Src/ERK activation of pro-osteocyte survival mechanisms. This was confirmed by inhibition of caveolin-1 that diminishes anti-apoptotic effects of mechanical stimulation due to disrupted ERK activation (Plotkin et al., 2005). The detailed underlying mechanisms around the role of caveolin-1 in mechanosensing in osteocytes are unclear, however, this integrin-dependent mechanism is intriguing.

MECHANOTRANSDUCTION PATHWAYS IN OSTEOCYTES AND THERAPEUTIC IMPLICATIONS

Although mechanically-induced osteocyte responses have been studied extensively, the precise signaling pathways underlying these responses are still unclear. Understanding the signaling pathways is critical due to the implications of the functional outcomes for both bone health and diseases, as well as more broadly for the other systemic role of osteocytes through their endocrine functions (Dallas et al., 2013). For the past decades, several signaling pathways have been identified, as potential therapeutic targets to improve bone health (**Table 2**).

Sphingolipid Signaling Pathway

In osteocyte cell models (MLO-Y4 and Ocy454 cell line), intracellular sphingosine-1-phosphatase (S1P) levels were found to be upregulated in response to fluid flow mechanical stimulation, with a corresponding downregulation of the enzymes for degradation/dephosphorylation of S1P (Sgp11, Sgpp11), as well as upregulation of Sphk1, responsible for phosphorylation of S1P leading to its activation (**Figure 3A**) (Zhang et al., 2015; Dobrosak and Gooi 2017). In response to mechanical load, S1P in osteocytes acts as a signaling molecule for modifying cellular Ca^{2+} levels and PGE_2, either directly via intracellular S1P or indirectly via S1P binding to G-protein-coupled receptors (Zhang et al., 2015; Meshcheryakova et al., 2017). In response to mechanical stimulations, osteocytes modulate S1P production and secretion that facilitate paracrine osteoblast-osteoclast crosstalk. In general, osteocyte-secreted S1P plays important role in both osteoblast and osteoclast activities (**Figure 3B**) (Zhang et al., 2020). The newly synthesized S1P is released intracellularly and acts like a second messenger, which induces Ca^{2+} release in an IP3-independent manner. The extracellular S1P can also bind to G-protein-coupled receptors (S1P receptors, SIPRs), which increases the mobilization of the intracellular level of Ca^{2+}. Furthermore, intracellular S1P can be released into circulation and binds to S1PRs on osteoblasts promoting cell differentiation and also inducing *RANKL* expression (Dobrosak and Gooi 2017). The osteoblast cells produce RANKL and this binds to the receptor RANK to activate osteoclasts, suggesting the crosstalk between osteoblasts-osteoclasts is important to mediate the balance between bone formation and resorption. The loop of this crosstalk is regulated by osteocytes since S1P secreted by osteoclasts is released and binds to S1PRs on osteocytes in a feedback loop mechanism. The sphingolipid signaling pathway is activated

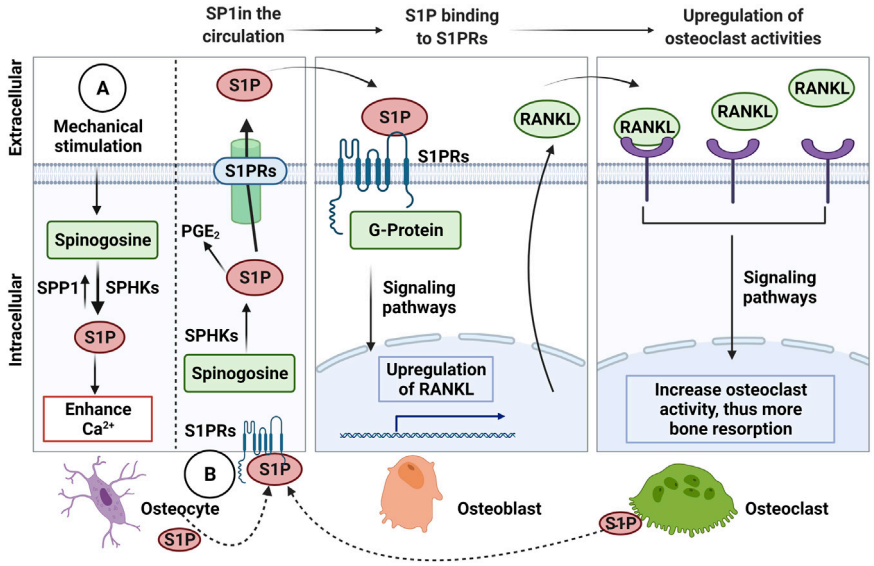

FIGURE 3 | The Sphingosine-1-Phosphate (S1P) signalling in osteocytic mechanotransduction and effects of osteocyte-mediated extracellular S1P on osteoblast-osteoclast crosstalk. **(A)** The endogenous S1P production in response to mechanical stimulation from Sphinogosine by the S1P phosphohydrolase (SPP1) and sphinogosine kinase (SPHKS) leading to increased cellular Ca^{2+}. **(B)** S1P can be released by osteocytes, which extracellular S1P can bind to S1P receptors (S1PRs) on osteoblasts that activate signaling pathways to upregulate receptor activator NF-κB (RANKL). Then, osteoblasts release RANKL that binds to RANK on osteoclasts to increase osteoclast activity for bone resorption. Osteoclasts are also known to release S1P, which binds to S1PRs on osteocytes as a feedback loop to increase intracellular S1P and prostaglandin E2 (PGE_2), Receptor activator NF-κB (RANKL), ligand (RANKL). Figure created using BioRender.

in response to oscillatory fluid flow-induced loading in bone (**Figure 4A**) (Tian et al., 2021; Thuy et al., 2014). The lipid mediator, S1P is the sphingolipid metabolite that acts as a signaling molecule for modifying intracellular Ca^{2+}, which was shown in both osteoblasts and osteoclasts previously (Meshcheryakova et al., 2017).

Interestingly, the increased S1P level in blood (>200 nM) is closely associated with bone fracture risk and low bone mineral density (Lee et al., 2012). The blood S1P plasma levels have been observed to be elevated in postmenopausal women compared to premenopausal women, with the postmenopausal women known to be at higher risk of bone loss (Ardawi et al., 2018). In pathological conditions, the S1P disrupts the equilibrium between osteoblast and osteoclast activities. Increased production of S1P by osteocytes in response to mechanical stimulation may also promote the osteoblast differentiation process, which results in a decreased level of osteoblast-produced RANKL inhibiting osteoclast differentiation (Dobrosak and Gooi 2017). There are S1P-targeted therapeutic approaches for osteoporosis using S1P lyase inhibitors (e.g., CYM5520 and LX2931) and a structural analog of sphingosine (e.g., FTY720, fingolimod) (Tian et al., 2021). These pharmacological treatments increase S1P at tissue levels, inducing new bone formation, which was confirmed in ovariectomized mice and rat studies (Huang et al., 2016; Weske et al., 2019). Currently, however, it remains unclear whether the expression of S1P receptors in osteocytes has a key regulatory role in response to S1P in the blood, and therefore further studies are required.

TGF-β Signaling Pathway

TGF-β signaling is also responsive to mechanical stimulation independent from TGF-β receptor-induced responses, which are initiated by Smad2/3 phosphorylation and downregulates sclerostin (**Figure 4B**) (Nguyen et al., 2013). The level of Smad2/3 phosphorylation was elevated even in the presence of the TGF-β receptor inhibitor, confirming fluid shear stress directly triggered TGF-β signaling (Monteiro et al., 2021). Also, the level of Smad2/3 phosphorylation was larger under fluid shear stress compared to osteocytes with TGF-β treatment, suggesting TGF-β signaling is largely induced by fluid shear stress. Impaired TGF-β signaling is often associated with aging, diminished mechanical adaptation and low bone mass. A recent *in vivo* study revealed that TGF-β signaling is important for osteocyte functions in LCN such as PLR, as mentioned previously (Schurman et al., 2021). Deletion of this specific TGF-β signaling compromised osteocytes functional response to mechanical stimulation, similar to that observed with aging.

Wnt/β-Catenin Signaling Pathway

The Wnt/β-catenin signaling has a crucial role in bone formation, not only for the effector cells but also in self-regulatory mechanisms for osteocytes (**Figure 4C**). Osteocytes increase the expression of the Wnt ligand in response to mechanical stimulation. Osteocyte-produced Wnt can then bind to the LRP6 receptor on osteocytes leading to intracellular β-catenin accumulation in the cytoplasm altering gene transcription changes for Wnt

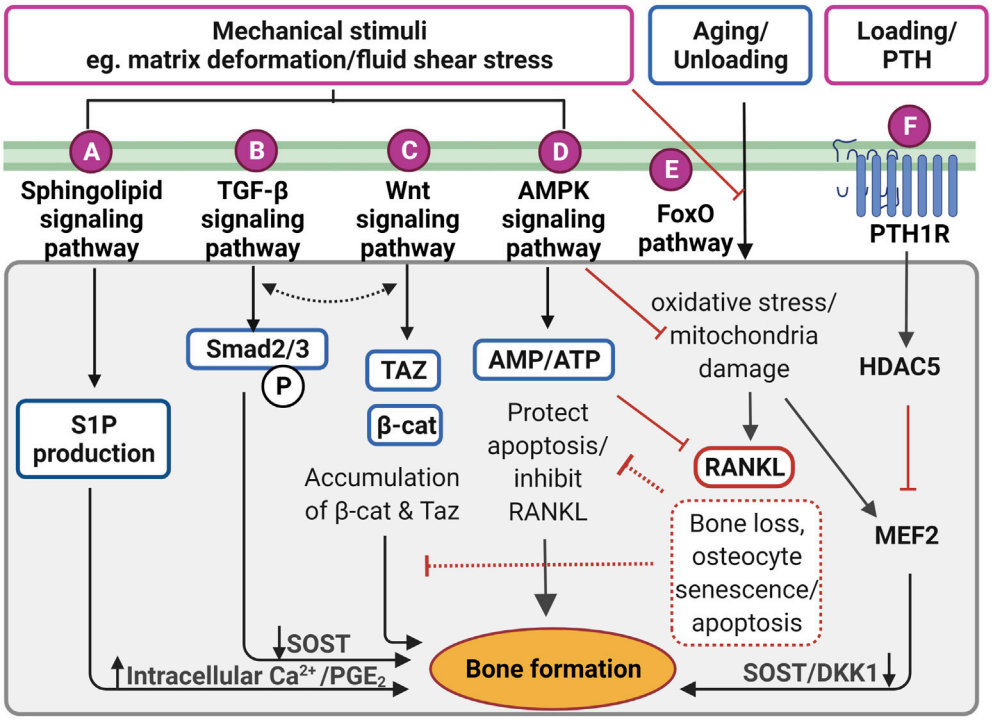

FIGURE 4 | Proposed mechanotransduction pathways in osteocytes for therapeutic targets showing intracellular signaling in response to the mechanical stimulation. **(A)** Pulsatile fluid flow triggered sphingolipid signaling to regulate the lipid mediators such as sphingosine-1-phosphate (S1P) production that upregulates the intracellular calcium ions (Ca^{2+}) levels and prostaglandin E2 (PGE_2) synthesis/release in osteocytes. **(B)** Fluid shear stress upregulates suppressor of mothers against decapentaplegic 2/3 (Smad2/3) phosphorylation triggering transforming growth factor-beta (TGF-β) signaling, resulting in sclerostin (SOST) downregulation. This is independent of TGF-β receptor-induced response. **(C)** Wnt/β-catenin signaling can be elicited by direct response to extracellular matrix deformation via integrins or fluid shear stress, which is important to maintain osteocyte viability and anabolic effect by accumulating Taz and β-catenin (β-cat). Interestingly, both TGF-β and Wnt/β signaling may interact with each other to induce bone formation, however, the exact mechanism is not clear. **(D)** Under mechanical stimuli, adenosine monophosphate (AMP)-activated protein kinase (AMPK) signaling governs energy homeostasis in osteocytes by increasing the AMP/adenosine triphosphate (ATP) ratio for inhibiting apoptosis and decrease receptor activator of nuclear factor-κB ligand (RANKL) expression. **(E)** Forkhead box O (FoxO) signaling is activated to protect osteocytes from oxidative stress and mitochondria damage caused by aging and reduced mechanical stimulation. Without FoxO activation, osteocytes lead to senescence and apoptosis. **(F)** Parathyroid hormone receptor (PTHr) is activated both by mechanical stimulation as well as parathyroid hormone. This receptor upregulates histone deacetylase 5 (HDAC5), which inhibits myocyte enhancer factor 2 (MEF2C), responsible for negative Wnt signaling molecules, SOST and dickkopf-related protein 1 (DKK1). Figure created using BioRender.

antagonists, *SOST*, and *DKK1* (Bonewald and Johnson 2008; Tu et al., 2015). In response to mechanical loading, the Wnt/β-catenin signaling pathway plays an important role, not only for bone anabolic effects but also in osteocyte viability (Bonewald and Johnson 2008). Glucocorticoid treatment (dexamethasone) can cause secondary osteoporosis by inducing apoptosis in osteocytes and interestingly, this glucocorticoid-induced apoptosis can be inhibited by a steady laminar fluid shear stress of 1.6 Pa for 2 h (Kitase et al., 2010). The protective mechanism is mediated through the release of an osteocyte-produced signaling molecule called PGE_2 associated with Wnt/β-catenin signaling by pulsatile fluid flow shear stress (0.2–2.4 Pa for 1 h), which is independent of LRP5 receptors in osteocytes (Kamel et al., 2010). This protective effect was induced through PGE_2 binding to EP2/4 receptors, which leads to Akt activation for glycogen synthesis kinase 3 (GSK-3β) inhibition. This results in an accumulation of intracellular β-catenin in osteocytes. Through this process, PGE_2 can also induce anabolic bone formation by crosstalk with Wnt/β-catenin pathway leading to downregulation of *SOST* and *DKK1* transcription levels and increased expression of *Wnt* in osteocytes. β-catenin is also known to bind to the Cx43 promoters, upregulating *Cx43* transcription. This enhances osteocyte cell–cell communication for osteocyte viability and increases PGE_2 levels in response to steady laminar flow of 1.6 Pa for 2 h (Cherian et al., 2003; Xia et al., 2010). This mechanism is also important to the integrin β1-caveolin-1 induced signaling, where vascular endothelial growth factor receptor 2 (VEGFR2) associated with caveolin-1 was reported to be responsive to 1 Pa fluid flow shear stress after 10 min, inducing Wnt/β-catenin signaling (de Castro et al., 2015). Another study also observed that VEGFR2 was activated by pulsatile fluid flow shear stress (1 Pa for 10 min) *via* caveolin, which induces ERK phosphorylation leading to β-catenin translocation to the cell membrane and triggering osteocyte prosurvival signaling. The deletion of caveolin-1 by siRNA impaired VEGFR2 activation, inducing osteocyte apoptosis (Gortazar et al., 2013).

It is known that the Wnt/β-catenin signaling pathway is in crosstalk with various other signaling pathways in response to mechanical stimulations. The TGF-β signaling pathway is known to interact with Wnt/β-catenin signaling in response to mechanical stimulation (Guo and Wang 2009; Rys et al., 2016). Although the mechanism behind the association is still not fully understood, these pathways are associating at multiple hierarchical levels to regulate common target genes, such as sclerostin. This mechanism is associated with the Forkhead box O (FoxO) signaling pathway to inhibit osteocyte apoptosis, which will be further explained later (Manolagas and Almeida 2007). From a therapeutic perspective, Wnt/β-catenin signaling can be induced by bisphosphonates, prostaglandin, estrogen, and anti-sclerostin antibodies, which are all known to prevent osteocyte apoptosis and have anabolic bone effects (Tomkinson et al., 1998; Plotkin et al., 1999; Kitase et al., 2010).

AMPK Signaling Pathway

RNA-sequencing analysis showed significantly up-regulated 5′adenosine monophosphate-activated protein kinase (AMPK) signaling pathways in osteocytes under fluid shear stress (**Figure 4D**) (Govey et al., 2015). Prior to this study, the same group also demonstrated the rapid release of ATP in response to fluid shear stress together with up-regulation of the ATP-producing enzyme, nucleoside diphosphate kinase B (NDK), suggesting initiation of AMPK signaling to generate more ATP (Govey et al., 2014). Osteocytes have also been shown to activate AMPK signaling pathway under energy imbalance conditions, like high oxidative stress or nutrient suppression as a protective mechanism (Tong et al., 2020). AMPK is a heterotrimeric complex including α, β, and γ subunits. This signaling pathway can be triggered by phosphorylation of AMPK via catalytic α subunit in low energy status, which can be detected *via* the increased ratio of adenosine monophosphate (AMP)/ATP, by turning on ATP-producing catabolic pathways and turning off ATP-consuming anabolic pathways to restore energy (Jeyabalan et al., 2012). This process is often found in autophagy, which is a survival mechanism to prevent osteocyte apoptosis that can be found under reduced mechanical stimulation. Interestingly, it was shown that AMPK activity is associated with bone metabolism by using a 5-Aminoimidazole-4-carboxyamide ribonucleotide (AICAR), an analog of AMP for AMPK activation (Yokomoto-Umakoshi et al., 2016). Osteocytes (MLO-Y4 cell line) with AICAR treatment induced the phosphorylation of AMPK α subunit leading to significantly reduced *RANKL* gene expression, suggesting inhibition of osteoclast activity (Yokomoto-Umakoshi et al., 2016; Tong et al., 2020). Interestingly, AMPK activation in osteocytes was found to regulate *FGF23* transcription in response to mineral metabolism (Komaba 2018). For example, deficient Ca^{2+} stores in the endoplasmic reticulum of osteocytes stimulate store-operated calcium entry (SOCE) *via* Orai1 on the cell membrane, which induces the influx of Ca^{2+} from the extracellular microenvironment leading to *FGF23* transcription. Conversely, in CKD, AMPK is activated due to decreased levels of ATP, which blocks the Ca^{2+} influx leading to inhibition of *FGF23* transcription in osteocytes leading to imbalanced serum calcium and phosphate levels. This mechanism, which still needs further investigation, may represent an important therapeutic target for CKD patients.

Fox Signaling Pathway

The protective (anti-apoptotic) action of the FoxO signaling pathway in osteocytes, as has been observed for other cell types, is also activated by mechanical stimulation (**Figure 4E**) (Ambrogini et al., 2010). Long-lived osteocytes experience oxidative stress and mitochondrial damage leading to apoptosis under physiological conditions such as reduced level of mechanical stimulation and aging. For example, increasing oxidative stress due to aging leads to bone loss, which is closely associated with reactive oxygen species (ROS), inhibiting the translocation of FoxO into the nucleus. However, in response to mechanical stimulation, FoxO is phosphorylated *via* PI3K/Akt signaling pathway, which increases β-catenin associated with the FoxO transcription factor. Osteocyte viability is important for balanced bone homeostasis as osteocyte apoptosis often leads to disease states and upregulation of bone resorption. Osteocyte apoptosis upregulates the expression of sclerostin and RANKL, promoting increased osteoclast activities (Zhang et al., 2019a). Interestingly, osteocytes located in deeper cortical bone showed abundant mitochondria with high levels of glycolytic enzymes, suggesting more protection against oxidative stress (Frikha-Benayed et al., 2016). Effective FoxO activation is closely associated with the Wnt/β-catenin signaling pathway, which is also responsible for osteocyte viability (Zhang et al., 2019b). An earlier study in FoxO-deficient mice showed increased osteocyte apoptosis leading to decreased osteoblast activities, resulting in reduced bone mass in these animals (Ambrogini et al., 2010). FoxO signaling pathway represents a potential target during aging and the observed decrease in osteocyte number that occurs, potentially through the use of antioxidant supplements such as polyphenols, anthocyanins to inhibit osteocyte apoptosis (Domazetovic et al., 2017; Ru and Wang 2020).

Osteocyte-secreted sclerostin expression was once thought to be regulated only by PTH, however, the recent findings demonstrate it is also induced by the fluid flow shear stress on osteocytes (**Figure 4F**) (Spatz et al., 2015; Sun et al., 2019; Sato et al., 2020). Upon stimulation, histone deacetylase 5 (HDAC5) inhibits myocyte enhancer factor 2 (MEF2C), responsible for *SOST* transcription in osteocytes. As expected, overexpression of HDAC5 in osteocyte cells downregulated *SOST* expression (Baertschi et al., 2014; Wein et al., 2015). Conversely, *HDAC5* knockout mice showed an upregulation of sclerostin mRNA levels, and of the number of sclerostin-positive cells leading to a diminished Wnt/β-catenin signaling pathway in osteoblasts (Wein et al., 2015).

OSTEOCYTE-RELATED DISEASES AND TREATMENTS

Abnormalities of bone strength and microstructure are common in bone diseases, where the bones become more fragile and are more likely to fracture (Feng and McDonald 2011). These disorders are often closely associated with the dysregulation of bone cells, especially osteocytes (Pathak et al., 2020). Specifically, the loss of osteocyte functional ability is linked to compromised bone

TABLE 3 | Treatment options for osteocyte-related diseases.

Treatment	Therapeutics	References
Antibody treatment	Sclerostin monoclonal antibody Romosozumab (AMG 785, CDP-785), Blosozumab, and BSP804 DKK1 antibody (BHQ880, DKN-01)	(McClung 2017; Morrell et al., 2021)
Bisphosphonates	Oral bisphosphonates (Fosamax, Boniva), intravenous bisphosphonates (Zoledronate, Pamidronate)	(Merlotti et al., 2007; Lewiecki 2010; Eriksen et al., 2014)
Anti-bone resorption	Cathepsin K inhibitors (Odanacatib), and Anti-RANKL (denosumab)	(Tanaka et al., 2017; Lu et al., 2018; Galvano et al., 2019)
Hormone replacement therapy	Estrogen receptor (Raloxifene) and parathyroid hormone peptide (teriparatide, abaloparatide)	(Deal et al., 2005; Leder, 2017)
Non-invasive, painless mechanotherapy	Low-intensity pulsed ultrasound (LIPUS), vibration therapy, whole-body vibration therapy	(Fritton et al., 2000; Thompson et al., 2014; Thompson et al., 2016; Camacho-Cardenosa et al., 2019; Jiang et al., 2019)

homeostasis. Osteocyte apoptosis has been proposed as a major risk factor caused by aging, reduced physical activity, hormone deficiency and inflammation resulting in dramatic decrease of osteocyte density (Almeida 2012). As a result, aged or dying cells are no longer able to carry out functional roles, which have an impact on the bone matrix quality (Shah et al., 2018). The accumulation of apoptotic osteocytes with aging is linked to several bone diseases such as osteonecrosis and the onset of age-related osteoporosis leading to increased fracture risk. During apoptosis, osteocytes secrete signals to osteoclasts to be recruited to the site for bone resorption (Schaffler et al., 2014). When apoptosis takes place, osteocytes release damage-associated molecular patterns (DAMPs) for osteoclast recruitment (McCutcheon et al., 2020). When dead osteocytes are removed, the empty lacunae are hyper-mineralized with calcium phosphate, leading to a condition called micropetrosis, resulting in more brittle bones (Qiu et al., 2002; Bell et al., 2008). The accumulation of mineralization in lacunae also interrupts the osteocytic cell–cell communication, leading to depletion of signals and nutrition due to disturbance of canalicular fluid flow (Hemmatian et al., 2017). This cascading process then inevitably further affects other osteocytes resulting in even more extensive osteocyte apoptosis. With less active osteocytes, the bone is less likely to be protected against microdamage. Microdamage triggers dying osteocytes to send signals for osteoclast activation, and at the same time, osteocytes also send anti-apoptotic factor, BAX to neighboring cells to protect their viability (Verborgt et al., 2000; Bonewald 2017). By doing this, the number of apoptotic osteocytes can be minimized around the damaged area. However, if there is a decreased number of viable cells, this mechanism is disrupted, leading to a large area of microcracks (Ma et al., 2008). Therefore, osteocyte cell viability plays a crucial role in the maintenance of bone health, and also protects against microdamage, which is a normal physiological process. The apoptosis process is closely associated with increased oxidative stress, which was confirmed with oxidative stress markers such as p53 and $p66^{Shc}$ in aged mice (Almeida et al., 2007). The oxidation process has been shown to be delayed by anti-oxidant *N*-acetyl Cysteine. Another noticeable change in aged osteocytes is the decreased level of autophagic activity, which is an important indicator for stress susceptibility (Ru and Wang 2020). For example, aged-osteocytes are less likely to produce autophagic proteins (e.g., Beclin-1) to suppress apoptotic proteins (e.g., cleaved-caspase-3). This mechanism is important especially for the anti-apoptotic activity of neighboring cells. However, prolonged stress will cause apoptosis eventually, which highlights the importance of the underlying mechanism between autophagy and apoptosis. Apart from aging, other factors such as estrogen deficiency and glucocorticoid treatment can also induce osteocyte apoptosis leading to osteoporosis (Jilka et al., 2013). Additionally, inflammatory cytokines such as interleukin 1 (IL-1) and tumor necrosis factor-alpha (TNF-α) increase osteocyte death (Marahleh et al., 2019; Wang et al., 2019). Some factors including parathyroid hormone, estrogen, bisphosphonates are known to protect osteocytes from apoptosis (Plotkin et al., 1999; Bellido and Plotkin 2011). Furthermore, as already mentioned above, unloading or decreased level of exercise often leads to decreased bone mass, which is well described in astronauts or bedridden patients (Bradbury et al., 2020; Stavnichuk et al., 2020). These findings are further illustrating, that osteocytes require mechanical stimulation, which can be introduced by mechanotherapy such as low-intensity pulsed ultrasound (LIPUS) treatments where this type of direct mechanical stimulation has been shown to improve bone healing (Thompson et al., 2016; Jiang et al., 2019). The vibration therapy studies demonstrated that high-frequency, low-magnitude vibration therapy (gravitational force = acceleration of 9.81 m/s^2, frequency >30 Hz) improved bone health (Thompson et al., 2014). These relative parameters were estimated based on the bone dynamics that experience low-frequency (1–3 Hz), high-frequency (10–50 Hz), and large-magnitude (2,000–3,000 microstrain) (Fritton et al., 2000). Whole-body vibration (WBV) has been recently introduced as a bone stimulation therapy (12.6 Hz for 30 s with 1-min rest for 4 times) with hypoxic stimuli (16.1% FiO_2) also showed improvement in bone mineral density (BMD) after 18 weeks (Camacho-Cardenosa et al., 2019).

Osteocyte cell death with age is one of the major factors for the onset of osteoporosis. Age-related osteoporosis is closely associated with a low level of autophagic activity, which was also shown in apoptotic osteocytes. There are several treatments for osteoporosis, reducing bone resorption, that are based on the administration of oral bisphosphonates (Fosamax, Boniva), intravenous bisphosphonates (Zoledronate, Pamidronate), Cathepsin K inhibitors (Odanacatib), and Anti-RANKL antibody therapy (denosumab) (Merlotti et al., 2007; Lewiecki 2010; Eriksen et al., 2014; Suen and Qin 2016; Tanaka et al., 2017; Lu et al., 2018; Galvano et al., 2019). Osteoblast-targeted hormone replacement therapy is also widely used, including estrogen receptor (Raloxifene) and parathyroid hormone peptide (teriparatide, abaloparatide),

however, these therapies also affect osteocytes (Deal et al., 2005; Bonewald 2017; Leder 2017). *In vivo* studies have confirmed that sclerostin monoclonal antibody (Scl-Ab) treatment induced bone formation, mass, and strength (Yao et al., 2016). Scl-Ab products are commercially available including Romosozumab (AMG 785, CDP-785), Blosozumab, and BSP804 (McClung 2017; Morrell et al., 2021). These antibody-based treatments are widely used for reducing fracture risk arising from various health conditions, including osteoporosis as well as post-menopause (Ominsky et al., 2011; MacNabb et al., 2016). Furthermore, a bispecific antibody for sclerostin and DKK1 has been shown to have synergistic effects for bone formation compared with monotherapies (Florio et al., 2016). These approaches try to inhibit the secretory signaling molecules produced by osteocytes that antagonize the Wnt-signaling pathway in the osteoblast lineage, affecting the anabolic bone formation.

Although these treatments are widely used, the long-term safety and efficacy have to be taken into consideration. The most commonly used treatment for osteoporosis is based on bisphosphonates (Drake et al., 2008). These are effective and safe treatments with persistent benefit even after taking a break from the treatment, however, there are no clear guidelines for "drug holiday" (Diab and Watts 2013). The United States Food and Drug Administration (FDA) proposed a reevaluation of continuing bisphosphonate therapy after 3–5 years, showing a small decrease in BMD without higher fracture risk (Whitaker et al., 2012). In contrast to the prolonged half-lives of bisphosphonates, anti-RANKL (denosumab) shows reduced efficacy after treatment discontinuation (Bone et al., 2011). The anti-sclerostin treatment with romosozumab showed a decrease in BMD after discontinuation followed by 2-years treatment (McClung et al., 2018). Similarly, blosozumab treatment showed a decline in BMD in both the femoral neck and the lumbar spine after the discontinuation suggesting there is an increased risk of fracture (Recknor et al., 2015). The treatment options are summarized in **Table 3**.

Osteogenesis imperfect (OI) is a congenital disease that exhibits brittle bone (Basel and Steiner 2009). This disorder is caused by alterations in type I collagen that was previously known to be associated with osteoblast activities (Wenstrup et al., 1990). As the type I collagen is the predominant ECM protein, its dysregulation influences bone mineralization, leading to the impairment of local-acting growth factors such as TGF-β (Morello 2018). A recent study revealed that the osteocyte transcriptome was dysregulated in OI mice including Wnt/β-catenin and TGF-β signaling pathways (Zimmerman et al., 2019). TGF-β is a crucial factor to regulate bone formation and bone resorption for maintaining bone mass. However, excessive activation of the TGF-β signaling pathway found in OI increases high bone turnover and low bone mass (Lim et al., 2017). This continuous activation of TGF-β signaling may disrupt osteoblast functions while increasing osteocyte density. Increased TGF-β signaling can be diminished by TGF-β neutralizing antibody (ID11) treatment leading to improved bone mass by decreasing osteoblast and osteoclast numbers while normalizing the osteocyte density. The exact mechanism of impaired TGF-β signaling in OI is not fully understood, but possibly through impaired binding of small leucine-rich proteoglycans (e.g., decorin) to TGF-β in collagen fibrils. OI mouse model showed abnormalities of type I collagen expression showing abnormal osteocyte phenotype with impaired dendritic formation. Impaired osteocyte phenotype may contribute to their functional roles by interrupting the cell–matrix interaction. As a consequence, osteocytes may increase osteoblast activities towards bone formation after detecting a defective matrix, possibly for the restoration process. The osteocyte transcriptome sequencing of OI compared to wild-type control mouse models demonstrated the differential expression of dysregulated collagen fibril organization, but also impaired osteocyte dendritic formation, ECM compositions, and integrin-mediated signaling (Zimmerman et al., 2019). This observation supports the role of impaired cell–matrix interaction promoting dysregulated dendritic formation and leading to changes in functional roles. Interestingly, the Wnt signaling pathway in osteocytes was also affected in OI mice as gene levels for Wnt ligands were significantly increased, however, the exact mechanism of Wnt upregulation in OI remains unclear (Fahiminiya et al., 2013). *In vivo* studies with the conditional Wnt inactivation in osteocytes showed increased bone fragility and low bone mass as a result of altered Wnt1 production (Joeng et al., 2017). Like osteoporotic therapeutics, anti-resorptive (e.g., cathepsin K inhibitors and Anti-RANKLtherapies) and bone anabolic treatments (e.g., Sci-Ab and PTH) are commonly used for OI patients (Drake et al., 2008; Morello 2018).

Apart from bone-related diseases, there is more evidence emerging that osteocytes are also associated with other diseases, facilitated *via* secretion of the FGF23 hormone (Guo and Yuan 2015). It was reported that highly elevated circulating FGF23 is closely associated with kidney dysfunction, and this was also linked to heart failures such as left ventricular hypertrophy and vascular calcification (Faul et al., 2011; Desjardins et al., 2012). Furthermore, FGF23 was linked to chronic hypophosphatemia, caused by impaired mineralization of the bone matrix leading to bone fragility (Murali et al., 2016). Circulating FGF23 controls serum phosphate levels, by suppressing reabsorption in the kidney, and excess FGF23 causes hypophosphatemia diseases. Hypophosphatemia with high levels of FGF23, can be treated with a monoclonal FGF23 antibody (anti-FGF23), for example, burosumab, which was recently approved by the FDA to stabilize serum phosphate levels. The alternative medication for hypophosphatemia is a combination of active vitamin D and phosphate salts, however, this treatment often leads to kidney failure (Kinoshita and Fukumoto 2018; Barratt et al., 2021).

DISCUSSION

Once considered inactive cells, the osteocytes are now attributed to have crucial roles in the overall bone remodeling process, local microenvironment regulation and systemic interactions with other organs. The tightly regulated bone homeostasis becomes dysregulated as we age and with reduced mechanical stimulation, shifting the balance towards more bone resorption, leading to bone

loss diseases such as osteopenia and osteoporosis, which increases fracture risk. As we move towards a more aging society, both intrinsic and extrinsic factors accelerate pathological signaling pathways causing disorders. Intrinsic factors (e.g., genetics, hormones, vasculature) and extrinsic factors (e.g., nutrition, physical activity, medications) are associated with the mechanisms that maintain healthy bone (Demontiero et al., 2012).

When the mechanosensitivity of osteocytes was first demonstrated, understanding the underlying modes of detection, the osteocyte-induced mechanotransduction pathways, and the functional outcomes for bone metabolism became significant research focuses in the field (Iolascon et al., 2013). The long life span of osteocytes (up to 25 years) and their important role in regulating the continuous coordinated cycle of bone formation and resorption and in the repair of bone damage makes them an ideal target for therapeutics. However, bone homeostasis is a complicated system involving multiple cell types that are signaling and coordinating each other. Until now, most studies on bone cells have focused on the more accessible effector cells, osteoblasts, and osteoclasts as compared to osteocytes (Liedert et al., 2005). The inaccessible location of osteocytes buried within the hydroxyapatite matrix, makes their visualization challenging, so studies have largely focused on *in vitro* cellular models to understand the mechanistic pathways that respond to mechanical stimuli.

Although *in vivo* studies provide more physiologically relevant outcomes, the various biological effects within more complex tissue responses are challenging to dissect and to attribute specific cellular roles given the complex microstructural organization of bone is hard to mimic. Targeting simplified approaches, focused on osteocyte-elicited mechanotransduction on 2D plastic or 2.5D using collagen coating, the *in vivo* three-dimensionality has been largely neglected in this field. Only recently, commercially available natural (e.g., collagen and fibrin), synthetic (e.g., polyethylene glycol hydrogels), and both animal and plant-derived (e.g., matrigel, gelatin, and alginate) matrices were used to construct 3D *in vitro* models (Langhans 2018; Zhang et al., 2019c; Aziz et al., 2020). The inorganic component, hydroxyapatite, is available as a ceramic composite with tricalcium/biphasic calcium phosphate (Boukhechba et al., 2009). Hydroxyapatite is widely used for coatings on metallic implants, bone fillings, and injectable bone substitutes (Ramesh et al., 2018). Alternative synthetic material, polystyrene is also available, and is tunable for various parameters such as pore sizes and thickness (Spatz et al., 2015). Direct cell-free bone tissue also becomes an option that represents the natural milieu, but again the mechanical properties are difficult to tune (Lyons et al., 2010; Li et al., 2019b).

Despite their inherent advantages, none of the cell models recapitulates the 3D dendritic morphology observed *in vivo*, indicating more ideal matrices need to be developed. This is especially important for osteocyte mechanotransduction studies, as the dendritic morphology is now considered an important mechanotransducer. Without providing an ideal microenvironment, this is not only limiting the morphology but also cellular responses, where better understanding of osteocyte mechanotransduction will provide significant opportunities for developing novel therapeutics for bone-related diseases.

The currently available treatments for bone disorders either target osteoclastic activity or osteoblastic activity (Rochefort 2014). Despite osteocytes abundance and their instrumental role in regulating bone metabolism, osteocyte-targeted treatments are not readily available. There are, however, some indirectly targeting antibody-based treatments to osteocyte-secreted molecules such as the recently FDA-approved sclerostin monoclonal antibody treatment for osteoporosis, promoting bone formation (Shakeri and Adanty 2020). Maintaining osteocyte viability is now considered one of the most important factors to maintain healthy bone (Bonewald 2017; Ru and Wang 2020). Aging, in particular, accelerates osteocyte apoptosis, resulting in fewer secretory factors, less bone matrix remodeling, and lower responsiveness to mechanical stimulation leading to impaired osteocyte functional roles in bone. Therefore, the development of novel osteocyte-specific therapeutics would be ideal to target osteocyte functions and signaling pathways including mechanisms to prevent apoptosis. Many of these pathways are still lacking a detailed understanding of, while others are more generic signaling pathways, such as the Wnt/β-catenin and TGF-β1 signaling, which are expressed in other cell types making therapies more challenging and less targeted (Janssens et al., 2005; Rys et al., 2016). In addition, the extra-skeletal roles of osteocytes in regulating distant organs, such as kidneys, heart, and parathyroid through secreted signaling molecules provides opportunities to target the associated dysfunctions in these organs through osteocyte manipulation.

The focus of this review was to highlight the fundamental role of osteocytes, the most mechanosensitive cells of the bone, by revealing how these cells detect mechanical stimuli through various mechanosensors and the proposed mechanotransduction pathways driving the functional responses that fundamentally affect bone metabolism. However, much detail around these mechanoresponsive pathways in osteocytes is still lacking. Therefore a greater understanding of these mechanisms will help us to identify more effective treatments for both chronic bone loss diseases such as osteoporosis as well as other genetic diseases affecting bone metabolism. This will also enable researchers to unravel, how these master regulators contribute to their important extraskeletal roles.

AUTHOR CONTRIBUTIONS

Literature search was conducted by JC and AK. Manuscript writing and editing were performed by JC, AK, JL, and AR. All authors contributed intellectual property to the work, and approved for publication.

FUNDING

This work was supported by the Australian Government Research Training Program (RTP) Scholarship/The University of Queensland Scholarships (JC) and the support from Australian Research Council (AR, ARC Laureate Fellowship FL160100139, ARC Discovery Project DP190102230).

REFERENCES

Aarden, E. M., Nijweide, P. J., van der Plas, A., Alblas, M. J., Mackie, E. J., Horton, M. A., et al. (1996). Adhesive Properties of Isolated Chick Osteocytes *In Vitro*. *Bone* 18, 305–313. doi:10.1016/8756-3282(96)00010-5

Aguilar-Perez, A., Pacheco-Costa, R., Atkinson, E. G., Deosthale, P., Davis, H. M., Essex, A. L., et al. (2019). Age- and Sex-dependent Role of Osteocytic Pannexin1 on Bone and Muscle Mass and Strength. *Sci. Rep.* 9, 13903. doi:10.1038/s41598-019-50444-1

Ajubi, N. E., Klein-Nulend, J., Alblas, M. J., Burger, E. H., and Nijweide, P. J. (1999). Signal Transduction Pathways Involved in Fluid Flow-Induced PGE2 Production by Cultured Osteocytes. *Am. J. Physiology-Endocrinology Metab.* 276, E171–E178. doi:10.1152/ajpendo.1999.276.1.e171

Ajubi, N. E., Klein-Nulend, J., Nijweide, P. J., Vrijheid-Lammers, T., Alblas, M. J., and Burger, E. H. (1996). Pulsating Fluid Flow Increases Prostaglandin Production by Cultured Chicken Osteocytes-A Cytoskeleton-dependent Process. *Biochem. Biophysical Res. Commun.* 225, 62–68. doi:10.1006/bbrc.1996.1131

Almeida, M. (2012). Aging Mechanisms in Bone. *Bonekey Rep.* 1, 1. doi:10.1038/bonekey.2012.102

Almeida, M., Han, L., Martin-Millan, M., Plotkin, L. I., Stewart, S. A., Roberson, P. K., et al. (2007). Skeletal Involution by Age-Associated Oxidative Stress and its Acceleration by Loss of Sex Steroids. *J. Biol. Chem.* 282, 27285–27297. doi:10.1074/jbc.m702810200

Ambrogini, E., Almeida, M., Martin-Millan, M., Paik, J.-H., Depinho, R. A., Han, L., et al. (2010). FoxO-Mediated Defense against Oxidative Stress in Osteoblasts Is Indispensable for Skeletal Homeostasis in Mice. *Cel. Metab.* 11, 136–146. doi:10.1016/j.cmet.2009.12.009

Ardawi, M.-S. M., Rouzi, A. A., Al-Senani, N. S., Qari, M. H., Elsamanoudy, A. Z., and Mousa, S. A. (2018). High Plasma Sphingosine 1-phosphate Levels Predict Osteoporotic Fractures in Postmenopausal Women: The Center of Excellence for Osteoporosis Research Study. *J. Bone Metab.* 25, 87–98. doi:10.11005/jbm.2018.25.2.87

Aziz, A. H., Wilmoth, R. L., Ferguson, V. L., and Bryant, S. J. (2020). IDG-SW3 Osteocyte Differentiation and Bone Extracellular Matrix Deposition Are Enhanced in a 3D Matrix Metalloproteinase-Sensitive Hydrogel. *ACS Appl. Bio Mater.* 3, 1666–1680. doi:10.1021/acsabm.9b01227

Bach-Gansmo, F. L., Wittig, N. K., Brüel, A., Thomsen, J. S., and Birkedal, H. (2016). Immobilization and Long-Term Recovery Results in Large Changes in Bone Structure and Strength but No Corresponding Alterations of Osteocyte Lacunar Properties. *Bone* 91, 139–147. doi:10.1016/j.bone.2016.07.005

Baertschi, S., Baur, N., Lueders-Lefevre, V., Voshol, J., and Keller, H. (2014). Class I and IIa Histone Deacetylases Have Opposite Effects on Sclerostin Gene Regulation. *J. Biol. Chem.* 289, 24995–25009. doi:10.1074/jbc.m114.564997

Balemans, W., Van Den Ende, J., Freire Paes-Alves, A., Dikkers, F. G., Willems, P. J., Vanhoenacker, F., et al. (1999). Localization of the Gene for Sclerosteosis to the Van Buchem Disease-Gene Region on Chromosome 17q12-Q21. *Am. J. Hum. Genet.* 64, 1661–1669. doi:10.1086/302416

Barratt, K. R., Sawyer, R. K., Atkins, G. J., St-Arnaud, R., and Anderson, P. H. (2021). Vitamin D Supplementation Improves Bone Mineralisation Independent of Dietary Phosphate in Male X-Linked Hypophosphatemic (Hyp) Mice. *Bone* 143, 115767. doi:10.1016/j.bone.2020.115767

Basel, D., and Steiner, R. D. (2009). Osteogenesis Imperfecta: Recent Findings Shed New Light on This once Well-Understood Condition. *Genet. Med.* 11, 375–385. doi:10.1097/gim.0b013e3181a1ff7b

Batra, N., Burra, S., Siller-Jackson, A. J., Gu, S., Xia, X., Weber, G. F., et al. (2012). Mechanical Stress-Activated Integrin 5 1 Induces Opening of Connexin 43 Hemichannels. *Proc. Natl. Acad. Sci.* 109, 3359–3364. doi:10.1073/pnas.1115967109

Baylink, D., and Wergedal, J. (1971). Bone Formation by Osteocytes. *Am. J. Physiology-Legacy Content* 221, 669–678. doi:10.1152/ajplegacy.1971.221.3.669

Bell, L. S., Kayser, M., and Jones, C. (2008). The Mineralized Osteocyte: a Living Fossil. *Am. J. Phys. Anthropol.* 137, 449–456. doi:10.1002/ajpa.20886

Bellido, T. (2014). Osteocyte-Driven Bone Remodeling. *Calcif. Tissue Int.* 94, 25–34. doi:10.1007/s00223-013-9774-y

Bellido, T., and Plotkin, L. I. (2011). Novel Actions of Bisphosphonates in Bone: Preservation of Osteoblast and Osteocyte Viability. *Bone* 49, 50–55. doi:10.1016/j.bone.2010.08.008

Bellido, T., Saini, V., and Pajevic, P. D. (2013). Effects of PTH on Osteocyte Function. *Bone* 54, 250–257. doi:10.1016/j.bone.2012.09.016

Benedetti, M. G., Furlini, G., Zati, A., and Letizia Mauro, G. (2018). The Effectiveness of Physical Exercise on Bone Density in Osteoporotic Patients. *Biomed. Res. Int.* 2018, 4840531. doi:10.1155/2018/4840531

Beno, T., Yoon, Y.-J., Cowin, S. C., and Fritton, S. P. (2006). Estimation of Bone Permeability Using Accurate Microstructural Measurements. *J. Biomech.* 39, 2378–2387. doi:10.1016/j.jbiomech.2005.08.005

Bone, H. G., Bolognese, M. A., Yuen, C. K., Kendler, D. L., Miller, P. D., Yang, Y.-C., et al. (2011). Effects of Denosumab Treatment and Discontinuation on Bone Mineral Density and Bone Turnover Markers in Postmenopausal Women with Low Bone Mass. *J. Clin. Endocrinol. Metab.* 96, 972–980. doi:10.1210/jc.2010-1502

Bonewald, L. F., and Johnson, M. L. (2008). Osteocytes, Mechanosensing and Wnt Signaling. *Bone* 42, 606–615. doi:10.1016/j.bone.2007.12.224

Bonewald, L. F. (2011). The Amazing Osteocyte. *J. Bone Miner. Res.* 26, 229–238. doi:10.1002/jbmr.320

Bonewald, L. F. (2017). The Role of the Osteocyte in Bone and Nonbone Disease. *Endocrinol. Metab. Clin. North America* 46, 1–18. doi:10.1016/j.ecl.2016.09.003

Bonewald, L. F., and Wacker, M. J. (2013). FGF23 Production by Osteocytes. *Pediatr. Nephrol.* 28, 563–568. doi:10.1007/s00467-012-2309-3

Boskey, A. L., and Coleman, R. (2010). Aging and Bone. *J. Dent. Res.* 89, 1333–1348. doi:10.1177/0022034510377791

Boukhechba, F., Balaguer, T., Michiels, J.-F., Ackermann, K., Quincey, D., Bouler, J.-M., et al. (2009). Human Primary Osteocyte Differentiation in a 3D Culture System. *J. Bone Mineral Res.* 24, 1927–1935. doi:10.1359/jbmr.090517

Bradbury, P., Wu, H., Choi, J. U., Rowan, A. E., Zhang, H., Poole, K., et al. (2020). Modeling the Impact of Microgravity at the Cellular Level: Implications for Human Disease. *Front. Cel. Dev. Biol.* 8, 96. doi:10.3389/fcell.2020.00096

Buenzli, P. R., and Sims, N. A. (2015). Quantifying the Osteocyte Network in the Human Skeleton. *Bone* 75, 144–150. doi:10.1016/j.bone.2015.02.016

Burnstock, G., Arnett, T. R., and Orriss, I. R. (2013). Purinergic Signalling in the Musculoskeletal System. *Purinergic Signal.* 9, 541–572. doi:10.1007/s11302-013-9381-4

Burr, D. B., Milgrom, C., Fyhrie, D., Forwood, M., Nyska, M., Finestone, A., et al. (1996). *In Vivo* measurement of Human Tibial Strains during Vigorous Activity. *Bone* 18, 405–410. doi:10.1016/8756-3282(96)00028-2

Burra, S., Nicolella, D. P., Francis, W. L., Freitas, C. J., Mueschke, N. J., Poole, K., et al. (2010). Dendritic Processes of Osteocytes Are Mechanotransducers that Induce the Opening of Hemichannels. *Proc. Natl. Acad. Sci.* 107, 13648–13653. doi:10.1073/pnas.1009382107

Burra, S., Nicolella, D. P., and Jiang, J. X. (2011). Dark Horse in Osteocyte Biology. *Communicative Integr. Biol.* 4, 48–50. doi:10.4161/cib.13646

Cabahug-Zuckerman, P., Stout, R. F., Jr., Majeska, R. J., Thi, M. M., Spray, D. C., Weinbaum, S., et al. (2018). Potential Role for a Specialized β3 Integrin-Based Structure on Osteocyte Processes in Bone Mechanosensation. *J. Orthop. Res.* 36, 642–652. doi:10.1002/jor.23792

Camacho-Cardenosa, M., Camacho-Cardenosa, A., Burtscher, M., Brazo-Sayavera, J., Tomas-Carus, P., Olcina, G., et al. (2019). Effects of Whole-Body Vibration Training Combined with Cyclic Hypoxia on Bone Mineral Density in Elderly People. *Front. Physiol.* 10, 1122. doi:10.3389/fphys.2019.01122

Candeliere, G. A., Liu, F., and Aubin, J. E. (2001). Individual Osteoblasts in the Developing Calvaria Express Different Gene Repertoires. *Bone* 28, 351–361. doi:10.1016/s8756-3282(01)00410-0

Canè, V., Marotti, G., Volpi, G., Zaffe, D., Palazzini, S., Remaggi, F., et al. (1982). Size and Density of Osteocyte Lacunae in Different Regions of Long Bones. *Calcif. Tissue Int.* 34, 558–563. doi:10.1007/BF02411304

Cao, H., Yan, Q., Wang, D., Lai, Y., Zhou, B., Zhang, Q., et al. (2020). Focal Adhesion Protein Kindlin-2 Regulates Bone Homeostasis in Mice. *Bone Res.* 8, 2. doi:10.1038/s41413-019-0073-8

Chen, J. S., and Sambrook, P. N. (2011). Antiresorptive Therapies for Osteoporosis: a Clinical Overview. *Nat. Rev. Endocrinol.* 8, 81–91. doi:10.1038/nrendo.2011.146

Cheng, B., Kato, Y., Zhao, S., Luo, J., Sprague, E., Bonewald, L. F., et al. (2001a). PGE2 Is Essential for Gap Junction-Mediated Intercellular Communication between Osteocyte-like MLO-Y4 Cells in Response to Mechanical Strain. *Endocrinology* 142, 3464–3473. doi:10.1210/endo.142.8.8338

Cheng, B., Zhao, S., Luo, J., Sprague, E., Bonewald, L. F., and Jiang, J. X. (2001b). Expression of Functional gap Junctions and Regulation by Fluid Flow in Osteocyte-like MLO-Y4 Cells. *J. Bone Miner. Res.* 16, 249–259. doi:10.1359/jbmr.2001.16.2.249

Cherian, P. P., Cheng, B., Gu, S., Sprague, E., Bonewald, L. F., and Jiang, J. X. (2003). Effects of Mechanical Strain on the Function of Gap Junctions in Osteocytes Are Mediated through the Prostaglandin EP2 Receptor. *J. Biol. Chem.* 278, 43146–43156. doi:10.1074/jbc.m302993200

Cherian, P. P., Siller-Jackson, A. J., Gu, S., Wang, X., Bonewald, L. F., Sprague, E., et al. (2005). Mechanical Strain Opens Connexin 43 Hemichannels in Osteocytes: A Novel Mechanism for the Release of Prostaglandin. *MBoC* 16, 3100–3106. doi:10.1091/mbc.e04-10-0912

Clarke, B. (2008). Normal Bone Anatomy and Physiology. *Clin. J. Am. Soc. Nephrol.* 3 (Suppl. 3), S131–S139. doi:10.2215/CJN.04151206

Collette, N. M., Genetos, D. C., Economides, A. N., Xie, L., Shahnazari, M., Yao, W., and Loots, G. G. (2012). Targeted Deletion of Sost Distal Enhancer Increases Bone Formation and Bone Mass. *Proc. Natl. Acad. Sci U. S. A.* 109 (35), 14092–14097. doi:10.1073/pnas.1207188109

Creecy, A., Damrath, J. G., and Wallace, J. M. (2021). Control of Bone Matrix Properties by Osteocytes. *Front. Endocrinol.* 11, 578477. doi:10.3389/fendo.2020.578477

Dai, R., Wu, Z., Chu, H. Y., Lu, J., Lyu, A., Liu, J., et al. (2020). Cathepsin K: The Action in and beyond Bone. *Front. Cel. Dev. Biol.* 8, 433. doi:10.3389/fcell.2020.00433

Dallas, S. L., Prideaux, M., and Bonewald, L. F. (2013). The Osteocyte: An Endocrine Cell ... and More. *Endocr. Rev.* 34, 658–690. doi:10.1210/er.2012-1026

Day, T. F., Guo, X., Garrett-Beal, L., and Yang, Y. (2005). Wnt/β-Catenin Signaling in Mesenchymal Progenitors Controls Osteoblast and Chondrocyte Differentiation during Vertebrate Skeletogenesis. *Developmental Cel.* 8, 739–750. doi:10.1016/j.devcel.2005.03.016

de Castro, L. F., Maycas, M., Bravo, B., Esbrit, P., and Gortazar, A. (2015). VEGF Receptor 2 (VEGFR2) Activation Is Essential for Osteocyte Survival Induced by Mechanotransduction. *J. Cel. Physiol.* 230, 278–285. doi:10.1002/jcp.24734

Deal, C., Omizo, M., Schwartz, E. N., Eriksen, E. F., Cantor, P., Wang, J., et al. (2005). Combination Teriparatide and Raloxifene Therapy for Postmenopausal Osteoporosis: Results from a 6-Month Double-Blind Placebo-Controlled Trial. *J. Bone Miner Res.* 20, 1905–1911. doi:10.1359/jbmr.050714

Demontiero, O., Vidal, C., and Duque, G. (2012). Aging and Bone Loss: New Insights for the Clinician. *Ther. Adv. Musculoskelet.* 4, 61–76. doi:10.1177/1759720x11430858

Denisov-Nikol'skiĭ, Iu. I., and Doktorov, A. A. (1987). Spatial Organization of the Lacunar-Canalicular System in the Structures of Bone Lamellae. *Arkh Anat. Gistol. Embriol.* 93, 37–43.

Desjardins, L., Liabeuf, S., Liabeuf, S., Renard, C., Lenglet, A., Lemke, H.-D., et al. (2012). FGF23 Is Independently Associated with Vascular Calcification but Not Bone mineral Density in Patients at Various CKD Stages. *Osteoporos. Int.* 23, 2017–2025. doi:10.1007/s00198-011-1838-0

Diab, D. L., and Watts, N. B. (2013). Bisphosphonate Drug holiday: Who, when and How Long. *Ther. Adv. Musculoskelet.* 5, 107–111. doi:10.1177/1759720x13477714

Dobrosak, C., and Gooi, J. H. (2017). Increased Sphingosine-1-Phosphate Production in Response to Osteocyte Mechanotransduction. *Bone Rep.* 7, 114–120. doi:10.1016/j.bonr.2017.10.002

Dole, N. S., Mazur, C. M., Acevedo, C., Lopez, J. P., Monteiro, D. A., Fowler, T. W., et al. (2017). Osteocyte-Intrinsic TGF-β Signaling Regulates Bone Quality through Perilacunar/Canalicular Remodeling. *Cel. Rep.* 21, 2585–2596. doi:10.1016/j.celrep.2017.10.115

Domazetovic, V., Marcucci, G., Iantomasi, T., Brandi, M. L., and Vincenzini, M. T. (2017). Oxidative Stress in Bone Remodeling: Role of Antioxidants. *ccmbm* 14, 209–216. doi:10.11138/ccmbm/2017.14.1.209

Drake, M. T., Clarke, B. L., and Khosla, S. (2008). Bisphosphonates: Mechanism of Action and Role in Clinical Practice. *Mayo Clinic Proc.* 83, 1032–1045. doi:10.4065/83.9.1032

Duan, P., and Bonewald, L. F. (2016). The Role of the Wnt/β-Catenin Signaling Pathway in Formation and Maintenance of Bone and Teeth. *Int. J. Biochem. Cel. Biol.* 77, 23–29. doi:10.1016/j.biocel.2016.05.015

Dussold, C., Gerber, C., White, S., Wang, X., Qi, L., Francis, C., et al. (2019). DMP1 Prevents Osteocyte Alterations, FGF23 Elevation and Left Ventricular Hypertrophy in Mice with Chronic Kidney Disease. *Bone Res.* 7, 12. doi:10.1038/s41413-019-0051-1

Eriksen, E. F., Díez-Pérez, A., and Boonen, S. (2014). Update on Long-Term Treatment with Bisphosphonates for Postmenopausal Osteoporosis: A Systematic Review. *Bone* 58, 126–135. doi:10.1016/j.bone.2013.09.023

Fahiminiya, S., Majewski, J., Mort, J., Moffatt, P., Glorieux, F. H., and Rauch, F. (2013). Mutations in WNT1 Are a Cause of Osteogenesis Imperfecta. *J. Med. Genet.* 50, 345–348. doi:10.1136/jmedgenet-2013-101567

Faibish, D., Ott, S. M., and Boskey, A. L. (2006). Mineral Changes in Osteoporosis. *Clin. Orthop. Relat. Res.* 443, 28–38. doi:10.1097/01.blo.0000200241.14684.4e

Faul, C., Amaral, A. P., Oskouei, B., Hu, M.-C., Sloan, A., Isakova, T., et al. (2011). FGF23 Induces Left Ventricular Hypertrophy. *J. Clin. Invest.* 121, 4393–4408. doi:10.1172/jci46122

Feng, X., and McDonald, J. M. (2011). Disorders of Bone Remodeling. *Annu. Rev. Pathol. Mech. Dis.* 6, 121–145. doi:10.1146/annurev-pathol-011110-130203

Florencio-Silva, R., Sasso, G. R., Sasso-Cerri, E., Simões, M. J., and Cerri, P. S. (2015). Biology of Bone Tissue: Structure, Function, and Factors that Influence Bone Cells. *Biomed. Res. Int.* 2015, 421746. doi:10.1155/2015/421746

Florio, M., Gunasekaran, K., Stolina, M., Li, X., Liu, L., Tipton, B., et al. (2016). A Bispecific Antibody Targeting Sclerostin and DKK-1 Promotes Bone Mass Accrual and Fracture Repair. *Nat. Commun.* 7, 11505. doi:10.1038/ncomms11505

Frikha-Benayed, D., Basta-Pljakic, J., Majeska, R. J., and Schaffler, M. B. (2016). Regional Differences in Oxidative Metabolism and Mitochondrial Activity Among Cortical Bone Osteocytes. *Bone* 90, 15–22. doi:10.1016/j.bone.2016.05.011

Fritton, S. P., J. McLeod, K., and Rubin, C. T. (2000). Quantifying the Strain History of Bone: Spatial Uniformity and Self-Similarity of Low-Magnitude Strains. *J. Biomech.* 33, 317–325. doi:10.1016/s0021-9290(99)00210-9

Galvano, A., Scaturro, D., Badalamenti, G., Incorvaia, L., Rizzo, S., Castellana, L., et al. (2019). Denosumab for Bone Health in Prostate and Breast Cancer Patients Receiving Endocrine Therapy? A Systematic Review and a Meta-Analysis of Randomized Trials. *J. Bone Oncol.* 18, 100252. doi:10.1016/j.jbo.2019.100252

Gardinier, J. D., Al-Omaishi, S., Morris, M. D., and Kohn, D. H. (2016). PTH Signaling Mediates Perilacunar Remodeling during Exercise. *Matrix Biol.* 52-54, 162–175. doi:10.1016/j.matbio.2016.02.010

Gaur, T., Lengner, C. J., Hovhannisyan, H., Bhat, R. A., Bodine, P. V. N., Komm, B. S., et al. (2005). Canonical WNT Signaling Promotes Osteogenesis by Directly Stimulating Runx2 Gene Expression. *J. Biol. Chem.* 280, 33132–33140. doi:10.1074/jbc.m500608200

Genetos, D. C., Kephart, C. J., Zhang, Y., Yellowley, C. E., and Donahue, H. J. (2007). Oscillating Fluid Flow Activation of gap junction Hemichannels Induces Atp Release from MLO-Y4 Osteocytes. *J. Cel. Physiol.* 212, 207–214. doi:10.1002/jcp.21021

Geoghegan, I. P., Hoey, D. A., and McNamara, L. M. (2019). Integrins in Osteocyte Biology and Mechanotransduction. *Curr. Osteoporos. Rep.* 17, 195–206. doi:10.1007/s11914-019-00520-2

Gerbaix, M., Gnyubkin, V., Farlay, D., Olivier, C., Ammann, P., Courbon, G., et al. (2017). One-month Spaceflight Compromises the Bone Microstructure, Tissue-Level Mechanical Properties, Osteocyte Survival and Lacunae Volume in Mature Mice Skeletons. *Sci. Rep.* 7, 2659. doi:10.1038/s41598-017-03014-2

Gluhak-Heinrich, J., Pavlin, D., Yang, W., MacDougall, M., and Harris, S. E. (2007). MEPE Expression in Osteocytes during Orthodontic Tooth Movement. *Arch. Oral Biol.* 52, 684–690. doi:10.1016/j.archoralbio.2006.12.010

Goldring, S. R. (2015). The Osteocyte: Key Player in Regulating Bone Turnover. *RMD Open* 1, e000049. doi:10.1136/rmdopen-2015-000049

Gortazar, A. R., Martin-Millan, M., Bravo, B., Plotkin, L. I., and Bellido, T. (2013). Crosstalk between Caveolin-1/Extracellular Signal-Regulated Kinase (ERK) and β-Catenin Survival Pathways in Osteocyte Mechanotransduction. *J. Biol. Chem.* 288, 8168–8175. doi:10.1074/jbc.m112.437921

Govey, P. M., Jacobs, J. M., Tilton, S. C., Loiselle, A. E., Zhang, Y., Freeman, W. M., et al. (2014). Integrative Transcriptomic and Proteomic Analysis of Osteocytic Cells Exposed to Fluid Flow Reveals Novel Mechano-Sensitive Signaling Pathways. *J. Biomech.* 47, 1838–1845. doi:10.1016/j.jbiomech.2014.03.022

Govey, P. M., Kawasawa, Y. I., and Donahue, H. J. (2015). Mapping the Osteocytic Cell Response to Fluid Flow Using RNA-Seq. *J. Biomech.* 48, 4327–4332. doi:10.1016/j.jbiomech.2015.10.045

Guo, X., and Wang, X.-F. (2009). Signaling Cross-Talk between TGF-β/BMP and Other Pathways. *Cell Res.* 19, 71–88. doi:10.1038/cr.2008.302

Guo, Y.-C., and Yuan, Q. (2015). Fibroblast Growth Factor 23 and Bone Mineralisation. *Int. J. Oral Sci.* 7, 8–13. doi:10.1038/ijos.2015.1

Hagan, M. L., Yu, K., Zhu, J., Vinson, B. N., Roberts, R. L., Montesinos Cartagena, M., et al. (2020). Decreased Pericellular Matrix Production and Selection for Enhanced Cell Membrane Repair May Impair Osteocyte Responses to Mechanical Loading in the Aging Skeleton. *Aging Cell* 19, e13056. doi:10.1111/acel.13056

Han, Y., Cowin, S. C., Schaffler, M. B., and Weinbaum, S. (2004). Mechanotransduction and Strain Amplification in Osteocyte Cell Processes. *Proc. Natl. Acad. Sci.* 101, 16689–16694. doi:10.1073/pnas.0407429101

Harris, S. E., Gluhak-Heinrich, J., Harris, M. A., Yang, W., Bonewald, L. F., Riha, D., et al. (2007). DMP1 and MEPE Expression Are Elevated in Osteocytes after Mechanical Loading *In Vivo*: Theoretical Role in Controlling mineral Quality in the Perilacunar Matrix. *J. Musculoskelet. Neuronal Interact* 7, 313–315.

Hart, N. H., Nimphius, S., Rantalainen, T., Ireland, A., Siafarikas, A., and Newton, R. U. (2017). Mechanical Basis of Bone Strength: Influence of Bone Material, Bone Structure and Muscle Action. *J. Musculoskelet. Neuronal Interact* 17, 114–139.

Haugh, M. G., Vaughan, T. J., and McNamara, L. M. (2015). The Role of Integrin αVβ3 in Osteocyte Mechanotransduction. *J. Mech. Behav. Biomed. Mater.* 42, 67–75. doi:10.1016/j.jmbbm.2014.11.001

Hellmich, C., and Ulm, F.-J. (2002). Micromechanical Model for Ultrastructural Stiffness of Mineralized Tissues. *J. Eng. Mech.* 128, 898–908. doi:10.1061/(asce)0733-9399(2002)128:8(898)

Hemmatian, H., Bakker, A. D., Klein-Nulend, J., and van Lenthe, G. H. (2017). Aging, Osteocytes, and Mechanotransduction. *Curr. Osteoporos. Rep.* 15, 401–411. doi:10.1007/s11914-017-0402-z

Huang, C., Ling, R., Li, F.-J., Li, E.-C., Huang, Q.-K., Liu, B.-G., et al. (2016). FTY720 Enhances Osteogenic Differentiation of Bone Marrow Mesenchymal Stem Cells in Ovariectomized Rats. *Mol. Med. Rep.* 14, 927–935. doi:10.3892/mmr.2016.5342

Iolascon, G., Resmini, G., and Tarantino, U. (2013). Mechanobiology of Bone. *Aging Clin. Exp. Res.* 25 (Suppl. 1), S3–S7. doi:10.1007/s40520-013-0101-2

Jacobs, C. R., Temiyasathit, S., and Castillo, A. B. (2010). Osteocyte Mechanobiology and Pericellular Mechanics. *Annu. Rev. Biomed. Eng.* 12, 369–400. doi:10.1146/annurev-bioeng-070909-105302

Jähn, K., Kelkar, S., Zhao, H., Xie, Y., Tiede-Lewis, L. M., Dusevich, V., et al. (2017). 'Osteocytes Acidify Their Microenvironment in Response to PTHrP *In Vitro* and in Lactating Mice *In Vivo*. *J. Bone Miner. Res.* 32, 1761–1772.

Janssens, K., ten Dijke, P., Janssens, S., and Van Hul, W. (2005). Transforming Growth Factor-B1 to the Bone. *Endocr. Rev.* 26, 743–774. doi:10.1210/er.2004-0001

Jeyabalan, J., Shah, M., Viollet, B., and Chenu, C. (2012). AMP-activated Protein Kinase Pathway and Bone Metabolism. *J. Endocrinol.* 212, 277–290. doi:10.1530/joe-11-0306

Jiang, X., Savchenko, O., Li, Y., Qi, S., Yang, T., Zhang, W., et al. (2019). A Review of Low-Intensity Pulsed Ultrasound for Therapeutic Applications. *IEEE Trans. Biomed. Eng.* 66, 2704–2718. doi:10.1109/tbme.2018.2889669

Jilka, R. L., Noble, B., and Weinstein, R. S. (2013). Osteocyte Apoptosis. *Bone* 54, 264–271. doi:10.1016/j.bone.2012.11.038

Joeng, K. S., Lee, Y.-C., Lim, J., Chen, Y., Jiang, M.-M., Munivez, E., et al. (2017). Osteocyte-specific WNT1 Regulates Osteoblast Function during Bone Homeostasis. *J. Clin. Invest.* 127, 2678–2688. doi:10.1172/jci92617

Johnson, M. W. (1984). Behavior of Fluid in Stressed Bone and Cellular Stimulation. *Calcif. Tissue Int.* 36, S72–S76. doi:10.1007/bf02406137

Joldersma, M., Burger, E. H., Semeins, C. M., and Klein-Nulend, J. (2000). Mechanical Stress Induces COX-2 mRNA Expression in Bone Cells from Elderly Women. *J. Biomech.* 33, 53–61. doi:10.1016/s0021-9290(99)00172-4

Jones, S. J., Gray, C., Sakamaki, H., Arora, M., Boyde, A., Gourdie, R., et al. (1993). The Incidence and Size of gap Junctions between the Bone Cells in Rat Calvaria. *Anat. Embryol. (Berl)* 187, 343–352. doi:10.1007/BF00185892

Kamel, M. A., Picconi, J. L., Lara-Castillo, N., and Johnson, M. L. (2010). Activation of β-catenin Signaling in MLO-Y4 Osteocytic Cells versus 2T3 Osteoblastic Cells by Fluid Flow Shear Stress and PGE2: Implications for the Study of Mechanosensation in Bone. *Bone* 47, 872–881. doi:10.1016/j.bone.2010.08.007

Kamel-ElSayed, S. A., Tiede-Lewis, L. M., Lu, Y., Veno, P. A., and Dallas, S. L. (2015). Novel Approaches for Two and Three Dimensional Multiplexed Imaging of Osteocytes. *Bone* 76, 129–140. doi:10.1016/j.bone.2015.02.011

Karner, C. M., and Long, F. (2017). Wnt Signaling and Cellular Metabolism in Osteoblasts. *Cell. Mol. Life Sci.* 74, 1649–1657. doi:10.1007/s00018-016-2425-5

Kawata, A., and Mikuni-Takagaki, Y. (1998). Mechanotransduction in Stretched Osteocytes-Temporal Expression of Immediate Early and Other Genes. *Biochem. Biophys. Res. Commun.* 246 (2), 404–408. doi:10.1006/bbrc.1998.8632

Kearns, A. E., Khosla, S., and Kostenuik, P. J. (2008). Receptor Activator of Nuclear Factor κB Ligand and Osteoprotegerin Regulation of Bone Remodeling in Health and Disease. *Endocr. Rev.* 29, 155–192. doi:10.1210/er.2007-0014

Kegelman, C. D., Coulombe, J. C., Jordan, K. M., Horan, D. J., Qin, L., Robling, A. G., et al. (2020). YAP and TAZ Mediate Osteocyte Perilacunar/Canalicular Remodeling. *J. Bone Miner. Res.* 35, 196–210. doi:10.1002/jbmr.3876

Kinoshita, Y., and Fukumoto, S. (2018). X-linked Hypophosphatemia and FGF23-Related Hypophosphatemic Diseases: Prospect for New Treatment. *Endocr. Rev.* 39, 274–291. doi:10.1210/er.2017-00220

Kitase, Y., Barragan, L., Qing, H., Kondoh, S., Jiang, J. X., Johnson, M. L., et al. (2010). Mechanical Induction of PGE2 in Osteocytes Blocks Glucocorticoid-Induced Apoptosis through Both the β-catenin and PKA Pathways. *J. Bone Miner. Res.* 25, 2657–2668. doi:10.1002/jbmr.168

Klein-Nulend, J., Burger, E. H., Semeins, C. M., Raisz, L. G., and Pilbeam, C. C. (1997). Pulsating Fluid Flow Stimulates Prostaglandin Release and Inducible Prostaglandin G/H Synthase mRNA Expression in Primary Mouse Bone Cells. *J. Bone Miner. Res.* 12, 45–51. doi:10.1359/jbmr.1997.12.1.45

Kogawa, M., Khalid, K. A., Wijenayaka, A. R., Ormsby, R. T., Evdokiou, A., Anderson, P. H., et al. (2018). Recombinant Sclerostin Antagonizes Effects of *Ex Vivo* Mechanical Loading in Trabecular Bone and Increases Osteocyte Lacunar Size. *Am. J. Physiology-Cell Physiol.* 314, C53–c61. doi:10.1152/ajpcell.00175.2017

Kogawa, M., Wijenayaka, A. R., Ormsby, R. T., Thomas, G. P., Anderson, P. H., Bonewald, L. F., et al. (2013). Sclerostin Regulates Release of Bone mineral by Osteocytes by Induction of Carbonic Anhydrase 2. *J. Bone Miner. Res.* 28, 2436–2448. doi:10.1002/jbmr.2003

Kohn, D. H., Sahar, N. D., Wallace, J. M., Golcuk, K., and Morris, M. D. (2009). Exercise Alters Mineral and Matrix Composition in the Absence of Adding New Bone. *Cells Tissues Organs* 189, 33–37. doi:10.1159/000151452

Komaba, H. (2018). Energy Sensor as a New Regulator of FGF23 Synthesis. *Kidney Int.* 94, 453–455. doi:10.1016/j.kint.2018.05.008

Krajisnik, T., Björklund, P., Marsell, R., Ljunggren, O., Akerström, G., Jonsson, K. B., et al. (2007). Fibroblast Growth Factor-23 Regulates Parathyroid Hormone and 1α-Hydroxylase Expression in Cultured Bovine Parathyroid Cells. *J. Endocrinol.* 195, 125–131. doi:10.1677/joe-07-0267

Kulkarni, R. N., Bakker, A. D., Everts, V., and Klein-Nulend, J. (2010). Inhibition of Osteoclastogenesis by Mechanically Loaded Osteocytes: Involvement of MEPE. *Calcif. Tissue Int.* 87, 461–468. doi:10.1007/s00223-010-9407-7

Langhans, S. A. (2018). Three-Dimensional *In Vitro* Cell Culture Models in Drug Discovery and Drug Repositioning. *Front. Pharmacol.* 9, 6. doi:10.3389/fphar.2018.00006

Leder, B. Z. (2017). Parathyroid Hormone and Parathyroid Hormone-Related Protein Analogs in Osteoporosis Therapy. *Curr. Osteoporos. Rep.* 15, 110–119. doi:10.1007/s11914-017-0353-4

Lee, S. H., Lee, S.-Y., Lee, Y.-S., Kim, B.-J., Lim, K.-H., Cho, E.-H., et al. (2012). Higher Circulating Sphingosine 1-Phosphate Levels Are Associated with Lower Bone Mineral Density and Higher Bone Resorption Marker in Humans. *J. Clin. Endocrinol. Metab.* 97, E1421–E1428. doi:10.1210/jc.2012-1044

Lewiecki, E. M. (2010). Bisphosphonates for the Treatment of Osteoporosis: Insights for Clinicians. *Ther. Adv. Chronic Dis.* 1, 115–128. doi:10.1177/2040622310374783

Li, J., Liu, D., Ke, H. Z., Duncan, R. L., and Turner, C. H. (2005). The P2X7 Nucleotide Receptor Mediates Skeletal Mechanotransduction. *J. Biol. Chem.* 280, 42952–42959. doi:10.1074/jbc.m506415200

Li, J., Rose, E., Frances, D., Sun, Y., and You, L. (2012). Effect of Oscillating Fluid Flow Stimulation on Osteocyte mRNA Expression. *J. Biomech.* 45, 247–251. doi:10.1016/j.jbiomech.2011.10.037

Li, J., Sarosi, I., Cattley, R. C., Pretorius, J., Asuncion, F., Grisanti, M., et al. (2006). Dkk1-mediated Inhibition of Wnt Signaling in Bone Results in Osteopenia. *Bone* 39, 754–766. doi:10.1016/j.bone.2006.03.017

Li, L., Lu, H., Zhao, Y., Luo, J., Yang, L., Liu, W., et al. (2019a). Functionalized Cell-free Scaffolds for Bone Defect Repair Inspired by Self-Healing of Bone Fractures: A Review and New Perspectives. *Mater. Sci. Eng. C* 98, 1241–1251. doi:10.1016/j.msec.2019.01.075

Li, M. C. M., Chow, S. K. H., Wong, R. M. Y., Qin, L., and Cheung, W. H. (2021). The Role of Osteocytes-specific Molecular Mechanism in Regulation of Mechanotransduction - A Systematic Review. *J. Orthopaedic Translation* 29, 1–9. doi:10.1016/j.jot.2021.04.005

Li, X., Han, L., Nookaew, I., Mannen, E., Silva, M. J., Almeida, M., et al. (2019b). 'Stimulation of Piezo1 by Mechanical Signals Promotes Bone Anabolism. *Elife* 8, 1. doi:10.7554/elife.49631

Liedert, A., Kaspar, D., Augat, P., Ignatius, A., and Claes, L. (2005). "Mechanobiology of Bone Tissue and Bone Cells," in *Mechanosensitivity in Cells and Tissues*. Editors A. Kamkin and I. Kiseleva (Moscow: Academia Publishing House Ltd.).

Lim, J., Grafe, I., Alexander, S., and Lee, B. (2017). Genetic Causes and Mechanisms of Osteogenesis Imperfecta. *Bone* 102, 40–49. doi:10.1016/j.bone.2017.02.004

Lin, X., Patil, S., Gao, Y.-G., and Qian, A. (2020). The Bone Extracellular Matrix in Bone Formation and Regeneration. *Front. Pharmacol.* 11, 757. doi:10.3389/fphar.2020.00757

Litzenberger, J. B., Kim, J.-B., Tummala, P., and Jacobs, C. R. (2010). β1 Integrins Mediate Mechanosensitive Signaling Pathways in Osteocytes. *Calcif. Tissue Int.* 86, 325–332. doi:10.1007/s00223-010-9343-6

Litzenberger, J. B., Tang, W. J., Castillo, A. B., and Jacobs, C. R. (2009). Deletion of β1 Integrins from Cortical Osteocytes Reduces Load-Induced Bone Formation. *Cel. Mol. Bioeng.* 2, 416–424. doi:10.1007/s12195-009-0068-4

Lotinun, S., Ishihara, Y., Nagano, K., Kiviranta, R., Carpentier, V. T., Neff, L., et al. (2019). Cathepsin K-Deficient Osteocytes Prevent Lactation-Induced Bone Loss and Parathyroid Hormone Suppression. *J. Clin. Invest.* 129, 3058–3071. doi:10.1172/jci122936

Lu, J., Wang, M., Wang, Z., Fu, Z., Lu, A., and Zhang, G. (2018). Advances in the Discovery of Cathepsin K Inhibitors on Bone Resorption. *J. Enzyme Inhib. Med. Chem.* 33, 890–904. doi:10.1080/14756366.2018.1465417

Lu, X. L., Huo, B., Chiang, V., and Guo, X. E. (2012). Osteocytic Network Is More Responsive in Calcium Signaling Than Osteoblastic Network under Fluid Flow. *J. Bone Miner. Res.* 27, 563–574. doi:10.1002/jbmr.1474

Lyons, F. G., Al-Munajjed, A. A., Kieran, S. M., Toner, M. E., Murphy, C. M., Duffy, G. P., et al. (2010). The Healing of Bony Defects by Cell-free Collagen-Based Scaffolds Compared to Stem Cell-Seeded Tissue Engineered Constructs. *Biomaterials* 31, 9232–9243. doi:10.1016/j.biomaterials.2010.08.056

Ma, Y.-L., Dai, R.-C., Sheng, Z.-F., Jin, Y., Zhang, Y.-H., Fang, L.-N., et al. (2008). Quantitative Associations between Osteocyte Density and Biomechanics, Microcrack and Microstructure in OVX Rats Vertebral Trabeculae. *J. Biomech.* 41, 1324–1332. doi:10.1016/j.jbiomech.2008.01.017

MacNabb, C., Patton, D., and Hayes, J. S. (20162016). Sclerostin Antibody Therapy for the Treatment of Osteoporosis: Clinical Prospects and Challenges. *J. Osteoporos.* 2016, 6217286. doi:10.1155/2016/6217286

Manolagas, S. C., and Almeida, M. (2007). Gone with the Wnts: β-Catenin, T-Cell Factor, Forkhead Box O, and Oxidative Stress in Age-dependent Diseases of Bone, Lipid, and Glucose Metabolism. *Mol. Endocrinol.* 21, 2605–2614. doi:10.1210/me.2007-0259

Marahleh, A., Kitaura, H., Ohori, F., Kishikawa, A., Ogawa, S., Shen, W.-R., et al. (2019). TNF-α Directly Enhances Osteocyte RANKL Expression and Promotes Osteoclast Formation. *Front. Immunol.* 10, 2925. doi:10.3389/fimmu.2019.02925

Martin, A. (2019). Bone and Heart Health in Chronic Kidney Disease. *Curr. Opin. Nephrol. Hypertens.* 28, 297–303. doi:10.1097/mnh.0000000000000512

Martin, A., David, V., and Quarles, L. D. (2012). Regulation and Function of the FGF23/Klotho Endocrine Pathways. *Physiol. Rev.* 92, 131–155. doi:10.1152/physrev.00002.2011

Maycas, M., Ardura, J. A., de Castro, L. F., Bravo, B., Gortázar, A. R., and Esbrit, P. (2015). Role of the Parathyroid Hormone Type 1 Receptor (PTH1R) as a Mechanosensor in Osteocyte Survival. *J. Bone Miner. Res.* 30 (7), 1231–1244. doi:10.1002/jbmr.2439

McClung, M. R., Brown, J. P., Diez-Perez, A., Resch, H., Caminis, J., Meisner, P., et al. (2018). Effects of 24 Months of Treatment with Romosozumab Followed by 12 Months of Denosumab or Placebo in Postmenopausal Women with Low Bone Mineral Density: A Randomized, Double-Blind, Phase 2, Parallel Group Study. *J. Bone Miner. Res.* 33, 1397–1406. doi:10.1002/jbmr.3452

McClung, M. R. (2017). Sclerostin Antibodies in Osteoporosis: Latest Evidence and Therapeutic Potential. *Ther. Adv. Musculoskelet.* 9, 263–270. doi:10.1177/1759720x17726744

McCreadie, B. R., and Hollister, S. J. (1997). Strain Concentrations Surrounding an Ellipsoid Model of Lacunae and Osteocytes. *Computer Methods Biomech. Biomed. Eng.* 1, 61–68. doi:10.1080/01495739708936695

McCutcheon, S., Majeska, R. J., Spray, D. C., Schaffler, M. B., and Vazquez, M. (2020). Apoptotic Osteocytes Induce RANKL Production in Bystanders via Purinergic Signaling and Activation of Pannexin Channels. *J. Bone Miner. Res.* 35, 966–977. doi:10.1002/jbmr.3954

McGarry, J. G., Klein-Nulend, J., and Prendergast, P. J. (2005). The Effect of Cytoskeletal Disruption on Pulsatile Fluid Flow-Induced Nitric Oxide and Prostaglandin E2 Release in Osteocytes and Osteoblasts. *Biochem. Biophysical Res. Commun.* 330, 341–348. doi:10.1016/j.bbrc.2005.02.175

McNamara, L. M., Majeska, R. J., Weinbaum, S., Friedrich, V., and Schaffler, M. B. (2009). Attachment of Osteocyte Cell Processes to the Bone Matrix. *Anat. Rec.* 292, 355–363. doi:10.1002/ar.20869

Merlotti, D., Gennari, L., Martini, G., Valleggi, F., De Paola, V., Avanzati, A., et al. (2007). Comparison of Different Intravenous Bisphosphonate Regimens for Paget's Disease of Bone. *J. Bone Miner. Res.* 22, 1510–1517. doi:10.1359/jbmr.070704

Meshcheryakova, A., Mechtcheriakova, D., and Pietschmann, P. (2017). Sphingosine 1-phosphate Signaling in Bone Remodeling: Multifaceted Roles and Therapeutic Potential. *Expert Opin. Ther. Targets* 21, 725–737. doi:10.1080/14728222.2017.1332180

Metz, L. N., Martin, R. B., and Turner, A. S. (2003). Histomorphometric Analysis of the Effects of Osteocyte Density on Osteonal Morphology and Remodeling. *Bone* 33, 753–759. doi:10.1016/s8756-3282(03)00245-x

Mirza, M. A. I., Larsson, A., Lind, L., and Larsson, T. E. (2009). Circulating Fibroblast Growth Factor-23 Is Associated with Vascular Dysfunction in the Community. *Atherosclerosis* 205, 385–390. doi:10.1016/j.atherosclerosis.2009.01.001

Monteiro, D. A., Dole, N. S., Campos, J. L., Kaya, S., Schurman, C. A., Belair, C. D., et al. (2021). 'Fluid Shear Stress Generates a Unique Signaling Response by Activating Multiple TGFβ Family Type I Receptors in Osteocytes. *Faseb j* 35, e21263. doi:10.1096/fj.202001998r

Morello, R. (2018). Osteogenesis Imperfecta and Therapeutics. *Matrix Biol.* 71-72, 294–312. doi:10.1016/j.matbio.2018.03.010

Morrell, A. E., Brown, G. N., Robinson, S. T., Sattler, R. L., Baik, A. D., Zhen, G., et al. (2018). Mechanically Induced Ca2+ Oscillations in Osteocytes Release Extracellular Vesicles and Enhance Bone Formation. *Bone Res.* 6, 6. doi:10.1038/s41413-018-0007-x

Morrell, A. E., Robinson, S. T., Ke, H. Z., Holdsworth, G., and Guo, X. E. (2021). Osteocyte Mechanosensing Following Short-Term and Long-Term Treatment with Sclerostin Antibody. *Bone* 149, 115967. doi:10.1016/j.bone.2021.115967

Murali, S. K., Andrukhova, O., Clinkenbeard, E. L., White, K. E., and Erben, R. G. (2016). Excessive Osteocytic Fgf23 Secretion Contributes to Pyrophosphate

Accumulation and Mineralization Defect in Hyp Mice. *Plos Biol.* 14, e1002427. doi:10.1371/journal.pbio.1002427

Nakamura, H., Kenmotsu, S.-i., Sakai, H., and Ozawa, H. (1995). Localization of CD44, the Hyaluronate Receptor; on the Plasma Membrane of Osteocytes and Osteoclasts in Rat Tibiae. *Cell Tissue Res.* 280, 225–233. doi:10.1007/bf00307793

Nakano, Y., Toyosawa, S., and Takano, Y. (2004). Eccentric Localization of Osteocytes Expressing Enzymatic Activities, Protein, and mRNA Signals for Type 5 Tartrate-Resistant Acid Phosphatase (TRAP). *J. Histochem. Cytochem.* 52, 1475–1482. doi:10.1369/jhc.4a6378.2004

Nguyen, J., Tang, S. Y., Nguyen, D., and Alliston, T. (2013). Load Regulates Bone Formation and Sclerostin Expression through a TGFβ-dependent Mechanism. *PLoS One* 8, e53813. doi:10.1371/journal.pone.0053813

Nicolella, D. P., Moravits, D. E., Gale, A. M., Bonewald, L. F., Gale, A. M., Bonewald, L. F., et al. (2006). Osteocyte Lacunae Tissue Strain in Cortical Bone. *J. Biomech.* 39, 1735–1743. doi:10.1016/j.jbiomech.2005.04.032

Nicolella, D. P., Nicholls, A. E., Lankford, J., and Davy, D. T. (2001). Machine Vision Photogrammetry: a Technique for Measurement of Microstructural Strain in Cortical Bone. *J. Biomech.* 34, 135–139. doi:10.1016/s0021-9290(00)00163-9

Noonan, K. J., Stevens, J. W., Tammi, R., Tammi, M., Hernandez, J. A., and Midura, R. J. (1996). Spatial Distribution of CD44 and Hyaluronan in the Proximal Tibia of the Growing Rat. *J. Orthop. Res.* 14, 573–581. doi:10.1002/jor.1100140411

Ominsky, M. S., Li, C., Li, X., Tan, H. L., Lee, E., Barrero, M., et al. (2011). Inhibition of Sclerostin by Monoclonal Antibody Enhances Bone Healing and Improves Bone Density and Strength of Nonfractured Bones. *J. Bone Miner. Res.* 26, 1012–1021. doi:10.1002/jbmr.307

Osterhoff, G., Morgan, E. F., Shefelbine, S. J., Karim, L., McNamara, L. M., and Augat, P. (2016). Bone Mechanical Properties and Changes with Osteoporosis. *Injury* 47 (Suppl. 2), S11–S20. doi:10.1016/s0020-1383(16)47003-8

Pajevic, P., Spatz, J., Garr, J., Adamson, C., and Misener, L. (2013). Osteocyte Biology and Space Flight. *Cbiot* 2, 179–183. doi:10.2174/2211550113029990017

Palumbo, C., Palazzini, S., and Marotti, G. (1990). Morphological Study of Intercellular Junctions during Osteocyte Differentiation. *Bone* 11, 401–406. doi:10.1016/8756-3282(90)90134-k

Pathak, J. L., Bravenboer, N., and Klein-Nulend, J. (2020). The Osteocyte as the New Discovery of Therapeutic Options in Rare Bone Diseases. *Front. Endocrinol.* 11, 405. doi:10.3389/fendo.2020.00405

Pathak, J. L., Bravenboer, N., Luyten, F. P., Verschueren, P., Lems, W. F., Klein-Nulend, J., et al. (2015). Mechanical Loading Reduces Inflammation-Induced Human Osteocyte-To-Osteoclast Communication. *Calcif. Tissue Int.* 97, 169–178. doi:10.1007/s00223-015-9999-z

Pittenger, M. F., Mackay, A. M., Beck, S. C., Jaiswal, R. K., Douglas, R., Mosca, J. D., et al. (1999). Multilineage Potential of Adult Human Mesenchymal Stem Cells. *Science* 284, 143–147. doi:10.1126/science.284.5411.143

Plotkin, L. I., and Bellido, T. (2013). Beyond gap Junctions: Connexin43 and Bone Cell Signaling. *Bone* 52, 157–166. doi:10.1016/j.bone.2012.09.030

Plotkin, L. I., Mathov, I., Aguirre, J. I., Parfitt, A. M., Manolagas, S. C., and Bellido, T. (2005). Mechanical Stimulation Prevents Osteocyte Apoptosis: Requirement of Integrins, Src Kinases, and ERKs. *Am. J. Physiology-Cell Physiol.* 289, C633–C643. doi:10.1152/ajpcell.00278.2004

Plotkin, L. I., Weinstein, R. S., Parfitt, A. M., Roberson, P. K., Manolagas, S. C., and Bellido, T. (1999). Prevention of Osteocyte and Osteoblast Apoptosis by Bisphosphonates and Calcitonin. *J. Clin. Invest.* 104, 1363–1374. doi:10.1172/jci6800

Portal-Núñez, S., de la Fuente, M., Díez, A., and Esbrit, P. (2016). Oxidative Stress as a Possible Therapeutic Target for Osteoporosis Associated with Ageing. *Rev. Osteoporos. Metab. Miner.* 8, 138–146.

Prideaux, M., Findlay, D. M., and Atkins, G. J. (2016). Osteocytes: The Master Cells in Bone Remodelling. *Curr. Opin. Pharmacol.* 28, 24–30. doi:10.1016/j.coph.2016.02.003

Qin, L., Liu, W., Cao, H., and Xiao, G. (2020). Molecular Mechanosensors in Osteocytes. *Bone Res.* 8, 23. doi:10.1038/s41413-020-0099-y

Qing, H., Ardeshirpour, L., Divieti Pajevic, P., Dusevich, V., Jähn, K., Kato, S., et al. (2012). Demonstration of Osteocytic Perilacunar/canalicular Remodeling in Mice during Lactation. *J. Bone Miner. Res.* 27, 1018–1029. doi:10.1002/jbmr.1567

Qing, H., and Bonewald, L. F. (2009). Osteocyte Remodeling of the Perilacunar and Pericanalicular Matrix. *Int. J. Oral Sci.* 1, 59–65. doi:10.4248/ijos.09019

Qiu, S., Rao, D. S., Palnitkar, S., and Parfitt, A. M. (2002). Age and Distance from the Surface but Not Menopause Reduce Osteocyte Density in Human Cancellous Bone. *Bone* 31, 313–318. doi:10.1016/s8756-3282(02)00819-0

Ramesh, N., Moratti, S. C., and Dias, G. J. (2018). Hydroxyapatite-polymer Biocomposites for Bone Regeneration: A Review of Current Trends. *J. Biomed. Mater. Res.* 106, 2046–2057. doi:10.1002/jbm.b.33950

Rath Bonivtch, A., Bonewald, L. F., and Nicolella, D. P. (2007). Tissue Strain Amplification at the Osteocyte Lacuna: A Microstructural Finite Element Analysis. *J. Biomech.* 40, 2199–2206. doi:10.1016/j.jbiomech.2006.10.040

Recknor, C. P., Recker, R. R., Benson, C. T., Robins, D. A., Chiang, A. Y., Alam, J., et al. (2015). The Effect of Discontinuing Treatment with Blosozumab: Follow-up Results of a Phase 2 Randomized Clinical Trial in Postmenopausal Women with Low Bone Mineral Density. *J. Bone Miner. Res.* 30, 1717–1725. doi:10.1002/jbmr.2489

Reilly, G. C., Haut, T. R., Yellowley, C. E., Donahue, H. J., and Jacobs, C. R. (2003). Fluid Flow Induced PGE2 Release by Bone Cells Is Reduced by Glycocalyx Degradation whereas Calcium Signals Are Not. *Biorheology* 40, 591–603.

Riquelme, M. A., Gu, S., Hua, R., and Jiang, J. X. (2021). Mechanotransduction via the Coordinated Actions of Integrins, PI3K Signaling and Connexin Hemichannels. *Bone Res.* 9, 8. doi:10.1038/s41413-020-00126-w

Riquelme, M. A., and Jiang, J. X. (2013). Elevated Intracellular Ca2+ Signals by Oxidative Stress Activate Connexin 43 Hemichannels in Osteocytes. *Bone Res.* 1, 355–361. doi:10.4248/br201304006

Rivadeneira, F., and Mäkitie, O. (2016). Osteoporosis and Bone Mass Disorders: From Gene Pathways to Treatments. *Trends Endocrinol. Metab.* 27, 262–281. doi:10.1016/j.tem.2016.03.006

Robling, A. G., and Turner, C. H. (2009). Mechanical Signaling for Bone Modeling and Remodeling. *Crit. Rev. Eukar Gene Expr.* 19, 319–338. doi:10.1615/critreveukargeneexpr.v19.i4.50

Rochefort, G. Y. (2014). The Osteocyte as a Therapeutic Target in the Treatment of Osteoporosis. *Ther. Adv. Musculoskelet.* 6, 79–91. doi:10.1177/1759720x14523500

Ru, J.-y., and Wang, Y.-f. (2020). Osteocyte Apoptosis: the Roles and Key Molecular Mechanisms in Resorption-Related Bone Diseases. *Cell Death Dis.* 11, 846. doi:10.1038/s41419-020-03059-8

Rubin, C. T., and Lanyon, L. E. (1984). Regulation of Bone Formation by Applied Dynamic Loads. *J. Bone Jt. Surg.* 66, 397–402. doi:10.2106/00004623-198466030-00012

Rys, J. P., Monteiro, D. A., and Alliston, T. (2016). Mechanobiology of TGFβ Signaling in the Skeleton. *Matrix Biol.* 52-54, 413–425. doi:10.1016/j.matbio.2016.02.002

Sandilos, J. K., Chiu, Y.-H., Chekeni, F. B., Armstrong, A. J., Walk, S. F., Ravichandran, K. S., et al. (2012). Pannexin 1, an ATP Release Channel, Is Activated by Caspase Cleavage of its Pore-Associated C-Terminal Autoinhibitory Region. *J. Biol. Chem.* 287, 11303–11311. doi:10.1074/jbc.m111.323378

Satir, P., Pedersen, L. B., and Christensen, S. T. (2010). The Primary Cilium at a Glance. *J. Cel. Sci.* 123, 499–503. doi:10.1242/jcs.050377

Sato, T., Verma, S., Andrade, C. D. C., Omeara, M., Campbell, N., Wang, J. S., et al. (2020). A FAK/HDAC5 Signaling axis Controls Osteocyte Mechanotransduction. *Nat. Commun.* 11, 3282. doi:10.1038/s41467-020-17099-3

Sauren, Y. M. H. F., Mieremet, R. H. P., Groot, C. G., and Scherft, J. P. (1992). An Electron Microscopic Study on the Presence of Proteoglycans in the Mineralized Matrix of Rat and Human Compact Lamellar Bone. *Anat. Rec.* 232, 36–44. doi:10.1002/ar.1092320105

Schaffler, M. B., Cheung, W.-Y., Majeska, R., and Kennedy, O. (2014). Osteocytes: Master Orchestrators of Bone. *Calcif. Tissue Int.* 94, 5–24. doi:10.1007/s00223-013-9790-y

Schaffler, M. B., and Kennedy, O. D. (2012). Osteocyte Signaling in Bone. *Curr. Osteoporos. Rep.* 10, 118–125. doi:10.1007/s11914-012-0105-4

Schurman, C. A., Verbruggen, S. W., and Alliston, T. (2021). Disrupted Osteocyte Connectivity and Pericellular Fluid Flow in Bone with Aging and Defective

TGF-β Signaling. *Proc. Natl. Acad. Sci. U S A.* 118, 1. doi:10.1073/pnas.2023999118

Scialla, J. J., Xie, H., Rahman, M., Anderson, A. H., Isakova, T., Ojo, A., et al. (2014). Fibroblast Growth Factor-23 and Cardiovascular Events in CKD. *Jasn* 25, 349–360. doi:10.1681/asn.2013050465

Sebastian, A., and Loots, G. G. (2018). Genetics of Sost/SOST in Sclerosteosis and Van Buchem Disease Animal Models. *Metabolism* 80, 38–47. doi:10.1016/j.metabol.2017.10.005

Seref-Ferlengez, Z., Urban-Maldonado, M., Sun, H. B., Schaffler, M. B., Suadicani, S. O., and Thi, M. M. (2019). Role of Pannexin 1 Channels in Load-Induced Skeletal Response. *Ann. N. Y Acad. Sci.* 1442, 79–90. doi:10.1111/nyas.13914

Shah, F. A., Thomsen, P., and Palmquist, A. (2018). A Review of the Impact of Implant Biomaterials on Osteocytes. *J. Dent. Res.* 97, 977–986. doi:10.1177/0022034518778033

Shakeri, A., and Adanty, C. (2020). Romosozumab (Sclerostin Monoclonal Antibody) for the Treatment of Osteoporosis in Postmenopausal Women: A Review. *jptcp* 27, e25–e31. doi:10.15586/jptcp.v27i1.655

Shekaran, A., Shoemaker, J. T., Kavanaugh, T. E., Lin, A. S., LaPlaca, M. C., Fan, Y., et al. (2014). The Effect of Conditional Inactivation of Beta 1 Integrins Using Twist 2 Cre, Osterix Cre and Osteocalcin Cre Lines on Skeletal Phenotype. *Bone* 68, 131–141. doi:10.1016/j.bone.2014.08.008

Sims, N. A. (2016). Senescent Osteocytes: Do They Cause Damage and Can They Be Targeted to Preserve the Skeleton? *J. Bone Miner. Res.* 31, 1917–1919. doi:10.1002/jbmr.2994

Spatz, J. M., Wein, M. N., Gooi, J. H., Qu, Y., Garr, J. L., Liu, S., et al. (2015). The Wnt Inhibitor Sclerostin Is Up-Regulated by Mechanical Unloading in Osteocytes *In Vitro*. *J. Biol. Chem.* 290, 16744–16758. doi:10.1074/jbc.m114.628313

Sroga, G. E., and Vashishth, D. (2012). Effects of Bone Matrix Proteins on Fracture and Fragility in Osteoporosis. *Curr. Osteoporos. Rep.* 10, 141–150. doi:10.1007/s11914-012-0103-6

Stavnichuk, M., Mikolajewicz, N., Corlett, T., Morris, M., and Komarova, S. V. (2020). A Systematic Review and Meta-Analysis of Bone Loss in Space Travelers. *Npj Microgravity* 6, 13. doi:10.1038/s41526-020-0103-2

Sterck, J. G. H., Klein-Nulend, J., Lips, P., and Burger, E. H. (1998). Response of normal and Osteoporotic Human Bone Cells to Mechanical Stress *In Vitro*. *Am. J. Physiology-Endocrinology Metab.* 274, E1113–E1120. doi:10.1152/ajpendo.1998.274.6.e1113

Sudo, K., Kanno, M., Miharada, K., Ogawa, S., Hiroyama, T., Saijo, K., et al. (2007). Mesenchymal Progenitors Able to Differentiate into Osteogenic, Chondrogenic, And/or Adipogenic Cells *In Vitro* Are Present in Most Primary Fibroblast-Like Cell Populations. *Stem Cells* 25, 1610–1617. doi:10.1634/stemcells.2006-0504

Suen, P. K., and Qin, L. (2016). Sclerostin, an Emerging Therapeutic Target for Treating Osteoporosis and Osteoporotic Fracture: A General Review. *J. Orthopaedic Translation* 4, 1–13. doi:10.1016/j.jot.2015.08.004

Sun, N., Uda, Y., Azab, E., Kochen, A., Santos, R. N. C. E., Shi, C., et al. (2019). Effects of Histone Deacetylase Inhibitor Scriptaid and Parathyroid Hormone on Osteocyte Functions and Metabolism. *J. Biol. Chem.* 294, 9722–9733. doi:10.1074/jbc.ra118.007312

Takata, S., Yonezu, H., Shibata, A., Enishi, T., Sato, N., Takahashi, M., et al. (2011). Mineral to Matrix Ratio Determines Biomaterial and Biomechanical Properties of Rat Femur -application of Fourier Transform Infrared Spectroscopy-. *J. Med. Invest.* 58, 197–202. doi:10.2152/jmi.58.197

Tanaka, M., Hashimoto, Y., Hasegawa, C., Deacon, S., and Eastell, R. (2017). Antiresorptive Effect of a Cathepsin K Inhibitor ONO-5334 and its Relationship to BMD Increase in a Phase II Trial for Postmenopausal Osteoporosis. *BMC Musculoskelet. Disord.* 18, 267. doi:10.1186/s12891-017-1625-y

Tavafoghi, M., and Cerruti, M. (2016). The Role of Amino Acids in Hydroxyapatite Mineralization. *J. R. Soc. Interf.* 13. doi:10.1098/rsif.2016.0462

Temiyasathit, S., and Jacobs, C. R. (2010). Osteocyte Primary Cilium and its Role in Bone Mechanotransduction. *Ann. N. Y Acad. Sci.* 1192, 422–428. doi:10.1111/j.1749-6632.2009.05243.x

Temiyasathit, S., Tang, W. J., Leucht, P., Anderson, C. T., Monica, S. D., Castillo, A. B., et al. (2012). Mechanosensing by the Primary Cilium: Deletion of Kif3A Reduces Bone Formation Due to Loading. *PLoS One* 7, e33368. doi:10.1371/journal.pone.0033368

Termine, J. D., Kleinman, H. K., Whitson, S. W., Conn, K. M., McGarvey, M. L., and Martin, G. R. (1981). Osteonectin, a Bone-specific Protein Linking mineral to Collagen. *Cell* 26, 99–105. doi:10.1016/0092-8674(81)90037-4

Teti, A., and Zallone, A. (2009). Do osteocytes Contribute to Bone mineral Homeostasis? Osteocytic Osteolysis Revisited. *Bone* 44, 11–16. doi:10.1016/j.bone.2008.09.017

Thi, M. M., Suadicani, S. O., Schaffler, M. B., Weinbaum, S., and Spray, D. C. (2013). Mechanosensory Responses of Osteocytes to Physiological Forces Occur along Processes and Not Cell Body and Require V 3 Integrin. *Proc. Natl. Acad. Sci.* 110, 21012–21017. doi:10.1073/pnas.1321210110

Thompson, W. R., Majid, A. S., Czymmek, K. J., Ruff, A. L., García, J., Duncan, R. L., et al. (2011a). Association of the α2δ1 Subunit with Cav3.2 Enhances Membrane Expression and Regulates Mechanically Induced ATP Release in MLO-Y4 Osteocytes. *J. Bone Miner. Res.* 26, 2125–2139. doi:10.1002/jbmr.437

Thompson, W. R., Modla, S., Grindel, B. J., Czymmek, K. J., Kirn-Safran, C. B., Wang, L., et al. (2011b). Perlecan/Hspg2 Deficiency Alters the Pericellular Space of the Lacunocanalicular System Surrounding Osteocytic Processes in Cortical Bone. *J. Bone Miner. Res.* 26, 618–629. doi:10.1002/jbmr.236

Thompson, W. R., Scott, A., Loghmani, M. T., Ward, S. R., and Warden, S. J. (2016). Understanding Mechanobiology: Physical Therapists as a Force in Mechanotherapy and Musculoskeletal Regenerative Rehabilitation. *Phys. Ther.* 96, 560–569. doi:10.2522/ptj.20150224

Thompson, W. R., Yen, S. S., and Rubin, J. (2014). Vibration Therapy. *Curr. Opin. Endocrinol. Diabetes Obes.* 21, 447–453. doi:10.1097/med.0000000000000111

Thuy, A. V., Reimann, C.-M., Hemdan, N. Y. A., and Gräler, M. H. (2014). Sphingosine 1-Phosphate in Blood: Function, Metabolism, and Fate. *Cell Physiol. Biochem.* 34, 158–171. doi:10.1159/000362992

Tian, J., Ma, S., Xie, W.-Q., Zhang, Y.-M., Tao, L., Li, Y.-S., et al. (2021). Sphingosine 1-phosphate and Osteoporosis: Pathophysiology and Therapeutic Aspects-A Narrative Review. *Ann. Palliat. Med.* 10, 4799–4805. doi:10.21037/apm-20-1255

Tomkinson, A., Gevers, E. F., Wit, J. M., Reeve, J., and Noble, B. S. (1998). The Role of Estrogen in the Control of Rat Osteocyte Apoptosis. *J. Bone Miner. Res.* 13, 1243–1250. doi:10.1359/jbmr.1998.13.8.1243

Tong, X., Zhang, C., Wang, D., Song, R., Ma, Y., Cao, Y., et al. (2020). Suppression of AMP-Activated Protein Kinase Reverses Osteoprotegerin-Induced Inhibition of Osteoclast Differentiation by Reducing Autophagy. *Cell Prolif.* 53, e12714. doi:10.1111/cpr.12714

Tsourdi, E., Jähn, K., Rauner, M., Busse, B., and Bonewald, L. F. (2018). Physiological and Pathological Osteocytic Osteolysis. *J. Musculoskelet. Neuronal Interact* 18, 292–303.

Tu, X., Delgado-Calle, J., Condon, K. W., Maycas, M., Zhang, H., Carlesso, N., et al. (2015). Osteocytes Mediate the Anabolic Actions of Canonical Wnt/β-Catenin Signaling in Bone. *Proc. Natl. Acad. Sci. USA* 112, E478–E486. doi:10.1073/pnas.1409857112

van Tol, A. F., Schemenz, V., Wagermaier, W., Roschger, A., Razi, H., Vitienes, I., et al. (2020). The Mechanoresponse of Bone Is Closely Related to the Osteocyte Lacunocanalicular Network Architecture. *Proc. Natl. Acad. Sci. USA* 117, 32251–32259. doi:10.1073/pnas.2011504117

Verborgt, O., Gibson, G. J., and Schaffler, M. B. (2000). Loss of Osteocyte Integrity in Association with Microdamage and Bone Remodeling after Fatigue *In Vivo*. *J. Bone Miner. Res.* 15, 60–67. doi:10.1359/jbmr.2000.15.1.60

Verbruggen, S. W., Mc Garrigle, M. J., Haugh, M. G., Voisin, M. C., and McNamara, L. M. (2015). Altered Mechanical Environment of Bone Cells in an Animal Model of Short- and Long-Term Osteoporosis. *Biophysical J.* 108, 1587–1598. doi:10.1016/j.bpj.2015.02.031

Verbruggen, S. W., Vaughan, T. J., and McNamara, L. M. (2012). Strain Amplification in Bone Mechanobiology: a Computational Investigation of the *In Vivo* Mechanics of Osteocytes. *J. R. Soc. Interf.* 9, 2735–2744. doi:10.1098/rsif.2012.0286

Wang, B., Lai, X., Price, C., Thompson, W. R., Li, W., Quabili, T. R., et al. (2014). Perlecan-Containing Pericellular Matrix Regulates Solute Transport and Mechanosensing within the Osteocyte Lacunar-Canalicular System. *J. Bone Miner. Res.* 29, 878–891. doi:10.1002/jbmr.2105

Wang, L., Dong, J., and Xian, C. J. (2015). Strain Amplification Analysis of an Osteocyte under Static and Cyclic Loading: a Finite Element Study. *Biomed. Res. Int.* 2015, 376474. doi:10.1155/2015/376474

Wang, T., Yu, X., and He, C. (2019). Pro-inflammatory Cytokines: Cellular and Molecular Drug Targets for Glucocorticoid-Induced-Osteoporosis via Osteocyte. *Curr. Drug Targets* 20, 1–15. doi:10.2174/1389450119666180405094046

Wang, Y., McNamara, L. M., Schaffler, M. B., and Weinbaum, S. (2007). A Model for the Role of Integrins in Flow Induced Mechanotransduction in Osteocytes. *Proc. Natl. Acad. Sci.* 104, 15941–15946. doi:10.1073/pnas.0707246104

Wein, M. N., Spatz, J., Nishimori, S., Doench, J., Root, D., Babij, P., et al. (2015). HDAC5 Controls MEF2C-Driven Sclerostin Expression in Osteocytes. *J. Bone Miner. Res.* 30, 400–411. doi:10.1002/jbmr.2381

Weinbaum, S., Cowin, S. C., and Zeng, Y. (1994). A Model for the Excitation of Osteocytes by Mechanical Loading-Induced Bone Fluid Shear Stresses. *J. Biomech.* 27, 339–360. doi:10.1016/0021-9290(94)90010-8

Weinbaum, S., Tarbell, J. M., and Damiano, E. R. (2007). The Structure and Function of the Endothelial Glycocalyx Layer. *Annu. Rev. Biomed. Eng.* 9, 121–167. doi:10.1146/annurev.bioeng.9.060906.151959

Wenstrup, R. J., Willing, M. C., Starman, B. J., and Byers, P. H. (1990). Distinct Biochemical Phenotypes Predict Clinical Severity in Nonlethal Variants of Osteogenesis Imperfecta. *Am. J. Hum. Genet.* 46, 975–982.

Weske, S., Vaidya, M., von Wnuck Lipinski, K., Keul, P., Manthe, K., Burkhart, C., et al. (2019). Agonist-induced Activation of the S1P Receptor 2 Constitutes a Novel Osteoanabolic Therapy for the Treatment of Osteoporosis in Mice. *Bone* 125, 1–7. doi:10.1016/j.bone.2019.04.015

Whitaker, M., Guo, J., Kehoe, T., and Benson, G. (2012). Bisphosphonates for Osteoporosis - where Do We Go from Here? *N. Engl. J. Med.* 366, 2048–2051. doi:10.1056/nejmp1202619

Wittkowske, C., Reilly, G. C., Lacroix, D., and Perrault, C. M. (2016). *In Vitro* Bone Cell Models: Impact of Fluid Shear Stress on Bone Formation. *Front. Bioeng. Biotechnol.* 4, 87. doi:10.3389/fbioe.2016.00087

Wu, D., Ganatos, P., Spray, D. C., and Weinbaum, S. (2011). On the Electrophysiological Response of Bone Cells Using a Stokesian Fluid Stimulus Probe for Delivery of Quantifiable Localized picoNewton Level Forces. *J. Biomech.* 44, 1702–1708. doi:10.1016/j.jbiomech.2011.03.034

Wysolmerski, J. J. (2012). Parathyroid Hormone-Related Protein: An Update. *J. Clin. Endocrinol. Metab.* 97 (9), 2947–2956. doi:10.1210/jc.2012-2142

Xia, X., Batra, N., Shi, Q., Bonewald, L. F., Sprague, E., and Jiang, J. X. (2010). Prostaglandin Promotion of Osteocyte Gap Junction Function through Transcriptional Regulation of Connexin 43 by Glycogen Synthase Kinase 3/β-Catenin Signaling. *Mol. Cel. Biol.* 30, 206–219. doi:10.1128/mcb.01844-08

Xiao, Z., Zhang, S., Mahlios, J., Zhou, G., Magenheimer, B. S., Guo, D., et al. (2006). Cilia-like Structures and Polycystin-1 in Osteoblasts/Osteocytes and Associated Abnormalities in Skeletogenesis and Runx2 Expression. *J. Biol. Chem.* 281, 30884–30895. doi:10.1074/jbc.m604772200

Xu, H., Zhang, J., Wu, J., Guan, Y., Weng, Y., and Shang, P. (2012). Oscillatory Fluid Flow Elicits Changes in Morphology, Cytoskeleton and Integrin-Associated Molecules in MLO-Y4 Cells, but Not in MC3T3-E1 Cells. *Biol. Res.* 45, 163–169. doi:10.4067/s0716-97602012000200008

Yao, W., Dai, W., Jiang, L., Lay, E. Y.-A., Zhong, Z., Ritchie, R. O., et al. (2016). Sclerostin-antibody Treatment of Glucocorticoid-Induced Osteoporosis Maintained Bone Mass and Strength. *Osteoporos. Int.* 27, 283–294. doi:10.1007/s00198-015-3308-6

Yavropoulou, M. P., and Yovos, J. G. (2016). The Molecular Basis of Bone Mechanotransduction. *J. Musculoskelet. Neuronal Interact* 16, 221–236.

Yokomoto-Umakoshi, M., Kanazawa, I., Takeno, A., Tanaka, K.-i., Notsu, M., and Sugimoto, T. (2016). Activation of AMP-Activated Protein Kinase Decreases Receptor Activator of NF-Kb Ligand Expression and Increases Sclerostin Expression by Inhibiting the Mevalonate Pathway in Osteocytic MLO-Y4 Cells. *Biochem. Biophysical Res. Commun.* 469, 791–796. doi:10.1016/j.bbrc.2015.12.072

You, J., Yellowley, C. E., Donahue, H. J., Zhang, Y., Chen, Q., and Jacobs, C. R. (2000). Substrate Deformation Levels Associated with Routine Physical Activity Are Less Stimulatory to Bone Cells Relative to Loading-Induced Oscillatory Fluid Flow. *J. Biomech. Eng.* 122, 387–393. doi:10.1115/1.1287161

You, L.-D., Weinbaum, S., Cowin, S. C., and Schaffler, M. B. (2004). Ultrastructure of the Osteocyte Process and its Pericellular Matrix. *Anat. Rec.* 278A, 505–513. doi:10.1002/ar.a.20050

You, L., Cowin, S. C., Schaffler, M. B., and Weinbaum, S. (2001). A Model for Strain Amplification in the Actin Cytoskeleton of Osteocytes Due to Fluid Drag on Pericellular Matrix. *J. Biomech.* 34, 1375–1386. doi:10.1016/s0021-9290(01)00107-5

Young, M. F. (2003). Bone Matrix Proteins: Their Function, Regulation, and Relationship to Osteoporosis. *Osteoporos. Int.* 14 (Suppl. 3), S35–S42. doi:10.1007/s00198-002-1342-7

Zambonin Zallone, A. Z., Teti, A., Nico, B., and Primavera, M. V. (1982). Osteoplastic Activity of Mature Osteocytes Evaluated by H-Proline Incorporation. *Basic Appl. Histochem.* 26, 65–67.

Zhang, C., Wei, W., Chi, M., Wan, Y., Li, X., Qi, M., et al. (2019b). FOXO1 Mediates Advanced Glycation End Products Induced Mouse Osteocyte-like MLO-Y4 Cell Apoptosis and Dysfunctions. *J. Diabetes Res.* 2019, 6757428. doi:10.1155/2019/6757428

Zhang, C., Bakker, A. D., Klein-Nulend, J., and Bravenboer, N. (2019a). Studies on Osteocytes in Their 3D Native Matrix versus 2D *In Vitro* Models. *Curr. Osteoporos. Rep.* 17, 207–216. doi:10.1007/s11914-019-00521-1

Zhang, C., Xu, S., Zhang, S., Liu, M., Du, H., Sun, R., et al. (2019c). Ageing Characteristics of Bone Indicated by Transcriptomic and Exosomal Proteomic Analysis of Cortical Bone Cells. *J. Orthop. Surg. Res.* 14, 129. doi:10.1186/s13018-019-1163-4

Zhang, J.-N., Zhao, Y., Liu, C., Han, E. S., Yu, X., Lidington, D., et al. (2015). The Role of the Sphingosine-1-Phosphate Signaling Pathway in Osteocyte Mechanotransduction. *Bone* 79, 71–78. doi:10.1016/j.bone.2015.05.017

Zhang, L., Dong, Y., Wang, Y., Hu, W., Dong, S., and Chen, Y. (2020). Sphingosine-1-phosphate (S1P) Receptors: Promising Drug Targets for Treating Bone-related Diseases. *J. Cel. Mol. Med.* 24, 4389–4401. doi:10.1111/jcmm.15155

Zhou, C., Wang, Q., Zhang, D., Cai, L., Du, W., and Xie, J. (2019). Compliant Substratum Modulates Vinculin Expression in Focal Adhesion Plaques in Skeletal Cells. *Int. J. Oral Sci.* 11, 18. doi:10.1038/s41368-019-0052-3

Zimmerman, D., Jin, F., Leboy, P., Hardy, S., and Damsky, C. (2000). Impaired Bone Formation in Transgenic Mice Resulting from Altered Integrin Function in Osteoblasts. *Developmental Biol.* 220, 2–15. doi:10.1006/dbio.2000.9633

Zimmerman, S. M., Dimori, M., Heard-Lipsmeyer, M. E., and Morello, R. (2019). The Osteocyte Transcriptome Is Extensively Dysregulated in Mouse Models of Osteogenesis Imperfecta. *JBMR Plus* 3, e10171. doi:10.1002/jbm4.10171

Conflict of Interest: The authors declare that the research was conducted in the absence of any commercial or financial relationships that could be construed as a potential conflict of interest.

Publisher's Note: All claims expressed in this article are solely those of the authors and do not necessarily represent those of their affiliated organizations, or those of the publisher, the editors and the reviewers. Any product that may be evaluated in this article, or claim that may be made by its manufacturer, is not guaranteed or endorsed by the publisher.

frontiers in Cell and Developmental Biology

ORIGINAL RESEARCH
published: 24 March 2022
doi: 10.3389/fcell.2022.767688

Modelling the Collective Mechanical Regulation of the Structure and Morphology of Epithelial Cell Layers

Hamid Khataee, Madeleine Fraser and Zoltan Neufeld*

School of Mathematics and Physics, The University of Queensland, Brisbane, QLD, Australia

The morphology and function of epithelial sheets play an important role in healthy tissue development and cancer progression. The maintenance of structure of closely packed epithelial layers requires the coordination of various mechanical forces due to intracellular activities and interactions with other cells and tissues. However, a general model for the combination of mechanical properties which determine the cell shape and the overall structure of epithelial layers remains elusive. Here, we propose a computational model, based on the Cellular Potts Model, to analyse the interplay between mechanical properties of cells and dynamical transitions in epithelial cell shapes and structures. We map out phase diagrams as functions of cellular properties and the orientation of cell division. Results show that monolayers of squamous, cuboidal, and columnar cells are formed when the axis of cell proliferation is perpendicular to the substrate or along the major axis of the cells. Monolayer-to-multilayer transition is promoted via cell extrusion, depending on the mechanical properties of cells and the orientation of cell division. The results and model predictions are discussed in the context of experimental observations.

Keywords: computational modeling, tissue modelling, mechanobiolgy, cell morphological analysis, cellular mechanics, stochastic modelling and simulation

OPEN ACCESS

Edited by:
Selwin K. Wu,
Mechanobiology Institute, National University of Singapore, Singapore

Reviewed by:
Keng-Hwee Chiam,
*Bioinformatics Institute (A*STAR), Singapore*
Romain Levayer,
Institut Pasteur, France

****Correspondence:***
Hamid Khataee
h.khataee@uq.edu.au

Specialty section:
This article was submitted to Cell Adhesion and Migration, a section of the journal Frontiers in Cell and Developmental Biology

Received: *31 August 2021*
Accepted: *28 February 2022*
Published: *24 March 2022*

Citation:
Khataee H, Fraser M and Neufeld Z (2022) Modelling the Collective Mechanical Regulation of the Structure and Morphology of Epithelial Cell Layers. Front. Cell Dev. Biol. 10:767688. doi: 10.3389/fcell.2022.767688

1 INTRODUCTION

Understanding the mechanisms of the development of various tissue morphologies is a major challenge in biology (Hannezo et al., 2014). Epithelial cell layers are the simplest living tissues that line organs throughout the body (Vincent et al., 2015) and play important roles in regulating embryo development, yet account for about 90% of all cancers (Pedersen et al., 2013). Morphogenesis of organ systems is driven by the ability of cells to survive and proliferate (Chen et al., 1997; Streichan et al., 2014), primarily regulated by cell growth factors and cell-substrate adhesion (Chen et al., 1997; Schwartz and Assoian, 2001; Brakebusch et al., 2002).

For many adherent cells, cell proliferation can only occur on a substrate (Adam Hacking et al., 2013). The substrate maintains a dynamic force balance between the cell and its microenvironment, and thus, the loss of substrate or its abnormal stiffness can results in aberrant cellular behaviours, e.g., breast tumor progression (Provenzano and Keely, 2011). As feedback loops, cells sense the stiffness of their environment by pulling against the extracellular matrix, through integrin-extracellular matrix linkages, and/or neighbouring cells (Chen et al., 1997; Provenzano and Keely, 2011). This process is dependent on cell–substrate and cell-cell adhesion, as well as the contractility of cell cortex (Provenzano and Keely, 2011). Therefore, both integrins and growth factor receptors use cytoplasmic signaling pathways to regulate cell cycle progression and growth (Schwartz and Assoian, 2001). It has been shown that the probability of cell proliferation increases with

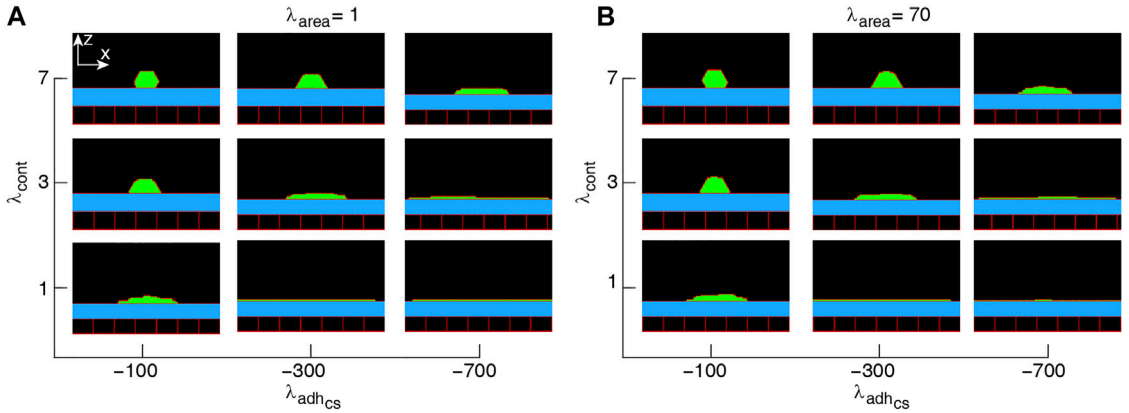

FIGURE 1 | Phase diagram of single-cell shapes **(A,B)**. *x-z* cross-section of the cell (green) placed on a substrate (blue) surrounded by an empty region (black) and wall cells (black squares). Simulations were run with the cell proliferation disabled. The range of parameter values are adopted from (Khataee et al., 2020). Snapshots were taken in the steady-states.

increasing substrate stiffness (Mohan et al., 2018) and cell area (Streichan et al., 2014). Yet, it remains inconclusive how different forces and regulatory mechanisms within cells can affect proliferation orientation; reviewed in (Collinet and Lecuit, 2013; Finegan and Bergstralh, 2019).

Earlier theoretical studies on epithelial morphology have explored two-dimensional (2D) mechanical model of a tubular epithelium (Hočevar Brezavšček et al., 2012; Krajnc et al., 2013), geometric patterning of apical junctions (Gibson et al., 2006; Farhadifar et al., 2007; Käfer et al., 2007; Hilgenfeldt et al., 2008), shapes of cells and the buckling of cell monolayers (Osterfield et al., 2013; Hannezo et al., 2014). Although these models are based on the mechanical properties of cells, they were mostly restricted to monolayers. To model the dynamic processes involved in the formation of epithelial cell layers, models of epidermal homeostasis were proposed based on probabilistic rules associated to different types of cells (Doupé et al., 2010; Doupé et al., 2012; Kostiou et al., 2020). However, these models do not consider the shape of the cells and the role of cellular mechanics in modelling the transition between monolayers to multilayers. Therefore, it remains elusive how the mechanical properties of cells and their interactions determine cell aspect ratios and the formation of mono- and multilayered epithelial structures. Further, the role of the orientation of the plane of cell division, in combination with mechanical properties of cells, in modelling collective tissue morphology has not been explored.

Here, we propose a computational model for analysing the development of collective epithelial morphologies using the Cellular Potts Model (CPM) (Graner and Glazier, 1992; Glazier and Graner, 1993). CPM is a computational modelling framework that can represent the essential features of the real-world epithelial cell dynamics, and allows general predictions of the behaviour and morphology of cells (Khataee et al., 2020; Kempf et al., 2021). Our model simulates the transition of cell shapes and the formation of mono- and multilayered structures by altering various mechanical properties of identical proliferative cells.

2 Theoretical Model

To simulate the collective morphology of cells emerging through their mechanical properties and interactions on a substrate, we use a two-dimensional CPM (Graner and Glazier, 1992; Glazier and Graner, 1993) which represents a cross-section of cells on a substrate on a plane perpendicular to the substrate. The CPM is an on-lattice model which is computationally simpler than most off-lattice models, e.g., vertex model (Osborne et al., 2017; Giniūnait et al., 2019) and has been used to capture essential realistic features of epithelial cell dynamics (Kempf et al., 2021), e.g., the dynamics of cell migration on short microlanes (Zhou et al., 2020), circular micropatterns (Segerer et al., 2015), and in a confluent sheet expanding into a free region (Khataee et al., 2020).

The cells are represented on a lattice, where each cell covers a set of connected lattice sites (or pixels) and each pixel can only be occupied by one cell at a time. Here, the lattice is a rectangular surface (480 × 195 pixels in length and height, respectively), representing a cross-sectional view to epithelial cells placed on a substrate. This means that the model is 2D in the *x-z* plane, where *x* and *z* axes are parallel and perpendicular to the substrate, respectively (see inset in **Figure 1A**, top left corner). The expansion and retraction of the cell boundaries are determined by minimising a phenomenological energy E, defined in terms of the area A_σ and perimeter L_σ of each cell σ of N cells (indices $\sigma = 1, \ldots, N$) (Farhadifar et al., 2007; Khataee et al., 2020; R. Noppe et al., 2015; Albert and Schwarz, 2016; Thüroff et al., 2019) as:

$$E=\lambda_{\text{area}}\sum_{\sigma}^{N}(A_\sigma-A_0)^2+\lambda_{\text{cont}}\sum_{\sigma}^{N}L_\sigma^2+\sum_{\vec{i},\vec{j}}J\left(\sigma_{\vec{i}},\sigma_{\vec{j}}\right)\left(1-\delta\left(\sigma_{\vec{i}},\sigma_{\vec{j}}\right)\right). \quad (1)$$

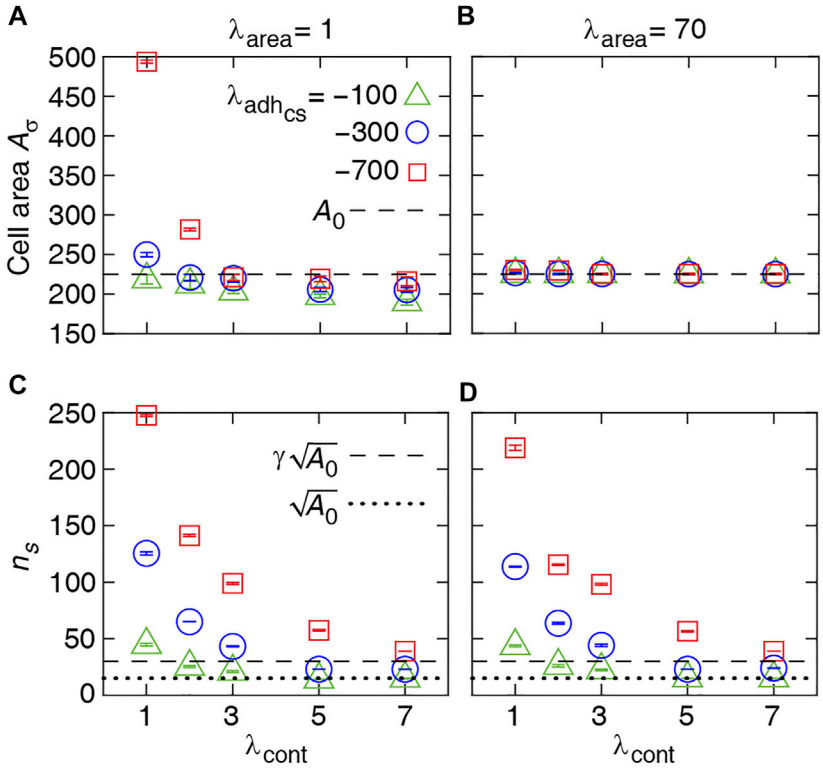

FIGURE 2 | Numerical results for single-cell properties. **(A, B)** Area of the cell in steady state versus contractility strength λ_{cont} at various λ_{area} and cell-substrate adhesion $\lambda_{adh_{cs}}$. **(C, D)** Number of cell-substrate adhesion sites n_s in the steady state versus λ_{cont} at various λ_{area} and $\lambda_{adh_{cs}}$. Each symbol is derived from an individual simulation run and corresponds to mean ± SD.

The first term models the compressibility of cells by penalising the deviation of cell areas from a target area A_0. The second term represents the contractility of the cell cortex as a spring with zero equilibrium length (i.e., the target length of the cell perimeter is zero). The penalty parameter λ_{cont} represents cortical actomyosin contractility, around the lateral cell membrane (Reffay et al., 2014). The last term describes the cell-cell adhesion mediated by adhesion molecules, such as E-cadherin (Charras and Yap, 2018). J is the boundary energy cost at neighbouring lattice sites $\vec{i}$ and $\vec{j}$. The Kronecker δ function prevents counting pixels that belong to the same cell. When both lattice sites $\vec{i}$ and $\vec{j}$ correspond to cells, $J(\sigma_{\vec{i}}, \sigma_{\vec{j}}) = \lambda_{adh_{cc}}$; when one lattice site corresponds to cell and another site corresponds to the substrate $J(\sigma_{\vec{i}}, \sigma_{\vec{j}}) = \lambda_{adh_{cs}}$; otherwise when one or both lattice sites represent empty space or boundary wall, the boundary energy cost J is set to zero. Note that $\lambda_{adh_{cc}} < 0$ and $\lambda_{adh_{cs}} < 0$ to represent that cells preferentially expand their boundaries shared with neighbouring cells or substrate. This is however balanced by the contractile tension along the cell cortex. The prefactors λ_{area}, λ_{cont}, and λ_{adh} reflect the relative importance of the corresponding cellular properties.

The dynamics of the CPM is defined by a stochastic series of elementary steps, where a cell expands or shrinks accommodated by a corresponding area change in the adjacent cell (or empty area) (Glazier and Graner, 1993; Swat et al., 2012). The algorithm randomly selects two adjacent lattice sites $\vec{i}$ and $\vec{j}$, occupied by different cells $\sigma_{\vec{i}} \neq \sigma_{\vec{j}}$. The elementary step is an attempt to copy $\sigma_{\vec{i}}$ into the adjacent lattice site $\vec{j}$, which takes place with probability

$$P\left(\sigma_{\vec{i}} \to \sigma_{\vec{j}}\right) = \begin{cases} 1 & \text{for } \Delta E \leq 0 \\ e^{-\Delta E/T} & \text{for } \Delta E > 0 \end{cases} \quad (2)$$

where ΔE is the change in functional (1) due to the elementary step considered, and the temperature parameter T is an arbitrary scaling factor. A Monte Carlo step (MCS) of the simulation, the natural unit of time in the model, is set to n elementary steps–where n is the total number of lattice sites in the simulated area (Swat et al., 2012). Together, **Eqs 1**, **2** imply that cell configurations which increase the energy in functional (1) are less likely to occur. Thus, the cell population evolves through stochastic rearrangements in accordance with the biological dynamics incorporated into the effective energy function E.

Among multiple environmental factors that can regulate cell proliferation, cell growth factors and cell-substrate adhesion are most crucial (Schwartz and Assoian, 2001; Brakebusch et al., 2002): the probability of cell proliferation for individual cells increases with the cell area (Streichan et al., 2014) and substrate stiffness (Mohan et al., 2018).We therefore

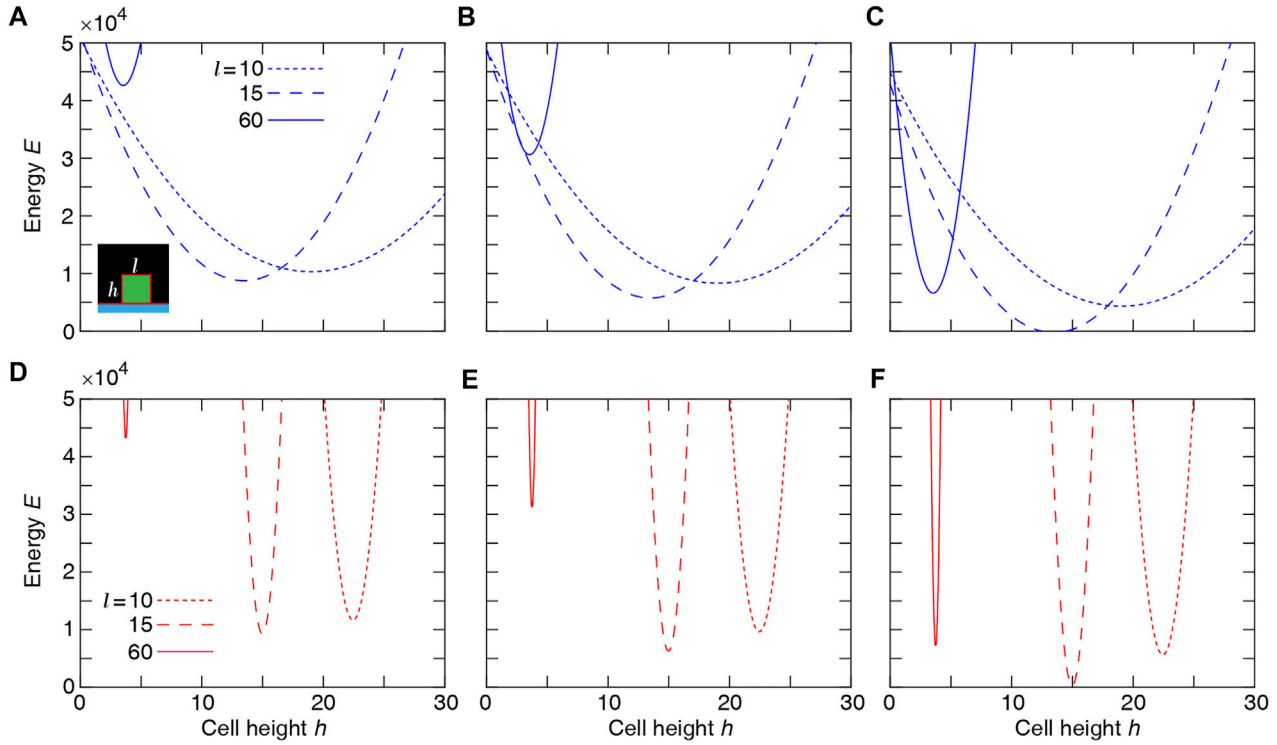

FIGURE 3 | Single-cell Potts energy E versus cell height h at various cell length l calculated using **Eq. 4**. Top row: $\lambda_{area} = 1$ and $\lambda_{cont} = 3$ at $\lambda_{adh_{cs}} = -100$ **(A)**, −300 **(B)**, −700 **(C)**. Bottom row: $\lambda_{area} = 70$ and $\lambda_{cont} = 3$ at $\lambda_{adh_{cs}} = -100$ **(D)**, −300 **(E)**, −700 **(F)**.

TABLE 1 | Model parameters.

Parameter	Value
Initial cell size (pixel × pixel)	15 × 15
Initial cell area, A_σ (pixel × pixel)	225
Preferred area, A_0 (pixel × pixel)	225
Temperature, T	50
Half-saturation constant, γ	2
Hill coefficient, k	10
Maximal proliferation probability, P_{max}	0.1

define cell proliferation probability as a function of cell area and adhesion to the substrate in the form of the Hill function, which is widely used in mathematical modelling of binding of molecular structures of cells (Santillán, 2008). At every MCS, if a cell σ reaches its target area (i.e., $A_\sigma \geq A_0$), the probability of proliferation is given by the following expression:

$$P_{\text{div}} = P_{\max}\frac{n_s^k}{n_s^k + \left(\gamma\sqrt{A_0}\right)^k} \tag{3}$$

where $P_{\max}$ is the maximum probability of proliferation and n_s denotes the number of boundary pixels of a cell adjacent to the substrate, representing cell-substrate adhesion sites (Paddillaya et al., 2019). We assume that the Hill half-saturation threshold is given by the dimension in pixels of a square shaped cell, i.e., $\gamma\sqrt{A_0}$ with a multiplicative factor γ. Together, **Eq. 3** expresses that the proliferation probability of a cell increases as the cell is more adhesive to the substrate. This is consistent with experiments (Chen et al., 1997; Provenzano and Keely, 2011; Mohan et al., 2018) where increased area of cell-substrate contact enhanced cell growth, and thus proliferation. Further, $P_{\text{div}} = 0$ for cells not adhered to the substrate, representing that cell proliferation can occur only on the substrate (Adam Hacking et al., 2013).

Our simulations are implemented using the open-source software package CompuCell3D (CC3D) (Swat et al., 2012). Each simulation starts with a single cell of the size 15 × 15 pixels placed on a substrate of width of 450 pixels and allowed to proliferate following **Eq. 3**. The simulation domain is surrounded by wall cells that prevent the cells from sticking to the lattice boundaries. The wall cells are excluded from participating in the pixel copies of the Potts model (Swat et al., 2009). If a cell division occurs, the cell is divided along a plane specified by a normal vector $n_{\text{div}} = (n_x, n_z)$, where n_x and n_z are the components normal to the plane. The division then results in two cells each with area $\approx A_0/2$. Then according to **Eqs 1**, **2** these two cells grow to reach the target area A_0. **Table 1** summarises the parameter values used in our computational simulations.

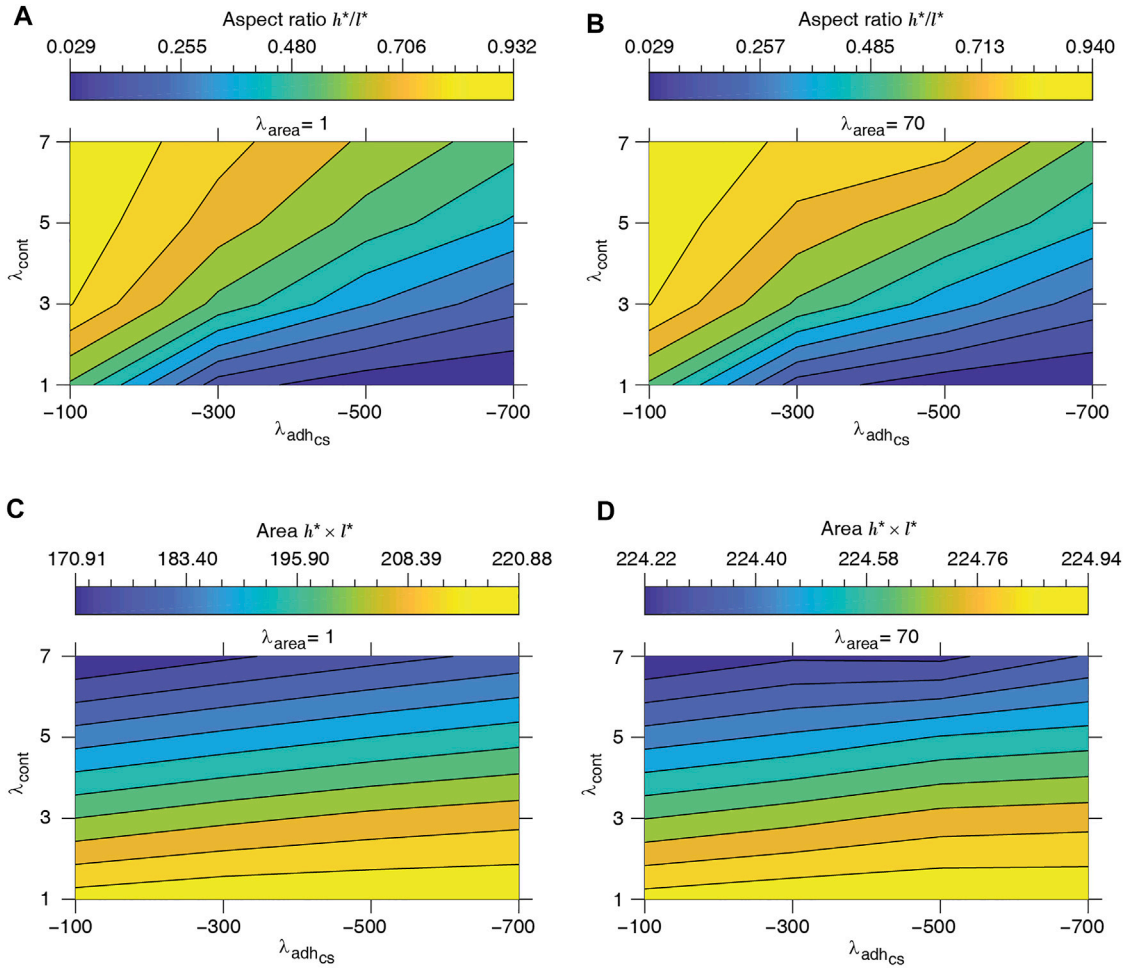

FIGURE 4 | Equilibrium single-cell aspect ratio h^*/l^* **(A, B)** and area $h^* \times l^*$ **(C, D)** versus cell-substrate adhesion $\lambda_{adh_{cs}}$ and contractility λ_{cont}. l^* and h^*: cell length and height at the mechanical equilibrium, respectively, corresponding to rectangular cell shape; see **Eq. 4**.

3 RESULTS AND DISCUSSION

3.1 Single Cell Morphology

Since the multicellular morphogenesis is partly driven by changes in the shape of individual cells (Widmann and Dahmann, 2009), our starting point for modelling collective epithelial cell morphology is to explore single-cell morphology in response to its mechanical properties, when cell proliferation is switched off. Typical snapshots of single-cell morphology in the steady-state are shown in **Figure 1**. We find that the squamous (i.e., flat)-to-cuboidal shape transition is promoted by increasing cell contractility. A similar shape transition is also found with decreasing cell-substrate adhesion; see **Figures 1A,B**.

To better understand how the single-cell morphology can influence the multi-cellular dynamics, we analyse the cell area and number of cell-substrate adhesion pixel (which affect the probability of cell proliferation) in response to the mechanical control parameters. This enables us to predict the combination of mechanical properties that can lead to different collective cell behaviors.

Figure 2A shows that the average cell area increases with cell-substrate adhesion, which is more evident with weak cell contractility. Contrarily, with strengthening cell contractility and decreasing cell-substrate adhesion, the average area of a cell falls below its target area A_0. On the other hand, with increasing λ_{area}, the average cell area remains close to A_0 at all λ_{cont} and $\lambda_{adh_{cs}}$; see **Figure 2B**. Further, increasing cell-substrate adhesion and weakening cell contractility expand cell-substrate adhesion sites; see **Figures 2C,D**. Together, these numerical results suggest that monolayers and multilayered structures are more likely to form with increasing cell-substrate adhesion and weaker cell contractility, due to increased proliferation probability of individual cells. Further, non-confluent structures are generated when cells have strong cortex contractility and low adhesion to the substrate.

We check the consistency of these simulation results with the estimated energy minimum determined for a simplified rectangular cell shape. The energy function for a single rectangular cell reads:

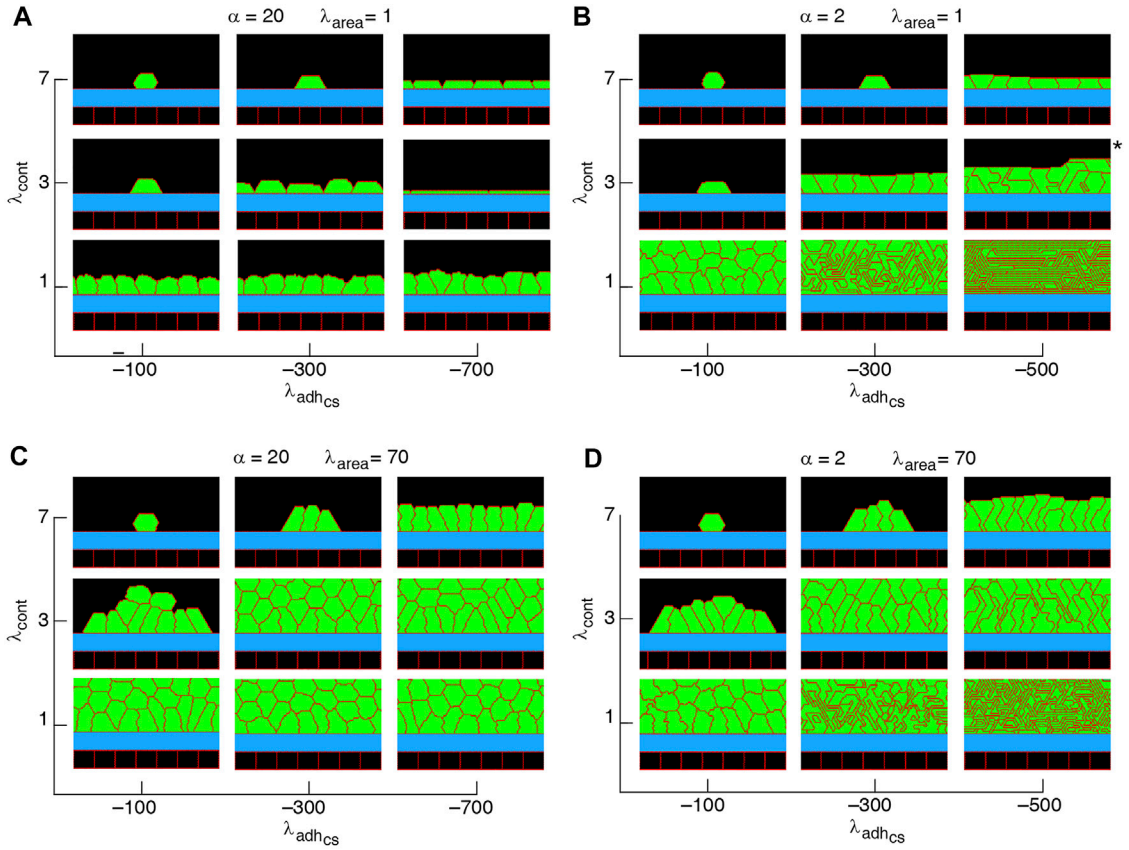

FIGURE 5 | Phase diagram of steady state collective cell morphology when the axis of division is perpendicular to the substrate, i.e., n_{div} = (1, 0); see **Eq. 3 (A–D)**. $\alpha = \lambda_{adh_{cs}}/\lambda_{adh_{cc}}$. *Slow-growing multilayers. See **Supplementary Movies S1–S5**.

$$E(l,h) = \lambda_{area}(lh - A_0)^2 + \lambda_{cont}(2l + 2h)^2 + \lambda_{adh_{cs}} l, \quad (4)$$

where l and h are cell length and height (see schematic inset, **Figure 3**). The minimum of the energy E is determined by solving the equations:

$$\frac{\partial E(l,h)}{\partial l} = 0, \quad \frac{\partial E(l,h)}{\partial h} = 0, \quad (5)$$

which results in

$$\begin{aligned} 2\lambda_{area} h(lh - A_0) + 8\lambda_{cont}(l + h) + \lambda_{adh_{cs}} &= 0, \\ 2\lambda_{area} l(lh - A_0) + 8\lambda_{cont}(l + w) &= 0, \end{aligned} \quad (6)$$

to define cell length l^* and height h^* at mechanical equilibrium. The typical dependence of the energy function on the cell height and width is illustrated in **Figure 3**. Assuming that the mechanical equilibrium at steady state can be approximately estimated from the minimisation of the energy function corresponding to a rectangular cell (**Eq. 4**), we calculate the steady cell aspect ratio and area. The results shown in **Figure 4** are consistent with the phase diagram of single-cell morphology in **Figure 1** and also show qualitative agreement with the CPM simulation results in **Figures 2A,B**.

3.2 Collective Multicellular Morphology

We now use the model to simulate a system of proliferating cells various combinations of mechanical parameters. The simulations are started with a single cell placed on the substrate in the middle of the domain and cell division is allowed according to the rules described above, i.e., when the cell area is larger than A_0 with a probability P_{div} dependent on the number cell adhesion sites (pixels) attached to the substrate.

During morphogenesis, oriented cell divisions are essential for the generation of cell diversity and for tissue shaping (Finegan and Bergstralh, 2019). The long-standing Hertwig's rule (or the long axis rule) states that cells tend to divide at their cytoplasmic centre perpendicular to their longest axis (Hertwig, 1884). More recent studies have revealed that the proliferation is oriented by additional cellular properties, e.g., spatial distribution of the cell–substrate adhesion sites (Théry et al., 2005) and actomyosin-based mechanical tension dependent (LeGoff et al., 2013) and independent (Scarpa et al., 2018; Finegan and Bergstralh, 2019) of cell shape. However, current evidence on the role of cell shape and different sets of intracellular mechanisms in orienting cell proliferation remains inconclusive (Collinet and Lecuit, 2013; Finegan and Bergstralh, 2019). Our model allows a convenient way to

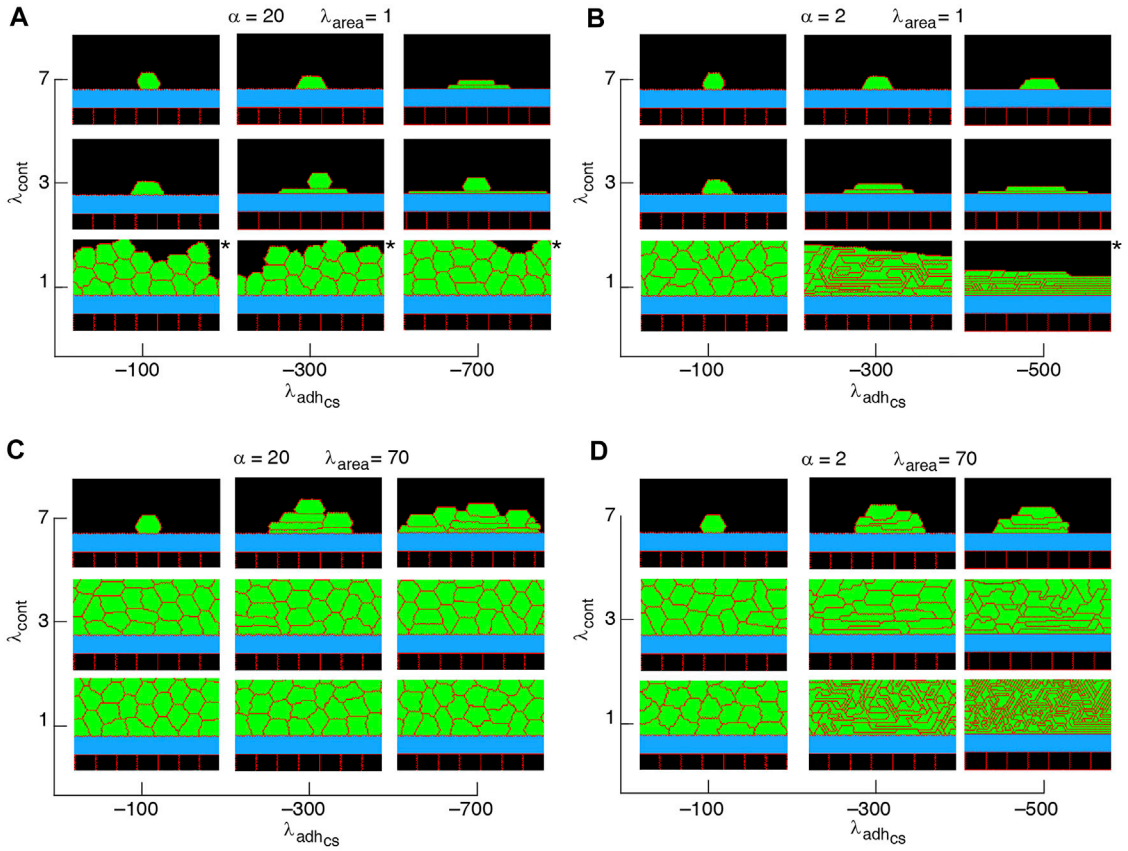

FIGURE 6 | Phase diagram of collective cell morphology with horizontal orientation of cell proliferation, where the axis of division is parallel to the substrate, i.e., n_{div} = (0, 1); see **Eq. 3 (A–D)**. $\alpha = \lambda_{adh_{cs}}/\lambda_{adh_{cc}}$. *Slow-growing multilayers. See **Supplementary Movies S6, S7**.

simulate collective cell morphologies by considering different orientations of cell division axis and varying mechanical properties of cells in various combinations.

Steady state phase diagrams of the collective morphology with horizontal, vertical, and random cell division orientation are presented in **Figures 5–7(A–D)**, **Supplementary Figure S1**. First, we note that the cell shapes in the multicellular system in most cases can be quite different from the shape of a single isolated cell obtained for the same set of mechanical parameters. We observe three main types of multi-cellular structures and behaviors developing in the simulations: 1) For certain parameter combinations, the cell division is either completely blocked or is very limited resulting in the formation of a small group of cells without forming a confluent cell layer along the substrate over the whole domain. 2) A cell monolayer can form through repeated cell divisions in such a way that cell proliferation stops in a self-regulated manner once a fully confluent layer is formed. This layer may be composed of flat or tall cells. 3) In multi-layered structures, the cell division continues indefinitely (although it is still restricted to the basal cells along the substrate) and the height of the cell layer increases over time. In a real multilayered epithelium, the height of such layer can be controlled by differentiation and death of the non-proliferating cells that are not adhered to the substrate. Since we focus on the emergence of the different cell layer structures and the corresponding cell shapes, we do not include cell death and differentiation in our model. The simulation results also show that for high cell-substrate adhesion and low contractility ($\lambda_{adh_{cs}} = -500$ and $\lambda_{cont} = 1$ in **Figures 5B–7B**,D) multicellular structures with irregular thin cell shapes develop. The formation of such structures is obviously not realistic and cannot appear in real tissues as it would be prevented by the internal cell cytoskeleton which is not included in the energy function of our model.

Non-confluent structures are formed at high cell contractility and reduced cell-substrate adhesion, independently of the proliferation orientation; see **Figures 5–7**, **Supplementary Figure S1**. This is due to reductions in both cell area and the number of cell-substrate adhesion sites in individual cells which reduce the probability of cell proliferation; see **Figure 2**.

Confluent monolayers and multilayered structures are formed with increasing cell-substrate adhesion and lowering cell contractility. With proliferation orientation perpendicular to the substrate, monolayers of squamous (flat), cuboidal, and columnar (tall) cells are found; see **Figure 5**. The expansion of monolayers typically happens through the division of border cells (at both edges of the monolayer) on the substrate, while the other

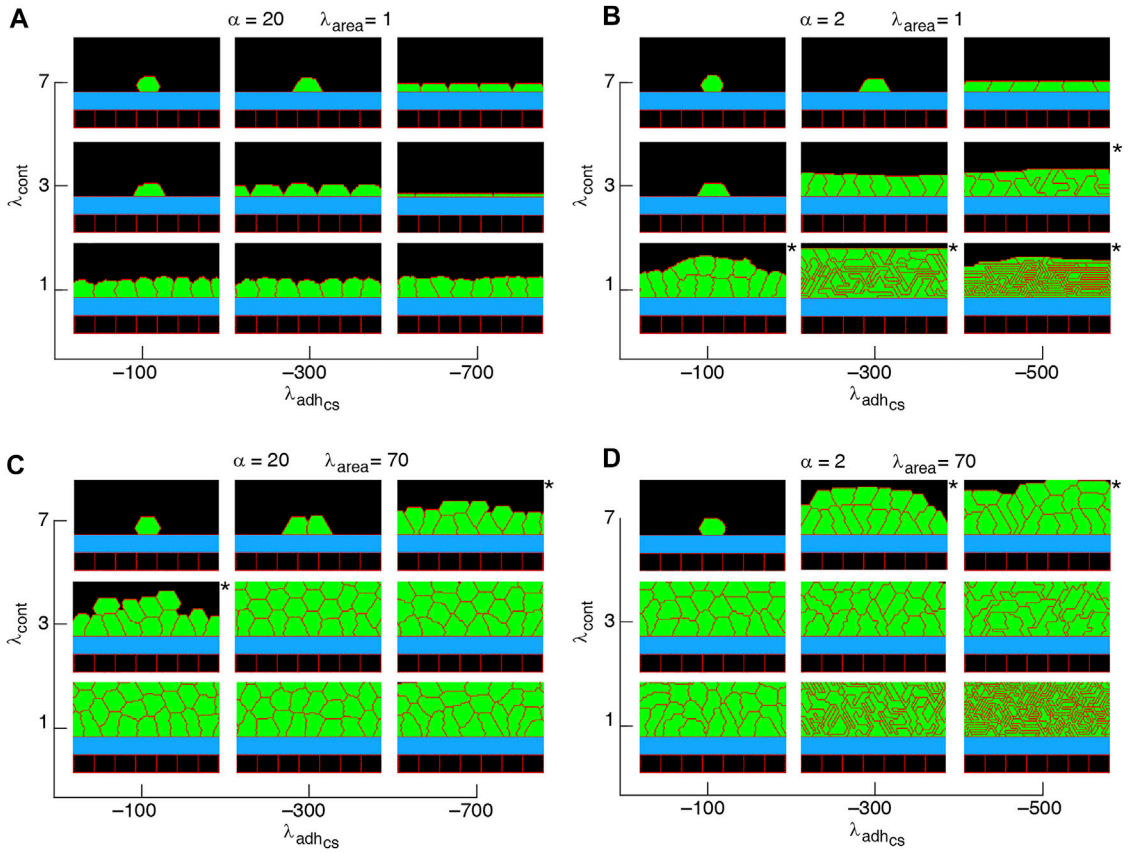

FIGURE 7 | Phase diagram of collective cell morphologies when orientation of cell proliferation is along the major axis of the cells **(A–D)**. $\alpha = \lambda_{adh_{cs}}/\lambda_{adh_{cc}}$. *Slow-growing multilayers. See **Supplementary Movie S8**.

cells inside the monolayer do not divide or only relatively rarely. Once the layer becomes confluent cell crowding limits the cell area and the cell-substrate adhesion sites, due to which the probability of proliferation decreases; see **Figures 8A–I**. At certain combinations of mechanical properties (summarised in **Figure 5** and analysed in **Figures 8A–I**), cells stop proliferating once a confluent monolayer is formed see **Supplementary Movies S1–S3, S5**. Squamous cells are mostly found for high cell-substrate adhesion (relative to cell-cell adhesion), increased cortex contractility and reduced λ_{area} parameter. Increasing λ_{area}, in this regime, leads to squamous-to-columnar shape transition.

A major factor that contributes to monolayer-to-multilayer transition is cell crowding. When the cell density cannot increase anymore in the basal layer, while cell deformations are likely, cells are extruded from the monolayer. Accordingly, cells at the basal layer can expand their area increasing the probability of their proliferation and further extrusion events; see **Figures 8J–L** and **Supplementary Movie S4**. Overall, monolayer-to-multilayer transition is more likely to appear with a combination of parameters that increase λ_{area}, increasing cell-substrate adhesion, reduced cortical contractility, and with proliferation orientation being parallel to the substrate, random, or along the major axis of the cell; see **Figures 6**, **7**, **Supplementary Figure S1**.

Our simulation results complement earlier findings on collective epithelial morphology. Simulation results characterise cell area strength λ_{area} as a major factor that influences collective morphology: increasing λ_{area} generates multilayer structures, whereas with reducing λ_{area} monolayer and non-confluent structures appear; see **Figures 5–7**, **Supplementary Figure S1**. Increasing λ_{area} promotes proliferation probability, by increasing cell area to approach the target area A_0; see **Eq. 1**. At a low λ_{area}, it is more likely that cell area deviates from A_0 resulting in smaller probability of proliferation. This effect is evident in the generation of monolayers, where cell proliferation is limited by cell area and the number of cell-substrate adhesion sites; see **Figures 8A–I**. However, in multilayer structures, the growth of cell area is facilitated (by λ_{area}, $\lambda_{adh_{cs}}$, and λ_{cont}) so that the crowding does not block cell proliferation events and continuous cell extrusions out of the basal layer lead to multilayered structure; see **Figures 8J–L**. At stronger cell-substrate adhesion $\lambda_{adh_{cs}}$, the extruded cells may return back to the basal layer; see inset in **Figure 8D**. Further, cortex contractility λ_{cont} affects cell proliferation probability through influencing cell size and shape. With lowering λ_{cont} and strengthening cellular adhesion, cell shapes become softer (i.e., stretched with dynamic boundaries), in contrast to the more rounded cell shapes with approximately static cell boundaries at

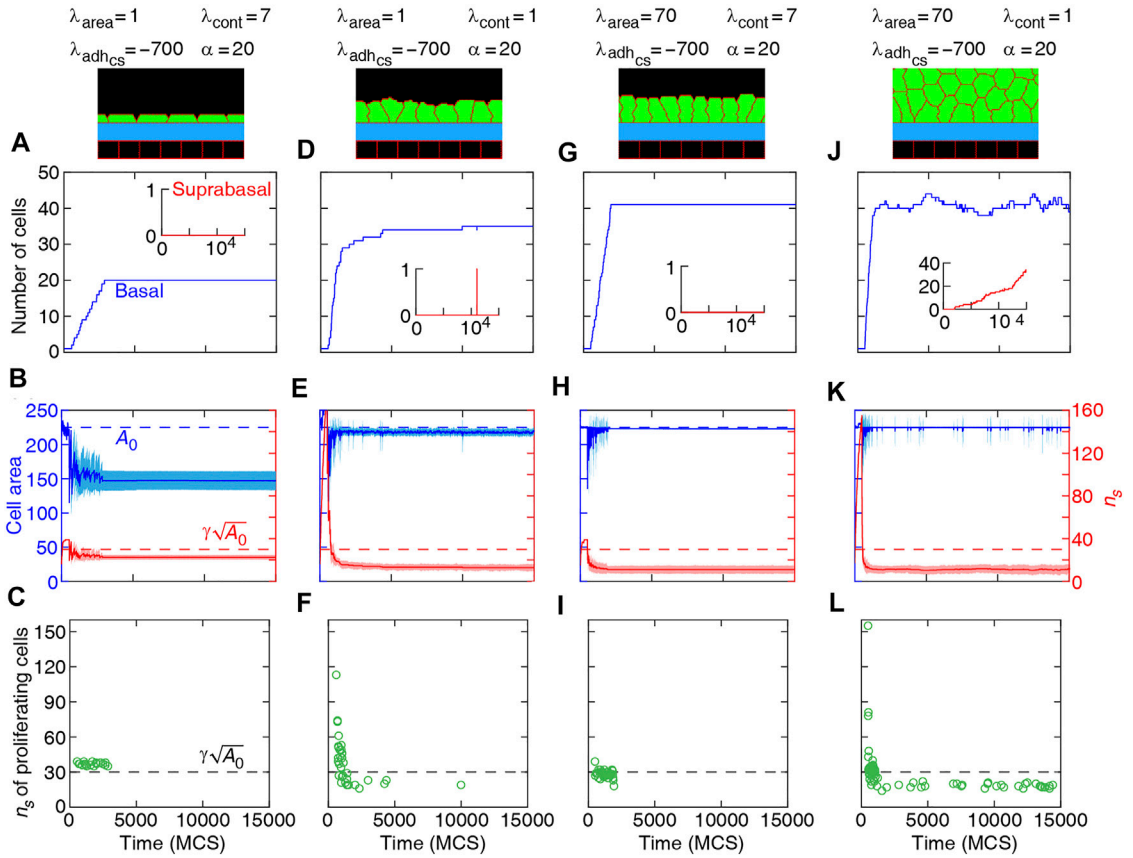

FIGURE 8 | Dynamics of basal cells in four different collective morphologies illustrated with snapshots and associated mechanical parameters. Top row **(A,D,G,J)**: number of basal cells (with adherence to the substrate) and suprabasal cells (without adherence to the substrate) versus time. Middle row **(B,E,H,K)**: area (left axis) and number of cell-substrate adhesion sites n_s (right axis) for basal cells versus time. Solid curves: mean. Shaded region: SD. Bottom row **(C,F,I,L)**: n_s of proliferating cells versus time. Orientation of cell proliferation is vertical, n_{div} = (1, 0). $\alpha = \lambda_{adh_{cs}}/\lambda_{adh_{cc}}$. See **Supplementary Movie S1–S4**.

higher λ_{cont} (Farhadifar et al., 2007; Khataee et al., 2020; R. Noppe et al., 2015). These fluctuations in the cell size then increase the probability of proliferation in the model.

The simulation results are consistent with experimental observations. It has been observed that the probability of cell proliferation increases with cell area (Streichan et al., 2014) and reduction in cell area (imposed by mechanical constraints on tissue expansion) inhibits cell proliferation (Chen et al., 1997; Puliafito et al., 2012). Further, substrate stiffness has been known to be positively correlated with cell proliferation increasing substrate stiffness (dependent on cell-substrate adhesion) and was found to increase the proliferation rate (García et al., 1999; Provenzano and Keely, 2011; Mohan et al., 2018). It was shown that when the cell density cannot increase anymore in a monolayer (due to cell crowding), while the proliferation events still occur, newly generated cells are extruded out of the monolayer where they remained without adhering to the substrate (Deforet et al., 2014). These suprabasal cells may slide over the basal cells such that they migrate in and become basal cells themselves (Rognoni and Watt, 2018; Haensel et al., 2020). Experiments have also provided evidence that mechanical stretching stimulates cell proliferation (Aragona et al., 2013). The proliferation is activated in cells with flattened geometry where the cell growth is promoted, whereas in cells with round geometry, cell growth and thus proliferation are limited (Dupont et al., 2011; Aragona et al., 2013). It was suggested that the rounded cell geometry, compared to spread geometry, may differently affect the adhesion sites and their associated F-actin cytoskeleton (Low et al., 2014).

The simulated cell shapes in monolayers are also consistent with experimental observations. For example, with intermediate cortical contractility λ_{cont} = 3 and $\lambda_{adh_{cs}}$ = −300, increasing adhesion ratio α from 2 to 20 reduces cell height by factor 1.88; compare middle snapshots in **Figures 5A,B**. For squamous cells (λ_{cont} = 7 and $\lambda_{adh_{cs}}$ = −700), cell height drops by factor 1.22; compare top right corner snapshots in **Figures 5A,B**. For columnar cells, a negligible reduction (by factor 1.10) in cell height is found with increasing α; compare top right corner snapshots in **Figures 5C,D**. These simulation results agree with experimental observations that lowering the lateral cell–cell adhesion decreases cell height (Weber et al., 2007; Melani et al., 2008; Montell, 2008; Gomez et al., 2012). It is also consistent with the theoretical prediction that the cell-cell

lateral adhesion is a crucial parameter to increase cell height (Hannezo et al., 2014; Dasbiswas et al., 2018).

Our results show that with altering the proliferation orientation from being perpendicular to the substrate to be along the major axis of the cells, monolayers of columnar cells transition into multilayered structures; compare **Figures 5**, **7C**,D, top right corner. With proliferation orientation perpendicular to the substrate, the new daughter cells are positioned to either left or right of the mother cell on the substrate. This way, cell crowding decreases the proliferation probability (see **Eq. 3**) and a monolayer of columnar cells are formed. However, when the proliferation orientation is along the major axis of the cells, new daughter cells can extrude from the basal layer, even before a confluent monolayer is formed (see **Supplementary Movie S8**). These extrusions then do not contribute to cell crowding on the basal layer and allow the basal cells to grow, so that further proliferation events occur and multilayered structures are formed. This is consistent with experimental observations (Chanet et al., 2017) showing that cell rounding is required for the division of columnar epithelial cells and without the cell rounding, cells remain elongated due to tight cell packing.

4 CONCLUSION

In this article, we introduced a 2D computational model to analyse the emergence of collective morphology of epithelial cells. The model allowed us to simulate diverse collective morphology using various combinations of mechanical properties of cells and the orientation of cell division axis. Our results suggest that non-confluent structures transition into confluent monolayers and multilayers with weakening cell contractility (λ_{cont}) and strengthening cell-substrate adhesion ($\lambda_{\text{adh}_{\text{cs}}}$), due to increase in probability of cell proliferation. Confluent monolayers of squamous, cuboidal, and columnar cells are formed with proliferation axis perpendicular to the substrate. It is further suggested that monolayer-to-multilayer transition occurs by cell extrusion from the basal layer as a result of the interplay between mechanical parameters (λ_{area}, λ_{cont}, and $\lambda_{\text{adh}_{\text{cs}}}$) and the orientation of cell proliferation. Taken together, our simulation results suggest that desirable biomechanical features of individual cells can regulate multicellular tissue morphology.

The extension of the energy function of the 2D model to 3D is relatively straightforward [e.g., see (Hannezo et al., 2014)], but including the third dimension would significantly increase the computational cost of the simulations. We expect that for most cases the computational results on the multicellular morphology would be at least qualitatively similar since the cell shapes are isotropic within the plane of the substrate (i.e., x-y plane). In addition, the cell proliferation steps defined here take into account the progressive increase of cell volume (through growing of lateral area of cell A_σ and approaching A_0) and the apical perimeter of the cells (through $\sqrt{A_0} = l$ in **Eq. 3**). Further, the presented 2D model is more amenable to efficient simulations (i.e., when performing parameter sweeps) and mathematical analysis, compared with that in 3D.

DATA AVAILABILITY STATEMENT

The theoretical model in this study is included within the article.

AUTHOR CONTRIBUTIONS

HK and ZN conceived the idea. HK performed the mathematical and numerical analyses. HK and MF implemented the computational simulations. All authors wrote the article.

FUNDING

HK and ZN was supported by ARC Discovery Project No. DP160104342.

SUPPLEMENTARY MATERIAL

The Supplementary Material for this article can be found online at: https://www.frontiersin.org/articles/10.3389/fcell.2022.767688/full#supplementary-material

REFERENCES

Adam Hacking, S., and Khademhosseini, A. (2013). "Cells and Surfaces *In Vitro*," in *Biomaterials Science an Introduction to Materials in Medicine*. Editors B. D. Ratner, A. S. Hoffman, F. J. Schoen, and J. E. Lemons (Elsevier), 408–427. doi:10.1016/b978-0-08-087780-8.00037-1

Albert, P. J., and Schwarz, U. S. (2016). Dynamics of Cell Ensembles on Adhesive Micropatterns: Bridging the gap between Single Cell Spreading and Collective Cell Migration. *Plos Comput. Biol.* 12, e1004863. doi:10.1371/journal.pcbi.1004863

Aragona, M., Panciera, T., Manfrin, A., Giulitti, S., Michielin, F., Elvassore, N., et al. (2013). A Mechanical Checkpoint Controls Multicellular Growth through YAP/TAZ Regulation by Actin-Processing Factors. *Cell* 154, 1047–1059. doi:10.1016/j.cell.2013.07.042

Brakebusch, C., Bouvard, D., Stanchi, F., Sakai, T., and Fässler, R. (2002). Integrins in Invasive Growth. *J. Clin. Invest.* 109, 999–1006. doi:10.1172/jci0215468

Chanet, S., Sharan, R., Khan, Z., and Martin, A. C. (2017). Myosin 2-Induced Mitotic Rounding Enables Columnar Epithelial Cells to Interpret Cortical Spindle Positioning Cues. *Curr. Biol.* 27, 3350–3358. doi:10.1016/j.cub.2017.09.039

Charras, G., and Yap, A. S. (2018). Tensile Forces and Mechanotransduction at Cell-Cell Junctions. *Curr. Biol.* 28, R445–R457. doi:10.1016/j.cub.2018.02.003

Chen, C. S., Mrksich, M., Huang, S., Whitesides, G. M., and Ingber, D. E. (1997). Geometric Control of Cell Life and Death. *Science* 276, 1425–1428. doi:10.1126/science.276.5317.1425

Collinet, C., and Lecuit, T. (2013). Stability and Dynamics of Cell-Cell Junctions. *Prog. Mol. Biol. Translational Sci.* 116, 25–47. doi:10.1016/b978-0-12-394311-8.00002-9

Dasbiswas, K., Hannezo, E., and Gov, N. S. (2018). Theory of Epithelial Cell Shape Transitions Induced by Mechanoactive Chemical Gradients. *Biophysical J.* 114, 968–977. doi:10.1016/j.bpj.2017.12.022

Deforet, M., Hakim, V., Yevick, H. G., Duclos, G., and Silberzan, P. (2014). Emergence of Collective Modes and Tri-dimensional Structures from Epithelial Confinement. *Nat. Commun.* 5, 3747. doi:10.1038/ncomms4747

Doupé, D. P., Alcolea, M. P., Roshan, A., Zhang, G., Klein, A. M., Simons, B. D., et al. (2012). A Single Progenitor Population Switches Behavior to Maintain and Repair Esophageal Epithelium. *Science* 337, 1091–1093. doi:10.1126/science.1218835

Doupé, D. P., Klein, A. M., Simons, B. D., and Jones, P. H. (2010). The Ordered Architecture of Murine Ear Epidermis Is Maintained by Progenitor Cells with Random Fate. *Dev. Cel* 18, 317–323.

Dupont, S., Morsut, L., Aragona, M., Enzo, E., Giulitti, S., Cordenonsi, M., et al. (2011). Role of YAP/TAZ in Mechanotransduction. *Nature* 474, 179–183. doi:10.1038/nature10137

Farhadifar, R., Röper, J.-C., Aigouy, B., Eaton, S., and Jülicher, F. (2007). The Influence of Cell Mechanics, Cell-Cell Interactions, and Proliferation on Epithelial Packing. *Curr. Biol.* 17, 2095–2104. doi:10.1016/j.cub.2007.11.049

Finegan, T. M., and Bergstralh, D. T. (2019). Division Orientation: Disentangling Shape and Mechanical Forces. *Cell Cycle* 18, 1187–1198. doi:10.1080/15384101.2019.1617006

García, A. J., Vega, M. D., and Boettiger, D. (1999). Modulation of Cell Proliferation and Differentiation through Substrate-dependent Changes in Fibronectin Conformation. *Mol. Biol. Cel* 10, 785–798. doi:10.1091/mbc.10.3.785

Gibson, M. C., Patel, A. B., Nagpal, R., and Perrimon, N. (2006). The Emergence of Geometric Order in Proliferating Metazoan Epithelia. *Nature* 442, 1038–1041. doi:10.1038/nature05014

Giniūnait, R., Baker, R. E., Kulesa, P. M., and Maini, P. K. (2019). Modelling Collective Cell Migration: Neural Crest as a Model Paradigm. *J. Math. Biol.* 80 (1-2), 481–504. doi:10.1007/s00285-019-01436-2

Glazier, J. A., and Graner, F. (1993). Simulation of the Differential Adhesion Driven Rearrangement of Biological Cells. *Phys. Rev. E* 47, 2128–2154. doi:10.1103/physreve.47.2128

Gomez, J. M., Wang, Y., and Riechmann, V. (2012). Tao Controls Epithelial Morphogenesis by Promoting Fasciclin 2 Endocytosis. *J. Cel Biol.* 199, 1131–1143. doi:10.1083/jcb.201207150

Graner, F., and Glazier, J. A. (1992). Simulation of Biological Cell Sorting Using a Two-Dimensional Extended Potts Model. *Phys. Rev. Lett.* 69, 2013–2016. doi:10.1103/physrevlett.69.2013

Haensel, D., Jin, S., Sun, P., Cinco, R., Dragan, M., Nguyen, Q., et al. (2020). Defining Epidermal Basal Cell States during Skin Homeostasis and Wound Healing Using Single-Cell Transcriptomics. *Cel Rep.* 30, 3932–3947. doi:10.1016/j.celrep.2020.02.091

Hannezo, E., Prost, J., and Joanny, J.-F. (2014). Theory of Epithelial Sheet Morphology in Three Dimensions. *Proc. Natl. Acad. Sci. U.S.A.* 111, 27–32. doi:10.1073/pnas.1312076111

Hertwig, O. (1884). Das problem der befruchtung und der isotropie des eies, eine theory der vererbung. *Jenaische Z. fuer Naturwissenschaft* 18, 276–318.

Hilgenfeldt, S., Erisken, S., and Carthew, R. W. (2008). Physical Modeling of Cell Geometric Order in an Epithelial Tissue. *Proc. Natl. Acad. Sci. U.S.A.* 105, 907–911. doi:10.1073/pnas.0711077105

Hočevar Brezavšček, A., Rauzi, M., Leptin, M., and Ziherl, P. (2012). A Model of Epithelial Invagination Driven by Collective Mechanics of Identical Cells. *Biophys. J.* 103, 1069–1077. doi:10.1016/j.bpj.2012.07.018

Käfer, J., Hayashi, T., Marée, A. F. M., Carthew, R. W., and Graner, F. (2007). Cell Adhesion and Cortex Contractility Determine Cell Patterning in the Drosophila Retina. *Proc. Natl. Acad. Sci. U.S.A.* 104, 18549–18554. doi:10.1073/pnas.0704235104

Kempf, F., Goychuk, A., and Frey, E. (2021). Tissue Flow through Pores: a Computational Study. *bioRxiv* 1–29.

Khataee, H., Czirok, A., and Neufeld, Z. (2020). Multiscale Modelling of Motility Wave Propagation in Cell Migration. *Sci. Rep.* 10, 8128. doi:10.1038/s41598-020-63506-6

Kostiou, V., Hall, M. W. J., Jones, P. H., and Hall, B. A. (2020). Different Responses to Cell Crowding Determine the Clonal Fitness of P53 and Notch Inhibiting Mutations in Squamous Epithelia. *bioRxiv*, 1–25.

Krajnc, M., Štorgel, N., Brezavšček, A. H., and Ziherl, P. (2013). A Tension-Based Model of Flat and Corrugated Simple Epithelia. *Soft Matter* 9, 8368. doi:10.1039/c3sm51588e

LeGoff, L., Rouault, H., and Lecuit, T. (2013). A Global Pattern of Mechanical Stress Polarizes Cell Divisions and Cell Shape in the Growing *drosophila* wing Disc. *Development* 140, 4051–4059. doi:10.1242/dev.090878

Low, B. C., Pan, C. Q., Shivashankar, G. V., Bershadsky, A., Sudol, M., and Sheetz, M. (2014). YAP/TAZ as Mechanosensors and Mechanotransducers in Regulating Organ Size and Tumor Growth. *FEBS Lett.* 588, 2663–2670. doi:10.1016/j.febslet.2014.04.012

Melani, M., Simpson, K. J., Brugge, J. S., and Montell, D. (2008). Regulation of Cell Adhesion and Collective Cell Migration by Hindsight and its Human Homolog RREB1. *Curr. Biol.* 18, 532–537. doi:10.1016/j.cub.2008.03.024

Mohan, A., Schlue, K. T., Kniffin, A. F., Mayer, C. R., Duke, A. A., Narayanan, V., et al. (2018). Spatial Proliferation of Epithelial Cells Is Regulated by E-Cadherin Force. *Biophysical J.* 115, 853–864. doi:10.1016/j.bpj.2018.07.030

Montell, D. J. (2008). Morphogenetic Cell Movements: Diversity from Modular Mechanical Properties. *Science* 322, 1502–1505. doi:10.1126/science.1164073

Osborne, J. M., Fletcher, A. G., Pitt-Francis, J. M., Maini, P. K., and Gavaghan, D. J. (2017). Comparing Individual-Based Approaches to Modelling the Self-Organization of Multicellular Tissues. *Plos Comput. Biol.* 13, e1005387. doi:10.1371/journal.pcbi.1005387

Osterfield, M., Du, X., Schüpbach, T., Wieschaus, E., and Shvartsman, S. Y. (2013). Three-Dimensional Epithelial Morphogenesis in the Developing Drosophila Egg. *Dev. Cel* 24, 400–410. doi:10.1016/j.devcel.2013.01.017

Paddillaya, N., Mishra, A., Kondaiah, P., Pullarkat, P., Menon, G. I., and Gundiah, N. (2019). Biophysics of Cell-Substrate Interactions under Shear. *Front. Cel Dev. Biol.* 7, 251. doi:10.3389/fcell.2019.00251

Pedersen, S. F., Hoffmann, E. K., and Novak, I. (2013). Cell Volume Regulation in Epithelial Physiology and Cancer. *Front. Physiol.* 4, 1–12. doi:10.3389/fphys.2013.00233

Provenzano, P. P., and Keely, P. J. (2011). Mechanical Signaling through the Cytoskeleton Regulates Cell Proliferation by Coordinated Focal Adhesion and Rho GTPase Signaling. *J. Cel Sci.* 124, 1195–1205. doi:10.1242/jcs.067009

Puliafito, A., Hufnagel, L., Neveu, P., Streichan, S., Sigal, A., Fygenson, D. K., et al. (2012). Collective and Single Cell Behavior in Epithelial Contact Inhibition. *Proc. Natl. Acad. Sci. U.S.A.* 109, 739–744. doi:10.1073/pnas.1007809109

Reffay, M., Parrini, M. C., Cochet-Escartin, O., Ladoux, B., Buguin, A., Coscoy, S., et al. (2014). Interplay of Rhoa and Mechanical Forces in Collective Cell Migration Driven by Leader Cells. *Nat. Cel Biol* 16, 217–223. doi:10.1038/ncb2917

R. Noppe, A., Roberts, A. P., Yap, A. S., Gomez, G. A., and Neufeld, Z. (2015). Modelling Wound Closure in an Epithelial Cell Sheet Using the Cellular Potts Model. *Integr. Biol.* 7, 1253–1264. doi:10.1039/c5ib00053j

Rognoni, E., and Watt, F. M. (2018). Skin Cell Heterogeneity in Development, Wound Healing, and Cancer. *Trends Cel Biol.* 28, 709–722. doi:10.1016/j.tcb.2018.05.002

Santillán, M. (2008). On the Use of the Hill Functions in Mathematical Models of Gene Regulatory Networks. *Math. Model. Nat. Phenomena* 3, 85–97.

Scarpa, E., Finet, C., Blanchard, G. B., and Sanson, B. (2018). Actomyosin-Driven Tension at Compartmental Boundaries Orients Cell Division Independently of Cell Geometry *In Vivo*. *Dev. Cel* 47, 727–740. doi:10.1016/j.devcel.2018.10.029

Schwartz, M. A., and Assoian, R. K. (2001). Integrins and Cell Proliferation. *J. Cel Sci.* 114, 2553–2560. doi:10.1242/jcs.114.14.2553

Segerer, F. J., Thüroff, F., Piera Alberola, A., Frey, E., and Rädler, J. O. (2015). Emergence and Persistence of Collective Cell Migration on Small Circular Micropatterns. *Phys. Rev. Lett.* 114, 228102. doi:10.1103/physrevlett.114.228102

Streichan, S. J., Hoerner, C. R., Schneidt, T., Holzer, D., and Hufnagel, L. (2014). Spatial Constraints Control Cell Proliferation in Tissues. *Proc. Natl. Acad. Sci. U.S.A.* 111, 5586–5591. doi:10.1073/pnas.1323016111

Swat, M. H., Hester, S. D., Balter, A. I., Heiland, R. W., Zaitlen, B. L., and Glazier, J. A. (2009). Multicell Simulations of Development and Disease Using the

CompuCell3D Simulation Environment. *Methods Mol. Biol.* 500, 361–428. doi:10.1007/978-1-59745-525-1_13

Swat, M. H., Thomas, G. L., Belmonte, J. M., Shirinifard, A., Hmeljak, D., and Glazier, J. A. (2012). Multi-scale Modeling of Tissues Using Compucell3d. *Methods Cel. Biol.* 110, 325–366. doi:10.1016/b978-0-12-388403-9.00013-8

Théry, M., Racine, V., Pépin, A., Piel, M., Chen, Y., Sibarita, J.-B., et al. (2005). The Extracellular Matrix Guides the Orientation of the Cell Division axis. *Nat. Cel Biol.* 7, 947–953. doi:10.1038/ncb1307

Thüroff, F., Goychuk, A., Reiter, M., and Frey, E. (2019). Bridging the gap between Single-Cell Migration and Collective Dynamics. *eLife* 8, e46842.

Vincent, R., Bazellières, E., Pérez-González, C., Uroz, M., Serra-Picamal, X., and Trepat, X. (2015). Active Tensile Modulus of an Epithelial Monolayer. *Phys. Rev. Lett.* 115, 248103. doi:10.1103/physrevlett.115.248103

Weber, K. L., Fischer, R. S., and Fowler, V. M. (2007). Tmod3 Regulates Polarized Epithelial Cell Morphology. *J. Cel Sci.* 120, 3625–3632. doi:10.1242/jcs.011445

Widmann, T. J., and Dahmann, C. (2009). Dpp Signaling Promotes the Cuboidal-To-Columnar Shape Transition of Drosophila wing Disc Epithelia by Regulating Rho1. *J. Cel Sci.* 122, 1362–1373. doi:10.1242/jcs.044271

Zhou, F., Schaffer, S. A., Schreiber, C., Segerer, F. J., Goychuk, A., Frey, E., et al. (2020). Quasi-periodic Migration of Single Cells on Short Microlanes. *PLOS ONE* 15, e0230679. doi:10.1371/journal.pone.0230679

Conflict of Interest: The authors declare that the research was conducted in the absence of any commercial or financial relationships that could be construed as a potential conflict of interest.

Publisher's Note: All claims expressed in this article are solely those of the authors and do not necessarily represent those of their affiliated organizations, or those of the publisher, the editors and the reviewers. Any product that may be evaluated in this article, or claim that may be made by its manufacturer, is not guaranteed or endorsed by the publisher.

frontiers in Cell and Developmental Biology

REVIEW
published: 28 March 2022
doi: 10.3389/fcell.2022.823857

Multiscale Mechanobiology in Brain Physiology and Diseases

Anthony Procès[1,2], *Marine Luciano*[1], *Yohalie Kalukula*[1], *Laurence Ris*[2] *and Sylvain Gabriele*[1]*

[1]Mechanobiology and Biomaterials group, Interfaces and Complex Fluids Laboratory, Research Institute for Biosciences, University of Mons, Mons, Belgium, [2]Neurosciences Department, Research Institute for Biosciences, University of Mons, Mons, Belgium

Increasing evidence suggests that mechanics play a critical role in regulating brain function at different scales. Downstream integration of mechanical inputs into biochemical signals and genomic pathways causes observable and measurable effects on brain cell fate and can also lead to important pathological consequences. Despite recent advances, the mechanical forces that influence neuronal processes remain largely unexplored, and how endogenous mechanical forces are detected and transduced by brain cells into biochemical and genetic programs have received less attention. In this review, we described the composition of brain tissues and their pronounced microstructural heterogeneity. We discuss the individual role of neuronal and glial cell mechanics in brain homeostasis and diseases. We highlight how changes in the composition and mechanical properties of the extracellular matrix can modulate brain cell functions and describe key mechanisms of the mechanosensing process. We then consider the contribution of mechanobiology in the emergence of brain diseases by providing a critical review on traumatic brain injury, neurodegenerative diseases, and neuroblastoma. We show that a better understanding of the mechanobiology of brain tissues will require to manipulate the physico-chemical parameters of the cell microenvironment, and to develop three-dimensional models that can recapitulate the complexity and spatial diversity of brain tissues in a reproducible and predictable manner. Collectively, these emerging insights shed new light on the importance of mechanobiology and its implication in brain and nerve diseases.

Keywords: mechanobiology, brain cells, brain tissues, mechanotransduction, brain diseases, extracellular matrix, cytoskeleton

OPEN ACCESS

Edited by:
Selwin K. Wu,
National University of Singapore, Singapore

Reviewed by:
Naotaka Nakazawa,
Kyoto University, Japan
Deok-Ho Kim,
Johns Hopkins University, United States

***Correspondence:**
Sylvain Gabriele
sylvain.gabriele@umons.ac.be

Specialty section:
This article was submitted to Signaling, a section of the journal Frontiers in Cell and Developmental Biology

Received: *28 November 2021*
Accepted: *08 March 2022*
Published: *28 March 2022*

Citation:
Procès A, Luciano M, Kalukula Y, Ris L and Gabriele S (2022) Multiscale Mechanobiology in Brain Physiology and Diseases. Front. Cell Dev. Biol. 10:823857. doi: 10.3389/fcell.2022.823857

INTRODUCTION

It is now well accepted that brain tissues are one of the most complex and compliant tissue in the human body (Budday et al., 2020). While neuroscience has mostly been limited to electrophysiological, biochemical, and genetic studies over the past few decades, emerging evidence confirms that mechanobiology plays a critical role in modulating brain function and dysfunction (Tyler, 2012). Indeed, accumulative works suggest that mechanical properties of the cell microenvironment can control developmental processes (Koser et al., 2016) and are involved in the progression of brain diseases (Ngo and Harley, 2021), while external mechanical forces can lead to brain injury (Meaney and Smith, 2011). Consequently, a better understanding of mechanobiological processes in brain tissues requires sophisticated *in vitro* models that capture more realistically the complex characteristics of brain tissues through engineered multi-scale platforms. These novel

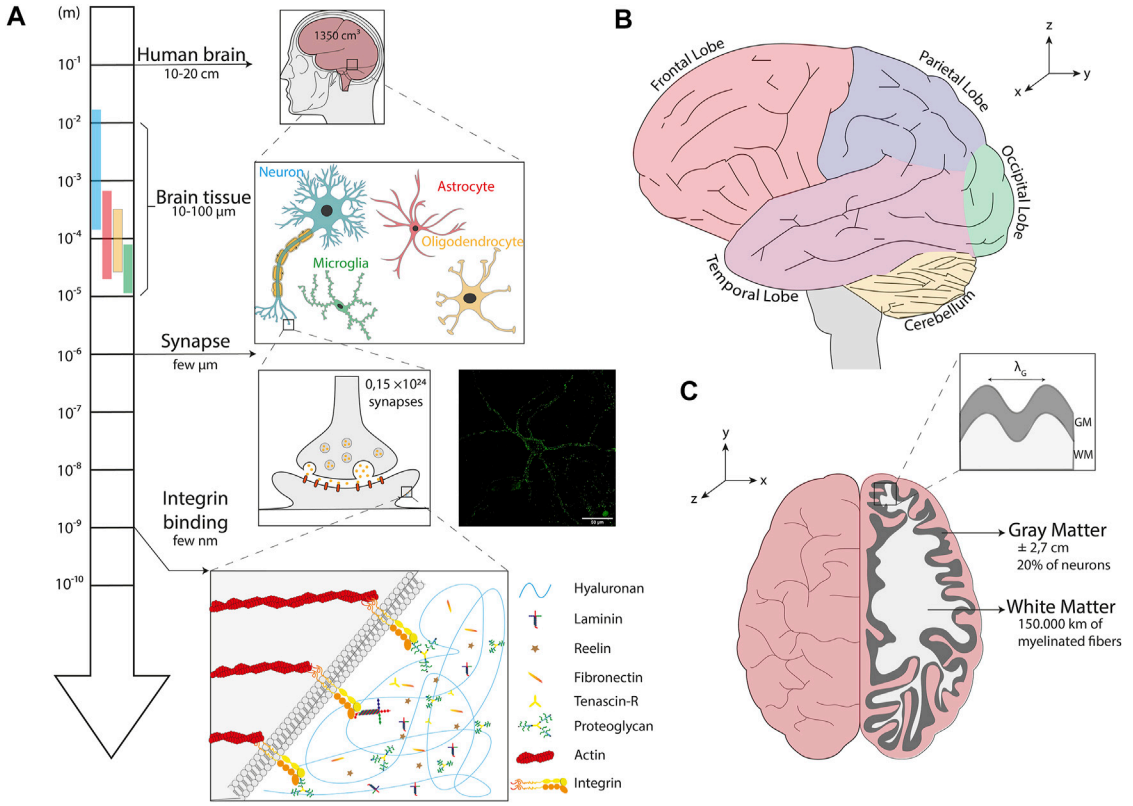

FIGURE 1 | The multi-scale structure of the human brain. **(A)** Homeostasis of brain tissues mainly relies on the interaction between four cell types: neurons, microglial cells, astrocytes and oligodendrocytes. At the subcellular scale, synapses allow the transmission of an electrical or chemical signal from a neuron to another one or to the target effector cell. The inset shows an image of a neuron isolated from an organotypic slice of hippocampus labeled with synaptotagmin (in green), a presynaptic calcium sensor. The scale bar is 50 µm. At the molecular scale, transmembrane integrins connect proteins of the extracellular matrix to cytoskeletal components. **(B)** Illustration of a sagittal section of a normal human brain whose different lobes are color-coded: the frontal lobe in red, the parietal lobe in blue, the occipital lobe in green, the temporal lobe in purple and the cerebellum in yellow. **(C)** Illustration of a top view of a normal human brain with a cross section of the right lobe showing the organization of the cerebral cortex (gray matter) and subcortical regions (white matter). The inset depicts the wavelength (λ_G) of cortical folds, the grey matter (GM) and the white matter (WM).

platforms must allow access to the molecular level, where transduction of mechanical signals occurs, to the cellular level, where mechanotransduction processes take place, and to inter-cellular interactions that control cross-talks between different brain cell types (**Figure 1A**).

Natural mechanical stimuli are part of the life of each individual and do not inevitably lead to brain injury. Indeed, the human nervous system is well organized and protected in many ways. It is divided into the central nervous system (CNS), which includes the brain and spinal cord, and the peripheric nervous system composed of the nerve, which connects the brain and spinal cord to tissues and organs (Barker et al., 2019). The first is enclosed by the skull, which provides an important physical barrier to all external aggressions and is also coated by three layers of membranes known as the meninges (dura mater, arachnoid mater, and pia mater), which protect the brain and spinal cord. The CNS is irrigated by the cerebrospinal fluid, which also assumes a role in the protection of neuronal tissue, both from an immunological and mechanical point of view (Saunders et al., 2016). The blood-brain barrier restricts the passage of pathogens, the diffusion of solutes in the blood, and large or hydrophilic molecules into the cerebrospinal fluid, while allowing the diffusion of hydrophobic molecules and small non-polar molecules (Daneman and Prat, 2015).

The high level of protection of the CNS allows to ensure the development is properly conducted through a precise orchestration sequence of genetic, biochemical, and physical events. For instance, rapid movements of the head or torsion of the backbone can be absorbed by the physical barriers, whereas inertia load is partially resorbed by the cerebrospinal fluid irrigating the meninges. Physical forces play a central role in translating the molecular and cellular mechanisms during neurodevelopment and maturation of the nervous system (Budday et al., 2015b). In some cases, the load can be above the limit leading to damaged cells and tissues (Bilston, 2011).

This review aims to describe the basic physical principles underlying brain function and to present our current understanding of the role of mechanical forces in physiological and pathological situations. We ambition to motivate further research in the field of brain and nerve mechanobiology by

highlighting the need for a global approach to brain mechanics at a multiscale level.

SCALE OF THE HUMAN BRAIN

Understanding how brain tissue mechanobiology is intimately linked with neurophysiology and brain disease progression requires to take the specificity and complexity of the human brain into account. Using a large sample of human brains from the general population, it has been established that the mean human brain weighs about 1,375 g for an average volume of ~1,350 cm^3, resulting in a volume mass of ~1,019 kg/m^3, which is comparable to calcium oxide. The total brain surface area is ~1,820 cm^2 and the average cortical thickness was found to be ~2.7 mm (Pakkenberg and Gundersen, 1997). Interestingly, about 20% of neurons are located in the cerebral cortex (Herculano-Houzel, 2009) and each cortical neuron forms an average of ~7,000 synaptic connections with other neurons, resulting in a total of 0.15 quadrillion synapses (Pakkenberg, 2003). These numbers allow to estimate that more than 150,000 kms of myelinated fibers browse the human brain, which is approximately the average distance covered by a car during its entire lifetime (**Figures 1A–C**).

Although the human brain makes up only ~2% of the body weight, it is well established that the human brain uses more energy than any other organ, accounting for up to 20% of the body's baseline energy (Shokri-Kojori et al., 2019). Until recently, it was widely accepted that this energy was mainly used to fuel electrical impulses that neurons use to communicate with neighbors. This concept was refined by using magnetic resonance spectroscopy (MRS) to measure the brain energy production during activity shifts. It was found that two-thirds of the brain's energy budget is used to support the firing of nerve cells, whereas the remaining third refers to cell-health maintenance (Raichle and Gusnard, 2002). This theory has been very recently confirmed by showing that synaptic vesicle (SV) pools are a major source of presynaptic basal energy consumption. Indeed, it was found that basal metabolic processes arise from SV-resident V-ATPases compensating for a hidden resting H+ efflux from the SV lumen, whereas that this steady-state H+ efflux is mediated by vesicular neurotransmitter transporters, is independent of the SV cycle, accounts for up to 44% of the resting synaptic energy consumption, and contributes substantially to nerve terminal intolerance of fuel deprivation (Pulido and Ryan, 2021).

It is usually reported in textbooks, reviews, and even original articles that the human brain is composed of about 100 billion neurons and about 10 more glial cells, even though no clear references are cited (Herculano-Houzel, 2009). The lack of original references for these numbers may lead the reader to believe that the cellular composition of the human brain has long been determined and can be used for developing new bioengineered platforms. Even if a direct estimation of the number of different cell types in the entire human brain is difficult to obtain, the relative abundance of each cell type in different parts of the brain is considered as a determinant of neural function and behavior (Williams and Herrup, 1988; Herculano-Houzel, 2011). However, determining glial cell counts is particularly challenging due to their small size and the difficulty to isolate them (von Bartheld et al., 2016).

To address this challenge, the isotropic fractionation method was introduced to transform an intact brain into a soup of nuclei (Gabi et al., 2016). Entire brains were sliced up into regions of interest (e.g., cerebellum, cerebral cortex, etc.), tissues were ground-up and then dissolved in saline detergent to harvest nuclei from both neurons and glia. An anti-NeuN antibody was used to bind specifically to proteins of neuronal nuclei and subtract that number from the total number of nuclei to determine the fraction of glial cells in each brain section. By using this method, it was found that the human brain contains about 170.68 billion cells, 86.1 billion of which are neurons and 84.6 billion of which are glial cells, thus debunking the myth there are at least 10 times as many glia as neurons in the human brain (Herculano-Houzel, 2005). Interestingly, it was also suggested that the ratio of glia to neurons differs significantly between different brain regions. In the cerebral cortex, 60.84 billion cells are glia, while only 16.34 billion cells are neurons, giving this large region glia to neuron ratio of about 3.72. An inversed situation was found in the cerebellum, that contains 69.03 billion neurons and only 16.04 glial cells, which means there are about 4.3 neurons for every glia in this region (Azevedo et al., 2009). The variations of the glia to neuron ratio is fascinating and it could be interesting to further investigate whether the difference of glia to neuron sub-populations can be involved in the modulation of the mechanical properties of brain tissue. In addition, it also highlights the importance of robust numbers for developing advanced engineering approaches to study the exact role of glial cells by considering their structural diversity, functional versatility, and the fact that they can change the behavior of firing neurons.

In this way, glial cells are extensively studied to understand whether they must be only considered as a "glue" for neurons or whether they also support them by providing a mechanical scaffold. To answer this question, the mechanobiology of brain tissues is intensively studied and many efforts focus on the determination of the individual mechanical characteristics of the main brain cell types.

MECHANOBIOLOGY OF BRAIN TISSUES

In vitro recapitulation of the native microenvironment of neurons and glial cells is crucial for studying cellular responses and creating biomaterials mimicking brain tissues. The brain is a complex tissue that is extremely soft and often considered as the softest tissue in the human body. Brain tissues are known to be incompressible (Brands et al., 2004) due to a large amounts of proteoglycans, which are heavily glycosylated proteins that bind water (Lau et al., 2013), leading to a relatively high amount of water of approximately 73–85% of the total mass. Interestingly, lipids account for roughly 60% of the total dry weight of the brain (O'Brien and Sampson, 1965; Chang et al., 2009).

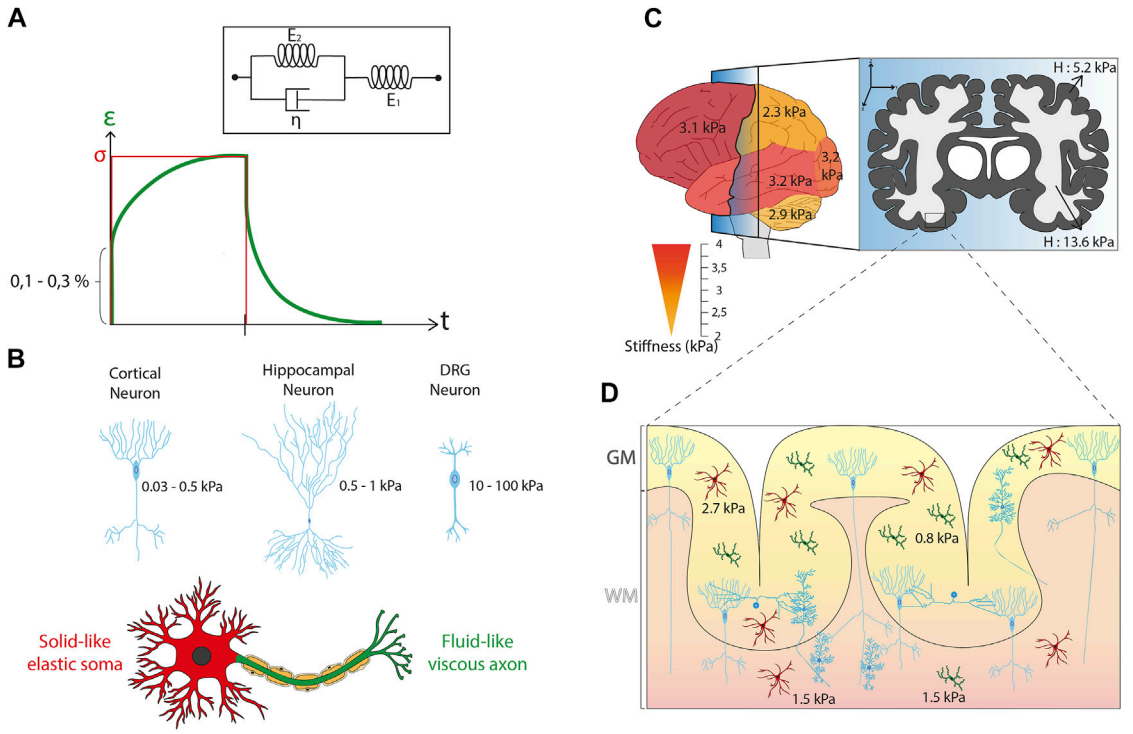

FIGURE 2 | Mechanical properties of brain cells and tissues. **(A)** Kelvin-Voigt representation of the Standard Linear Solid (SLS) model that describes a viscoelastic material with two systems in series. The first system is called the Kelvin arm and is formed by a spring (E_2) and a dashpot (η) in parallel. The other arm is only made of a spring (E_1). These SLS model predicts the temporal evolution of the strain (ε, solid black curve) in response to the application of a constant stress (σ) depicted in red line. **(B)** Sagittal view of the normal human brain color-coded with a gradient of stiffness starting from yellow (~2 kPa) to red (~4 kPa) that illustrates the differences of mechanical properties in brain tissues according to the different regions of interest. Parietal lobe and cerebellum are softer than frontal, parietal, and occipital lobes. The frontal section illustrates the anatomical distribution of white (~13.6 kPa) and grey (~5.2 kPa) matter. **(C)** Illustration of the mean stiffness observed in different neuron types. A cortical neuron exhibits a typical stiffness between 0.03 and 0.5 kPa, a neuron from the hippocampus shows a stiffness of 0.5–1 kPa, and a DRG neuron is characterized by a mean stiffness of 10–100 kPa. The mechanical compartmentalization of a neuron is presented with a solid-like elastic Soma (in red) and a fluid-like viscous axon (in green). **(D)** Cross-section of the cerebral cortex indicating the individual mechanical properties of the glial cells as well as their spatial differences with values of ~0.85 kPa for cortical microglia cells, ~1.5 kPa for subcortical microglia cells, ~2.7 kPa for cortical astrocytes and ~1.5 kPa for subcortical astrocytes. It is interesting to note the non-homogeneous distribution of glial cells in brain tissues with a larger cell density in grey matter.

This very specific composition of brain tissues leads to elaborated rheological properties. Although mechanical properties of brain tissues are difficult to test experimentally and to model theoretically (Goriely et al., 2015), it is now well accepted that brain stiffness increases with age, starting at the developing brain (Antonovaite et al., 2021). As a matter of fact, brain tissue acts as a linear viscoelastic material under very small strain in order of ~0.1–0.3% (Bilston et al., 1997; Nicolle et al., 2005) (See **Box 1** and **Figure 2A**). Interestingly, storage (i.e. the elastic part) and loss (i.e. the viscous part) moduli of brain tissues both increase with frequency (Bilston et al., 1997). When the strain goes beyond the limit of linear viscoelastic strain, brain tissues behave in a complex non-linear mode, with an apparent stiffness depending on both the strain and the type of loading. Low mechanical inputs induce reversible deformations, which are characteristic of elastic behavior. Under high deformations, brain tissues exhibit a plastic deformation as observed in non-linear viscoelastic materials (Budday et al., 2017). Moreover, brain tissues are unable to adapt over short time scales and can be therefore subject to damage and injury (Mc Intosh et al., 1998).

Brain rheological properties are a key ingredient of the cortical folding process, by which brain tissues undergo morphological changes in terms of waving. Indeed, the brain cortex starts to form convex gyri and concave sulci, whose depth and length increase during development, which starts at the third trimester of gestation in humans. Different models of cortical folding have been reported that rely on a combination of biological and mechanical properties of brain tissues: i) axonal tension-driven folding which assumes that tension driven by axons triggers the buckling of the cortical layer (Essen, 1997), ii) differential tangential growth, which explains buckling by the more rapid growth of the external layer of the cortical plate than the inner layer lying on the elastic core (Richman et al., 1975; Tallinen et al., 2016) and iii) viscoelastic instability in a model of stress-induced growth, which includes a growing core under the resulting stresses from outer layer expansion producing a stress-growth relationship between inner and outer layer (white and gray matter) (Bayly et al., 2013). Altogether, these models illustrate the importance of mechanobiology to further understand fundamental biological mechanisms such as cortical folding.

BOX 1 | Viscoelastic properties

Viscoelasticity is a time-dependent mechanical property of synthetic and living materials that exhibit both viscous and elastic characteristics when undergoing deformation. Viscoelastic properties are usually evaluated by recording over time the degree of deformation of an object upon constant force application (i.e., creep) and then its recovery (i.e., relaxation). Purely elastic materials (Hookean solids) are described with a spring model that relates linearly stress (σ) to strain (ε) by the elastic modulus (E in N/m^2 or Pa), such as $E = \sigma/\varepsilon$. The stress (σ, in Pa) is defined as the exerted force (in Newtons) per unit area (in m^2), while the strain (ε, adimensional) is defined as changes in length with respect to initial length. The response of purely elastic materials to a creep-relaxation test is to undergo an instantaneous elastic strain upon loading, to maintain that strain as long as the load is applied, and then to undergo an instantaneous recovery upon removal of the load. Purely viscous fluids (Newtonian fluids) are described with a dashpot model that represents a piston-cylinder filled with a viscous fluid (η expressed in Pa.s). The dashpot responds with a strain-rate proportional to stress. Viscoelastic materials exhibit mechanical characteristics of both solids and fluids: at short time scales, they deform elastically, while they behave as viscous fluids at long time scales. Basically, viscoelastic materials can therefore be described as composite structures containing an elastic spring connected to a viscous dashpot, either in series (Maxwell configuration) or in parallel (Kelvin-Voigt configuration). By using more complex combinations of springs and dashpots, many different viscoelastic models were developed, such as the standard linear solid model (SLSM), to determine the viscoelastic properties of materials based on creep-relaxation experiments. Here we show the Kelvin form of the SLSM model (**Figure 2A**) that consists of two systems in series: the first contains a spring (E_2) and a dashpot (η) in parallel and the second contains only a spring (E_1). Upon loading the right-hand spring (E_1) stretches immediately. The dashpot (η) then takes up the stress, transferring the load to the second spring (E_2) as it slowly opens over time. Upon unloading the right-hand spring (E_1) contracts immediately and then the left-hand spring (E_2) slowly contracts, being held back by the dashpot. As shown in **Figure 2A**, the Kelvin form of the SLSM model allows to describe more realistically the viscoelastic responses of cells and tissues than simplest viscoelastic models (Wang and Kuhl, 2020).

However, inconsistency in sample preparation, postmortem timing, and testing conditions in most of the previous experiments prevents a reliable mechanical characterization of brain tissues (Hrapko et al., 2008). Despite this technical difficulty, the mechanical characterization of specific part of brain tissues is considered as an important issue for understanding the individual properties of white and gray matter. White matter is mostly composed of bundled myelinated axons, whereas gray matter contains numerous cellular bodies and relatively few myelinated axons. Interestingly, this structural difference is directly correlated with changes in mechanical properties. Indeed, white matter is approximately 30% stiffer than grey matter, with a stiffness of ~1.9 kPa for white matter and ~1.4 kPa for gray matter for bovine tissues in compression mode (Budday et al., 2015a). Magnetic resonance elastography (MRE) on the human brain has shown a shear modulus of ~13.6 kPa for white matter and ~5.2 kPa for grey matter (Kruse et al., 2008), while another group (Green et al., 2008) showed more similar shear stiffness values for white (~3.1 kPa) and gray (~2.7 kPa) matter (**Figure 2B**). White matter have also higher regional variations of stiffnesses, is more viscous, and shows longer relaxation times than gray matter (Pervin and Chen, 2009; Budday et al., 2015a). Even in the mature brain, significant differences in brain tissue stiffness were found between different regions, including the cerebellum, medulla, cortex, and pons (MacManus et al., 2017). Using MRE, cerebellum (~2.9 kPa) and parietal (~2.4 kPa) lobes were found to be softer than frontal (~3.2 kPa), occipital (~3.2 kPa), or temporal (~3.2 kPa) lobes (Murphy et al., 2013) (**Figure 2B**). Interestingly, a correlation has been issued between the local stiffness and the underlying morphological properties with regions of high nuclear densities that appear softer than those with lower nuclear densities. For instance, the stiffness of the CA3 stratum pyramidal (CA3-SP) (high nuclear density) was found to be softer (~1.5 kPa) than the stratum radiatum (CA3-SR) (low nuclear density) of ~3 kPa.

These differences in mechanical properties between brain regions result from complex combinations of different cell types, which are embedded in an extracellular matrix (ECM) whose composition varies depending on the brain zone (Lam et al., 2019). Determining the mechanical properties of each brain cell type and ECM is therefore crucial for understanding how mechanical forces acting on the brain could be involved in the brain functioning and the development of pathological situations.

MECHANOBIOLOGY OF BRAIN CELLS

Neurons conduct nerve impulses and for this reason they are considered as the central functional unit of the brain, while glial cells maintain the biochemical homeostasis and serve as physical support to neurons (Franze et al., 2013). We will present in this section the current mechanical picture of neuronal and glial cells and how both cell types adapt to physico-chemical changes (topography, stiffness, or composition) of their microenvironment.

Mechanical Properties of Neurons

Neurons are highly specialized cells that are primarily responsible for transmitting information through chemical and electrical signaling, in both the central and peripheral nervous systems. Since there is a broad range of functions performed by different types of neurons, there is also a wide variety of morphologies. The typical morphology of neurons are composed of a cell body, also called the Soma, that contains the nucleus and two other compartments: the dendrites, which are fine and branched cell processes that receive synaptic input from other neurons, and one axon that can reach a length of several meters with presynaptic terminals (Franze and Guck, 2010). The structural and mechanical properties of neurons are essentially defined by the spatial organization of their cytoskeletal filaments, which governs growth and regeneration processes, including axonal extension and the generation of traction forces, but also interactions with the surrounding environment, such as the ECM, glial cells, or other neurons (Marinval and Chew, 2021).

Several rheological studies have been conducted on different neuronal cell types and from different species, resulting in a discrepancy in stiffness values. Atomic Force Microscopy (AFM) measurements of mouse hippocampal neurons reported a

stiffness between 480 and 970 Pa for the Soma (Lu et al., 2006). Cortical neurons were found to be softer, with a typical stiffness ranging from 30 to 500 Pa (Bernick et al., 2011; Spedden et al., 2012a; Spedden et al., 2012b). Interestingly, recent investigations with optical tweezers confirmed a very low stiffness for cortical neurons with a Young's modulus around 50 Pa (Ayala et al., 2016). Dorsal root ganglion (DRG) neurons, which are a cluster of neurons (a ganglion) in a dorsal root of a spinal nerve, were found to be stiffer with a mean stiffness ranging from 10 to 100 kPa (Mustata et al., 2010; Spedden et al., 2012a; Martin et al., 2013). As discussed previously, neurons are compartmentalized cells which can exhibit different sub-cellular mechanical properties. By combining protein micropatterns and magnetic tweezers, it was found that the cell body is soft with a solid-like and stress-stiffening response, whereas the neurite compartment is stiffer and viscous-like (Grevesse et al., 2015). The growth cone, which directs the migration of neurons and mediates the formation of synapses (Kalil and Dent, 2014), was reported to have a Young's modulus ranging from ~0.4 to ~40 kPa (Martin et al., 2013) (Xiong et al., 2009) (**Figure 2C**).

An intriguing question concerns the influence of the mechanical properties of individual neuronal and non-neuronal cells on the stiffness of specific regions of the brain. To address this question, the spatiotemporal stiffness of the mouse embryonic cerebral cortex and isolated cells from the same brain region was probed with AFM (Iwashita et al., 2014). A gradual stiffening of specific layers of the embryonic brain was observed over time, whereas the rigidity of neuronal progenitor cells remained constant over time. In addition, the cortical plate showed an initial increase in stiffness until E18.5 (embryonic stage) where it started to decrease, whereas the neuronal population of this layer showed a constant increase in their stiffness according to the maturation of microtubules (Iwashita et al., 2014). Altogether these results demonstrated that the mechanical behavior of individual cells cannot explain the temporal evolution of the tissue stiffness. Other reports performed on the cortical plate of mice and ferrets confirmed that this observation and suggested that the density of the cell population could modulate the mechanical properties of brain tissues (Nagasaka et al., 2016). To get a step further in understanding the temporal behaviour of brain tissue mechanics, future studies will have to focus on the variation of cell density across brain tissues and consider the composition and the stiffness of the cell matrix.

Mechanical Properties of Glial Cells

Glial cells participate to form the microenvironment of neurons by filling most of the interstitial space. They ensure the maintenance of homeostasis, produce myelin and play a role in supporting and protecting nervous tissues by providing nutrients and oxygen, eliminating dead cells, and fighting pathogens (Jäkel and Dimou, 2017). Glial cells find the origin of their name from the Greek word "γλια" meaning "glue" and they were long considered as the glue of brain tissues, acting as a paste between neurons. This theory was challenged by probing with AFM the viscoelastic properties of individual glial cells and neurons in the CNS (Lu et al., 2006). Both cell types were found to exhibit predominant elastic properties but very low elastic moduli (<1 kPa). Glial cells were twice softer than neurons, with an elastic modulus of 300–520 Pa for astrocytes and 480–970 Pa for neurons. Interestingly, similar results were obtained for Müller glial cells, which are a type of retinal glial cells (Lu et al., 2006). Very recently, the stiffness of microglial cells was reported to be even softer with an elastic modulus ranging from 40 to 100 Pa (Rheinlaender et al., 2020). Interestingly, microglia derived from gray matter are intrinsically softer (842 Pa) than microglia derived from white matter (1,429 Pa), suggesting that their mechanical properties depend on their spatial location (van Wageningen et al., 2021). This characteristic was also recently confirmed for astrocytes. Indeed, astrocytes from the white matter (~1.5 kPa) were found to be approximatively 1.8 times softer than astrocytes derived from the gray matter (~2.7 kPa) (Antonovaite et al., 2020) (**Figure 2D**).

Taken together, these findings indicate that neuronal cells are surrounded by softer glial cells, which are constantly subjected to physical forces. It was shown recently that Schwann cells (SCs), which have a dense vimentin network, have a great ability to resist mechanical deformation with nuclei that are hard to deform, suggesting that adults SCs can mechanically protect the neurons they encase (Rosso et al., 2019). To further confirm this hypothesis, future studies should investigate the mechanical properties of the nucleus of glial cells and focus on nucleoskeletal interactions to better understand their mechanosensing properties and identify the mechanotransduction pathways in glial cells, which in turn may have an impact on neuronal network activity.

Cytoskeleton, Nucleus and Molecular Clutch in Brain Cells

Even if it has been demonstrated very recently that the cortical stiffness of microglial cells is independent of substrate mechanics (Rheinlaender et al., 2020), the reorganization of the cell cytoskeleton allows many cell types to adapt their stiffness to that of their surroundings (Doss et al., 2020). Adherent cells can sense their mechanical environment through focal adhesions, which connect the cytoskeletal filaments to the ECM via transmembrane integrins and act as a mechanosensor (see **Box 2**). In addition, cells can also use adherens junctions to adapt their mechanical properties to the intercellular stress and the spatial confinement (Mohammed et al., 2019) imposed by neighbouring cells (Takeichi, 2007). Interestingly, adherens junctions bridge neighboring cells and the actin-myosin cytoskeleton, thereby contributing to mechanical coupling between cells (Indra et al., 2020). Adherent cells must adapt their shape and their mechanical properties in response to the physico-chemical properties of the ECM to perform their tasks, such as migration or differentiation. Much effort has gone into identify mechanotransduction pathways and the molecular process used by brain cells to convert mechanical stimuli into biochemical signals.

Emerging evidence suggests that the nucleus of brain cells must be considered as a key mechanical ingredient. Mechanical properties of the nucleus are mostly related to the chromatin state

BOX 2 | Cytoskeleton of neuronal cells: structure and function

The cytoskeleton of neuronal cells is composed of three main polymers: microtubules (MTs), intermediate or neurofilaments (NFs), and actin filaments or microfilaments (MFs). While they form an actin mesh in the dendritic spines (Star et al., 2002), MFs can be described as highly repeated patterns in the axons known as actin rings spaced of approximatively 180–200 nm and be linked by α-β-spectrin dimers (Xu et al., 2013; Vassilopoulos et al., 2019). Neurofilaments are approximately 10 nm in diameter and are made of heteropolymers, composed of subunits of variable molecular weight as well as internexin or peripherin intermediate filaments (Leterrier et al., 2017). They are in high density in axon from 170/μm^2 in internodes to 209/μm^2 in nodes (Reles and Friede, 1991). NFs are heteropolymers forming arms when glial filaments (GFs) are homopolymers without any arms (Pigino et al., 2012). MTs lead to the formation of highly dynamic regions, as well as stable regions, made of α-tubulin and β-tubulin heteropolymer. MTs have a diameter of ~25 nm and are polar structures, with a fast-growing 'plus' end and a slower-growing 'minus' end. MTs stabilize the cellular architecture during rest and movement thanks to their ability to bear mechanical loading (**Figure 3**). Furthermore, they serve as tracks for the movement of mitochondria, lipids, synaptic vesicles, proteins, and other organelles (Ciocanel et al., 2020). Axonal transport is divided into the slow transport of cytoplasmic proteins (including enzymes and cytoskeletal structures such as NFs) and the fast transport of membrane-bounded organelles along microtubules. Fast axonal transport is based on the predominant role of kinesin and dynein with a transport rate of 50–400 mm/day (Cyr and Brady, 1992; Maday et al., 2014). Although dynein and kinesin role has been revealed in fast axonal transport, a new hypothesis have been proposed that consists on a "stop and go" process to explain the slower transport rate by the pausing of molecular cargoes (Brown et al., 2005; Brown and Jung, 2013). This intracellular traffic can be described as anterograde flow (toward the synapses) supported by the kinesin and retrograde flow (toward the Soma) mainly produced by the dynein molecular motors (Guillaud et al., 2020).

and the nuclear lamina, which is connected to the cell cytoskeleton by LINC complexes (Corne et al., 2017). The nuclear lamina is an intermediate filament meshwork, composed largely of lamins A and C (A-type lamins) and lamins B1 and B2 (B-type lamins), that is located immediately adjacent to the inner nuclear membrane and provides a structural scaffolding for the cell nucleus. Among the different lamin types, the expression level of A-type lamins mainly determines nuclear stiffness and viscoelastic properties (Swift et al., 2013). Nonetheless, B-type lamins also contribute to nuclear stiffness and stability, and loss of either lamin type results in abnormal nuclear shape and increased nuclear envelope (NE) rupture. However, the level of A-type lamin expression in the human brain is unclear. It was shown recently that cortical glial cells and neurons in the cortex of rat brains both express more lamin C than lamin A (Takamori et al., 2018). Interestingly, astrocytes and oligodendrocytes, both mature glial cells, showed a similar balance of lamins A and C, whereas microglia showed low expression of lamins A and C. Oligodendrocyte progenitor cells showed a weak lamin C immunoreactivity but an intense lamin B1 immunoreactivity. The staining intensity of lamin B2 in all glial cells was found to be relatively weak compared with cortical neurons. These data indicate that glial cells in the adult cerebral cortex showed cell type specific lamin expression patterns (Takamori et al., 2018). However, deregulation of lamin expression can lead to pathologies such as Huntington's disease and to was shown recently that neurons overexpressing B-type lamin contributes to nuclear dysfunction in Huntington's disease (Alcalá-Vida et al., 2021). Further studies will be needed to determine the exact role of lamins in the establishment of the mechanical properties of brain tissues. Indeed, the hetero-distribution of the isoforms of lamin can be considered as both static and dynamic biomarkers of mechanophenotype (González-Cruz et al., 2018). Considering that stiff cells express higher ratio of lamin A/C:B than soft cells, it could be interesting to further study lamin expression in brain cells which could be considered as a key factor to the overall brain tissue mechanical properties.

The nucleus is also an interesting organelle for understanding other cellular events such the migration of brain cells. Indeed, migration is a complex cellular process that requires the cytoskeleton to translocate the nucleus through interstitial pores of submicron size. In many situations, dynein and kinesin molecular motors directly interact with the nuclear lamina via the LINC complex and steer directional nuclear movement, while actomyosin contractility and its global flow exert forces to deform and move the nucleus (**Figure 2**). There is growing evidence that the clutch machinery mediates neuronal migration, which is regulated by extracellular guidance cues. In this context, recent efforts have been made to refine the molecular clutch model that describes the mechanosensing mechanism during axon outgrowth and cell migration (Elosegui-Artola et al., 2018). During such processes, the cytoskeleton is constantly polymerizing, and actomyosin generates contractile forces that push against the membrane. This constant flow of actin is called the "retrograde flow" and is directed from cell edge to nucleus. The motor-clutch was introduced to describe the mechanism that the force imparted to the ECM counteracts myosin contractility, slows down retrograde actin flow, and promotes actin protrusion away from the cell center (Mitchison and Kirschner, 1988). The motor-clutch model predicts how cell migration is affected by the matrix stiffness by considering the number of myosin II molecular motors and clutches to predict the traction force dynamics (Chan and Odde, 2008; Bangasser et al., 2013; Riaz et al., 2016). In the molecular-clutch mechanism, ligand-bound adhesion receptors are mechanically coupled to the actin network to transmit traction forces to the substrate, resulting in a local diminution of the retrograde flow and forward progression. This model was then refined to consider the role of N-cadherin adhesion molecules in the axon outgrowth mechanism. Indeed, it was shown that the growth cone velocity and the mechanical coupling are strongly correlated with N-cadherin receptors and the retrograde actin flow (Bard et al., 2008). To get further insight into this mechanism, experiments using optical tweezers and microneedle were performed to control the motion of microspheres coated with purified recombinant N-cadherin. These experiments have shown a slippage of cadherin-cytoskeletal bonds at low forces and a local actin accumulation with a strengthening of nascent N-cadherin contacts at higher forces (Bard et al., 2008), demonstrating that a molecular clutch between the actin flow and N-cadherin adhesions drives growth cone advance and neurite extension. In addition, motor-clutch models must also include microtubule dynamics and to explain why microtubules-targeting agents (MTAs) can influence cell migration in tumors. Indeed, it was shown that the human glioma sensitivity to stiffness

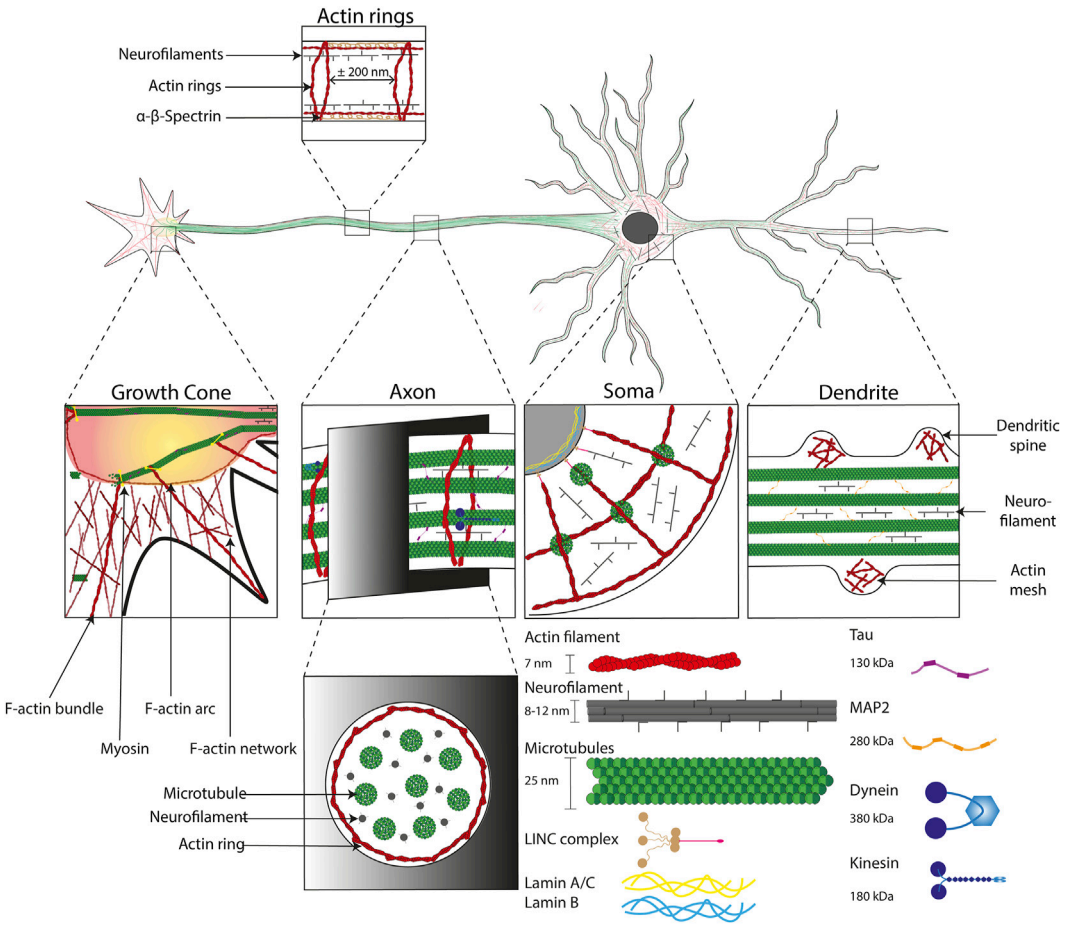

FIGURE 3 | Cytoskeletal organization in neuronal cells. Illustration of the cytoskeletal organization into the four major subcellular compartments of neuronal cells. From left to right: the growth cone, the axon, the cell body (Soma) and the dendrites. The cytoskeleton is composed of i) actin filaments (~7 nm in diameter, in red) that form specific structures, such as: bundles in growth cones, actin rings (interspace of ~200 nm) in axons, F-actin arcs in Soma and dendritic spines, ii) neurofilaments (8–12 nm in diameter) which have a supporting role and iii) microtubules (~25 nm in diameter) stabilized by the Tau protein (130 kDa) in axons and the MAP2 protein (280 kDa) in dendrites. The microtubule network enables the formation of tracks in axons that support axonal transport through molecular motors allowing a retrograde transport (from the growth cone to the Soma) with dynein (380 kDa) and anterograde transport (from the Soma to the Soma) with kinesin (180 kDa). Cytoskeletal components are intimately linked to the nucleus with LINC complex, which is itself anchored to the lamin network (14–30 nm thick) inside the nucleus.

was impaired in MTAs, such as paclitaxel and vinblastine (Prahl et al., 2018). Interestingly, MTAs did not only influence microtubule dynamics but also cell traction forces in an opposite way. Motor-clutch model predictions obtained by computational simulations suggested that MTAs indirectly influence motor-clutch parameters rather than acting directly on tension exerted by the actomyosin network (Prahl et al., 2018). To better identify the clutch molecules involved in neuronal migration and to discriminate from those involved in axonal guidance, recent works have studied the role of Shootin molecules, which are neuronal polarization molecules. Shootin1a was identified as an axonal clutch molecule that accumulates at the leading edge of the axonal growth cone and couples the actin retrograde flow *via* L1-CAM adhesion molecules (Toriyama et al., 2006). Interestingly, a mechanical motor-clutch mechanism based on Shootin1a was recently reported on dendritic spines and highlights the role of synaptic activation in enhancing the actin-adhesion coupling in spines (Kastian et al., 2021). Indeed L1-CAM, laminin, and N-cadherin molecules cooperatively contribute to shootin1a-mediated actin-adhesion coupling to promote robust spine plasticity. In addition to Shootin1a, Shootin1b which is a splicing isoform of Shootin1a, was reported as an important mediator of the mechanical clutch by coupling F-actin retrograde flow at the growth cone with cell adhesions to produce the requisite force for the neuronal movement (Minegishi et al., 2018).

Remarkably, some studies have reported that non-neuronal cells migrating in 3D environments can use a wide range of alternative migration modes that may not involve F-actin-adhesion coupling (Petrie et al., 2014; Stroka et al., 2014), thereby raising the question of whether molecular-clutch models can describe the migration of neuronal cells *in vivo*. To answer this, live *in situ* imaging, super-resolution microscopy and 3D-traction force microscopy were performed on axon growth in 3D microenvironments (Santos et al., 2020). It was shown that neurons grow in an amoeboid mode without the

need for adhesions, suggesting that regeneration of adult CNS axons might be facilitated by an amoeboid mode of growth rather than the actomyosin contractive mesenchymal migration mode. This study highlighted the need for a better understanding of the cytomechanics underlying axon growth and to refine molecular-clutch models to 3D microenvironments. Further investigations will require to develop computational and mathematical models at the filament level to consider forces and deformations of individual cytoskeletal components of neuronal cells (Rutkowski and Vavylonis, 2021). Moreover, additional work using mechanobiology assays, such as substrate stretching and optical tweezers, are required to gain quantitative insight into the role of the rate of force application, which has been recently identified as a key component of the mechanosensing mechanism in mouse embryonic fibroblasts (Andreu et al., 2021).

Altogether these findings demonstrate that the nucleus can play an important role in brain tissue mechanics and highlight the importance of the spatial location of brain cells in the establishment of their mechanical properties. To better understand why brain cell mechanics could be modulated by their place of origin, we will describe in the next section the role of the ECM in the modulation of brain cell function.

ECM MODULATES BRAIN CELL FUNCTION

There is growing evidence that the mechanical properties of the cell microenvironment are involved in the normal brain tissue functioning but also in neuropathological situations. Neurons propagate signals through axons and dendrites via complex biochemicals and ionic transfer between extra- and intra-cellular compartments. Action potentials lead to volumetric changes by propagating membrane deformations along the axon (Hill, 1950). Moreover, it was shown that dendritic spines twitch (Crick, 1982) and that rapid actin-mediated contractions occurred after a synaptic activity (Star et al., 2002). These mechanical cues are supported by the cytoskeleton of neuronal cells, which interacts with ECM components via transmembrane integrins (**Figure 3**).

The brain ECM, which is considered as the softest matrix of the human body, is composed of a variety of proteins that combine to create a complex network of specific biochemical and mechanical properties. The brain ECM is mainly composed of glycosaminoglycans, either bound to proteins, thus forming proteoglycans, or unbound in the form of hyaluronan (Maeda, 2015). The last is a high-molecular-weight protein that acts as a diffusional barrier. Its role is to modulate the diffusion of proteins and nutrients in the extracellular space locally. Consequent to the matrix degradation, hyaluronan fragments are released to the extracellular space where they passively act as pro-inflammatory molecules and give rise to resident immune cells activation, such as microglia (Soria et al., 2020). Brain ECM contains also a small number of fibrous proteins, such as laminins or fibronectin, which have an essential role in cell anchoring (Novak and Kaye, 2000). Although the overall composition of the brain ECM has been mostly determined, the spatial distribution of ECM components is still unclear. Indeed ECM networks in the brain differ in composition, and are spatially distributed (Dauth et al., 2016). The distribution of specific proteins such as aggrecan, brevican, and tenascin-R indicated the presence of large numbers of perineuronal nets (PNNs) in the isocortex, which correlated with clusters of aggrecan (Dauth et al., 2016). This observation suggests that aggrecan in the isocortex is mainly part of PNNs but less abundant in the interstitial matrix, whereas the brevican was observed in the hippocampus at high intensity levels, but not colocalized with PNNs (Dauth et al., 2016). Another important component of the ECM is the large glycoprotein reelin, which is an essential building block of the brain ECM that is secreted by Cajal-Retzius cells in the developing cerebral cortex and hippocampus (Tissir and Goffinet, 2003). Reelin acts as a key regulator of neuronal migration, axonal and dendritic branching, cell aggregation, dendrite formation and synaptic plasticity (Fatemi, 2005; Santana and Marzolo, 2017). It was suggested recently that the migration of multipolar neurons in the developing neocortex follows a multi-step mechanism in which Reelin activates Rap1, Rap1 up-regulates N-cadherin, and N-cadherin is needed to orient cell migration. In addition, it has been observed that Reelin is expressed in several adult neuronal cells, including glutamatergic cerebellar granule neurons and specific GABAergic interneurons of the cerebral cortex and hippocampus (Pesold et al., 1999). Furthermore, accumulative evidence indicates that in the adult brain reelin modulates hippocampal long-term potentiation (LTP) (Herz and Chen, 2006) and synaptic activity (Qiu et al., 2006), promotes hippocampal dendrite and spine development and enhances cognitive ability (Rogers et al., 2011). Dysfunctions in reelin signaling were associated with brain lamination defects such as lissencephaly and with neuropsychiatric diseases as autism, schizophrenia, and depression (Ishii et al., 2016), demonstrating that distinct ECM compositions form specific cellular microenvironments that contribute to brain pathologies (Hemphill et al., 2011).

In addition to the modulation of the biochemical composition of the ECM, modifications of its mechanical properties can affect the spreading, differentiation, migration, or even the epigenetic expression of brain cells (Soria et al., 2020). Using Xenopus retinal ganglion cells (RGCs), it was shown that mechanosensing is critical for axon growth in the developing brain (Koser et al., 2016). Axonal migration was found more persistent on stiff substrates (1 kPa), while it was significantly reduced on softer substrates (0.1 kPa). This result agrees with the presence of a stiffness gradient in the developing brain tissue that should guide the axon growth towards the softer brain tissues. Interestingly, the axonal mechanosensing process was observed to be mediated by piezo1 stretch-activated ion channels (Koser et al., 2016). Aberrant axon growth in response to the softening of brain tissue obtained by manipulating the ECM component, suggesting the reorganization the ECM during the developmental brain can lead to an impaired development. Altogether, these results demonstrate that the local tissue stiffness, which is read out by the piezo1 mechanosensitive ion channels, is critically involved in instructing neuronal growth *in vivo*.

Recent efforts have been made to decipher the role of matrix deformations on glial cells differentiation and more precisely on oligodendrocytes, which are part of the interstitial neuroglia. The main function of oligodendrocytes is the formation of the myelin sheath that wrap the axons of the CNS, whereas this function is assumed by Schwann cells in the peripheral nervous system (PNS) (Marton et al., 2019). While chemical cues are well known to enhance the differentiation oligodendrocytes, recent evidence suggests that biophysical properties of the ECM such as stiffness, topography or strain can also be involved (Jagielska et al., 2012; Shah et al., 2014). For instance, a mechanical strain can stimulate oligodendrocyte differentiation in a ligand-dependent manner, whereas it can inhibit its proliferation through changes of the nuclear shape and global gene expression (Jagielska et al., 2017; Makhija et al., 2018). Modifications of matrix stiffness can be detected by cells that exert traction forces on their substrate through the establishment of focal adhesions (Lampi and Reinhart-King, 2018). In response to stiffness changes, the contractile actomyosin network adapts the cortical tension at the global cell scale acting on the overall tissue stiffening (Clark et al., 2007; Fouchard et al., 2011).

In neurobiology, important efforts have been made to understand how mechanical events can establish physiological cellular functions. For example, it has been demonstrated that matrix stiffness can modulate the formation and activity of cortical neurons *in vitro* (Lantoine et al., 2016). Indeed, the migration of cortical neurons was found to be enhanced on soft substrates, leading to a faster formation of neuronal networks. However, pre-synaptic density, number of action potentials, and miniature synaptic currents were enhanced on stiff substrates (Lantoine et al., 2016). Other works reported that stiff substrates promote neurite outgrowth of cortical and hippocampal neurons (Flanagan et al., 2002; Kostic et al., 2007; Athamneh and Suter, 2015) and enhance neuronal activity (Zhang et al., 2015). Despite these efforts, the mechanotransduction pathways involved in neuronal cell migration and neurite outgrowth are not clear yet. Axonal elongation is mediated by the growth cone, which can be influenced by chemical and physical ECM cues. Forces generated by the growth cone pulling itself are thought to be the motor that pulls the axon along the substrate by actomyosin-mediated contraction (Short et al., 2016).

Mechanical and functional properties of brain tissues are modulated by a set of tunable features. The composition of the ECM can modulate the cell mechanical properties through a spatial reorganization of the cell cytoskeleton, which can in turn modify the mechanical properties of brain tissues. Despite recent advances, how brain cells can sense the physico-chemical changes of their microenvironment and how these changes can lead to a regulation of their functions are still open questions in brain cell mechanotransduction.

MECHANOSENSITIVITY AND MECHANOSENSING

The mechanical properties of the ECM of the CNS have some distinctive and unique features regarding mechanics, structure, and composition that differ substantially from the ECM of other organs and tissues. The process of converting mechanical stimuli into biochemical signals is called mechanotransduction (Martinac and Cox, 2017) and is critical for the function and survival of brain cells. In the following, we will therefore focus on the mechanosensing machinery, which is used sense and interpret microenvironmental biophysical features, highlighting recent findings in neuromechanics. Brain ECM stiffness has been recently studied by observing the activation of astrocytes in response to matrix softening, while matrix stiffening reverted the process (Hu et al., 2021). Interestingly, changes of the brain ECM stiffness were also observed to impact microglia, which is the first line of defense after infection or trauma and is an active actor of synapses remodeling (Yates, 2020). Indeed, changes in matrix stiffness were found to induce a morphological adaptation of microgliocytes. It was reported that soft substrates enhanced microglia polarization and increased their proliferation (Blaschke et al., 2020). Similar to other cell types, microglial cells were observed to migrate towards the stiffer zone of a mechanical gradient (Bollmann et al., 2015). However, few works have reported that neurons migrate toward a softer environment, a process known as negative or inverse durotaxis. This mechanism first observed in the developing embryonic brain of *Xenopus* (Franze et al., 2013; Koser et al., 2016) was also found recently in human glioblastoma cells. Interestingly, inverse durotaxis was not observed to be related to focal adhesion kinase (FAK), extracellular signal-regulated kinase (ERK) or Yes-associated proteins (YAP) signaling. A better understanding of the molecular pathways implicated in the mechanosensing process of brain cells will be substantial for designing new implants or enhancing therapeutic strategies for neurodegenerative pathologies or traumatic brain injuries.

Topotaxis is another process related to ECM fibers that mediates directional cell migration in response to the gradients of the density of extracellular matrix fibers (Park et al., 2016). Studies on hippocampal neurons showed that neuronal growth was random compared to culture on pillared surfaces. They observed the longest neurites lengths on pillars with the smallest inter-pillar space (2 μm) (Dowell-Mesfin et al., 2004). These observations were confirmed by observing that neurons formed longer axons on lines than on holes and smooth surfaces, but independently of their orientation (Fozdar et al., 2010). More precise micropillar arrays fabricated with a laser were able to control the direction of neurite outgrowth of DRGs neurons and Swann cells (Simitzi et al., 2015). However, the underlying mechanosensing mechanisms are not yet elucidated. To better understand how nanotopographical features affect neuronal adhesion, morphology, and neurite outgrowth, a proteomic analysis reported that important proteins were upregulated, while many others were downregulated on surfaces with nanoscale topographical features (Schulte et al., 2016). A myriad of axon-guidance signaling pathways, including synaptogenesis and synaptic regulation, were found to be upregulated (Baranes et al., 2019). Altogether these observations demonstrate the importance of mechanosensing mechanisms in physiological processes of brain cells. The emerging role of substrate topography in brain cell fate allows promising opportunities towards a better understanding of

complex developmental processes or the design of new regenerative platforms.

Mechanosensitivity of Brain Cells

It has been shown that neuronal membranes and membrane channels can be modulated by mechanical stimuli, which affect neuronal activity (Morris, 2011; Tyler, 2012) and indicate that neuronal cells are mechanosensitive cells. Mechanosensing can be described as an active cellular process through which cells detect changes of external forces or mechanical properties of their microenvironment (Chalfie, 2009). However, little is known about the magnitude of forces required for neurons to respond to internal and external mechanical stimuli. It has been shown that forces experienced during a collision, or a shock can lead to diffuse axonal injury (DAI) (Hemphill et al., 2011), membrane poration (Kilinc et al., 2008), and ultimately apoptosis (Serbest et al., 2005, 2006). However, how sub-traumatic forces are sensed by brain cells (Gaub et al., 2020) and transduced in activity changes remain to be described. In this context, identification of novel mechano-gated ion channels and their modulators is essential for understanding mechanosensitivity in neurons and other brain cells.

The first experimental demonstration that mechanical forces could directly activate ion channels was the activation of ionic currents in auditory epithelial cells by Hudspeth and Corey in 1979 (Corey and Hudspeth, 1979). Subsequently, ionic channels in the membrane of tissue-cultured pectoral muscle were observed to be activated by membrane stretch (Guharay and Sachs, 1984). Ion channels that are directly (i.e., sub-millisecond range) activated by a mechanical stimulation are classified as mechanically activated channels. Among the 15 members of the K_{2P} channel family, TREK1 (also known as potassium channel subfamily K member 2) was the first identified mechanically activated mammalian ion channel. Subsequently, TREK2 (also known as potassium channel subfamily K member 10) and TRAAK (also known as potassium channel subfamily K member 4) were discovered (Maingret et al., 1999). K_{2P} activation suppresses neuronal excitability in the sensory system by hyperpolarizing the membrane potential, whereas asymmetric tension induced by membrane curvature is sufficient to activate K_{2P} channels (Ranade et al., 2015). Transient receptor potential (TRP) channels could modulate ion entry driving forces and Ca^{2+} and Mg^{2+} transport machinery in the plasma membrane (Clapham, 2003). Among them, TRPV4 was reported insensitive to mechanical indentation and membrane stretch, but to open in response to elastomeric pillar array-mediated membrane stretch (Rocio Servin-Vences et al., 2017). In addition, TMEM150C/Tentonin3 was proposed to act as an ion channel mediating slowly inactivating mechano-evoked current in proprioceptive neurons in mouse DRG neurons but heterologous expression of TMEM150C fails to generate MA currents in cells with genomic ablation of the PIEZO1 gene (Hong et al., 2016; Dubin et al., 2017). By cloning TMEM150C from the trigeminal neurons of the tactile-foraging domestic duck it was shown that TMEM150C must be considered as a general regulator of mechano-gated ion channels from different classes (Anderson et al., 2018).

Piezo channels family is formed by two genes: Piezo1 and Piezo2 that share half amino acid composition when the protein is expressed in vertebrates, and are the largest known pore-forming multimeric ion channels, with ~2,500 amino acids in each subunit (Murthy et al., 2017). Mechanical activation of the Piezo channel results in influx of Na^{2+} and Ca^{2+}, which can lead to the propagation of electrical signals and initiate intracellular secondary messenger pathways. PIEZO1 is expressed mainly in non-neuronal cells, whereas PIEZO2 is expressed in sensory neurons and specialized mechanosensory structures. PIEZO1 and PIEZO2 were found to be active players in mechanically-activated currents in Neuro2A and DRG neurons (Coste et al., 2010). Using Yoda1 and Capsaicin agonists, longer mechanical hyperalgesia was observed *in vivo* with the activation of Piezo1 rather than TRPV1, suggesting that Piezo1 is a promising candidate for mechano-nociception (Wang et al., 2019). Piezo1 has been observed to adopt an activated state after axonal injury and during axonal regeneration where chemical activation of Piezo1 by Yoda1 agonist has shown slight inhibition of axonal regeneration via the CamKII-Nos-PKG pathway (Song et al., 2019). In addition, the upregulation of astrocytic Piezo1 may dampen neuroinflammation (Velasco-Estevez et al., 2020). Indeed, activating Piezo1 channels can inhibit the release of cytokines and chemokines, such as IL-1β, TNFα, and fractalkine (CX3 CL1) in activated astrocyte cultures. Furthermore, LPS-stimulated astrocytes exposed to Yoda1 (Piezo1 channel activation) versus GsMTx4 (Piezo1 channel inhibition) indicated that Piezo1 channel activation in reactive astrocytes decreases their migration speed (Velasco-Estevez et al., 2020), suggesting a key role of PIEZO1 in astrocyte functioning. Force from lipid (FFL) models have been used to explain that forces arising from actin-mediated contractility and within the lipid bilayer act synergistically to regulate PIEZO1 activation (Bavi et al., 2019). The FFL gating paradigm implies that mechanical force activates MS channels through the lipid bilayer alone with no requirement for other cellular components (Ridone et al., 2019).

Despite the recent surge in Piezo-dependent mechanotransduction research, several aspects of Piezo channel architecture and physiology are still unknown (Murthy et al., 2017) and the role of Piezo channels in brain functioning remains elusive. Intracellular mechanobiology was largely thought to be mediated by transmembrane proteins such as integrins, but the emerging role of the PIEZO1 ion channel in traction force sensing can potentially remodel this concept. Furthermore, we envision that the identification of phenotypes associated with human brain mutations in PIEZO channels will have a significant impact on our understanding of the key role of mechanotransduction-based processes.

Integrin-Mediated Mechanosensing

Brain cells interact with the surrounding matrix by using transmembrane integrins, which consist of a 24 heterodimers transmembrane protein family composed of 18 α- and 8 β-subunit (Moreno-Layseca et al., 2019). These integrin heterodimers are not found uniformly in the brain and do not bind the same ECM proteins (Wu and Reddy, 2012). Integrin

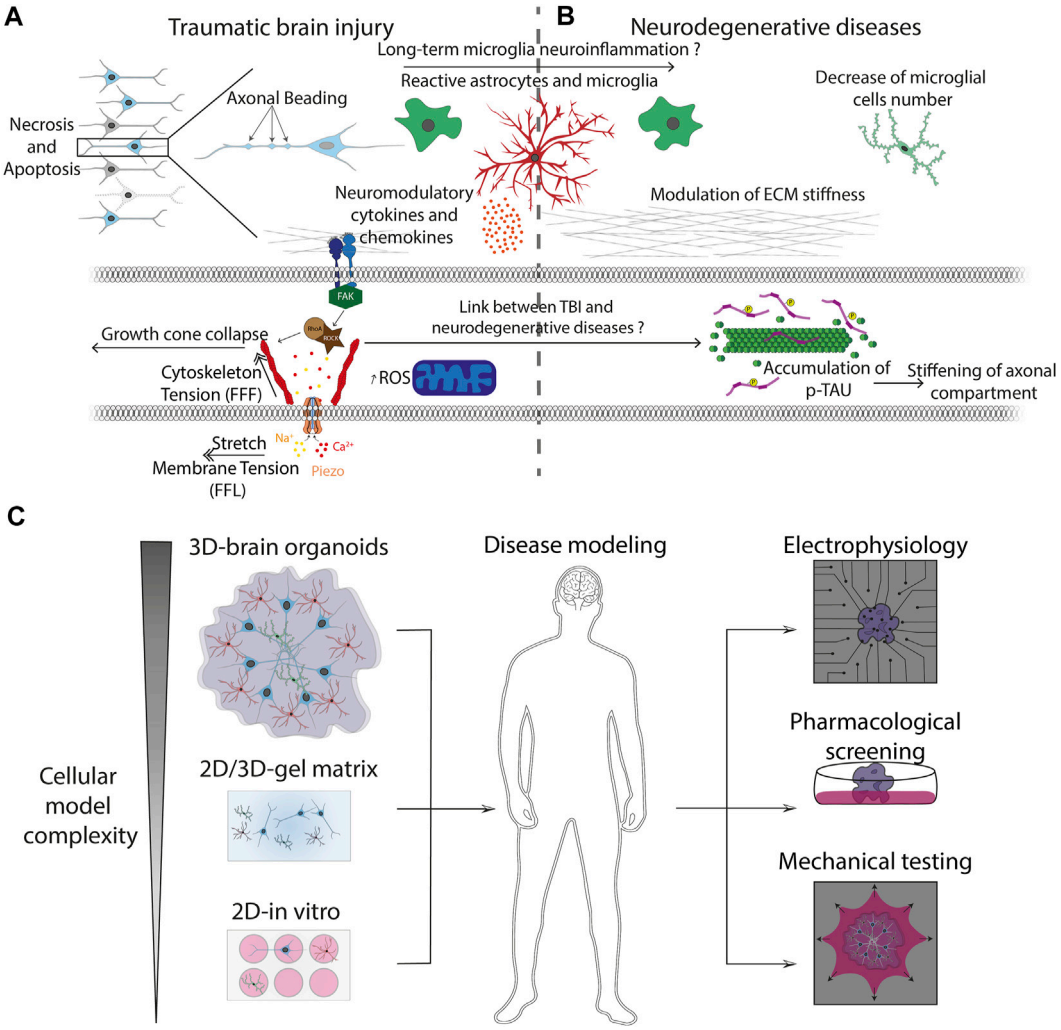

FIGURE 4 | Pathophysiological processes and advanced *in vitro* models **(A)** Mechanically-induced diseases, such as TBI, leads to axonal beading and activation of glial cells. Reactive astrocytes and microglia trigger the release of cytokines and neuromodulatory chemokines that are involved into the long-term neuroinflammation process observed in neurodegenerative diseases. Injury forces applied to neuronal and glial cells are transmitted from the ECM to the cytoskeleton through transmembrane integrins. Focal adhesion kinase (FAK) is a cytoplasmic tyrosine kinase that plays critical roles in integrin-mediated signal transduction and can trigger the activation of the Rho-ROCK pathways, leading to rearrangement of actin filaments and ultimately to the axonal growth cone collapse. **(B)** Cytoskeletal changes are related to the formation of protein aggregates such as phosphorylated the neuronal microtubule Tau protein, which is a hallmark of many neurodegenerative diseases. This process can be followed by a stiffening of the axonal compartment and major modifications of the ECM mechanical properties. **(C)** Advanced bioengineered systems allow to increase the complexity of conventional 2D culture models to obtain physiologically relevant 3D pluricellular models such as brain organoids. The 3D culture models can be combined with mechanical assays and new electrophysiological methods such as microelectrode arrays (MEA) for investigating brain development, neurodegenerative diseases and to improve the screening of pharmacological drug candidates.

activation can either be induced by integrin ligand binding itself (outside-in signaling) or intracellular cascades (inside-out signaling) (Mohammed et al., 2019). Interestingly, activation of integrin can also be triggered by a change in membrane tension resulting from mechanical forces or by cytoskeletal forces generated by the actomyosin complex linked to integrins *via* adaptors proteins (Gingras and Ginsberg, 2020). The integrin-ECM has been described as a catch-bond which significates that receptor-ligand liaison strengthens under increasing forces until a threshold (Kong et al., 2009). Cell-matrix adhesion is therefore ruled by the nature of integrins and the stability of the binding. Interestingly, the binding stability has been observed to depend on the level of applied forces which influence in return the integrin clustering (Gauthier and Roca-Cusachs, 2018). This ligand-binding mechanism provides mechanical properties sensitivity for brain cells which means that they can adapt to the mechanical environment such as stiffness and topography. It was shown that talin binds the β-integrin subunit (Shattil et al., 2010; Kim et al., 2012) which destabilizes the interaction with the α-subunit, whereas kindlin seems to act as an indirect activator of integrins by cooperation with talin (Theodosiou et al., 2016).

A large number of studies indicated that soft substrates promote neurite outgrowth for a variety of neuronal cell types (Balgude, 2001; Teixeira et al., 2009; Franze et al., 2013; Kerstein et al., 2015; Lantoine et al., 2016; Mosley et al., 2017). However, other studies reported conflicting results about the sensitivity of cortical (Zhang et al., 2015) and hippocampal (Koch et al., 2012) neuronal cells towards matrix stiffness, suggesting that mechanosensitivity can vary between different neuronal cell types. Interestingly, the intrinsic electrical properties of neurons were observed to change in response to the modifications of the mechanical environment (Lantoine et al., 2016; Wen et al., 2018). Mouse hippocampal neurons cultured on stiff substrates displayed enhanced voltage-gated Ca^{2+} channel currents compared to neurons cultured on soft substrates (Wen et al., 2018). In addition, matrix stiffness can alter mechanically gated ion channels, such as Piezo1, conduct calcium and sodium ions (Coste et al., 2012). In addition to the study of the matrix stiffness, further works are needed to understand whether viscoelastic properties of the matrix (Chaudhuri et al., 2020) can modulate the membrane potential and tune the electrophysiological properties of neurons. Indeed, emerging evidence suggests a time dependence of cellular mechanosensing and the influence of viscous dissipation of the ECM on cell phenotype (Chaudhuri et al., 2016; Janmey et al., 2020). For instance, if this hypothesis is valid, altered tissue mechanics may contribute to calcium dysregulations in the aging or neurodegenerative brains.

MECHANOBIOLOGY IN BRAIN AND NERVE DISEASES

In addition to the important role of biophysical cues in neurophysiological processes, external mechanical forces and changes in the physico-chemical properties of the ECM were also observed to be involved in the development of brain and nerve pathologies. We will discuss in this section how perturbation of the cell microenvironment and modification of the mechanical properties of brain and nerve tissues can contribute to the emergence of specific diseases by focusing on three specific examples: traumatic brain injury, neurodegenerative diseases, and neuroblastoma.

Traumatic Brain Injury

Traumatic brain injury (TBI) is a nondegenerative and noncongenitally insult to the brain arising from an external mechanical shock, which can lead to permanent or temporary impairment of cognitive, physical, and psychosocial functions (Sandsmark and Diaz-Arrastia, 2021). TBI can be associated with a diminished or altered state of consciousness and its molecular mechanisms have been extensively studied during the last few decades using innovative *in vitro* assays (Puntambekar et al., 2018). TBI can be separated between primary and secondary injuries. Primary injuries are the direct mechanical consequences of the traumatic event occurring on the brain. It can be described as disruption of cortical parenchyma, axotomy, and massive cellular death (Kaur and Sharma, 2018). The secondary injury is more complex and is triggered by glutamate excitotoxicity (Luo et al., 2019) along with inflammation neuromodulator (Simon et al., 2017), astrogliosis (Burda and Sofroniew, 2014; Burda et al., 2016), and ion dysregulation (Weber, 2012). Primary injury can be described as contusion (Ct) and pericontusion (PCt) (Harish et al., 2015). Ct is the center of TBI where occurs hemorrhage, shrunken neurons, and inflammatory changes. PCt is more the seat of oedema, axonal loss, and dystrophic changes in neurons and astrocytes and where microglial activation occurs. DAI and neurotoxicity, which are key players of the secondary injury, are associated with the dysregulation of glutamate transmission and the release of proteins in extracellular compartments, leading to massive tissue necrosis and apoptosis (Akamatsu and Hanafy, 2020). In addition, axonal mitochondria can be injured, leading to massive formation of reactive oxygen species (Kumar Sahel et al., 2019). Furthermore, accumulative evidence underlines the role of the immune system in microglial activation and astrogliosis in response to inflammation signals in the CNS (Karve et al., 2016). TBI is also implicated in memory loss due to dysregulation of the dopaminergic pathway (Chen et al., 2017). All these features are characteristic of the secondary injury that progresses over time after the traumatic event (**Figure 4A**).

Among these biochemical events, accumulative evidence suggests a key role of the impact of mechanical forces on tissue remodeling and cellular adaptation. Loading forces can be applied on brain tissues directly (i.e., physical insult) or indirectly (i.e., acceleration-deceleration forces). Although the amount of loading forces applied to the brain is a critical factor, the nature and direction of loading are also important parameters. Indeed, longitudinal, transversal, or rotational stresses can lead to different degrees of severity (Ivancevic, 2009). In addition, TBI can result from a direct impact caused by contact between an object of high energy or from the rapid movement of the head in the space characterized by fast acceleration and deceleration phases (Brazinova et al., 2016). Inertial forces apply longitudinal tension and compression to brain tissues and can cause shear stress when the acceleration is not longitudinal to the axis of the head and neck (Blennow et al., 2012). The mechanical loading of brain tissues often results in focal injuries (skull fracture, contusion, or hemorrhage) and/or diffuse injuries such as diffuse vascular injury, diffuse brain swelling, and DAI.

In response to intense stretching forces, axons can break and neurons can go under cell-autonomous death pathways like Wellerian degeneration (Kanamori et al., 2012). Distal axotomy can also have an influence on injured neurons by enhancing retrograde presynaptic excitability via transsynaptic signaling (Nagendran et al., 2017). Secondary axotomy can be triggered by a stretch of at least 10%, occuring in 100 ms or less (Di Pietro et al., 2013). During the secondary injury, forces are translated to the cytoskeleton by the focal adhesions and detected by mechanosensory proteins inducing intracellular signal pathways. By using stretch assays and optical magnetic tweezers, it was found that ECM-integrin specific interaction activates the RhoA-ROCK signaling pathways (Hemphill et al., 2011), which is known to be implicated in growth cone collapse, therefore inhibiting the growth and repair of axons (Dupraz et al.,

2019). When loading exceeds the mechanical limit of the cell, cytoskeletal components can break leading for instance to the fracture of microtubules and compaction of neurofilaments (Chen et al., 1999). Axonal transport is therefore impaired and proteins such as βAPP and phosphorylated Tau protein are accumulated in "retractation bulbs" also called "axonal beading" (Tang-Schomer et al., 2012). We can also witness a rapid and important intake of calcium which can alter the permeability of mitochondrial membrane through activation of calcineurin and therefore activate caspase-mediated apoptosis (Mu et al., 2015). Furthermore, mechanical activation of glial cells has an important role in the outcome of TBI. It was shown in injured neocortex and spinal cord injury that brain tissues altered their mechanical properties and softened, suggesting a soft mechanical signature of glial scars following brain injury (Moeendarbary et al., 2017). The release of cytokines and chemokines triggers the loss of presynaptic vesicles in cortical neuronal networks and modulates the balance between TNFR1 and TNFR2 receptors (Lantoine et al., 2021).

In addition to immediate complications and the development of a neuroinflammatory context, TBI involves not only short- but also long-term consequences, including an increased risk for patients to develop neurodegenerative disorders such as Alzheimer's disease, chronic traumatic encephalopathy, and amyotrophic lateral sclerosis in later stages of life (Gupta and Sen, 2016). A better consideration of mechanobiological aspects of TBI is critical to move the field forward. Indeed, most of the current injury models are not representative of human injury and thus fail to replicate mechanisms of primary and secondary damages. The development of advanced *in vitro* models that integrate mechanobiology assays is critical to improve our understanding of the cellular response to neurotrauma and to address current open questions, such as determining the molecular pathway involved in stress propagation through brain tissues or establishing effective pharmacological treatments that can be clinically translated.

Neurodegenerative Diseases

Aging is the main risk factor for humans to develop neurodegenerative diseases, which are defined by progressive degeneration of the structure and function of the central or peripheral nervous system. Neurodegenerative diseases are a group of pathologies, which have cellular and sub-cellular similitudes with programmed cell death, such as protein accumulation within the neurons (Rubinsztein, 2006).

Accumulation of hyaluronic acid, one of the constituents of the ECM, in the dentate gyrus of the hippocampus is correlated with a reduced number of dendritic spines but also with spatial memory impairment (Yoshino et al., 2017, 2018). In addition the accumulation of hyaluronic acid in the cortex and cerebellum of aged mice, suggests that remodeling of the brain ECM with time is not suitable for synaptic plasticity (Foscarin et al., 2017; Reed et al., 2018). Accumulative evidence shows a positive correlation between increasing amyloid load and reduced brain stiffness in mild cognitive impairment (Murphy et al., 2016) and magnetic resonance elastography (MRE) images of Alzheimer patients show a decrease in brain stiffness compared to healthy controls (Murphy et al., 2016; Hiscox et al., 2020).

In addition to ECM changes, many neurodegenerative diseases were associated with important changes in cell composition and cell mechanics. The decrease in the neuron-to-glial cell ratio could contribute to the overall softening of AD brains, at least on the macroscale of MRE elastograms (**Figure 4B**). Furthermore, several MRE studies revealed a continuous softening of the human brain tissues with age from ~4 to ~2 kPa (Sack et al., 2011). Increasing age is the single greatest risk factor for the development of AD (Hou et al., 2019) that is associated with the loss of neurons and synapses in the cerebral cortex and certain subcortical structures (e.g., hippocampus). The loss of neurons results in a volume decrease of different regions of the brain, including the temporal lobe, parietal lobe, and parts of the frontal cortex and cingulate gyrus (Wenk, 2003). Alteration of the viscoelastic properties of the brain ECM was observed occurring in AD (Murphy et al., 2011; Hiscox et al., 2020), with specific differences according to the different brain regions. For instance, association cortices (frontal with 2.65 versus 2.47 kPa and temporal with 2.69 versus 2.58 kPa) showed a significant softening, whereas other region remained unaffected (occipital, sensory/motor, deep gray and white matter, and the cerebellum) (Murphy et al., 2016).

There is now accumulative evidence linking TBI to dementia (Fann et al., 2018; Gardner et al., 2018) and neurodegenerative diseases (DeKosky and Asken, 2017; Brett et al., 2021) that involves the gradual and chronic hyperphosphorylation, misfolding, and missorting of the microtubule-associated protein, tau. When tau is phosphorylated, it detaches from microtubules at the axon initial segment and breaks down the barrier that normally prevents retrograde flow of axonal tau (Hatch et al., 2017). This may cause the neuron to become stiffer due to the accumulation of tau in the somatodendritic compartment (Hagestedt et al., 1989; Zempel et al., 2017). Therefore, hyperphosphorylation of tau causes intrinsic mechanical disturbances in damaged neurons. Because axonal transport is dependent on a normal functioning cytoskeleton, marked tau-associated changes in neuron stiffness may be a novel biomarker of neurodegenerative disease associated with a severe breakdown in axonal transport machinery (Millecamps and Julien, 2013).

Neuroblastoma

In addition to be involved in CNS diseases, mechanobiology was also found to be a key parameter of other nerve diseases that affect predominantly the peripheral nervous system. Human neuroblastoma (NB) is the most common extracranial solid tumor occurring during infancy (Allen-Rhoades et al., 2018). NB is a neurodevelopmental disorder that can be viewed as resulting from the failure of neural crest differentiation (Ratner et al., 2016). This sympathetic nervous system tumor displays several unique features: the early age of onset, high incidence of metastatic cases at diagnosis, and proneness for spontaneous regression of tumors (Matthay et al., 2016). The origin of NB remains unknown, but accumulative evidence suggests that neural crest cell-derived neuroblasts may be one

cell of origin and amplification of the oncogenic transcription factor MYCN was found as the main characteristic of a subset of human NBs (Ratner et al., 2016).

The migratory and aggressiveness potential of NB cells appear to be intrinsically related to their stem cell-like characteristics, such as self-renewal and migratory potential. Consistently, I-type NB cells in tumors present the highest level of progress and the highest malignant potential *in vitro* (Matthay et al., 2016). It was observed recently that a lack of lamin A/C could predispose cells towards stem-like phenotype (Nardella et al., 2015), which is suggested to be involved in therapy failure. This is particularly interesting considering that lamin A/C expression is known to scale with the differentiation state (Swift et al., 2013) and that low lamin A/C level correlates with softer nuclei, which is essential for fast amoeboid migration (Heo et al., 2020). Interestingly, clinical behavior of NB is correlated with high-level amplification of the MYCN oncogene, whose expression was found to inversely relate to lamin A/C expression in tumor-initiating cells (Nardella et al., 2015).

Upon differentiation, the elastic modulus of human-derived NB was observed to increase significantly (approximately 3-fold increase) (Zhao et al., 2015) and to scale with the cell differentiation state. This mechanism is not well understood and it has been suggested that it could originate from an increase in the heterochromatin after differentiation (Bergqvist et al., 2020) or due to structural modifications in the actomyosin cortex after differentiation. Several studies demonstrated that the degree of tubulin polymerization can be four to five times higher in differentiated NB cells possessing microtubule-filled neurites (Van de Water and Olmsted, 1980; Olmsted and Lyon, 1981). Interestingly, the average young's modulus of NB was shown to increase from 5 to 10 kPa after the induction of neurodegeneration. This cell stiffening was correlated to the activation of the RhoA signaling pathway and induced a consequent increase in contractile forces within the cytoskeleton (Fang et al., 2014). It is likely to assume that elastic moduli of human NB cells can significantly vary during the disease progression and these variations could be correlated with the different malignant potential in NB cell types, as they are associated with different differentiation states (Mescola et al., 2012). Further mechanical experiments need to be conducted to better determine the mechanical properties of NB cells according to their metastatic potential. This could help to understand their migratory potential as they might be more deformable during migration and may constitute a basis for sorting according to metastatic potentials. In addition, novel 3D *in vitro* platforms that efficiently sustain patient-derived tumor cell growth are required for assessing drug-specific responses and performing more robust pre-clinical testing (Corallo et al., 2020).

BRAIN-TISSUE-LIKE BIOMATERIALS

One of the major limitations in the study of brain and nerve diseases is the lack of *in vitro* systems that faithfully recapitulates the complexity and delicacy of human brain and nerve tissues. A better understanding of the modulation of brain and nerve function in response to physico-chemical changes of the surrounding matrix or external forces requires to create novel biomaterials with similar mechanical and biochemical properties to the native tissues. Indeed, recapitulating *in vitro* the complex microenvironment of neuron and glial cells is crucial to study their cellular responses to chemical signals, to develop new pharmacological candidates, and to expand cells for therapeutic applications.

Due to the softness and a large amount of water in brain tissues, hydrogels are promising candidates and offer the possibility of delivering drugs in a sustained release manner (Appel et al., 2012; Mol et al., 2019). Hydrogels are water-swollen biomacromolecules that possess up to 90% of water, while exhibiting the physical properties of elastic solids. The high-water content allows the diffusion of biomolecules secreted by cells. Hydrogels are 3D networks that are promising tools for brain tissue regeneration due to their tunable physico-chemical properties. Conventional biomaterials such as autologous bones and titanium meshes are rather stiff, with young's modulus values ranging from dozen of kPa up to GPa and have poor stretchability. Hydrogel scaffolds can overcome these drawbacks and adapt to intracranial pressure changes and degrade after few weeks (Che et al., 2019). In the past few years, injections of hydrogel directly into the brain have been used in the treatment of nervous system damage diseases (kun Zhang et al., 2018; Sun et al., 2020). Injectable peptide hydrogels in a zebrafish model enable angiogenesis that promotes new blood vessel growth and neurogenesis by increasing neural growth both *in vitro* and *in vivo* (Wang et al., 2017). An injectable self-assembling peptide-based hydrogel that mimics a vascular endothelial growth factor was used recently to create a regenerative microenvironment for neovascularization at the injured brain tissues (Ma et al., 2020). Indeed, brain damage following significant TBI commonly results in extensive tissue loss and long-term disability. However, there are currently no clinical treatments to prevent the resulting cognitive impairments or tissue loss. To address this limitation, chondroitin sulfate glycosaminoglycan (CS-SAG) matrices were developed to act as a scaffolding for transplanted stem cells, which are capable of repairing damaged tissue in a more natural healing environment (Betancur et al., 2017). Injection of CS-SAG matrices into rats with TBI has led to a significantly enhanced retention of neural stem cells. In addition, CS-SAG matrices were implanted into rats with severe TBI, who after 20 weeks exhibited enhanced cell repair and improvement of motor function (Latchoumane et al., 2021), providing evidence that the hydrogel protects against brain tissue loss, but also actively regenerates functional neurons at the lesion cavity after a TBI.

In addition to these advanced culture matrices that can recapitulate important characteristics of the native microenvironment of neuron and glial cells, the emergence of 3D organoids has attracted great attention in fundamental neurosciences and regenerative medicine. Brain organoids are a type of organoids that tend to reproduce specific brain structures which are characteristic of different human brain regions such as the hippocampus (Sakaguchi et al., 2015), hypothalamus (Qian et al., 2016), or the cerebellum

(Muguruma et al., 2015). Interestingly, microfluidic chips have simplified the manufacturing process of brain organoids and micro-pillar array devices are used for *in situ* formations of plentiful brain organoids (Zhu et al., 2017). Brain organoids are now considered as a versatile tool for screening therapeutic compounds for neurodegenerative diseases that allow for instance to observe the aggregation of amyloid-beta and tau pathology (Kim et al., 2019). Recently, human cerebellar organoids were shown to be an effective model to explore *in vitro* the role of genetic mechanisms in glioma patients (Ballabio et al., 2020) and are expected to be relevant models for mechanical testing and electrophysiological studies (**Figure 4C**).

FUTURE PERSPECTIVES AND CHALLENGES IN MECHANOBIOLOGY OF BRAIN TISSUES

Over the last decade, neuroscience studies have extensively used electrophysiology, molecular biology, biochemistry, and genetics. At the same time, the emergence of cell mechanobiology gained many other fields and the role of mechanical forces in mediating neuronal processes remained unexplored. Accumulative evidence shows that the brain is a mechanically sensitive organ and that its structure and functioning can be regulated by external and internal forces (Tallinen et al., 2016), for instance during neural migration (Abuwarda and Pathak, 2020) and formation and pruning of synapses (Sakai, 2020). Studying the consequences of endogenous forces exerted on glial cells will help to understand how mechanical injuries to the brain can be lead to the emergence of neurodegenerative diseases via the establishment of a neuroinflammatory context (Kokiko-Cochran and Godbout, 2018).

Among mechanical stimuli, the physico-chemical properties of the matrix stiffness contribute significantly to the neuronal cell fate. Interestingly, changes in tissue mechanics contribute to age-related cognitive decline and neurodegenerative states. Future works are required to understand how changes in composition and mechanical properties of the matrix are linked with neurophysiology and cognition. In this context, a large effort is required to understand how neuronal and glial cell mechanics and brain tissue mechanobiology are intimately connected. An emerging theme concerns the role of the physical changes in the tumor microenvironment that can activate signaling pathways leading to ECM remodeling, which can in turn enhance pro-tumorigenic mechanosignaling. A closer examination of the mechanoreciprocity circuit is required to understand the role of ECM changes in therapy resistance, poor prognosis and to identify new therapeutic targets.

Conventional 2D cell cultures have allowed to identify important cellular signaling pathways, determine potential drug targets and establish the design of drug candidates for brain pathologies. However, cell culture performed in plastic flasks or flat Petri dishes also have many limitations, such as the disturbance of interactions between the cellular and extracellular environments, changes in cell morphology, culture in homogeneous media or limited cell interactions that mainly depend on cell distribution and proximity. To address these drawbacks and facilitate the translation to the clinic, many research efforts have been dedicated to design compartmentalized microsystems (Hur et al., 2011; Bhatia and Ingber, 2014; De Vitis et al., 2021). Microengineering culture platforms represent a promising technology for the study of complex spatiotemporal signals, cell dynamic and pharmacologic response with unprecedented levels of control (Polini et al., 2019). Through the years, microengineering platforms had experienced few variations and are now considered as a powerful tool to study the structure-function relationship and the complex communication between the different brain cell populations in standardized conditions. Promising models combine engineering methods with stem cells, such as embryonic stem cells (ESCs) or human-induced pluripotent stem cells (hiPSCs), to create patterned brain organoids (Geraili et al., 2018; Smith et al., 2020) that will represent a unique opportunity for biopharmaceuticals, cell-based therapies, and personalized medicine.

Despite significant advances in the development of brain organoid cultures (Strzyz, 2021), there are still some issues that need to be addressed such as the harvest difficulty after long cultures or the variability in size and composition (Shou et al., 2020; Passaro and Stice, 2021). Recently, cerebral organoids derived from human, gorilla and chimpanzee cells were used to study developmental mechanisms driving evolutionary brain expansion (Benito-Kwiecinski et al., 2021). Early cell shape transition of the neuroepithelial cells was associated with apical constrictions and elongation and correlated with a slowing down of the cell cycle and DNA transcription. This phenomenon happened at earlier stage in ape-derived organoids than in human-derived organoids, assessing the fundamental mechanisms driven evolutionary expansion of the human forebrain.

We envision that the next generation of microengineered platforms will integrate mechanical assays and advanced synthetic matrices with human brain organoids (Sato et al., 2009; Takasato et al., 2015; Turco et al., 2017; Fujii et al., 2018; Pérez-González et al., 2021) to form an effective preclinical platform that can test and guide personalized treatment in a reproducible and predictable manner. These advanced engineered platforms will bridge the gap between 2D human cell cultures and non-human animal models. Moreover, by integrating relevant surrounding matrices and mechanical constraints they will open the door for a variety of studies including development and disease modeling and high-throughput screening. Finally, a significant effort will be required to overcome the limitations posed by the three-dimensionality of brain organoids in order to develop robust functional analysis methods, such new as electrophysiological approaches (Passaro and Stice, 2021).

AUTHOR CONTRIBUTIONS

The article was written and corrected by all authors. AP and SG designed the figures.

FUNDING

SG acknowledges funding from FEDER Prostem Research Project no. 1510614 (Wallonia DG06), the F.R.S.-FNRS Epiforce Project no. T.0092.21 and the Interreg MAT(T)ISSE project, which is financially supported by Interreg France-Wallonie-Vlaanderen (Fonds Européen de Développement Régional, FEDER-ERDF). AP, ML, and YK are financially supported by FRIA (F.R.S.-FNRS). AP and YK are financially supported by the FRMH (Fonds de la Recherche Mons-Hainaut).

REFERENCES

Abuwarda, H., and Pathak, M. M. (2020). Mechanobiology of Neural Development. *Curr. Opin. Cel Biol.* 66, 104–111. doi:10.1016/j.ceb.2020.05.012

Akamatsu, Y., and Hanafy, K. A. (2020). Cell Death and Recovery in Traumatic Brain Injury. *Neurotherapeutics* 17, 446–456. doi:10.1007/s13311-020-00840-7

Alcalá-Vida, R., Garcia-Forn, M., Castany-Pladevall, C., Creus-Muncunill, J., Ito, Y., Blanco, E., et al. (2021). Neuron Type-specific Increase in Lamin B1 Contributes to Nuclear Dysfunction in Huntington's Disease. *EMBO Mol. Med.* 13. doi:10.15252/emmm.202012105

Allen-Rhoades, W., Whittle, S. B., and Rainusso, N. (2018). Pediatric Solid Tumors of Infancy: An Overview. *Pediatr. Rev.* 39, 57–67. doi:10.1542/pir.2017-0057

Anderson, E. O., Schneider, E. R., Matson, J. D., Gracheva, E. O., and Bagriantsev, S. N. (2018). TMEM150C/Tentonin3 Is a Regulator of Mechano-Gated Ion Channels. *Cel Rep.* 23, 701–708. doi:10.1016/j.celrep.2018.03.094

Andreu, I., Falcones, B., Hurst, S., Chahare, N., Quiroga, X., Le Roux, A.-L., et al. (2021). The Force Loading Rate Drives Cell Mechanosensing through Both Reinforcement and Cytoskeletal Softening. *Nat. Commun.* 12, 4229. doi:10.1038/s41467-021-24383-3

Antonovaite, N., Hulshof, L. A., Hol, E. M., Wadman, W. J., and Iannuzzi, D. (2021). Viscoelastic Mapping of Mouse Brain Tissue: Relation to Structure and Age. *J. Mech. Behav. Biomed. Mater.* 113, 104159. doi:10.1016/j.jmbbm.2020.104159

Antonovaite, N., van Wageningen, T. A., Paardekam, E. J., van Dam, A.-M., and Iannuzzi, D. (2020). Dynamic Indentation Reveals Differential Viscoelastic Properties of white Matter versus gray Matter-Derived Astrocytes upon Treatment with Lipopolysaccharide. *J. Mech. Behav. Biomed. Mater.* 109, 103783. doi:10.1016/j.jmbbm.2020.103783

Appel, E. A., Loh, X. J., Jones, S. T., Dreiss, C. A., and Scherman, O. A. (2012). Sustained Release of Proteins from High Water Content Supramolecular Polymer Hydrogels. *Biomaterials* 33, 4646–4652. doi:10.1016/j.biomaterials.2012.02.030

Athamneh, A. I. M., and Suter, D. M. (2015). Quantifying Mechanical Force in Axonal Growth and Guidance. *Front. Cel. Neurosci.* 9. doi:10.3389/fncel.2015.00359

Ayala, Y. A., Pontes, B., Ether, D. S., Pires, L. B., Araujo, G. R., Frases, S., et al. (2016). Rheological Properties of Cells Measured by Optical Tweezers. *BMC Biophys.* 9, 5. doi:10.1186/s13628-016-0031-4

Azevedo, F. A. C., Carvalho, L. R. B., Grinberg, L. T., Farfel, J. M., Ferretti, R. E. L., Leite, R. E. P., et al. (2009). Equal Numbers of Neuronal and Nonneuronal Cells Make the Human Brain an Isometrically Scaled-Up Primate Brain. *J. Comp. Neurol.* 513, 532–541. doi:10.1002/cne.21974

Balgude, A. (2001). Agarose Gel Stiffness Determines Rate of DRG Neurite Extension in 3D Cultures. *Biomaterials* 22, 1077–1084. doi:10.1016/S0142-9612(00)00350-1

Ballabio, C., Anderle, M., Gianesello, M., Lago, C., Miele, E., Cardano, M., et al. (2020). Modeling Medulloblastoma *In Vivo* and with Human Cerebellar Organoids. *Nat. Commun.* 11, 583. doi:10.1038/s41467-019-13989-3

Bangasser, B. L., Rosenfeld, S. S., and Odde, D. J. (2013). Determinants of Maximal Force Transmission in a Motor-Clutch Model of Cell Traction in a Compliant Microenvironment. *Biophysical J.* 105, 581–592. doi:10.1016/j.bpj.2013.06.027

Baranes, K., Hibsh, D., Cohen, S., Yamin, T., Efroni, S., Sharoni, A., et al. (2019). Comparing Transcriptome Profiles of Neurons Interfacing Adjacent Cells and Nanopatterned Substrates Reveals Fundamental Neuronal Interactions. *Nano Lett.* 19, 1451–1459. doi:10.1021/acs.nanolett.8b03879

Bard, L., Boscher, C., Lambert, M., Mege, R.-M., Choquet, D., and Thoumine, O. (2008). A Molecular Clutch between the Actin Flow and N-Cadherin Adhesions Drives Growth Cone Migration. *J. Neurosci.* 28, 5879–5890. doi:10.1523/JNEUROSCI.5331-07.2008

Barker, R. A., Cicchetti, F., Robinson, E. S. J., and Leistedt, S. (2019). *Neuroanatomie et neurosciences*.

Bavi, N., Richardson, J., Heu, C., Martinac, B., and Poole, K. (2019). PIEZO1-Mediated Currents Are Modulated by Substrate Mechanics. *ACS Nano* 13, 13545–13559. doi:10.1021/acsnano.9b07499

Bayly, P. V., Okamoto, R. J., Xu, G., Shi, Y., and Taber, L. A. (2013). A Cortical Folding Model Incorporating Stress-dependent Growth Explains Gyral Wavelengths and Stress Patterns in the Developing Brain. *Phys. Biol.* 10, 016005. doi:10.1088/1478-3975/10/1/016005

Benito-Kwiecinski, S., Giandomenico, S. L., Sutcliffe, M., Riis, E. S., Freire-Pritchett, P., Kelava, I., et al. (2021). An Early Cell Shape Transition Drives Evolutionary Expansion of the Human Forebrain. *Cell* 184, 2084–2102. e19. doi:10.1016/j.cell.2021.02.050

Bergqvist, C., Servy, A., Servy, A., Valeyrie-Allanore, L., Ferkal, S., Combemale, P., et al. (2020). Neurofibromatosis 1 French National Guidelines Based on an Extensive Literature Review since 1966. *Orphanet J. Rare Dis.* 15, 37. doi:10.1186/s13023-020-1310-3

Bernick, K. B., Prevost, T. P., Suresh, S., and Socrate, S. (2011). Biomechanics of Single Cortical Neurons. *Acta Biomater.* 7, 1210–1219. doi:10.1016/j.actbio.2010.10.018

Betancur, M. I., Mason, H. D., Alvarado-Velez, M., Holmes, P. V., Bellamkonda, R. V., and Karumbaiah, L. (2017). Chondroitin Sulfate Glycosaminoglycan Matrices Promote Neural Stem Cell Maintenance and Neuroprotection Post-Traumatic Brain Injury. *ACS Biomater. Sci. Eng.* 3, 420–430. doi:10.1021/acsbiomaterials.6b00805

Bhatia, S. N., and Ingber, D. E. (2014). Microfluidic Organs-On-Chips. *Nat. Biotechnol.* 32, 760–772. doi:10.1038/nbt.2989

Bilston, L. E., Liu, Z., and Phan-Thien, N. (1997). Linear Viscoelastic Properties of Bovine Brain Tissue in Shear. *Bir* 34, 377–385. doi:10.3233/BIR-1997-34603

Blaschke, S. J., Demir, S., König, A., Abraham, J.-A., Vay, S. U., Rabenstein, M., et al. (2020). Substrate Elasticity Exerts Functional Effects on Primary Microglia. *Front. Cel. Neurosci.* 14, 590500. doi:10.3389/fncel.2020.590500

Blennow, K., Hardy, J., and Zetterberg, H. (2012). The Neuropathology and Neurobiology of Traumatic Brain Injury. *Neuron* 76, 886–899. doi:10.1016/j.neuron.2012.11.021

Bollmann, L., Koser, D. E., Shahapure, R., Gautier, H. O. B., Holzapfel, G. A., Scarcelli, G., et al. (2015). Microglia Mechanics: Immune Activation Alters Traction Forces and Durotaxis. *Front. Cel. Neurosci.* 9. doi:10.3389/fncel.2015.00363

Brands, D. W. A., Peters, G. W. M., and Bovendeerd, P. H. M. (2004). Design and Numerical Implementation of a 3-D Non-linear Viscoelastic Constitutive Model for Brain Tissue during Impact. *J. Biomech.* 37, 127–134. doi:10.1016/S0021-9290(03)00243-4

Brazinova, A., Rehorcikova, V., Taylor, M. S., Buckova, V., Majdan, M., Psota, M., et al. (2021). Epidemiology of Traumatic Brain Injury in Europe: A Living Systematic Review. *J. Neurotrauma* 38, 1411–1440. doi:10.1089/neu.2015.4126

Brett, B. L., Gardner, R. C., Godbout, J., Dams-O'Connor, K., and Keene, C. D. (2022). Traumatic Brain Injury and Risk of Neurodegenerative Disorder. *Biol. Psychiatry* 91, 498–507. doi:10.1016/j.biopsych.2021.05.025

Brown, A., and Jung, P. (2013). A Critical Reevaluation of the Stationary Axonal Cytoskeleton Hypothesis. *Cytoskeleton* 70, 1–11. doi:10.1002/cm.21083

Brown, A., Wang, L., and Jung, P. (2005). Stochastic Simulation of Neurofilament Transport in Axons: The "Stop-And-Go" Hypothesis. *MBoC* 16, 4243–4255. doi:10.1091/mbc.e05-02-0141

Budday, S., Nay, R., de Rooij, R., Steinmann, P., Wyrobek, T., Ovaert, T. C., et al. (2015a). Mechanical Properties of gray and white Matter Brain Tissue by Indentation. *J. Mech. Behav. Biomed. Mater.* 46, 318–330. doi:10.1016/j.jmbbm.2015.02.024

Budday, S., Ovaert, T. C., Holzapfel, G. A., Steinmann, P., and Kuhl, E. (2020). Fifty Shades of Brain: A Review on the Mechanical Testing and Modeling of Brain

Tissue. *Arch. Computat Methods Eng.* 27, 1187–1230. doi:10.1007/s11831-019-09352-w

Budday, S., Sommer, G., Haybaeck, J., Steinmann, P., Holzapfel, G. A., and Kuhl, E. (2017). Rheological Characterization of Human Brain Tissue. *Acta Biomater.* 60, 315–329. doi:10.1016/j.actbio.2017.06.024

Budday, S., Steinmann, P., and Kuhl, E. (2015b). Physical Biology of Human Brain Development. *Front. Cel. Neurosci.* 9. doi:10.3389/fncel.2015.00257

Burda, J. E., Bernstein, A. M., and Sofroniew, M. V. (2016). Astrocyte Roles in Traumatic Brain Injury. *Exp. Neurol.* 275, 305–315. doi:10.1016/j.expneurol.2015.03.020

Burda, J. E., and Sofroniew, M. V. (2014). Reactive Gliosis and the Multicellular Response to CNS Damage and Disease. *Neuron* 81, 229–248. doi:10.1016/j.neuron.2013.12.034

Chalfie, M. (2009). Neurosensory Mechanotransduction. *Nat. Rev. Mol. Cel Biol.* 10, 44–52. doi:10.1038/nrm2595

Chan, C. E., and Odde, D. J. (2008). Traction Dynamics of Filopodia on Compliant Substrates. *Science* 322, 1687–1691. doi:10.1126/science.1163595

Chang, C. Y., Ke, D. S., and Chen, J. Y. (2009). Essential Fatty Acids and Human Brain. *Acta Neurol. Taiwan* 18, 231–241.

Chaudhuri, O., Cooper-White, J., Janmey, P. A., Mooney, D. J., and Shenoy, V. B. (2020). Effects of Extracellular Matrix Viscoelasticity on Cellular Behaviour. *Nature* 584, 535–546. doi:10.1038/s41586-020-2612-2

Chaudhuri, O., Gu, L., Klumpers, D., Darnell, M., Bencherif, S. A., Weaver, J. C., et al. (2016). Hydrogels with Tunable Stress Relaxation Regulate Stem Cell Fate and Activity. *Nat. Mater* 15, 326–334. doi:10.1038/nmat4489

Che, L., Lei, Z., Wu, P., and Song, D. (2019). A 3D Printable and Bioactive Hydrogel Scaffold to Treat Traumatic Brain Injury. *Adv. Funct. Mater.* 29, 1904450. doi:10.1002/adfm.201904450

Chen, X.-H., Meaney, D. F., Xu, B.-N., Nonaka, M., Mcintosh, T. K., Wolf, J. A., et al. (1999). Evolution of Neurofilament Subtype Accumulation in Axons Following Diffuse Brain Injury in the Pig. *J. Neuropathol. Exp. Neurol.* 58, 588–596. doi:10.1097/00005072-199906000-00003

Chen, Y.-H., Huang, E. Y.-K., Kuo, T.-T., Miller, J., Chiang, Y.-H., and Hoffer, B. J. (2017). Impact of Traumatic Brain Injury on Dopaminergic Transmission. *Cel Transpl.* doi:10.3727/096368917X694787

Ciocanel, M.-V., Jung, P., and Brown, A. (2020). A Mechanism for Neurofilament Transport Acceleration through Nodes of Ranvier. *MBoC* 31, 640–654. doi:10.1091/mbc.E19-09-0509

Clapham, D. E. (2003). TRP Channels as Cellular Sensors. *Nature* 426, 517–524. doi:10.1038/nature02196

Clark, K., Langeslag, M., Figdor, C. G., and van Leeuwen, F. N. (2007). Myosin II and Mechanotransduction: a Balancing Act. *Trends Cel Biol.* 17, 178–186. doi:10.1016/j.tcb.2007.02.002

Corallo, D., Frabetti, S., Candini, O., Gregianin, E., Dominici, M., Fischer, H., et al. (2020). Emerging Neuroblastoma 3D *In Vitro* Models for Pre-clinical Assessments. *Front. Immunol.* 11, 584214. doi:10.3389/fimmu.2020.584214

Corey, D. P., and Hudspeth, A. J. (1979). Ionic Basis of the Receptor Potential in a Vertebrate Hair Cell. *Nature* 281, 675–677. doi:10.1038/281675a0

Corne, T. D. J., Sieprath, T., Vandenbussche, J., Mohammed, D., Te Lindert, M., Gevraert, K., et al. (2017). Deregulation of Focal Adhesion Formation And Cytoskeletal Tension Due To Loss of A-Type Lamins. *Cell Adhes. Migrat.* 11, 447–463. doi:10.1080/19336918.2016.1247144

Coste, B., Mathur, J., Schmidt, M., Earley, T. J., Ranade, S., Petrus, M. J., et al. (2010). Piezo1 and Piezo2 Are Essential Components of Distinct Mechanically Activated Cation Channels. *Science* 330, 55–60. doi:10.1126/science.1193270

Coste, B., Xiao, B., Santos, J. S., Syeda, R., Grandl, J., Spencer, K. S., et al. (2012). Piezo Proteins Are Pore-Forming Subunits of Mechanically Activated Channels. *Nature* 483, 176–181. doi:10.1038/nature10812

Crick, F. (1982). Do dendritic Spines Twitch? *Trends Neurosciences* 5, 44–46. doi:10.1016/0166-2236(82)90020-0

Cyr, J. L., and Brady, S. T. (1992). Molecular Motors in Axonal Transport. *Mol. Neurobiol.* 6, 137–155. doi:10.1007/BF02780549

Daneman, R., and Prat, A. (2015). The Blood-Brain Barrier. *Cold Spring Harb. Perspect. Biol.* 7, a020412. doi:10.1101/cshperspect.a020412

Dauth, S., Grevesse, T., Pantazopoulos, H., Campbell, P. H., Maoz, B. M., Berretta, S., et al. (2016). Extracellular Matrix Protein Expression Is Brain Region Dependent. *J. Comp. Neurol.* 524, 1309–1336. doi:10.1002/cne.23965

De Vitis, E., La Pesa, V., Gervaso, F., Romano, A., Quattrini, A., Gigli, G., et al. (2021). A Microfabricated Multi-Compartment Device for Neuron and Schwann Cell Differentiation. *Sci. Rep.* 11, 7019. doi:10.1038/s41598-021-86300-4

DeKosky, S. T., and Asken, B. M. (2017). Injury Cascades in TBI-Related Neurodegeneration. *Brain Inj.* 31, 1177–1182. doi:10.1080/02699052.2017.1312528

Di Pietro, V., Amorini, A. M., Tavazzi, B., Hovda, D. A., Signoretti, S., Giza, C. C., et al. (2013). Potentially Neuroprotective Gene Modulation in an *In Vitro* Model of Mild Traumatic Brain Injury. *Mol. Cel. Biochem.* 375, 185–198. doi:10.1007/s11010-012-1541-2

Doss, B. L., Pan, M., Gupta, M., Grenci, G., Mège, R.-M., Lim, C. T., et al. (2020). Cell Response to Substrate Rigidity Is Regulated by Active and Passive Cytoskeletal Stress. *Proc. Natl. Acad. Sci. U.S.A.* 117, 12817–12825. doi:10.1073/pnas.1917555117

Dowell-Mesfin, N. M., Abdul-Karim, M.-A., Turner, A. M. P., Schanz, S., Craighead, H. G., Roysam, B., et al. (2004). Topographically Modified Surfaces Affect Orientation and Growth of Hippocampal Neurons. *J. Neural Eng.* 1, 78–90. doi:10.1088/1741-2560/1/2/003

Dubin, A. E., Murthy, S., Lewis, A. H., Brosse, L., Cahalan, S. M., Grandl, J., et al. (2017). Endogenous Piezo1 Can Confound Mechanically Activated Channel Identification and Characterization. *Neuron* 94, 266–270. e3. doi:10.1016/j.neuron.2017.03.039

Dupraz, S., Hilton, B. J., Husch, A., Santos, T. E., Coles, C. H., Stern, S., et al. (2019). RhoA Controls Axon Extension Independent of Specification in the Developing Brain. *Curr. Biol.* 29, 3874–3886. e9. doi:10.1016/j.cub.2019.09.040

Elosegui-Artola, A., Trepat, X., and Roca-Cusachs, P. (2018). Control of Mechanotransduction by Molecular Clutch Dynamics. *Trends Cel Biol.* 28, 356–367. doi:10.1016/j.tcb.2018.01.008

Essen, D. C. V. (1997). A Tension-Based Theory of Morphogenesis and Compact Wiring in the central Nervous System. *Nature* 385, 313–318. doi:10.1038/385313a0

Fang, Y., Iu, C. Y. Y., Lui, C. N. P., Zou, Y., Fung, C. K. M., Li, H. W., et al. (2014). Investigating Dynamic Structural and Mechanical Changes of Neuroblastoma Cells Associated with Glutamate-Mediated Neurodegeneration. *Sci. Rep.* 4, 7074. doi:10.1038/srep07074

Fann, J. R., Ribe, A. R., Pedersen, H. S., Fenger-Grøn, M., Christensen, J., Benros, M. E., et al. (2018). Long-term Risk of Dementia Among People with Traumatic Brain Injury in Denmark: a Population-Based Observational Cohort Study. *The Lancet Psychiatry* 5, 424–431. doi:10.1016/S2215-0366(18)30065-8

Fatemi, S. H. (2005). Reelin Glycoprotein: Structure, Biology and Roles in Health and Disease. *Mol. Psychiatry* 10, 251–257. doi:10.1038/sj.mp.4001613

Flanagan, L. A., Ju, Y.-E., Marg, B., Osterfield, M., and Janmey, P. A. (2002). Neurite Branching on Deformable Substrates. *Neuroreport* 13, 2411–2415. doi:10.1097/00001756-200212200-00007

Foscarin, S., Raha-Chowdhury, R., Fawcett, J. W., and Kwok, J. C. F. (2017). Brain Ageing Changes Proteoglycan Sulfation, Rendering Perineuronal Nets More Inhibitory. *Aging* 9, 1607–1622. doi:10.18632/aging.101256

Fouchard, J., Mitrossilis, D., and Asnacios, A. (2011). Acto-myosin Based Response to Stiffness and Rigidity Sensing. *Cell Adhes. Migration* 5, 16–19. doi:10.4161/cam.5.1.13281

Fozdar, D. Y., Lee, J. Y., Schmidt, C. E., and Chen, S. (2010). Hippocampal Neurons Respond Uniquely to Topographies of Various Sizes and Shapes. *Biofabrication* 2, 035005. doi:10.1088/1758-5082/2/3/035005

Franze, K., and Guck, J. (2010). The Biophysics of Neuronal Growth. *Rep. Prog. Phys.* 73, 094601. doi:10.1088/0034-4885/73/9/094601

Franze, K., Janmey, P. A., and Guck, J. (2013). Mechanics in Neuronal Development and Repair. *Annu. Rev. Biomed. Eng.* 15, 227–251. doi:10.1146/annurev-bioeng-071811-150045

Fujii, M., Matano, M., Toshimitsu, K., Takano, A., Mikami, Y., Nishikori, S., et al. (2018). Human Intestinal Organoids Maintain Self-Renewal Capacity and Cellular Diversity in Niche-Inspired Culture Condition. *Cell Stem Cell* 23, 787–793. e6. doi:10.1016/j.stem.2018.11.016

Gabi, M., Neves, K., Masseron, C., Ribeiro, P. F. M., Ventura-Antunes, L., Torres, L., et al. (2016). No Relative Expansion of the Number of Prefrontal Neurons in Primate and Human Evolution. *Proc. Natl. Acad. Sci. U.S.A.* 113, 9617–9622. doi:10.1073/pnas.1610178113

Gardner, R. C., Byers, A. L., Barnes, D. E., Li, Y., Boscardin, J., and Yaffe, K. (2018). Mild TBI and Risk of Parkinson Disease. *Neurology* 90, e1771–e1779. doi:10.1212/WNL.0000000000005522

Gaub, B. M., Kasuba, K. C., Mace, E., Strittmatter, T., Laskowski, P. R., Geissler, S. A., et al. (2020). Neurons Differentiate Magnitude and Location of Mechanical Stimuli. *Proc. Natl. Acad. Sci. U.S.A.* 117, 848–856. doi:10.1073/pnas.1909933117

Gauthier, N. C., and Roca-Cusachs, P. (2018). Mechanosensing at Integrin-Mediated Cell-Matrix Adhesions: from Molecular to Integrated Mechanisms. *Curr. Opin. Cel Biol.* 50, 20–26. doi:10.1016/j.ceb.2017.12.014

Geraili, A., Jafari, P., Hassani, M. S., Araghi, B. H., Mohammadi, M. H., Ghafari, A. M., et al. (2018). Controlling Differentiation of Stem Cells for Developing Personalized Organ-On-Chip Platforms. *Adv. Healthc. Mater.* 7, 1700426. doi:10.1002/adhm.201700426

Gingras, A. R., and Ginsberg, M. H. (2020). Signal Transduction: Physical Deformation of the Membrane Activates Integrins. *Curr. Biol.* 30, R397–R400. doi:10.1016/j.cub.2020.02.068

González-Cruz, R. D., Dahl, K. N., and Darling, E. M. (2018). The Emerging Role of Lamin C as an Important LMNA Isoform in Mechanophenotype. *Front. Cel Dev. Biol.* 6, 151. doi:10.3389/fcell.2018.00151

Goriely, A., Budday, S., and Kuhl, E. (2015). "Neuromechanics," in *Advances in Applied Mechanics* (Elsevier), 79–139. doi:10.1016/bs.aams.2015.10.002

Green, M. A., Bilston, L. E., and Sinkus, R. (2008). In Vivobrain Viscoelastic Properties Measured by Magnetic Resonance Elastography. *NMR Biomed.* 21, 755–764. doi:10.1002/nbm.1254

Grevesse, T., Dabiri, B. E., Parker, K. K., and Gabriele, S. (2015). Opposite Rheological Properties of Neuronal Microcompartments Predict Axonal Vulnerability in Brain Injury. *Sci. Rep.* 5. doi:10.1038/srep09475

Guharay, F., and Sachs, F. (1984). Stretch-activated Single Ion Channel Currents in Tissue-Cultured Embryonic Chick Skeletal Muscle. *J. Physiol.* 352, 685–701. doi:10.1113/jphysiol.1984.sp015317

Guillaud, L., El-Agamy, S. E., Otsuki, M., and Terenzio, M. (2020). Anterograde Axonal Transport in Neuronal Homeostasis and Disease. *Front. Mol. Neurosci.* 13, 556175. doi:10.3389/fnmol.2020.556175

Gupta, R., and Sen, N. (2016). Traumatic Brain Injury: a Risk Factor for Neurodegenerative Diseases. *Rev. Neurosci.* 27, 93–100. doi:10.1515/revneuro-2015-0017

Hagestedt, T., Lichtenberg, B., Wille, H., Mandelkow, E. M., and Mandelkow, E. (1989). Tau Protein Becomes Long and Stiff upon Phosphorylation: Correlation between Paracrystalline Structure and Degree of Phosphorylation. *J. Cel Biol.* 109, 1643–1651. doi:10.1083/jcb.109.4.1643

Harish, G., Mahadevan, A., Pruthi, N., Sreenivasamurthy, S. K., Puttamallesh, V. N., Keshava Prasad, T. S., et al. (2015). Characterization of Traumatic Brain Injury in Human Brains Reveals Distinct Cellular and Molecular Changes in Contusion and Pericontusion. *J. Neurochem.* 134, 156–172. doi:10.1111/jnc.13082

Hatch, R. J., Wei, Y., Xia, D., and Götz, J. (2017). Hyperphosphorylated Tau Causes Reduced Hippocampal CA1 Excitability by Relocating the Axon Initial Segment. *Acta Neuropathol.* 133, 717–730. doi:10.1007/s00401-017-1674-1

Hemphill, M. A., Dabiri, B. E., Gabriele, S., Kerscher, L., Franck, C., Goss, J. A., et al. (2011). A Possible Role for Integrin Signaling in Diffuse Axonal Injury. *PLoS ONE* 6, e22899. doi:10.1371/journal.pone.0022899

Heo, S.-J., Song, K. H., Thakur, S., Miller, L. M., Cao, X., Peredo, A. P., et al. (2020). Nuclear Softening Expedites Interstitial Cell Migration in Fibrous Networks and Dense Connective Tissues. *Sci. Adv.* 6, eaax5083. doi:10.1126/sciadv.aax5083

Herculano-Houzel, S. (2005). Isotropic Fractionator: A Simple, Rapid Method for the Quantification of Total Cell and Neuron Numbers in the Brain. *J. Neurosci.* 25, 2518–2521. doi:10.1523/JNEUROSCI.4526-04.2005

Herculano-Houzel, S. (2011). Not All Brains Are Made the Same: New Views on Brain Scaling in Evolution. *Brain Behav. Evol.* 78, 22–36. doi:10.1159/000327318

Herculano-Houzel, S. (2009). The Human Brain in Numbers: a Linearly Scaled-Up Primate Brain. *Front. Hum. Neurosci.* 3. doi:10.3389/neuro.09.031.2009

Herz, J., and Chen, Y. (2006). Reelin, Lipoprotein Receptors and Synaptic Plasticity. *Nat. Rev. Neurosci.* 7, 850–859. doi:10.1038/nrn2009

Hill, D. K. (1950). The Volume Change Resulting from Stimulation of a Giant Nerve Fibre. *J. Physiol.* 111, 304–327. doi:10.1113/jphysiol.1950.sp004481

Hiscox, L. V., Johnson, C. L., McGarry, M. D. J., Marshall, H., Ritchie, C. W., van Beek, E. J. R., et al. (2020). Mechanical Property Alterations across the Cerebral Cortex Due to Alzheimer's Disease. *Brain Commun.* 2, fcz049. doi:10.1093/braincomms/fcz049

Hong, G.-S., Lee, B., Wee, J., Chun, H., Kim, H., Jung, J., et al. (2016). Tentonin 3/TMEM150c Confers Distinct Mechanosensitive Currents in Dorsal-Root Ganglion Neurons with Proprioceptive Function. *Neuron* 91, 107–118. doi:10.1016/j.neuron.2016.05.029

Hou, Y., Dan, X., Babbar, M., Wei, Y., Hasselbalch, S. G., Croteau, D. L., et al. (2019). Ageing as a Risk Factor for Neurodegenerative Disease. *Nat. Rev. Neurol.* 15, 565–581. doi:10.1038/s41582-019-0244-7

Hrapko, M., van Dommelen, J. A. W., Peters, G. W. M., and Wismans, J. S. H. M. (2008). The Influence of Test Conditions on Characterization of the Mechanical Properties of Brain Tissue. *J. Biomech. Eng.* 130, 031003. doi:10.1115/1.2907746

Hu, Y., Huang, G., Tian, J., Qiu, J., Jia, Y., Feng, D., et al. (2021). Matrix Stiffness Changes Affect Astrocyte Phenotype in an *In Vitro* Injury Model. *NPG Asia Mater.* 13, 35. doi:10.1038/s41427-021-00304-0

Hur, E.-M., Yang, I. H., Kim, D.-H., Byun, J., SaijilafuXu, W.-L., Xu, W.-L., et al. (2011). Engineering Neuronal Growth Cones to Promote Axon Regeneration over Inhibitory Molecules. *Proc. Natl. Acad. Sci. U.S.A.* 108, 5057–5062. doi:10.1073/pnas.1011258108

Indra, I., Troyanovsky, R. B., Shapiro, L., Honig, B., and Troyanovsky, S. M. (2020). Sensing Actin Dynamics through Adherens Junctions. *Cel Rep.* 30, 2820–2833.e3. doi:10.1016/j.celrep.2020.01.106

Ishii, K., Kubo, K.-i., and Nakajima, K. (2016). Reelin and Neuropsychiatric Disorders. *Front. Cel. Neurosci.* 10. doi:10.3389/fncel.2016.00229

Ivancevic, V. G. (2009). New Mechanics of Traumatic Brain Injury. *Cogn. Neurodyn.* 3, 281–293. doi:10.1007/s11571-008-9070-0

Iwashita, M., Kataoka, N., Toida, K., and Kosodo, Y. (2014). Systematic Profiling of Spatiotemporal Tissue and Cellular Stiffness in the Developing Brain. *Development* 141, 3793–3798. doi:10.1242/dev.109637

Jagielska, A., Lowe, A. L., Makhija, E., Wroblewska, L., Guck, J., Franklin, R. J. M., et al. (2017). Mechanical Strain Promotes Oligodendrocyte Differentiation by Global Changes of Gene Expression. *Front. Cel. Neurosci.* 11, 93. doi:10.3389/fncel.2017.00093

Jagielska, A., Norman, A. L., Whyte, G., Vliet, K. J. V., Guck, J., and Franklin, R. J. M. (2012). Mechanical Environment Modulates Biological Properties of Oligodendrocyte Progenitor Cells. *Stem Cell Development* 21, 2905–2914. doi:10.1089/scd.2012.0189

Jäkel, S., and Dimou, L. (2017). Glial Cells and Their Function in the Adult Brain: A Journey through the History of Their Ablation. *Front. Cel. Neurosci.* 11. doi:10.3389/fncel.2017.00024

Janmey, P. A., Fletcher, D. A., and Reinhart-King, C. A. (2020). Stiffness Sensing by Cells. *Physiol. Rev.* 100, 695–724. doi:10.1152/physrev.00013.2019

Kalil, K., and Dent, E. W. (2014). Branch Management: Mechanisms of Axon Branching in the Developing Vertebrate CNS. *Nat. Rev. Neurosci.* 15, 7–18. doi:10.1038/nrn3650

Kanamori, A., Catrinescu, M.-M., Belisle, J. M., Costantino, S., and Levin, L. A. (2012). Retrograde and Wallerian Axonal Degeneration Occur Synchronously after Retinal Ganglion Cell Axotomy. *Am. J. Pathol.* 181, 62–73. doi:10.1016/j.ajpath.2012.03.030

Karve, I. P., Taylor, J. M., and Crack, P. J. (2016). The Contribution of Astrocytes and Microglia to Traumatic Brain Injury. *Br. J. Pharmacol.* 173, 692–702. doi:10.1111/bph.13125

Kastian, R. F., Minegishi, T., Baba, K., Saneyoshi, T., Katsuno-Kambe, H., Saranpal, S., et al. (2021). Shootin1a-mediated Actin-Adhesion Coupling Generates Force to Trigger Structural Plasticity of Dendritic Spines. *Cel Rep.* 35, 109130. doi:10.1016/j.celrep.2021.109130

Kaur, P., and Sharma, S. (2018). Recent Advances in Pathophysiology of Traumatic Brain Injury. *Cn* 16, 1224–1238. doi:10.2174/1570159X15666170613083606

Kerstein, P. C., Nichol IV, R. H., and Gomez, T. M. (2015). Mechanochemical Regulation of Growth Cone Motility. *Front. Cel. Neurosci.* 9. doi:10.3389/fncel.2015.00244

Kilinc, D., Gallo, G., and Barbee, K. A. (2008). Mechanically-induced Membrane Poration Causes Axonal Beading and Localized Cytoskeletal Damage. *Exp. Neurol.* 212, 422–430. doi:10.1016/j.expneurol.2008.04.025

Kim, C., Ye, F., Hu, X., and Ginsberg, M. H. (2012). Talin Activates Integrins by Altering the Topology of the β Transmembrane Domain. *J. Cel Biol.* 197, 605–611. doi:10.1083/jcb.201112141

Kim, H., Park, H. J., Choi, H., Chang, Y., Park, H., Shin, J., et al. (2019). Modeling G2019S-LRRK2 Sporadic Parkinson's Disease in 3D Midbrain Organoids. *Stem Cel Rep.* 12, 518–531. doi:10.1016/j.stemcr.2019.01.020

Koch, D., Rosoff, W. J., Jiang, J., Geller, H. M., and Urbach, J. S. (2012). Strength in the Periphery: Growth Cone Biomechanics and Substrate Rigidity Response in Peripheral and Central Nervous System Neurons. *Biophysical J.* 102, 452–460. doi:10.1016/j.bpj.2011.12.025

Kokiko-Cochran, O. N., and Godbout, J. P. (2018). The Inflammatory Continuum of Traumatic Brain Injury and Alzheimer's Disease. *Front. Immunol.* 9, 672. doi:10.3389/fimmu.2018.00672

Kong, F., García, A. J., Mould, A. P., Humphries, M. J., and Zhu, C. (2009). Demonstration of Catch Bonds between an Integrin and its Ligand. *J. Cel Biol.* 185, 1275–1284. doi:10.1083/jcb.200810002

Koser, D. E., Thompson, A. J., Foster, S. K., Dwivedy, A., Pillai, E. K., Sheridan, G. K., et al. (2016). Mechanosensing Is Critical for Axon Growth in the Developing Brain. *Nat. Neurosci.* 19, 1592–1598. doi:10.1038/nn.4394

Kostic, A., Sap, J., and Sheetz, M. P. (2007). RPTPα Is Required for Rigidity-dependent Inhibition of Extension and Differentiation of Hippocampal Neurons. *J. Cel Sci.* 120, 3895–3904. doi:10.1242/jcs.009852

Kruse, S. A., Rose, G. H., Glaser, K. J., Manduca, A., Felmlee, J. P., Jack, C. R., et al. (2008). Magnetic Resonance Elastography of the Brain. *NeuroImage* 39, 231–237. doi:10.1016/j.neuroimage.2007.08.030

Kumar Sahel, D., Kaira, M., Raj, K., Sharma, S., and Singh, S. (2019). Mitochondrial Dysfunctioning and Neuroinflammation: Recent Highlights on the Possible Mechanisms Involved in Traumatic Brain Injury. *Neurosci. Lett.* 710, 134347. doi:10.1016/j.neulet.2019.134347

Lam, D., Enright, H. A., Cadena, J., Peters, S. K. G., Sales, A. P., Osburn, J. J., et al. (2019). Tissue-specific Extracellular Matrix Accelerates the Formation of Neural Networks and Communities in a Neuron-Glia Co-culture on a Multi-Electrode Array. *Sci. Rep.* 9, 4159. doi:10.1038/s41598-019-40128-1

Lampi, M. C., and Reinhart-King, C. A. (2018). Targeting Extracellular Matrix Stiffness to Attenuate Disease: From Molecular Mechanisms to Clinical Trials. *Sci. Transl. Med.* 10, eaao0475. doi:10.1126/scitranslmed.aao0475

Lantoine, J., Grevesse, T., Villers, A., Delhaye, G., Mestdagh, C., Versaevel, M., et al. (2016). Matrix Stiffness Modulates Formation and Activity of Neuronal Networks of Controlled Architectures. *Biomaterials* 89, 14–24. doi:10.1016/j.biomaterials.2016.02.041

Lantoine, J., Procès, A., Villers, A., Halliez, S., Buée, L., Ris, L., et al. (2021). Inflammatory Molecules Released by Mechanically Injured Astrocytes Trigger Presynaptic Loss in Cortical Neuronal Networks. *ACS Chem. Neurosci.* 12, 3885–3897. 1c00488. doi:10.1021/acschemneuro.1c00488

Latchoumane, C.-F. V., Betancur, M. I., Simchick, G. A., Sun, M. K., Forghani, R., Lenear, C. E., et al. (2021). Engineered Glycomaterial Implants Orchestrate Large-Scale Functional Repair of Brain Tissue Chronically after Severe Traumatic Brain Injury. *Sci. Adv.* 7, eabe0207. doi:10.1126/sciadv.abe0207

Lau, L. W., Cua, R., Keough, M. B., Haylock-Jacobs, S., and Yong, V. W. (2013). Pathophysiology of the Brain Extracellular Matrix: a New Target for Remyelination. *Nat. Rev. Neurosci.* 14, 722–729. doi:10.1038/nrn3550

L. E. Bilston (Editor) (2011). *Neural Tissue Biomechanics* (Berlin, Heidelberg: Springer Berlin Heidelberg). doi:10.1007/978-3-642-13890-4

Leterrier, C., Dubey, P., and Roy, S. (2017). The Nano-Architecture of the Axonal Cytoskeleton. *Nat. Rev. Neurosci.* 18, 713–726. doi:10.1038/nrn.2017.129

Lu, Y.-B., Franze, K., Seifert, G., Steinhäuser, C., Kirchhoff, F., Wolburg, H., et al. (2006). Viscoelastic Properties of Individual Glial Cells and Neurons in the CNS. *Proc. Natl. Acad. Sci. U.S.A.* 103, 17759–17764. doi:10.1073/pnas.0606150103

Luo, P., Li, X., Wu, X., Dai, S., Yang, Y., Xu, H., et al. (2019). Preso Regulates NMDA Receptor-Mediated Excitotoxicity via Modulating Nitric Oxide and Calcium Responses after Traumatic Brain Injury. *Cell Death Dis* 10, 496. doi:10.1038/s41419-019-1731-x

Ma, X., Agas, A., Siddiqui, Z., Kim, K., Iglesias-Montoro, P., Kalluru, J., et al. (2020). Angiogenic Peptide Hydrogels for Treatment of Traumatic Brain Injury. *Bioactive Mater.* 5, 124–132. doi:10.1016/j.bioactmat.2020.01.005

MacManus, D. B., Pierrat, B., Murphy, J. G., and Gilchrist, M. D. (2017). Region and Species Dependent Mechanical Properties of Adolescent and Young Adult Brain Tissue. *Sci. Rep.* 7, 13729. doi:10.1038/s41598-017-13727-z

Maday, S., Twelvetrees, A. E., Moughamian, A. J., and Holzbaur, E. L. F. (2014). Axonal Transport: Cargo-specific Mechanisms of Motility and Regulation. *Neuron* 84, 292–309. doi:10.1016/j.neuron.2014.10.019

Maeda, N. (2015). Proteoglycans and Neuronal Migration in the Cerebral Cortex during Development and Disease. *Front. Neurosci.* 9. doi:10.3389/fnins.2015.00098

Maingret, F., Fosset, M., Lesage, F., Lazdunski, M., and Honoré, E. (1999). TRAAK Is a Mammalian Neuronal Mechano-Gated K+Channel. *J. Biol. Chem.* 274, 1381–1387. doi:10.1074/jbc.274.3.1381

Makhija, E., Jagielska, A., Zhu, L., Bost, A. C., Ong, W., Chew, S. Y., et al. (2018). Mechanical Strain Alters Cellular and Nuclear Dynamics at Early Stages of Oligodendrocyte Differentiation. *Front. Cel. Neurosci.* 12, 59. doi:10.3389/fncel.2018.00059

Marinval, N., and Chew, S. Y. (2021). Mechanotransduction Assays for Neural Regeneration Strategies: A Focus on Glial Cells. *APL Bioeng.* 5, 021505. doi:10.1063/5.0037814

Martin, M., Benzina, O., Szabo, V., Végh, A.-G., Lucas, O., Cloitre, T., et al. (2013). Morphology and Nanomechanics of Sensory Neurons Growth Cones Following Peripheral Nerve Injury. *PLoS ONE* 8, e56286. doi:10.1371/journal.pone.0056286

Martinac, B., and Cox, C. D. (2017). "Mechanosensory Transduction: Focus on Ion Channels ☆ ☆," in *Reference Module in Life Sciences* (0: Elsevier). B9780128096338082000. doi:10.1016/B978-0-12-809633-8.08094-8

Marton, R. M., Miura, Y., Sloan, S. A., Li, Q., Revah, O., Levy, R. J., et al. (2019). Differentiation and Maturation of Oligodendrocytes in Human Three-Dimensional Neural Cultures. *Nat. Neurosci.* 22, 484–491. doi:10.1038/s41593-018-0316-9

Matthay, K. K., Maris, J. M., Schleiermacher, G., Nakagawara, A., Mackall, C. L., Diller, L., et al. (2016). Neuroblastoma. *Nat. Rev. Dis. Primers* 2, 16078. doi:10.1038/nrdp.2016.78

McINTOSH, T. K., Juhler, M., and Wieloch, T. (1998). Novel Pharmacologic Strategies in the Treatment of Experimental Traumatic Brain Injury: 1998. *J. Neurotrauma* 15, 731–769. doi:10.1089/neu.1998.15.731

Meaney, D. F., and Smith, D. H. (2011). Biomechanics of Concussion. *Clin. Sports Med.* 30, 19–31. doi:10.1016/j.csm.2010.08.009

Mescola, A., Vella, S., Scotto, M., Gavazzo, P., Canale, C., Diaspro, A., et al. (2012). Probing Cytoskeleton Organisation of Neuroblastoma Cells with Single-Cell Force Spectroscopy. *J. Mol. Recognit.* 25, 270–277. doi:10.1002/jmr.2173

Millecamps, S., and Julien, J.-P. (2013). Axonal Transport Deficits and Neurodegenerative Diseases. *Nat. Rev. Neurosci.* 14, 161–176. doi:10.1038/nrn3380

Minegishi, T., Uesugi, Y., Kaneko, N., Yoshida, W., Sawamoto, K., and Inagaki, N. (2018). Shootin1b Mediates a Mechanical Clutch to Produce Force for Neuronal Migration. *Cel Rep.* 25, 624–639. e6. doi:10.1016/j.celrep.2018.09.068

Mitchison, T., and Kirschner, M. (1988). Cytoskeletal Dynamics and Nerve Growth. *Neuron* 1, 761–772. doi:10.1016/0896-6273(88)90124-9

Moeendarbary, E., Weber, I. P., Sheridan, G. K., Koser, D. E., Soleman, S., Haenzi, B., et al. (2017). The Soft Mechanical Signature of Glial Scars in the central Nervous System. *Nat. Commun.* 8, 14787. doi:10.1038/ncomms14787

Mohammed, D., Charras, G., Vercruysse, E., Versaevel, M., Lantoine, J., Alaimo, L., et al. (2019). Substrate Area Confinement Is a Key Determinant of Cell Velocity in Collective Migration. *Nat. Phys.* 15, 858–866. doi:10.1038/s41567-019-0543-3

Mohammed, D., Versaevel, M., Bruyere, C., Alaimo, L., Luciano, M., Vercruysse, E., et al. (2019). Innovative Tools For Mechanobiology: Unraveling Outside-In And Inside-Out Mechanotransduction. *Front. Bioeng. Biotech.* 7, 162. doi:10.3389/fbioe.2019.00162

Mol, E. A., Lei, Z., Roefs, M. T., Bakker, M. H., Goumans, M. J., Doevendans, P. A., et al. (2019). Injectable Supramolecular Ureidopyrimidinone Hydrogels Provide Sustained Release of Extracellular Vesicle Therapeutics. *Adv. Healthc. Mater.* 8, 1900847. doi:10.1002/adhm.201900847

Moreno-Layseca, P., Icha, J., Hamidi, H., and Ivaska, J. (2019). Integrin Trafficking in Cells and Tissues. *Nat. Cel Biol.* 21, 122–132. doi:10.1038/s41556-018-0223-z

Morris, C. E. (2011). Voltage-Gated Channel Mechanosensitivity: Fact or Friction? *Front. Physio.* 2. doi:10.3389/fphys.2011.00025

Mosley, M. C., Lim, H. J., Chen, J., Yang, Y.-H., Li, S., Liu, Y., et al. (2017). Neurite Extension and Neuronal Differentiation of Human Induced Pluripotent Stem Cell Derived Neural Stem Cells on Polyethylene Glycol Hydrogels Containing a Continuous Young's Modulus Gradient. *J. Biomed. Mater. Res.* 105, 824–833. doi:10.1002/jbm.a.35955

Mu, J., Song, Y., Zhang, J., Lin, W., and Dong, H. (2015). Calcium Signaling Is Implicated in the Diffuse Axonal Injury of Brain Stem. *Int. J. Clin. Exp. Pathol.* 8, 4388–4397.

Muguruma, K., Nishiyama, A., Kawakami, H., Hashimoto, K., and Sasai, Y. (2015). Self-Organization of Polarized Cerebellar Tissue in 3D Culture of Human Pluripotent Stem Cells. *Cel Rep.* 10, 537–550. doi:10.1016/j.celrep.2014.12.051

Murphy, M. C., Huston, J., Jack, C. R., Glaser, K. J., Manduca, A., Felmlee, J. P., et al. (2011). Decreased Brain Stiffness in Alzheimer's Disease Determined by Magnetic Resonance Elastography. *J. Magn. Reson. Imaging* 34, 494–498. doi:10.1002/jmri.22707

Murphy, M. C., Huston, J., Jack, C. R., Glaser, K. J., Senjem, M. L., Chen, J., et al. (2013). Measuring the Characteristic Topography of Brain Stiffness with Magnetic Resonance Elastography. *PLoS ONE* 8, e81668. doi:10.1371/journal.pone.0081668

Murphy, M. C., Jones, D. T., Jack, C. R., Glaser, K. J., Senjem, M. L., Manduca, A., et al. (2016). Regional Brain Stiffness Changes across the Alzheimer's Disease Spectrum. *NeuroImage: Clin.* 10, 283–290. doi:10.1016/j.nicl.2015.12.007

Murthy, S. E., Dubin, A. E., and Patapoutian, A. (2017). Piezos Thrive under Pressure: Mechanically Activated Ion Channels in Health and Disease. *Nat. Rev. Mol. Cel Biol.* 18, 771–783. doi:10.1038/nrm.2017.92

Mustata, M., Ritchie, K., and McNally, H. A. (2010). Neuronal Elasticity as Measured by Atomic Force Microscopy. *J. Neurosci. Methods* 186, 35–41. doi:10.1016/j.jneumeth.2009.10.021

Nagasaka, A., Shinoda, T., Kawaue, T., Suzuki, M., Nagayama, K., Matsumoto, T., et al. (2016). Differences in the Mechanical Properties of the Developing Cerebral Cortical Proliferative Zone between Mice and Ferrets at Both the Tissue and Single-Cell Levels. *Front. Cel Dev. Biol.* 4. doi:10.3389/fcell.2016.00139

Nagendran, T., Larsen, R. S., Bigler, R. L., Frost, S. B., Philpot, B. D., Nudo, R. J., et al. (2017). Distal Axotomy Enhances Retrograde Presynaptic Excitability onto Injured Pyramidal Neurons via Trans-synaptic Signaling. *Nat. Commun.* 8, 625. doi:10.1038/s41467-017-00652-y

Nardella, M., Guglielmi, L., Musa, C., Iannetti, I., Maresca, G., Amendola, D., et al. (2015). Down-regulation of the Lamin A/C in Neuroblastoma Triggers the Expansion of Tumor Initiating Cells. *Oncotarget* 6, 32821–32840. doi:10.18632/oncotarget.5104

Ngo, M. T., and Harley, B. A. C. (2021). Progress in Mimicking Brain Microenvironments to Understand and Treat Neurological Disorders. *APL Bioeng.* 5, 020902. doi:10.1063/5.0043338

Nicolle, S., Lounis, M., Willinger, R., and Palierne, J. F. (2005). Shear Linear Behavior of Brain Tissue over a Large Frequency Range. *Biorheology* 42, 209–223.

Novak, U., and Kaye, A. H. (2000). Extracellular Matrix and the Brain: Components and Function. *J. Clin. Neurosci.* 7, 280–290. doi:10.1054/jocn.1999.0212

O'Brien, J. S., and Sampson, E. L. (1965). Lipid Composition of the normal Human Brain: gray Matter, white Matter, and Myelin. *J. Lipid Res.* 6, 537–544.

Olmsted, J. B., and Lyon, H. D. (1981). A Microtubule-Associated Protein Specific to Differentiated Neuroblastoma Cells. *J. Biol. Chem.* 256, 3507–3511. doi:10.1016/s0021-9258(19)69638-9

Pakkenberg, B. (2003). Aging and the Human Neocortex. *Exp. Gerontol.* 38, 95–99. doi:10.1016/S0531-5565(02)00151-1

Pakkenberg, B., and Gundersen, H. J. r. G. (1997). Neocortical Neuron Number in Humans: Effect of Sex and Age. *J. Comp. Neurol.* 384, 312–320. doi:10.1002/(sici)1096-9861(19970728)384:2<312::aid-cne10>3.0.co;2-k

Park, J., Kim, D.-H., Kim, H.-N., Wang, C. J., Kwak, M. K., Hur, E., et al. (2016). Directed Migration of Cancer Cells Guided by the Graded Texture of the Underlying Matrix. *Nat. Mater* 15, 792–801. doi:10.1038/nmat4586

Passaro, A. P., and Stice, S. L. (2021). Electrophysiological Analysis of Brain Organoids: Current Approaches and Advancements. *Front. Neurosci.* 14, 622137. doi:10.3389/fnins.2020.622137

Pérez-González, C., Ceada, G., Greco, F., Matejčić, M., Gómez-González, M., Castro, N., et al. (2021). Mechanical Compartmentalization of the Intestinal Organoid Enables Crypt Folding and Collective Cell Migration. *Nat. Cel Biol.* 23, 745–757. doi:10.1038/s41556-021-00699-6

Pervin, F., and Chen, W. W. (2009). Dynamic Mechanical Response of Bovine gray Matter and white Matter Brain Tissues under Compression. *J. Biomech.* 42, 731–735. doi:10.1016/j.jbiomech.2009.01.023

Pesold, C., Liu, W. S., Guidotti, A., Costa, E., and Caruncho, H. J. (1999). Cortical Bitufted, Horizontal, and Martinotti Cells Preferentially Express and Secrete Reelin into Perineuronal Nets, Nonsynaptically Modulating Gene Expression. *Proc. Natl. Acad. Sci.* 96, 3217–3222. doi:10.1073/pnas.96.6.3217

Petrie, R. J., Koo, H., and Yamada, K. M. (2014). Generation of Compartmentalized Pressure by a Nuclear Piston Governs Cell Motility in a 3D Matrix. *Science* 345, 1062–1065. doi:10.1126/science.1256965

Pigino, G., Song, Y., Kirkpatrick, L. L., and Brady, S. T. (2012). "The Cytoskeleton of Neurons and Glia," in *Basic Neurochemistry* (Elsevier), 101–118. doi:10.1016/B978-0-12-374947-5.00006-7

Polini, A., del Mercato, L. L., Barra, A., Zhang, Y. S., Calabi, F., and Gigli, G. (2019). Towards the Development of Human Immune-System-On-A-Chip Platforms. *Drug Discov. Today* 24, 517–525. doi:10.1016/j.drudis.2018.10.003

Prahl, L. S., Bangasser, P. F., Stopfer, L. E., Hemmat, M., White, F. M., Rosenfeld, S. S., et al. (2018). Microtubule-Based Control of Motor-Clutch System Mechanics in Glioma Cell Migration. *Cel Rep.* 25, 2591–2604. e8. doi:10.1016/j.celrep.2018.10.101

Pulido, C., and Ryan, T. A. (2021). Synaptic Vesicle Pools Are a Major Hidden Resting Metabolic burden of Nerve Terminals. *Sci. Adv.* 7, eabi9027. doi:10.1126/sciadv.abi9027

Puntambekar, S. S., Saber, M., Lamb, B. T., and Kokiko-Cochran, O. N. (2018). Cellular Players that Shape Evolving Pathology and Neurodegeneration Following Traumatic Brain Injury. *Brain Behav. Immun.* 71, 9–17. doi:10.1016/j.bbi.2018.03.033

Qian, X., Nguyen, H. N., Song, M. M., Hadiono, C., Ogden, S. C., Hammack, C., et al. (2016). Brain-Region-Specific Organoids Using Mini-Bioreactors for Modeling ZIKV Exposure. *Cell* 165, 1238–1254. doi:10.1016/j.cell.2016.04.032

Qiu, S., Zhao, L. F., Korwek, K. M., and Weeber, E. J. (2006). Differential Reelin-Induced Enhancement of NMDA and AMPA Receptor Activity in the Adult Hippocampus. *J. Neurosci.* 26, 12943–12955. doi:10.1523/JNEUROSCI.2561-06.2006

Raichle, M. E., and Gusnard, D. A. (2002). Appraising the Brain's Energy Budget. *Proc. Natl. Acad. Sci. U.S.A.* 99, 10237–10239. doi:10.1073/pnas.172399499

Ranade, S. S., Syeda, R., and Patapoutian, A. (2015). Mechanically Activated Ion Channels. *Neuron* 87, 1162–1179. doi:10.1016/j.neuron.2015.08.032

Ratner, N., Brodeur, G. M., Dale, R. C., and Schor, N. F. (2016). The "neuro" of Neuroblastoma: Neuroblastoma as a Neurodevelopmental Disorder. *Ann. Neurol.* 80, 13–23. doi:10.1002/ana.24659

Reed, M. J., Damodarasamy, M., Pathan, J. L., Erickson, M. A., Banks, W. A., and Vernon, R. B. (2018). The Effects of Normal Aging on Regional Accumulation of Hyaluronan and Chondroitin Sulfate Proteoglycans in the Mouse Brain. *J. Histochem. Cytochem.* 66, 697–707. doi:10.1369/0022155418774779

Reles, A., and Friede, R. L. (1991). Axonal Cytoskeleton at the Nodes of Ranvier. *J. Neurocytol.* 20, 450–458. doi:10.1007/BF01252273

Rheinlaender, J., Dimitracopoulos, A., Wallmeyer, B., Kronenberg, N. M., Chalut, K. J., Gather, M. C., et al. (2020). Cortical Cell Stiffness Is Independent of Substrate Mechanics. *Nat. Mater.* 19, 1019–1025. doi:10.1038/s41563-020-0684-x

Riaz, M., Versaevel, M., Mohammed, D., Glinel, K., and Gabriele, S. (2016). Persistence of Fan-Shaped Keratocytes Is a Matrix-rigidity-dependent Mechanism that Requires α5β1 Integrin Engagement. *Sci. Rep.* 6, 34141. doi:10.1038/srep34141

Richman, D. P., Stewart, R. M., Hutchinson, J., and Caviness, V. S. (1975). Mechanical Model of Brain Convolutional Development. *Science* 189, 18–21. doi:10.1126/science.1135626

Ridone, P., Vassalli, M., and Martinac, B. (2019). Piezo1 Mechanosensitive Channels: what Are They and Why Are They Important. *Biophys. Rev.* 11, 795–805. doi:10.1007/s12551-019-00584-5

Rocio Servin-Vences, M., Moroni, M., Lewin, G. R., and Poole, K. (2017). Direct Measurement of TRPV4 and PIEZO1 Activity Reveals Multiple Mechanotransduction Pathways in Chondrocytes. *eLife* 6, e21074. doi:10.7554/eLife.21074

Rogers, J. T., Rusiana, I., Trotter, J., Zhao, L., Donaldson, E., Pak, D. T. S., et al. (2011). Reelin Supplementation Enhances Cognitive Ability, Synaptic Plasticity, and Dendritic Spine Density. *Learn. Mem.* 18, 558–564. doi:10.1101/lm.2153511

Rosso, G., Liashkovich, I., and Shahin, V. (2019). *In Situ* Investigation of Interrelationships between Morphology and Biomechanics of Endothelial and Glial Cells and Their Nuclei. *Adv. Sci.* 6, 1801638. doi:10.1002/advs.201801638

Rubinsztein, D. C. (2006). The Roles of Intracellular Protein-Degradation Pathways in Neurodegeneration. *Nature* 443, 780–786. doi:10.1038/nature05291

Rutkowski, D. M., and Vavylonis, D. (2021). Discrete Mechanical Model of Lamellipodial Actin Network Implements Molecular Clutch Mechanism and Generates Arcs and Microspikes. *PLOS Comput. Biol.* 17, e1009506. doi:10.1371/journal.pcbi.1009506

Sack, I., Streitberger, K.-J., Krefting, D., Paul, F., and Braun, J. (2011). The Influence of Physiological Aging and Atrophy on Brain Viscoelastic Properties in Humans. *PLoS ONE* 6, e23451. doi:10.1371/journal.pone.0023451

Sakaguchi, H., Kadoshima, T., Soen, M., Narii, N., Ishida, Y., Ohgushi, M., et al. (2015). Generation of Functional Hippocampal Neurons from Self-Organizing Human Embryonic Stem Cell-Derived Dorsomedial Telencephalic Tissue. *Nat. Commun.* 6, 8896. doi:10.1038/ncomms9896

Sakai, J. (2020). How Synaptic Pruning Shapes Neural Wiring during Development and, Possibly, in Disease. *Proc. Natl. Acad. Sci. U.S.A.* 117, 16096–16099. doi:10.1073/pnas.2010281117

Sandsmark, D. K., and Diaz-Arrastia, R. (2021). Advances in Traumatic Brain Injury Research in 2020. *Lancet Neurol.* 20, 5–7. doi:10.1016/S1474-4422(20)30455-5

Santana, J., and Marzolo, M.-P. (2017). The Functions of Reelin in Membrane Trafficking and Cytoskeletal Dynamics: Implications for Neuronal Migration, Polarization and Differentiation. *Biochem. J.* 474, 3137–3165. doi:10.1042/BCJ20160628

Santos, T. E., Schaffran, B., Broguière, N., Meyn, L., Zenobi-Wong, M., and Bradke, F. (2020). Axon Growth of CNS Neurons in Three Dimensions Is Amoeboid and Independent of Adhesions. *Cel Rep.* 32, 107907. doi:10.1016/j.celrep.2020.107907

Sato, T., Vries, R. G., Snippert, H. J., van de Wetering, M., Barker, N., Stange, D. E., et al. (2009). Single Lgr5 Stem Cells Build Crypt-Villus Structures *In Vitro* without a Mesenchymal Niche. *Nature* 459, 262–265. doi:10.1038/nature07935

Saunders, N. R., Habgood, M. D., Møllgård, K., and Dziegielewska, K. M. (2016). The Biological Significance of Brain Barrier Mechanisms: Help or Hindrance in Drug Delivery to the central Nervous System? *F1000Res* 5, 313. doi:10.12688/f1000research.7378.1

Schulte, C., Ripamonti, M., Maffioli, E., Cappelluti, M. A., Nonnis, S., Puricelli, L., et al. (2016). Scale Invariant Disordered Nanotopography Promotes Hippocampal Neuron Development and Maturation with Involvement of Mechanotransductive Pathways. *Front. Cel. Neurosci.* 10. doi:10.3389/fncel.2016.00267

Serbest, G., Horwitz, J., and Barbee, K. (2005). The Effect of Poloxamer-188 on Neuronal Cell Recovery from Mechanical Injury. *J. Neurotrauma* 22, 119–132. doi:10.1089/neu.2005.22.119

Serbest, G., Horwitz, J., Jost, M., and Barbee, K. A. (2006). Mechanisms of Cell Death and Neuroprotection by Poloxamer 188 after Mechanical Trauma. *FASEB j.* 20, 308–310. doi:10.1096/fj.05-4024fje

Shah, S., Yin, P. T., Uehara, T. M., Chueng, S.-T. D., Yang, L., and Lee, K.-B. (2014). Guiding Stem Cell Differentiation into Oligodendrocytes Using Graphene-Nanofiber Hybrid Scaffolds. *Adv. Mater.* 26, 3673–3680. doi:10.1002/adma.201400523

Shattil, S. J., Kim, C., and Ginsberg, M. H. (2010). The Final Steps of Integrin Activation: the End Game. *Nat. Rev. Mol. Cel Biol.* 11, 288–300. doi:10.1038/nrm2871

Shokri-Kojori, E., Tomasi, D., Alipanahi, B., Wiers, C. E., Wang, G.-J., and Volkow, N. D. (2019). Correspondence between Cerebral Glucose Metabolism and BOLD Reveals Relative Power and Cost in Human Brain. *Nat. Commun.* 10, 690. doi:10.1038/s41467-019-08546-x

Short, C. A., Suarez-Zayas, E. A., and Gomez, T. M. (2016). Cell Adhesion and Invasion Mechanisms that Guide Developing Axons. *Curr. Opin. Neurobiol.* 39, 77–85. doi:10.1016/j.conb.2016.04.012

Shou, Y., Liang, F., Xu, S., and Li, X. (2020). The Application of Brain Organoids: From Neuronal Development to Neurological Diseases. *Front. Cel Dev. Biol.* 8, 579659. doi:10.3389/fcell.2020.579659

Simitzi, C., Efstathopoulos, P., Kourgiantaki, A., Ranella, A., Charalampopoulos, I., Fotakis, C., et al. (2015). Laser Fabricated Discontinuous Anisotropic Microconical Substrates as a New Model Scaffold to Control the Directionality of Neuronal Network Outgrowth. *Biomaterials* 67, 115–128. doi:10.1016/j.biomaterials.2015.07.008

Simon, D. W., McGeachy, M. J., Bayır, H., Clark, R. S. B., Loane, D. J., and Kochanek, P. M. (2017). The Far-Reaching Scope of Neuroinflammation after Traumatic Brain Injury. *Nat. Rev. Neurol.* 13, 171–191. doi:10.1038/nrneurol.2017.13

Smith, A. S. T., Choi, E., Gray, K., Macadangdang, J., Ahn, E. H., Clark, E. C., et al. (2020). NanoMEA: A Tool for High-Throughput, Electrophysiological Phenotyping of Patterned Excitable Cells. *Nano Lett.* 20, 1561–1570. doi:10.1021/acs.nanolett.9b04152

Song, Y., Li, D., Farrelly, O., Miles, L., Li, F., Kim, S. E., et al. (2019). The Mechanosensitive Ion Channel Piezo Inhibits Axon Regeneration. *Neuron* 102, 373–389. doi:10.1016/j.neuron.2019.01.050

Soria, F. N., Paviolo, C., Doudnikoff, E., Arotcarena, M.-L., Lee, A., Danné, N., et al. (2020). Synucleinopathy Alters Nanoscale Organization and Diffusion in the Brain Extracellular Space through Hyaluronan Remodeling. *Nat. Commun.* 11, 3440. doi:10.1038/s41467-020-17328-9

Spedden, E., White, J. D., Kaplan, D., and Staii, C. (2012a). Young's Modulus of Cortical and P19 Derived Neurons Measured by Atomic Force Microscopy. *MRS Proc.* 1420, mrsf11–1420-oo04-04. doi:10.1557/opl.2012.485

Spedden, E., White, J. D., Naumova, E. N., Kaplan, D. L., and Staii, C. (2012b). Elasticity Maps of Living Neurons Measured by Combined Fluorescence and Atomic Force Microscopy. *Biophysical J.* 103, 868–877. doi:10.1016/j.bpj.2012.08.005

Star, E. N., Kwiatkowski, D. J., and Murthy, V. N. (2002). Rapid Turnover of Actin in Dendritic Spines and its Regulation by Activity. *Nat. Neurosci.* 5, 239–246. doi:10.1038/nn811

Stroka, K. M., Jiang, H., Chen, S.-H., Tong, Z., Wirtz, D., Sun, S. X., et al. (2014). Water Permeation Drives Tumor Cell Migration in Confined Microenvironments. *Cell* 157, 611–623. doi:10.1016/j.cell.2014.02.052

Strzyz, P. (2021). Shaping the Human Brain. *Nat. Rev. Mol. Cel Biol.* 22, 304–305. doi:10.1038/s41580-021-00364-8

Sun, Y., Nan, D., Jin, H., and Qu, X. (2020). Recent Advances of Injectable Hydrogels for Drug Delivery and Tissue Engineering Applications. *Polym. Test.* 81, 106283. doi:10.1016/j.polymertesting.2019.106283

Swift, J., Ivanovska, I. L., Buxboim, A., Harada, T., Dingal, P. C. D. P., Pinter, J., et al. (2013). Nuclear Lamin-A Scales with Tissue Stiffness and Enhances Matrix-Directed Differentiation. *Science* 341, 1240104. doi:10.1126/science.1240104

Takamori, Y., Hirahara, Y., Wakabayashi, T., Mori, T., Koike, T., Kataoka, Y., et al. (2018). Differential Expression of Nuclear Lamin Subtypes in the Neural Cells of the Adult Rat Cerebral Cortex. *IBRO Rep.* 5, 99–109. doi:10.1016/j.ibror.2018.11.001

Takasato, M., Er, P. X., Chiu, H. S., Maier, B., Baillie, G. J., Ferguson, C., et al. (2015). Kidney Organoids from Human iPS Cells Contain Multiple Lineages and Model Human Nephrogenesis. *Nature* 526, 564–568. doi:10.1038/nature15695

Takeichi, M. (2007). The Cadherin Superfamily in Neuronal Connections and Interactions. *Nat. Rev. Neurosci.* 8, 11–20. doi:10.1038/nrn2043

Tallinen, T., Chung, J. Y., Rousseau, F., Girard, N., Lefèvre, J., and Mahadevan, L. (2016). On the Growth and Form of Cortical Convolutions. *Nat. Phys* 12, 588–593. doi:10.1038/nphys3632

Tang-Schomer, M. D., Johnson, V. E., Baas, P. W., Stewart, W., and Smith, D. H. (2012). Partial Interruption of Axonal Transport Due to Microtubule Breakage Accounts for the Formation of Periodic Varicosities after Traumatic Axonal Injury. *Exp. Neurol.* 233, 364–372. doi:10.1016/j.expneurol.2011.10.030

Teixeira, A. I., Ilkhanizadeh, S., Wigenius, J. A., Duckworth, J. K., Inganäs, O., and Hermanson, O. (2009). The Promotion of Neuronal Maturation on Soft Substrates. *Biomaterials* 30, 4567–4572. doi:10.1016/j.biomaterials.2009.05.013

Theodosiou, M., Widmaier, M., Böttcher, R. T., Rognoni, E., Veelders, M., Bharadwaj, M., et al. (2016). Kindlin-2 Cooperates with Talin to Activate Integrins and Induces Cell Spreading by Directly Binding Paxillin. *eLife* 5, e10130. doi:10.7554/eLife.10130

Tissir, F., and Goffinet, A. M. (2003). Reelin and Brain Development. *Nat. Rev. Neurosci.* 4, 496–505. doi:10.1038/nrn1113

Toriyama, M., Shimada, T., Kim, K. B., Mitsuba, M., Nomura, E., Katsuta, K., et al. (2006). Shootin1: a Protein Involved in the Organization of an Asymmetric Signal for Neuronal Polarization. *J. Cel Biol.* 175, 147–157. doi:10.1083/jcb.200604160

Turco, M. Y., Gardner, L., Hughes, J., Cindrova-Davies, T., Gomez, M. J., Farrell, L., et al. (2017). Long-term, Hormone-Responsive Organoid Cultures of Human Endometrium in a Chemically Defined Medium. *Nat. Cel Biol.* 19, 568–577. doi:10.1038/ncb3516

Tyler, W. J. (2012). The Mechanobiology of Brain Function. *Nat. Rev. Neurosci.* 13, 867–878. doi:10.1038/nrn3383

Van de Water, L., and Olmsted, J. B. (1980). The Quantitation of Tubulin in Neuroblastoma Cells by Radioimmunoassay. *J. Biol. Chem.* 255, 10744–10751. doi:10.1016/s0021-9258(19)70370-6

van Wageningen, T. A., Antonovaite, N., Paardekam, E., Brevé, J. J. P., Iannuzzi, D., and van Dam, A.-M. (2021). Viscoelastic Properties of white and gray Matter-Derived Microglia Differentiate upon Treatment with Lipopolysaccharide but Not upon Treatment with Myelin. *J. Neuroinflammation* 18, 83. doi:10.1186/s12974-021-02134-x

Vassilopoulos, S., Gibaud, S., Jimenez, A., Caillol, G., and Leterrier, C. (2019). Ultrastructure of the Axonal Periodic Scaffold Reveals a Braid-like Organization of Actin Rings. *Nat. Commun.* 10, 5803. doi:10.1038/s41467-019-13835-6

Velasco-Estevez, M., Rolle, S. O., Mampay, M., Dev, K. K., and Sheridan, G. K. (2020). Piezo1 Regulates Calcium Oscillations and Cytokine Release from Astrocytes. *Glia* 68, 145–160. doi:10.1002/glia.23709

von Bartheld, C. S., Bahney, J., and Herculano-Houzel, S. (2016). The Search for True Numbers of Neurons and Glial Cells in the Human Brain: A Review of 150 Years of Cell Counting. *J. Comp. Neurol.* 524, 3865–3895. doi:10.1002/cne.24040

Wang, J., La, J.-H., and Hamill, O. P. (2019). PIEZO1 Is Selectively Expressed in Small Diameter Mouse DRG Neurons Distinct from Neurons Strongly Expressing TRPV1. *Front. Mol. Neurosci.* 12, 178. doi:10.3389/fnmol.2019.00178

Wang, L. M., and Kuhl, E. (2020). Viscoelasticity of the Axon Limits Stretch-Mediated Growth. *Comput. Mech.* 65, 587–595. doi:10.1007/s00466-019-01784-2

Wang, Y., Gunasekara, D. B., Reed, M. I., DiSalvo, M., Bultman, S. J., Sims, C. E., et al. (2017). A Microengineered Collagen Scaffold for Generating a Polarized Crypt-Villus Architecture of Human Small Intestinal Epithelium. *Biomaterials* 128, 44–55. doi:10.1016/j.biomaterials.2017.03.005

Weber, J. T. (2012). Altered Calcium Signaling Following Traumatic Brain Injury. *Front. Pharmacol.* 3. doi:10.3389/fphar.2012.00060

Wen, Y.-Q., Gao, X., Wang, A., Yang, Y., Liu, S., Yu, Z., et al. (2018). Substrate Stiffness Affects Neural Network Activity in an Extracellular Matrix Proteins Dependent Manner. *Colloids Surf. B: Biointerfaces* 170, 729–735. doi:10.1016/j.colsurfb.2018.03.042

Wenk, G. L. (2003). Neuropathologic Changes in Alzheimer's Disease. *J. Clin. Psychiatry* 64 (Suppl. 9), 7–10.

Williams, R. W., and Herrup, K. (1988). The Control of Neuron Number. *Annu. Rev. Neurosci.* 11, 423–453. doi:10.1146/annurev.ne.11.030188.002231

Wu, X., and Reddy, D. S. (2012). Integrins as Receptor Targets for Neurological Disorders. *Pharmacol. Ther.* 134, 68–81. doi:10.1016/j.pharmthera.2011.12.008

Xiong, Y., Lee, A. C., Suter, D. M., and Lee, G. U. (2009). Topography and Nanomechanics of Live Neuronal Growth Cones Analyzed by Atomic Force Microscopy. *Biophysical J.* 96, 5060–5072. doi:10.1016/j.bpj.2009.03.032

Xu, K., Zhong, G., and Zhuang, X. (2013). Actin, Spectrin, and Associated Proteins Form a Periodic Cytoskeletal Structure in Axons. *Science* 339, 452–456. doi:10.1126/science.1232251

Yates, D. (2020). Remodelling the Matrix. *Nat. Rev. Neurosci.* 21, 449. doi:10.1038/s41583-020-0356-5

Yoshino, Y., Ishisaka, M., Tsuruma, K., Shimazawa, M., Yoshida, H., Inoue, S., et al. (2017). Distribution and Function of Hyaluronan Binding Protein Involved in Hyaluronan Depolymerization (HYBID, KIAA1199) in the Mouse central Nervous System. *Neuroscience* 347, 1–10. doi:10.1016/j.neuroscience.2017.01.049

Yoshino, Y., Shimazawa, M., Nakamura, S., Inoue, S., Yoshida, H., Shimoda, M., et al. (2018). Targeted Deletion of HYBID (Hyaluronan Binding Protein Involved in Hyaluronan Depolymerization/KIAA1199/CEMIP) Decreases Dendritic Spine Density in the Dentate Gyrus through Hyaluronan Accumulation. *Biochem. Biophysical Res. Commun.* 503, 1934–1940. doi:10.1016/j.bbrc.2018.07.138

Zempel, H., Dennissen, F. J. A., Kumar, Y., Luedtke, J., Biernat, J., Mandelkow, E.-M., et al. (2017). Axodendritic Sorting and Pathological Missorting of Tau Are Isoform-specific and Determined by Axon Initial Segment Architecture. *J. Biol. Chem.* 292, 12192–12207. doi:10.1074/jbc.M117.784702

Zhang, K., Shi, Z., Zhou, J., Xing, Q., Ma, S., Li, Q., et al. (2018). Potential Application of an Injectable Hydrogel Scaffold Loaded with Mesenchymal Stem Cells for Treating Traumatic Brain Injury. *J. Mater. Chem. B* 6, 2982–2992. doi:10.1039/c7tb03213g

Zhang, Q.-Y., Zhang, Y.-Y., Xie, J., Li, C.-X., Chen, W.-Y., Liu, B.-L., et al. (2015). Stiff Substrates Enhance Cultured Neuronal Network Activity. *Sci. Rep.* 4, 6215. doi:10.1038/srep06215

Zhao, S., Stamm, A., Lee, J. S., Gruverman, A., Lim, J. Y., and Gu, L. (2015). Elasticity of Differentiated and Undifferentiated Human Neuroblastoma Cells Characterized by Atomic Force Microscopy. *J. Mech. Med. Biol.* 15, 1550069. doi:10.1142/S0219519415500694

Zhu, Y., Wang, L., Yu, H., Yin, F., Wang, Y., Liu, H., et al. (2017). *In Situ* generation of Human Brain Organoids on a Micropillar Array. *Lab. Chip* 17, 2941–2950. doi:10.1039/C7LC00682A

Conflict of Interest: The authors declare that the research was conducted in the absence of any commercial or financial relationships that could be construed as a potential conflict of interest.

Publisher's Note: All claims expressed in this article are solely those of the authors and do not necessarily represent those of their affiliated organizations, or those of the publisher, the editors and the reviewers. Any product that may be evaluated in this article, or claim that may be made by its manufacturer, is not guaranteed or endorsed by the publisher.

frontiers | Frontiers in Cell and Developmental Biology

MINI REVIEW
published: 25 April 2022
doi: 10.3389/fcell.2022.874840

Mechanobiology in the Comorbidities of Ehlers Danlos Syndrome

Shaina P. Royer[1] *and Sangyoon J. Han*[1,2,3]*

[1]Department of Biomedical Engineering, Michigan Technological University, Houghton, MI, United States, [2]Department of Mechanical Engineering, Michigan Technological University, Houghton, MI, United States, [3]Health Research Institute, Michigan Technological University, Houghton, MI, United States

Ehlers-Danlos Syndromes (EDSs) are a group of connective tissue disorders, characterized by skin stretchability, joint hypermobility and instability. Mechanically, various tissues from EDS patients exhibit lowered elastic modulus and lowered ultimate strength. This change in mechanics has been associated with EDS symptoms. However, recent evidence points toward a possibility that the comorbidities of EDS could be also associated with reduced tissue stiffness. In this review, we focus on mast cell activation syndrome and impaired wound healing, comorbidities associated with the classical type (cEDS) and the hypermobile type (hEDS), respectively, and discuss potential mechanobiological pathways involved in the comorbidities.

Keywords: mechanobiology, classical Ehlers-Danlos syndrome, hypermobile Ehlers-Danlos Syndrome, collagen V, extracellular matrix, stiffness, mast cell degranulation

OPEN ACCESS

Edited by:
Guillermo Alberto Gomez, University of South Australia, Australia

Reviewed by:
Tero Anssi Järvinen, Tampere University, Finland

***Correspondence:**
Sangyoon J. Han
sjhan@mtu.edu

Specialty section:
This article was submitted to Cell Adhesion and Migration, a section of the journal Frontiers in Cell and Developmental Biology

Received: *13 February 2022*
Accepted: *16 March 2022*
Published: *25 April 2022*

Citation:
Royer SP and Han SJ (2022) Mechanobiology in the Comorbidities of Ehlers Danlos Syndrome. Front. Cell Dev. Biol. 10:874840. doi: 10.3389/fcell.2022.874840

INTRODUCTION

Ehlers-Danlos Syndromes (EDSs) are a group of connective tissue disorders (Malfait et al., 2017). Currently, within the 2017 classification system, the disorders are grouped into 7 different subclasses with one more recently discovered type having yet to be named and fitted in the classification system (Malfait et al., 2017; Blackburn et al., 2018). The genes involved in every type except one have been identified (Malfait et al., 2017). Most of identified genes, if not all, are associated with components within collagen matrix, e.g., collagen I, III, V, or with assembly or crosslinking of the procollagen fibrils, e.g., procollagen N-proteinases, lysyl hydroxylase or tenascin XB, etc. Accordingly, all EDS subclasses exhibit some level of changes in collagen microarchitecture (Royce et al., 1990; Hausser and Anton-Lamprecht, 1994; Burch et al., 1997; Colige et al., 2004; Malfait et al., 2007; Fukada et al., 2008; Rohrbach et al., 2011; Hermanns-Lê et al., 2012; Kapferer-Seebacher et al., 2016; Blackburn et al., 2018; Van Damme et al., 2018; Ayoub et al., 2020; Delbaere et al., 2020; Kosho et al., 2020). Each EDS subclass is associated with stretchiness or rupture of skin and artery or hypermobility of joint (Bowen et al., 2017; Brady et al., 2017; Byers et al., 2017; Tinkle et al., 2017; Blackburn et al., 2018). Despite identified genetic defects, molecular explanation of how the genetic defects lead to clinical phenotypes that are assessed for EDS subclass determination has been unclear (Malek and Köster, 2021). Since defected genes are related to collagen formation, it has been assumed that microarchitectural changes due to those genetic defects can give rise to clinical abnormality exhibited in the EDS patients (Kobayasi, 2004). However, recent evidence shows that the structure alone is not a sole factor that determines clinical severity (Proske et al., 2006; Hermanns-Lê et al., 2012; Angwin et al., 2019). As an alternative, mechanobiological factors appear to be a key player that induces the EDS symptoms. For example, changes in adhesion and cytoskeletal organization, key mediators for mechanotransduction, are observed, along with defects in migration and contractility, in dermal fibroblasts from cEDS, hEDS and vEDS (Viglio et al., 2008; Zoppi et al., 2018). How EDS affects fibroblast dysfunction has been well discussed in a recent review article (Malek and Köster, 2021).

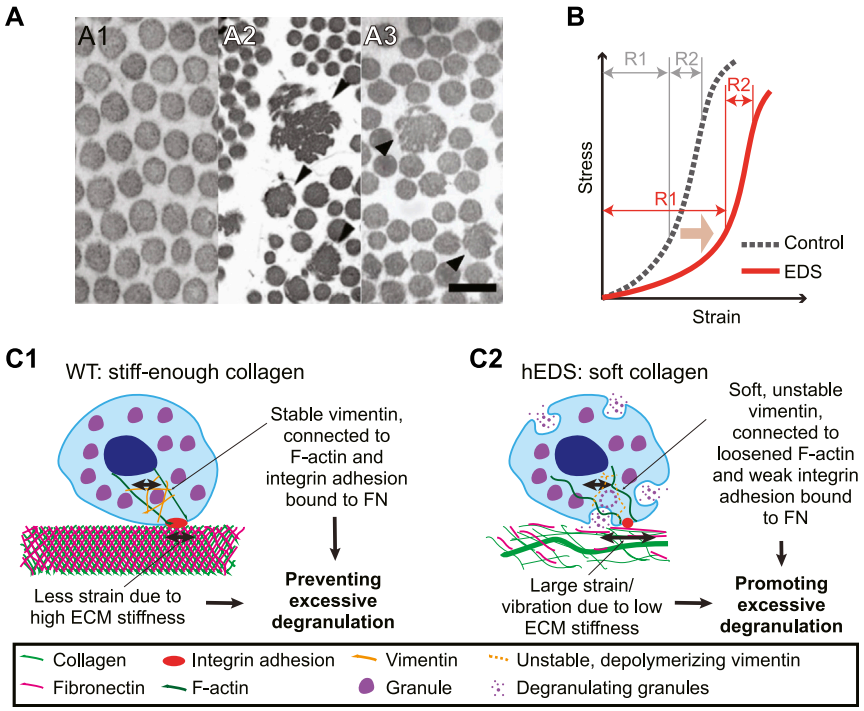

FIGURE 1 | Collagen in EDS is irregular in microarchitecture, softer in mechanical behavior, and might induce mast cell degranulation. **(A)** Transmission electron microscopy images of normal skin biopsy **(A1)**, adapted from (Malfait et al., 2013), cEDS skin biopsy **(A2)**, adapted from (Angwin et al., 219), and hEDS skin biopsy (A3), adapted from (Hermanns-Lê et al., 2012). Note that collagen fibrils are enlarged (black arrowheads) and have irregular shapes in **(A2)**, and that occasional irregular fibrils depicted by black arrowheads in **(A3)**. Scale bar: 200 nm for all panels. **(B)** A typical nonlinear stress-strain curve of a skin tissue of control (dotted line) and EDS (red line). Note that EDS shifts the curve to the softer regime (light brown arrow) and that the softening is distinctly present only in the small stress regime (R1). For high stress regime (R2), there is no significant difference between control vs. EDS skin. Illustrated graph recreated by adapting (Grahame and Beighton, 1969). **(C)** Potential mechanobiological mechanism for MCAS in hEDS. **(C1)** In extracellular environment from control cases, stiff-enough collagen, intertwined with fibronectin, provides small strain or small magnitude of vibration. A mast cell adjusts its own stiffness by adjusting expression level and organization of vimentin intermediate filaments (orange), which help secure granules inside the cell. Vimentin is connected to F-actin and integrin $\alpha_V\beta_3$, $\alpha_5\beta_1$, and $\alpha_{IIb}\beta_3$.*via* plectin. F-actin could also be in high tension due to the stiffness sensing via integrin adhesions. The stable vimentin and increased cell stiffness allows only small strain or vibration, which can help prevent excessive degranulation. **(C2)** In hEDS, irregular collagen organization results in overall low ECM stiffness, allowing large strain or vibration. The low ECM stiffness is sensed by integrin adhesions, which induces down-regulation of F-actin tension and cell stiffness by poor vimentin expression and polymerization. This results in poor vimentin organization around granules, unstable immobilization of granules, and ultimately promotion of excessive degranulation. Vimentin filaments were illustrated for only one part of a cell to contrast the encapsulation vs. loose organization between WT vs. hEDS, respectively.

However, how extracellular changes in EDS, particularly in the two most common types, hypermobile type (hEDS) and classical type (cEDS), can promote comorbidities of EDS have just begun to be revealed. In this review, we discuss how aberrant collagen mechanics can lead to mast cell activation syndrome and impaired wound healing, comorbidities found in hEDS and cEDS, respectively. The review begins with introducing findings about changes in tissue stiffness and extensibility in both EDS types. Then we summarize recent discoveries regarding potential linkages between mechanics and the two comorbidities and predict potential mechanobiological pathways involved in each comorbidity.

Ehlers-Danlos Syndrome Pathophysiology Associated With Altered Collagen Microstructure

Out of 14 types (Malfait et al., 2017), most patients have one of the two most common types, hEDS and cEDS (Malfait et al., 2010; Tinkle et al., 2017). hEDS is characterized by hypermobile joints and joint instability along with other minor signs of reduced strength of connective tissues such as mitral valve prolapse, piezogenic papules, and soft stretchy skin (Tinkle et al., 2017). cEDS has similar symptoms to hEDS although cEDS-induced joint involvement is generally less severe whereas skin involvement is more severe than ones by hEDS. Skin in patients with cEDS is fragile, soft, and stretchy. Wounds take longer to heal and result in atrophic scaring (Bowen et al., 2017).

One common component that is altered in both patients with hEDS and cEDS is collagen fibril structure. In both types, large, irregularly shaped collagen fibrils have been observed from the skin biopsy samples (**Figure 1A**). In addition, in patients with cEDS, overall collagen fibril diameter has been found to be larger than patients without EDS (Hausser and Anton-Lamprecht, 1994). In cEDS, the increase in diameter is caused by haploinsufficiency in collagen V. Unlike collagen I, which has a straight triple helix structure, the N-terminal end of the collagen

V is globular. This structural difference results in steric hindrance limiting the diameter of collagen fibrils (Mak et al., 2016). Collagen V haploinsufficiency thus increases collagen diameter by allowing parallel collagen fibril assembly. The cause for the abnormal morphology in collagen fibrils in hEDS tissue is unknown (Tinkle et al., 2017). This altered collagen architecture appears to trigger different adhesion and cytoskeletal response by fibroblasts within connective tissue (Zoppi et al., 2018). For example, in hEDS, cEDS, and vEDS, which have different sources for altered collagen architectures, fibroblasts display similar changes in gene expression for integrin heterodimer expressions (Chiarelli et al., 2019b). This finding suggests that regardless of underlying cause of abnormal ECM architecture, the altered ECM architecture itself can induce fibroblasts dysfunction. One important parameter controlled by the microarchitecture is the mechanical stiffness, which we will focus in this review.

Soft Tissue Mechanical Properties

Thick fibers in collagen gel have been putatively associated with high local stiffness. Collagen gels *in vitro* with thicker fibrils has been measured stiffer than collagen consisting of thin fibers, which has also been computationally modeled *via* fiber-based mechanics model (Seo et al., 2020). In cEDS tissue, however, this positive correlation has not been observed. Rather, the cEDS connective tissue, where collagen fibrils are larger than normal, has been reported softer than normal (Hausser and Anton-Lamprecht, 1994; Nielsen et al., 2014). A rheological measurement, done by measuring skin deformation curve over time in response to a sudden constant vacuum force followed by relaxation, has also shown that cEDS tissue is consistently softer than normal skin (Catala-Pétavy et al., 2009). This finding implies that the fiber diameter alone cannot predict the bulk mechanical property when it co-resides with other cells and ECM components as in the skin. The findings also suggests that reconstituted collagen gel might not represent the mechanical properties of collagen in the skin because it lacks the bundling of fibrils into fibers and the anisotropic orientation of collagen fibrils (Piérard and Lapière, 1987; Salvatore et al., 2021). Moreover, as seen in **Figure 1A2**, not all of collagen fibrils in skin appear to be larger in diameter in cEDS, but there are significant number of thinner fibers as well. Yet further systematic study is needed to elucidate the functional relationship between heterogeneous collagen organization and gel stiffness.

In hEDS, it is likely that the skin tissue is soft and hyperextensible, but not as much as in cEDS. When measured using a soft tissue stiffness meter, which measures the percentage change in distance between two dots drawn on the back of the hand when the skin is stretched (Farmer et al., 2010), a significant increase in extensibility has been observed in the hEDS group compared to control group (Remvig et al., 2009). However, depending on the test methods or the sample size, such significant extensibility has not been always guaranteed. When a suction cup method (Piérard et al., 2013) was used, for example, the increase in extensibility became statistically insignificant (Remvig et al., 2009). Using the same method, the reduction in the elasticity has been observed only in cEDS but not in hEDS (Catala-Pétavy et al., 2009). It is worth noting that small sample sizes were used in both studies, e.g., with 6 and 18 people, respectively, in the hEDS groups, which may not have provided sufficient statistical power. For hEDS, the connective tissue in other tissues than in the skin appears to be more distinctly and consistently softer than control group. When non-invasively measured using dynamometer during isometric plantar flexion, reduction in Achilles tendon stiffness has been observed from hEDS patients, along with larger maximal joint angle (Rombaut et al., 2012). Similarly, when the strain elastography, which estimates tissue elasticity by measuring perpendicular deformation in response to small strain induced by ultrasound, was used, the relative stiffness, represented by strain ratio and strain index, has been found to be lower in the brachioradialis muscle, patellar tendon, and Achilles tendons of patients with hypermobile disorder (Alsiri et al., 2019).

Importantly, as in typical animal soft tissue, the human skin tissue exhibits a nonlinear mechanical behavior (**Figure 1B**, dotted line) (Fung, 1993; Xu et al., 2008; Annaidh et al., 2012). Strain-stiffening behavior has been associated with continuous alignment of collagen with stretch (Bancelin et al., 2015). EDS, especially classical type, lowers and widens the stress-strain curve in low stress regime (**Figure 1B**, red line), likely due to altered microstructural change in collagen organization (Bancelin et al., 2015). Accordingly, depending on the strain regime where the skin-extending test is performed, the acquired tissue elasticity can be widely variable. When the second strain regime was used for the elastic modulus estimation, the estimated stiffness displayed no statistical difference between EDS specimen and control ones (Grahame and Beighton, 1969). In contrast, the EDS tissue's elastic modulus is significantly reduced when it is estimated from the first, i.e., small, strain regime (Grahame and Beighton, 1969).

Mast Cell Activation Syndrome and Mechanosensitivity of Mast Cells Within Hypermobile Type Ehlers-Danlos Syndromes

Mast cell activation disorder (MCAD) is a family of immunological disorders in which mast cells degranulate, i.e., release their granules containing histamine and other substances, unusually easily (Hamilton, 2018). Mast cells are derived from multipotential hematopoietic stem cells (MHSCs) which then differentiate into mast cell progenitors (MCPs). These MCPs then leave the circulatory system and migrate into connective and mucosal tissue where they proliferate and differentiate into mast cells (Kitamura et al., 2007). Mast cells are filled with granules filled histamine, heparin, and various cytokines among other pro inflammatory molecules. When triggered, mast cells degranulate, i.e., release the contents of their granules into the surrounding tissues (Krystel-Whittemore et al., 2016). Accordingly, too early and/or too much degranulation, which is the case of MCAD, can cause allergic reactions. Typical symptoms of these reactions are pain, fatigue, itching, flushing, dizziness, abdominal cramps, and diarrhea (Jennings et al., 2018).

Mast cell activation syndrome (MCAS) is a subtype of MCAD characterized by mast cell activation due to abnormal sensitivity of mast cells without being associated with mast cell proliferation. Around 25% percent of patients with hEDS have MCAS (Mcgillis et al., 2020). However, the MCAS-hEDS association has not been robustly supported with clinical evidence partly due to changing criteria of hEDS classification (Kohn and Chang, 2020). MCAS causes allergic symptoms when a patient is exposed to 'a trigger' (Hamilton, 2018). The antigen within the trigger promotes immunoglobulin E production. Binding of antigen to IgE triggers degranulation process (Krystel-Whittemore et al., 2016). The trigger includes matters that cause classical allergic responses such as food. However, it also includes heat and mechanical stimuli.

One mechanical stimulus is the physical vibration (Jennings et al., 2018). hEDS, by being easily deformable, likely increases probability to allow higher magnitude of vibration that triggers degranulation. A mediator for this vibration-induced degranulation is a transmembrane protein adhesion G protein-coupled receptor E2 (ADGRE2). ADGRE2 consists of an extracellular α subunit and a transmembrane β subunit. The protein is initially expressed as one unit but undergoes posttranslational modification by cleaving itself into an α subunit and a β subunit, held together by non-covalent bonds. While the α subunit is attached to the β subunit, it remains in its inactive state. Vibration can activate ADGRE2 by breaking its α subunit away from β subunit, which triggers degranulation (Olivera et al., 2018). Whether ADGRE2 is overexpressed in hEDS, or whether the magnitude of the vibration is a determinant of ADGRE2's conformational change is yet to be determined. An *ex vivo* study supports the idea in the latter by showing that the magnitude of mechanical strain is a determinant of degranulation. When fibrotic rat lungs were ventilated at either low, control pressure of 5 cmH_2O or high pressure of 30 cmH_2O, more mast cell degranulation was observed in the high pressure-based ventilation group than in a lower pressure condition. This demonstrates that strain-induced degranulation is also strain magnitude-dependent (Shimbori et al., 2019).

Another component that may endow degranulation process with mechano-sensitivity is an intermediate filament vimentin. Intermediate filaments play a role in determining cell stiffness by resisting compression (Brown et al., 2001; Ingber, 2003). In mast cells, vimentin encapsulates the granules and immobilize them within the cytoplasm (Dráber et al., 2012). Upon degranulation, vimentin filaments rapidly depolymerize, which facilitates exocytosis of the granule's contents (Dráber et al., 2012). Mast cells in a vimentin-deficient mouse model have shown easier degranulation than the control (Dráber et al., 2012). Cells adapt their own stiffness to the stiffness of their underlying substrate via remodeling of the cytoskeleton (Yeung et al., 2005; Solon et al., 2007). Although not explicitly reported, it is possible that mast cell stiffness could be lowered due to reduced elasticity of the collagen and the ECM, which could elicit remodeling of the vimentin filaments. Vimentin expression is correlated with substrate stiffness (Murray et al., 2014). This makes vimentin a protein of particular interest in the investigation of the pathophysiology behind in the link between hEDS and MCAS.

To be mechanosensitive, cells need to anchor themselves to the ECM. Mast cells anchor themselves to fibronectin in the ECM using integrins $\alpha_V\beta_3$, $\alpha_5\beta_1$, and $\alpha_{IIb}\beta_3$ that bind to the RGD motif (Fowlkes et al., 2013). When treated with echistatin, an inhibitor for $\alpha_V\beta_3$, $\alpha_5\beta_1$, and $\alpha_{IIb}\beta_3$ by competing with RGD sequence for integrin binding, mast cells have shown reduction in degranulation in a dose-dependent manner: cells treated with the highest dose of echistatin has shown the least degranulation, comparable to the static control (Fowlkes et al., 2013). This evidence suggests that the RGD-binding family of integrins are mediators for strain-induced degranulation in mast cells. As these RGD-binding integrins do not bind collagen (Humphries et al., 2006), it is possible that the "softness" of the collagen is sensed by mast cells through cells' binding to fibronectin and fibronectin-collagen binding. It is worth being reminded of the mechanics that the resultant stiffness of the two materials connected in series is lower than that of the softer material.

These pieces of evidence point toward a potential mechanobiological interpretation about how mast cells in hEDS tissue might be easier to degranulate. As illustrated in **Figure 1C**, wild-type (WT) ECM is relatively stiff enough owing to well-organized collagen network. WT mast cells bind the ECM *via* fibronectin-binding integrins. Potential strain or vibration, in response to the cell-generated force or external forces, is relatively small due to high ECM stiffness. Mast cells adapt to the high ECM stiffness by upregulating F-actin tension and vimentin expression and stiffness. The stable and stiff-enough vimentin protect mast cells from excessive degranulation (**Figure 1C1**). In hEDS, however, a large strain or vibration magnitude is possible due to irregular collagen network and resulting softness in the ECM. Low stiffness might disable the contractility in F-actin and expression and organization of vimentin, which ultimately facilitate the cytoplasm mechanically unstable. The larger strain and unstable vimentin potentially help promote excessive degranulation (**Figure 1C2**). Another possibility is that the integrin adhesions can be a direct input for IgE's activation because a study with rat basophilic leukemia mast cells has shown the adhesion protein (e.g., talin, vinculin and paxillin)-IgE colocalization and connection to F-actin (Torres et al., 2008). Softened ECM can thus induce a more direct effect on IgE via weak integrin adhesions forming in hEDS.

Wound Healing in Classical Type Ehlers-Danlos Syndromes

One of the more challenging dermatological issues caused by EDS to treat is impaired wound management. Because of the fragility, the skin of cEDS patients splits open easily (Malfait et al., 2010). Surgical repair of these wounds is complicated by the fragility of skin in cEDS, e.g., stitches ripping through the skin. Once occurred, wounds in cEDS tend to take significantly longer to heal than wounds in control patients (Bowen et al., 2017). Furthermore, even after closure, widening of the scars tends to occur if tension is placed on them. Scars in cEDS are frequently widened and atrophic (Bowen et al., 2017).

Collagen V mutations present in cEDS have been recently associated with downregulation (e.g., SPP1, EDIL3, and PAPPA)

or upregulation (e.g., IGFBP2 and C3) of genes in fibroblasts, which encode soluble and matricellular proteins involved in wound healing *in vivo* (Chiarelli et al., 2019a). Reduced migration and impaired wound healing have been observed from *in vitro* fibroblasts as well (Viglio et al., 2008). Chiarelli and colleagues have found that the changes in gene expressions can be replicated by mutated collagen V expression (Chiarelli et al., 2019a). Pathways from collagen V mutation to gene expression for wound healing, however, have remained to be investigated.

A factor that might play a critical role in the impaired wound healing in cEDS is the ECM stiffness that is significantly lowered in the case of cEDS due to lack of collagen V. The change in stiffness can affect the wound healing in many ways. First, fibroblasts' differentiation to myofibroblasts, which plays an important role in wound healing, is regulated by the ECM stiffness (Huang et al., 2012). During wound healing, fibroblasts migrate from the edges of the wound and differentiate into myofibroblasts. Myofibroblasts contract the edges of the wounds, lay down the ECM and compact the ECM by exerting high contractile force (Darby et al., 2014). Similar to mesenchymal stem cell differentiation into bone lineage (Engler et al., 2006), fibroblasts are differentiated into myofibroblasts at a higher degree in stiff ECM than in soft substrates (Walraven and Hinz, 2018; Seo et al., 2020). Thus, we speculate that the reduced ECM stiffness in cEDS impairs myofibroblast differentiation, which again diminishes the overall wound healing process. This possibility needs further controlled experiments to evaluate.

Second, wound healing requires fibroblasts to actively migrate into the wound site. Although fibroblasts migration is directed by chemical cues such as cytokines and growth factors, it is also well established that it is strongly regulated by mechanical properties, e.g., stiffness, of the ECM. Most cell types including fibroblasts display durotaxis, that is the tendency to migrate in the direction of a stiffer surface (Lo et al., 2000; Sunyer et al., 2016). There are currently two main models for explaining durotaxis: the random walk model and the molecular clutch model. In the random walk model, the cell creates protrusions in all directions. Since the adhesions that form to stiffer substrates are more persistent than those formed on softer substrates, the net movement of the cell is in the direction of the stiffer substrate (Novikova et al., 2017). In the molecular clutch model, on stiff substrates, there is frictional slippage between flowing actin and adhesion protein (e.g., talin) whereas the interaction between actin and adhesion periodically builds up load on softer substrates until the strain reaches their failure point at which point it fails catastrophically allowing the substrate to snap back to its original position. The load-and-fail dynamics promote faster retrograde flow of actin than the frictional slippage, resulting in retraction of the cell on softer substrates and protrusion on stiffer thereby causing the cell to move in the direction of the stiffer substrate (Chan and Odde, 2008). Therefore, the lowered ECM stiffness observed in cEDS might impair wound healing by slowing down fibroblast migration.

Phenotypically, collagen V allows for cell adhesion to fibroblasts (Yamamoto et al., 1992; Kihara et al., 2004), and promotes fibroblast contractility (Berendsen et al., 2006), implying that absence of collagen V synthesis in cEDS downregulates fibroblast adhesion and contractility. Fibroblasts from a cEDS-exhibiting mouse, thus unable to synthesize collagen V, have shown reduction in migration and proliferation as well (Denigris et al., 2016). Similarly, cells derived from skin biopsies from patients with cEDS display significant reduction in expression of $\alpha_2\beta_1$ and $\alpha_5\beta_1$ integrins, major receptors for collagen types I-VI and fibronectin, respectively, via less-organized collagen network (Zoppi et al., 2004). Despite this reduction, cells can survive by increased expression of $\alpha_V\beta_3$ integrins and avoiding anoikis, a type of apoptosis that is the result of an adherent cell becoming detached from its substrate (Zoppi et al., 2004). This has been associated with pathways independent of focal adhesion kinase (FAK). Typically, in adherent cells, FAK signaling prevent anoikis by inhibiting p53 activity which is responsible for cell cycle arrest and apoptosis (Lim et al., 2008). FAK is recruited to integrin adhesions after integrins' binding to the ECM, is activated by integrin and undergoes autophosphorylation (Frisch et al., 1996; Zhan et al., 2004), and initiates a signaling cascade preventing anoikis (Hungerford et al., 1996; Gilmore, 2005; Zouq et al., 2009). However, FAK is not associated with the most common integrin $\alpha_V\beta_3$ (Zoppi et al., 2008; Kuonen et al., 2018) but with $\alpha_5\beta_1$ integrin that is expressed in wild-type fibroblasts (Zoppi et al., 2004). Instead, $\alpha_V\beta_3$ acts together with endothelial growth

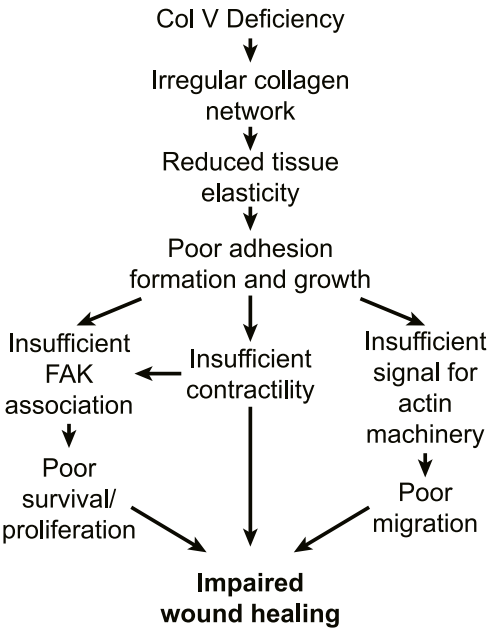

FIGURE 2 | Potential pathways for impaired wound healing in cEDS tissue. In cEDS, collagen V deficiency results in irregular collagen microarchitecture, which features reduced tissue mechanics. Fibroblasts respond to the low ECM stiffness by exhibiting poor integrin adhesion formation and growth, which is unable to accommodate FAK binding. Signals from weak adhesion downregulate myosin contractility and actin polymerization, which again downregulates survival, proliferation and migration, which all impacts impaired wound healing.

factor receptor (EGFR) to trigger a separate pathway that involves the phosphorylation of paxillin, paxillin's pp60src binding, which ultimately helps prevent anoikis (Zoppi et al., 2008).

The impaired cell adhesion and proliferation in cEDS as well as downregulated expressions of actin and focal adhesions can be output from mechanosensing of the ECM architecture abnormally organized by mutated/lacked collagen V. One key evidence supports this idea by exogenously expressing collagen V and showing the cEDS cells' phenotypic change. For example, cEDS cells are restored to the wildtype phenotype with normal integrin expression and fibronectin secretion by providing an exogenous source of collagen V (Zoppi et al., 2004). Also, the cEDS-like phenotype, e.g., with the altered integrin expression, and impaired fibronectin expression, is induced in wildtype fibroblasts when their collagen V expression is blocked by collagen V-blocking antibody (Zoppi et al., 2004). Altogether, the impaired wound healing in cEDS tissue can be still attributed to softened, irregular ECM structure by lack of collagen V's contribution, which induces poor cell-ECM adhesion formation and growth, which again transduce insufficient mechanotransduction signals that supports cell migration, survival, and proliferation (**Figure 2**). Detailed studies on how collagen V changes microarchitecture of the collagen network and overall ECM would shed light on further insight to the cEDS's main comorbidity.

CONCLUSION

We have reviewed the two most popular types of Ehlers-Danlos syndrome, hEDS and cEDS in a perspective of mechanobiology. We attempted to link the common mechanical feature in both hEDS and cEDS, e.g., connective tissue being softer to comorbidities associated with hEDS and cEDS: MCAS and impaired wound healing, respectively. For MCAS, we identify ADGRE2, vimentin, and the RGD binding family of integrins $\alpha_V\beta_3$, $\alpha_5\beta_1$, and $\alpha_{IIb}\beta_3$ as mechanosensitive proteins that are altered in hEDS. For impaired wound healing, the reduced ECM stiffness, due to lack of collagen V, may be the main contributor to impaired myofibroblast differentiation, altered integrin expression and fibronectin secretion in cEDS. Beyond the current focus in the EDS field on uncovering the cause of hEDS and better defining what MCAS is, our review suggests that mechanobiological research using hEDS mast cells or cEDS fibroblasts would advance mechanistic understanding of phenotypic changes in the two comorbidities.

AUTHOR CONTRIBUTIONS

SR and SH contributed to the conception and design of the study, wrote all sections of the manuscript. All authors contributed to manuscript revision, read, and approved the submitted version

FUNDING

This work was funded by NIH 1R15GM135806-01 and Michigan Tech's Research Excellence Fund (REF) award. and Portage Health Foundation's Undergraduate Research Internship Program (URIP).

REFERENCES

Alsiri, N., Al-Obaidi, S., Asbeutah, A., Almandeel, M., and Palmer, S. (2019). The Impact of Hypermobility Spectrum Disorders on Musculoskeletal Tissue Stiffness: an Exploration Using Strain Elastography. *Clin. Rheumatol.* 38, 85–95. doi:10.1007/s10067-018-4193-0

Angwin, C., Brady, A. F., Colombi, M., Ferguson, D. J. P., Pollitt, R., Pope, F. M., et al. (2019). Absence of Collagen Flowers on Electron Microscopy and Identification of (Likely) Pathogenic COL5A1 Variants in Two Patients. *Genes* 10, 762. doi:10.3390/genes10100762

Annaidh, A. N., Bruyère, K., Destrade, M., Gilchrist, M. D., and Otténio, M. (2012). Characterization of the Anisotropic Mechanical Properties of Excised Human Skin. *J. Mechanic. Behav. Biomed. Mater.* 5 (1), 139–148. doi:10.1016/j.jmbbm.2011.08.016

Ayoub, S., Ghali, N., Angwin, C., Baker, D., Baffini, S., Brady, A. F., et al. (2020). Clinical Features, Molecular Results, and Management of 12 Individuals with the Rare Arthrochalasia Ehlers-Danlos Syndrome. *Am. J. Med. Genet.* 182, 994–1007. doi:10.1002/ajmg.a.61523

Bancelin, S., Lynch, B., Bonod-Bidaud, C., Ducourthial, G., Psilodimitrakopoulos, S., Dokládal, P., et al. (2015). Ex Vivo Multiscale Quantitation of Skin Biomechanics in Wild-Type and Genetically-Modified Mice Using Multiphoton Microscopy. *Sci. Rep.* 5, 17635. doi:10.1038/srep17635

Berendsen, A. D., Bronckers, A. L. J. J., Smit, T. H., Walboomers, X. F., and Everts, V. (2006). Collagen Type V Enhances Matrix Contraction by Human Periodontal Ligament Fibroblasts Seeded in Three-Dimensional Collagen Gels. *Matrix Biol.* 25, 515–522. doi:10.1016/j.matbio.2006.07.006

Blackburn, P. R., Xu, Z., Tumelty, K. E., Zhao, R. W., Monis, W. J., Harris, K. G., et al. (2018). Bi-allelic Alterations in AEBP1 lead to Defective Collagen Assembly and Connective Tissue Structure Resulting in a Variant of Ehlers-Danlos Syndrome. *Am. J. Hum. Genet.* 102, 696–705. doi:10.1016/j.ajhg.2018.02.018

Bowen, J. M., Sobey, G. J., Burrows, N. P., Colombi, M., Lavallee, M. E., Malfait, F., et al. (2017). "Ehlers-Danlos Syndrome, Classical Type," in *American Journal of Medical Genetics Part C: Seminars in Medical Genetics* (Wiley Online Library), 27–39. doi:10.1002/ajmg.c.31548

Brady, A. F., Demirdas, S., Fournel-Gigleux, S., Ghali, N., Giunta, C., Kapferer-Seebacher, I., et al. (2017). "The Ehlers-Danlos Syndromes, Rare Types," in *American Journal of Medical Genetics Part C: Seminars in Medical Genetics* (Wiley Online Library), 70–115. doi:10.1002/ajmg.c.31550

Brown, M. J., Hallam, J. A., Colucci-Guyon, E., and Shaw, S. (2001). Rigidity of Circulating Lymphocytes Is Primarily Conferred by Vimentin Intermediate Filaments. *J. Immunol.* 166, 6640–6646. doi:10.4049/jimmunol.166.11.6640

Burch, G. H., Gong, Y., Liu, W., Dettman, R. W., Curry, C. J., Smith, L., et al. (1997). Tenascin-X Deficiency Is Associated with Ehlers-Danlos Syndrome. *Nat. Genet.* 17, 104–108. doi:10.1038/ng0997-104

Byers, P. H., Belmont, J., Black, J., De Backer, J., Frank, M., Jeunemaitre, X., et al. (2017). "Diagnosis, Natural History, and Management in Vascular Ehlers-Danlos Syndrome," in *American Journal of Medical Genetics Part C: Seminars in Medical Genetics* (Wiley Online Library), 40–47. doi:10.1002/ajmg.c.31553

Catala-Petavy, C., Machet, L., Georgesco, G., Pétavy, F., Maruani, A., and Vaillant, L. (2009). Contribution of Skin Biometrology to the Diagnosis of the Ehlers–Danlos Syndrome in a Prospective Series of 41 Patients. *Skin Res. Tech.* 15, 412–417. doi:10.1111/j.1600-0846.2009.00379.x

Chan, C. E., and Odde, D. J. (2008). Traction Dynamics of Filopodia on Compliant Substrates. *Science* 322, 1687–1691. doi:10.1126/science.1163595

Chiarelli, N., Carini, G., Zoppi, N., Ritelli, M., and Colombi, M. (2019a). Molecular Insights in the Pathogenesis of Classical Ehlers-Danlos Syndrome from Transcriptome-wide Expression Profiling of Patients' Skin Fibroblasts. *PLoS One* 14, e0211647. doi:10.1371/journal.pone.0211647

Chiarelli, N., Ritelli, M., Zoppi, N., and Colombi, M. (2019b). Cellular and Molecular Mechanisms in the Pathogenesis of Classical, Vascular, and Hypermobile Ehlers–Danlos Syndromes. *Genes* 10, 609. doi:10.3390/genes10080609

Colige, A., Nuytinck, L., Hausser, I., Van Essen, A. J., Thiry, M., Herens, C., et al. (2004). Novel Types of Mutation Responsible for the Dermatosparactic Type of Ehlers-Danlos Syndrome (Type VIIC) and Common Polymorphisms in the ADAMTS2 Gene. *J. Invest. Dermatol.* 123, 656–663. doi:10.1111/j.0022-202x.2004.23406.x

Darby, I. A., Laverdet, B., Bonté, F., and Desmoulière, A. (2014). Fibroblasts and Myofibroblasts in Wound Healing. *Clin. Cosmet. Investig. Dermatol.* 7, 301–311. doi:10.2147/CCID.S50046

Delbaere, S., Dhooge, T., Syx, D., Petit, F., Goemans, N., Destrée, A., et al. (2020). Novel Defects in Collagen XII and VI Expand the Mixed myopathy/Ehlers-Danlos Syndrome Spectrum and lead to Variant-specific Alterations in the Extracellular Matrix. *Genet. Med.* 22, 112–123. doi:10.1038/s41436-019-0599-6

Denigris, J., Yao, Q., Birk, E. K., and Birk, D. E. (2016). Altered Dermal Fibroblast Behavior in a Collagen V Haploinsufficient Murine Model of Classic Ehlers-Danlos Syndrome. *Connect. Tissue Res.* 57, 1–9. doi:10.3109/03008207.2015.1081901

Dráber, P., Sulimenko, V., and Dráberová, E. (2012). Cytoskeleton in Mast Cell Signaling. *Front. Immun.* 3, 130. doi:10.3389/fimmu.2012.00130

Engler, A. J., Sen, S., Sweeney, H. L., and Discher, D. E. (2006). Matrix Elasticity Directs Stem Cell Lineage Specification. *Cell* 126, 677–689. doi:10.1016/j.cell.2006.06.044

Farmer, A. D., Douthwaite, H., Gardiner, S., Aziz, Q., and Grahame, R. (2010). A Novelin VivoSkin Extensibility Test for Joint Hypermobility. *J. Rheumatol.* 37, 1513–1518. doi:10.3899/jrheum.091192

Fowlkes, V., Wilson, C. G., Carver, W., and Goldsmith, E. C. (2013). Mechanical Loading Promotes Mast Cell Degranulation via RGD-Integrin Dependent Pathways. *J. Biomech.* 46, 788–795. doi:10.1016/j.jbiomech.2012.11.014

Frisch, S. M., Vuori, K., Ruoslahti, E., and Chan-Hui, P. Y. (1996). Control of Adhesion-dependent Cell Survival by Focal Adhesion Kinase. *J. Cel. Biol.* 134, 793–799. doi:10.1083/jcb.134.3.793

Fukada, T., Civic, N., Furuichi, T., Shimoda, S., Mishima, K., Higashiyama, H., et al. (2008). The Zinc Transporter SLC39A13/ZIP13 Is Required for Connective Tissue Development; its Involvement in BMP/TGF-β Signaling Pathways. *PloS one* 3, e3642. doi:10.1371/journal.pone.0003642

Fung, Y. C. (1993). *Biomechanics. Mechanical Properties of Living Tissues*. Springer-Verlag.

Gilmore, A. P. (2005). Anoikis. *Cell Death Differ* 12, 1473–1477. doi:10.1038/sj.cdd.4401723

Grahame, R., and Beighton, P. (1969). Physical Properties of the Skin in the Ehlers-Danlos Syndrome. *Ann. Rheum. Dis.* 28, 246–251. doi:10.1136/ard.28.3.246

Hamilton, M. J. (2018). Nonclonal Mast Cell Activation Syndrome. *Immunol. Allergy Clin. North America* 38, 469–481. doi:10.1016/j.iac.2018.04.002

Hausser, I., and Anton-Lamprecht, I. (1994). Differential Ultrastructural Aberrations of Collagen Fibrils in Ehlers-Danlos Syndrome Types I-IV as a Means of Diagnostics and Classification. *Hum. Genet.* 93, 394–407. doi:10.1007/BF00201664

Hermanns-Le, T., Reginster, M.-A., Piérard-Franchimont, C., Delvenne, P., Piérard, G. E., and Manicourt, D. (2012). Dermal Ultrastructure in Low Beighton Score Members of 17 Families with Hypermobile-type Ehlers-Danlos Syndrome. *J. Biomed. Biotechnol.* 2012, 1–3. doi:10.1155/2012/878107

Huang, X., Yang, N., Fiore, V. F., Barker, T. H., Sun, Y., Morris, S. W., et al. (2012). Matrix Stiffness-Induced Myofibroblast Differentiation Is Mediated by Intrinsic Mechanotransduction. *Am. J. Respir. Cel Mol Biol* 47, 340–348. doi:10.1165/rcmb.2012-0050oc

Humphries, J. D., Byron, A., and Humphries, M. J. (2006). Integrin Ligands at a Glance. *J. Cel. Sci.* 119, 3901–3903. doi:10.1242/jcs.03098

Hungerford, J. E., Compton, M. T., Matter, M. L., Hoffstrom, B. G., and Otey, C. A. (1996). Inhibition of pp125FAK in Cultured Fibroblasts Results in Apoptosis. *J. Cel. Biol.* 135, 1383–1390. doi:10.1083/jcb.135.5.1383

Ingber, D. E. (2003). Tensegrity I. Cell Structure and Hierarchical Systems Biology. *J. Cel. Sci.* 116, 1157–1173. doi:10.1242/jcs.00359

Jennings, S. V., Slee, V. M., Zack, R. M., Verstovsek, S., George, T. I., Shi, H., et al. (2018). Patient Perceptions in Mast Cell Disorders. *Immunol. Allergy Clin. North America* 38, 505–525. doi:10.1016/j.iac.2018.04.006

Kapferer-Seebacher, I., Pepin, M., Werner, R., Aitman, T. J., Nordgren, A., Stoiber, H., et al. (2016). Periodontal Ehlers-Danlos Syndrome Is Caused by Mutations in C1R and C1S , Which Encode Subcomponents C1r and C1s of Complement. *Am. J. Hum. Genet.* 99, 1005–1014. doi:10.1016/j.ajhg.2016.08.019

Kihara, T., Takemura, Y., Imamura, Y., Mizuno, K., and Hayashi, T. (2004). Reconstituted Type V Collagen Fibrils as Cementing Materials in the Formation of Cell Clumps in Culture. *Cell Tissue Res* 318, 343–352. doi:10.1007/s00441-004-0959-6

Kitamura, Y., Oboki, K., and Ito, A. (2007). Development of Mast Cells. *Proc. Jpn. Acad. Ser. B: Phys. Biol. Sci.* 83, 164–174. doi:10.2183/pjab.83.164

Kobayasi, T. (2004). Abnormality of Dermal Collagen Fibrils in Ehlers Danlos Syndrome. Anticipation of the Abnormality for the Inherited Hypermobile Disorders. *Eur. J. Dermatol.* 14, 221–229.

Kohn, A., and Chang, C. (2020). The Relationship Between Hypermobile Ehlers-Danlos Syndrome (hEDS), Postural Orthostatic Tachycardia Syndrome (POTS), and Mast Cell Activation Syndrome (MCAS). *Clin. Rev. Allergy Immunol.* 58(3), 273–297. doi:10.1007/s12016-019-08755-8

Kosho, T., Mizumoto, S., Watanabe, T., Yoshizawa, T., Miyake, N., and Yamada, S. (2020). Recent Advances in the Pathophysiology of Musculocontractural Ehlers-Danlos Syndrome. *Genes* 11, 43. doi:10.3390/genes11010043

Krystel-Whittemore, M., Dileepan, K. N., and Wood, J. G. (2016). Mast Cell: a Multi-Functional Master Cell. *Front. Immunol.* 6, 620. doi:10.3389/fimmu.2015.00620

Kuonen, F., Surbeck, I., Sarin, K. Y., Dontenwill, M., Rüegg, C., Gilliet, M., et al. (2018). TGFβ, Fibronectin and Integrin α5β1 Promote Invasion in Basal Cell Carcinoma. *J. Invest. Dermatol.* 138, 2432–2442. doi:10.1016/j.jid.2018.04.029

Lim, S.-T., Chen, X. L., Lim, Y., Hanson, D. A., Vo, T.-T., Howerton, K., et al. (2008). Nuclear FAK Promotes Cell Proliferation and Survival through FERM-Enhanced P53 Degradation. *Mol. Cel.* 29, 9–22. doi:10.1016/j.molcel.2007.11.031

Lo, C.-M., Wang, H.-B., Dembo, M., and Wang, Y.-L. (2000). Cell Movement Is Guided by the Rigidity of the Substrate. *Biophysical J.* 79, 144–152. doi:10.1016/s0006-3495(00)76279-5

Mak, K. M., Png, C. Y. M., and Lee, D. J. (2016). Type V Collagen in Health, Disease, and Fibrosis. *Anat. Rec.* 299, 613–629. doi:10.1002/ar.23330

Malek, S., and Koster, D. V. (2021). The Role of Cell Adhesion and Cytoskeleton Dynamics in the Pathogenesis of the Ehlers-Danlos Syndromes and Hypermobility Spectrum Disorders. *Front. Cel Dev. Biol.* 9, 883. doi:10.3389/fcell.2021.649082

Malfait, F., Symoens, S., De Backer, J., Hermanns-Lê, T., Sakalihasan, N., Lapière, C. M., et al. (2007). Three Arginine to Cysteine Substitutions in the Pro-alpha (I)-collagen Chain Cause Ehlers-Danlos Syndrome with a Propensity to Arterial Rupture in Early Adulthood. *Hum. Mutat.* 28, 387–395. doi:10.1002/humu.20455

Malfait, F., Wenstrup, R. J., and De Paepe, A. (2010). Clinical and Genetic Aspects of Ehlers-Danlos Syndrome, Classic Type. *Genet. Med.* 12, 597–605. doi:10.1097/gim.0b013e3181eed412

Malfait, F. (2013). Helical mutations in type I collagen that affect the processing of the amino-propeptide result in an Osteogenesis Imperfecta/Ehlers-Danlos Syndrome overlap syndrome. *Orphan. J. Rare Dis.* 8(1), 1–10. doi:10.1111/j.1600-0846.2009.00379.x

Malfait, F., Francomano, C., Byers, P., Belmont, J., Berglund, B., Black, J., et al. (2017). "The 2017 International Classification of the Ehlers-Danlos Syndromes," in *American Journal of Medical Genetics Part C: Seminars in Medical Genetics* (Wiley Online Library), 8–26. doi:10.1002/ajmg.c.31552

Mcgillis, L., Mittal, N., Santa Mina, D., So, J., Soowamber, M., Weinrib, A., et al. (2020). Utilization of the 2017 Diagnostic Criteria for hEDS by the Toronto GoodHope Ehlers-Danlos Syndrome Clinic: A Retrospective Review. *Am. J. Med. Genet.* 182, 484–492. doi:10.1002/ajmg.a.61459

Murray, M. E., Mendez, M. G., and Janmey, P. A. (2014). Substrate Stiffness Regulates Solubility of Cellular Vimentin. *MBoC* 25, 87–94. doi:10.1091/mbc.e13-06-0326

Nielsen, R. H., Couppé, C., Jensen, J. K., Olsen, M. R., Heinemeier, K. M., Malfait, F., et al. (2014). Low Tendon Stiffness and Abnormal Ultrastructure Distinguish Classic Ehlers-Danlos Syndrome from Benign Joint Hypermobility Syndrome in Patients. *FASEB J.* 28, 4668–4676. doi:10.1096/fj.14-249656

Novikova, E. A., Raab, M., Discher, D. E., and Storm, C. (2017). Persistence-driven Durotaxis: Generic, Directed Motility in Rigidity Gradients. *Phys. Rev. Lett.* 118, 078103. doi:10.1103/physrevlett.118.078103

Olivera, A., Beaven, M. A., and Metcalfe, D. D. (2018). Mast Cells Signal Their Importance in Health and Disease. *J. Allergy Clin. Immunol.* 142, 381–393. doi:10.1016/j.jaci.2018.01.034

Piérard, G. E., and Lapiére, C. M. (1987). Microanatomy of the Dermis in Relation to Relaxed Skin Tension Lines and Langer's Lines. *The Am. J. dermatopathology* 9, 219–224. doi:10.1097/00000372-198706000-00007

Piérard, G. E., Piérard, S., Delvenne, P., and Piérard-Franchimont, C. (2013). In vivo evaluation of the skin tensile strength by the suction method: pilot study coping with hysteresis and creep extension. *ISRN Dermatol.* 2013, 841217. doi:10.1097/00000372-198706000-00007

Proske, S., Hartschuh, W., Enk, A., and Hausser, I. (2006). Ehlers-Danlos Syndrome - 20 Years Experience with Diagnosis and Classification. *JDDG* 4, 308–318. doi:10.1111/j.1610-0387.2006.05958.x

Remvig, L., Duhn, P. H., Ullman, S., Kobayasi, T., Hansen, B., Juul-Kristensen, B., et al. (2009). Skin Extensibility and Consistency in Patients with Ehlers-Danlos Syndrome and Benign Joint Hypermobility Syndrome. *Scand. J. Rheumatol.* 38, 227–230. doi:10.1080/03009740802520714

Rohrbach, M., Vandersteen, A., Yiş, U., Serdaroglu, G., Ataman, E., Chopra, M., et al. (2011). Phenotypic Variability of the Kyphoscoliotic Type of Ehlers-Danlos Syndrome (EDS VIA): Clinical, Molecular and Biochemical Delineation. *Orphanet J. Rare Dis.* 6, 46–49. doi:10.1186/1750-1172-6-46

Rombaut, L., Malfait, F., De Wandele, I., Mahieu, N., Thijs, Y., Segers, P., et al. (2012). Muscle-tendon Tissue Properties in the Hypermobility Type of Ehlers-Danlos Syndrome. *Arthritis Care Res.* 64, 766–772. doi:10.1002/acr.21592

Royce, P. M., Steinmann, B., Vogel, A., Steinhorst, U., and Kohlschuetter, A. (1990). Brittle Cornea Syndrome: an Heritable Connective Tissue Disorder Distinct from Ehlers-Danlos Syndrome Type VI and Fragilitas Oculi, with Spontaneous Perforations of the Eye, Blue Sclerae, Red Hair, and normal Collagen Lysyl Hydroxylation. *Eur. J. Pediatr.* 149, 465–469. doi:10.1007/bf01959396

Salvatore, L., Gallo, N., Natali, M. L., Terzi, A., Sannino, A., and Madaghiele, M. (2021). Mimicking the Hierarchical Organization of Natural Collagen: Toward the Development of Ideal Scaffolding Material for Tissue Regeneration. *Front. Bioeng. Biotechnol.* 9, 258. doi:10.3389/fbioe.2021.644595

Seo, B. R., Chen, X., Ling, L., Song, Y. H., Shimpi, A. A., Choi, S., et al. (2020). Collagen Microarchitecture Mechanically Controls Myofibroblast Differentiation. *Proc. Natl. Acad. Sci. U.S.A.* 117, 11387–11398. doi:10.1073/pnas.1919394117

Shimbori, C., Upagupta, C., Bellaye, P.-S., Ayaub, E. A., Sato, S., Yanagihara, T., et al. (2019). Mechanical Stress-Induced Mast Cell Degranulation Activates TGF-B1 Signalling Pathway in Pulmonary Fibrosis. *Thorax* 74, 455–465. doi:10.1136/thoraxjnl-2018-211516

Solon, J., Levental, I., Sengupta, K., Georges, P. C., and Janmey, P. A. (2007). Fibroblast Adaptation and Stiffness Matching to Soft Elastic Substrates. *Biophysical J.* 93, 4453–4461. doi:10.1529/biophysj.106.101386

Sunyer, R., Conte, V., Escribano, J., Elosegui-Artola, A., Labernadie, A., Valon, L., et al. (2016). Collective Cell Durotaxis Emerges from Long-Range Intercellular Force Transmission. *Science* 353, 1157–1161. doi:10.1126/science.aaf7119

Tinkle, B., Castori, M., Berglund, B., Cohen, H., Grahame, R., Kazkaz, H., et al. (2017). Hypermobile Ehlers-Danlos Syndrome (a.k.a. Ehlers-Danlos Syndrome Type III and Ehlers-Danlos Syndrome Hypermobility Type): Clinical Description and Natural History. *Am. J. Med. Genet.* 175, 48–69. doi:10.1002/ajmg.c.31538

Torres, A. J., Vasudevan, L., Holowka, D., and Baird, B. A. (2008). Focal Adhesion Proteins Connect IgE Receptors to the Cytoskeleton as Revealed by Micropatterned Ligand Arrays. *Proc. Natl. Acad. Sci. U.S.A.* 105, 17238–17244. doi:10.1073/pnas.0802138105

Van Damme, T., Pang, X., Guillemyn, B., Gulberti, S., Syx, D., De Rycke, R., et al. (2018). Biallelic B3GALT6 Mutations Cause Spondylodysplastic Ehlers-Danlos Syndrome. *Hum. Mol. Genet.* 27, 3475–3487. doi:10.1093/hmg/ddy234

Viglio, S., Zoppi, N., Sangalli, A., Gallanti, A., Barlati, S., Mottes, M., et al. (2008). Rescue of Migratory Defects of Ehlers-Danlos Syndrome Fibroblasts *In Vitro* by Type V Collagen but Not Insulin-like Binding Protein-1. *J. Invest. Dermatol.* 128, 1915–1919. doi:10.1038/jid.2008.33

Walraven, M., and Hinz, B. (2018). Therapeutic Approaches to Control Tissue Repair and Fibrosis: Extracellular Matrix as a Game Changer. *Matrix Biol.* 71-72, 205–224. doi:10.1016/j.matbio.2018.02.020

Xu, F., Lu, T. J., and Seffen, K. A. (2008). Biothermomechanical Behavior of Skin Tissue. *Acta Mech. Sinica* 24, 1–23.

Yamamoto, K., Yamamoto, M., and Noumura, T. (1992). Disassembly of F-Actin Filaments in Human Endothelial Cells Cultured on Type V Collagen. *Exp. Cel. Res.* 201, 55–63. doi:10.1016/0014-4827(92)90347-b

Yeung, T., Georges, P. C., Flanagan, L. A., Marg, B., Ortiz, M., Funaki, M., et al. (2005). Effects of Substrate Stiffness on Cell Morphology, Cytoskeletal Structure, and Adhesion. *Cell Motil. Cytoskeleton* 60, 24–34. doi:10.1002/cm.20041

Zhan, M., Zhao, H., and Han, Z. C. (2004). Signalling mechanisms of anoikis. *Cell Motil. Cytoskeleton* 19(3), 973–983. doi:10.14670/HH-19.973

Zoppi, N., Gardella, R., De Paepe, A., Barlati, S., and Colombi, M. (2004). Human Fibroblasts with Mutations in COL5A1 and COL3A1 Genes Do Not Organize Collagens and Fibronectin in the Extracellular Matrix, Down-Regulate α2β1 Integrin, and Recruit αvβ3 Instead of α5β1 Integrin. *J. Biol. Chem.* 279, 18157–18168. doi:10.1074/jbc.m312609200

Zoppi, N., Barlati, S., and Colombi, M. (2008). FAK-independent αvβ3 Integrin-EGFR Complexes rescue from Anoikis Matrix-Defective Fibroblasts. *Biochim. Biophys. Acta (Bba) - Mol. Cel Res.* 1783, 1177–1188. doi:10.1016/j.bbamcr.2008.03.003

Zoppi, N., Chiarelli, N., Binetti, S., Ritelli, M., and Colombi, M. (2018). Dermal Fibroblast-To-Myofibroblast Transition Sustained by αvß3 Integrin-ILK-Snail1/Slug Signaling Is a Common Feature for Hypermobile Ehlers-Danlos Syndrome and Hypermobility Spectrum Disorders. *Biochim. Biophys. Acta (Bba) - Mol. Basis Dis.* 1864, 1010–1023. doi:10.1016/j.bbadis.2018.01.005

Zouq, N. K., Keeble, J. A., Lindsay, J., Valentijn, A. J., Zhang, L., Mills, D., et al. (2009). FAK Engages Multiple Pathways to Maintain Survival of Fibroblasts and Epithelia - Differential Roles for Paxillin and p130Cas. *J. Cel. Sci.* 122, 357–367. doi:10.1242/jcs.030478

Conflict of Interest: The authors declare that the research was conducted in the absence of any commercial or financial relationships that could be construed as a potential conflict of interest.

Publisher's Note: All claims expressed in this article are solely those of the authors and do not necessarily represent those of their affiliated organizations, or those of the publisher, the editors, and the reviewers. Any product that may be evaluated in this article, or any claim that may be made by its manufacturer, is not guaranteed or endorsed by the publisher.

frontiers | Frontiers in Cell and Developmental Biology

ORIGINAL RESEARCH
published: 16 May 2022
doi: 10.3389/fcell.2022.871326

Lung Cancer Induces NK Cell Contractility and Cytotoxicity Through Transcription Factor Nuclear Localization

Darren Chen Pei Wong[1,2†], *E Hui Clarissa Lee*[1], *Junzhi Er*[1], *Ivan Yow*[2], *Ricky Abdi Gunawan Koean*[1], *Owen Ang*[1], *Jingwei Xiao*[2], *Boon Chuan Low*[1,2,3†] *and Jeak Ling Ding*[1,4*†]

[1]*Department of Biological Sciences, National University of Singapore, Singapore, Singapore,* [2]*Mechanobiology Institute Singapore, National University of Singapore, Singapore, Singapore,* [3]*University Scholars Programme, National University of Singapore, Singapore, Singapore,* [4]*Integrative Sciences and Engineering Programme, National University of Singapore, Singapore, Singapore*

Actomyosin-mediated cellular contractility is highly conserved for mechanotransduction and signalling. While this phenomenon has been observed in adherent cell models, whether/how contractile forces regulate the function of suspension cells like natural killer (NK) cells during cancer surveillance, is unknown. Here, we demonstrated in coculture settings that the evolutionarily conserved NK cell transcription factor, Eomes, undergoes nuclear shuttling during lung cancer cell surveillance. Biophysical and biochemical analyses revealed mechanistic enhancement of NK cell actomyosin-mediated contractility, which is associated with nuclear flattening, thus enabling nuclear entry of Eomes associated with enhanced NK cytotoxicity. We found that NK cells responded to the presumed immunosuppressive TGFβ in the NK-lung cancer coculture medium to sustain its intracellular contractility through myosin light chain phosphorylation, thereby promoting Eomes nuclear localization. Therefore, our results demonstrate that lung cancer cells provoke NK cell contractility as an early phase activation mechanism and that Eomes is a plausible mechano-responsive protein for increased NK cytotoxicity. There is scope for strategic application of actomyosin-mediated contractility modulating drugs *ex vivo,* to reinvigorate NK cells prior to adoptive cancer immunotherapy *in vivo* (177 words).

Keywords: cellular contractility of natural killer (NK) cell, transcription factor shuttling, Eomesdermin (Eomes), non-small cell lung cancer (NSCLC, invasive and non-invasive subtypes), NK-cancer cell interaction, TGFβ disparate role, mechanotransduction in NK cells, actin cytoskeleton

OPEN ACCESS

Edited by:
Guillermo Alberto Gomez, University of South Australia, Australia

Reviewed by:
Rosa Molfetta, Sapienza University of Rome, Italy
Clément Thomas, Luxembourg Institute of Health, Luxembourg

***Correspondence:**
Jeak Ling Ding
dbsdjl@nus.edu.sg

†These authors share senior authorship

Specialty section:
This article was submitted to Signaling, a section of the journal Frontiers in Cell and Developmental Biology

Received: *08 February 2022*
Accepted: *19 April 2022*
Published: *16 May 2022*

Citation:
Wong DCP, Lee EHC, Er J, Yow I, Koean RAG, Ang O, Xiao J, Low BC and Ding JL (2022) Lung Cancer Induces NK Cell Contractility and Cytotoxicity Through Transcription Factor Nuclear Localization. Front. Cell Dev. Biol. 10:871326. doi: 10.3389/fcell.2022.871326

INTRODUCTION

The innate immune Natural Killer (NK) cells do not require antigen sensitization and are fast-acting first-line responders to pathophysiological conditions of infection and cancer. Nevertheless, the prowess of NK cells is mediated by expression and balance of its activating and inhibitory surface receptors along with transcriptional control of cytotoxic molecules which, altogether, regulate NK cell cytotoxic activity (Brennan et al., 1994; Stabile et al., 2017; Frutoso and Mortier, 2019). The evolutionarily conserved Tbr1 subfamily of T-box transcription factors (TFs) (Papaioannou, 2014), Eomes and T-bet, are the only

T-box proteins expressed in cells of hematopoietic origin (Simonetta et al., 2016; Wagner et al., 2020), and are known to regulate of immune cell development and functions.

Earlier studies in murine models purported redundant roles of Eomes and T-bet in CD8 T-cells (Weder et al., 2014; Zhang et al., 2018). However, in the context of NK cells, the study of Eomes and T-bet has been mainly restricted to their roles in the regulation of stage-specific NK cell maturation, with the expression of Eomes being crucial to functional maturation (Simonetta et al., 2016; Wagner et al., 2020; Zhang et al., 2018, 2021). Interestingly, although much focus on NK maturation has been on the balance of expression of Eomes and T-bet (Zhang et al., 2018), information is lacking on how Eomes and T-bet are compartmentalized for NK cells to elicit anticancer activities. Understanding the molecular and/or biophysical mechanisms and triggers that influence Eomes and T-bet localization is relevant since previous studies in CD8 T-cells highlighted preferential nuclear localization of Eomes or T-bet based on either CD8 exhausted (McLane et al., 2021) or memory T-cells (McLane et al., 2013). These findings indicate a context-specific determinant in the regulation of Eomes and T-bet cytoplasmic/nuclear compartmentalization. Furthermore, whilst Eomes was reported to partially restore dysfunctional NK cell activity (Gill et al., 2012) by a weak suppression of the inhibitory receptor PD1 in T-cells (McLane et al., 2021), a persistently high Eomes expression has also been associated with increased expression of inhibitory receptor TIGIT in NK cells (Yu et al., 2021). Hence, understanding the pathophysiological triggers for nuclear localization of Eomes will help to conceptualize NK cell function versus exhaustion, for therapeutic purposes. In this study, we used non-small cell lung cancer (NSCLC) cells to delineate the cancer context-specific trigger for Eomes and/or T-bet nuclear localization, and the consequential outcome on NK functions.

The tumour microenvironment (TME) is hypertonic due to high levels of inflammatory cytokines and cations (Burgdorf et al., 2020). The osmolarity of the extracellular compartment has traditionally been known to affect intracellular contractility, with the hypertonic environment triggering increased contractility and vice versa (Guan et al., 2007; Malek et al., 2007). For example, hypertonicity can trigger RhoA-dependent actin reassembly that generates contractile force in endothelial cells (Malek et al., 2007). However, the functional consequences of hypertonicity of the TME on the intracellular contractility of NK cell for mechanosignaling is unknown, especially since the NK cells are non-adherent circulating cells which lack force transduction focal adhesion complexes. Furthermore, mechanotransduction events triggered by intracellular force are able to direct protein structure, function and localization, such as the case of force-induced talin activation at the focal adhesion complex in adherent cells (Lombardi et al., 2011; Carisey et al., 2013; Yao et al., 2016; Elosegui-Artola et al., 2017). However, there is no evidence on whether the cytoplasmic/nuclear localization of transcription factors can be directly influenced by the perturbation of cellular force in non-adherent circulating immune cells like NK when undergoing anti-cancer activities. The activation of NK cells requires actin retrograde flow (Matalon et al., 2018; Santoni et al., 2021) and the convergence and activation of various contractility-promoting proteins such as myosin IIA (Krzewski et al., 2006). Moreover, degranulation of NK cells requires Arp2/3-mediated cytoskeleton rearrangement (Carisey et al., 2018; Santoni et al., 2021). These observations hint that cellular contractility, which awaits exploration, may play a role in regulating protein localization in the activation of NK cells, especially since NK cells harbour abundant cytoplasmic content (Carpen et al., 1982).

NK cells express the TGFβ receptor 1 (TGFβR1) which is activated by TGFβ (Viel et al., 2016), and cancer cells are known to generate high levels of TGFβ (Li et al., 2019). Ample evidence suggests that prolonged exposure to TGFβ downmodulates NK cytotoxicity and promotes its exhaustion (Viel et al., 2016; Zaiatz-Bittencourt et al., 2018). Furthermore, high levels of TGFβ has been associated with poor prognosis of non-small cell lung cancer cell (NSCLC) patients (Li et al., 2019). However, a recent study of peripheral blood γδ T cells showed enhancement of T-cell cytotoxicity with short-term addition of TGFβ (Peters et al., 2019). Collectively, these evidence support a more nuanced view; that the functional impact of TGFβ in immune cells may be spatiotemporally regulated, which may be dissected into potentiating and prolonged phases. Given the important roles of actomyosin-associated proteins in promoting NK cytotoxicity at the immune synapse (Krzewski et al., 2006; Carisey et al., 2018; Matalon et al., 2018), we hypothesized that Eomes and/or T-bet nuclear localization may be associated with NK intracellular contractility beyond the immune synapse, potentially triggered by TGFβ, and this might influence NK cytotoxicity against cancer cells.

Using interdisciplinary approaches of biochemical, biophysical and imaging analyses, we first characterized the expression and localization of Eomes and T-bet in healthy donor NK cells that were challenged with NSCLCs. We found a relatively constant expression of Eomes and T-bet proteins, along with a sustained nuclear localization of Eomes (and to a lesser extent, T-bet). Our findings also demonstrated the non-redundant roles of T-bet and Eomes, where Eomes expression and nuclear localization were specifically associated with enhanced NK cytotoxicity against the NSCLCs. However, prolonged exposure to NSCLCs resulted in imbalance of NK activating and inhibitory receptors, which plausibly reduced the cytotoxic capacity to eliminate the lung cancer cells. Secondly, we performed laser ablation experiments in non-adherent NK cells to demonstrate the presence of actomyosin-mediated intracellular contractility even though the NK cells lack force transduction focal adhesion complexes. We showed that Eomes nuclear localization is driven by enhanced NK intracellular contractility. This is demonstrated by increased F-actin intensity and actomyosin-mediated tensional force, as indicated by a higher F-actin recoil velocity induced by laser-ablation and increased myosin light chain phosphorylation. These observations along with NK cell nuclear flattening, are indicative of increased nuclear pore permeability and higher permissibility for Eomes nuclear localization. Pharmacological perturbation of NK intracellular contractility further confirmed Eomes as the first transcription factor identified to directly respond to cellular forces, resulting in its nuclear localization

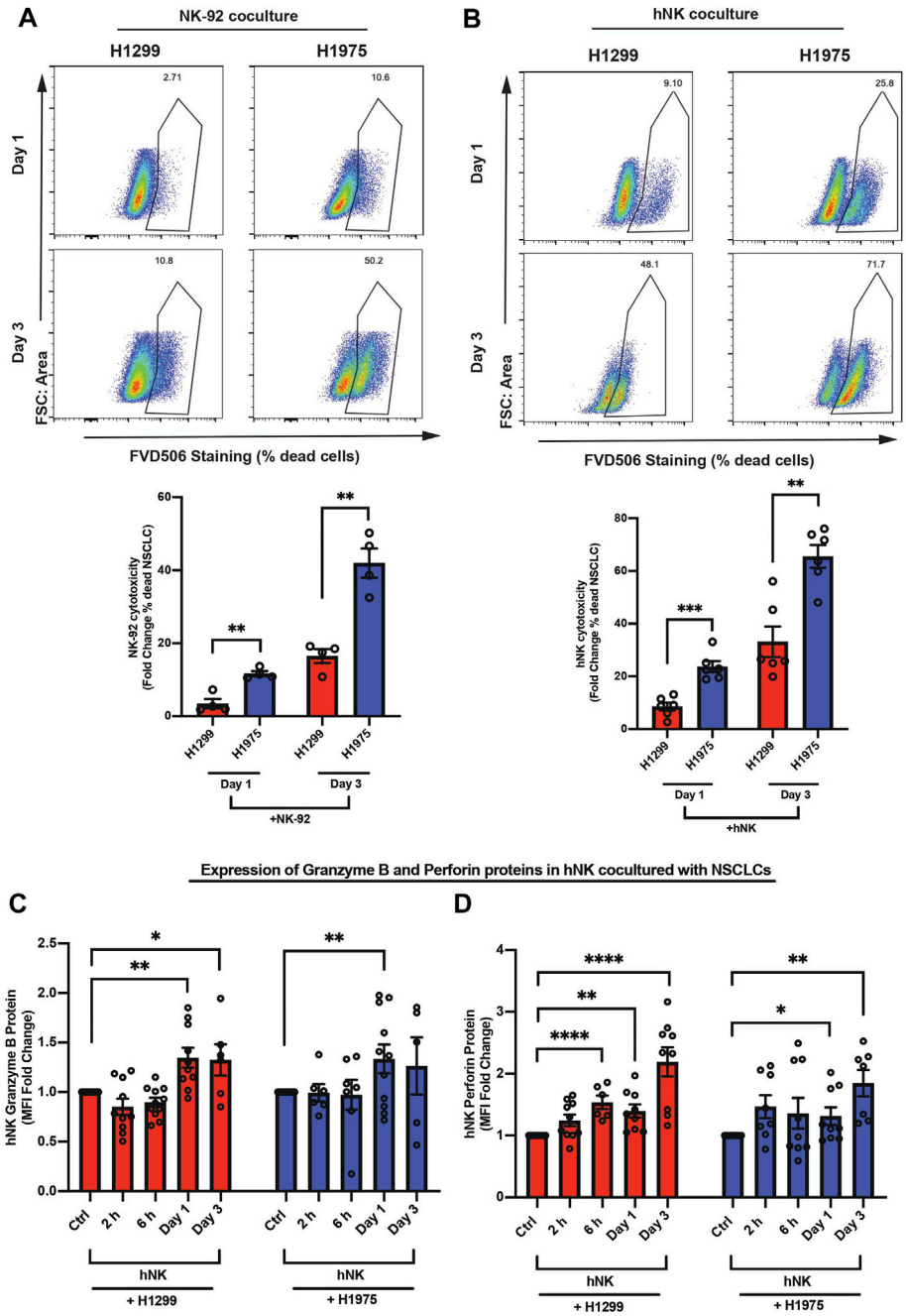

FIGURE 1 | NSCLCs were susceptible to NK cell killing. Flow cytometry analyses show: **(A,B)** Representative and quantified percentage of dead NSCLCs (FVD506 positive). The NSCLCs were CFSE stained prior to coculture with NK-92 **(A)** or hNK **(B)** cells; *n* = 4 for NK-92 coculture. *n* = 6 for hNK coculture. Data are representative of three donors for hNK cells; Gating strategy is presented in **Supplementary Figure 1C**. **(C,D)** The hNK median fluorescence intensity (MFI) fold change of granzyme B and perforin proteins in hNK cells cocultured with NSCLCs were analyzed by flow cytometry at indicated time points and compared to control hNK cells. The graphs represent means ± SEM; n ≥ 6 and representative of four donors. One way ANOVA test was used to compare across conditions.

in NK cells. Thirdly and unexpectedly, we revealed that NK-cancer cell interaction triggered a new disparate role of TGFβ; instead of being immunosuppressive to NK cells, TGFβ sustained an increase in myosin light chain phosphorylation in NK cells, resulting in NK cell contractility which mediated Eomes nuclear localization leading to the enhancement of NK cytotoxicity.

RESULTS

NSCLCs Were Susceptible to NK Cell Killing

The transcription factors, Eomes and T-bet, share a consensus DNA binding T-box domain, but other parts of their sequences are unique (Zhang et al., 2018). To study the mechanistic roles of Eomes and

T-bet in NK cells during cancer surveillance, we tested: 1) primary human NK (hNK) cells, which are $CD3^{-}CD56^{+}Tbet^{+}Eomes^{+}$ (**Supplementary Figure S1A**), and 2) NK-92 cell line, which is $Tbet^{+}Eomes^{+}$ (**Supplementary Figure S1B**), on their anti-cancer capacity against two non-small cell lung cancer cell (NSCLC) subtypes, H1299 (aggressive invasive subtype) and H1975 (less invasive subtype) cells. A coculture setting of cell-cell ratio of 2.5: 1 as determined previously (Verma et al., 2020) was established for NK and lung cancer cells, respectively. We found differential killing capacity of hNK and NK-92 against H1299 and H1975 NSCLCs, where H1975 was more susceptible to NK killing (**Figures 1A,B**). To exclude the possibility that the differential killing capacities of NK cells was due to different proliferation rates of the two NSCLC subtypes, we verified the proliferation marker, Ki67, on NSCLCs cocultured with NK cell. Interestingly, both NSCLC subtypes showed a significant and comparable drop in Ki67 expression in coculture conditions (**Supplementary Figures S2A,B**). We further verified the invasiveness of the two NSCLC subtypes by comparing their migratory displacements and colony-formation abilities in soft agar. H1299 was significantly more invasive than H1975 (**Supplementary Figures S2C,D**), which is consistent with a previous report (Shen et al., 2018). Interestingly, at days 1 and 3 of coculture the more invasive H1299 NSCLC induced hNK to produce significantly higher fold-increase in two key targets of Eomes (Araki et al., 2008), perforin (≈2.5 fold) and granzyme b (≈1.5 fold), compared to control hNK cells which were not challenged with NSCLCs (**Figures 1C,D**). These observations suggest that NK cytotoxicity was upregulated over 1–3 days during which NK cells attempted to kill the NSCLCs, and that there may be an increase in Eomes nuclear localization, resulting in the higher production of perforin and granzyme b. Henceforth, we focused on: 1) the impact of aggressive invasive metastatic NSCLC on NK T-box transcription factors and cytotoxicity, and 2) intrinsic mechanistic characteristics of NK cells during their interaction with the two NSCLC subtypes.

NSCLC Induced Nuclear Localization of Eomes Within 1 day in NK Cells

We had previously demonstrated that Eomes-low Group 1 ILCs, which contain both NK and ILC1 cell subtypes, are associated with poorer cancer surveillance and worse clinical outcomes for lung cancer patients (Verma et al., 2020). Hence, Eomes probably plays an essential role in the regulation of NK anti-cancer cytotoxicity. Since murine models showed differential expressions of Eomes and T-bet in Group 1 ILCs located in the TME or periphery (Verma et al., 2020), we first analyzed the protein expression of Eomes and T-bet in hNK cocultured *ex vivo* with the NSCLCs. Interestingly, coculture with NSCLCs induced a slight reduction in Eomes expression in hNK and this only occurred after 3 days of coculture with H1299 cells (**Supplementary Figures S3A,E**). On the other hand, T-bet showed a slight increase at day 3 of coculture with H1975 (**Supplementary Figure S3B,F**). Nevertheless, these results suggested that any increase in Eomes nuclear localization would not be due to an increase in Eomes protein expression. This is also relevant to translational applications since KIR educating/licensing does not affect T-box protein expression in NK cells (Pradier et al., 2016), and would most likely not affect their expression in NK cells challenged by cancer cells that might experience KIR mismatch issues.

Since the localization of T-bet and Eomes was previously reported to change in CD8 cytotoxic T cells depending on their activation status (McLane et al., 2013, 2021), we next used a spinning disk microscope equipped with a super-resolution module (Live-SR) to delineate the subcellular localization of Eomes in comparison to T-bet, in three NK cell types (hNK, NK-92 and KHYG-1) cocultured with the NSCLCs. Since there was only a marginal increase in hNK perforin and granzyme b after 2 and 6 h of coculture with NSCLCs (**Figures 1C,D**), we reasoned that Eomes and T-bet localization would not likely display localization differences at such time-points. Indeed, Eomes or T-bet did not show significant increase in nuclear signals (**Supplementary Figure S4A,B**). Next, we focused on days 1, 3 and 6 because of significantly higher perforin and granzyme b production observable by day 1 of coculture (monitored from 2 h to 3 days, **Figures 1C,D**). Consistently, we observed a more prominent nuclear localization of Eomes across all NK cell types (**Figures 2** and **Supplementary Figure S5**) up to 3 days of coculture**.** Interestingly, only T-bet in hNK cells displayed nuclear localization at day 3. However, the nuclear-cytoplasmic ratio of T-bet (≈1.25) (**Supplementary Figure S5B)** was still lower than that of Eomes (≈2.0). Although both NSCLC subtypes induced Eomes nuclear localization in NK cells to different extents, we observed a particularly prominent nuclear localization when hNK cells were primed by the highly invasive metastatic NSCLC, H1299 (**Figure 2**), corresponding to up to 2.0-fold change in the production of perforin and granzyme b (**Figures 1C,D**). These results suggest that Eomes nuclear localization (and to a lesser extent, T-bet), may be an attempt by NK cells to upregulate its cytotoxicity. To corroborate these observations, we next cocultured NK-92 cells with two breast cancer cell lines (MCF7 and MDA-MB-231) that were reported to display different susceptibility to NK cell killing (Absi et al., 2018). As expected, the more metastatic and resistant MDA-MD-231 breast cancer cells were able to induce faster and more prominent Eomes nuclear localization in NK-92 cells (**Supplementary Figure S4C**).

Since Eomes nuclear localization is associated with potentiating NK cytotoxicity (e.g., increased perforin and granzyme b production, **Figures 1C,D**), we performed cytotoxicity assay against a model target lymphoblast cell line (K562) using two NK cell lines (NK-92 and KHYG-1) which overexpress either Eomes or T-bet, to corroborate that Eomes specifically promotes NK cytotoxicity. In both NK cell types, only Eomes (but not T-bet) overexpression indeed resulted in significantly higher killing of K562 target cells (**Supplementary Figure S6**).

NSCLCs are one of the leading causes of cancer mortality (Li et al., 2019). Our observation that Eomes did not further display prominent nuclear localization at day 6 of coculture with the invasive H1299 NSCLC (**Figure 2**), is consistent with reduced NK cytotoxicity after prolonged encounter of NKs with NSCLCs. One possible explanation is the regulation of surface activating and

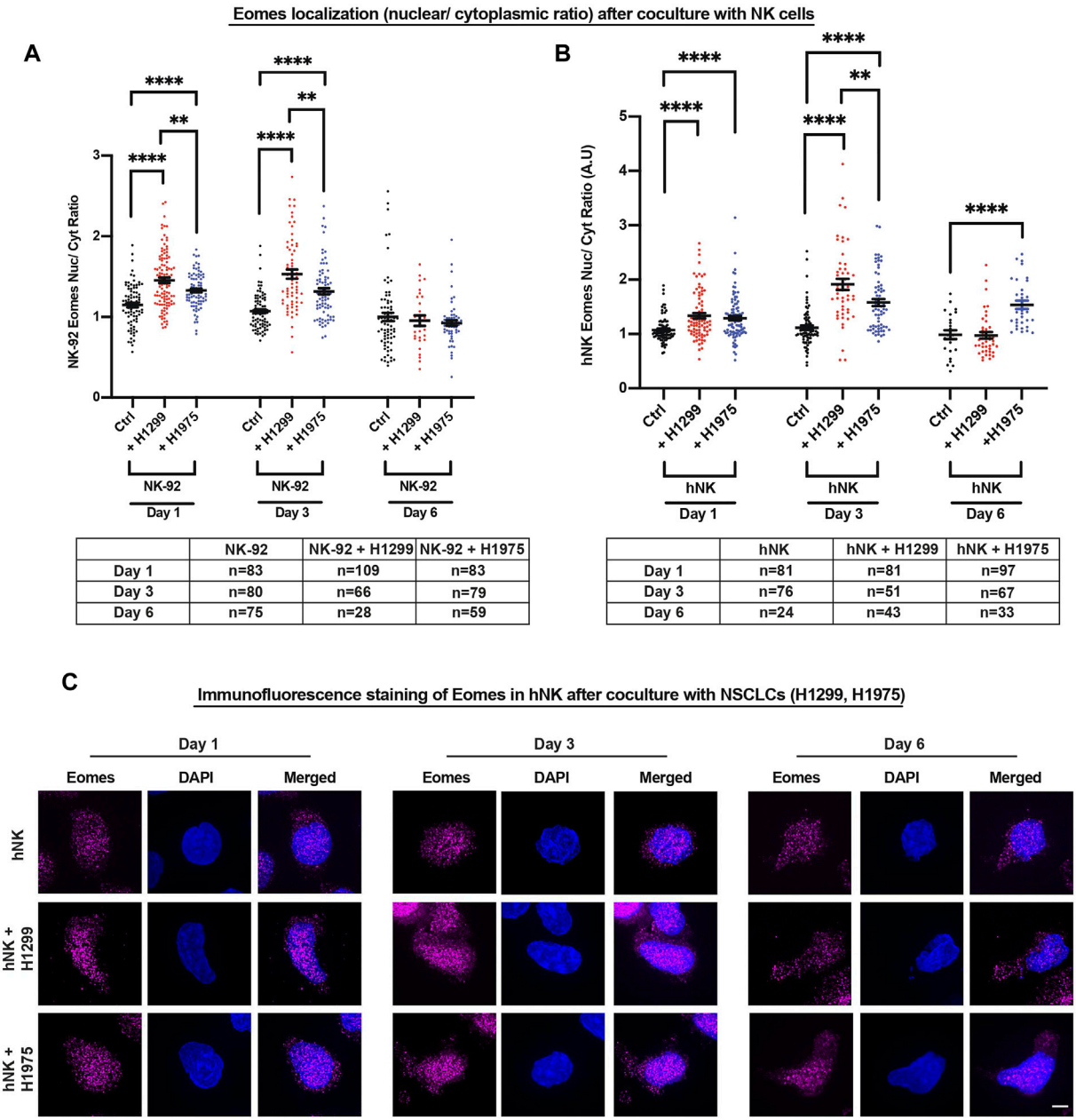

	NK-92	NK-92 + H1299	NK-92 + H1975
Day 1	n=83	n=109	n=83
Day 3	n=80	n=66	n=79
Day 6	n=75	n=28	n=59

	hNK	hNK + H1299	hNK + H1975
Day 1	n=81	n=81	n=97
Day 3	n=76	n=51	n=67
Day 6	n=24	n=43	n=33

FIGURE 2 | NSCLCs induced nuclear localization of Eomes within 1 day in NK cells**. (A,B)** NK-92 and hNK cells cocultured with NSCLCs showed preferential nuclear localization of Eomes, particularly strongly on day 3 for NK cells cocultured with H1299 NSCLC. The graphs represent means ± SEM; *n* is tabulated below the graphs. For hNK cells, n values are representative of individual cells representative of three donors. One way ANOVA was used to compare the means of each group. **(C)** Representative SIM images of Eomes in hNK cocultured with NSCLCs. Increasing nuclear (DAPI stained) Eomes signal (magenta) is detected in hNK cocultured with NSCLCs. Scale bar = 5 μm.

inhibitory receptors of NK cells, which is well-associated with NK exhaustion and reduced function (Gill et al., 2012; Lee et al., 2021). To verify this possibility, we analyzed the surface expression of various inhibitory (PD-1, TIGIT, NKG2A) and activating (NKG2D) receptors on viable (FVD506-negatively stained) hNK and NK-92 cells cocultured with NSCLCs. Interestingly, there was a consistent reduction in all receptors analyzed, and especially so for hNK cells (**Supplementary Figure S7**). These results suggest that prolonged exposure to invasive metastatic NSCLCs progressively imbalances NK receptors, rendering Eomes nuclear localization insufficient to overcome invasive cancer cells. Taken together, these data suggest a specific role of Eomes, in activating a dormant cytotoxic machinery by translocating into NK nucleus. However, such mechanism was undermined in prolonged coculture setting, possibly due to the imbalance in activating and inhibitory receptors. These

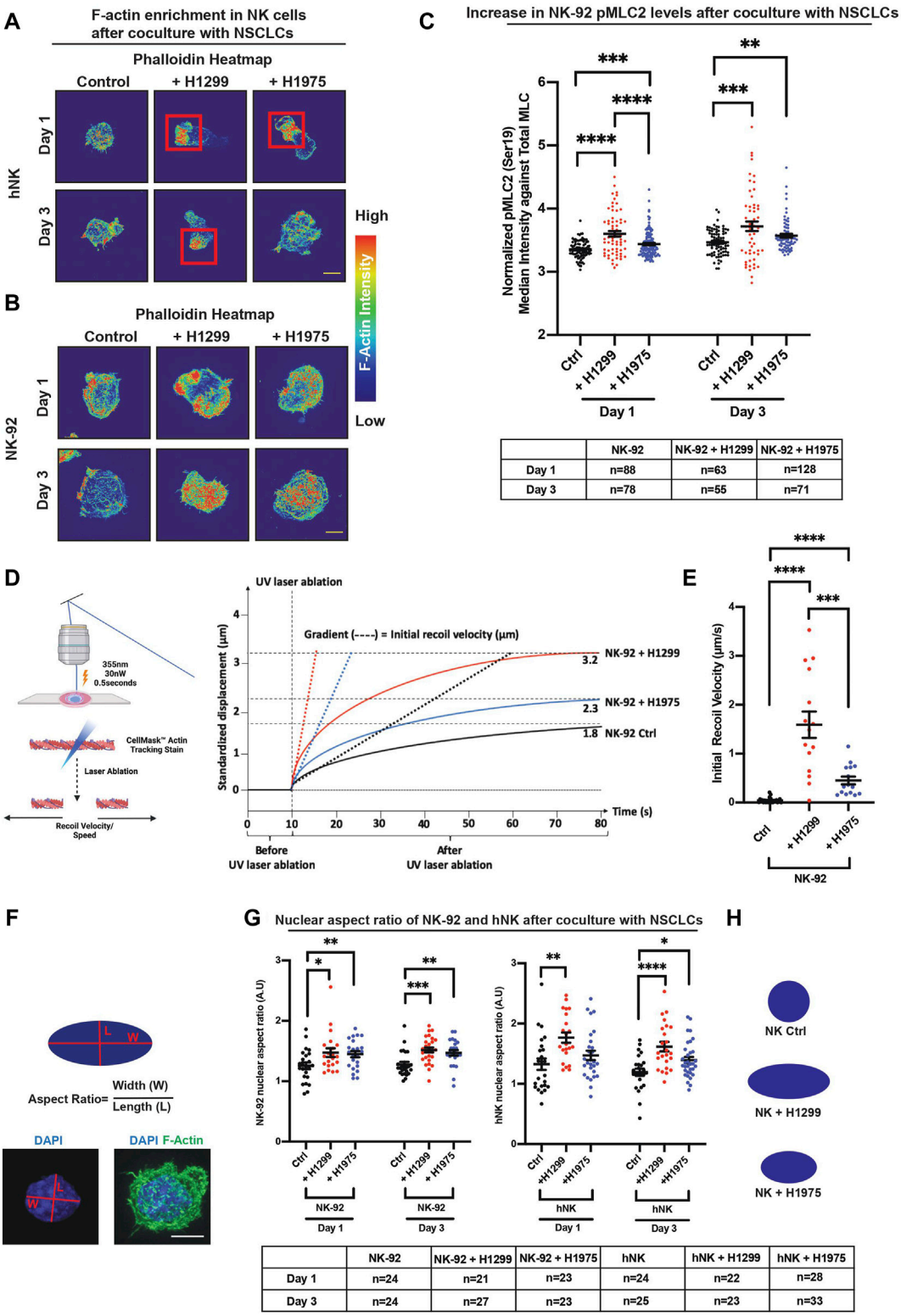

FIGURE 3 | NSCLCs activated NK cellular contractility and induced nuclear flattening. **(A)** SIM super-resolution images show localised enhancement of F-actin concentration in hNK cells that were cocultured with NSCLCs. Red squares highlight areas of F-actin enrichment in hNK cells that were cocultured with NSCLCs. All samples were stained with a master mix of phalloidin, specific for F-actin, and laser power and exposure settings were kept constant across samples imaged. Scale bar = 5 µm. **(B)** NK-92 cells showed an increase in F-actin intensity after coculture with NSCLC, corresponding to an increase in F-actin heatmap on the right. All samples

(*Continued*)

FIGURE 3 | were stained with a master mix of phalloidin and laser power and exposure settings were kept constant across samples imaged. Scale bar = 5 μm. **(C)** Cocultures of NK-92 cells with NSCLCs increased phosphorylation of myosin light chain 2 at Ser19 (pMLC2) in NK-92 cells. All samples were stained with a master mix of respective primary and secondary antibodies and imaged with same laser power and exposure time. Representative images are shown in **Supplementary Figure S8B**. Unpaired students *t*-test was used to compare between conditions. The graphs represent means ± SEM and n is tabulated below the graph. **(D)** Schematics showing laser ablation of NK cells, and representative graph showing maximum recoil displacement (Ctrl = 1.8 μm, + H1299 = 3.2 μm, and + H1975 = 2.3 μm) of laser ablated actin, and the derivation of initial recoil velocity. Detailed experimental and quantification procedures are documented in the materials and methods section. **(E)** NK cells cocultured with NSCLCs show higher F-actin recoil velocity compared to control NK cells unchallenged by NSCLCs. Unpaired students *t*-test was used to compare F-actin recoil velocities between conditions. The graphs represent means ± SEM and $n = 24$ for control, and $n = 15$ for NSCLC coculture. **(F)** Schematic showing quantification of aspect ratio as a representative indicator for nuclear flattening. Blue signal represents the nucleus. Scale bar = 5 μm. **(G)** NK-92 and hNK cocultured with NSCLCs consistently showed increased nuclear aspect ratio (nuclear flattening). The graphs represent means ± SEM, n is tabulated below the graph. Unpaired students *t*-test was used. **(H)** Schematic representing nuclear flattening with an increased aspect ratio after NK coculture with NSCLCs. Dark blue schematic represents the nucleus of NK cells.

observations warrant a deeper understanding on the extrinsic and intrinsic signaling mechanism that trigger NK Eomes nuclear localization when they encounter NSCLCs.

NSCLCs Activated NK Cellular Contractility and Induced Nuclear Flattening

The biological roles of actomyosin in NK cells has thus far been focused on its regulation of the immune synapse (Krzewski et al., 2006; Carisey et al., 2018; Jankowska et al., 2018). However, information on how global regulation of actomyosin-mediated cellular contractility may affect NK function, is unexplored albeit important. Intracellular actomyosin-based contractility has been proposed to regulate protein activities through focal adhesion complex present in adherent cells (Elosegui-Artola et al., 2017). Yet, such contractility-based regulation of protein activation and localization still remains an undefined physiological trigger. Based on our preliminary findings, we hypothesized that when NK cells encounter NSCLCs, the actin dynamics would impel NK cell contractility, which will in turn impact the subcellular compartmentalization of Eomes. To investigate this possibility, we first cocultured NK cells with the two NSCLC subtypes, H1299 and H1975, for 1 and 3 days. A high Eomes nuclear localization signal and high levels of perforin and granzyme b were observed at these timepoints (**Figures 1C,D**, **Figure 2**). We next characterized the F-actin organization in NK cells after coculture. In the absence of NSCLC, the F-actin in the hNK cell was observed to be relatively homogeneous in the cell body with occasional filipodia-like structures (**Figure 3A**). However, for hNK cocultured with NSCLCs, we observed a notable display of F-actin polarization and condensation (**Figure 3A**, red box and **Supplementary Figure S8A**). Interestingly, the invasive metastatic H1299 cells were found to sustain such polarization over 3 days whereas the less invasive H1975 reverted hNK to a control-like phenotype (**Figure 3A** and **Supplementary Figure S8A**). Similar observations were made with NK92-NSCLC coculture, where NK92 displayed an increase in F-actin intensity (**Figure 3B**). With the less invasive H1975, the NK cell displayed a correspondingly lower intensity of actin at day 3, which was also consistent with lower translocation of Eomes to the nucleus (**Figure 2**). These observations suggest enhancement of intracellular contractility in NK cells upon encountering NSCLCs.

Since high nuclear localization of Eomes is associated with more pronounced condensation of F-actin in NK cells (**Figure 2**, **Figures 3A,B**), we next sought to understand the functional association between higher F-actin and intracellular contractility on the localization of Eomes. The Rho-ROCK-Myosin pathway is known to increase cellular contractility, and myosin has been identified to stabilize cellular F-actin (Amano et al., 1996, 2010; Yamashiro et al., 2018). Thus, we analyzed the phosphorylation status of the non-muscle myosin II light chain 2 (MLC2) in NK cells cocultured with NSCLCs to ascertain if there was an increase in cellular contractility. Indeed, despite relatively constant staining of total MLC2 (**Supplementary Figure S8B,C**), we observed a prominent rise in the normalized expression (intensity) of phosphorylated MLC2 (pMLC2) in NK cells cocultured with NSCLCs (**Figure 3C** and **Supplementary Figure S8B**). Consistently, H1299 NSCLC appeared to have primed NK cells to sustain a significantly higher level of pMLC2 for up to 3 days, concurrent with the peak of nuclear Eomes localization (**Figure 2A**).

To directly determine whether the increase in F-actin intensity and myosin light chain phosphorylation result in enhanced NK intracellular contractility, we analyzed the recoil velocity of F-actin by performing a laser-ablation experiment on NK-92 cells cocultured with NSCLCs (**Figure 3D**). Corroboratively, we found that NK cells cocultured with NSCLCs displayed profound and significant recoil velocities compared to control NK cells alone, which is a direct indication of a stronger intracellular contractile force generated by the actomyosin complex (**Figure 3E**). Consistently, we observed a higher recoil velocity in NK cells cocultured with H1299 compared to H1975, and this corresponds to higher F-actin intensity and myosin light chain phosphorylation when NK cells encounter the more aggressive NSCLC.

Since the nucleus is mechanically coupled to the cytoskeleton via the LINC complex (Guilluy et al., 2014), an increase in intracellular contractility will tether mechanical force transmission to the nucleus and result in nuclear flattening with consequential increase in the nuclear aspect ratio (Elosegui-Artola et al., 2017; Alisafaei et al., 2019). Changes in nuclear geometric parameters would favour increase in nuclear pore permeability and protein import (Elosegui-Artola et al., 2017; Alisafaei et al., 2019). Thus, we compared the aspect ratios (length/width) of the NK nucleus, between control NK and NK + NSCLC cocultures (**Figure 3F**). Interestingly, the more

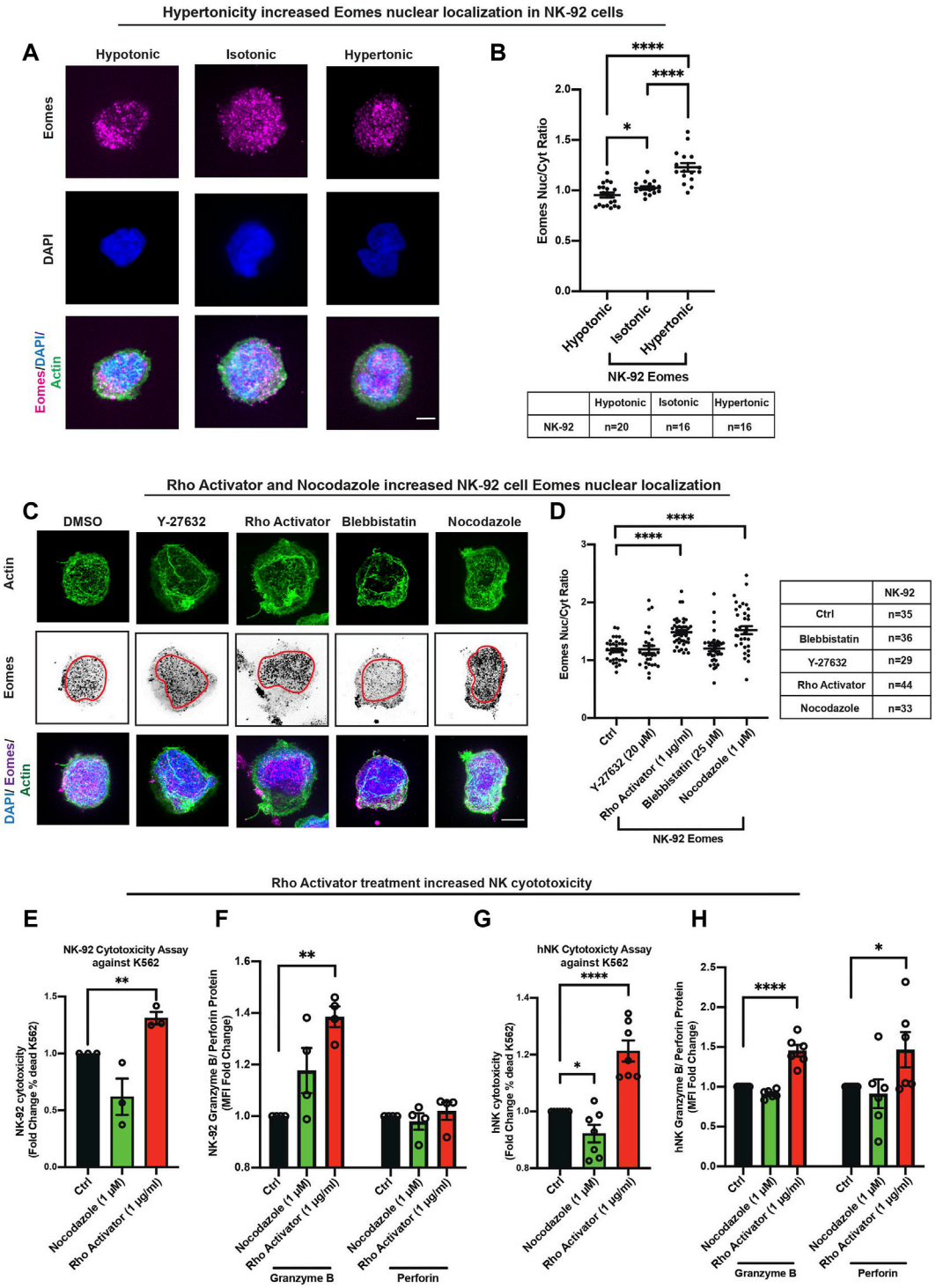

FIGURE 4 | Eomes is the first transcription factor identified to respond to cellular contractility**. (A,B)** Hypertonic treatment significantly increased NK-92 Eomes nuclear localization. Representative images and quantification of Eomes intracellular localisation after 30 min of tonicity treatment. The graph represents means ± SEM, *n* is tabulated below the graph. Scale bar = 5 µm. Unpaired students *t*-test was used. **(C,D)** Representative images and quantification on the right show increased nuclear localisation of Eomes with Rho activator and nocodazole treatment. The graph represents means ± SEM, *n* is tabulated beside the graph. Scale bar = 5 µm. Unpaired students *t*-test was used. **(E,G)** Increased cellular contractility due to treatment with Rho activator enhanced NK-92 and hNK cytotoxicity (reflected as percentage killing) against model target K562 cells, effector (NK): target (K562) ratio was 3:1 for NK-92 and 1:1 for hNK cells. *n* = 3 for NK-92 and *n* = 7 for hNK, representative of three donors. **(F,H)** Rho activator increased the production of granzyme B in NK-92 **(F)** and hNK **(H)** cells cocultured with K562 cells, whereas only hNK cells showed an increase in perforin expression with Rho activator treatment. *n* = 4 for NK-92 cells and *n* = 6 independent experiments representative of three donors for hNK cells. All graphs are represented by means ± SEM and unpaired students *t*-test was used.

aggressive metastatic H1299 NSLC flattened the NK nucleus starting from day 1, yielding a more prominent aspect ratio (≈40% more than control) by day 3 (**Figures 3G,H**). On the other hand, hNK cocultured with H1975 showed a moderate nuclear flattening at day 3 (**Figures 3G,H**), again corresponding to the lesser nuclear Eomes observed at day 3 (**Figure 2**). Similar observations were made with NK-92 cocultures (**Figures 3G,H**). Altogether, these data suggest that compounding factors in the coculture media could have resulted in a graded response within NK cells that differentiates between invasive and less invasive cancer cell lines. For instance, the fine tuning of cellular contractility through myosin light chain phosphorylation could be one of the mechanisms involved. Nevertheless, nuclear flattening observed in NK cells suggested that this is associated with mechanical deformation of NK nucleus which favours shuttling of Eomes into the nucleus.

Eomes Is the First Transcription Factor Identified to Respond to Cellular Contractility

Because enhanced NK intracellular contractility is associated with increased Eomes nuclear localization, we reasoned that intracellular contractility alone might be sufficient to drive Eomes nuclear shuttling. To test this hypothesis, we subjected NK-92 cells to iso-, hypo-, or hyper-osmotic shocks and stained for actin with phalloidin (**Supplementary Figure S9A**). Since the *in vivo* TME (represented partially in these experiments by the conditioned coculture medium) is hypertonic due to chronic inflammation which supports an intratumoral osmotic pressure (Sirtl et al., 2018; Burgdorf et al., 2020), there is a direct physiological link to the role of increased NK cell contractility in promoting Eomes nuclear localization, which plausibly regulates NK cytotoxicity. Thus, we employed a hypertonic treatment, which will induce a flaccid membrane with a concurrent increase in intracellular contractility, and vice versa with hypotonic treatment (Gonano et al., 2014). Interestingly again, only Eomes (and not T-bet) specifically responded to hypertonicity associated with increased nuclear localization observed (**Figures 4A,B**). In fact, T-bet only displayed moderate localization differences between extreme osmolarities, viz, hypotonic and hypertonic conditions (**Supplementary Figures 9B,C**).

The phosphorylation of the myosin light chain directly contributes to actomyosin-based intracellular contractility (Ridley, 2001), which is conceivably associated with Eomes nuclear localization. Thus, we performed pharmacological perturbation of this pathway to ascertain Eomes (using T-bet as control) nuclear localization in response to altered intracellular contractility. We treated NK-92 cells with contractility perturbation drugs, Y-27632 (ROCK inhibitor) and Rho Activator, targeting the Rho-ROCK-Myosin pathway, and quantified Eomes and T-bet nuclear localization. Although Rho activation could have induced several molecular pathways (Bros et al., 2019; Wurzer et al., 2019), its constitutive activation was shown to induce abundant stress fiber and enhance intracellular contractility (Hodge and Ridley, 2016). As expected, treatment with Y-27632 marginally reduced the nuclear localization of Eomes (**Figures 4C,D**) and T-bet (**Supplementary Figures S9D,E**). Notably, Rho activator, the upstream small GTPase that activates myosin through ROCK kinase, significantly increased Eomes nuclear localization (**Figures 4C,D**). To corroborate this, we verified NK-92 Eomes localization by treating the cells with blebbistatin and nocodazole. Blebbistatin inhibits myosin activity and nocodazole induces the release of the Rho GTPase exchange factor, GEF-H1, which increases intracellular contractility (Pan et al., 2020). Indeed, there was a significant increase in Eomes nuclear localization with nocodazole treatment (**Figures 4C,D**).

Since increased intracellular contractility specifically impels Eomes into the nucleus, and upregulates NK cytotoxicity (**Supplementary Figure S6**), we hypothesized that an increase in contractility would functionally upregulate NK cytotoxicity. Indeed, cytotoxicity assay of NK cells pre-treated with Rho activator was shown to significantly increase NK cytotoxicity against the target K562 lymphoblast cell line, and this was associated with increased production of the Eomes transcription target, granzyme B (**Figures 4F,H**). Furthermore, there was a consistent reduction in the surface expression of the inhibitory receptors TIGIT and NKG2A (**Supplementary Figure S9F**). Although nocodazole pre-treatment increases contractility and Eomes nuclear localization, it is a potent microtubule depolymerization reagent that could have affected multiple cellular processes. This explains a reduction in NK cytotoxicity with nocodazole pre-treatment (**Figures 4E,G**).

Taken together, we demonstrate for the first time that a transcription factor, Eomes, responds directly to intracellular contractility perturbations via the Rho-ROCK-Myosin pathway. Although the NK cells are a non-adherent circulating cell type, which lack the force transduction focal adhesion, their ability to summon intracellular contractility for Eomes to gain traction into the nucleus, is unique and interesting in view of NK cell reactivation. This prompted us to further identify the extrinsic and/or intrinsic trigger(s) of intracellular contractility-mediated Eomes nuclear localization induced in *ex vivo* NK-NSCLC coculture, with a view to elucidating the mechanisms underlying such a promotion of NK cytotoxicity against the invasive NSCLC subtype.

TGFβ Induced NK Cell Contractility and Eomes Nuclear Localization

Metastatic NSCLCs are known to be associated with high levels of the presumably immunosuppressive cytokine TGFβ (Ye et al., 2015). Nonetheless, observations in non-immune systems suggest the induction and activation of contractile genes (Birukova et al., 2005; Ojiaku et al., 2018; Gladilin et al., 2019), which has yet to be proven in immune cells. This prompted us to examine a potential opposing/disparate role of TGFβ during the early phase of NK anti-cancer coculture, which may facilitate the activation of NK cytotoxicity.

Since coculturing with NSCLC induced myosin light chain phosphorylation in NK cells (**Figure 3C**), we first verified if blocking the TGFβR1 receptor will affect MLC2

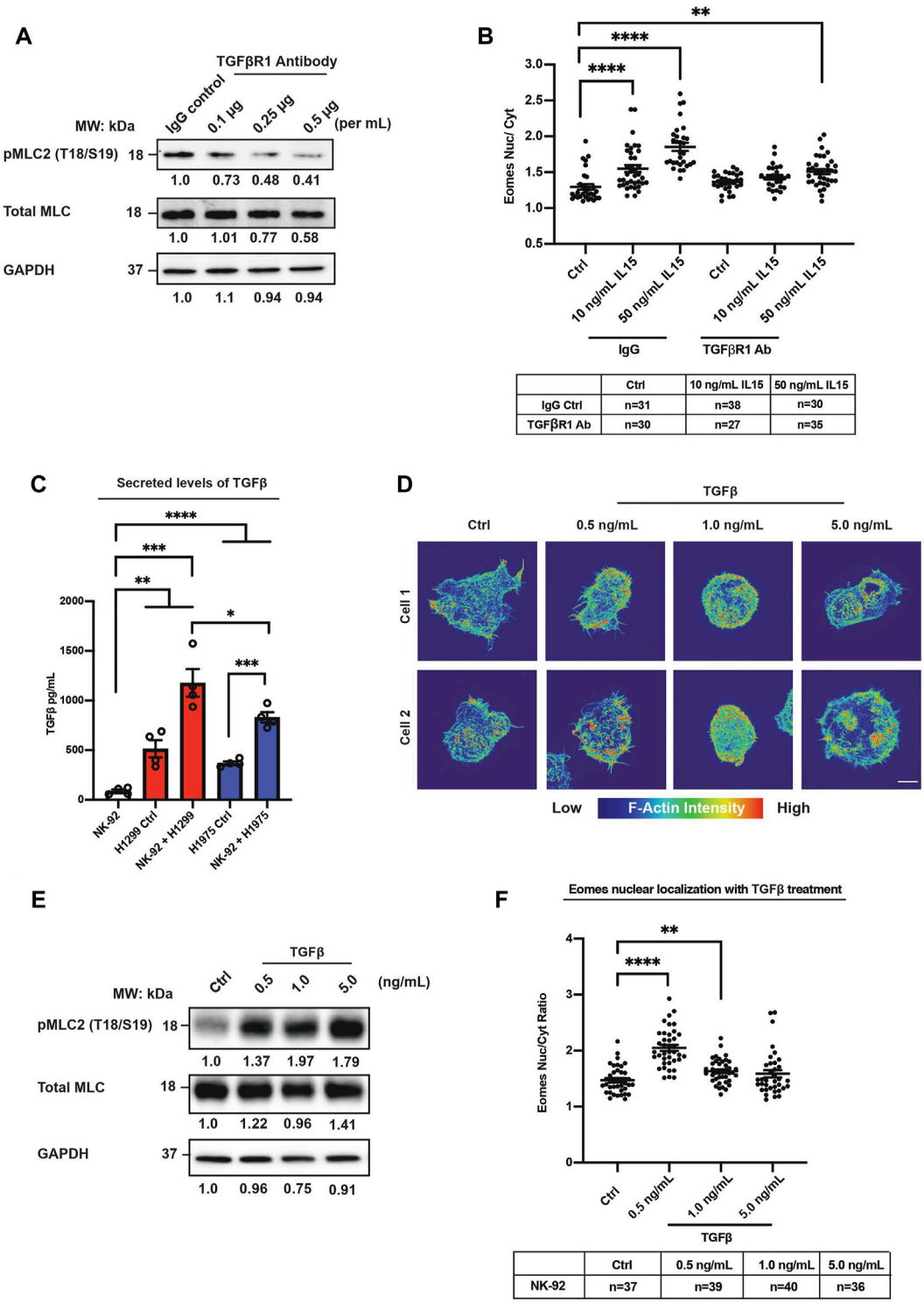

FIGURE 5 | TGFβ-induced myosin light chain phosphorylation is associated with Eomes nuclear localization**. (A)** Western blot with densitometric quantification (numerically represented below each band) shows that TGFβ1R antibody blocking reduced pMLC2 (Thr18/Ser19) expression in a dose-dependent manner, $n = 3$. **(B)** IL15 induced dose-dependent increase in Eomes nuclear localization in NK-92 cells, whereas TGFβR1 antibody blocking (compared to control IgG) suppressed IL15-induced nuclear localization of Eomes in NK-92 cells. n is represented in the table below the graph. One way ANOVA was used to compare the means of each group. **(C)** ELISA quantification of TGFβ in supernatants from individual cultures and cocultures showed higher TGFβ levels in the presence of H1299 cells, $n = 4$. Unpaired students *t*-test was used to compare between groups. **(D)** SIM super-resolution images show enhancement of F-actin concentration in NK-92 cells that were pre-treated with TGFβ. The scale below represents the color coding for actin intensity. All samples were stained with a master mix of phalloidin, specific for F-actin, and

(*Continued*)

FIGURE 5 | laser power and exposure settings were kept constant across samples imaged. Scale bar = 5 μm. **(E)** Western blot with densitometric quantification (numerically represented below each band) shows TGFβ increased pMLC2 (Thr18/Ser19) expression in a dose-dependent manner, $n = 3$. **(F)** TGFβ treatment promoted nuclear localization of Eomes in NK-92 cells in a dose-dependent manner as indicated by higher Eomes nuc/cyt ratio. n is tabulated below the graph. All graphs are represented by means ± SEM and unpaired students *t*-test was used.

phosphorylation in NK cells. Indeed, treatment with anti-TGFβ1R blocking antibody exhibited a dose-dependent reduction of pMLC2 in NK-92 cells (**Figure 5A**), suggesting that TGFβR1 activation is responsible for maintaining NK contractility through myosin light chain phosphorylation. Importantly, we showed that blocking TGFβR1 with a high dose of anti-TGFβR1 antibody did not affect Eomes and T-bet expression levels (**Supplementary Figure S10A**), implying that any observed regulation of Eomes and/or T-bet localization through TGFBR signaling is not attributed to changes in their protein levels. Next, we directly verified if blocking TGFβ1R on NK cells would affect Eomes nuclear localization (using T-bet as control). Consistent with our hypothesis, we demonstrated that inhibition of TGFβ1R specifically reduced Eomes nuclear localization in NK-92 cells stimulated with PMA/Ionomycin, conceivably attributable to reduced cellular contractility (**Supplementary Figure S10B**), whereas again, there was no change in T-bet nuclear localization (**Supplementary Figure S10C**). To corroborate the finding that TGFβ1R blocking could affect Eomes nuclear localization, we stimulated NK-92 cells with a physiological stimulant, IL15. IL15 was previously shown to synergize TGFβ activities in immune cells (Hawke et al., 2020). We found that treatment of NK-92 with IL15 induced a dose-dependent increase in Eomes nuclear localization. However, such increase was less prominent when NK cells were pre-treated with TGFβ1R blocking antibody (**Figure 5B**). These results suggest that there could be an increased TGFβ production and/or TGFβ1R surface expression in coculture conditions which might have facilitated the increase in cellular contractility in NK cells.

The above findings prompted us to analyze the mRNA expressions of *TGFB1* and *TGFBR1* genes from the flow sorted NK-92 and NSCLCs after coculture (**Supplementary Figures S10D,F**). Consistently, H1299 cells expressed a higher level of *TGFB1* mRNA compared to H1975 cells in both control and coculture conditions (**Supplementary Figure S10F**). Interestingly, H1299 cells induced >10-fold increase in *TGFBR1* mRNA in NK-92 cells (**Supplementary Figure S10D**) compared to that induced by H1975. These results suggest that the innately high level of TGFβ1 produced by the invasive metastatic NSCLC (H1299) markedly induced the expression of NK cell TGFβR1, to further enhance NK cell contractility through myosin light chain phosphorylation. To corroborate these observations, we further verified surface level of TGFβR1, which indeed showed a higher expression on NK-92 cells that were cocultured with the invasive metastatic H1299 NSCLC compared to that of coculture with H1975 NSCLC (**Supplementary Figure 10E**).

Next, we performed an ELISA to determine the secreted levels of TGFβ in NK-92, H1299 and H1975 alone cultures and in coculture conditions. As shown in **Figure 5C**, both cocultures with H1299 and H1975 significantly increased the secreted levels of TGFβ1, with the more invasive H1299 inducing a substantially higher level of secreted TGFβ1. Interestingly, the secreted levels of TGFβ in NK-92 or NSCLC alone media did not add up to that of the coculture conditions (**Figure 5C**). Furthermore, there was an increase in NK-92 *TGFB1 mRNA in* coculture conditions (**Supplementary Figure 10D**). These observations suggest that the source of TGFβ could be contributed by both NK and NSCLCs and we cannot rule out autocrine regulation of NK cells by its TGFβ secreted into the media. However, this warrants full scale studies in future investigations.

Since the enhanced contractility and Eomes nuclear localization may be in part due to TGFβ1 in the culture media, we reasoned that the TGFβ1 level determined by ELISA (**Figure 5C**) should be able to stimulate actin reorganization, myosin light chain phosphorylation and induce significant Eomes nuclear localization. We first asked whether actin reorganization and density would be affected. We found that treatment with a low dose (0.5 ng/ml) of TGFβ1 was sufficient to induce significant increase in actin reorganization and filopodia-like protrusions from NK-92 cells (**Figure 5D**), which was indicative of RhoA activation (Heasman and Ridley, 2010). Furthermore, actin reorganization after treatment with TGFβ1 was also associated with a prominent increase in myosin light chain phosphorylation (**Figure 5E**). Finally, we verified that Eomes displayed highest nuclear localization at the doses of 0.5 ng/ml and 1.0 ng/ml (**Figure 5F**), corresponding to TGFβ levels in the culture supernatants of H1299 alone and coculture with H1299, respectively (**Figure 5C**).

To recapitulate, we have shown that in the presence of NSCLCs, the NK cells increased their cellular contractility which potentiated Eomes nuclear localization associated with enhanced cytolytic activity against the NSCLCs. Mechanistically, Eomes responds to actomyosin-mediated contractility, and preferentially localizes to the nucleus of NK cells. The sustained NK cell contractility is explained by the trigger from secreted TGFβ (ligand) from NK and NSCLCs, and NK cell TGFβ1R (receptor) which evoked pMLC2-mediated NK cell contractility to increase Eomes nuclear localization. Overall, the basal cytotoxicity of NK cell with moderate Eomes nuclear localization was only sufficient to subdue the less invasive NSCLC (e.g., H1975). It is plausible that NK cells exploit and contravene the seemingly immunosuppressive tumor microenvironment (represented here as conditioned culture medium from NK + NSCLC coculture) to potentiate its cytolytic response over 1–3 days, but this diminished thereafter due to the imbalance in NK activating and inhibitory receptors. **Figure 6** illustrates our findings in a schematic model.

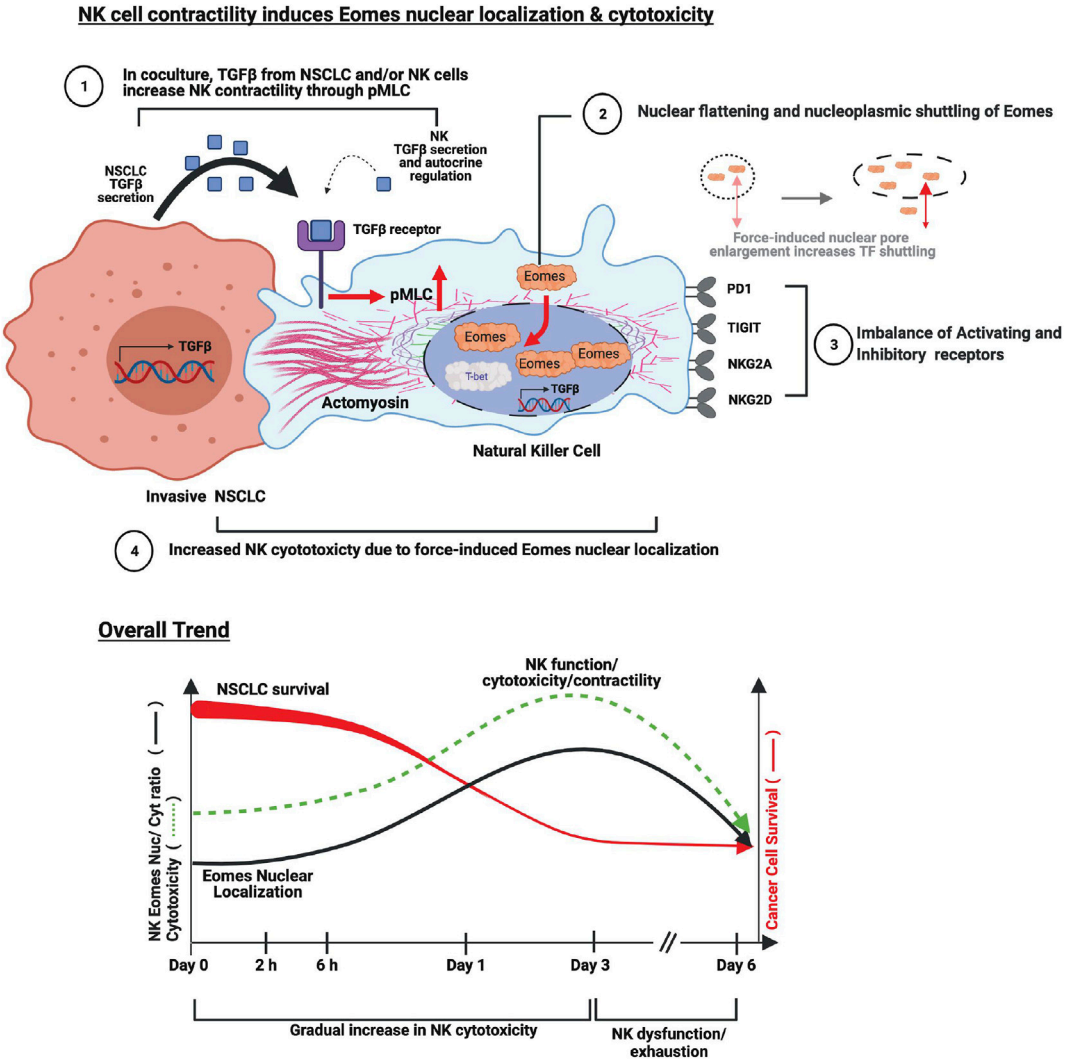

FIGURE 6 | A model summarizing NK cellular contractility which induces Eomes nuclear localization and provokes antitumor surveillance. (Cell-molecular mechanism) Metastatic invasive NSCLC (e.g., H1299) produces higher levels of TGFβ to which NK cells respond by increasing TGFβR1 expression, which activates downstream signal transduction events. (1) Continuous production and secretion of TGFβ persistently increases NK cell contractility through TGFβR1 upregulation and MLC phosphorylation (pMLC). The source of TGFβ could be from NSCLCs and/or NK cells, the latter of which could conceivably mediate autocrine regulation of NK cell activity, as evident by an increase in TGFβ mRNA; (2) Enhanced cellular contractility (as indicated by actin-recoil) promotes actin re-organization and Eomes nuclear shuttling. One mechanism is through mechanical stretching of the nuclear pore, which promotes transcription factor (TF) shuttling (Elosegui-Artola et al., 2017); (3 and 4) Imbalance of activating and inhibitory receptors on NK cell surface reduced the cytotoxicity of NK cells despite increased Eomes nuclear localization, which compromises NK cell killing of metastatic NSCLC. The insufficiency/exhaustion of NK cells is exacerbated by continuous TGFβ secretion by the resistant invasive NSCLC. (Overall Trend) NSCLCs increase NK contractility which is accompanied by nuclear shuttling of Eomes that surged from day 1. The increase in NK cytotoxicity is sufficient to subdue the less invasive H1975 NSCLC and partially eliminate the more invasive H1299. However, as Eomes nuclear residency peaked at day 3, NK cytotoxicity against the more invasive metastatic H1299 wanes, possibly due to compounding factors present in the highly immunosuppressive microenvironment, eventually leading to exhaustion-like phenotype.

DISCUSSION

In our previous study, we found that Eomes-low Group 1 ILCs in mice, which contain both NK and ILC1 cell subtypes, are associated with poorer lung cancer surveillance and worse clinical outcomes (Verma et al., 2020). However, recent evidence shows that human NK cells in the TME display similar Eomes and T-bet expression compared to those in the periphery (Russick et al., 2020). Hence, by using hNK cells from healthy donors, we characterized differential intracellular localization of these transcription factors that exist in the context of anti-NSCLC activities and provide a mechanistic insight on the extrinsic roles of TGFβ in the regulation of NK actomyosin contractility during this process. We discovered that compared to the less invasive H1975, the more invasive H1299 NSCLC could increase and sustain Eomes nuclear localization, which was associated with increased NK cytotoxicity (indicated by granzyme b and perforin production) against NSCLCs.

Furthermore, when in the presence of H1299, higher levels of TGFβ triggered phosphorylation of myosin light chain 2 (pMLC2), resulting in an increase in F-actin condensation, which upregulated NK intracellular contractility for nuclear localization of Eomes. However, prolonged exposure to uncleared NSCLC ultimately led to an imbalance in cell surface activating and inhibitory receptors on the NK cells. Collectively, we propose an alternative view - that at the appropriate and subtle concentration, TGFβ spatiotemporally acts as an NK cell activator through the activation of actomyosin-mediated contractility for Eomes nuclear localization. Additionally, we propose Eomes in NK cells to be the first mechanosensitive transcription factor identified to regulate anti-cancer activities.

In agreement with an earlier study (Chang et al., 2011) which reported that T-bet was predominantly localized to the T-cell nucleus, we observed only little compartment shuttling of T-bet in NK cells undergoing antitumor activities. However, in contrast to a study on human CD8 T-cells (McLane et al., 2013), we demonstrated a key and novel mechanistic finding, that with human NK cells, Eomes specifically displays nuclear compartmentalization preference when challenged by NSCLCs and this was not due to an increase in Eomes protein expression. Intriguingly, despite an increase in the level of nuclear Eomes, the NK cells were somewhat constrained in eliminating the more invasive NSCLC H1299. This seemed to undermine our initial finding that overexpression of Eomes promoted cytotoxicity against the lymphoblast model target cell line, K562. It also seemed counter-intuitive of the expectation that Eomes overexpression in adoptively transferred murine NK cells increases cytotoxicity (Gill et al., 2012). On the other hand, we have also shown that Eomes nuclear localization is associated with reduction of PD-1 expression, agreeing partially with the previous finding that Eomes and T-bet are suppressors of the *PDCD1* gene in CD8 T-cells (McLane et al., 2021).

Although it was reported that Eomes sustained or enhanced the expression of several inhibitory receptors and promoted NK (Gill et al., 2012) and T cell (Kurtulus et al., 2015) exhaustion, these experiments typically entail long durations (e.g., 17 days). Furthermore, the effects observed were attributed to Eomes overexpression or downregulation. We have shown in our studies that Eomes expression in NK cells remained relatively constant throughout the coculture period. Hence, any perceived change (generally decreasing trend) to receptor expressions could be due to direct or indirect consequences of the subcellular localization of Eomes (nuclear/cytoplasmic translocation). Interestingly, it was reported that PD-1 blockade in CD8 T-cells induced higher expression of Eomes related genes, and this process was proposed to be a consequence of increased Eomes nuclear localization after PD-1 blockade (McLane et al., 2021), which corroborates our inference. Although progressive exhaustion cannot be ruled out as a possible mechanism that limited NK cytotoxicity, we did not observe an upregulation of inhibitory receptors, but rather, downregulation of both the inhibitory and activating receptors in prolonged cocultures. Such observations suggest that either: 1) NK cells reduced their cytotoxicity for self-preservation; this prevents over-activation due to persistent reduction in inhibitory receptors and/or 2) the inhibitory and activating receptors might co-regulate the activities of NK cells when overwhelmed by the persistently immunosuppressive condition. Indeed, several NK cell activating and inhibitory receptors were identified to share/compete for the same ligands (Chauvin and Zarour, 2020; Holder and Grant, 2020), suggesting additional fine-tuning of downstream signaling. In addition, actin remodeling in more invasive NSCLCs could also be a limiting factor against NK cytotoxicity. For instance, it was recently reported that metastatic breast cancer cells were enriched in synaptic actin responses that served as a protective barrier against NK cell attack (Absi et al., 2018). Interestingly, we have also shown in our study that Eomes nuclear localization was more prominent in NK cells challenged with the more invasive breast cancer cells, MDA-MB-231 (see **Supplementary Figure S4C**). Such consistent observations on NK cell response against different cancer types (lung and breast cancers) are interesting and warrant future investigation since synaptic actin responses in target cells are associated with altered NK receptor ligand density (Absi et al., 2018). It is also entirely possible that any increase in TGFβ levels in the coculture could similarly induce activation of cancer cell contractility, which could in turn affect cancer cell ligand density to facilitate the evasion from NK cell killing.

Our findings also highlight two plausible physiological triggers (hypertonicity and TGFβ) and their functional consequences which promoted the contractility-induced nuclear compartmentalization of Eomes. The pathophysiological TME is hypertonic due to chronic inflammation which supports an intratumoral osmotic pressure (Sirtl et al., 2018; Burgdorf et al., 2020). Hypertonicity was earlier demonstrated to increase adherent cell intracellular contractility (Gauthier et al., 2011; Gonano et al., 2014). Here, we provide the first evidence that human circulating immune cells are mechanosensitive and harness contractility as a means to induce nuclear translocation of transcription factors to elicit cytotoxicity against NSCLCs. This may explain why previous studies showed a positive graded response of immune response genes (including *IFNG*) when immune cells (e.g., T-cells) were cultured on substrates of increasing stiffness (Saitakis et al., 2017; Santoni et al., 2021). Also, our findings help explain why an increase in osmolarity due to hemorrhages (Pirkle and Gann, 1976) can result in the activation of infiltrating NK cells that exhibit increased cytotoxicity and chemokine production versus peripheral NK cells (Li et al., 2020).

We further identified a spatiotemporally graded response initiated by the TGFβ, to sustain intracellular contractility by promoting myosin light chain phosphorylation, thereby evoking Eomes nuclear entry. This is supported by decreased Eomes nuclear localization upon blocking of the TGFβR1 receptor and increased Eomes nuclear localization with TGFβ treatment. Our data seem to contradict immune studies showcasing TGFβ as a potent immunosuppressive cytokine, particularly towards NK cells (Foltz et al., 2018; Zaiatz-Bittencourt et al., 2018). However, it is noteworthy that most immune studies in murine models involved long treatment regimes, which may have limited data on early phase effects of

the TME on the NK cells. In addition, we demonstrated that a high dosage of TGFβ could not sustain or increase Eomes nuclear localization, which may mirror long treatment regimens that likely harbor high TGFβ concentrations. This could also partially explain why TGFβ has been viewed as immunosuppressive. Moreover, it is not uncommon for cells to undergo desensitization due to persistently high levels of TGFβ, and that the TGFβR receptor could have been internalized due to high levels of TGFβ (Mitchell et al., 2004; Duan and Derynck, 2019). Furthermore, it was previously reported that high NKG2D ligands in endothelial cells resulted in NKG2D receptor internalization in NK cells (Thompson et al., 2017). Additionally, by super-resolution imaging of NK actin reorganization, we found that only treatment with low dosage of TGFβ showed filopodia-like structure and homogeneous increase in actin intensities (indicative of dynamic RhoA activation). By contrast, higher dosages induced intense local enhancement of actin condensation. It is well known that contractility induced by RhoA is dynamic and spatio-temporally coordinated (Pertz, 2010; Narumiya and Thumkeo, 2018). A persistent and global activation of RhoA with high dosage of TGFβ could have fired aberrant signaling pathways that masked the perceived effects of RhoA-MLC contractility-induced Eomes nuclear localization. Further works are required to understand whether and how RhoA activation is tightly controlled to specifically enhance NK cell contractility for Eomes nuclear localization.

What else could be the trigger for intracellular contractility in NK cells that lack focal adhesions for force transduction? One possibility is the force transmission at the immune synapse/other surfaces. For instance, the KLRG1 receptor on NK cells recognizes E-cadherin on target cells (Nakamura et al., 2009), and it has been demonstrated that E-cadherins adhesive clusters at cell junctions are mechanically coupled to actomyosin cortex to generate junctional tension (Wu et al., 2015). Hence, future work may identify whether an interplay of different biological parameters co-regulate such intracellular contractility in non-adherent immune cells.

Since the nucleus of eukaryotic cells is mechanically coupled to the focal adhesion complex and the actin cytoskeleton by the LINC complex (Guilluy et al., 2014), enhanced intracellular contractility exerts a mechanical force on the nuclear membrane. Such force exertion deforms the nuclear membrane and increases nuclear pore exposure to the cytosolic versus nuclear side of the membrane to favour protein import (Elosegui-Artola et al., 2017). Our results indicate that the NSCLCs induce significant nuclear flattening, which we demonstrated to be a consequence of enhanced contractility. Hence, we propose that such mechanical deformation of the nucleus is recapitulated in mechanosensitive NK cells undergoing anticancer activities; this action facilitates Eomes transcription factor nuclear shuttling. NK cells lack focal adhesion complexes to couple force transmission from ECM to actomyosin complex; therefore, the ability to intrinsically fine-tune its intracellular contractility according to the aggressiveness of cancer cells, and apply the induced mechanoforce for Eomes to gain traction into the nucleus is a novel attribute for translational therapeutics consideration. Future studies may ascertain whether the LINC complex, which couples cytoskeletal force to nuclear pore enlargement, is directly involved in Eomes nuclear entry. In addition to ultimately defining how Eomes can be mechanistically regulated, it would be pertinent in future, to identify pathways that simultaneously engage cytoskeletal remodeling and dynamism. For example, both the activating receptors, NKG2D and DNAM-1, are known to induce actin polymerization through Vav1 (Xiong et al., 2015), which will influence the dynamism of the NK cytoskeletal network. Likewise, the recognition of target cells through β1 and β2 integrins will most likely synergize mechano-responsively in NK cells (Zhang et al., 2020; Santoni et al., 2021).

In conclusion, our results support that Eomes nuclear entry is associated with F-actin re-organization and force-induced nuclear flattening that can be influenced by osmolarity and TGFβ. Our findings offer a vivid mechanism (see **Figure 6**) on how NK cells attempt to regain cytotoxicity via intracellular contractility which promoted early and prominent accumulation of Eomes (and possibly other mechanosensitive proteins) in the nucleus. Awaiting further exploration is the augmentation of NK cellular contractility though myosin light chain phosphorylation, which could act as a potential "*biological rheostat*" to facilitate activation of dormant NK cytotoxicity against pathophysiological events and prevent excessive metabolic expenditures that may undermine NK activities. Our results also caution researchers that well-studied cytotoxicity promoting TFs in *vitro* investigations may be insufficient to yield highly desirable results *in vivo* when there is a lack of context-dependent understanding of the TFs and cell dynamics. Overall, our findings provide a new avenue for the development of potential immunotherapeutic strategies, for example, through the use of contractility modulating drugs to perform *ex vivo* enhancement of NK cytotoxicity prior to *in vivo* administration in clinical settings.

MATERIALS AND METHODS

The general methodologies on cell culture, transfection (plasmids & siRNAs), flow cytometry, ELISA, Western blot, RT-PCR, soft agar assay and antibody list with Resource Reference IDs (RRIDs) are in the "**Supplementary Material**".

Isolation of PBMCs and Primary NK Cells

Apheresis cones from healthy donors were obtained from the Health Sciences Authority Singapore (HSA), under protocols approved by HSA and NUS Institutional Review Board (201706-06 and H-17-028E). Peripheral blood mononuclear cells (PBMCs) were isolated from blood samples using Ficoll-Paque (GE Healthcare, Cat# 17144003) gradient centrifugation. Primary human NK cells were enriched from PBMCs by negative selection using the EasySep Human NK Cell Enrichment Kit

(StemCell Technologies, Cat# 19055), following the manufacturer's protocol.

NK Cell Coculture With Lung and Breast Cancer Cells

hNK, KHYG-1 and NK-92 cells were co-cultured with NSCLCs: NCI-H1299 or NCI- H1975 at 2.5:1 effector (NK) to target (NSCLC) ratio as was previously determined by the group (Verma et al., 2020). hNK or NK-92 were cocultured with breast cancer cell lines MCF7 or MDA-MB-231 at 2.5:1 effector (NK) to target (breast cancer cell) ratio. Coculture was carried out in NK MACS media supplemented with 25 ng/ml IL2 for primary human NK cells, or 10% RPMI supplemented with 10 ng/ml IL-2 for KHYG-1 and NK-92 cell lines. hNK, KHYG-1 and NK-92 cell lines were pre-stained with CFSE (Sigma), which was able to perpetuate for 6 days as determined by CFSE + population from flow cytometry, following the manufacturer's protocol for all co-culture setups except for those used for cytotoxicity assay against model target cell line, K562.

NK Cell Cytotoxicity Assay

Target K562 cells were pre-stained with CFSE prior to coculture with NK cells for cytotoxicity assay. Effector (NK) to target (K562) ratio used was 1:1 for hNK cells and KHYG-1 cells and 3:1 for NK-92 cells. After a 4-h incubation period maintained at 37°C with 5% CO2, cells were stained with fixable viability dye eFluor506 (eBioscience, Cat# 65–0866–14) on ice for 30 min and immediately analysed by flow cytometry for fixable viability dye eFluor506 staining.

Tonicity Treatment

NK-92 cells were incubated with warm 1x PBS (isotonic), 2X PBS (hypertonic) or 0.5x PBS (hypotonic) for 30 min at 37°C with 5% CO2. Subsequently, NK-92 cells were fixed with warm 4% PFA (Electron Microscopy Sciences, Cat# 15710) for imaging.

Immunofluorescence Staining and Structured Illumination Microscopy

For immunofluorescence staining, cells were centrifuged and fixed with 4% PFA for 15 min at 37°C. After fixation, free aldehydes were quenched with freshly prepared sodium borohydride (0.01%; Sigma-Aldrich, Cat# 452882) dissolved in 1x PBS for 5 min. Samples were washed thrice with 1x PBS at 5-min intervals and incubated with blocking and permeabilising solution (3% bovine serum albumin and 0.2% Triton X-100 in 1× PBS) for 30 min. After fixation, permeabilization and blocking, samples were incubated with appropriately diluted primary antibodies (1:200 for T-bet and Eomes, and 1: 500 for all other antibodies) in blocking solution for 40 min at room temperature. This was followed by washing thrice with 1× PBS, and incubating with Goat anti-Rabbit IgG (H + L) Highly Cross-Adsorbed Secondary Antibody, Alexa Fluor– 647 conjugated secondary antibodies (ThermoFisher Scientific, Cat# A32733, RRID:AB_2535805), Goat anti-Mouse IgG (H + L) Highly Cross-Adsorbed Secondary Antibody, Alexa Fluor Plus 555) (ThermoFisher Scientific, Cat# A32727, RRID:AB_2633276), and DAPI (ThermoFisher Scientific, Cat# D1306, RRID:AB_2629482)). The cells were washed thrice with 1× PBS. Cells were placed in an iBidi glass-bottom dish (iBidi, Cat# 81218–200) pre-coated with 0.01% poly-L-lysine (Invitrogen, Cat# P8920), and centrifuged at 700 xg for 5 min using a swing-out bucket rotor. The cells were then imaged by confocal or structured illumination microscopy (SIM). For visualisation of actin, Alexa Fluor 488 Phalloidin (ThermoFisher Scientific, Cat# A12379) stain was used together with the secondary antibodies at 1:500 dilution. Imaging was performed on Yokogawa CSU-W1 (Nikon TiE system) using a 1.40 numerical aperture (NA) oil immersion ×100 objective. For SIM imaging, Live-SR module (Roper Scientific) on the spinning disk microscope was engaged during imaging. Post-processing of the images was performed with Live-SR algorithm. For comparison between samples, the binning, laser powers and exposure time were kept constant.

Laser Ablation

Thirty minutes prior to imaging, suspension NK-92 cells were stained with CellMask™ Actin Tracking Stain (ThermoFisher Scientific, Cat# A57243). The NK-92 cells were then centrifuged onto a PLL coated glass bottom dish at 500 g for 5 min. All subsequent imaging were performed within 30 min after NK-92 cells were centrifuged onto the glass bottom dish to prevent any diminishing effects due to removal of NK-92 cells from cancer cells. To measure recoil velocity due to tensional release of actin network mesh within the cells, distinctive features were monitored before, during and after UV laser ablation. Spatiotemporal information of the distinctive features after UV ablation was obtained and quantified as shown in **Figure 3D**, using MTrackJ plugin in Fiji ImageJ. Fitting of calculated distance between points of distinctive features was carried out using a linear function and a single exponential function. The single exponential function was used for datasets with slow recoil velocity to obtain slow elastic response of the actin network mesh upon ablation. Next, recoil velocity was calculated as the derivative of the above mentioned functions using methods mentioned in earlier literatures (Meijering et al., 2012; Hara et al., 2016).The linear function is:

$$f(t) = p_1 t + p_2$$

Where t is the approximate time when UV laser shutter is opened, p_1 is the deformation speed for linear model, and p_2 is the initial length between points of distinctive features at t = 0 s for linear model.

The single exponential model is:

$$f(t) = a + Ae^{\left(\frac{-1(t-b)}{\tau}\right)}$$

Where t is the approximate time when UV laser shutter is opened, a is the initial length between points of distinctive features at $t = 0\,s$ for exponential model, τ is the ratio of Young's modulus to viscosity, and A, and b are arbitrary constants.

TGFβ ELISA

To validate the concentration TGFβ, the supernatants of H1299, H1975 and NK-92 cells alone and after cocultures were harvested after 24 h. Supernatant was diluted and TGFβ was measured using TGF-β1 Human ELISA kit (Invitrogen, Cat# 88-8350-86), according to the manufacturer's instructions. Briefly, the supernatants were diluted 2-fold with ELISA kit diluent and further diluted 1.4 fold with 1N HCl and 1N NaOH. The supernatant was allowed to incubate overnight with a pre-coated 96 well plate and absorbance readings were measured at 459 and 570 nm.

Treatment of NK Cells With TGFβ for Contractility Assessment

Recombinant human TGFβ protein (Cat # 240-B-002) was obtained from RnD Systems and diluted at 20 μg/ml in sterile 4 mM HCl containing 1 mg/ml human or bovine serum albumin, according to manufacturer's protocol. NK-92 cells were treated overnight with TGFβ or control (4 mM HCl containing 1 mg/ml human or bovine serum albumin) before fixing with warm 4% PFA for downstream imaging analysis or lysed with RIPA buffer for western blot analysis.

TGFβR1 Antibody Blocking

TGFβR1 antibody of various concentrations or IgG isotype control were prepared by diluting in incomplete RPMI media (without serum and antibiotics). NK cells were incubated with the TGFβR1 antibody or IgG isotype control for 90 min at 37°C with 5% CO_2. Subsequently, NK cells were stimulated with PMA/Ionomycin or human recombinant IL15 for 3 and 4 h, respectively before fixing with warm 4% PFA for imaging.

Measurement of Nuclear-Cytoplasmic Ratio

Confocal and SIM images obtained were analysed using ImageJ V2.0. The nuclear/cytosolic ratio was analysed as previously described (Elosegui-Artola et al., 2017), with slight modifications to accommodate to the smaller cytoplasmic areas in NK cells. CFSE-stained NK cells were identified in cocultures with lung/breast cancer cells at E (NK): T (cancer cell) ratio of 2.5 : 1. DAPI staining was used to identify the nucleus of NK cells. A Z-stacked image (step size 0.2 μm) encompassing the whole cell was obtained and the stacks demarcated by nuclear DAPI staining were Z-stacked for quantification of nuclear/cytoplasmic ratio. The DIC image, CFSE, DAPI, and T-bet/Eomes channels were then merged to demarcate, respectively, the cell cytoplasm (CFSE and DIC areas without DAPI stain), the nucleus (DAPI) and Eomes/Tbet. To avoid measurement of an ROI (Region on Interest) in the nucleus that exceeded the cytoplasmic ROI, the biggest possible ROI drawn in the cytosol next to the DAPI-stained nucleus was first measured. The same ROI was then shifted inside the nucleus to measure the mean intensity of Eomes/T-bet within the nucleus. The nuclear-cytoplasmic ratio was derived by dividing the nuclear intensity by cytosol intensity.

Quantification of Intracellular Protein Staining in NK cells

To quantify fluorescence intensity of proteins in NK cells, the cells were first identified as CFSE-positive cells (if NK cells were from cocultures) in confocal imaging. The median fluorescence intensity was quantified from an ROI which resembled the cell shape as demarcated by CFSE/DIC in the 488 nm laser/wide field channel. The ROI was then moved to an area without any cells to measure the median fluorescence intensity of the background. The final median intensity was measured as median fluorescence within the cell bound by the ROI minus that of the background. For quantification of pMLC2, the acquired pMLC2 median fluorescence intensity was divided by the median fluorescence intensity of total MLC2 and presented as 'Normalized pMLC2 median intensity against Total MLC2'. For the quantification of Eomes median fluorescence intensity, individual values were normalized to the mean value of control condition.

NSCLC Displacement/Migration Analysis

NCI-H1299 and NCI-H1975 NSCLCs were seeded on iBidi glass bottom dish at 10% confluency for 24 h before imaging. Mitomycin C (Sigma, Cat# M0503) was added to the media 1 h before imaging for cell migratory profiles. Nikon Biostation IMQ was used to capture migratory profiles of H1299 and H1975 NSCLCs using a ×20 objective. Images were captured at 10-min intervals over 8 h with cells incubated at 37 °C with 5% CO_2. ImageJ (RRID: RRID:SCR_003070) plugin 'Manual tracking' was used to capture individual cell movements. Displacement profile was generated using Matlab 2021b with in-house code.

Statistical Analysis

All graphs are presented as mean ± SEM. Statistical analysis was carried out using Prism 7.04 (GraphPad Software), with a p-value < 0.05 considered as significant. $^{*}p < 0.05$, $^{**}p < 0.01$, $^{***}p < 0.001$, $^{****}p < 0.0001$. Two-tailed Student's T-tests were used when two cases were compared, and analysis of variance (ANOVA) test was used when more cases were analysed. When data did not meet normality criteria, equivalent non-parametric tests were applied. For all experiments with hNK cells, results were obtained from biological repeats of at least three donors as indicated in the individual legends.

DATA AVAILABILITY STATEMENT

The original contributions presented in the study are included in the article/**Supplementary Material**, further inquiries can be directed to the corresponding author, upon reasonable request.

ETHICS STATEMENT

The studies involving human participants were reviewed and approved by Health Sciences Authority Singapore (HSA), under protocols approved by HSA and NUS Institutional Review Board

(201706-06 and H-17-028E). The patients/participants provided their written informed consent to participate in this study.

AUTHOR CONTRIBUTIONS

DW, EL, RK, OA, IY, and JX conducted the experiments; JE, BL, and JD provided advice and samples or reagents; DW, EL, JE, and JD designed the experiments and wrote the manuscript.

FUNDING

This project is supported by the National Research Foundation, Singapore, under its funding to NUS for RIE-Related Roles for the SGUnited Jobs Initiative (NRF-MP-2020-0004).

ACKNOWLEDGMENTS

We thank the core facilities of the Department of Biological Sciences (NUS), Confocal Microscopy Unit and Flow Cytometry Laboratory (NUS) and Mechanobiology Institute of Singapore, and Centre for BioImaging Sciences (NUS) for technical support. We thank M.X. Yao for advice and some reagents for the research. We thank H.T. Ong for providing in-house matlab code for cell displacement and trajectory analysis.

SUPPLEMENTARY MATERIAL

The Supplementary Material for this article can be found online at: https://www.frontiersin.org/articles/10.3389/fcell.2022.871326/full#supplementary-material

REFERENCES

Absi, A. Al., Wurzer, H., Guerin, C., Hoffmann, C., Moreau, F., Mao, X., et al. (2018). Actin Cytoskeleton Remodeling Drives Breast Cancer Cell Escape from Natural Killer-Mediated Cytotoxicity. *Cancer Res.* 78 (19), 5631–5643. doi:10.1158/0008-5472.can-18-0441

Alisafaei, F., Jokhun, D. S., Shivashankar, G. V., and Shenoy, V. B. (2019). Regulation of Nuclear Architecture, Mechanics, and Nucleocytoplasmic Shuttling of Epigenetic Factors by Cell Geometric Constraints. *Proc. Natl. Acad. Sci. U.S.A.* 116, 13200–13209. doi:10.1073/pnas.1902035116

Amano, M., Ito, M., Kimura, K., Fukata, Y., Chihara, K., Nakano, T., et al. (1996). Phosphorylation and Activation of Myosin by Rho-Associated Kinase (Rho-Kinase). *J. Biol. Chem.* 271, 20246–20249. doi:10.1074/jbc.271.34.20246

Amano, M., Nakayama, M., and Kaibuchi, K. (2010). Rho-kinase/ROCK: A Key Regulator of the Cytoskeleton and Cell Polarity. *Cytoskeleton* 67, 545–554. doi:10.1002/cm.20472

Araki, Y., Fann, M., Wersto, R., and Weng, N.-p. (2008). Histone Acetylation Facilitates Rapid and Robust Memory CD8 T Cell Response through Differential Expression of Effector Molecules (Eomesodermin and its Targets: Perforin and Granzyme B). *J. Immunol.* 180, 8102–8108. doi:10.4049/jimmunol.180.12.8102

Birukova, A. A., Adyshev, D., Gorshkov, B., Birukov, K. G., and Verin, A. D. (2005). ALK5 and Smad4 Are Involved in TGF-B1-Induced Pulmonary Endothelial Permeability. *FEBS Lett.* 579 (18), 4031–4037. doi:10.1016/j.febslet.2005.06.018

Brennan, J., Mager, D., Jefferies, W., and Takei, F. (1994). Expression of Different Members of the Ly-49 Gene Family Defines Distinct Natural Killer Cell Subsets and Cell Adhesion Properties. *J. Exp. Med.* 180, 2287–2295. doi:10.1084/jem.180.6.2287

Bros, M., Haas, K., Moll, L., and Grabbe, S. (2019). RhoA as a Key Regulator of Innate and Adaptive Immunity. *Cells* 8 (7), 733. doi:10.3390/cells8070733

Burgdorf, S., Porubsky, S., Marx, A., and Popovic, Z. V. (2020). Cancer Acidity and Hypertonicity Contribute to Dysfunction of Tumor-Associated Dendritic Cells: Potential Impact on Antigen Cross-Presentation Machinery. *Cancers (Basel)* 12, 1–13. doi:10.3390/cancers12092403

Carisey, A. F., Mace, E. M., Saeed, M. B., Davis, D. M., and Orange, J. S. (2018). Nanoscale Dynamism of Actin Enables Secretory Function in Cytolytic Cells. *Curr. Biol.* 28, 489–502. e9. doi:10.1016/j.cub.2017.12.044

Carisey, A., Tsang, R., Greiner, A. M., Nijenhuis, N., Heath, N., Nazgiewicz, A., et al. (2013). Vinculin Regulates the Recruitment and Release of Core Focal Adhesion Proteins in a Force-dependent Manner. *Curr. Biol.* 23 (4), 271–281. doi:10.1016/j.cub.2013.01.009

Carpen, O., Virtanen, I., and Saksela, E. (1982). Ultrastructure of Human Natural Killer Cells: Nature of the Cytolytic Contacts in Relation to Cellular Secretion. *J. Immunol.* 128, 2691–2697.

Chang, J. T., Ciocca, M. L., Kinjyo, I., Palanivel, V. R., McClurkin, C. E., DeJong, C. S., et al. (2011). Asymmetric Proteasome Segregation as a Mechanism for Unequal Partitioning of the Transcription Factor T-Bet during T Lymphocyte Division. *Immunity* 34 (4), 492–504. doi:10.1016/j.immuni.2011.03.017

Chauvin, J. M., and Zarour, H. M. (2020). TIGIT in Cancer Immunotherapy. *J. Immunother. Cancer* 8 (2), e000957. doi:10.1136/jitc-2020-000957

Duan, D., and Derynck, R. (2019). Transforming Growth Factor-β (TGF-B)-Induced Up-Regulation of TGF-β Receptors at the Cell Surface Amplifies the TGF-β Response. *J. Biol. Chem.* 294 (21), 8490–8504. doi:10.1074/jbc.ra118.005763

Elosegui-Artola, A., Andreu, I., Beedle, A. E. M., Lezamiz, A., Uroz, M., Kosmalska, A. J., et al. (2017). Force Triggers YAP Nuclear Entry by Regulating Transport across Nuclear Pores. *Cell* 171, 1397–1410. e14. doi:10.1016/j.cell.2017.10.008

Foltz, J. A., Moseman, J. E., Thakkar, A., Chakravarti, N., and Lee, D. A. (2018). Tgfβ Imprinting during Activation Promotes Natural Killer Cell Cytokine Hypersecretion. *Cancers (Basel)* 10 (11), 423. doi:10.3390/cancers10110423

Frutoso, M., and Mortier, E. (2019). NK Cell Hyporesponsiveness: More Is Not Always Better. *Int. J. Mol. Sci.* 20, 4514. doi:10.3390/ijms20184514

Gauthier, N. C., Fardin, M. A., Roca-Cusachs, P., and Sheetz, M. P. (2011). Temporary Increase in Plasma Membrane Tension Coordinates the Activation of Exocytosis and Contraction during Cell Spreading. *Proc. Natl. Acad. Sci. U.S.A.* 108, 14467–14472. doi:10.1073/pnas.1105845108

Gill, S., Vasey, A. E., De Souza, A., Baker, J., Smith, A. T., Kohrt, H. E., et al. (2012). Rapid Development of Exhaustion and Down-Regulation of Eomesodermin Limit the Antitumor Activity of Adoptively Transferred Murine Natural Killer Cells. *Blood* 119, 5758–5768. doi:10.1182/blood-2012-03-415364

Gladilin, E., Ohse, S., Boerries, M., Busch, H., Xu, C., Schneider, M., et al. (2019). Tgfβ-Induced Cytoskeletal Remodeling Mediates Elevation of Cell Stiffness and Invasiveness in NSCLC. *Sci. Rep.* 9, 7667. doi:10.1038/s41598-019-43409-x

Gonano, L. A., Morell, M., Burgos, J. I., Dulce, R. A., De Giusti, V. C., Aiello, E. A., et al. (2014). Hypotonic Swelling Promotes Nitric Oxide Release in Cardiac Ventricular Myocytes: Impact on Swelling-Induced Negative Inotropic Effect. *Cardiovasc. Res.* 104, 456–466. doi:10.1093/cvr/cvu230

Guan, Y.-f., Chen, R.-h., Wang, P., Qin, Y., Su, D.-f., and Miao, C.-y. (2007). Hypertonic and Isotonic Potassium Solutions Have Different Effects on Vessel Contractility Resulting in Differences in Optimal Resting Tension in Rat Aorta. *Acta Pharmacol. Sin.* 28, 643–650. doi:10.1111/j.1745-7254.2007.00548.x

Guilluy, C., Osborne, L. D., Van Landeghem, L., Sharek, L., Superfine, R., Garcia-Mata, R., et al. (2014). Isolated Nuclei Adapt to Force and Reveal a Mechanotransduction Pathway in the Nucleus. *Nat. Cell Biol.* 16, 376–381. doi:10.1038/ncb2927

Hara, Y., Shagirov, M., and Toyama, Y. (2016). Cell Boundary Elongation by Non-autonomous Contractility in Cell Oscillation. *Curr. Biol.* 26 (17), 2388–2396. doi:10.1016/j.cub.2016.07.003

Hawke, L. G., Mitchell, B. Z., and Ormiston, M. L. (2020). TGF-β and IL-15 Synergize through MAPK Pathways to Drive the Conversion of Human NK Cells to an Innate Lymphoid Cell 1–like Phenotype. *J. Immunol.* 204 (12), 3171–3181. doi:10.4049/jimmunol.1900866

Heasman, S. J., and Ridley, A. J. (2010). Multiple Roles for RhoA during T Cell Transendothelial Migration. *Small GTPases* 1, 174. doi:10.4161/sgtp.1.3.14724

Hodge, R. G., and Ridley, A. J. (2016). Regulating Rho GTPases and Their Regulators. *Nat. Rev. Mol. Cell Biol.* 17 (8), 496–510. doi:10.1038/nrm.2016.67

Holder, K. A., and Grant, M. D. (2020). TIGIT Blockade: A Multipronged Approach to Target the HIV Reservoir. *Front. Cell. Infect. Microbiol.* 10, 175. doi:10.3389/fcimb.2020.00175

Jankowska, K. I., Williamson, E. K., Roy, N. H., Blumenthal, D., Chandra, V., Baumgart, T., et al. (2018). Integrins Modulate T Cell Receptor Signaling by Constraining Actin Flow at the Immunological Synapse. *Front. Immunol.* 1, 1. doi:10.3389/fimmu.2018.00025

Krzewski, K., Chen, X., Orange, J. S., and Strominger, J. L. (2006). Formation of a WIP-, WASp-, Actin-, and Myosin IIA-Containing Multiprotein Complex in Activated NK Cells and its Alteration by KIR Inhibitory Signaling. *J. Cell Biol.* 173, 121–132. doi:10.1083/jcb.200509076

Kurtulus, S., Sakuishi, K., Ngiow, S. F., Joller, N., Tan, D. J., Teng, M. W. L., et al. (2015). TIGIT Predominantly Regulates the Immune Response via Regulatory T Cells. *J. Clin. Invest.* 125 (11), 4053–4062. doi:10.1172/jci81187

Lee, E. H. C., Wong, D. C. P., and Ding, J. L. (2021). NK Cells in a Tug-Of-War with Cancer: The Roles of Transcription Factors and Cytoskeleton. *Front. Immunol.* 12, 1–15. doi:10.3389/fimmu.2021.734551

Li, J., Shen, C., Wang, X., Lai, Y., Zhou, K., Li, P., et al. (2019). Prognostic Value of TGF-β in Lung Cancer: Systematic Review and Meta-Analysis. *BMC Cancer* 19, 691. doi:10.1186/s12885-019-5917-5

Li, Z., Li, M., Shi, S. X., Yao, N., Cheng, X., Guo, A., et al. (2020). Brain Transforms Natural Killer Cells that Exacerbate Brain Edema after Intracerebral Hemorrhage. *J. Exp. Med.* 217 (12), e20200213. doi:10.1084/jem.20200213

Lombardi, M. L., Jaalouk, D. E., Shanahan, C. M., Burke, B., Roux, K. J., and Lammerding, J. (2011). The Interaction between Nesprins and Sun Proteins at the Nuclear Envelope Is Critical for Force Transmission between the Nucleus and Cytoskeleton. *J. Biol. Chem.* 286, 26743–26753. doi:10.1074/jbc.m111.233700

Malek, A. M., Xu, C., Kim, E. S., and Alper, S. L. (2007). Hypertonicity Triggers RhoA-dependent Assembly of Myosin-Containing Striated Polygonal Actin Networks in Endothelial Cells. *Am. J. Physiol. Cell Physiol.* 292, C1645–C1659. doi:10.1152/ajpcell.00533.2006

Matalon, O., Ben-Shmuel, A., Kivelevitz, J., Sabag, B., Fried, S., Joseph, N., et al. (2018). Actin Retrograde Flow Controls Natural Killer Cell Response by Regulating the Conformation State of SHP-1. *EMBO J.* 37, e96264. doi:10.15252/embj.201696264

McLane, L. M., Ngiow, S. F., Chen, Z., Attanasio, J., Manne, S., Ruthel, G., et al. (2021). Role of Nuclear Localization in the Regulation and Function of T-Bet and Eomes in Exhausted CD8 T Cells. *Cell Rep.* 35, 109120. doi:10.1016/j.celrep.2021.109120

McLane, L. M., Banerjee, P. P., Cosma, G. L., Makedonas, G., Wherry, E. J., Orange, J. S., et al. (2013). Differential Localization of T-Bet and Eomes in CD8 T Cell Memory Populations. *J. I.* 190, 3207–3215. doi:10.4049/jimmunol.1201556

Meijering, E., Dzyubachyk, O., and Smal, I. (2012). "Methods for Cell and Particle Tracking," in *Methods in Enzymology*. doi:10.1016/b978-0-12-391857-4.00009-4

Mitchell, H., Choudhury, A., Pagano, R. E., and Leof, E. B. (2004). Ligand-dependent and -independent Transforming Growth Factor-β Receptor Recycling Regulated by Clathrin-Mediated Endocytosis and Rab11. *Mol. Biol. Cell* 8, 25. doi:10.1091/mbc.e04-03-0245

Nakamura, S., Kuroki, K., Ohki, I., Sasaki, K., Kajikawa, M., Maruyama, T., et al. (2009). Molecular Basis for E-Cadherin Recognition by Killer Cell Lectin-like Receptor G1 (KLRG1). *J. Biol. Chem.* 284, 27327–27335. doi:10.1074/jbc.m109.038802

Narumiya, S., and Thumkeo, D. (2018). Rho Signaling Research: History, Current Status and Future Directions. *FEBS Lett.* 592, 1763–1776. doi:10.1002/1873-3468.13087

Ojiaku, C. A., Cao, G., Zhu, W., Yoo, E. J., Shumyatcher, M., Himes, B. E., et al. (2018). TGF-β1 Evokes Human Airway Smooth Muscle Cell Shortening and Hyperresponsiveness via Smad3. *Am. J. Respir. Cell Mol. Biol.* 58, 575–584. doi:10.1165/rcmb.2017-0247oc

Pan, M., Chew, T. W., Wong, D. C. P., Xiao, J., Ong, H. T., Chin, J. F. L., et al. (2020). BNIP-2 Retards Breast Cancer Cell Migration by Coupling Microtubule-Mediated GEF-H1 and RhoA Activation. *Sci. Adv.* 6, eaaz1534–14. doi:10.1126/sciadv.aaz1534

Papaioannou, V. E. (2014). The T-Box Gene Family: Emerging Roles in Development, Stem Cells and Cancer. *Dev* 141, 3819–3833. doi:10.1242/dev.104471

Pertz, O. (2010). Spatio-temporal Rho GTPase Signaling - where Are We Now? *J. Cell Sci.* 123 (Pt 11), 1841–1850. doi:10.1242/jcs.064345

Peters, C., Meyer, A., Kouakanou, L., Feder, J., Schricker, T., Lettau, M., et al. (2019). TGF-β Enhances the Cytotoxic Activity of Vδ2 T Cells. *Oncoimmunology* 8, e1522471. doi:10.1080/2162402X.2018.1522471

Pirkle, J. C., and Gann, D. S. (1976). Restitution of Blood Volume after Hemorrhage: Role of the Adrenal Cortex. *Am. J. Physiol.* 230 (6), 1683–1687. doi:10.1152/ajplegacy.1976.230.6.1683

Pradier, A., Simonetta, F., Waldvogel, S., Bosshard, C., Tiercy, J. M., and Roosnek, E. (2016). Modulation of T-Bet and Eomes during Maturation of Peripheral Blood NK Cells Does Not Depend on Licensing/educating KIR. *Front. Immunol.* 7, 299. doi:10.3389/fimmu.2016.00299

Ridley, A. J. (2001). Rho GTPases and Cell Migration. *J. Cell Sci.* 114, 2713–2722. doi:10.1242/jcs.114.15.2713

Russick, J., Joubert, P. E., Gillard-Bocquet, M., Torset, C., Meylan, M., Petitprez, F., et al. (2020). Natural Killer Cells in the Human Lung Tumor Microenvironment Display Immune Inhibitory Functions. *J. Immunother. Cancer* 8 (2), e001054. doi:10.1136/jitc-2020-001054

Saitakis, M., Dogniaux, S., Goudot, C., Bufi, N., Asnacios, S., Maurin, M., et al. (2017). Different TCR-Induced T Lymphocyte Responses Are Potentiated by Stiffness with Variable Sensitivity. *Elife* 6, e23190. doi:10.7554/eLife.23190

Santoni, G., Amantini, C., Santoni, M., Maggi, F., Morelli, M. B., and Santoni, A. (2021). Mechanosensation and Mechanotransduction in Natural Killer Cells. *Front. Immunol.* 12, 688918. doi:10.3389/fimmu.2021.688918

Shen, M., Zhao, X., Zhao, L., Shi, L., An, S., Huang, G., et al. (2018). Met Is Involved in TIGAR-Regulated Metastasis of Non-small-cell Lung Cancer. *Mol. Cancer* 17, 88. doi:10.1186/s12943-018-0839-4

Simonetta, F., Pradier, A., and Roosnek, E. (2016). T-bet and Eomesodermin in NK Cell Development, Maturation, and Function. *Front. Immunol.* 7, 241. doi:10.3389/fimmu.2016.00241

Sirtl, S., Knoll, G., Trinh, D. T., Lang, I., Siegmund, D., Gross, S., et al. (2018). Hypertonicity-enforced BCL-2 Addiction Unleashes the Cytotoxic Potential of Death Receptors. *Oncogene* 37, 4122–4136. doi:10.1038/s41388-018-0265-5

Stabile, H., Fionda, C., Gismondi, A., and Santoni, A. (2017). Role of Distinct Natural Killer Cell Subsets in Anticancer Response. *Front. Immunol.* 8, 293. doi:10.3389/fimmu.2017.00293

Thompson, T. W., Kim, A. B., Li, P. J., Wang, J., Jackson, B. T., Huang, K. T. H., et al. (2017). Endothelial Cells Express NKG2D Ligands and Desensitize Antitumor NK Responses. *Elife* 6, e30881. doi:10.7554/elife.30881

Verma, R., Er, J. Z., Pu, R. W., Sheik Mohamed, J., Soo, R. A., Muthiah, H. M., et al. (2020). Eomes Expression Defines Group 1 Innate Lymphoid Cells during Metastasis in Human and Mouse. *Front. Immunol.* 11, 1190. doi:10.3389/fimmu.2020.01190

Viel, S., Marçais, A., Guimaraes, F. S., Loftus, R., Rabilloud, J., Grau, M., et al. (2016). TGF-β Inhibits the Activation and Functions of NK Cells by Repressing the mTOR Pathway. *Sci. Signal.* 9, ra19. doi:10.1126/scisignal.aad1884

Wagner, J. A., Wong, P., Schappe, T., Berrien-Elliott, M. M., Cubitt, C., Jaeger, N., et al. (2020). Stage-Specific Requirement for Eomes in Mature NK Cell Homeostasis and Cytotoxicity. *Cell Rep.* 31, 107720. doi:10.1016/j.celrep.2020.107720

Weder, N., Zhang, H., Jensen, K., Yang, B. Z., Simen, A., Jackowski, A., et al. (2014). Child Abuse, Depression, and Methylation in Genes Involved with Stress, Neural Plasticity, and Brain Circuitry. *J. Am. Acad. Child. Adolesc. Psychiatry* 53, 417–e5. doi:10.1016/j.jaac.2013.12.025

Wu, S. K., Lagendijk, A. K., Hogan, B. M., Gomez, G. A., and Yap, A. S. (2015). Active Contractility at E-Cadherin Junctions and its Implications for Cell Extrusion in Cancer. *Cell Cycle* 14, 315–322. doi:10.4161/15384101.2014.989127

Wurzer, H., Hoffmann, C., Al Absi, A., and Thomas, C. (2019). Actin Cytoskeleton Straddling the Immunological Synapse between Cytotoxic Lymphocytes and Cancer Cells. *Cells* 8, 463. doi:10.3390/cells8050463

Xiong, P., Sang, H.-W., and Zhu, M. (2015). Critical Roles of Co-activation Receptor DNAX Accessory Molecule-1 in Natural Killer Cell Immunity. *Immunology* 146, 369–378. doi:10.1111/imm.12516

Yamashiro, S., Tanaka, S., McMillen, L. M., Taniguchi, D., Vavylonis, D., and Watanabe, N. (2018). Myosin-dependent Actin Stabilization as Revealed by Single-Molecule Imaging of Actin Turnover. *MBoC* 29, 1941–1947. doi:10.1091/mbc.e18-01-0061

Yao, M., Goult, B. T., Klapholz, B., Hu, X., Toseland, C. P., Guo, Y., et al. (2016). The Mechanical Response of Talin. *Nat. Commun.* 7, 11966. doi:10.1038/ncomms11966

Ye, Y., Liu, S., Wu, C., and Sun, Z. (2015). TGFβ Modulates Inflammatory Cytokines and Growth Factors to Create Premetastatic Microenvironment and Stimulate Lung Metastasis. *J. Mol. Hist.* 46, 365–375. doi:10.1007/s10735-015-9633-4

Yu, L., Liu, X., Wang, X., Yan, F., Wang, P., Jiang, Y., et al. (2021). TIGIT+ TIM-3+ NK Cells Are Correlated with NK Cell Exhaustion and Disease Progression in Patients with Hepatitis B Virus-Related Hepatocellular Carcinoma. *Oncoimmunology* 10, 1942673. doi:10.1080/2162402x.2021.1942673

Zaiatz-Bittencourt, V., Finlay, D. K., and Gardiner, C. M. (2018). Canonical TGF-β Signaling Pathway Represses Human NK Cell Metabolism. *J. I.* 200, 3934–3941. doi:10.4049/jimmunol.1701461

Zhang, J., Le Gras, S., Pouxvielh, K., Faure, F., Fallone, L., Kern, N., et al. (2021). Sequential Actions of EOMES and T-BET Promote Stepwise Maturation of Natural Killer Cells. *Nat. Commun.* 1, 1. doi:10.1038/s41467-021-25758-2

Zhang, J., Marotel, M., Fauteux-Daniel, S., Mathieu, A.-L., Viel, S., Marçais, A., et al. (2018). T-bet and Eomes Govern Differentiation and Function of Mouse and Human NK Cells and ILC1. *Eur. J. Immunol.* 48, 738–750. doi:10.1002/eji.201747299

Zhang, X., Kim, T. H., Thauland, T. J., Li, H., Majedi, F. S., Ly, C., et al. (2020). Unraveling the Mechanobiology of Immune Cells. *Curr. Opin. Biotechnol.* 1, 1. doi:10.1016/j.copbio.2020.09.004

Conflict of Interest: The authors declare that the research was conducted in the absence of any commercial or financial relationships that could be construed as a potential conflict of interest.

Publisher's Note: All claims expressed in this article are solely those of the authors and do not necessarily represent those of their affiliated organizations, or those of the publisher, the editors and the reviewers. Any product that may be evaluated in this article, or claim that may be made by its manufacturer, is not guaranteed or endorsed by the publisher.

frontiers | Frontiers in Cell and Developmental Biology

MINI REVIEW
published: 23 May 2022
doi: 10.3389/fcell.2022.864522

Emerging Role of Mechanical Forces in Cell Fate Acquisition

Yanina Alvarez and Michael Smutny**

Centre for Mechanochemical Cell Biology and Division of Biomedical Sciences, Warwick Medical School, University of Warwick, Coventry, United Kingdom

Mechanical forces are now recognized as key cellular effectors that together with genetic and cellular signals physically shape and pattern tissues and organs during development. Increasing efforts are aimed toward understanding the less explored role of mechanical forces in controlling cell fate decisions in embryonic development. Here we discuss recent examples of how differential forces feedback into cell fate specification and tissue patterning. In particular, we focus on the role of actomyosin-contractile force generation and transduction in affecting tissue morphogenesis and cell fate regulation in the embryo.

Keywords: mechanical forces, cell fate acquisition, morphogenesis, embryonic development, patterning, actomyosin

OPEN ACCESS

Edited by:
Anne Karine Lagendijk,
University of Queensland, Australia

Reviewed by:
René-Marc Mège,
Centre National de la Recherche Scientifique (CNRS), France
Vivian Tang,
University of Illinois at Urbana-Champaign, United States
Akankshi Munjal,
School of Medicine, Duke University, United States
Yusuke Toyama,
National University of Singapore, Singapore

****Correspondence:***
Yanina Alvarez
Yanina.Alvarez@warwick.ac.uk
Michael Smutny
michael.smutny@warwick.ac.uk

Specialty section:
This article was submitted to Cell Adhesion and Migration, a section of the journal Frontiers in Cell and Developmental Biology

Received: *28 January 2022*
Accepted: *07 April 2022*
Published: *23 May 2022*

Citation:
Alvarez Y and Smutny M (2022) Emerging Role of Mechanical Forces in Cell Fate Acquisition. Front. Cell Dev. Biol. 10:864522. doi: 10.3389/fcell.2022.864522

INTRODUCTION

A complex interplay between biochemical and physical events on multiple lengths and time scales regulates the formation of tissues and organs during embryonic development. Mechanical forces are now recognized as central players in tissue morphogenesis that drive changes in cell shape, size, proliferation, and movement (Heisenberg and Bellaiche, 2013; Mammoto et al., 2013). These processes rely on dynamic feedback of mechanochemical signals whereby forces are transduced into biochemical signals which in turn control mechanical mechanisms (Hannezo and Heisenberg, 2019; Collinet and Lecuit, 2021). Forces that lead to changes in cell form and function can either be intracellularly generated by contractile actomyosin networks or extrinsically received from the surrounding microenvironment through cell adhesive complexes (cell-cell or cell-extracellular matrix (ECM) receptors) (Lecuit et al., 2011; Heisenberg and Bellaiche, 2013; Mammoto et al., 2013; Vining and Mooney, 2017; Goodwin and Nelson, 2021). Further, cells can also respond to stresses from changes in hydrostatic or hydraulic fluid pressure as observed during early embryonic development (Dumortier et al., 2019; Mosaliganti et al., 2019). Coordination and transmission of mechanical forces allow cells to change shape and position, thereby producing morphogenetic changes at the tissue and organ level.

A crucial event during early embryonic development is the establishment of different cell identities (fates) for specialized function and patterning of tissues and organs. Numerous studies have now established the view that large-scale patterning is achieved by short- or long-range morphogen signaling in tissues in a dose-dependent manner, thereby controlling local activation of transcription factors and modulation of gene expression to determine cell fate (Gilmour et al., 2017). Apart from genetic control of tissue patterning, recent studies highlight a significant role for mechanical forces in cell fate specification, adding another distinct layer of control over cell fate decision making (Mammoto et al., 2011; Brunet et al., 2013; Gordon et al., 2015). Forces generated inside the cell, modulating cell contractility and mechanics (Samarage et al., 2015; Le et al., 2016; Maitre et al., 2016; Mitrossilis et al., 2017) as well as stresses outside the cell such as those produced

through hydrostatic pressure can impact on cell fate regulation and tissue patterning (Planas-Paz et al., 2012; Chan et al., 2019). Notably, mechanical signaling through cell–cell and cell–ECM adhesions seems to play a significant role in the interplay between forces and cell fate specification (Martin-Bermudo, 2000; Kuriyama and Mayor, 2009; Maître et al., 2012; Taylor-Weiner et al., 2015; Steed et al., 2016; Barone et al., 2017). Given the multitude of forces present during tissue morphogenesis and the numerous mechanosensitive proteins that can potentially affect cell fate decisions, a major challenge is to delineate which force inputs and which specific effectors are functionally relevant to control cell fate.

In the following chapters, we will briefly discuss the relationship between forces and cell fate and their consequences for tissue and organ development on the basis of recent discoveries in the field with a specific focus on two processes during vertebrate development that serve as excellent model systems of how contractility can control cell fate decisions.

Feedback Between Cell Fate and Mechanical Forces

The link between forces and cell fate specification is essential for understanding the underlying mechanisms that regulate robust tissue patterning during development (Gilmour et al., 2017). Identifying the mechanical pathways that are responsible for cell fate specification requires quantitative force measurements which are often intricate to accomplish in the embryo. Hence, key findings originate from studies using cultured cells that enable better access and control to investigate the contribution of mechanical signals to changes in cell behavior (Engler et al., 2006; Astudillo, 2020; Petzold and Gentleman, 2021). Such findings revealed, for example, that environmental mechanical cues such as matrix stiffness are key modulators of embryonic stem cell (ESC) differentiation (Engler et al., 2006; McBride and Knothe Tate, 2008; Huebsch et al., 2010; El-Mohri et al., 2017). Furthermore, actomyosin contractility and membrane tension have been shown to guide cell fate and patterning (Fu et al., 2010; Bergert et al., 2021; De Belly et al., 2021), indicating that cortex and membrane tension can actively contribute to cell fate decisions. However, given the precise spatiotemporally controlled biochemical and physical signals together with geometric cues in the embryo, recent studies highlight the need to investigate functional relationships between force and cell fate *in vivo* (Yang et al., 2000; Hove et al., 2003; Desprat et al., 2008; Adamo et al., 2009; Barone et al., 2017).

Notably, mechanical forces controlling cell fate is not a strictly unidirectional pathway. Cell fate can feedback into cytoskeletal tension generation, and this regulatory loop appears to be crucial for robust morphogenesis during development. This typically includes cell–cell adhesion complexes which relay physical signals between cells and are therefore an integral part for integrating mechanosensitive responses at the tissue level. For example, a positive feedback loop between cell–cell contact duration, morphogen signaling, and mesendoderm cell fate specification was observed during early zebrafish gastrulation (Barone et al., 2017). Moreover, compressive forces by the global extension of

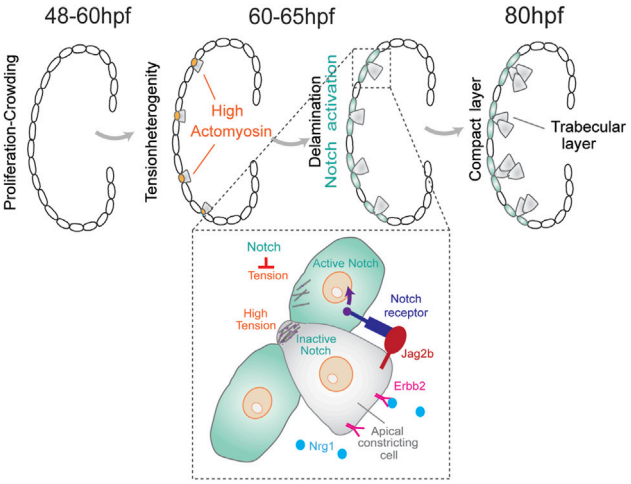

FIGURE 1 | During cardiac trabeculation in zebrafish (between 60 and 65 hpf), proliferation-induced crowding leads to tension heterogeneity in cardiomyocytes. CMs with higher tension constrict their apical domain and delaminate to seed the trabecular layer. This delamination triggers activation of Notch signaling in adjacent compact layer CMs, thereby establishing a distinct CM fate for these two layers. The coordination between Notch and Erbb2 pathways between neighboring cells produces a distinctive pattern of cell shape and fate for the trabecular and compact layer formation.

the germband in *Drosophila* were shown to generate a stretching of the β-catenin-E-cadherin binding site, resulting in the expression of β-catenin target genes including the mesodermal marker *twist* (Desprat et al., 2008). In turn, Twist can control the expression of upstream regulators of actomyosin contractility such as the activation of the Rho-family GTPase RhoGEF2 (Leptin, 1991; Dawes-Hoang et al., 2005; Kolsch et al., 2007; Sandmann et al., 2007). Other known examples of feedback loops between forces and cell fate come from processes regulated by effectors of the Hippo signaling pathway that control organ size during development. Here, the transcriptional co-activator proteins YAP (Yes-associated protein 1) and TAZ (transcriptional coactivator with PDZ-binding motif) are associated with cell proliferation and fate specification and can mechanically be controlled by extracellular matrix rigidity and cell shape (Dupont et al., 2011; Elosegui-Artola et al., 2017). For instance, recent work elegantly demonstrated that cell specification of the micropyle precursor cell (MPC) within the follicular epithelium during zebrafish oogenesis is controlled by nuclear translocation of TAZ (Xia et al., 2019). TAZ triggers massive growth of the MPC, which leads to mechanical compression and deformation of its neighboring cells and, consequently, the depletion of nuclear TAZ in these cells. This lateral inhibition mechanism triggers a positive feedback loop, facilitating TAZ-dependent growth of the dominant cell while at the same time limiting growth in the surrounding cells (Xia et al., 2019).

In the next chapters, we will discuss recent findings on how actomyosin anisotropies can lead to different cell fates during embryogenesis with a particular focus on early heart development in zebrafish and first lineage segregation in the mouse.

Trabeculation During Zebrafish Heart Development

Heart development in vertebrates undergoes complex morphogenetic transformations during cardiac trabeculation, a process where sheet-like muscular structures form as a result of cardiomyocytes' extrusion and expansion into the lumen of the ventricular chambers (Staudt and Stainier, 2012). Although the zebrafish heart has only two chambers instead of four as the mammalian counterpart, the major components are conserved and similar cellular and molecular pathways are implicated during heart development (Moorman and Christoffels, 2003). In zebrafish, the myocardium transforms from a monolayer at 48 h post-fertilization (hpf) to a complex three-dimensional (3D) structure that consists of two cell types: the outer compact layer (CL) cardiomyocytes encircling the inner trabecular layer (TL) cardiomyocytes (**Figure 1**). The Notch signaling pathway has been reported to play an important role in fate specification during trabecular morphogenesis (Samsa et al., 2015). A zebrafish line with a Notch reporter from the Epstein–Barr virus terminal protein 1 (TP1) gene was utilized to study cell fate specification during trabecular morphogenesis. Notch reporter TP1 was shown to be activated in CL cardiomyocytes but not in TL cardiomyocytes (Han et al., 2016; Jimenez-Amilburu et al., 2016). Moreover, abrogating myocardial Notch led to ectopic trabeculation (Han et al., 2016). In mouse embryos, however, Notch signaling activation is essential for ventricular trabeculation initiation, but the inactivation of myocardial Notch does not affect heart development (Grego-Bessa et al., 2007; Salguero-Jimenez et al., 2018), which points to differences in Notch-dependent regulation of heart development across species. In zebrafish, differential myocardial fate requires binding of epidermal growth factor neuregulin 1 (Ngr1) to Erb-B2 receptor tyrosine kinase 2 (Erbb2) which leads to its phosphorylation and downstream signaling (Han et al., 2016). Endocardial Nrg1 activates myocardial Erbb2 signaling, which triggers the expression of the Notch receptor ligand, Jag2b. In turn, Jag2b activates Notch signaling in neighboring cardiomyocytes, which inhibits Erbb2 expression. This regulatory feedback mechanism prevents excessive cell internalization of the embryonic outer cell layer to generate a distinctive morphology and fate during early heart development (**Figure 1**).

A recent study discovered that cardiomyocytes with higher contractility delaminate even in the absence of the Nrg–Erbb2 pathway (Priya et al., 2020). In this model, tissue crowding induces local differences in cell shape and tension to initiate cardiomyocytes with higher contractility to segregate by apical constriction. Moreover, changes in actomyosin contractility were shown to be sufficient to trigger differential apicobasal polarity and fate (Priya et al., 2020). This hypothesis is based on the fact that myocardial Notch reporter expression correlates with the apical surface area of cardiomyocytes. Apical domain length quantifications showed that cells with higher expression levels of TP1 in the CL layer have larger apical domains than those in delaminating cardiomyocytes (Priya et al., 2020). Lastly, myocardial wall patterning was postulated to rely on a Notch signaling feedback pathway. In particular, Notch signaling is activated in neighboring CL cardiomyocytes which suppresses the actomyosin machinery in these cells and limits excessive delamination (**Figure 1**). The mechanism for the Notch-mediated lateral inhibition is still unknown, but a model considering contact area dependence predicts that smaller cells are more likely to be selected by the lateral inhibition process than larger cells (Shaya and Sprinzak, 2011).

Although major advances in understanding heart morphogenesis have been achieved, high-resolution 3D imaging of beating hearts during developmental stages remains challenging. Recent advances in live imaging of a developing mouse heart coupled with computational segmentation accomplished precise tracking of cell fate decisions during embryonic development (Yue et al., 2020). This is a crucial first step in modeling heart morphogenesis at a single-cell resolution in order to enhance our understanding of heart development.

First Lineage Segregation in Mouse Embryos

During the preimplantation stages of mammalian embryonic development, cells of the embryo physically segregate into the pluripotent inner cell mass (ICM), which contains the precursors for all cells in the body, and the outer trophectoderm (TE) layer that will form the placenta (White et al., 2018). In the mouse embryo, this lineage segregation starts after the 8-cell stage. It has been suggested that asymmetric cell divisions are the main mechanism to ensure ICM formation (Yamanaka et al., 2006; Zernicka-Goetz et al., 2009). However, asymmetric divisions are infrequent, and the first inner cells originate primarily from cell internalization events. During this process, blastomeres divide with tilted angles, and one daughter internalizes gradually via cortical tension-dependent apical constriction (Samarage et al., 2015) (**Figure 2**). Apicobasal polarity and Hippo signaling are believed to be the key molecular mechanisms by which outer and inner cells control their fate (Plusa et al., 2005; Sasaki, 2017; White et al., 2018). The establishment of apical polarity by Par-aPKC components in the outer (polar) cells was shown to promote the nuclear localization of YAP, which upregulates the expression of Cdx2, a transcription factor essential for TE-fate maturation (Strumpf et al., 2005; Ralston and Rossant, 2008). In contrast, inner (apolar) cells lack apical polarity and YAP remains cytoplasmic through phosphorylation by the Hippo signaling pathway component Lats. Cytoplasmic YAP fails to activate homeobox transcription factor Cdx2 expression to promote a pluripotent fate (Nishioka et al., 2009; Sasaki 2017). Yet, it is unclear when YAP and Cdx2 start to be differentially regulated during inner-outer segregation (Hirate et al., 2015; Sasaki 2017). Recent reports indicate that the F-actin-rich apical domain might be asymmetrically inherited during cell division to differentially control YAP and Cdx2 (Maitre et al., 2016; Korotkevich et al., 2017). According to this model, segregation of the apical domain generates both polarized and unpolarized blastomeres, which are defined by the different levels of apical aPKC and myosin 2. Unpolarized cells showed higher cortical levels of myosin 2 than polarized ones, and the differences

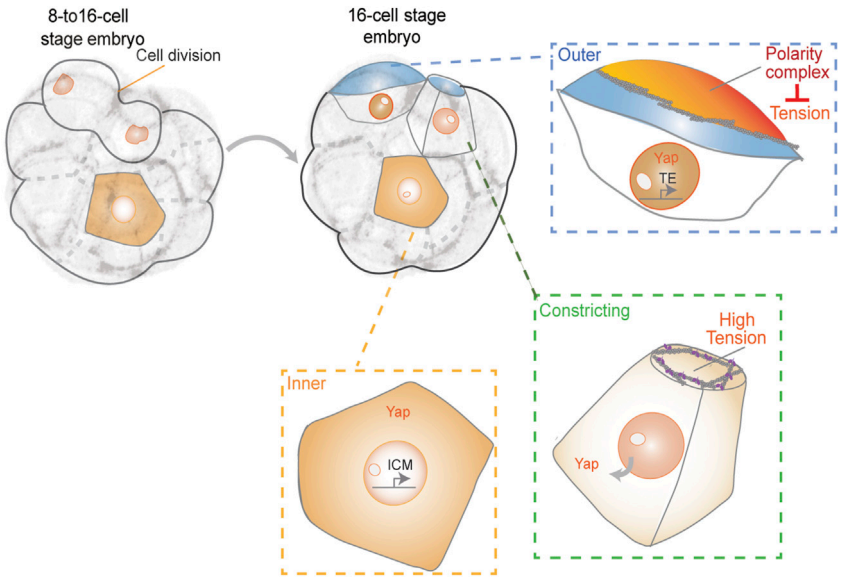

FIGURE 2 | First lineage segregation during 8- to 16-cell transition. The resulting daughter cells show differences in polarity, contractility, and exposed surface area. Together, these properties may control cell fate acquisition, resulting in appropriate partitioning of ICM and TE cells during patterning of the blastocyst.

in contractility determined their sorting into inner and outer positions (Maitre et al., 2016). Polar daughter cells that inherited the apical domain displayed lower contractility and remained in the outer position whereas apolar cells internalized.

Furthermore, by using a reduced system in which two blastomeres are isolated from a 16-cell stage embryo, it was shown that the apical domain recruits a spindle pole to ensure its differential distribution upon division (Korotkevich et al., 2017). According to this model, the inheritance of the apical domain is sufficient for the daughter cell to adopt TE fate. In contrast to this model, the apical domain seems to disassemble when blastomeres divide before being re-established *de novo* after cytokinesis (Zenker et al., 2018). These results demonstrate that polarity establishment does not occur immediately after division. In agreement with these observations, it was recently reported that keratins form long-lived filaments that become asymmetrically retained by outer daughter cells. Keratin filaments may stabilize the cortex to promote the subsequent establishment of apical Par-aPKC components (Lim et al., 2020). Despite direct links between the Hippo pathway and F-actin (Leung and Zernicka-Goetz 2013; Sasaki 2017), the direct role of actomyosin-generated tension in controlling cell fate during early mouse embryonic development remains unclear. Yet, the observation that cortical contractility causes blastomeres to become inner cell-like with respect to phosphorylated YAP localization and Cdx2 levels and independent of their external position, favors such an idea (Maitre et al., 2016). These results suggest the possibility that YAP may sense cortical tension independently of apical polarity. Moreover, in a recent work, a correlation between levels of nuclear YAP and the proportion of the exposed apical surface area of each blastomere at the 16-cell stage was observed (Royer et al., 2020). This suggests that cells may sense the proportion of their surface area exposed and signal to the nucleus by modulating the subcellular localization of YAP. The authors suggested a possible feedback loop between apical cell surface area and YAP localization. Certain cells that exhibited a lower proportion of exposed surface area after cell divisions from 8- to 16-cell stage, displayed lower nuclear YAP levels and subsequently internalized (Royer et al., 2020). However, the precise underlying mechanisms of regulation remain unclear and future studies will be needed to gain a complete understanding of this process.

DISCUSSION

Understanding the crosstalk between cell- and tissue-scale mechanics and cell fate specification is essential to uncover the key mechanisms that regulate robust tissue patterning during development. Mechanical forces are now recognized as essential control mechanisms for tissue integrity and function by regulating cellular processes such as tension, polarity, and adhesion during development. In this mini-review, we revisited recent studies that illustrate the impact of forces on cell-fate specification during embryonic development with a particular focus on zebrafish heart development and first lineage segregation in the mouse. Notably, the establishment of force anisotropies seems to be a conserved feature in both systems to drive changes in cell identities and suggests that local differences in cell shape and contractility might be a more general mechanism in mechanical regulation of cell fate across various species. In this regard, it will also be critical to identify mechanosensitive proteins and their specific contribution to cell fate changes

such as mechanosensitive ion channels at the plasma membrane including TRP (Liu and Montell, 2015) and Piezo1 (Ridone et al., 2019), or mechanoresponsive proteins at cell adhesion sites such as α-catenin and vinculin.

Moreover, recent work revealed that mechanical forces also impact nuclear morphology and processes within the nucleus (Kirby and Lammerding, 2018; Lomakin et al., 2020; Venturini et al., 2020). Nuclear responses to mechanical force include adaptations in chromatin architecture and transcriptional activity that trigger changes in cell state (Hampoelz and Lecuit, 2011). These force-driven changes also influence the mechanical properties of chromatin and nuclei themselves to prevent aberrant alterations in nuclear shape and maintain genome integrity (Uhler and Shivashankar 2017). Linking cell and nuclear mechanics to events directly controlling gene expression involved in cell-fate specification will be an important endeavor for future studies to completely understand developmental programs.

AUTHOR CONTRIBUTIONS

YA and MS wrote the manuscript. YA made figures.

FUNDING

YA is supported by a BBSRC research grant (BB/T016493/1). MS is supported by the Quantitative Biomedicine Program (QBP) funded by the Wellcome Trust Institutional Strategic Support Fund (ISSF) and a BBSRC research grant (BB/T016493/1).

ACKNOWLEDGMENTS

The authors apologize for any omissions due to space limitations. We thank the members of our lab for critical discussions and reading of the manuscript.

REFERENCES

Adamo, L., Naveiras, O., Wenzel, P. L., McKinney-Freeman, S., Mack, P. J., Gracia-Sancho, J., et al. (2009). Biomechanical Forces Promote Embryonic Haematopoiesis. *Nature* 459 (7250), 1131–1135. doi:10.1038/nature08073

Astudillo, P. (2020). Extracellular Matrix Stiffness and Wnt/β-Catenin Signaling in Physiology and Disease. *Biochem. Soc. Trans.* 48 (3), 1187–1198. doi:10.1042/BST20200026

Barone, V., Lang, M., Krens, S. F. G., Pradhan, S. J., Shamipour, S., Sako, K., et al. (2017). An Effective Feedback Loop between Cell-Cell Contact Duration and Morphogen Signaling Determines Cell Fate. *Develop. Cell* 43 (2), 198–211. e112. doi:10.1016/j.devcel.2017.09.014

Bergert, M., Lembo, S., Sharma, S., Russo, L., Milovanović, D., Gretarsson, K. H., et al. (2021). Cell Surface Mechanics Gate Embryonic Stem Cell Differentiation. *Cell Stem Cell* 28 (2), 209–216. e204. doi:10.1016/j.stem.2020.10.017

Brunet, T., Bouclet, A., Ahmadi, P., Mitrossilis, D., Driquez, B., Brunet, A.-C., et al. (2013). Evolutionary Conservation of Early Mesoderm Specification by Mechanotransduction in Bilateria. *Nat. Commun.* 4, 2821. doi:10.1038/ncomms3821

Chan, C. J., Costanzo, M., Ruiz-Herrero, T., Mönke, G., Petrie, R. J., Bergert, M., et al. (2019). Hydraulic Control of Mammalian Embryo Size and Cell Fate. *Nature* 571 (7763), 112–116. doi:10.1038/s41586-019-1309-x

Collinet, C., and Lecuit, T. (2021). Programmed and Self-Organized Flow of Information during Morphogenesis. *Nat. Rev. Mol. Cell Biol* 22 (4), 245–265. doi:10.1038/s41580-020-00318-6

Dawes-Hoang, R. E., Parmar, K. M., Christiansen, A. E., Phelps, C. B., Brand, A. H., and Wieschaus, E. F. (2005). Folded Gastrulation, Cell Shape Change and the Control of Myosin Localization. *Development* 132 (18), 4165–4178. doi:10.1242/dev.01938

De Belly, H., Stubb, A., Yanagida, A., Labouesse, C., Jones, P. H., Paluch, E. K., et al. (2021). Membrane Tension Gates ERK-Mediated Regulation of Pluripotent Cell Fate. *Cell Stem Cell* 28 (2), 273–284. doi:10.1016/j.stem.2020.10.018

Desprat, N., Supatto, W., Pouille, P.-A., Beaurepaire, E., and Farge, E. (2008). Tissue Deformation Modulates Twist Expression to Determine Anterior Midgut Differentiation in Drosophila Embryos. *Develop. Cell* 15 (3), 470–477. doi:10.1016/j.devcel.2008.07.009

Dumortier, J. G., Le Verge-Serandour, M., Tortorelli, A. F., Mielke, A., de Plater, L., Turlier, H., et al. (2019). Hydraulic Fracturing and Active Coarsening Position the Lumen of the Mouse Blastocyst. *Science* 365 (6452), 465–468. doi:10.1126/science.aaw7709

Dupont, S., Morsut, L., Aragona, M., Enzo, E., Giulitti, S., Cordenonsi, M., et al. (2011). Role of YAP/TAZ in Mechanotransduction. *Nature* 474 (7350), 179–183. doi:10.1038/nature10137

El-Mohri, H., Wu, Y., Mohanty, S., and Ghosh, G. (2017). Impact of Matrix Stiffness on Fibroblast Function. *Mater. Sci. Eng. C* 74, 146–151. doi:10.1016/j.msec.2017.02.001

Elosegui-Artola, A., Andreu, I., Beedle, A. E. M., Lezamiz, A., Uroz, M., Kosmalska, A. J., et al. (2017). Force Triggers YAP Nuclear Entry by Regulating Transport across Nuclear Pores. *Cell* 171 (6), 1397–1410. e1314. doi:10.1016/j.cell.2017.10.008

Engler, A. J., Sen, S., Sweeney, H. L., and Discher, D. E. (2006). Matrix Elasticity Directs Stem Cell Lineage Specification. *Cell* 126 (4), 677–689. doi:10.1016/j.cell.2006.06.044

Fu, J., Wang, Y.-K., Yang, M. T., Desai, R. A., Yu, X., Liu, Z., et al. (2010). Mechanical Regulation of Cell Function with Geometrically Modulated Elastomeric Substrates. *Nat. Methods* 7 (9), 733–736. doi:10.1038/nmeth.1487

Gilmour, D., Rembold, M., and Leptin, M. (2017). From Morphogen to Morphogenesis and Back. *Nature* 541 (7637), 311–320. doi:10.1038/nature21348

Goodwin, K., and Nelson, C. M. (2021). Mechanics of Development. *Develop. Cell* 56 (2), 240–250. doi:10.1016/j.devcel.2020.11.025

Gordon, W. R., Zimmerman, B., He, L., Miles, L. J., Huang, J., Tiyanont, K., et al. (2015). Mechanical Allostery: Evidence for a Force Requirement in the Proteolytic Activation of Notch. *Develop. Cell* 33 (6), 729–736. doi:10.1016/j.devcel.2015.05.004

Grego-Bessa, J., Luna-Zurita, L., del Monte, G., Bolós, V., Melgar, P., Arandilla, A., et al. (2007). Notch Signaling Is Essential for Ventricular Chamber Development. *Develop. Cell* 12 (3), 415–429. doi:10.1016/j.devcel.2006.12.011

Hampoelz, B., and Lecuit, T. (2011). Nuclear Mechanics in Differentiation and Development. *Curr. Opin. Cell Biol.* 23 (6), 668–675. doi:10.1016/j.ceb.2011.10.001

Han, P., Bloomekatz, J., Ren, J., Zhang, R., Grinstein, J. D., Zhao, L., et al. (2016). Coordinating Cardiomyocyte Interactions to Direct Ventricular Chamber Morphogenesis. *Nature* 534 (7609), 700–704. doi:10.1038/nature18310

Hannezo, E., and Heisenberg, C.-P. (2019). Mechanochemical Feedback Loops in Development and Disease. *Cell* 178 (1), 12–25. doi:10.1016/j.cell.2019.05.052

Heisenberg, C.-P., and Bellaïche, Y. (2013). Forces in Tissue Morphogenesis and Patterning. *Cell* 153 (5), 948–962. doi:10.1016/j.cell.2013.05.008

Hirate, Y., Hirahara, S., Inoue, K. i., Kiyonari, H., Niwa, H., and Sasaki, H. (2015). Par- aPKC -dependent and -independent Mechanisms Cooperatively Control Cell Polarity, Hippo Signaling, and Cell Positioning in 16-cell Stage Mouse Embryos. *Develop. Growth Differ.* 57 (8), 544–556. doi:10.1111/dgd.12235

Hove, J. R., Köster, R. W., Forouhar, A. S., Acevedo-Bolton, G., Fraser, S. E., and Gharib, M. (2003). Intracardiac Fluid Forces Are an Essential Epigenetic Factor for Embryonic Cardiogenesis. *Nature* 421 (6919), 172–177. doi:10.1038/nature01282

Huebsch, N., Arany, P. R., Mao, A. S., Shvartsman, D., Ali, O. A., Bencherif, S. A., et al. (2010). Harnessing Traction-Mediated Manipulation of the Cell/matrix

Interface to Control Stem-Cell Fate. *Nat. Mater* 9 (6), 518–526. doi:10.1038/nmat2732

Jiménez-Amilburu, V., Rasouli, S. J., Staudt, D. W., Nakajima, H., Chiba, A., Mochizuki, N., et al. (2016). *In Vivo* Visualization of Cardiomyocyte Apicobasal Polarity Reveals Epithelial to Mesenchymal-like Transition during Cardiac Trabeculation. *Cell Rep.* 17 (10), 2687–2699. doi:10.1016/j.celrep.2016.11.023

Kirby, T. J., and Lammerding, J. (2018). Emerging Views of the Nucleus as a Cellular Mechanosensor. *Nat. Cell Biol* 20 (4), 373–381. doi:10.1038/s41556-018-0038-y

Korotkevich, E., Niwayama, R., Courtois, A., Friese, S., Berger, N., Buchholz, F., et al. (2017). The Apical Domain Is Required and Sufficient for the First Lineage Segregation in the Mouse Embryo. *Develop. Cell* 40 (3), 235–247. doi:10.1016/j.devcel.2017.01.006

Kölsch, V., Seher, T., Fernandez-Ballester, G. J., Serrano, L., and Leptin, M. (2007). Control of Drosophila Gastrulation by Apical Localization of Adherens Junctions and RhoGEF2. *Science* 315 (5810), 384–386. doi:10.1126/science.1134833

Kuriyama, S., and Mayor, R. (2009). A Role for Syndecan-4 in Neural Induction Involving ERK- and PKC-dependent Pathways. *Development* 136 (4), 575–584. doi:10.1242/dev.027334

Le, H. Q., Ghatak, S., Yeung, C.-Y. C., Tellkamp, F., Günschmann, C., Dieterich, C., et al. (2016). Mechanical Regulation of Transcription Controls Polycomb-Mediated Gene Silencing during Lineage Commitment. *Nat. Cell Biol* 18 (8), 864–875. doi:10.1038/ncb3387

Lecuit, T., Lenne, P.-F., and Munro, E. (2011). Force Generation, Transmission, and Integration during Cell and Tissue Morphogenesis. *Annu. Rev. Cell Dev. Biol.* 27, 157–184. doi:10.1146/annurev-cellbio-100109-104027

Leptin, M. (1991). Twist and Snail as Positive and Negative Regulators during Drosophila Mesoderm Development. *Genes Dev.* 5 (9), 1568–1576. doi:10.1101/gad.5.9.1568

Leung, C. Y., and Zernicka-Goetz, M. (2013). Angiomotin Prevents Pluripotent Lineage Differentiation in Mouse Embryos via Hippo Pathway-dependent and -independent Mechanisms. *Nat. Commun.* 4, 2251. doi:10.1038/ncomms3251

Lim, H. Y. G., Alvarez, Y. D., Gasnier, M., Wang, Y., Tetlak, P., Bissiere, S., et al. (2020). Keratins Are Asymmetrically Inherited Fate Determinants in the Mammalian Embryo. *Nature* 585 (7825), 404–409. doi:10.1038/s41586-020-2647-4

Liu, C., and Montell, C. (2015). Forcing Open TRP Channels: Mechanical Gating as a Unifying Activation Mechanism. *Biochem. Biophysical Res. Commun.* 460 (1), 22–25. doi:10.1016/j.bbrc.2015.02.067

Lomakin, A. J., Cattin, C. J., Cuvelier, D., Alraies, Z., Molina, M., Nader, G. P. F., et al. (2020). The Nucleus Acts as a Ruler Tailoring Cell Responses to Spatial Constraints. *Science* 370 (6514), eaba2894. doi:10.1126/science.aba2894

Maître, J.-L., Berthoumieux, H., Krens, S. F. G., Salbreux, G., Jülicher, F., Paluch, E., et al. (2012). Adhesion Functions in Cell Sorting by Mechanically Coupling the Cortices of Adhering Cells. *Science* 338 (6104), 253–256. doi:10.1126/science.1225399

Maître, J.-L., Turlier, H., Illukkumbura, R., Eismann, B., Niwayama, R., Nédélec, F., et al. (2016). Asymmetric Division of Contractile Domains Couples Cell Positioning and Fate Specification. *Nature* 536 (7616), 344–348. doi:10.1038/nature18958

Mammoto, T., Mammoto, A., and Ingber, D. E. (2013). Mechanobiology and Developmental Control. *Annu. Rev. Cell Dev. Biol.* 29, 27–61. doi:10.1146/annurev-cellbio-101512-122340

Mammoto, T., Mammoto, A., Torisawa, Y.-s., Tat, T., Gibbs, A., Derda, R., et al. (2011). Mechanochemical Control of Mesenchymal Condensation and Embryonic Tooth Organ Formation. *Develop. Cell* 21 (4), 758–769. doi:10.1016/j.devcel.2011.07.006

Martin-Bermudo, M. D. (2000). Integrins Modulate the Egfr Signaling Pathway to Regulate Tendon Cell Differentiation in the Drosophila Embryo. *Development* 127 (12), 2607–2615. doi:10.1242/dev.127.12.2607

McBride, S. H., and Knothe Tate, M. L. (2008). Modulation of Stem Cell Shape and Fate A: the Role of Density and Seeding Protocol on Nucleus Shape and Gene Expression. *Tissue Eng. A* 14 (9), 1561–1572. doi:10.1089/ten.tea.2008.0112

Mitrossilis, D., Röper, J.-C., Le Roy, D., Driquez, B., Michel, A., Ménager, C., et al. (2017). Mechanotransductive cascade of Myo-II-dependent Mesoderm and Endoderm Invaginations in Embryo Gastrulation. *Nat. Commun.* 8, 13883. doi:10.1038/ncomms13883

Moorman, A. F. M., and Christoffels, V. M. (2003). Cardiac Chamber Formation: Development, Genes, and Evolution. *Physiol. Rev.* 83 (4), 1223–1267. doi:10.1152/physrev.00006.2003

Mosaliganti, K. R., Swinburne, I. A., Chan, C. U., Obholzer, N. D., Green, A. A., Tanksale, S., et al. (2019). Size Control of the Inner Ear via Hydraulic Feedback. *Elife* 8, e39596. doi:10.7554/eLife.39596

Nishioka, N., Inoue, K.-i., Adachi, K., Kiyonari, H., Ota, M., Ralston, A., et al. (2009). The Hippo Signaling Pathway Components Lats and Yap Pattern Tead4 Activity to Distinguish Mouse Trophectoderm from Inner Cell Mass. *Develop. Cell* 16 (3), 398–410. doi:10.1016/j.devcel.2009.02.003

Petzold, J., and Gentleman, E. (2021). Intrinsic Mechanical Cues and Their Impact on Stem Cells and Embryogenesis. *Front. Cell Dev. Biol.* 9, 761871. doi:10.3389/fcell.2021.761871

Planas-Paz, L., Strilić, B., Goedecke, A., Breier, G., Fässler, R., and Lammert, E. (2012). Mechanoinduction of Lymph Vessel Expansion. *EMBO J.* 31 (4), 788–804. doi:10.1038/emboj.2011.456

Plusa, B., Frankenberg, S., Chalmers, A., Hadjantonakis, A.-K., Moore, C. A., Papalopulu, N., et al. (2005). Downregulation of Par3 and aPKC Function Directs Cells towards the ICM in the Preimplantation Mouse Embryo. *J. Cell Sci* 118 (Pt 3), 505–515. doi:10.1242/jcs.01666

Priya, R., Allanki, S., Gentile, A., Mansingh, S., Uribe, V., Maischein, H.-M., et al. (2020). Tension Heterogeneity Directs Form and Fate to Pattern the Myocardial wall. *Nature* 588 (7836), 130–134. doi:10.1038/s41586-020-2946-9

Ralston, A., and Rossant, J. (2008). Cdx2 Acts Downstream of Cell Polarization to Cell-Autonomously Promote Trophectoderm Fate in the Early Mouse Embryo. *Develop. Biol.* 313 (2), 614–629. doi:10.1016/j.ydbio.2007.10.054

Ridone, P., Vassalli, M., and Martinac, B. (2019). Piezo1 Mechanosensitive Channels: what Are They and Why Are They Important. *Biophys. Rev.* 11 (5), 795–805. doi:10.1007/s12551-019-00584-5

Royer, C., Leonavicius, K., Kip, A., Fortin, D., Nandi, K., Vincent, A., et al. (2020). Establishment of a Relationship between Blastomere Geometry and YAP Localisation during Compaction. *Development* 147 (19), dev189449. doi:10.1242/dev.189449

Salguero-Jiménez, A., Grego-Bessa, J., D'Amato, G., Jiménez-Borreguero, L. J., and de la Pompa, J. L. (2018). Myocardial Notch1-Rbpj Deletion Does Not Affect NOTCH Signaling, Heart Development or Function. *PLoS One* 13 (12), e0203100. doi:10.1371/journal.pone.0203100

Samarage, C. R., White, M. D., Álvarez, Y. D., Fierro-González, J. C., Henon, Y., Jesudason, E. C., et al. (2015). Cortical Tension Allocates the First Inner Cells of the Mammalian Embryo. *Develop. Cell* 34 (4), 435–447. doi:10.1016/j.devcel.2015.07.004

Samsa, L. A., Givens, C., Tzima, E., Stainier, D. Y. R., Qian, L., and Liu, J. (2015). Cardiac Contraction Activates Endocardial Notch Signaling to Modulate Chamber Maturation in Zebrafish. *Development* 142 (23), 4080–4091. doi:10.1242/dev.125724

Sandmann, T., Girardot, C., Brehme, M., Tongprasit, W., Stolc, V., and Furlong, E. E. M. (2007). A Core Transcriptional Network for Early Mesoderm Development in *Drosophila melanogaster*. *Genes Dev.* 21 (4), 436–449. doi:10.1101/gad.1509007

Sasaki, H. (2017). Roles and Regulations of Hippo Signaling during Preimplantation Mouse Development. *Develop. Growth Differ.* 59 (1), 12–20. doi:10.1111/dgd.12335

Shaya, O., and Sprinzak, D. (2011). From Notch Signaling to fine-grained Patterning: Modeling Meets Experiments. *Curr. Opin. Genet. Develop.* 21 (6), 732–739. doi:10.1016/j.gde.2011.07.007

Staudt, D., and Stainier, D. (2012). Uncovering the Molecular and Cellular Mechanisms of Heart Development Using the Zebrafish. *Annu. Rev. Genet.* 46, 397–418. doi:10.1146/annurev-genet-110711-155646

Steed, E., Faggianelli, N., Roth, S., Ramspacher, C., Concordet, J.-P., and Vermot, J. (2016). klf2a Couples Mechanotransduction and Zebrafish Valve Morphogenesis through Fibronectin Synthesis. *Nat. Commun.* 7, 11646. doi:10.1038/ncomms11646

Strumpf, D., Mao, C.-A., Yamanaka, Y., Ralston, A., Chawengsaksophak, K., Beck, F., et al. (2005). Cdx2 Is Required for Correct Cell Fate Specification and Differentiation of Trophectoderm in the Mouse Blastocyst. *Development* 132 (9), 2093–2102. doi:10.1242/dev.01801

Taylor-Weiner, H., Ravi, N., and Engler, A. J. (2015). Traction Forces Mediated by Integrin Signaling Are Necessary for Definitive Endoderm Specification. *J. Cell Sci* 128 (10), 1961–1968. doi:10.1242/jcs.166157

Uhler, C., and Shivashankar, G. V. (2017). Regulation of Genome Organization and Gene Expression by Nuclear Mechanotransduction. *Nat. Rev. Mol. Cell Biol* 18 (12), 717–727. doi:10.1038/nrm.2017.101

Venturini, V., Pezzano, F., Català Castro, F., Häkkinen, H.-M., Jiménez-Delgado, S., Colomer-Rosell, M., et al. (2020). The Nucleus Measures Shape Changes for Cellular Proprioception to Control Dynamic Cell Behavior. *Science* 370 (6514), eaba2644. doi:10.1126/science.aba2644

Vining, K. H., and Mooney, D. J. (2017). Mechanical Forces Direct Stem Cell Behaviour in Development and Regeneration. *Nat. Rev. Mol. Cell Biol* 18 (12), 728–742. doi:10.1038/nrm.2017.108

White, M. D., Zenker, J., Bissiere, S., and Plachta, N. (2018). Instructions for Assembling the Early Mammalian Embryo. *Develop. Cell* 45 (6), 667–679. doi:10.1016/j.devcel.2018.05.013

Xia, P., Gütl, D., Zheden, V., and Heisenberg, C.-P. (2019). Lateral Inhibition in Cell Specification Mediated by Mechanical Signals Modulating TAZ Activity. *Cell* 176 (6), 1379–1392. e1314. doi:10.1016/j.cell.2019.01.019

Yamanaka, Y., Ralston, A., Stephenson, R. O., and Rossant, J. (2006). Cell and Molecular Regulation of the Mouse Blastocyst. *Dev. Dyn.* 235 (9), 2301–2314. doi:10.1002/dvdy.20844

Yang, Y., Beqaj, S., Kemp, P., Ariel, I., and Schuger, L. (2000). Stretch-induced Alternative Splicing of Serum Response Factor Promotes Bronchial Myogenesis and Is Defective in Lung Hypoplasia. *J. Clin. Invest.* 106 (11), 1321–1330. doi:10.1172/JCI8893

Yue, Y., Zong, W., Li, X., Li, J., Zhang, Y., Wu, R., et al. (2020). Long-term, In Toto Live Imaging of Cardiomyocyte Behaviour during Mouse Ventricle Chamber Formation at Single-Cell Resolution. *Nat. Cell Biol* 22 (3), 332–340. doi:10.1038/s41556-020-0475-2

Zenker, J., White, M. D., Gasnier, M., Alvarez, Y. D., Lim, H. Y. G., Bissiere, S., et al. (2018). Expanding Actin Rings Zipper the Mouse Embryo for Blastocyst Formation. *Cell* 173 (3), 776–791. e717. doi:10.1016/j.cell.2018.02.035

Zernicka-Goetz, M., Morris, S. A., and Bruce, A. W. (2009). Making a Firm Decision: Multifaceted Regulation of Cell Fate in the Early Mouse Embryo. *Nat. Rev. Genet.* 10 (7), 467–477. doi:10.1038/nrg2564

Conflict of Interest: The authors declare that the research was conducted in the absence of any commercial or financial relationships that could be construed as a potential conflict of interest.

frontiers | Frontiers in Cell and Developmental Biology

MINI REVIEW
published: 14 June 2022
doi: 10.3389/fcell.2022.908799

Modelling the Tumor Microenvironment: Recapitulating Nano- and Micro-Scale Properties that Regulate Tumor Progression

*Danielle Vahala and Yu Suk Choi**

School of Human Sciences, The University of Western Australia, Perth, WA, Australia

Breast cancer remains a significant burden with 1 in 8 women affected and metastasis posing a significant challenge for patient survival. Disease progression involves remodeling of the extracellular matrix (ECM). In breast cancer, tissue stiffness increases owing to an increase in collagen production by recruited cancer-associated fibroblasts (CAFs). These stromal modifications are notable during primary tumor growth and have a dualistic action by creating a hard capsule to prevent penetration of anti-cancer therapies and forming a favorable environment for tumor progression. Remodeling of the tumor microenvironment immediately presented to cells can include changes in protein composition, concentration and structural arrangement and provides the first mechanical stimuli in the metastatic cascade. Not surprisingly, metastatic cancer cells possess the ability to mechanically adapt, and their adaptability ensures not only survival but successful invasion within altered environments. In the past decade, the importance of the microenvironment and its regulatory role in diseases have gained traction and this is evident in the shift from plastic culture to the development of novel biomaterials that mimic *in vivo* tissue. With these advances, elucidations can be made into how ECM remodeling and more specifically, altered cell-ECM adhesions, regulate tumor growth and cancer cell plasticity. Such enabling tools in mechanobiology will identify fundamental mechanisms in cancer progression that eventually help develop preventative and therapeutic treatment from a clinical perspective. This review will focus on current platforms engineered to mimic the micro and nano-properties of the tumor microenvironment and subsequent understanding of mechanically regulated pathways in cancer.

Keywords: extracellular matrix, mechanobiology, invasion, hydrogel, stiffness, adhesion

OPEN ACCESS

Edited by:
Samantha Jane Stehbens, The University of Queensland, Australia

Reviewed by:
Sarah Boyle, Centre for Cancer Biology (CCB), Australia

***Correspondence:**
Yu Suk Choi
yusuk.choi@uwa.edu.au

Specialty section:
This article was submitted to Cell Adhesion and Migration, a section of the journal Frontiers in Cell and Developmental Biology

Received: *31 March 2022*
Accepted: *20 May 2022*
Published: *14 June 2022*

Citation:
Vahala D and Choi YS (2022) Modelling the Tumor Microenvironment: Recapitulating Nano- and Micro-Scale Properties that Regulate Tumor Progression. Front. Cell Dev. Biol. 10:908799. doi: 10.3389/fcell.2022.908799

1 INTRODUCTION

As cancer, particularly metastasis, remains a leading cause of death globally (WHO, 2021), there is a call to action for researchers to develop novel approaches to enable new treatments. While the biochemical and genetic drivers of metastasis have been extensively studied, (Chatterjee et al., 2018; De Francesco et al., 2018; Siegel et al., 2018), there is a growing appreciation for the regulatory roles that biophysical cues play in tumor progression and the onset of metastasis. Changes to mechanical inputs such as stiffness (Sherman-Baust et al., 2003; Paszek and Weaver, 2004; Lu et al., 2011; Gierach et al., 2012) and ligand presentation (Allinen et al., 2004; Larsen et al., 2006; Oskarsson, 2013) are

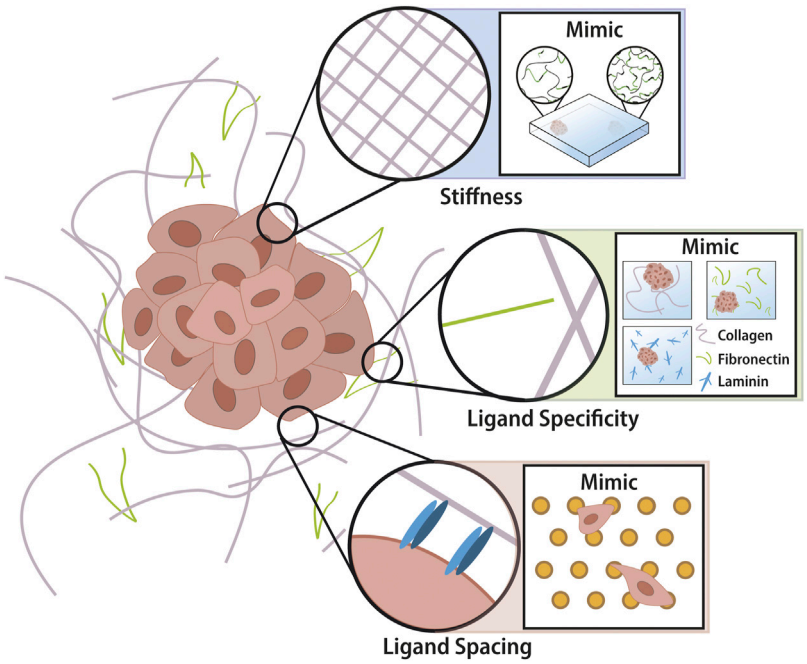

FIGURE 1 | Tumor extracellular matrix in nano- and micro-scale. Properties of tumor ECM include microscale stiffness and ligand chemistry changes as well as nanoscale ligand spacing changes. The intelligent design of biomaterials allows recapitulation of these properties into tuneable devices for the study of cancer phenotypes. Hydrogels utilise cross-linking technology which investigators can control spatially across one gel by altering UV penetration. There is a multitude of biomaterials each utilising different backbones and employing different ligands for cells to adhere to (i.e. collagen = GFOGER and GelMA = RGD). Novel advancements in nanotechnology have enabled the production of a platform whereby the nano-spacing of ligands can be altered according to the micelle-nano-array of gold-nanoparticles that have attached peptides.

transduced to the cell nucleus via a process coined mechanotransduction. The microenvironment is composed of micro-and nanoscale features which undergo extensive remodeling during tumor development (Leiss et al., 2008; Wang et al., 2017). While these aberrant mechanical stimuli are acknowledged in tumor progression, the contribution and specific mechanism for this is still largely unknown. Understanding how mechanical stimuli regulate cancer cell fate largely relies on enabling biomimetic and tuneable materials that precisely recapitulate specific properties of the tumor microenvironment (TME) and more specifically the ECM. In this review, we discuss the functional consequences that alterations of the ECM, at the nano- and micro-scale, have on cancer cell growth and invasion and the platforms allowing the study of this complex disease.

2 WHAT IS THE TUMOR MICROENVIRONMENT (TME)

TME refers to the cellular (fibroblasts, immune cells, endothelial cells, and adipocytes, etc) and non-cellular (proteins that make up the ECM) components that form the microenvironment of a tumour. In this review, we focus on the non-cellular component, the ECM, present in all tissues and providing the physical scaffolding and biomechanical cues required for tissue morphogenesis, differentiation and homeostasis. The ECM consists of a multitude of proteins (e.g. collagen, laminin, and fibronectin) and glycosaminoglycans/proteoglycan (e.g. hyaluronic acid, heparin). Utilising certain cell membrane receptors (e.g., mainly integrins) cells can adhere to specific ligands expressed on the ECM. In this way, cells and the microenvironment maintain a dynamic dialogue, whereby healthy tissues remain in a state of homeostasis. This crosstalk is disrupted in tumorigenesis, where extensive remodification to the TME results in altered cell behaviour (Lu et al., 2011). The ECM is remodelled by ECM modifying factors (MMP and LOX) which alter cross-linking of the matrix or by paracrine signalling to cancer-associated fibroblasts (CAFs) resulting in increased deposition of ECM proteins (Özdemir et al., 2014; Rhim et al., 2014; Sahai et al., 2020; Lee and Chaudhuri, 2021). Changes in ECM composition by prolonged cross-linking/degradation will present altered mechanical properties (e.g., stiffness), cell-ECM ligand specificity (e.g., fibronectin dominant to collagen dominant), and altered spacing between ligands (e.g., nano-spacing of GFOGER, peptide in collagen that binds integrins α1β1 and α2β1) (**Figure 1**). As physical properties of the ECM influence cell behaviour via mechanotransduction and these properties are altered in cancer, acknowledging the cancer ECM and its regulatory role in controlling cell behaviour are critical for understanding cancer progression. (Young et al., 2016).

2.1 ECM Stiffness Activates Mechanotransduction Pathways to Regulate Cancer Fate

Changes to tissue stiffness following tumor development is one of the most well-established characteristics of the TME and this knowledge is exploited during cancer screening (e.g., palpation) (Khaled et al., 2004). Tumor stiffening is a downstream effect of increased deposition of ECM proteins (such as collagen) by the recruitment and activation of CAFs (Tlsty and Coussens, 2006). Collagen is increasingly more crosslinked by lysyl oxidase (LOX) which is implicated with increasing tension between cytoskeletal components and integrins and mediating cell-matrix focal adhesions (FA) (Choquet et al., 1997; Cox et al., 2013). Establishing a mechanical connection between cell and ECM, via FA, will result in the activation of various signalling cascades and the generation of intracellular force through actin-myosin. This process, coined mechanotransduction, begins at the cell-ECM interface whereby specific integrins bind to the ECM proteins to recruit and form actin stress fibers which maintain the cytoskeletal tension (Bershadsky et al., 2003). Filamentous Actin binds to Lamin-A within the nuclear membrane via adaptor proteins such as Nesprin and SUN (Wang et al., 2009), translating mechanical input to the nucleus of the cell. Tension applied to nuclear lamina (Lamin-A is one of the key building blocks) leads to translocation of mechanosensitive proteins such as transcriptional coactivator with PDZ-binding motif (TAZ) and yes-associated protein (YAP). This mechanotransduction pathway utilises biochemical and biomechanical signals to alter cancer cell growth, modes of invasion and eventually govern the fate of cells in the TME. Increased ECM stiffness enhances YAP and TAZ activity which evidence suggests can drive tumour-initiating cells (cancer stem cells (CSCs) to maintain self-renewal and tumor-initiation capacities of breast cancer cells and induce EMT (Cordenonsi et al., 2011; Dupont et al., 2011; Maugeri-Saccà et al., 2015). Alongside integrin-mediated mechanotransduction, increasing traction force not only regulates Rho-associated protein kinase (ROCK), a protein largely responsible for actin cytoskeleton dynamics and regulating breast cancer epithelial cell differentiation (Wozniak et al., 2003), but also activates mitogen-activated protein kinase (MAPK), which is responsible for many diverse cellular programs including cell proliferation, differentiation, motility and survival (Provenzano et al., 2009; Cargnello and Roux, 2011). Overall, a stiff ECM activates mechanotransduction which induces a gene expression signature in cancer cells that is associated with a greater risk for invasive breast carcinoma (Habel et al., 2004; Provenzano et al., 2009).

2.2 TME Stiffness is Dynamic at the Nanoscale

Previous investigations into the effects of stiffening on cancer phenotypes arose from the common consensus that tumors are stiffer than their healthy counterpart. However, the TME, and more specifically the ECM, has displayed levels of complexity not previously appreciated. A recent investigation into the nanoscale stiffness of breast explants revealed non-metastatic tumors with this characteristic increase in stiffness, but metastatic tumors with a "softer" more "heterogenous" stiffness profile with 3 distinct mechanical properties (Plodinec et al., 2012). These nanoscale measurements translate to clinical measurements, with high mammographic density associated with a greater risk of developing breast cancer, whilst low density is linked to an increased risk of cancer invasion (Ye et al., 2014). An examination of transgenic mice showed initial stiffening following tumor growth (spatially heterogeneous) followed by tissue softening at the onset of tumor dissemination as a result of ECM digestion (Sameni et al., 2000). These studies highlight the complexity of the TME and more importantly the dynamic nature of cancer ECM at the nanoscale.

2.3 Tumour Progression Involves Altered ECM Composition

2.3.1 Protein Composition Changes and Integrin Specificity

In diseases where ECM is misregulated, changes to ECM composition results in changes to the ligand presentation (e.g., density (Sherman-Baust et al., 2003; Paszek and Weaver, 2004; Gierach et al., 2012) chemistry and geometry (Allinen et al., 2004; Larsen et al., 2006; Oskarsson, 2013)) which mediates integrin binding. Integrins are a family of transmembrane glycoproteins receptors consisting of 18 α and 8 β units which form heterodimers that mediate cell-matrix interactions (Ruoslahti, 1991; Hynes, 1992). As receptors, integrins mediate recognition of ECM constituents (e.g., cells that express α1β1 and α2β1 bind to GFOGER), recruiting focal adhesion complexes to establish traction force generation and actin filament assembly (Massia and Hubbell, 1991; Arnold et al., 2004). For this reason, integrin-mediated mechanotransduction has gained traction as a highly specific process that regulates cytoskeletal tension, intracellular signalling and gene expression related to proliferation, migration and survival. In breast cancer, an aberrant ECM can destabilise integrin-mediated adhesion resulting in enhanced metastatic potential and drug resistance (Young et al., 2020).

In the majority of cancers, significant accumulation of collagen has been associated with metastatic recurrence, aggressive behaviour, and chemoresistance (Lochter and Bissell, 1995; Ramaswamy et al., 2003; Oskarsson, 2013; Holle et al., 2016; Ondeck et al., 2019). Integrins α1β1 and α2β1 are known to be primarily collagen receptors and their expression has shown to play a role in melanoma cell migration in 3D collagen matrices (Koistinen and Heino, 2013). Increased expression of these two heterodimers is noted in melanoma metastatic cells when compared to cells in the primary tumor (Klein et al., 1991). Interestingly, studies utilising mammary epithelium and aorta-derived smooth muscles have shown collagen to activate distinct signalling pathways and alter cell behaviour independent of mechanical stimuli (stiffness) (Giancotti and Ruoslahti, 1999; Engler et al., 2004; Brownfield et al., 2013). Accompanying increased collagen deposition during a fibrotic response is the deposition of fibronectin. Fibronectin is a glycoprotein known to

enhance the growth of breast epithelial cells (McIntosh et al., 2010), increase breast cancer invasion (via STAT3 and MAPK pathways) (Balanis et al., 2013) and is upregulated in circulating tumor cells (Raimondi et al., 2011). Cells adhere to RGD motifs expressed on fibronectin via the α5β1 receptor and αVβ3 which have emerged as essential mediators in many human carcinomas and are largely implicated in tumour proliferation and metastasis, with αVβ3 identified as a melanoma tumour progression marker (Hsu et al., 1998; Koistinen and Heino, 2013; Hou et al., 2020).

2.3.2 Glycosaminoglycan Expression During Tumor Progression

Aside from ECM proteins, glycosaminoglycans (GAGs) have also proven essential in cancer progression. Hyaluronan is a GAG that is highly expressed in breast cancer (Karousou et al., 2014). Hyaluronan can interact with cancer cells via cell surface receptors CD44 and RHAMM (Toole, 2004). CD44 is a cell surface adhesion receptor (not an integrin) and is largely recognized as a cancer stem cell (CSC) marker expressed by almost every tumour cell (Jaggupilli and Elkord, 2012; Lin and Ding, 2017; Wang et al., 2018). Employing alternative signaling cascades then integrin-driven adhesion, CD44 has shown regulatory roles in the Hippo pathway (Wang et al., 2014) and interacts with RHAMM and ERK (Hamilton et al., 2007) as well as Rho-ROCK (Chellaiah et al., 2003; Ohata et al., 2012) to mediate breast cancer cell motility and enhance stemness of colon cancer-initiating cells. This offers an alternative perspective on the regulatory roles of GAGs and less understood cell-ECM interactions. Overall, these studies emphasize the specificity of cell-ECM adhesions which promote sustained altered signaling cascades and govern particular cell fates.

2.3.3 Altered Nano-Spacing of Ligands in TME

Compositional remodeling due to increased deposition of ECM proteins, enhanced cross-linking by LOX and localized degradation by secreted MMP factors, has an implication in altering the spacing between individual ligands (e.g. GFOGER). Cells sense the variations in the spacing of ECM proteins through either single integrin proteins or recruitment of larger integrin-containing adhesion complexes (Oria et al., 2017). This spatial sensing has shown to play a role in physiological and pathological states (Daley et al., 2008). Oria et al., 2017 demonstrated that human breast myoepithelial integrin clustering and subsequent recruitment of focal adhesion is inhibited when cell-ECM interactions are separated by more than a few tens of nanometers. These nanometer-scale alterations have regulatory roles in cellular migration, morphology, focal adhesion assembly, cell adhesion and traction force generation (Arnold et al., 2004; Cavalcanti-Adam et al., 2006; Cavalcanti-Adam et al., 2007; Selhuber-Unkel et al., 2010; Oria et al., 2017). Interestingly, breast cancer cell survival, in response to chemotherapeutic treatment, is highly dependent on the nanoscale ligand spacing (Young et al., 2020).

Collagen fibres interact with each other at defined spacing intervals termed periodicity (Gelse et al., 2003; Young et al., 2016). This periodicity has shown intervals ranging from 63 to 72 nm and is the interval at which cells interact with the protein (Wallace et al., 2010; Young et al., 2016). *In vitro* studies have shown when periodicity is increased above 73 nm melanocytes and osteoclasts were inhibited in their ability to cluster integrins (Arnold et al., 2004). Fibronectin, also implicated in cancer, has shown a regular fibril arrangement of 42 nm in thick fibres and 84 nm in thin fibres. The fibrils at 84 nm will be unfolded and at a state of extension whilst the thick fibres are a result of staggered fibronectin dimers (Dzamba and Peters, 1991). It is hypothesized that the latter could be exacerbated in cancer due to the highly dense protein structures in the TME (Young et al., 2016). As the spatial organization of the available ligand binding partner changes, this mediates integrin clustering affecting force-mediated contractility of the cell and governing cell fate (Li et al., 2015). To confirm this theory, cartilage cells were placed on ligands of discreet spacing; the result was significantly greater cell area on the smaller nano-spaced ligands, inferring aberrant integrin-clustering on the larger nano-spacing (Li et al., 2015). In breast cancer cells, altering the nano-spacing of ligands showed altered cellular properties including morphology, focal adhesion formation, migration and chemoprotection (smaller ligand spacing hinders survival against chemotherapeutic drugs) (Young et al., 2020).

3 TOOLS FOR RECAPITULATING THE TUMOR MICROENVIRONMENT

3.1 Stiffness Tunable Hydrogels

The TME offers a complex assortment of biochemical and biomechanical inputs that dynamically change following cancer progression and onset of metastasis. To better understand the functional consequences of ECM mechanics on cell phenotype, investigators have employed a combination of 2D and 3D hydrogel-based platforms. Being highly water-based and tunable, hydrogels offer superior recapitulation of specific characteristics of the ECM including stiffness, composition, and ligand spacing (**Supplementary Table S1**).

As mentioned previously, one of the most well-established characteristics of the TME is changes in tissue stiffness which is largely correlated with the risk of breast cancer development (Habel et al., 2004; Provenzano et al., 2008). Because of this, the production of biomaterials was largely centred around hydrogels whose chemistry would allow easy manipulation of stiffness. Synthetic gels such as polyacrylamide can produce discrete, static 2D gels of different stiffnesses and spatial gradients which offer greater biomimicry of the spatial heterogeneity seen *in vivo* (Engler et al., 2006; Insua-Rodríguez and Oskarsson, 2016; Hadden et al., 2017; Chin et al., 2021). Seeding metastatic breast cancer cells on uniform stiffness hydrogels which varied from 2.4–10.6 kPa demonstrated stiffness-dependent differences in traction forces, strain energies, and morphologies (Massalha and Weihs, 2017). As

robust as PA is, the presence of free radicals during polymerization inhibits cell encapsulation and limits translatability from a 3D perspective.

Appreciation for the 3D architecture and its regulatory role on cell phenotype has geared the development of novel 3D-capable hydrogels. Collagen, being the primary constituent and major structural component in many tissues is very attractive for cell-ECM studies. Formed mainly from fibrous protein collagen type I, fabrication involves manipulating collagen concentration and raising the solution temperature until gelation occurs. Their soft mesh-like matrix makes collagen hydrogels ideal for invasion assays, with the most recent investigation showing collective cancer cell migration inhibited in the stiffest microenvironment (2.5 mg/ml) (Raghuraman et al., 2022). The drawback of this platform includes limited stiffness ranges (up to ~5 kPa) and temporal tuneability, with reduced long-term stability and high batch-batch variability.

For these reasons, semi-synthetic materials such as gelatin methacryloyl (GelMA), synthesized from denatured collagen, has gained significant traction (Bertlein et al., 2017). Containing cross-linkable methacrylate groups, GelMA, will undergo polymerization upon the addition of a photoinitiator (Irgacure 2,959) and exposure to UV light. In this way, investigators gain greater tuneability over GelMA whilst still maintaining biological relevance (contains RGD). GelMA can also employ a gradient stiffness model which allows for a more holistic understanding of mechanically driven cell phenotypes (Major et al., 2019; Kim et al., 2020).

The use of these hydrogels allows for high throughput fabrication of readily adaptable and physiologically relevant environments, making it appealing for the study of ECM for cancer proliferation and invasion. Other approaches to mimicking the 3D microenvironment include 3D bioprinting which is beneficial in creating an exact replication of target tissue with consideration for cellular components, ECM and 3D spatial components (for reviews see; (Charbe et al., 2017; Ro et al., 2022)). Alternatively, the decellularization of tumors also offers a new Frontier in tissue engineering that maintains not only the mechanical components of the ECM but also the composition and structure (for review see; (García-Gareta et al., 2022)).

Stiffness is just one ECM characteristic supplying biophysical input to the cell. Tumor progression also proceeds extensive modification to ECM composition (i.e., going from fibronectin-laminin rich matrix to primarily collagen dominated) which alters the integrin profile and at the nanoscale alters the spacing at which cells are interacting with ECM proteins (Sherman-Baust et al., 2003; Allinen et al., 2004; Paszek and Weaver, 2004; Larsen et al., 2006; Gierach et al., 2012; Oskarsson, 2013).

3.2 Tools to Control ECM Composition

Polyacrylamide is inert in nature and requires conjugation with proteins to enable cell attachment. Using a bifunctional cross-linker sulfo-SANPAH, proteins can be covalently bound to the PA and enable cell attachment (Caliari and Burdick, 2016). Because of this, PA is an attractive choice when investigating the effects of specific adhesive ligands, as cell-ECM interactions can be tightly controlled (Tse and Engler, 2010). For 3D investigation different biomaterials which utilize different ligands can be employed. Collagen as mentioned previously expresses abundant GFOGER which will activate integrins α1β1 and α2β1. GelMA, adapted from native gelatin, contains RGD binding motifs (Bertlein et al., 2017) which will recruit integrins α5β1 and αVβ3. Alginate and polyethylene glycol diacrylate (PEGDA), do not express native ligands, similar to PA, and offers a "blank canvas" allowing preferential modification with adhesive ligands within a 3D context (Caliari and Burdick, 2016).

Hyaluronic acid (HA) as a hydrogel has several important advantages including its biological relevance and chemical tunability. HA functional groups can be modified to enable a wide range of cross-linking chemistries, useful for cellular mechanotransduction investigations (Fraser et al., 1997). Unlike collagen and GelMA, HA lacks integrin-mediated cell adhesion but presents cell surface markers including CD44 which can be beneficial when studying alternative cell-ECM adhesions and indirect pathways interacting with integrin-mediated mechanotransduction.

3.3 Tools for Investigating Ligand Nano-Spacing

Recapitulating and controlling for the nanoscale properties of the microenvironment remains a great challenge in biomaterials. Photolithography and optical lithography are the two most commonly used techniques in nanofabrication (Lohmüller et al., 2011). However, these two methods rely on light and achieving structural dimensions below 100 nm is hardly feasible (Lohmüller et al., 2011). Alternative methods, such as block copolymer micelle lithography (BCMN), rely on the self-organization of molecules to generate structural materials and can reach these sub-nanometer resolutions (Gates et al., 2004). BCMN involves the formation of spontaneous microphase-separated morphologies from amphiphilic block copolymers (Lohmüller et al., 2011). The distribution of nanoparticles due to block copolymer micelle self-assembly can be manipulated by changing micelle size, the concentration of polymer solution, the amount of metal precursor and the retraction speed from the substrate. Once the micro-arrays are established, peptides can be adhered to the nanoparticles enabling precise control over ligand spacing. Seeding cancer cells atop this platform has shown to influence key cellular properties such as morphology, focal adhesion formation, migration as well as drug sensitivity (Young et al., 2020).

4 CONCLUSION AND FUTURE PERSPECTIVES

The phenomenon responsible for the successful spread of primary cancer cells from their tumor microenvironment to secondary sites is still largely uncharacterized at the molecular level. Universally, the metastatic cascade employs mechanical challenges in which cancer cells will morphologically adapt to survive in these altered environments (Amos and Choi, 2021). Numerous *in vivo* and *in vitro* studies have examined the initial stages of tumor growth and invasion and begun to outline some of the nano- and micro-scale changes occurring in the TME–including changes to ECM stiffness, ligand chemistry and ligand nanospacing. Micro-scale changes, such as stiffness and ligand chemistry, have shown greater advancements in biomaterials than nano-scale properties where the primary obstacle

has been developing tools *in vivo* to examine these changes and establishing platforms *in vitro* that allow for tuneability at this level. Overall, intelligent design of synthetic and biological biomaterials should incorporate these properties so that investigators can focus on the crucial differences between these properties and appreciate the role of the ECM and its regulation of cell fate even at the smallest, and perhaps most crucial, of metrics.

AUTHOR CONTRIBUTIONS

DV and YC drafted manuscript.

FUNDING

This work was supported by Heart Foundation Future Leader Fellowship 101173 (to YC) and Australian Government Research Training Program (to DV)

SUPPLEMENTARY MATERIAL

The Supplementary Material for this article can be found online at: https://www.frontiersin.org/articles/10.3389/fcell.2022.908799/full#supplementary-material

REFERENCES

Allinen, M., Beroukhim, R., Cai, L., Brennan, C., Lahti-Domenici, J., Huang, H., et al. (2004). Molecular Characterization of the Tumor Microenvironment in Breast Cancer. *Cancer Cell* 6, 17–32. doi:10.1016/j.ccr.2004.06.010

Amos, S. E., Choi, Y. S., and Glass, R. (2021). The Cancer Microenvironment: Mechanical Challenges of the Metastatic Cascade. *Front. Bioeng. Biotechnol.* 9, 56.

Arnold, M., Cavalcanti-Adam, E. A., Glass, R., Blümmel, J., Eck, W., Kantlehner, M., et al. (2004). Activation of Integrin Function by Nanopatterned Adhesive Interfaces. *Chem. Phys. Chem.* 5, 383–388. doi:10.1002/cphc.200301014

Balanis, N., Wendt, M. K., Schiemann, B. J., Wang, Z., Schiemann, W. P., and Carlin, C. R. (2013). Epithelial to Mesenchymal Transition Promotes Breast Cancer Progression via a Fibronectin-dependent STAT3 Signaling Pathway. *J. of Biol. Chem.* 288, 17954–17967. doi:10.1074/jbc.m113.475277

Bershadsky, A. D., Balaban, N. Q., and Geiger, B. (2003). Adhesion-dependent Cell Mechanosensitivity. *Annu. Rev. Cell. Dev. Biol.* 19, 677–695. doi:10.1146/annurev.cellbio.19.111301.153011

Bertlein, S., Brown, G., Lim, K. S., Jungst, T., Boeck, T., Blunk, T., et al. (2017). Thiol-Ene Clickable Gelatin: A Platform Bioink for Multiple 3D Biofabrication Technologies. *Adv. Mat.* 29, 1703404. doi:10.1002/adma.201703404

Brownfield, D. G., Venugopalan, G., Lo, A., Mori, H., Tanner, K., Fletcher, D. A., et al. (2013). Patterned Collagen Fibers Orient Branching Mammary Epithelium through Distinct Signaling Modules. *Curr. Biol.* 23, 703–709. doi:10.1016/j.cub.2013.03.032

Caliari, S. R., and Burdick, J. A. (2016). A Practical Guide to Hydrogels for Cell Culture. *Nat. Methods* 13, 405–414. doi:10.1038/nmeth.3839

Cargnello, M., and Roux, P. P. (2011). Activation and Function of the MAPKs and Their Substrates, the MAPK-Activated Protein Kinases. *Microbiol. Mol. Biol. Rev.* 75, 50–83. doi:10.1128/mmbr.00031-10

Cavalcanti-Adam, E. A., Micoulet, A., Blümmel, J., Auernheimer, J., Kessler, H., and Spatz, J. P. (2006). Lateral Spacing of Integrin Ligands Influences Cell Spreading and Focal Adhesion Assembly. *Eur. J. of Cell Biol.* 85, 219–224. doi:10.1016/j.ejcb.2005.09.011

Cavalcanti-Adam, E. A., Volberg, T., Micoulet, A., Kessler, H., Geiger, B., and Spatz, J. P. (2007). Cell Spreading and Focal Adhesion Dynamics Are Regulated by Spacing of Integrin Ligands. *Biophysical J.* 92, 2964–2974. doi:10.1529/biophysj.106.089730

Charbe, N., McCarron, P. A., and Tambuwala, M. M. (2017). Three-dimensional Bio-Printing: A New Frontier in Oncology Research. *Wjco* 8, 21. doi:10.5306/wjco.v8.i1.21

Chatterjee, A., Rodger, E. J., and Eccles, M. R. (2018). "Epigenetic Drivers of Tumourigenesis and Cancer Metastasis," in *Seminars in Cancer Biology* (Netherlands: Elsevier), 51, 149–159. doi:10.1016/j.semcancer.2017.08.004

Chellaiah, M. A., Biswas, R. S., Rittling, S. R., Denhardt, D. T., and Hruska, K. A. (2003). Rho-dependent Rho Kinase Activation Increases CD44 Surface Expression and Bone Resorption in Osteoclasts. *J. of Biol. Chem.* 278, 29086–29097. doi:10.1074/jbc.m211074200

Chin, I. L., Hool, L., and Choi, Y. S. (2021). Interrogating Cardiac Muscle Cell Mechanobiology on Stiffness Gradient Hydrogels. *Biomater. Sci.* 9, 6795–6806. doi:10.1039/d1bm01061a

Choquet, D., Felsenfeld, D. P., and Sheetz, M. P. (1997). Extracellular Matrix Rigidity Causes Strengthening of Integrin-Cytoskeleton Linkages. *Cell.* 88, 39–48. doi:10.1016/s0092-8674(00)81856-5

Cordenonsi, M., Zanconato, F., Azzolin, L., Forcato, M., Rosato, A., Frasson, C., et al. (2011). The Hippo Transducer TAZ Confers Cancer Stem Cell-Related Traits on Breast Cancer Cells. *Cell.* 147, 759–772. doi:10.1016/j.cell.2011.09.048

Cox, T. R., Bird, D., Baker, A.-M., Barker, H. E., Ho, M. W.-Y., Lang, G., et al. (2013). LOX-mediated Collagen Crosslinking Is Responsible for Fibrosis-Enhanced Metastasis. *Cancer Res.* 73, 1721–1732. doi:10.1158/0008-5472.can-12-2233

Daley, W. P., Peters, S. B., and Larsen, M. (2008). Extracellular Matrix Dynamics in Development and Regenerative Medicine. *J. of Cell Sci.* 121, 255–264. doi:10.1242/jcs.006064

De Francesco, E. M., Sotgia, F., and Lisanti, M. P. (2018). Cancer Stem Cells (CSCs): Metabolic Strategies for Their Identification and Eradication. *Biochem. J.* 475, 1611–1634. doi:10.1042/bcj20170164

Dupont, S., Morsut, L., Aragona, M., Enzo, E., Giulitti, S., Cordenonsi, M., et al. (2011). Role of YAP/TAZ in Mechanotransduction. *Nature* 474, 179–183. doi:10.1038/nature10137

Dzamba, B. J., and Peters, D. M. (1991). Arrangement of Cellular Fibronectin in Noncollagenous Fibrils in Human Fibroblast Cultures. *J. of Cell Sci.* 100, 605–612. doi:10.1242/jcs.100.3.605

Engler, A., Bacakova, L., Newman, C., Hategan, A., Griffin, M., and Discher, D. (2004). Substrate Compliance versus Ligand Density in Cell on Gel Responses. *Biophysical J.* 86, 617–628. doi:10.1016/s0006-3495(04)74140-5

Engler, A. J., Sen, S., Sweeney, H. L., and Discher, D. E. (2006). Matrix Elasticity Directs Stem Cell Lineage Specification. *Cell.* 126, 677–689. doi:10.1016/j.cell.2006.06.044

Fraser, J. R. E., Laurent, T. C., and Laurent, U. B. G. (1997). Hyaluronan: its Nature, Distribution, Functions and Turnover. *J. of Intern. Med.* 242, 27–33. doi:10.1046/j.1365-2796.1997.00170.x

García-Gareta, E., Pérez, M. Á., and García-Aznar, J. M. (2022). Decellularization of Tumours: A New Frontier in Tissue Engineering. *J. of Tissue Eng.* 13, 20417314221091682. doi:10.1177/20417314221091682

Gates, B. D., Xu, Q., Love, J. C., Wolfe, D. B., and Whitesides, G. M. (2004). Unconventional Nanofabrication. *Annu. Rev. Mat. Res.* 34, 339–372. doi:10.1146/annurev.matsci.34.052803.091100

Gelse, K., Pöschl, E., and Aigner, T. (2003). Collagens-structure, Function, and Biosynthesis. *Adv. drug Deliv. Rev.* 55, 1531–1546. doi:10.1016/j.addr.2003.08.002

Giancotti, F. G., and Ruoslahti, E. (1999). Integrin Signaling. *science* 285, 1028–1033. doi:10.1126/science.285.5430.1028

Gierach, G. L., Ichikawa, L., Kerlikowske, K., Brinton, L. A., Farhat, G. N., Vacek, P. M., et al. (2012). Relationship between Mammographic Density and Breast Cancer Death in the Breast Cancer Surveillance Consortium. *J. of Natl. Cancer Inst.* 104, 1218–1227. doi:10.1093/jnci/djs327

Habel, L. A., Dignam, J. J., Land, S. R., Salane, M., Capra, A. M., and Julian, T. B. (2004). Mammographic Density and Breast Cancer after Ductal Carcinoma *In Situ*. *JNCI J. of Natl. Cancer Inst.* 96, 1467–1472. doi:10.1093/jnci/djh260

Hadden, W. J., Young, J. L., Holle, A. W., McFetridge, M. L., Kim, D. Y., Wijesinghe, P., et al. (2017). Stem Cell Migration and Mechanotransduction

on Linear Stiffness Gradient Hydrogels. *Proc. Natl. Acad. Sci. U.S.A.* 114, 5647–5652. doi:10.1073/pnas.1618239114

Hamilton, S. R., Fard, S. F., Paiwand, F. F., Tolg, C., Veiseh, M., Wang, C., et al. (2007). The Hyaluronan Receptors CD44 and Rhamm (CD168) Form Complexes with ERK1,2 that Sustain High Basal Motility in Breast Cancer Cells. *J. of Biol. Chem.* 282, 16667–16680. doi:10.1074/jbc.m702078200

Holle, A. W., Young, J. L., and Spatz, J. P. (2016). *In Vitro* cancer Cell-ECM Interactions Inform *In Vivo* Cancer Treatment. *Adv. drug Deliv. Rev.* 97, 270–279. doi:10.1016/j.addr.2015.10.007

Hou, J., Yan, D., Liu, Y., Huang, P., and Cui, H. (2020). The Roles of Integrin α5β1 in Human Cancer. *Ott* 13, 13329–13344. doi:10.2147/ott.s273803

Hsu, M.-Y., Shih, D.-T., Meier, F. E., Van Belle, P., Hsu, J.-Y., Elder, D. E., et al. (1998). Adenoviral Gene Transfer of β3 Integrin Subunit Induces Conversion from Radial to Vertical Growth Phase in Primary Human Melanoma. *The Am. J. of pathology* 153, 1435–1442. doi:10.1016/s0002-9440(10)65730-6

Hynes, R. O. (1992). Integrins: Versatility, Modulation, and Signaling in Cell Adhesion. *Cell.* 69, 11–25. doi:10.1016/0092-8674(92)90115-s

Insua-Rodríguez, J., and Oskarsson, T. (2016). The Extracellular Matrix in Breast Cancer. *Adv. drug Deliv. Rev.* 97, 41–55. doi:10.1016/j.addr.2015.12.017

Jaggupilli, A., and Elkord, E. (2012). Significance of CD44 and CD24 as Cancer Stem Cell Markers: an Enduring Ambiguity. *Clin. Dev. Immunol.* 2012, 708036. doi:10.1155/2012/708036

Karousou, E., D'Angelo, M. L., Kouvidi, K., Vigetti, D., Viola, M., Nikitovic, D., et al. (2014). Collagen VI and Hyaluronan: the Common Role in Breast Cancer. *BioMed Res. Int.* 2014, 606458. doi:10.1155/2014/606458

Khaled, W., Reichling, S., Bruhns, O., Boese, H., Baumann, M., Monkman, G., et al. (2004). "Palpation Imaging Using a Haptic System for Virtual Reality Applications in Medicine," in *Perspective in Image-Guided Surgery* (Singapore: World Scientific), 407–414. doi:10.1142/9789812702678_0055

Kim, C., Young, J. L., Holle, A. W., Jeong, K., Major, L. G., Jeong, J. H., et al. (2020). Stem Cell Mechanosensation on Gelatin Methacryloyl (GelMA) Stiffness Gradient Hydrogels. *Ann. Biomed. Eng.* 48, 893–902. doi:10.1007/s10439-019-02428-5

Klein, C. E., Dressel, D., Steinmayer, T., Mauch, C., Eckes, B., Krieg, T., et al. (1991). Integrin Alpha 2 Beta 1 Is Upregulated in Fibroblasts and Highly Aggressive Melanoma Cells in Three-Dimensional Collagen Lattices and Mediates the Reorganization of Collagen I Fibrils. *The J. of Cell Biol.* 115, 1427–1436. doi:10.1083/jcb.115.5.1427

Koistinen, P., and Heino, J. (2013). "Integrins in Cancer Cell Invasion," in *Madame Curie Bioscience Database* (Texas(United States): Landes Bioscience). Internet.

Larsen, M., Artym, V. V., Green, J. A., and Yamada, K. M. (2006). The Matrix Reorganized: Extracellular Matrix Remodeling and Integrin Signaling. *Curr. Opin. Cell Biol.* 18, 463–471. doi:10.1016/j.ceb.2006.08.009

Lee, J. Y., and Chaudhuri, O. (2021). Modeling the Tumor Immune Microenvironment for Drug Discovery Using 3D Culture. *Apl. Bioeng.* 5, 010903. doi:10.1063/5.0030693

Leiss, M., Beckmann, K., Girós, A., Costell, M., and Fässler, R. (2008). The Role of Integrin Binding Sites in Fibronectin Matrix Assembly *In Vivo*. *Curr. Opin. Cell Biol.* 20, 502–507. doi:10.1016/j.ceb.2008.06.001

Li, S., Wang, X., Cao, B., Ye, K., Li, Z., and Ding, J. (2015). Effects of Nanoscale Spatial Arrangement of Arginine-Glycine-Aspartate Peptides on Dedifferentiation of Chondrocytes. *Nano Lett.* 15, 7755–7765. doi:10.1021/acs.nanolett.5b04043

Lin, J., and Ding, D. (2017). The Prognostic Role of the Cancer Stem Cell Marker CD44 in Ovarian Cancer: a Meta-Analysis. *Cancer Cell. Int.* 17, 8–11. doi:10.1186/s12935-016-0376-4

Lochter, A., and Bissell, M. J. (1995). "Involvement of Extracellular Matrix Constituents in Breast Cancer," in *Seminars in Cancer Biology* (Berkeley, CA (United States): Lawrence Berkeley National Lab.), 6. doi:10.1006/scbi.1995.0017

Lohmüller, T., Aydin, D., Schwieder, M., Morhard, C., Louban, I., Pacholski, C., et al. (2011). Nanopatterning by Block Copolymer Micelle Nanolithography and Bioinspired Applications. *Biointerphases* 6, MR1–MR12. doi:10.1116/1.3536839

Lu, P., Takai, K., Weaver, V. M., and Werb, Z. (2011). Extracellular Matrix Degradation and Remodeling in Development and Disease. *Cold Spring Harb. Perspect. Biol.* 3, a005058. doi:10.1101/cshperspect.a005058

Major, L. G., Holle, A. W., Young, J. L., Hepburn, M. S., Jeong, K., Chin, I. L., et al. (2019). Volume Adaptation Controls Stem Cell Mechanotransduction. *ACS Appl. Mat. Interfaces* 11, 45520–45530. doi:10.1021/acsami.9b19770

Massalha, S., and Weihs, D. (2017). Metastatic Breast Cancer Cells Adhere Strongly on Varying Stiffness Substrates, Initially without Adjusting Their Morphology. *Biomech. Model. Mechanobiol.* 16, 961–970. doi:10.1007/s10237-016-0864-4

Massia, S. P., and Hubbell, J. A. (1991). An RGD Spacing of 440 Nm Is Sufficient for Integrin Alpha V Beta 3-mediated Fibroblast Spreading and 140 Nm for Focal Contact and Stress Fiber Formation. *The J. of Cell Biol.* 114, 1089–1100. doi:10.1083/jcb.114.5.1089

Maugeri-Saccà, M., Barba, M., Pizzuti, L., Vici, P., Di Lauro, L., Dattilo, R., et al. (2015). The Hippo Transducers TAZ and YAP in Breast Cancer: Oncogenic Activities and Clinical Implications. *Expert Rev. Mol. Med.* 17, e14. doi:10.1017/erm.2015.12

McIntosh, J., Dennison, G., Holly, J. M. P., Jarrett, C., Frankow, A., Foulstone, E. J., et al. (2010). IGFBP-3 Can Either Inhibit or Enhance EGF-Mediated Growth of Breast Epithelial Cells Dependent upon the Presence of Fibronectin. *J. of Biol. Chem.* 285, 38788–38800. doi:10.1074/jbc.m110.177311

Ohata, H., Ishiguro, T., Aihara, Y., Sato, A., Sakai, H., Sekine, S., et al. (2012). Induction of the Stem-like Cell Regulator CD44 by Rho Kinase Inhibition Contributes to the Maintenance of Colon Cancer-Initiating Cells. *Cancer Res.* 72, 5101–5110. doi:10.1158/0008-5472.can-11-3812

Ondeck, M. G., Kumar, A., Placone, J. K., Plunkett, C. M., Matte, B. F., Wong, K. C., et al. (2019). Dynamically Stiffened Matrix Promotes Malignant Transformation of Mammary Epithelial Cells via Collective Mechanical Signaling. *Proc. Natl. Acad. Sci. U.S.A.* 116, 3502–3507. doi:10.1073/pnas.1814204116

Oria, R., Wiegand, T., Escribano, J., Elosegui-Artola, A., Uriarte, J. J., Moreno-Pulido, C., et al. (2017). Force Loading Explains Spatial Sensing of Ligands by Cells. *Nature* 552, 219–224. doi:10.1038/nature24662

Oskarsson, T. (2013). Extracellular Matrix Components in Breast Cancer Progression and Metastasis. *The Breast* 22, S66–S72. doi:10.1016/j.breast.2013.07.012

Özdemir, B. C., Pentcheva-Hoang, T., Carstens, J. L., Zheng, X., Wu, C.-C., Simpson, T. R., et al. (2014). Depletion of Carcinoma-Associated Fibroblasts and Fibrosis Induces Immunosuppression and Accelerates Pancreas Cancer with Reduced Survival. *Cancer Cell* 25, 719–734. doi:10.1016/j.ccr.2014.04.005

Paszek, M. J., and Weaver, V. M. (2004). The Tension Mounts: Mechanics Meets Morphogenesis and Malignancy. *J. Mammary Gland. Biol. Neoplasia* 9, 325–342. doi:10.1007/s10911-004-1404-x

Plodinec, M., Loparic, M., Monnier, C. A., Obermann, E. C., Zanetti-Dallenbach, R., Oertle, P., et al. (2012). The Nanomechanical Signature of Breast Cancer. *Nat. Nanotech* 7, 757–765. doi:10.1038/nnano.2012.167

Provenzano, P. P., Inman, D. R., Eliceiri, K. W., and Keely, P. J. (2009). Matrix Density-Induced Mechanoregulation of Breast Cell Phenotype, Signaling and Gene Expression through a FAK-ERK Linkage. *Oncogene* 28, 4326–4343. doi:10.1038/onc.2009.299

Provenzano, P. P., Inman, D. R., Eliceiri, K. W., Trier, S. M., and Keely, P. J. (2008). Contact Guidance Mediated Three-Dimensional Cell Migration Is Regulated by Rho/ROCK-dependent Matrix Reorganization. *Biophysical J.* 95, 5374–5384. doi:10.1529/biophysj.108.133116

Raghuraman, S., Schubert, A. S., Bröker, S., Jurado, A., Müller, A., Brandt, M., et al. (2022). Pressure Drives Rapid Burst-Like Coordinated Cellular Motion from 3D Cancer Aggregates. *Adv. Sci.* 9, 2104808. doi:10.1002/advs.202104808

Raimondi, C., Gradilone, A., Naso, G., Vincenzi, B., Petracca, A., Nicolazzo, C., et al. (2011). Epithelial-mesenchymal Transition and Stemness Features in Circulating Tumor Cells from Breast Cancer Patients. *Breast Cancer Res. Treat.* 130, 449–455. doi:10.1007/s10549-011-1373-x

Ramaswamy, S., Ross, K. N., Lander, E. S., and Golub, T. R. (2003). A Molecular Signature of Metastasis in Primary Solid Tumors. *Nat. Genet.* 33, 49–54. doi:10.1038/ng1060

Rhim, A. D., Oberstein, P. E., Thomas, D. H., Mirek, E. T., Palermo, C. F., Sastra, S. A., et al. (2014). Stromal Elements Act to Restrain, rather Than Support, Pancreatic Ductal Adenocarcinoma. *Cancer Cell* 25, 735–747. doi:10.1016/j.ccr.2014.04.021

Ro, J., Kim, J., and Cho, Y.-K. (2022). Recent Advances in Spheroid-Based Microfluidic Models to Mimic Tumour Microenvironment. *Analyst* 147, 2023–2034. doi:10.1039/D2AN00172A

Ruoslahti, E. (1991). Integrins. *J. Clin. Invest.* 87, 1–5. doi:10.1172/jci114957

Sahai, E., Astsaturov, I., Cukierman, E., DeNardo, D. G., Egeblad, M., Evans, R. M., et al. (2020). A Framework for Advancing Our Understanding of Cancer-Associated Fibroblasts. *Nat. Rev. Cancer* 20, 174–186. doi:10.1038/s41568-019-0238-1

Sameni, M., Moin, K., and Sloane, B. F. (2000). Imaging Proteolysis by Living Human Breast Cancer Cells. *Neoplasia* 2, 496–504. doi:10.1038/sj.neo.7900116

Selhuber-Unkel, C., Erdmann, T., López-García, M., Kessler, H., Schwarz, U. S., and Spatz, J. P. (2010). Cell Adhesion Strength Is Controlled by Intermolecular Spacing of Adhesion Receptors. *Biophysical J.* 98, 543–551. doi:10.1016/j.bpj.2009.11.001

Sherman-Baust, C. A., Weeraratna, A. T., Rangel, L. B. A., Pizer, E. S., Cho, K. R., Schwartz, D. R., et al. (2003). Remodeling of the Extracellular Matrix through Overexpression of Collagen VI Contributes to Cisplatin Resistance in Ovarian Cancer Cells. *Cancer Cell* 3, 377–386. doi:10.1016/s1535-6108(03)00058-8

Siegel, M. B., He, X., Hoadley, K. A., Hoyle, A., Pearce, J. B., Garrett, A. L., et al. (2018). Integrated RNA and DNA Sequencing Reveals Early Drivers of Metastatic Breast Cancer. *The J. of Clin. investigation* 128, 1371–1383. doi:10.1172/jci96153

Tlsty, T. D., and Coussens, L. M. (2006). Tumor Stroma and Regulation of Cancer Development. *Annu. Rev. Pathol. Mech. Dis.* 1, 119–150. doi:10.1146/annurev.pathol.1.110304.100224

Toole, B. P. (2004). Hyaluronan: from Extracellular Glue to Pericellular Cue. *Nat. Rev. Cancer* 4, 528–539. doi:10.1038/nrc1391

Tse, J. R., and Engler, A. J. (2010). Preparation of Hydrogel Substrates with Tunable Mechanical Properties. *Curr. Protoc. Cell. Biol.* 10. Unit 10.16. doi:10.1002/0471143030.cb1016s47

Wallace, J. M., Chen, Q., Fang, M., Erickson, B., Orr, B. G., and Banaszak Holl, M. M. (2010). Type I Collagen Exists as a Distribution of Nanoscale Morphologies in Teeth, Bones, and Tendons. *Langmuir* 26, 7349–7354. doi:10.1021/la100006a

Wang, K., Wu, F., Seo, B. R., Fischbach, C., Chen, W., Hsu, L., et al. (2017). Breast Cancer Cells Alter the Dynamics of Stromal Fibronectin-Collagen Interactions. *Matrix Biol.* 60-61, 86–95. doi:10.1016/j.matbio.2016.08.001

Wang, L., Zuo, X., Xie, K., and Wei, D. (2018). "The Role of CD44 and Cancer Stem Cells," in *Cancer Stem Cells* (Berlin(Germany): Springer), 31–42. doi:10.1007/978-1-4939-7401-6_3

Wang, N., Tytell, J. D., and Ingber, D. E. (2009). Mechanotransduction at a Distance: Mechanically Coupling the Extracellular Matrix with the Nucleus. *Nat. Rev. Mol. Cell. Biol.* 10, 75–82. doi:10.1038/nrm2594

Wang, Z., Wu, Y., Wang, H., Zhang, Y., Mei, L., Fang, X., et al. (2014). Interplay of Mevalonate and Hippo Pathways Regulates RHAMM Transcription via YAP to Modulate Breast Cancer Cell Motility. *Proc. Natl. Acad. Sci. U. S. A.* 111, E89–E98. doi:10.1073/pnas.1319190110

WHO (2021). *Breast Cancer*. Minnesota(United States): Mayo Clinic.

Wozniak, M. A., Desai, R., Solski, P. A., Der, C. J., and Keely, P. J. (2003). ROCK-generated Contractility Regulates Breast Epithelial Cell Differentiation in Response to the Physical Properties of a Three-Dimensional Collagen Matrix. *The J. of Cell Biol.* 163, 583–595. doi:10.1083/jcb.200305010

Ye, J., Wu, D., Wu, P., Chen, Z., and Huang, J. (2014). The Cancer Stem Cell Niche: Cross Talk between Cancer Stem Cells and Their Microenvironment. *Tumor Biol.* 35, 3945–3951. doi:10.1007/s13277-013-1561-x

Young, J. L., Holle, A. W., and Spatz, J. P. (2016). Nanoscale and Mechanical Properties of the Physiological Cell-ECM Microenvironment. *Exp. Cell. Res.* 343, 3–6. doi:10.1016/j.yexcr.2015.10.037

Young, J. L., Hua, X., Somsel, H., Reichart, F., Kessler, H., and Spatz, J. P. (2020). Integrin Subtypes and Nanoscale Ligand Presentation Influence Drug Sensitivity in Cancer Cells. *Nano Lett.* 20, 1183–1191. doi:10.1021/acs.nanolett.9b04607

Conflict of Interest: The authors declare that the research was conducted in the absence of any commercial or financial relationships that could be construed as a potential conflict of interest.

Publisher's Note: All claims expressed in this article are solely those of the authors and do not necessarily represent those of their affiliated organizations, or those of the publisher, the editors and the reviewers. Any product that may be evaluated in this article, or claim that may be made by its manufacturer, is not guaranteed or endorsed by the publisher.

frontiers | Frontiers in Cell and Developmental Biology

TYPE Original Research
PUBLISHED 06 September 2022
DOI 10.3389/fcell.2022.927631

OPEN ACCESS

EDITED BY
Selwin K. Wu,
National University of Singapore,
Singapore

REVIEWED BY
Sangappa B. Chadchan,
Baylor College of Medicine,
United States
Maryse Bailly,
University College London,
United Kingdom

*CORRESPONDENCE
Junaid Afzal,
junaid.afzal@ucsf.edu
Kshitiz,
kshitiz@uchc.edu

†These authors have contributed equally to this work

SPECIALTY SECTION
This article was submitted to Signaling, a section of the journal Frontiers in Cell and Developmental Biology

RECEIVED 24 April 2022
ACCEPTED 09 August 2022
PUBLISHED 06 September 2022

CITATION
Afzal J, Du W, Novin A, Liu Y, Wali K, Murthy A, Garen A, Wagner G, Kshitiz (2022), Paracrine HB-EGF signaling reduce enhanced contractile and energetic state of activated decidual fibroblasts by rebalancing SRF-MRTF-TCF transcriptional axis.
Front. Cell Dev. Biol. 10:927631.
doi: 10.3389/fcell.2022.927631

Paracrine HB-EGF signaling reduce enhanced contractile and energetic state of activated decidual fibroblasts by rebalancing SRF-MRTF-TCF transcriptional axis

Junaid Afzal[1]*, Wenqiang Du[2†], Ashkan Novin[2†], Yamin Liu[2], Khadija Wali[2], Anarghya Murthy[2], Ashley Garen[2], Gunter Wagner[3,4] and Kshitiz[2,4]*

[1]Division of Cardiology, Department of Medicine, University of California San Francisco, San Francisco, CA, United States, [2]Department of Biomedical Engineering, University of Connecticut Health, Farmington, CT, United States, [3]Department of Ecology and Evolution, Yale University West Campus, West Haven, CT, United States, [4]Systems Biology Institute, Yale University, West Haven, CT, United States

Multiple parallels exist between placentation and cancer dissemination at molecular, cellular, and anatomical levels, presenting placentation as a unique model to mechanistically understand the onset of cancer metastasis. In humans, interaction of placenta and the endometrium results eventually in deep invasion of placental extravillous trophoblasts (EVTs) into the maternal stroma, a process similar to stromal trespass by disseminating carcinoma cells. In anticipation of implantation, endometrial fibroblasts (ESFs) undergo a process called decidualization during the secretory phase of the menstrual cycle. Decidualization, among other substantial changes associated with ESF differentiation, also involves a component of fibroblast activation, and myofibroblast transformation. Here, using traction force microscopy, we show that increased cellular contractility in decidualized ESFs is reversed after interaction with EVTs. We also report here the large changes in energetic state of ESFs upon decidualization, showing increased oxidative phosphorylation, mitochondrial competency and ATP generation, as well as enhanced aerobic glycolysis, presenting mechanical contractility and energetic state as new functional hallmarks for decidualization. These energetic changes accompanying the marked increase in contractile force generation in decidualization were reduced in the presence of EVTs. We also show that increase in decidual contractility and mechanical resistance to invasion is achieved by SRF-MRTF transcriptional activation, achieved via increased phosphorylation of fibroblast-specific myosin light chain 9 (MYL9). EVT induced paracrine secretion of Heparin Binding Epidermal Growth Factor (HBEGF), a potent MAPK activator, which shifts the balance of SRF association away from MRTF based transcription, reducing decidual ESF contractility and mechanical resistance to placental invasion. Our results identify a new axis of intercellular communication in the placental bed

modulating stromal force generation and resistance to invasion with concurrent downregulation of cellular energetics. These findings have important implications for implantation related disorders, as well as stromal control of cancer dissemination.

KEYWORDS

contractility, energetics, cell-cell communication, cancer-stroma crosstalk, fetal maternal interface, placental invasion, paracrine HB-EGF signaling, SRF-Mrtf/Tcf axis

Introduction

Parallels between placental invasion into the endometrium, and cancer metastasis has long been recognized (Costanzo et al., 2018; Coorens et al., 2021; Wagner et al., 2022). These parallels exist at multiple biological scales: genetic, molecular, cellular, and anatomical, and manifest in many similarities in the biochemical, immunological, or physical nature of interaction between cancer and stroma in one context, and placenta and endometrium in another (Suhail et al., 2021; Wagner et al., 2021). In humans, the endometrial fibroblasts (ESFs) undergo a cyclic pattern of differentiation, wherein ESFs differentiate into decidual ESFs (dESFs), resulting in increased cellular hypertrophy, transcriptional changes, increased secretion of hormones, and contractile force generation, in anticipation of implantation (Christian et al., 2002; Gellersen et al., 2007). For long, it was still not settled whether decidualization supports, or resists trophoblast invasion (Gleeson et al., 2001; Menkhorst et al., 2012; Pollheimer et al., 2018). In recent works, we have shown that decidualization significantly reduces trophoblast invasion, suggesting that the advent of dESFs is an evolutionary response to limit excessive invasion. We have also shown that decidualization as a process has evolved by incorporating a classical fibroblast activation response to wounding (Wu et al., 2020), which occurs in response to the degradation of uterine epithelium by trophoblasts, and their invasion into the maternal stroma.

Fibroblast activation generically results in increased actomyosin assembly and force generation, followed by remodeling of the extracellular matrix. Contractile force generation by fibroblasts, when coupled with fibroblast-epithelium interaction, is now understood to be important in instigating dissemination of epithelial tumors (Labernadie et al., 2017; Ansardamavandi and Tafazzoli-Shadpour, 2021). However, contractile forces may also be resistive (Wang et al., 2021). Drawing parallels between cancer-fibroblast interaction, and trophoblast-ESF interaction (Kshitiz et al., 2019), we asked how the decidual stromal contractile force generation change after interaction with trophoblasts. Generation of contractile force is an energy intensive phenomenon. We found that decidualization is accompanied by a marked increase in the energetic state, increasing both oxidative phosphorylation (OxPhos) and glycolysis. We also found that the EVT induced reduction in contractile force generation is also accompanied by correlated reduction in glycolysis, as well as oxidative phosphorylation.

We have also identified a cell-cell paracrine interaction axis between EVTs and dESFs, which mediated the reversal in dESF contractile force generation, and increased invasability. Specifically, we found that secretion of HB-EGF (heparin bound-endocrine growth factor) by HTR8 resulted in rewiring of SRF (serum response factor) association from MRTF (myocardin related transcription factor) to TCF (ternary complex factor). Reduced SRF-MRTF transcriptional regulation reduces phosphorylation of myosin light chain 9 (MYL9) resulting in decreased contractile force generation in dESFs. HB-EGF is an abundantly secreted growth factor in many cancers (Sethuraman et al., 2018), but its role in regulating stromal contractility, and invasability has not been studied. Our study underlines that fibroblast mechanics and energetic state are crucial in the stromal containment of epithelial invasion, and that both invasive cells, here trophoblasts, can evade the mechanical resistance offered by stromal fibroblasts by paracrine modulation of their contractile machinery.

Results

Extravillous trophoblasts reduce mechanical force generation by decidual endometrial fibroblasts

Extravillous trophoblasts (EVTs), which are notably of recent evolutionary origin (Carter, 2012, 2021), invade through the decidual stroma, to reach the maternal spiral arteries. In the process, EVTs interact with the decidual endometrial fibroblasts (dESFs) (Figure 1A). We have previously reported that decidualization is evolutionarily derived from fibroblast activation (Wu et al., 2020). Indeed, we had found that differentiation of ESFs involves an interim stage which mimics activation of fibroblasts in response to wounding, which gets extended to a larger program of decidualization (Wu et al., 2020). Early decidualization, therefore, appeared to be mimicking increase in ESF contractility and generation of mechanical forces. We therefore asked if interaction of dESFs with EVTs may influence dESF mechanical force generation. We have previously reported that EVTs could modulate the matricellular homeostasis achieved by decidualization, which

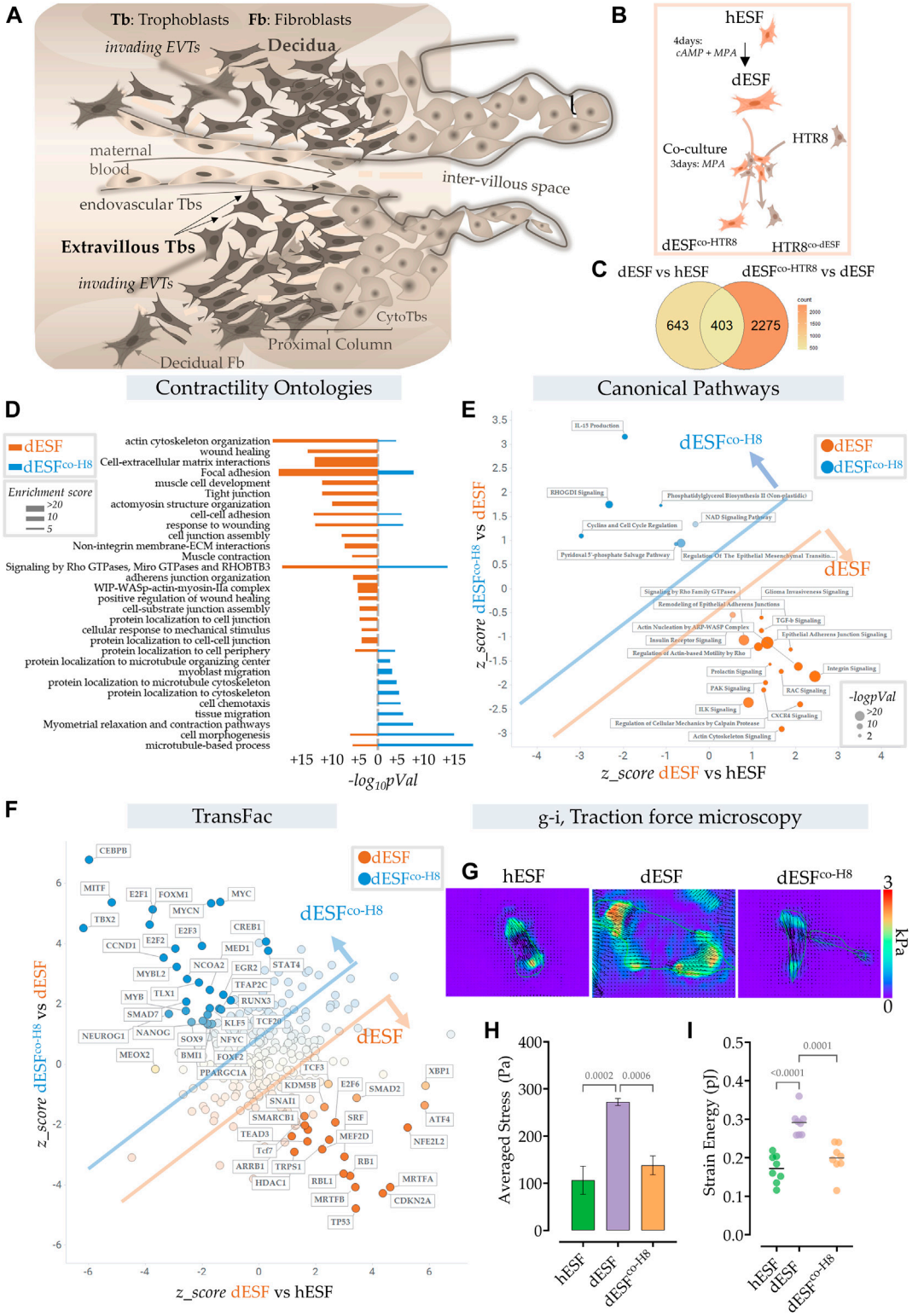

FIGURE 1
Extravillous trophoblasts reduce contractile force generation by decidual endometrial fibroblasts. **(A)** Schematic showing the maternal fetal interface during placentation, wherein EVTs escape into the maternal stroma and deeply invade into the endometrium to eventually reach the spiral arteries. **(B)** Schematic showing the experimental plan for co-culture of dESFs with fluorescently labeled HTR8; cells were separated by fluorescent assisted cell sorting after 3 days of co-culture and sequenced. **(C)** Venn diagram showing gene counts differentially regulated between

(*Continued*)

FIGURE 1
undifferentiated ESFs (hESFs), and decidualized ESFs (dESFs), and between dESFs co-cultured with HTR8 (dESFco-H8) and dESFs. **(D)** Activation of Contractility related ontologies in dESFs and dESF^{co-H8}. Thickness of bar plot shows enrichment score of the relevant ontology. **(E)**. Activation of canonical pathways in dESFs compared to hESFs or in dESFco-H8 vs. dESFs; Axes represent the activation or inhibition (z-score) of relevant ontologies; Ontologies that are upregulated in dESFs (compared to hESFs) but go down with co-culture (dESF^{co-H8}) are labeled orange, and ontologies upregulated in dESF^{co-H8} are labeled blue. Size of the bubble reflect -log (p-Val) in that quadrant. Calculated using Ingenuity Pathway (IPA) analysis. **(F).** Transcriptional factors (TransFac) upregulated in dESFs and then downregulated after co-culture are labeled orange) or downregulated with decidualization (dESFs), and then upregulated with co-culture (dESF^{co-H8}) are labeled blue. Calculated using Ingenuity Pathway (IPA) analysis. **(H–I)**. Traction force microscopy: **(H)**. Representative traction force vector maps and strain energy maps in hESF with decidualization (dESF) and after co-culture treatment (dESFco-H8). Anova with Tukey's correction was used for quantification of average cellular stress **(H)**, and strain energy **(I)**; $n >$ 10 cells per condition.

directly reverses the decidual-specific resistance to placental invasion. Here, we focused on fibroblast force generation, and associated fibroblast metabolism to ask if interaction with EVTs may modulate the force generation capability of decidualized ESFs.

We used RNAseq data obtained from ESFs decidualized for 4 days and co-cultured for 2 days with fluorescently labeled HTR8, an EVT cell line. After incubation, ESFs and EVTs were seperated using fluorescence assisted cell sorting (FACS) (Figure 1B). Co-culture with HTR8 resulted in significant change in gene expression of dESFs, with many genes that were reversed in expression after co-culture (Figure 1C). Focusing on biomechanical pathways associated with fibroblast activation, we found that overall there was a significant effect of HTR8 co-culture on dESF gene expression (Figure 1D).

To confirm whether co-culture induced reduction in dESF gene expression related to biomechanical force was systemic, we computed activation of canonical pathways of contractile force generation in decidualization, and after co-culture with HTR8 (Figure 1E). We found that many gene ontologies related to cellular contractile force generation, including TGFβ signaling, actin nucleation, Rho mediated action-based motility, Rac signaling, and Calpain protease mediated cellular mechanics were upregulated in dESFs vs. hESFs. Their activation were markedly reduced after co-culture with HTR8 in dESF^{co-H8} (Figure 1E). Transfac based Transcription Factor activation scoring also showed that key transcriptional regulators associated with cellular motility, contractile force generation, and fibroblast activation were initially upregulated in dESFs, and showed reversal when dESFs were in co-culture with HTR8. These included myocardin related TFs, MRTF-A/B, and serum response factor (SRF), which together can form a transcriptional factor complex activating expression of many genes mediating cellular force generation (Gualdrini et al., 2016). Others included SNAI1, a key factor regulating epithelial to mesenchymal transformation, as well as MEF2D encoding myocyte enhancer factor 2D, a key TF regulating genes encoding myosin based contractile machinery.

To functionally confirm that co-culture with HTR8 had indeed resulted in reduction in force generation by dESFs, we used traction force microscopy, which computes contractile forces generated by adhered cells from displacement of fluorescent beads embedded in a pliable hydrogel based cell substratum. dESFs were cultured, either after decidualization, or conditioned with supplemented medium from HTR8. We found that contractile force generation in dESFs was markedly higher than in hESFs, and treatment with conditioned medium from HTR8 reduced it significantly (Figures 1G,H). Strain energy density, normalized to cell area also showed a similar trend of an initial increase, and then decrease after co-culture (Figure 1I). Reduction in the contractile force generated by dESFs by conditioned medium suggested involvement of paracrine signals from HTR8 in regulating fibroblast mechanics.

Decidualization enhances oxidative phosphorylation and mitochondrial ATP generation in ESFs, which is reduced after co-culture with EVTs

Large contractile force generation is a highly energetically intensive process, necessitating rewiring of the metabolic flux in a cell. As decidualization involves an early onset of fibroblast activation, accompanied by increase in mechanical force generation (Figures 2A–C), we expected an increase in energy demand in the cell (Sleep et al., 2005). To functionally test if glucose uptake and force generation are linked, we took advantage of the inherent diversity in strain energy in a population of dESFs, and correlatively measured NBDG (glucose) uptake and contractile force generation (Figures 1A,B). We found a high correlation between NBDG uptake and strain energy within dESFs (Figure 2C), confirming that increased contractile force generation poses higher energy demands on the cell (Figure 2D). How decidualization affects metabolism and energy requirement in ESFs has not been well studied, and there is little understanding of the energetic transitions in dESFs as they interact with EVTs during placentation. We therefore systematically tested the energetic state of ESFs in response to decidualization, as well as subsequent co-culture with HTR8s.

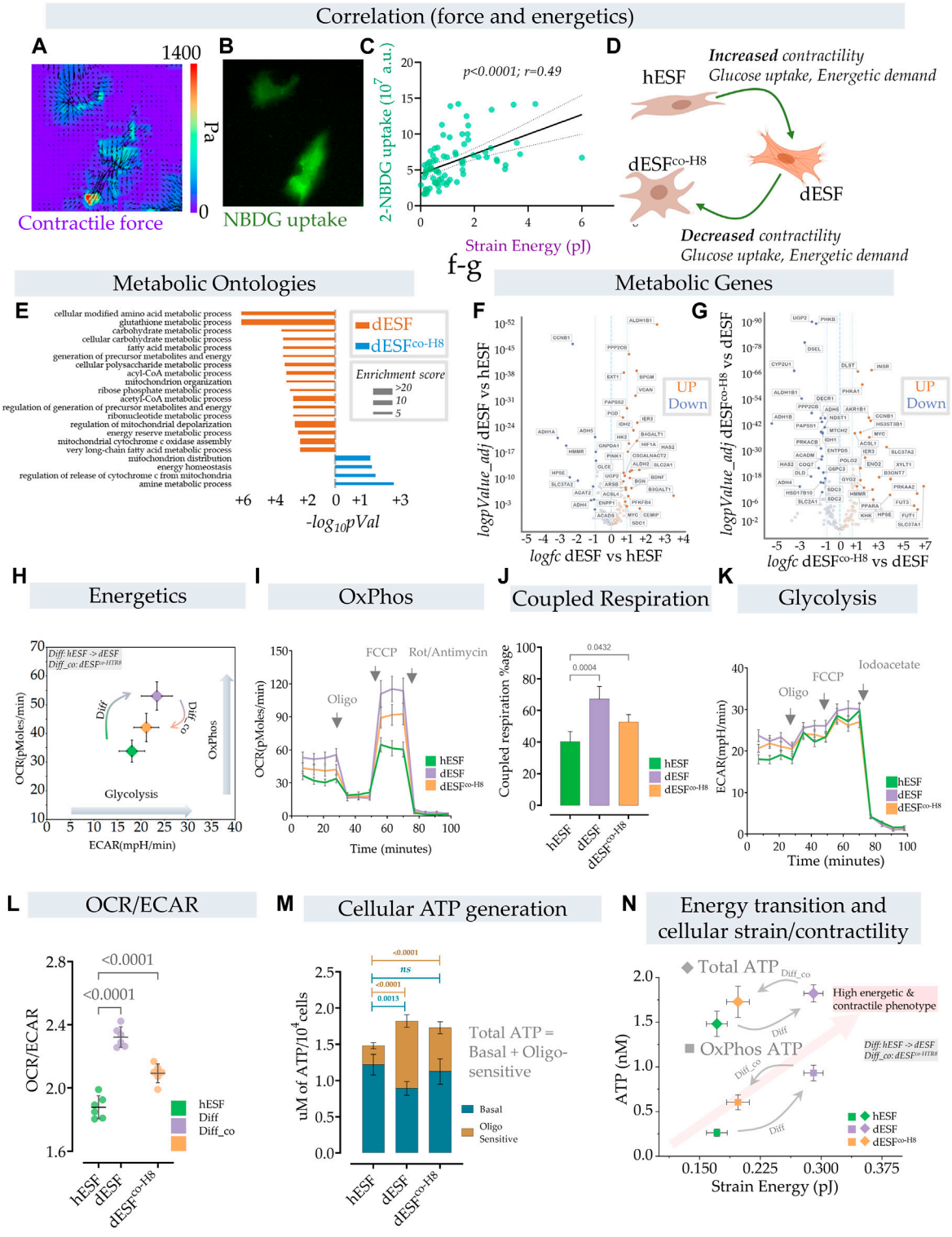

FIGURE 2
Energetic transition in decidual ESF reflect changes in contractility which is reversed by EVT. **(A–D)** Traction force microscopy and glucose uptake: **(A)** Glucose uptake was monitored within a population of decidualized ESFs (dESF) with NBDG along with cellular contractility, Representative figure of two contracting cells with **(A)** traction force vector maps and **(B)** NBDG fluorescence **(B)**; **(C)** Correlation of strain energy of contracting cells and glucose uptake; $n > 70$. **(D)** Schematic showing increased contractility, glucose uptake, and energetic demand in decidualized cells (dESF) that is reduced with co-culture ($dESF^{co-H8}$). **(E)** Metabolic ontologies that are activated in dESF or $dESF^{co-H8}$ with their

(*Continued*)

FIGURE 2
enrichment score **(F,G)**. Volcano plot of differential metabolic genes in combined ontologies of ATP generation, Oxidative phosphorylation, and glycolysis: Significant number of metabolic genes are upregulated (highlighted genes are < $p0.001$) with differentiation and several key TCA (citric acid cycle) genes are downregulated after co-culture with hTR8. **(H,I)** Energetics data in hESF, decidualized hESFs (dESF) and co-culture condition (dESFco-H8) using XF analyzer. **(H)** Basal oxygen consumption rate (OCR) and extracellular acidification rate (ECAR) shows an increase in OxPhos and glycolysis with decidualization which is partially reversed with co-culture condition. Basal data is presented with mean and SD. **(I)** Increase in oxygen consumption rate (OCR) at basal levels, enhanced coupled (oligomycin sensitive) and uncoupled respiration (FCCP) with decidualization. **(J)** Percentage of coupled respiration: oligomycin sensitive respiration is significantly increased in dESFs compared to hESF and $dESF^{co-H8}$. **(K)** Extracellular acidification rate: Increase in ECAR with decidualization reflects increase in glycolysis which is confirmed after inhibition with iodoacetate. n = 6 in each XF experiment with data reported as mean ± SD and statistical significance calculated using Anova followed by Dunnett's test. **(L)** OCR/ECAR ratio at basal levels reflects increased reliance on oxygen consumption in dESFs. n = 6 in each XF experiment with data reported as mean ± SD and statistical significance calculated using Anova followed by Dunnett's test. **(M)** Increase in total cellular ATP generation with decidualization. Oligomycin sensitive ATP generation which reflects ATP generation from OxPhos indicates increased utilization of oxidative phosphorylation for ATP generation in dESFs. n = 6 in ATP experiment and the data is presented as mean ± SD. Statistical significance was calculated using Anova followed by Šídák's test. **(N)** Transition of cellular contractility (strain energy) and ATP levels per cell (total and Oxphos) show high energetic and contractile phenotype with decidualization.

Although enhanced glucose uptake suggested increase in aerobic glycolysis, gene set analysis for metabolic ontologies showed that decidualization also resulted in enrichment of several ontologies related to mitochondrial respiration (Figure 2E). Key metabolic genes and mitochondrial transcripts that regulate citric acid cycle (TCA) and ATP generation through mitochondria were also increased with decidualization (Figures 2F,G). Increase in mitochondrial ATP generation is an efficient process whereby ATP generation per glucose molecule is significantly increased from 2–4 mol/glucose molecule to 32–36 mol of ATP. Increase in ATP however limits cellular substrate (glucose) uptake (Blodgett et al., 2007). To keep the high glucose levels for proliferative or other needs, cells have adaptive mechanisms to increase the pyruvate to lactate flux, limit OxPhos and/or increase ATP utilization (Melo et al., 1998; Hardie, 2000; Garcia-Cao et al., 2012).

In order to understand the parallel increase in glucose uptake, as well as several key mitochondrial energetics transcripts, we performed a comprehensive energetic measurement in decidualized ESFs, as well as after subsequent treatment with HTR8 conditioned medium. Using XF analyzer to simultaneously measure oxidative phosphorylation (OxPhos) and glycolysis, we asked whether the increase in energy substrate uptake with concomitant increase in cellular contractility also leads to a parallel increase in aerobic glycolysis (Figure 2H). Surprisingly, we observed an increase in both Oxphos and aerobic glycolysis with decidualization. Both the basal mitochondrial respiration rate and extracellular acidification rate (ECAR), indicative of OxPhos and aerobic glycolysis respectively, were increased in decidualization, suggesting the transition of cells towards high energy state (Figure 2H). Interestingly, treatment with HTR8 conditioned medium resulted in a decrease of both Oxphos and aerobic glycosis (Figure 2H).

Furthermore, decidualization not only resulted in increased basal respiration but also caused a significant increase in coupled respiration (with ATP synthase inhibitor oligomycin) and maximum respiratory chain capacity (FCCP) (Figure 2I). The increase in respiration that was coupled to ATP generation (coupled respiration) was close to ~67% in decidualized cells compared to ~40% in hESFs, and ~52% with co-culture condition (Figures 2I,J). These results indicate not only increase in mitochondrial respiration, but also increase in mitochondrial efficiency with decidualization. Extracellular acidification rate (ECAR) was also increased with decidualization (Figure 2K). Although increase in both OxPhos and aerobic glycolysis suggest high energetic state of cells in decidualized stage, the OCR/ECAR ratio which is independent of cell number indicated preferential increase in mitochondrial respiration in decidualized cells (Figure 2L). Interestingly, although the total ATP levels were increased with decidualization from ~1.47 nM/cell to ~1.72 nM, a significant increase in ATP generation was observed through mitochondria which were sensitive to oligomycin (Figure 2M).

These results show that decidualization involves large changes in the energetic state of fibroblasts, both in ATP generation within the mitochondria, as well as large increase in carbon flux, likely for anabolic processes. Oxphos is increased typically as cells differentiate and leave the undifferentiated proliferative state (Zheng et al., 2016). However, the large increase in ATP generation in dESFs suggest that Oxphos produced ATP likely primarily fuels large increase in contractile force generation. HTR8s cause a significant reversal in both these fundamental changes in the energetic state of dESFs. Indeed, increase in glucose flux after decidualization does not result in a significant contribution towards ATP generation through glycolysis. The increase in cellular energy demand (ATP) with decidualization is primarily met with an increase in energy efficient OxPhos pathway. Significantly high ATP generation in dESFs vs. hESFs, also more proportionately met by Oxphos, indicate the metabolic flux meeting the needs for the marked increase in contractile force generation (Figure 2M). Correlating the strain energy, and ATP generation showed that increased mechanical strain energy generation in response to decidualization also results in large increase in ATP generation in the mitochondria (OxPhos), and treatment with conditioned

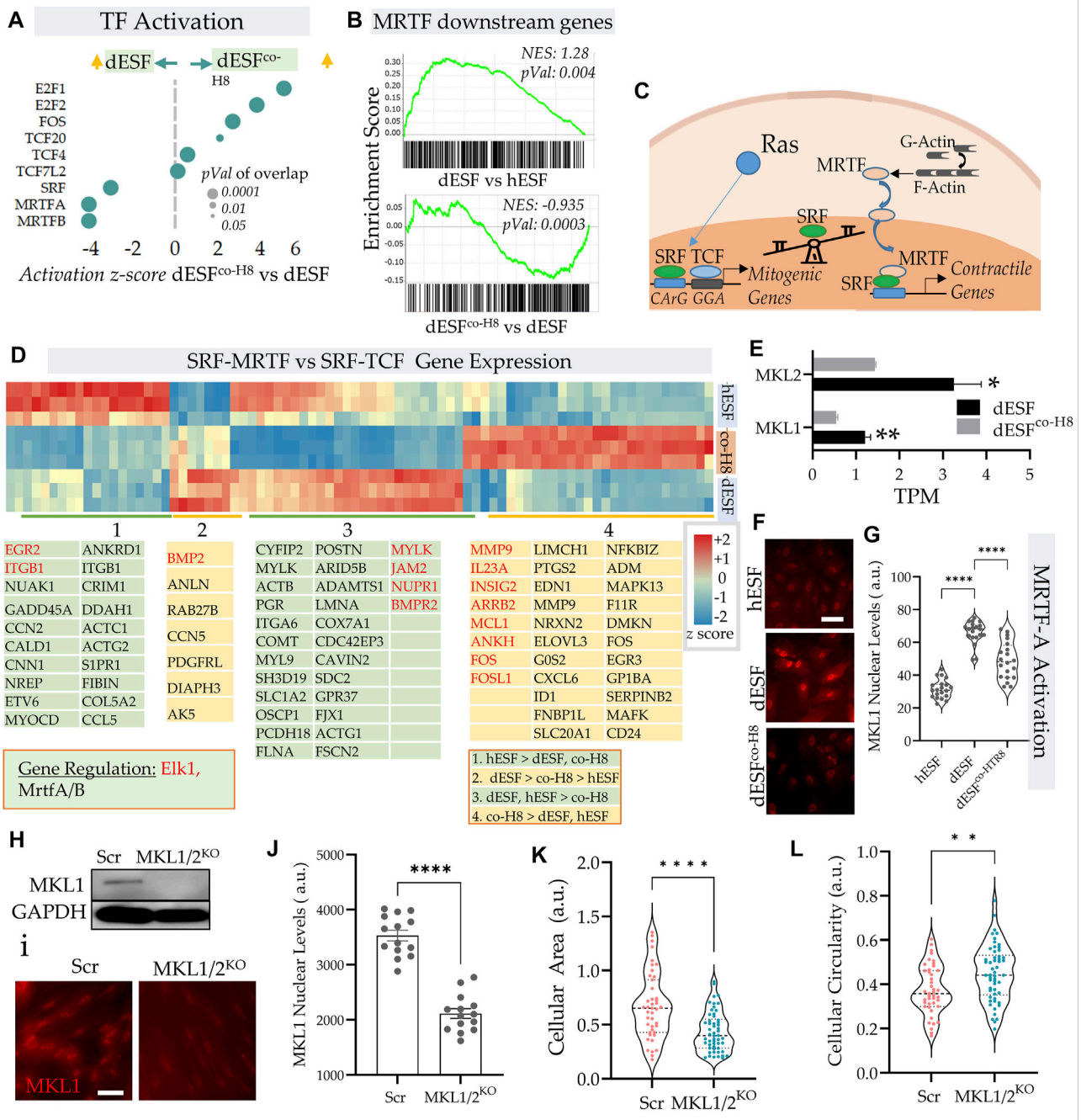

FIGURE 3
EVTs reverse MRTF activation in decidual fibroblasts. **(A)** Predicted IPA based activation scores of top transcription factors which are reduced in dESFs co-cultured with HTR8 feature MRTF-A, and MRTF-B, as well as SRF. Bubble size reflects *p*-value overlap of genes. **(B)** Gene set enrichment analysis (GSEA) of SRF-MRTF downstream genes in dESF vs. hESF (top), and dESF^{co-H8} vs. dESF (bottom); Enrichment score, and *p*-value shown in inset; leading edge genes for both comparisons shown at the bottom. **(C)** Schematic showing a balance of contractile and mitogen phenotype maintained by association of MRTA or TCF co-factors with SRF. **(D)** Heatmap showing z-scores genes activated by SRF in hESF, dESF and dESF^{co-H8}. Hierarchical clustering by Euclidian distance revealed 4 main clusters that were either upregulated in hESF, dESF, both hESF and dESF, or in co-culture condition. Genes that are downstream of Elk1 activation are coded with red color and MRTFA/B are coded with black color. Color intensity bar shows z score calculated from TPM values. **(E)** Transcripts per million (TPM) for MKL1 and MKL2 in dESF, and dESF^{co-H8}; n = 3 samples. **(F)** Representative immunofluorescence images showing MKL1 (MRTF-A) expression in hESF, dESFs, and dESF^{co-H8}, with quantification of fluorescence levels in the nuclei shown in **(G)**; significance was calculated using Anova followed by Tukey's test; *n* = 20 for each condition. **(H)** Immunoblot showing reduced MKL1 abundance in dESFs before, and after silencing of both MKL1 and MKL2 genes (MKL1/2), lower lane shows abundance of GAPDH; also confirmed with immunofluorescence **(I,J)**. **(K,L)** Morphological changes in dESFs in response to MKL1 and MKL2 gene silencing in dESFs, showing single cell area **(K)**, and cellular circularity **(L)**.

medium from HTR8 restored the low ATP generation energetic state in the mitochondria, correlatively with reduced strain energy (Figure 2N).

Overall, increase in both glucose uptake and mitochondrial respiration capacity/mitochondrial ATP generation indicates an increase in ATP demand that is met by OxPhos and a possible diversion of glucose carbon towards biosynthetic needs as indicated in upregulation of several metabolic ontologies, transcripts and increase ECM/collagen production with decidualization (Figure 2N). The concomitant increase in glycolysis and activation of several biosynthetic gene ontologies with decidualization indicate a shift in metabolic pathways towards biosynthetic processes (Vander Heiden et al., 2009), which was partially reversed by interaction with EVTs.

EVTs reverse decidualization induced increase in activation of MRTF transcriptional regulation

IPA pathway analysis revealed an increased activation of serum response factor (SRF) and myocardin-related transcription factors (MRTFs) (Figure 1F). Indeed, both MRTF-A and MRTF-B, as well as SRF were among the top transcription factors that were predicted to be activated with decidualization, and then decreased after EVT co-culture (Figure 3A). GSEA analysis revealed a significant enrichment of MRTF downstream genes in dESF vs. hESF, which was also reduced in dESF^{co-H8} (Figure 3B). MRTFs in association with SRF are key TFs regulating muscle machinery adaptation to workload (Montel et al., 2019), and along with YAP-TAZ, impart contractile properties to cancer associated fibroblasts (Foster et al., 2017). Activation of SRF-MRTF, as well as SRF independent MRTF activation are important mediators of mechanical forces essential for cancer cell migration through dense extracellular matrix (Gau and Roy, 2018). MRTFs competitively associate with serum response factor (SRF) against TCFs (Erk regulated ternary complex factors), in response to actin polymerization. Upon actin polymerization, MRTFs can localize in the nucleus, and bind to SRF to activate gene transcription of several genes regulating cellular contractility and force generation (Gualdrini et al., 2016; Gau and Roy, 2018) (Figure 3C). Indeed, many genes downstream of MRTFs showed increased expression with decidualization, while genes downstream of TCF factors were preferentially expressed after co-culture (Figure 3D). RNAseq showed significant reduction in the transcripts levels of both MKL1 and MKL2 (Figure 3E), while immunofluorescence showed that MRTF-A (MKL1) localization was primarily nuclear in dESFs compared to hESFs, and treatment with conditioned medium from HTR8 reversed the trend (Figures 3F,G), corroborating the predicted transcriptional activation of SRF-MRTF signaling in dESFs and its reduction after EVT interaction. CRISPR Cas9 mediated gene silencing of both MKL1 and MKL2 showed reduced MKL1 abundance and nuclear localization (Figures 3H–J). Gene silencing for MKL1 and MKL2 also resulted in significant reduction in cell area (Figure 3K), while cellular circularity which negatively correlates with the elongated spindle shape formation was significantly increased (Figure 3L). Overall, gene expression data indicated increased SRF-MRTF mediated transcriptional activation in decidual cells, which was reversed after interaction with EVTs.

MRTFs regulate mechanical resistance in decidual fibroblasts to trophoblast invasion

Traction force microscopy showed that silencing both MRTF-A (encoding MKL1) and MRTF-B (encoding MKL2) genes resulted in significant reduction in strain energy density (Figures 4A,B). We sought to identify how MRTFs may regulate actomyosin contractility at a molecular level. Upon being phosphorylated, myosin light chain homologues engage with actin filaments, generating contractile forces in cells. MYL9 is the chief homologue of myosin light chain encoding genes within fibroblasts, and has been described to be transcriptionally regulated by MRTFs. However, immunostaining for MYL9 did not show much difference between control dESFs, and those silenced for MKL1 and MKL2 genes (Figures 4A,B). Immunofluorescence also showed expectedly that MYL9 did not colocalize with F-actin fibers. However, phosphorylated MYL9 (pMYL9) was significantly lower in dESFs with MKL1 and MKL2 silenced (MKL1/2^{KO}) (Figures 4C,D). Notably, myosin light chain kinase (MYLK) is also transcriptionally expressed by MRTFs (Johnson et al., 2014 #67), and was significantly reduced in dESFs after co-culture of conditioning with HTR8 (Figure 4E), suggesting that MRTFs may increase phosphorylated MYL9 in dESFs. Colocalization analysis also showed that pMYL9 was associated strongly with F-actin fibers, and this association reduced significantly in MKL1/2^{KO} cells (Figure 4F). Overall, these data indicated that MRTFs may be regulating dESF contractile forces via increased phosphorylation of MYL9, likely by transcription of MYLK.

Could the increased contractile force generation likely by downstream targets regulated by MRTFs contribute to increased decidual resistance to trophoblast invasion? Although, contractile force generation by cancer associated fibroblasts has been shown to be critical in inducing dissemination of epithelial cancer (Ansardamavandi and Tafazzoli-Shadpour, 2021), the actual response of collective fibroblast activation in a wound, or in response to decidualization, in resisting epithelial invasion is not well understood. Both epithelial-fibroblast coupling via N- and E-Cadherin heterotypic adhesion

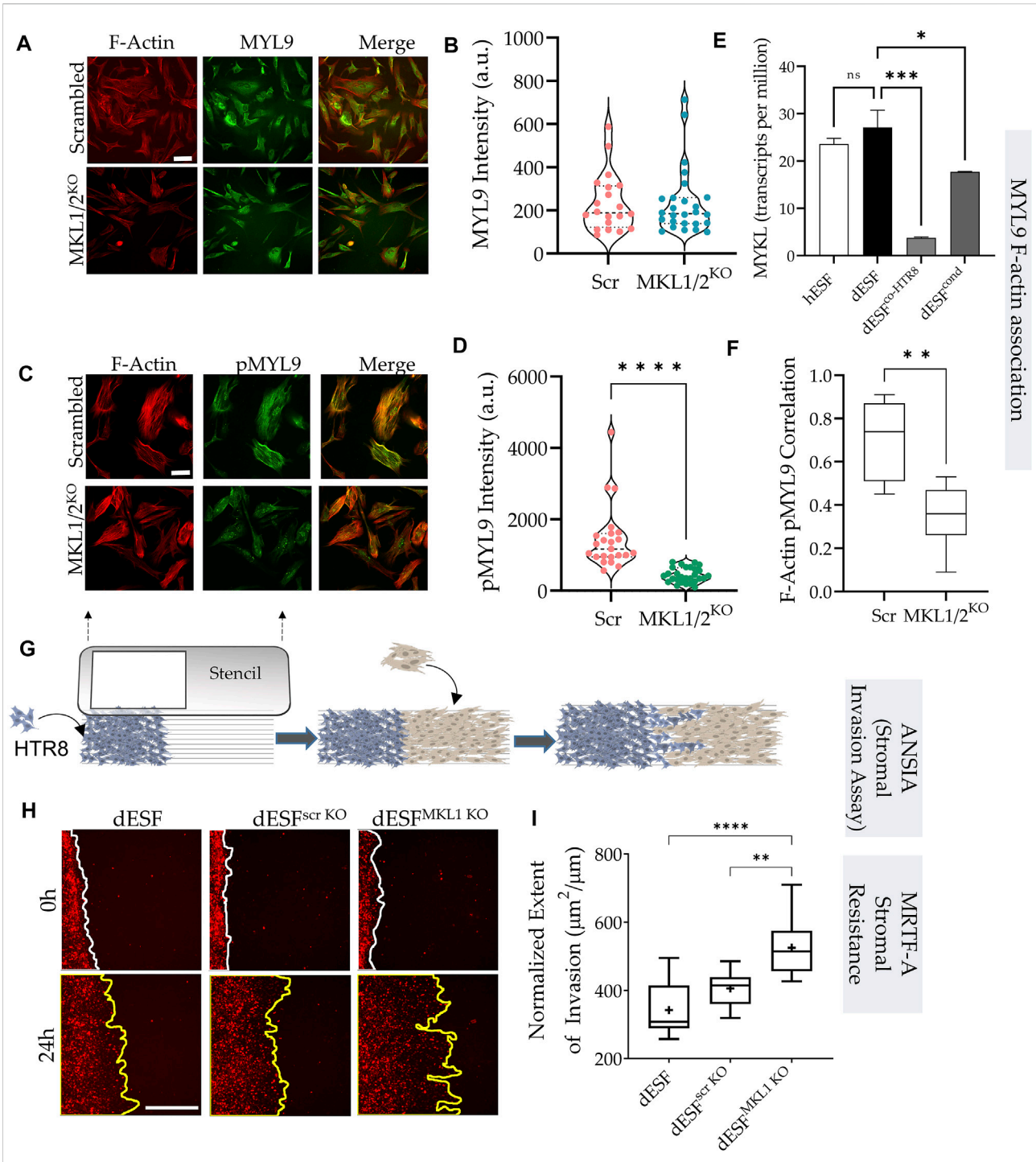

FIGURE 4
MRTF silencing in decidual fibroblasts reduces actomyosin contractility and resistance to trophoblast invasion. **(A)** Immunofluorescence of dESFs with CRISPR/Cas9 based gene silencing for scrambled control, and MKL1 & MKL2 (MKL1/2^{KO}) showing F-actin and myosin light chain-9 (MYL9), quantification of intensity per cell for MYL9 shows no statistical difference **(B)**; scale bar = 25 μm. **(C)** Immunofluorescence images showing reduced abundance of phospho-MYL9 in MKL1/2^{KO} dESFs **(D)**; scale bar = 20 μm. **(E)** Relative expression of myosin light chain kinase (MYLK) hESF, dESF, as well as dESFs co-cultured or conditioned with HTR8. **(F)** Pearson's coefficient of phospho-MYL9 (green) co-localization with F-actin fibers (red) in Scrambled control, and MKL1/2^{KO} dESFs. **(G)** Schematic showing the setting of the ANSIA assay to measure stromal invasion of H2B-mCherry expressing HTR8s in the dESF monolayer on a nanopatterned substrate with the anisotropic nanoridges aligned orthogonal to the patterned HTR8-dESF interface. **(H)** Representative time-stamped images of HTR8 (red)-dESF (unlabeled) interface at 0 and 24 h, with dESFs either silenced with scrambled gRNA, or gRNA targeted towards MKL1. **(I)** Extent of stromal invasion by H2B-mCherry labeled HTR8 cells into the dESF monolayer for conditions in e, and significance is calculated using Anova followed by Tukey's test; $n > 10$ per condition.

(Labernadie et al., 2017), as well as the collective directionality of force presentation against the invading front because of remodeled matrix may contribute to the process of stromal resistance (Erdogan and Webb, 2017; Asif et al., 2021).

Harnessing the large differences in comparative placentation across mammals, we have demonstrated that stromal invasion is both an outcome of the invading cells, as well as the active resistance, or assistance, offered by the stromal fibroblasts (Kshitiz et al., 2019). Indeed, across mammals, the large differences in placental invasion is primarily an outcome of differential stromal invasability, a selected and genetically regulated phenotype (Kshitiz et al., 2019; Suhail et al., 2019). We have shown that decidualization results in significantly high resistance to invasion by trophoblasts, also borne from the observation that ectopic pregnancies in non-decidualized regions of the uterus are highly invasive (Randall et al., 1987). We therefore asked whether decreased MRTF activation in response to EVT co-culture may also regulate decidual invasability.

Towards this objective, we used a quantitative and high sensitivity assay to measure stromal invasability which we have previously described, called Accelerated Nanopatterned Stromal Invasion Assay (ANSIA) (Novin et al., 2021). As stromal invasion is a very slow phenotype to observe at cellular and subcellular resolution, we have used a collagen matrix mimicking anisotropic pattern to align the actomyosin assemblies in individual cells in a single direction (Figure 4G). H2B-mCherry labeled HTR8 and unlabeled dESFs are patterned using a stencil to create an interface orthogonal to the direction of the underlying nanoridges (Figure 4G). Before plating, dESFs were either left untreated, or silenced with scrambled control, or gRNA targeted against MKL1 gene. HTR8 invasion was observed for 24 h using fluorescence live microscopy, and invasive spread measured and normalized to the initial interface length between HTR8 and dESFs. We found that MKL1 gene knockout significantly decreased the resistance offered by dESFs to HTR8 invasion, with HTR8 forging deep collective fronts into the stroma (Figures 4H,I). These data showed that co-culture with HTR8 resulted in decreased SRF-MRTF downstream gene expression, and that MRTF regulates stromal actomyosin force generation and resistance to trophoblast invasion.

HB-EGF secreted by HTR8 rewire SRF association with MRTFs in decidual fibroblasts

The effect of EVTs on reduction of dESF contractility was maintained both in co-culture, as well as from conditioned medium from HTR8, suggesting that paracrine signals from HTR8 may play a role in regulating dESF contractility. Because SRF-MRTF signaling was predicted to be highly active in dESF, and was also reduced significantly by HTR8 conditioned medium (Figure 3B), we sought to identify secreted factors that could potentially regulate MRTF activation.

Protein kinases are essential in regulation of cellular contractility and motility, and RNA seq data indicated that MAPK were top kinases activated on PTMsigDB (Figure 5A). Further, several of the MAPK were also putatively activated as predicted by IPA analysis (Figure 5B) in decidualized cells (Krug et al., 2019; Kuleshov et al., 2021). As described earlier, TCF components, which are Erk activated act as antagonists to SRF-MRTF signaling, by competitive binding to SRF in the nucleus (Gau and Roy, 2018). We therefore sought to identify paracrine sources from HTR8 which could activate MAPK signaling in dESF, and potentially reduce SRF-MRTF signaling. Using RNAseq of HTR8 we identified the genes encoding secreted ligands which may be responsible for modulating MRTF signaling (Figure 5C). We identified heparin bound epidermal growth factor (HB-EGF), a key enzyme implicated in implantation and placentation, and a potent activator of Erk signaling, which could regulate TCF localization in the nucleus antagonizing SRF-MRTF interaction (Figure 5C). As gene enrichment analysis had revealed a marked activation of MAPK pathway in dESFs after HTR8 co-culture (Figure 5B), it laid credence to the hypothesis that intercellular signaling through HB-EGF may modulate intracellular dESF signaling. We therefore tested if HB-EGF could indeed alter MRTF signaling in dESFs. Immunofluorescence revealed that treatment of dESFs with recombinant human HB-EGF resulted in a marked decrease in the nuclear localization of MKL1 (MRTF-A), as well as concomitantly, increased nuclear localization of Elk1, suggesting that HB-EGF is capable of tipping the balance in dESF from SRF-MRTF to SRF-TCF signaling (Figures 5D–F). Additionally, HB-EGF treatment also reduced cell size (Figure 5G), similar to what was observed in MRTF gene silencing (Figure 3K).

HB-EGF reduces actomyosin contractility and stromal resistance acquired in decidual fibroblasts

HB-EGF produced by EVTs rewired the SRF axis from SRF-MRTF mediated to likely SRF-TCF mediated gene expression. Earlier results also suggested reduction of SRF-MRTF signaling to decrease contractile force generation. Immunofluorescence in dESFs showed a marked reduction in phospho-MYL9 intensity after treatment with HB-EGF, as well as colocalization with F-Actin (Figures 6A–C). The dramatic reduction in phosphor-MYL9 levels was also matched phenotypically in a profound reduction in contractile force generation in dESF after HB-EGF

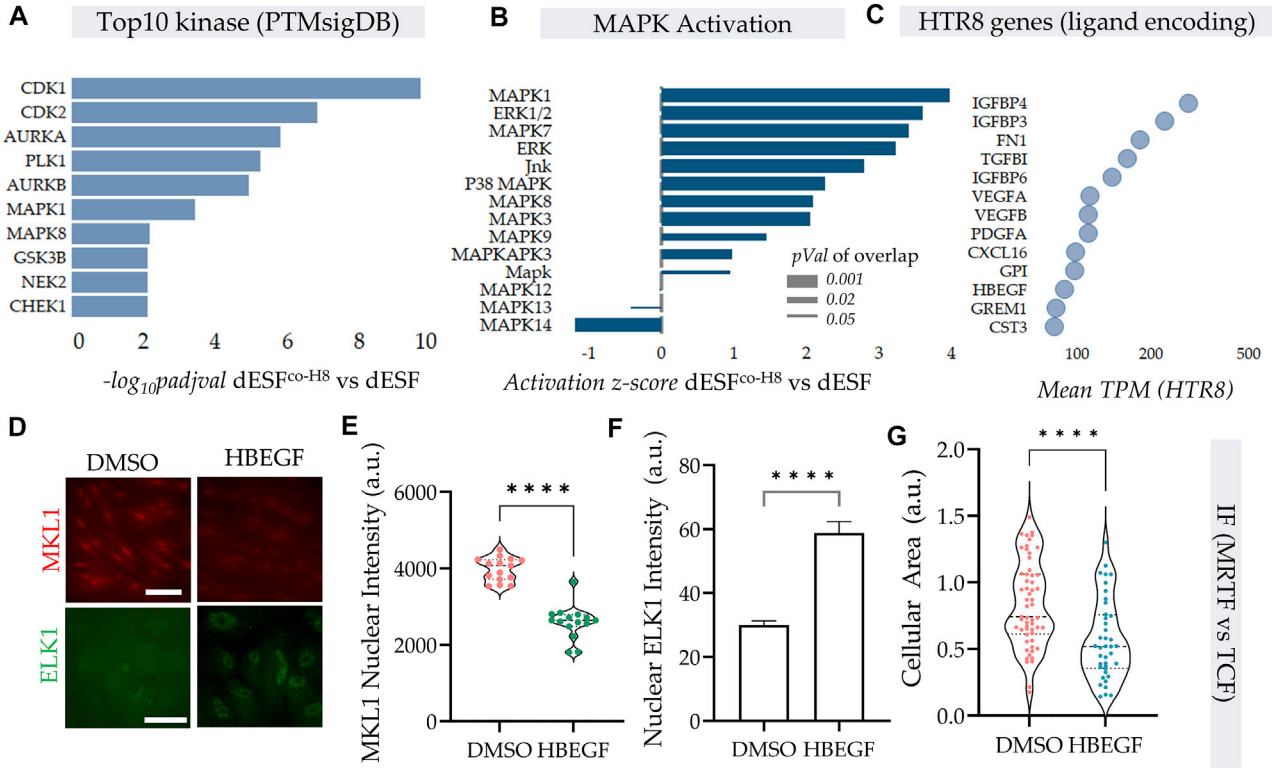

FIGURE 5
HB-EGF secreted from EVTs shift SRF-MRTF to SRF-TCF transcription. **(A–C)** HTR8 secreted HB-EGF activate MAPK signaling in dESF. **(A)** Top 10 kinases that are activated with HTR8 co-culture (dESF^{co-H8} vs. dESF) based on differential genes that are downstream of the predicted kinases, evaluated using PTM signatures database; Data presented with FDR correction of pVal. **(B)** IPA predicted activation score of MAPK species in dESFco-H8 vs. dESFs. **(C)** Bubble plot showing TPM values of genes encoding ligands expressed in HTR8. **(D)** Immunofluorescence images showing MKL1 (encoded by *MRTFA*) and ELK1 (component of TCF complex) localization in dESF without, or with treatment with recombinant HB-EGF, with quantification for MKL1 nuclear levels shown in **(E)**, and Elk1 cytoplasmic and nuclear intensities shown in **(F,G)**.

treatment. Traction force microscopy confirmed that treatment of dESFs with HB-EGF decreased cellular contractility by nearly 3 folds, a remarkable effect on cell mechanics (Figures 6D,E). Strain energy also showed a rapid decrease in dESFs after treatment with recombinant HB-EGF (Figure 6F).

We finally asked if HB-EGF mediated change in MRTF regulated dESF contractility and resistance to invasion. Using ANSIA, we tested the effect of dESF resistance after pre-conditioning with medium from HTR8, wild-type or those with silenced HB-EGF. We found that when dESFs were pre-conditioned with medium from HTR8 with HBEGF gene silencing, their resistance to invasion was significantly increased (Figures 6G,H). Overall these data suggested an intercellular signaling communication between EVTs and dESFs, wherein HB-EGF produced by EVTs rewire the balance of contractile signaling from SRF-MRTF to SRF-TCF transcription in dESFs, reducing mechanical resistance to invasion, thereby facilitating EVT invasion into the maternal stroma.

Discussion

Collective migration of epithelial cells into the stromal compartment underlines many physiological processes, including gastrulation (Dumortier et al., 2012), wound healing (Li et al., 2013), placentation (Knofler and Pollheimer, 2013), as well as cancer dissemination (Gaggioli, 2008). For long, the invading cells, either trophoblasts in placentation, or cancer cells in metastatic initiation, were considered as the primary agents in stromal invasion, with the stroma considered as a passive barrier to breach (Hanahan and Weinberg, 2000, 2011). Recent decade has increased our appreciation of the role of cancer associated fibroblasts in abetting tumor dissemination, but it is not yet clear whether fibroblasts assist, or resist cancer invasion, as evidence point to either scenario. It is however recognized that cancer cells themselves can prime stromal fibroblasts, incorporating them to facilitate stromal invasion (Ansardamavandi and Tafazzoli-Shadpour, 2021).

Here, we report a mechanism used by the invading extravillous trophoblasts (EVTs) to reduce the decidual

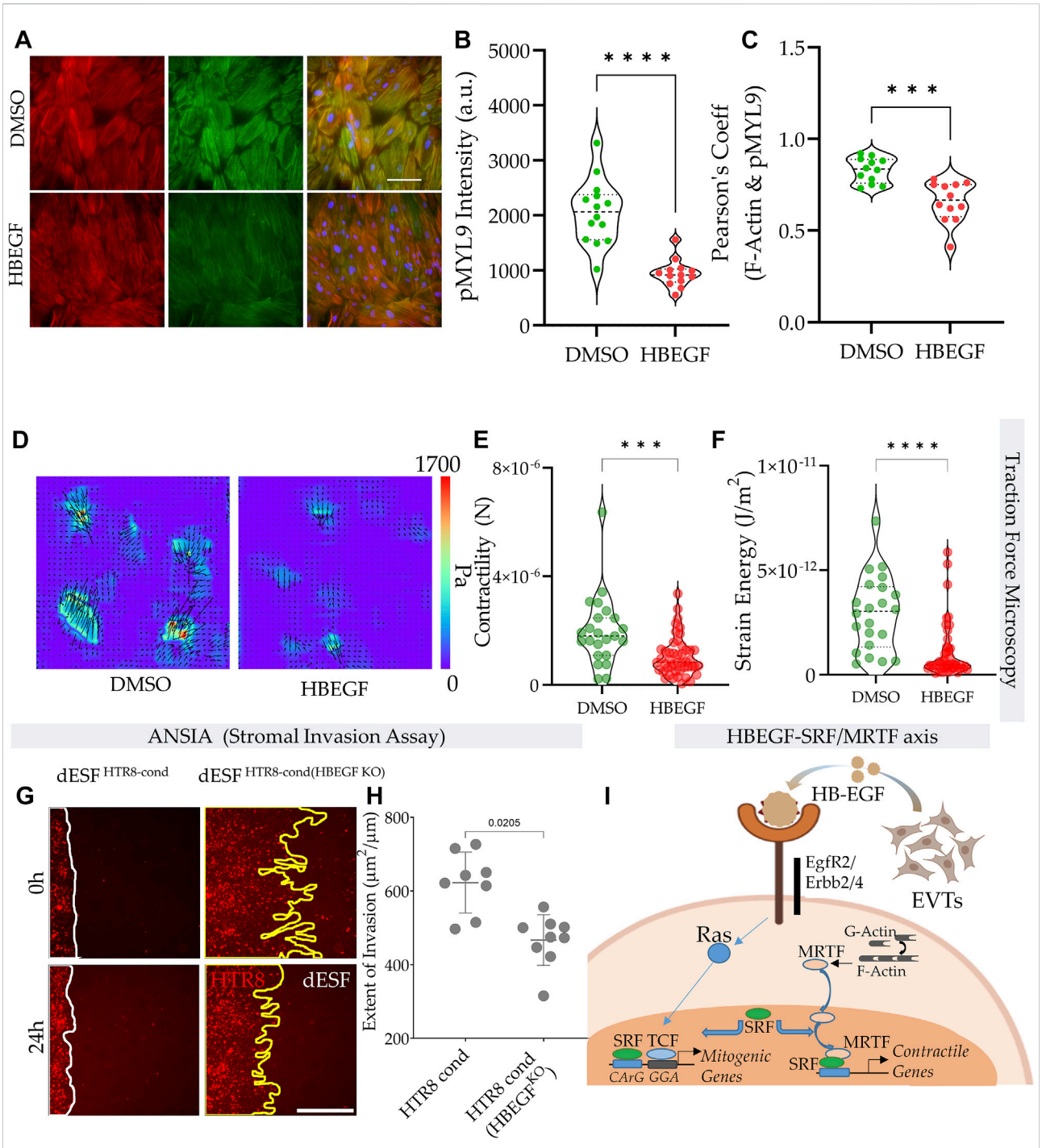

FIGURE 6
HB-EGF from EVTs reduce contractile force generation in dESFs reducing decidual resistance to invasion. **(A)** Immunofluorescence images of dESFs treated with DMSO control, and HB-EGF (HBEGF) showing F-actin, phospho-MYL9, and combined expression; scale bar = 25 mm. **(B–C)** Average intensity per cell for phospho-MYL9, and Pearson's coefficient showing F-actin and phospho-MYL9 colocalization. **(D–F)** HB-EGF reduces dESF contractile force generation. **(D)** Stress vector spatial maps showing representative examples of dESFs treated without, or with HB-EGF for 24 h. Individual cell contractility shown in **(E)**, and strain energy density shown in **(F)**; $n > 20$. **(G–H)** HB-EGF decreases dESF resistance to HTR8 invasion. **(G)** Representative images of HTR8-dESF interface at time 0 and 24 h shown for dESFs pre-treated with conditioned medium from wild-type HTR8, or from HTR8 with gene silencing for HB-EGF. **(H)** Quantification of the extent of stromal invasion by HTR8 for conditions in j; $n > 10$. **(I)** Schematic showing the balance of SRF transcriptional association with either TCF co-factors acting through CaRG response element, or with MRTF-A/B co-factors present in nucleus upon release by polymerized actin in the cytosol.

resistance to invasion, specifically by decreasing the high contractile forces in decidual endometrial fibroblasts (dESFs) which phenocopy the mechanics of activated fibroblasts. It is notable that extravillous trophoblasts (EVTs) are a recently evolved cell type present in great apes, characterized by excessively deep placental invasion during pregnancy. It would be interesting to test if trophoblasts which are of more ancestral lineage also employ a similar strategy to reduce mechanical resistance by decidual fibroblasts.

A key finding in this report is the metabolic transition of ESFs in response to decidualization and their subsequent interaction with EVTs. Cellular contractility is an intense energetic process requiring high ATP levels to maintain steady state of ATP hydrolysis required for actomyosin cycling (Dos Remedios et al., 2003; Sleep et al., 2005). Harnessing the variance in cellular contractility within dESF populations, we showed that cellular glucose uptake and strain energy were highly correlated. Increase in contractile phenotype in decidualization was also paralleled by a transition towards energy efficient OxPhos pathway for ATP generation. However, concomitant increase in glycolysis, glucose uptake and activation of biosynthetic pathways suggested that other biosynthetic processes associated with decidualization were likely sustained through increased glucose uptake. Increase in OxPhos can also lead to higher reactive oxygen species generation and oxidized cellular state, but enhanced mitochondrial competency and glycolytic flux can keep the reduced cellular state which is necessary to maintain the cellular collagen production (Heid et al., 2017). We found that interaction with EVTs both reduced glycolysis, as well as Oxphos, reducing the energetic state of the dESFs, paralleling the reduction in contractile force generation. A comprehensive metabolic assessment of decidualization has not been presented before, and our data can set the metabolic and mechanical hallmarks to measure decidualization phenotype.

We identified a key paracrine axis recruit decidual fibroblasts as EVT's partners in invasion. A marked activation of SRF-MRTF transcriptional activity indicated its role in the increased contractile force generation during decidualization of ESFs. Somewhat surprisingly, we found that the effect of SRF-MRTF activation on cellular contractility was achieved not directly via transcription of the fibroblast specific myosin light chain 9 (MYL9) (Zhang et al., 2013), but by its increased phosphorylation. This is likely achieved by increased MRTF induced transcription of the upstream myosin light chain kinase (MLCK) (Johnson et al., 2014).

Because SRF is known to competitively bind either to MRTF, or TCF, a transcriptional co-regulator activated by MAPK signaling (Gau and Roy, 2018), we searched for potential ligands encoding genes expressed in the trophoblasts itself which could potentially activate MAPK signaling in the recipient dESF cells. We found that HTR8 expressed a key secreted ligand for the epidermal growth factor receptor signaling, HBEGF (heparin binding epidermal growth factor like growth factor), which could potentially rebalance the SRF association with MRTF in the nucleus. Decidual ESFs expressed genes encoding receptors which HBEGF could bind to, and pathway analysis suggested a strong activation of MAPK signaling in dESFs after co-culture with HTR8. Other evidence, including immunocytochemistry, also pointed towards a shift in the transcription of genes in dESFs from the initial SRF-MRTF activated genes to the SRF-TCF activated CARGome genes, which contain a consensus CARG sequence in their promoter regions (Sun et al., 2006). Treatment of dESFs with HB-EGF resulted in significant and substantial reduction of cellular contractile forces and mechanical strain energy, highlighting its novel role as a key paracrine mechanoregulator. We also quantitatively tested the effect of HB-EGF on regulating decidual resistance to invasion using ANSIA, a platform we have developed to quantitatively measure stromal invasability as a phenotype with high sensitivity (Novin et al., 2021). These data indicate that HBEGF secreted by EVTs rebalance SRF transcription from the decidual specific MRTF mediated to MAPK driven TCF mediated, resulting in significantly reduced contractile force generation and increasing invasability.

Being a potent activator of the mitogenic MAPK signaling, HB-EGF has been studied primarily in cancers as an oncogenic target, for its role in activating cell proliferation and anchorage-independent growth through autocrine signaling (Ray et al., 2014; Hsieh et al., 2017). HB-EGF autocrine signaling is associated with breast cancer intravasation and metastasis in macrophage independent fashion, and owing to its activity on MAPK signaling, is a potent mitogen in many cancers, including lung (Yotsumoto et al., 2017; Wang et al., 2020), pancreatic (Ray et al., 2014), and breast tumors (Sethuraman et al., 2018). HB-EGF is frequently referred to as an "immediate early gene" owing to its rapid transcription in response to cytoprotective or oncogenic stimuli, including ischemia reperfusion in the heart (Xia et al., 2003), and in tumorogenesis (Mccarthy et al., 1995). Although AP-1 related transcription in response to stretch in smooth muscle cells can induce transcription of HB-EGF (Park et al., 1999) the role of HB-EGF as a modulator of myofibroblast transformation are not well studied. We found that HB-EGF can tilt the balance from a high contractility promoting state in a myofibroblast like decidual fibroblasts to a less mechanically resistive cell, primarily by shifting association of SRF to the MAPK induced TCF signaling. Again, this was achieved by reduced phosphorylation of MYL9 which engages with actin bundles to promote actomyosin contractility. The effect of HB-EGF on dESF mechanics was profound, reducing their contractility and strain energy density by 3 folds, as well as reducing their mechanical resistance to trophoblast invasion. This finding may shed light on previous reports where HB-EGF was found to be a suppressor of liver fibrosis (Huang et al., 2012).

In light of placental invasion and cancer metastasis being parallel models, in so far as the stromal fibroblast response is

concerned in regulating the process of invasion, we show that invading cells can use paracrine signals to modulate mechanical forces in the resistive cells, facilitating invasion. As HB-EGF is produced by the invading cells themselves, it presents a therapeutic target to control the transformation of fibroblasts to reduce their mechanical resistance to invasion by cancer, or to modulate placental invasion in pregnancy related disorders.

Methods

Cell isolation and maintenance

Human endometrial stromal fibroblasts (hESFs) were isolated from normal patient biopsies obtained by Charles Lockwood Lab at Yale, and obtained from Gil Mor group (Krikun et al., 2004; Graham et al., 1993), as well as from patient biopsies obtained from UCHC Biorepository. HTR8 and BeWo cells were obtained from ATCC. hESF cells were maintained in phenol-red free DMEM/F12 50: 50 containing 25 mM glucose, and supplemented with 10% calf serum (charcoal stripped), 1% antibiotic/antimycotic, and ITS (insulin, transferrin, and selenium). hESFs were decidualized with 0.5 mM 8-B-cAMP (Cayman), and 0.5 mM medroxy-progesterone acetate (MPA) for 4 days in DMEM/F12 supplemented with 2% charcoal stripped calf serum.

For co-culture, trophoblasts were labeled with DiI (or stably transduced with plasmid expressing H2B-bound mCherry driven by CMV promoter), washed multiple times with PBS and mixed with decidual ESFs (dESFs) at 1:1 ratio for 3 days. During co-culture cAMP was withdrawn owing to its toxicity to HTR8. For co-culture controls, dESFs were also maintained in decidualization medium without cAMP. Conditioned medium from HTR8 was supplemented with MPA to maintain consistency across all experimental conditions.

Fluorescence assisted flow sorting

After co-culture, cells were detached from the substrate with 0.25% Trypsin-EDTA, and protease was neutralized with excess medium when all cells were detached. Serum free medium at 4°C was used for cell suspension, and sorting was performed using BD FacsARIA II in UConn Health Flow Core. PE. Cy5 channel was used to separate HTR8, and dESFs using conservative gating (thereby only selecting DiI^{lo} and DiI^{hi} cells, leaving most cells in the middle spectrum to avoid trace potential chance of cell fusion, or dye uptake from apoptotic cells). FACSDiva 6.0. or Flowjo was used for anlaysis. After sorting, cells were directly collected in RNASelect to stabilize RNA, or were collected in 10% FBS containing medium for further experiments. The same procedure was applied on control cells, even though there were only one type of cells in the monoculture dESFs.

RNA sequencing and transcriptomic analysis

Cells were lysed with buffer RLT, and RNA was isolated using RNeasy Mini Kit (Qiagen) following manufacturer's instructions. RNA integrity was evaluated with Bioanalyzer 2100 (Agilent) and samples with RIN ~8 were used for library preparation. Library prep and RNA sequencing were performed by Novogene Inc. NCBI GRCh38 genome assembly were used to align the Reads using HISAT2 pipeline with default parameters. Reads were counted using HTSeq, and DESeq2 was used to estimate the Fold changes and statistical significance (p-values) for differential expression. Wald test was used to calculate p-values for differential expression and the moderated log2 fold change was used for the differential analysis. To calculate the gene sets (Gene Ontology/KEGG) enriched in the DE genes upon decidualization or HTR8, Fisher exact test was used to calculate the over-representative of terms using hypergeometric test followed by correction for multiple testing (Kolberg et al., 2020). Activation scores of transcription factors and canonical pathways analysis were performed using Ingenuity Pathway Analysis (IPA, Qiagen Inc.). Gene set enrichment analysis (GSEA) (Subramanian et al., 2005) were performed on the genes that are downstream of Mrtf (Gualdrini et al., 2016). Hierarchical clustering was performed using UPGMA method with Euclidian distance on z-scores as mentioned earlier (Afzal et al., 2022). Briefly, a subset of genes was selected for clustering that were differentially expressed in either condition, and are known to be downstream of SRF-MRTF or SRF-TCF axis (Gualdrini et al., 2016; Esnault et al., 2017).

Traction force microscopy: Traction force gels were fabricated using protocols previously described (Colin-York et al., 2017). Briefly, coverslips for gel attachment were cleaned using ethanol as well as sonication, followed by treatment with air plasma, and activated with 0.5% glutaraldehyde and 0.5% (3-Aminopropyl) triethoxysilane. Coverslips to be used in beads coating were treated with air plasma, and were coated with 0.01% poly-L-lysine (PLL) before another coating of carboxylate-modified microspheres (diameters = 0.2 um) (Thermo Fisher). Gel precursor solution containing 7.5% acrylamide and 0.15% bis-acrylamide was degassed for 30 min s and thereafter mixed with 0.1% tetramethylethylenediamine and 0.1% ammonium persulfate, and sandwiched between silane-activated coverslips and bead-coated coverslips for 20 min s. After polymerization of polyacrylamide in between the coverslips, bead-coated coverslips were peeled, and the resulting traction force gels coated with 50 ug/ml collagen type I using sulfo-SANPAH (Thermo Fisher) overnight at 4°C. UV was used to sterilize gels for at least 2 h before cell seeding. Images containing microbeads location before and after cells trypsinization were recorded using Zeiss Observer A1 microscope. Traction forces were calculated using protocols previously described (Bauer et al., 2021).

Measurement of oxidative phosphorylation and glycolysis: XF analyzer from Agilent Technologies was used to monitor cellular energetics (Reid et al., 2013; Afzal et al., 2017; Afzal et al.,

2022). Cells were cultured in 96 wells XF plate and the assay was repeated three times to estimate the energetics of cells. Oxygen consumption rate (OCR) which reflect the rate of change of dissolved O_2 in each well was used to estimate OxPhos and change in extracellular acidification rate which is measured as a change in extracellular pH change was used to estimate glycolysis. Basal rates reflect respiration or pH in the absence of added compounds or metabolic inhibitors. Oligomycin (4 μM) was used to inhibit mitochondrial F1Fo-ATP synthase, rotenone (2 μM) was used to inhibit Complex 1 of ETC, antimycin A (2 μM) was used to inhibit complex 3 of ETC, FCCP (500 nM) was used to uncouple mitochondria to estimate maximum respiratory capacity, and iodoacetate (100 μM) was used to inhibit glycolysis (glyceraldehyde-3-phosphate dehydrogenase). Fresh compounds were prepared and dissolved in the XF assay media immediately before the experiment.

Respiration fractions were calculated as follows (Pesta and Gnaiger, 2012; Afzal et al., 2017).

1) *Coupled respiration*: OCR sensitive to oligomycin inhibition which represents OCR used for mitochondrial phosphorylation of ADP.
2) *Uncoupled respiration*: Increase in OCR after FCCP addition which reflects maximal oxygen consumption capacity of mitochondria.
3) *Total mitochondrial respiration*: OCR fraction sensitive to inhibition by rotenone + antimycin.
4) *Glycolytic fraction*: ECAR fraction sensitive to iodoacetate.

OCR/ECAR ratios were used to estimate relative contribution of OxPhos versus glycolysis to cellular energetics as it is independent of cell number. To normalize the respiratory rates, we lysed the cells after the XF assay and quantified the cell number using Picogreen DNA assay (ThermoFisher Scientific) following manufacturer's instructions.

Cellular ATP quantification: ATP was measured using the ATP Determination Kit (A22066, ThermoFisher scientific) using previously published protocols (Afzal et al., 2017). Reaction solution was prepared for 100 μL reaction volume per well. Cells were lysed using passive lysis buffer (Cat. #E1941, Promega) in cultured well for 15 min, and a reaction solution was added in each well and signal was immediately monitored using luminometer. Standard curves were used to estimate the amount of ATP/well and ATP signal was normalized to cell number using the Picogreen DNA assay (ThermoFisher Scientific). Following ATP measurements were performed using inhibition of metabolic pathways in the cultured cells just before the ATP assays as mentioned in detail (Afzal et al., 2017).

Oligo-sensitive ATP %: ATP levels that were sensitive to the inhibition of ATP synthase using oligomycin (4 μM) for 30 min on live cultured cells. This ATP fraction reflects the ATP produced by cells when OxPhos is inhibited. Ox-Phos ATP percentage is calculated as follows: Oligo-sensitive ATP/basal ATP × 100 in each of three experiments.

Fluorescence microscopy: Invasion assay, as well as immunofluorescence imaging was performed on Zeiss AxioObserver, Z1 microscope with either 10 × or ×20 objectives (EC Plan-Neofluar ×10/0.3, and Plan-Apochromat 20x/0.8 M27) and Hamamatsu ORCA Flash camera. The light source used was SOLA light engine, and image acquisition was performed using Zeiss Zen 2.6 software.

Gene silencing

Gene knockout was achieved by using pre-prepared synthetic sgRNA (IDT). hESF (or HTR8) were transfected with sgRNA and recombinant Cas9 (IDT) using CRISPRmax reagent (Invitrogen). Specifically, a cocktail was created by mixing 1) solution1: 24 μL OPTIMEM and 1 uL CRISPRMAX, and 2) solution 2: 10 nmol gRNA, 15 nmol Cas9, 1.5 μL CRISPRMAX Plus reagent and remaining OptiMEM to make a 30 μL solution. Solution 1 and 2 were mixed and incubated for 15 min before being drop dispensed for a 24 well containing hESF, dESF, or HTR8 cells at 70%–80% confluency in culture medium with no serum. Cells were used after 48 h of transfection, and observation completed within 48 h thereafter.

Immunoblot

Cells were lysed in RIPA lysis buffer (Cell Signaling Technology 9806) containing protease inhibitors (Sigma-Aldrich P8340). BCA kit (Thermo Fisher Scientific) was used for protein quantification. 20 ug denatured proteins (95°C for 2 min in SDS) were loaded on 4%–12% NuPAGE Bis-Tris Gel (Thermo Fisher Scientific NP0322BOX), transferred to polyvinylidene difluoride (PVDF) membranes and blocked with 5% BSA for 1 h at room temperature. Antibodies used were: anti-MKL1 (Cusabio G0615A), MYL9 (Proteintech, Inc. 29504-1-AP), phosphor-MYL9 (Proteintech, Inc. 15354-1-AP). Primary antibodies were incubated overnight at 4°C, followed by incubation with GAPDH (Cell Signaling Technology 5174) for 1 h at room temperature. Subsequently, samples were incubated with HRP-linked anti-rabbit secondary antibody (GE healthcare NA9340) for 1 h at room temperature. An enhanced chemiluminescence reagent (Thermo Fisher Scientific 34095) was used to visualize the bands.

Fabrication of ANSIA platform

ANSIA platform was fabricated by methods previously described (Novin et al., 2021). Briefly, nanotextured substrate was fabricated using pre-fabricated molds, or created using

photoresist spun on silicon wafers, and patterned using electron-beam lithography. After developing the photoresist, the exposed silicon was etched with a deep-reactive ion etcher, allowing for the formation of submicron parallel ridges. Residual photoresist was removed using ashing, and diced into silica master for replica molding. Polyurethane was drop-dispensed onto the silicon master and thereafter pressed with a polyethylene terephthalate (PET) film, and subsequently cured with UV (λ= 200–400 nm, 100 mJ/cm^2) for 1 min. After peeling the mold, the revealed patterned PUA was overcured overnight with UV to terminate residual acrylate groups. Patterns were also purchased from Nanobiosurface for some experiments.

The PET-PUA mold was employed as a replica mold to transfer nanotopographic pattern on glass substrate using capillary force lithography (CFL). Glass coverslip was cleaned using NaOH (0.1 M for 1 h), washed with DIH$_2$O, and dried. Propylene glycol monomethyl ether acetate and phosphoric acrylate were mixed in a ratio of 10:1 as a primer and spin coated on the coverslip. The coverslip was baked for 40 min at 68°C. After dispensing PUA precursor dropwise on the primed coverslip, the mold was placed reversibly, and cured in UV (λ= 250–400 nm, 100 mJ/cm^2) for 1 min, peeled, and overcured in UV overnight.

Fabricated or procured substrates were then seeded with cells in the described pattern to create well defined juxtaposed interfaces between fluorescently labeled trophoblasts, and unlabeled stromal fibroblasts using stencils. A stereolithographic plastic mold was used to create polydimethylsiloxane (PDMS) stencil. The stencil was casted in the mold by mixing monomer and cross-linker in a 1: 10 ratio, degassing, and curing at 80°C for 4 h. Topographic substrates were coated with 0.1% w/v collagen type I overnight after corona treatment for 30 s. PDMS stencil was placed, while keeping the setup in a vacuum chamber to allow air under the stencil to escape. H2B-mCherry expressing HTR8 were seeded on the stencil at a density of 10^7 cells/ml, allowed to attach and form a monolayer in 8 h. Unattached cells were washed out 3 times with PBS, the stencil removed to reveal a cleared area. This cleared area was then seeded with stromal fibroblasts at a typical density of 5×10^7 cells/ml. Unattached cells were washed after 4–6 h of seeding, and live cell microscopy performed immediately in a basal medium consisting of 1:1 ratio of HTR8 and ESF medium without cAMP. Any additional factors were added to the medium according to experimental requirement.

Analysis of stromal invasion & determination of invasive parameters: For each time stamp, images were converted to binary using OTSU thresholding technique (Otsu, 1979). Images were dilated employing a 2 × 4 kernel iteratively ~15 times. Remaining black interspersed holes were thereafter closed using a trapezoidal 9 × 9 kernel applied in 40 iterations. Dilation and closing resulted in an almost completely whitened mask, which marked the region occupied by invading trophoblasts, and another almost completely black region occupied by stromal fibroblasts, also containing interspersed white regions occupied by the escaped trophoblasts. Approximating a polygon to the contour of the largest connected segment then provided the final invasion region. The escaped cells outside this region were isolated using watershed segmentation (Najman and Schmitt, 1994). By identifying the convex vertices of the polygon, the invasive forks were marked, and the extent of invasion was determined by calculating the area occupied by the main region of the trophoblasts for each time point. For each invasive fork, we then calculated the horizontal distance it travelled starting from its initial positon.

Statistical analysis

Statistical analysis was performed using students *t*-test unless otherwise mentioned with each result. Data is presented as ± SD, or ±SEM as mentioned in each results section and only significant *pvalues* are reported with each test.

Data availability statement

The data presented in the study is deposited in the NCBI's Gene Expression Omnibus repository, and is accessible through GEO Series accession number: GSE197810 (use token: kripqmwozfitliv).

Author contributions

JA conducted energetics experiments, performed bioinformatics analysis, developed the manuscript. WD performed mechanical experiments, AN performed invasion experiments, YL assisted in bioinformatics analysis, GW helped in developing and editing the manuscript, Kshitiz conceived, and wrote the manuscript.

Funding

Research Enhancement Funding from OVPR, University of Connecticut.

Conflict of interest

The authors declare that the research was conducted in the absence of any commercial or financial relationships that could be construed as a potential conflict of interest.

Publisher's note

References

Afzal, J., Chan, A., Karakas, M. F., Woldemichael, K., Vakrou, S., Guan, Y., et al. (2017). Cardiosphere-derived cells demonstrate metabolic flexibility that is influenced by adhesion status. *JACC. Basic Transl. Sci.* 2, 543–560. doi:10.1016/j.jacbts.2017.03.016

Afzal, J., Liu, Y., Du, W., Suhail, Y., Zong, P., Feng, J., et al. (2022). Cardiac ultrastructure inspired matrix induces advanced metabolic and functional maturation of differentiated human cardiomyocytes. *Cell Rep.* 40, 111146. doi:10.1016/j.celrep.2022.111146

Ansardamavandi, A., and Tafazzoli-Shadpour, M. (2021). The functional cross talk between cancer cells and cancer associated fibroblasts from a cancer mechanics perspective. *Biochim. Biophys. Acta. Mol. Cell Res.* 1868, 119103. doi:10.1016/j.bbamcr.2021.119103

Asif, P. J., Longobardi, C., Hahne, M., and Medema, J. P. (2021). The role of cancer-associated fibroblasts in cancer invasion and metastasis. *Cancers (Basel)* 13, 4720. doi:10.3390/cancers13184720

Bauer, A., Prechova, M., Fischer, L., Thievessen, I., Gregor, M., and Fabry, B. (2021). pyTFM: A tool for traction force and monolayer stress microscopy. *PLoS Comput. Biol.* 17, e1008364. doi:10.1371/journal.pcbi.1008364

Blodgett, D. M., De Zutter, J. K., Levine, K. B., Karim, P., and Carruthers, A. (2007). Structural basis of GLUT1 inhibition by cytoplasmic ATP. *J. Gen. Physiol.* 130, 157–168. doi:10.1085/jgp.200709818

Carter, A. M. (2012). Evolution of placental function in mammals: The molecular basis of gas and nutrient transfer, hormone secretion, and immune responses. *Physiol. Rev.* 92, 1543–1576. doi:10.1152/physrev.00040.2011

Carter, A. M. (2021). Unique aspects of human placentation. *Int. J. Mol. Sci.* 22, 8099. doi:10.3390/ijms22158099

Christian, M., Mak, I., White, J. O., and Brosens, J. J. (2002). Mechanisms of decidualization. *Reprod. Biomed. Online* 4 (3), 24–30. doi:10.1016/s1472-6483(12)60112-6

Colin-York, H., Eggeling, C., and Fritzsche, M. (2017). Dissection of mechanical force in living cells by super-resolved traction force microscopy. *Nat. Protoc.* 12, 783–796. doi:10.1038/nprot.2017.009

Coorens, T. H. H., Oliver, T. R. W., Sanghvi, R., Sovio, U., Cook, E., Vento-Tormo, R., et al. (2021). Inherent mosaicism and extensive mutation of human placentas. *Nature* 592, 80–85. doi:10.1038/s41586-021-03345-1

Costanzo, V., Bardelli, A., Siena, S., and Abrignani, S. (2018). Exploring the links between cancer and placenta development. *Open Biol.* 8, 180081. doi:10.1098/rsob.180081

Dos Remedios, C. G., Chhabra, D., Kekic, M., Dedova, I. V., Tsubakihara, M., Berry, D. A., et al. (2003). Actin binding proteins: Regulation of cytoskeletal microfilaments. *Physiol. Rev.* 83, 433–473. doi:10.1152/physrev.00026.2002

Dumortier, J. G., Martin, S., Meyer, D., Rosa, F. M., and David, N. B. (2012). Collective mesendoderm migration relies on an intrinsic directionality signal transmitted through cell contacts. *Proc. Natl. Acad. Sci. U. S. A.* 109, 16945–16950. doi:10.1073/pnas.1205870109

Erdogan, B., and Webb, D. J. (2017). Cancer-associated fibroblasts modulate growth factor signaling and extracellular matrix remodeling to regulate tumor metastasis. *Biochem. Soc. Trans.* 45, 229–236. doi:10.1042/BST20160387

Esnault, C., Gualdrini, F., Horswell, S., Kelly, G., Stewart, A., East, P., et al. (2017). ERK-induced activation of TCF family of SRF cofactors initiates a chromatin modification cascade associated with transcription. *Mol. Cell* 65, 1081–1095. e1085. doi:10.1016/j.molcel.2017.02.005

Foster, C. T., Gualdrini, F., and Treisman, R. (2017). Mutual dependence of the MRTF-SRF and YAP-TEAD pathways in cancer-associated fibroblasts is indirect and mediated by cytoskeletal dynamics. *Genes Dev.* 31, 2361–2375. doi:10.1101/gad.304501.117

Gaggioli, C. (2008). Collective invasion of carcinoma cells: When the fibroblasts take the lead. *Cell adh. Migr.* 2, 45–47. doi:10.4161/cam.2.1.5705

Garcia-Cao, I., Song, M. S., Hobbs, R. M., Laurent, G., Giorgi, C., De Boer, V. C., et al. (2012). Systemic elevation of PTEN induces a tumor-suppressive metabolic state. *Cell* 149, 49–62. doi:10.1016/j.cell.2012.02.030

Gau, D., and Roy, P. (2018). SRF'ing and SAP'ing - the role of MRTF proteins in cell migration. *J. Cell Sci.* 131, jcs218222. doi:10.1242/jcs.218222

Gellersen, B., Brosens, I. A., and Brosens, J. J. (2007). Decidualization of the human endometrium: Mechanisms, functions, and clinical perspectives. *Semin. Reprod. Med.* 25, 445–453. doi:10.1055/s-2007-991042

Gleeson, L. M., Chakraborty, C., Mckinnon, T., and Lala, P. K. (2001). Insulin-like growth factor-binding protein 1 stimulates human trophoblast migration by signaling through alpha 5 beta 1 integrin via mitogen-activated protein Kinase pathway. *J. Clin. Endocrinol. Metab.* 86, 2484–2493. doi:10.1210/jcem.86.6.7532

Graham, C. H., Hawley, T. S., Hawley, R. G., Macdougall, J. R., Kerbel, R. S., Khoo, N., et al. (1993). Establishment and characterization of first trimester human trophoblast cells with extended lifespan. *Exp. Cell Res.* 206, 204–211. doi:10.1006/excr.1993.1139

Gualdrini, F., Esnault, C., Horswell, S., Stewart, A., Matthews, N., and Treisman, R. (2016). SRF Co-factors control the balance between cell proliferation and contractility. *Mol. Cell* 64, 1048–1061. doi:10.1016/j.molcel.2016.10.016

Hanahan, D., and Weinberg, R. A. (2011). Hallmarks of cancer: The next generation. *Cell* 144, 646–674. doi:10.1016/j.cell.2011.02.013

Hanahan, D., and Weinberg, R. A. (2000). The hallmarks of cancer. *Cell* 100, 57–70. doi:10.1016/s0092-8674(00)81683-9

Hardie, D. G. (2000). Metabolic control: A new solution to an old problem. *Curr. Biol.* 10, R757–R759. doi:10.1016/s0960-9822(00)00744-2

Heid, J., Cencioni, C., Ripa, R., Baumgart, M., Atlante, S., Milano, G., et al. (2017). Age-dependent increase of oxidative stress regulates microRNA-29 family preserving cardiac health. *Sci. Rep.* 7, 16839. doi:10.1038/s41598-017-16829-w

Hsieh, C. H., Chou, Y. T., Kuo, M. H., Tsai, H. P., Chang, J. L., and Wu, C. W. (2017). A targetable HB-EGF-CITED4 axis controls oncogenesis in lung cancer. *Oncogene* 36, 2946–2956. doi:10.1038/onc.2016.465

Huang, G., Besner, G. E., and Brigstock, D. R. (2012). Heparin-binding epidermal growth factor-like growth factor suppresses experimental liver fibrosis in mice. *Lab. Invest.* 92, 703–712. doi:10.1038/labinvest.2012.3

Johnson, L. A., Rodansky, E. S., Haak, A. J., Larsen, S. D., Neubig, R. R., and Higgins, P. D. (2014). Novel Rho/MRTF/SRF inhibitors block matrix-stiffness and TGF-beta-induced fibrogenesis in human colonic myofibroblasts. *Inflamm. Bowel Dis.* 20, 154–165. doi:10.1097/01.MIB.0000437615.98881.31

Knofler, M., and Pollheimer, J. (2013). Human placental trophoblast invasion and differentiation: A particular focus on wnt signaling. *Front. Genet.* 4, 190. doi:10.3389/fgene.2013.00190

Kolberg, L., Raudvere, U., Kuzmin, I., Vilo, J., and Peterson, H. (2020). gprofiler2 -- an R package for gene list functional enrichment analysis and namespace conversion toolset g:Profiler. *F1000Res* 9, 1. doi:10.12688/f1000research.24956.2

Krikun, G., Mor, G., Alvero, A., Guller, S., Schatz, F., Sapi, E., et al. (2004). A novel immortalized human endometrial stromal cell line with normal progestational response. *Endocrinology* 145, 2291–2296. doi:10.1210/en.2003-1606

Krug, K., Mertins, P., Zhang, B., Hornbeck, P., Raju, R., Ahmad, R., et al. (2019). A curated resource for phosphosite-specific signature analysis. *Mol. Cell. Proteomics* 18, 576–593. doi:10.1074/mcp.TIR118.000943

KshitizAfzal, J., Maziarz, J. D., Hamidzadeh, A., Liang, C., Erkenbrack, E. M., et al. (2019). Evolution of placental invasion and cancer metastasis are causally linked. *Nat. Ecol. Evol.* 3, 1743–1753. doi:10.1038/s41559-019-1046-4

Kuleshov, M. V., Xie, Z., London, A. B. K., Yang, J., Evangelista, J. E., Lachmann, A., et al. (2021). KEA3: Improved kinase enrichment analysis via data integration. *Nucleic Acids Res.* 49, W304–W316. doi:10.1093/nar/gkab359

Labernadie, A., Kato, T., Brugues, A., Serra-Picamal, X., Derzsi, S., Arwert, E., et al. (2017). A mechanically active heterotypic E-cadherin/N-cadherin adhesion enables fibroblasts to drive cancer cell invasion. *Nat. Cell Biol.* 19, 224–237. doi:10.1038/ncb3478

Li, L., He, Y., Zhao, M., and Jiang, J. (2013). Collective cell migration: Implications for wound healing and cancer invasion. *Burns Trauma* 1, 21–26. doi:10.4103/2321-3868.113331

Mccarthy, S. A., Samuels, M. L., Pritchard, C. A., Abraham, J. A., and Mcmahon, M. (1995). Rapid induction of heparin-binding epidermal growth factor/diphtheria toxin receptor expression by Raf and Ras oncogenes. *Genes Dev.* 9, 1953–1964. doi:10.1101/gad.9.16.1953

Melo, R. F., Stevan, F. R., Campello, A. P., Carnieri, E. G., and De Oliveira, M. B. (1998). Occurrence of the Crabtree effect in HeLa cells. *Cell biochem. Funct.* 16, 99–105. doi:10.1002/(SICI)1099-0844(199806)16:2<99::AID-CBF773>3.0.CO;2-2

Menkhorst, E. M., Lane, N., Winship, A. L., Li, P., Yap, J., Meehan, K., et al. (2012). Decidual-secreted factors alter invasive trophoblast membrane and secreted proteins implying a role for decidual cell regulation of placentation. *PLoS One* 7, e31418. doi:10.1371/journal.pone.0031418

Montel, L., Sotiropoulos, A., and Henon, S. (2019). The nature and intensity of mechanical stimulation drive different dynamics of MRTF-A nuclear redistribution after actin remodeling in myoblasts. *PLoS One* 14, e0214385. doi:10.1371/journal.pone.0214385

Najman, L., and Schmitt, M. (1994). Watershed of a continuous function. *Signal Process.* 38, 99–112. doi:10.1016/0165-1684(94)90059-0

Novin, A., Suhail, Y., Ajeti, V., Goyal, R., Wali, K., Seck, A., et al. (2021). Diversity in cancer invasion phenotypes indicates specific stroma regulated programs. *Hum. Cell* 34, 111–121. doi:10.1007/s13577-020-00427-6

Otsu, N. (1979). A threshold selection method from gray-level histograms. *IEEE Trans. Syst. Man. Cybern.* 9, 62–66. doi:10.1109/tsmc.1979.4310076

Park, J. M., Adam, R. M., Peters, C. A., Guthrie, P. D., Sun, Z., Klagsbrun, M., et al. (1999). AP-1 mediates stretch-induced expression of HB-EGF in bladder smooth muscle cells. *Am. J. Physiol.* 277, C294–C301. doi:10.1152/ajpcell.1999.277.2.C294

Pesta, D., and Gnaiger, E. (2012). High-resolution respirometry: OXPHOS protocols for human cells and permeabilized fibers from small biopsies of human muscle. *Methods Mol. Biol.* 810, 25–58. doi:10.1007/978-1-61779-382-0_3

Pollheimer, J., Vondra, S., Baltayeva, J., Beristain, A. G., and Knofler, M. (2018). Regulation of placental extravillous trophoblasts by the maternal uterine environment. *Front. Immunol.* 9, 2597. doi:10.3389/fimmu.2018.02597

Randall, S., Buckley, C. H., and Fox, H. (1987). Placentation in the fallopian tube. *Int. J. Gynecol. Pathol.* 6, 132–139. doi:10.1097/00004347-198706000-00005

Ray, K. C., Moss, M. E., Franklin, J. L., Weaver, C. J., Higginbotham, J., Song, Y., et al. (2014). Heparin-binding epidermal growth factor-like growth factor eliminates constraints on activated Kras to promote rapid onset of pancreatic neoplasia. *Oncogene* 33, 823–831. doi:10.1038/onc.2013.3

Reid, B., Afzal, J. M., Mccartney, A. M., Abraham, M. R., O'rourke, B., and Elisseeff, J. H. (2013). Enhanced tissue production through redox control in stem cell-laden hydrogels. *Tissue Eng. Part A* 19, 2014–2023. doi:10.1089/ten.TEA.2012.0515

Sethuraman, A., Brown, M., Krutilina, R., Wu, Z. H., Seagroves, T. N., Pfeffer, L. M., et al. (2018). BHLHE40 confers a pro-survival and pro-metastatic phenotype to breast cancer cells by modulating HBEGF secretion. *Breast Cancer Res.* 20, 117. doi:10.1186/s13058-018-1046-3

Sleep, J., Irving, M., and Burton, K. (2005). The ATP hydrolysis and phosphate release steps control the time course of force development in rabbit skeletal muscle. *J. Physiol.* 563, 671–687. doi:10.1113/jphysiol.2004.078873

Subramanian, A., Tamayo, P., Mootha, V. K., Mukherjee, S., Ebert, B. L., Gillette, M. A., et al. (2005). Gene set enrichment analysis: A knowledge-based approach for interpreting genome-wide expression profiles. *Proc. Natl. Acad. Sci. U. S. A.* 102, 15545–15550. doi:10.1073/pnas.0506580102

Suhail, Y., Afzal, J., and Kshitiz (2021). Evolved resistance to placental invasion secondarily confers increased survival in melanoma patients. *J. Clin. Med.* 10, 595. doi:10.3390/jcm10040595

Suhail, Y., Cain, M. P., Vanaja, K., Kurywchak, P. A., Levchenko, A., Kalluri, R., et al. (2019). Systems Biology of cancer metastasis. *Cell Syst.* 9, 109–127. doi:10.1016/j.cels.2019.07.003

Sun, Q., Chen, G., Streb, J. W., Long, X., Yang, Y., Stoeckert, C. J., Jr., et al. (2006). Defining the mammalian CArGome. *Genome Res.* 16, 197–207. doi:10.1101/gr.4108706

Vander Heiden, M. G., Cantley, L. C., and Thompson, C. B. (2009). Understanding the warburg effect: The metabolic requirements of cell proliferation. *Science* 324, 1029–1033. doi:10.1126/science.1160809

Wagner, G. P., KshitizDighe, A., and Levchenko, A. (2021). The coevolution of placentation and cancer. *Annu. Rev. Anim. Biosci.* 10, 259–279. doi:10.1146/annurev-animal-020420-031544

Wagner, G. P., KshitizDighe, A., and Levchenko, A. (2022). The coevolution of placentation and cancer. *Annu. Rev. Anim. Biosci.* 10, 259–279. doi:10.1146/annurev-animal-020420-031544

Wang, L., Lu, Y. F., Wang, C. S., Xie, Y. X., Zhao, Y. Q., Qian, Y. C., et al. (2020). HB-EGF activates the EGFR/HIF-1α pathway to induce proliferation of arsenic-transformed cells and tumor growth. *Front. Oncol.* 10, 1019. doi:10.3389/fonc.2020.01019

Wang, Z., Yang, Q., Tan, Y., Tang, Y., Ye, J., Yuan, B., et al. (2021). Cancer-associated fibroblasts suppress cancer development: The other side of the coin. *Front. Cell Dev. Biol.* 9, 613534. doi:10.3389/fcell.2021.613534

Wu, L., Stadtmauer, D. J., Maziarz, J. D., and Wagner, G. (2020). *Decidual cell differentiation is evolutionarily derived from fibroblast activation*. Newyork City: BioRxiv (Cold Spring Harbor Laboratory).

Xia, G., Rachfal, A. W., Martin, A. E., and Besner, G. E. (2003). Upregulation of endogenous heparin-binding EGF-like growth factor (HB-EGF) expression after intestinal ischemia/reperfusion injury. *J. Invest. Surg.* 16, 57–63. doi:10.1080/08941930390194389

Yotsumoto, F., Fukagawa, S., Miyata, K., Nam, S. O., Katsuda, T., Miyahara, D., et al. (2017). HB-EGF is a promising therapeutic target for lung cancer with secondary mutation of EGFR(T790M). *Anticancer Res.* 37, 3825–3831. doi:10.21873/anticanres.11761

Zhang, C., Luo, X., Liu, L., Guo, S., Zhao, W., Mu, A., et al. (2013). Myocardin-related transcription factor A is up-regulated by 17β-estradiol and promotes migration of MCF-7 breast cancer cells via transactivation of MYL9 and CYR61. *Acta Biochim. Biophys. Sin.* 45, 921–927. doi:10.1093/abbs/gmt104

Zheng, X., Boyer, L., Jin, M., Kim, Y., Fan, W., Bardy, C., et al. (2016). Alleviation of neuronal energy deficiency by mTOR inhibition as a treatment for mitochondria-related neurodegeneration. *Elife* 5, e13378. doi:10.7554/eLife.13378

Frontiers in
Cell and Developmental Biology

Explores the fundamental biological processes of life, covering intracellular and extracellular dynamics.

The world's most cited developmental biology journal, advancing our understanding of the fundamental processes of life. It explores a wide spectrum of cell and developmental biology, covering intracellular and extracellular dynamics.

Discover the latest Research Topics

See more →

Frontiers

Avenue du Tribunal-Fédéral 34
1005 Lausanne, Switzerland
frontiersin.org

Contact us

+41 (0)21 510 17 00
frontiersin.org/about/contact